Geometric and surface energy balance change affecting Kårsaglaciären, northern Sweden, over the past century

Christopher Neil Williams

Submitted in accordance with the
requirements for the degree of

Doctor of Philosophy

The University of Leeds

School of Geography

September 2013

Declaration

The candidate confirms that the work submitted is his own, except where work which has formed part of jointly-authored publications has been included. The contribution of the candidate and the other authors to this work has been explicitly indicated below. The candidate confirms that appropriate credit has been given within the thesis where reference has been made to the work of others.

The candidate contributed work to the article outlined below, which was published in the Journal of Glaciology. The candidate is a co-author of the article. The article was published in October 2011.

The 2008 glacier outline presented in chapter 7 was used throughout Rippin *et al.* (2011) to support their observational analysis. The observational analysis presented in Rippin *et al.* (2011) is not the work of the author of this thesis and was performed by David Rippin. As such, where the observations from Rippin *et al.* (2011) have been discussed in this thesis, they have been referenced accordingly.

Publication details:
Rippin, D.M. and Carrivick, J.L. and Williams, C. 2011. Evidence towards a thermal lag in the response of Kårsaglaciären, northern Sweden, to climate change. *Journal of Glaciology*, 57(205), pp895-903.

Acknowledgements

There are many people I would like to thank who have made this thesis possible. Firstly a big thank you to my supervisors — Dr Jonathan Carrivick, Dr Andrew Evans and Dr Steve Carver — for their ideas, enthusiasm, help, assistance and patience throughout my time at Leeds. Thanks to Daniel Carrivick for all of the help in the field — you made loads considerably lighter to carry. At the Abisko Naturvetenskapliga station, my thanks to Linnia Wanhatalo and Annika Kristoffersson for their accommodation during the field work in Sweden and their assistance with acquiring meteorological data records. At the University of York, Dr David Rippin for his assistance and advice both in and out of the field. At the University of Stockholm, Professor Peter Jansson and Professor Per Holmlund for their advice and for opening the vaults of the department of Physical Geography and Quaternary Geology so that I could access the original maps of Dr Wallén and Dr Bodin. At Utrecht University, Dr Rianne Giesen for all of her advice on distributed surface energy balance modelling. At the University of Leeds my thanks to the School of Geography and in particular David Appleyard, Lee Coothoopermal and David Ashley for sorting out everything computer and field equipment related.

My nomadic PhD approach since 2012 would not have been possible if it were not for the very accommodating Dr Lewis Gilbert at the University of Minnesota, USA and the staff at the Max Planck Institute for Biogeochemistry, Jena, Germany. A special thanks also to those who provide the excellent working environments available as part of the German library system - both in Karlsruhe and Jena.

I am blessed to have great family and friends who have always supported me and without whom I would not be where I am today. A huge thanks to Mum, Dad, Tom and Charlie for always being there and always believing in me; Franzi for consistently putting up with me and standing by me; Ed Turner for all of his wisdom; Aaron O'Leary for the good times and Bethan White for all of the physics related advice and climbing. Thanks also to Nikée Groot, Tom Kelly, Ant Blundell and all of the other PhD students and post-docs at the University of Leeds who have provided a great environment in which to study.

Finally I would like to thank Professor Andrew Russell for introducing me to glaciology on the first field trip I ever made to Iceland — even if it did rain all of the time.

Abstract

Glacier mass balance depends upon the dynamic change of glacier geometry. Despite this effect being recognised as important, few modelling studies have addressed and quantified it specifically. This study presents a 99 year reconstruction and mass balance response analysis of Kårsaglaciären, a small (0.89 km^2) mountain glacier located in Arctic Sweden, using a number of techniques in order to overcome this limitation.

A geodetic approach was used to assess changing mass balance over time. Data were derived from topographic maps and contemporary field surveys. These data were used to interpolate a number of DEMs and full 3D reconstructions were derived, providing information on spatial change for the period 1909-2010. A long term trend of negative mass balance was identified. The glacier retreated 1292 m, thinned by 0.35 m w.e. yr^{-1} and reduced in volume by 1.33 km^3 yr^{-1}.

The 3D reconstructions provided the input for a user friendly, simple distributed surface energy balance model, aimed at facilitating the assessment of the effect of geometry change on mass balance — designed specifically for this study and made available to other researchers online (`https://github.com/Chris35Wills/SEB_model_java_files`). Using the reference balance approach, it was possible to assess change in mass balance over time both with and without dynamic surface adjustment, allowing disentanglement of these effects with climate. Geometry change on an annual basis had little effect on glacier mass balance response to climate but has a significant dampening effect for the period 1926-1943.

These results provide evidence of Kårsaglaciären showing a strong pattern of retreat throughout the 20th and early 21st century. From these analyses it is apparent that the effects of glacier geometry on mass balance response are not simply linked by time. Future mass balance studies should consider changes in glacier geometry for accurate assessments of glacier response to climate.

Abbreviations and Symbols

ANS	Abisko Naturvetenskapliga Station
T_a	Air temperature
ALS	Airborne Laser Scanner
α	Albedo (general)
α_{ice}	Albedo (ice)
α_{snow}	Albedo (snow)
τ	Atmospheric Transmissivity
AWS	Automatic Weather Station
z_{bed}	Bed elevation
ψ	Bulk flux
ψ_{min}	Constant Bulk Flux value
CLR	Constant Lapse Rate
$dGPS$	Differential Global Positioning System
ELA	Equilibrium Line Altitude
GIS	Geographic Information System
$z_{glacier\ thickness}$	Glacier thickness
GPS	Global Positioning System
GUI	Graphical User Interface
GCP	Ground Control Point
GPR	Ground Penetrating Radar
H	Hillshade value
HEP	Hydroelectric Power
ρ_{ice}	Ice density
$z_{ice\ surface}$	Ice surface elevation
I	Incident Radiation

R	Instantaneous sun earth distance
km^3	Kilometres cubed
km^2	Kilometres squared
LR	Lapse Rate
L_f	Latent heat of fusion
η	Latitude
MB	Mass Balance
Rm	Mean sun earth distance
Q	Melt energy
$mw.e.$	Melt water equivalent
m	Metres
$ma.s.l.$	Metres above sea level
$MALR$	Moist Adiabatic Lapse Rate
yr^-1	Per year
RPA	Raster Planar Surface Area
c	Rate of increase of Bulk Flux
SLR	Sea Level Rise
ρ_{snow}	Snow density
T_{Thresh}	Snowfall threshold
ϕ	Solar azimuth
I_0	Solar constant
δ	Solar declination
ω	Solar hour angle
θ	Solar zenith
A	Surface aspect
SEB	Surface Energy Balance
β	Surface slope
T_{Tip}	Temperature Tipping point
TLS	Terrestrial Laser Scanner
ρ_{water}	Water density

WGI	World Glacier Inventory
$WGMS$	World Glacier Monitoring Service

Contents

List of Figures

List of Tables

Chapter 1

Introduction

Small mountain glaciers are extremely important indicators of climate change due to their small size and fast response times (Dyurgerov & Meier, 1997, 2000; Dyurgerov, 2003; Raper & Braithwaite, 2006; Haeberli *et al.*, 2007). Many Arctic glaciers have been found to be particularly responsive to climate, especially those in northern Europe due to their location relative to warm, north trending Atlantic ocean currents (James *et al.*, 2012). Recent studies have concluded that the mass loss of relatively small glaciers in mountain regions could be much more important for contributions to sea level in the short term than contributions from the large ice sheets of Greenland and Antarctica (Meier *et al.*, 2007). The retreat of small mountain glaciers also has immediate regional and local implications because changes in meltwater magnitude and timing affects power generation, irrigation, riparian ecology and even tourism.

This study is an investigation into mountain glacier mass loss with a specific focus on the control that changing glacier geometry has on both the surface energy balance and mass balance. Glacier geometry modifies energy contributions of the different elements of the surface energy balance which in turn affects mass balance. An understanding of the surface energy balance (SEB) is vital if one is to calculate, understand and eventually predict changes to the volume of small mountain glaciers. Modelling is an important way of understanding surface/atmosphere interactions and the potential effects that climate change may consequently have

on local and global hydrology (Michlmayr *et al.*, 2008).

There has long been a focus on the effect of climate on glacier mass balance with early work by Finsterwalder & Schunk (1887) and Ångstrom (1933) in the early 20th Century. This work identified the relationship between glacier fluctuations and climatic variations and led to an understanding of the surface energy balance which manifests itself over a glacier surface at the glacier/atmosphere interface (Hock, 2005). The surface energy balance exists as a pool of energy over a glacier that can either be in surplus or deficit relative to the energy needed to maintain the glacier in a steady state. The SEB exists through energy contributions from a variety of components including air temperature and solar radiation. Where the energy balance is in surplus, melting of snow and ice can occur. However, if the energy balance is in deficit, melting will not occur as there is not enough energy available to facilitate this process. The SEB is inextricably linked to climate and is the link between climate change and glacier mass change.

A wealth of glacial mass balance models exist (e.g. Hock & Noetzli, 1997; Braithwaite & Zhang, 2000; Michlmayr *et al.*, 2008; MacDougall & Flowers, 2010; Paul, 2010) which account for changes in the mass of a glacier in relation to the surface energy-balance and which have different distributions (local/regional/global) and data requirements. These models vary between being point and grid (distributed) based (Hock, 2005) and many are finely tuned to best-fit individual glaciers. Issues relating to the use of fixed digital elevation models (DEMs) — and therefore non-dynamic glacier surface geometry — in modelling studies with regard to elevation effects have been considered in the work of others including e.g. Gerbaux *et al.* (2005). However, many existing models do not consider dynamic geometric effects, particularly with regard to changes in slope and aspect from those inherent to the initial input surface (e.g. Paul, 2004; Harrison *et al.*, 2009; Huss *et al.*, 2012).

Investigation of the effects of dynamic geometric change and the resultant response of mass balance is vital to enable further understanding of mountain glacier response to changes in climate. Knowledge derived from this study will ultimately enable better modelling and prediction of how glaciers will change in accordance

with changing climate and what effects this will have both globally, such as affecting sea level rise (SLR), and locally, such as affecting power generation and with regard to tourism where mountain glaciers are present in more populated areas such as the European Alps.

The aims of this study are to:

1. Provide a full 3D glacier geometry reconstruction and assessment of a small mountain glacier, since the beginning of the 20th century, over decadal and annual time scales (see chapters 6 and 7)

2. Assess the sensitivity of the surface energy balance and mass balance change to meteorological and topographical forcing (see chapter 8)

3. Assess the effect of changing glacier geometry on the surface energy balance and mass balance of a small mountain glacier throughout the 20th and early 21st century with focus on solar radiation contributions and glacier-topography relationships (see chapter 9)

These aims are addressed via the following objectives:

1. Collate historic topographic maps and reports as well as data from the field to ascertain glacier geometry, meteorological conditions and snow pack characteristics (see chapter 4)

2. Apply geostatistical methods to reconstruct 3D glacier geometry and enable geometry and geometric change analyses (through development of a GIS) (see chapter 4)

3. Account for sensitivity of applied geostatistical techniques on reconstructed surface properties (see chapter 4)

4. Develop a user friendly grid based distributed surface energy balance model which uses reconstructed surfaces as an input, combined with meteorological data from the field (see chapter 5)

5. Conduct model scenarios with the developed model to assess the effects of meteorological and topographic forcing as well as geometry change on surface energy balance and mass balance change (see chapter 5)

Chapter 2

Literature review

2.1 Mountain glaciers, climate change and sea level rise

Mountain glaciers include all of those outside of the Greenland and Antarctic ice sheets, with them sometimes being referred to as small glaciers and ice caps (Paterson, 1994; Raper & Braithwaite, 2006; De Woul, 2008). Approximately 10% of the Earths land surface is covered in ice of which only approximately 3% is from outside of the two major ice caps (Church, 2001; Solomon *et al.*, 2007). These smaller glaciers and ice caps cover an area between 512 x 10^3 and 546 x 10^3 km^2 which is equal to a sea level equivalent (SLE) rise of 0.15 - 0.37 m respectively (Lemke, 2007). Although covering only a small amount of the globe, they contribute significantly to SLR due to their short response times and large mass turn-over (Oerlemans *et al.*, 1998).

Throughout the 20th century and to the present there has been a generally negative trend in mountain glacier mass balance across the globe resulting in large reductions in volume (Dyurgerov & Meier, 2000; Zemp *et al.*, 2006; Diolaiuti *et al.*, 2011; Gardner *et al.*, 2011; Lenaerts *et al.*, 2013). The global retreat of glaciers in recent decades is a clear sign of accelerating environmental change and this is, rightly or wrongly, frequently accepted as a clear manifestation of global warming (Kuhn, 1981; Haeberli *et al.*, 1999; Dyurgerov & Meier, 2000;

Oerlemans, 2005; Zemp *et al.*, 2006; Citterio *et al.*, 2007; Diolaiuti *et al.*, 2011). Glacier retreat relates directly to the glacier/climate transfer function concept whereby a change in one over time, results in equivalent change in the other (Oerlemans, 2005; Diolaiuti *et al.*, 2011). Glacier change is directly governed by the mass balance (MB) — where negative, this results in glacier mass loss (associated with glacier thinning and retreat) and where positive, this results in glacier mass gain (associated with glacier thickening and advance). Change in the MB is controlled predominantly by the surface energy balance (SEB). These two balances are discussed in detail in section 2.2.

Between 20-25% of global continental land masses are orographic, supporting 10% of the Earths population and indirectly affecting 50% (Haeberli & Beniston, 1998; Barry, 2008). Decreases in mountain glaciers and ice caps not only increase melt water contribution to SLR (Jacob *et al.*, 2012), but also affect settlements within glacier locales which rely upon glaciers for irrigation and resource supplies (Chen & Ohmura, 1990; Granshaw & Fountain, 2006). In Switzerland, 56% of the national energy mix is from hydroelectric power and remains the main renewable energy component. This figure was at 90% in the 1970s, reducing as a consequence of the introduction of nuclear power (BFE, 2013). Further relating climate change to mountain regions specifically, there have been observations made of elevation-dependent climate change occurrences in some areas, with some exhibiting seasonal warming rates greater than at sea level (Rangwala & Miller, 2012). However the use of such observations in support of climate change is controversial, due to the relative lack of understanding of meteorological processes in mountain environments (e.g. Barry, 1992; Rangwala & Miller, 2012). A full understanding of glacial systems is required in order to assess the effect that a changing climate will have upon them (Huss *et al.*, 2012) and to predict future contributions from these glaciers in the most accurate way possible.

Small mountain glaciers are of special interest as they have been identified as extremely useful indicators of climate perturbations. Compared to all other ice masses, small glaciers are the first to respond to changes in climate (Grudd, 1990). Studies have identified that smaller glaciers respond much quicker to climate

perturbations compared to their larger counterparts in Greenland and Antarctica (Granshaw & Fountain, 2006; DeBeer & Sharp, 2009), and this helps to explain their large proportional contribution to 20th century SLR (see below) (Raper & Braithwaite, 2006). Over the past century, the largest area reductions of ice in the Alps are manifest over glaciers of area less than 1 km^2 (Citterio *et al.*, 2007; Diolaiuti *et al.*, 2011). Faster response times of smaller glaciers are supported by kinematic wave theory which has been used to identify valley glacier response times to be within the order of 10 - 70 years (Folland, 2001).

The Arctic has been attributed to be particularly sensitive to climate change (Bates *et al.*, 2008), and this in part can be contributed to the number of small mountain glaciers and their related fast response times, within the region. The World Glacier Inventory (WGI) was used to identify that in 2009 64.2% of Arctic glaciers were $\leq$2 km^2 (Rippin *et al.*, 2011). The contribution of glaciers in these regions to SLR is expected to propagate over the next century (Arendt *et al.*, 2002; Raper & Braithwaite, 2006; Rippin *et al.*, 2011). The relative juxtaposition of Arctic glaciers, such as in Svalbard, to the north of warm North Atlantic currents further enhances sensitivity of these glaciers to climate change (Fleming *et al.*, 1997; Lefauconnier *et al.*, 1999; James *et al.*, 2012).

Current estimates of mass balance in terms of SLR for Antarctica and Greenland are in the range of -0.12 to +0.38 mm yr^{-1}, which is equivalent to a +42 to -139 Gton yr^{-1} of mass gain or loss (Shepherd & Wingham, 2007; Lee *et al.*, 2013). This compares to estimates from mountain glaciers in the range of 0.52 to 1.4 mm yr^{-1} (Kaser *et al.*, 2006; Meier *et al.*, 2007; Bahr *et al.*, 2009; Cogley, 2009; Hock *et al.*, 2009; Cogley, 2011; Radić & Hock, 2011; Jacob *et al.*, 2012). A best approximation of mountain glaciers and ice cap contribution throughout the 20th century is equal to approximately 0.028 m (Church, 2001; Raper & Braithwaite, 2006). Increasingly negative mass balance values are a cause for concern with regard to SLR (e.g. Solomon *et al.*, 2007) as this is important with regard to planning as well as with regard to those that live in the immediate vicinity of glaciers (Xu *et al.*, 2009). In model runs with warming running from 1998 - 2100,

mountain glaciers appear to decline much faster than ice caps, therefore contributing proportionally more to SLR; ice caps did not appear to contribute until the 21st Century (Raper & Braithwaite, 2006). The contribution from mountain glaciers and ice caps to SLR is expected to be prolific for at least the next 100 years (Meier *et al.*, 2007; Glasser *et al.*, 2011; Radić & Hock, 2011) however some authors argue that specific contributions are yet to be calculated (Glasser *et al.*, 2011; Radić & Hock, 2011). The contribution to SLR from mountain glaciers and ice caps is an order of magnitude greater than for both the Greenland and Antarctic ice sheets when compared to calculations made by Zwally *et al.* (2005) and discussed in Carrivick & Chase (2011), contributing to an SLR of 0.5 mm yr^{-1} over the past 50 years (Kaser *et al.*, 2006; Raper & Braithwaite, 2006; Carrivick & Chase, 2011).

Thus, despite acknowledgment of the importance of the sensitivity of small mountain glaciers, there is still a lot left to be understood and it is critical to reduce such uncertainties to enable more effective planning, such as for resources and energy policy. Contemporary and future projections of glacier contributions to SLR and thus to hydroelectric power (HEP) and irrigation, are still uncertain and this is linked to data gaps in global information on the size and locations of glaciers (Paul, 2011). Such gaps explain the large errors that have been for example associated with attempts at estimating total SLR contributions by the end of the 21st century which range between 0.05 - 0.24 m (Hock *et al.*, 2009; Paul, 2011).

Following a critical study of the literature, a number of common themes have been identified, highlighting a variety of issues that contribute to inaccuracies associated with assessments of mountain glacier melt (Gardner *et al.*, 2013; Kerr, 2013; Zemp *et al.*, 2013). The key issues with regard to the difficulties and errors associated with estimating mountain glacier and ice cap meltwater contributions that need to be addressed include:

1. Geodetic ice loss calculations (see section 2.4) for individual glaciers are distorted where surface interpolations are based on sparse point networks resulting in poor reconstructions of glacier dimensions (Barrand *et al.*,

2010; Carrivick & Chase, 2011). Such issues fail to acknowledge the effects introduced by glacier hypsometry and climatic gradients (Førland & Hanssen-Bauer, 2003);

2. Knowledge of geometric, topographic and climatic conditions of individual glaciers is required to understand and more accurately accounting for local glacier change (Oerlemans, 1987; Granshaw & Fountain, 2006; Salinger *et al.*, 2008). Neglecting these factors can result in highly erroneous melt and resultant SLR estimates (Barrand *et al.*, 2010). To scale up measurements from only a few glaciers to provide catchment wide values, risks inaccuracies being introduced as such scaling will often not effectively account for true inter-catchment variability (Carrivick & Rushmer, 2009).

3. Poor understanding of the variability in mass-balance gradients leads to poor melt estimates from modelling routines, as mass-balance sensitivities are inaccurately represented (Raper & Braithwaite, 2006). Despite these uncertainties — which can be related to limitations of existing studies — volume changes are still calculated which will only emulate these issues. (Carrivick & Chase, 2011);

4. Glacier volume can easily be overestimated as a function of the methodological approach taken to derive a value. Volumes are often calculated from only a few point measurements or the use of *center-line* analyses (e.g. Shugar *et al.*, 2010) which results in an inadequate quantification of spatial variability (Barrand *et al.*, 2010; Berthier *et al.*, 2010; Carrivick & Chase, 2011) (see section 2.4). Volume inaccuracies can be further introduced as a result of the application of fixed density functions, resulting in incorrect acknowledgments of true glacier water content and therefore contribution to SLR (Huss, 2013);

More recently, many inconsistencies have been found between local and satellite based measurements of glacier mass balance, the former often providing more negative results. This is discussed with the methodology of this study in chapter 10.

2.2 The driver of glacier change - the relationship between surface energy balance (SEB) and mass balance (MB)

The sum of the different energy fluxes that exist across the surface of a glacier at a given point in time amounts to the *surface energy balance* (SEB) (Hock, 2005; Benn & Evans, 2010). The energy fluxes are contributed by different meteorological factors as well as changes of state and geological components. The SEB directly affects the glacier mass balance (MB). Where the mass of a glacier is in balance, this is indicative of conditions where accumulation and ablation processes are equal over a year. Such a positive MB indicates accumulation processes are dominant over ablation processes. Accumulation processes include addition of mass through a number of processes (which are site specific), including precipitation, avalanching and snow drifting. A negative MB indicates ablation processes exceed the contribution of accumulation processes. At a given point in time, positive SEB conditions, whereby there is a surplus of energy available at the surface, will drive snow and ice melt. Equally, where there is an energy surplus available to drive ice/snow melt, there will be mass loss through melting. These varying states of SEB contribute directly to the overall MB change of the glacier resulting in more or less mass loss respectively. However, the relationship between SEB and MB is not simple, resulting in an array of complex feedbacks, as by the SEB affecting MB, the SEB is itself modified by resultant changes and evolution of the glacier surface, as well as the relationship between the glacier and the topography that surrounds it. Here an assessment of the different terms and calculations associated with MB are discussed as well as the construction of the SEB equation and acknowledgments of contributions to it. Modelling is not discussed here, being the focus of section 2.5.

2.2.1 Glacier mass balance

Glacier mass balance is equal to the difference between net accumulation and net ablation measured over a given time period, which is usually a year. This can also be called the cumulative mass balance, as it is calculated by the addition of the

winter and summer balances, the latter usually having a negative sign. A value of 0 from such a calculation denotes a glacier in balance, with a negative value indicating negative balance and a positive value indicating a positive balance. The *year* over which mass balance is calculated is better described as being between specific glacier stances whereby two stances define the "year" time step. In this case it is better to refer to the time step as the balance-year (Benn & Evans, 1998). Here, we define $t1$ and $t2$ as the glacier minimum surface at time step 1, succeeded by the glacier minimum surface at time step 2. Regarding nomenclature, the following terms are used to define mass balance:

1. Specific net balance: mass change per unit area (not glacier wide) relative to the previous minimum surface $t2$ (b_n)

2. Annual glacier balance: mass change for the entire glacier relative to the previous minimum surface $t2$ (B_n)

3. Mean glacier balance: mass change for the entire glacier relative to the previous minimum surface $t2$ divided by the glacier area ($\bar{b_n}$)

There is a lot of confusion in the literature between different terms for mass balance (Cuffey & Paterson, 2010), where ultimately specific, mean and annual balance all mean the same - the only factor changing being the area over which they are integrated. The calculation of these values are defined in equations 2.1, 2.2 and 2.3 (Cuffey & Paterson, 2010).

$$b_n = \mathrm{t2} - \mathrm{t1} \tag{2.1}$$

$$B_n = \int_A \mathrm{b_a}\,\mathrm{d}A \tag{2.2}$$

$$\bar{b_n} = \frac{B_n}{A} \tag{2.3}$$

Where b_n has been calculated for a surface where data on surface change is only available over large time steps, the value calculated for b_n using equation 2.1 is then divided by the number of years in the interval between $t1$ and $t2$. To convert

changes in mass to m w.e. (melt water equivalent) values, changes in terms of ice thickness are considered. Glacier ice density is assumed to be 900 kg m^{-3} compared to water at 1000 kg m^{-3}. Where B_n or $\bar{b_n}$ are in m (ice), m w.e. is calculated using:

$$m\ w.e.\ =\ \Delta m_{ice}\ \text{x}\ 0.9 \tag{2.4}$$

where Δm_{ice} is the change in mass in m of ice per the area defined. Δm_{ice} is derived from either equation 2.2 or 2.3. The m w.e. calculations here assume no change in total ice density, with it being fixed at 900 kg m^{-3}. Fixing ice density for m w.e. volume change assessment is common (Braithwaite, 2002) and has been carried out in other studies over long periods including a 50 year reconstruction and comparison for Glacier de Sarennes, French Alps, from 1952-2003 (Thibert *et al.*, 2008).

2.2.2 Conventional and reference glacier mass balance

The aforementioned description and equations 2.1 - 2.3 pertain to the *conventional mass balance* and such values are derived from different studies of mass balance change (see section 2.4) and modelling efforts. These studies assume the glacier itself changes in accordance to its state of mass balance, although this may not be explicitly stated (Huss *et al.*, 2012). This is mentioned, as following Elsberg *et al.* (2001), a second term — the *reference balance* — was also defined.

The reference balance calculation was originally used in situations where little spatial information relating to a glacier was available (perhaps a single map from the beginning of a long term mass balance assessment). The issue identified was that mass balance at specific points could only be translated to the available map, despite the glacier surface having changed (requiring an updated glacier map) — ultimately giving incorrect information regarding mass balance, especially where mass balance change was not linearly related to elevation (Elsberg *et al.*, 2001). Such limitations are overcome when considering conventional and reference balance approaches together. Where a conventional balance is calculated using a dynamic surface which changes in relation to changing meteorological conditions

and mass loss, the reference balance is calculated using a fixed reference surface for which the geometry is held fixed and the surface does not change. Thus, all geometric components of a reference surface will remain the same for a given period. The amount of mass loss which may be expected over the set time frame for such a surface can still be calculated, but the specific geometric considerations relating to — for example — elevation, slope and aspect which are considered in the calculation of different fluxes, do not alter. For the conventional surface, these values do alter. By comparing dynamic (conventional) surfaces and fixed (reference) surfaces, the effects of changes in surface geometries can be considered in terms of their effect on mass loss and therefore mass balance processes affecting a given glacier.

The calculation of the reference balance provides information on a hypothetical glacier state, providing the mass balance at a given time whilst assuming glacier geometry has remained fixed since a given reference period. The reference balance therefore isolates the effects that any dynamic glacier geometric changes may have on MB change. This differs to the conventional balance which changes in time with glacier geometry. Thus, the reference balance method is extremely useful for climatic and dynamics based problems (Elsberg *et al.*, 2001). However, due to its fixed nature, it does not represent real changes and thus is no replacement for the contemporary mass balance which gives knowledge of real mass changes, thus being of use when considering melt water output such as for SLR. The reference balance can be acquired using a SEB model approach as in Huss *et al.* (2010) or by extrapolating mass-balance profiles of different years to the reference surface as engineered in the studies of Elsberg *et al.* (2001) and Harrison *et al.* (2009).

Few studies have made use of the reference mass balance approach (Huss *et al.*, 2008; Harrison *et al.*, 2009; Paul, 2010; Huss *et al.*, 2012) with no such studies having been carried out on small mountain glaciers in sub-polar/polar regions. Nevertheless, the method of conventional/reference mass balance comparison is powerful in its ability to allow for an assessment of geometrical change and its effect on SEB and therefore MB.

An important consideration when applying the method, as mentioned in Harrison *et al.* (2009), concerns what specific elements of the *reference* surface remain fixed. Harrison *et al.* (2009) state that their application of the reference balance method corrects for both elevation and area and that where area alone is fixed, this should be given another name such as the reference-area balance, specifically so that the two types of reference balance can be differentiated.

2.2.3 The surface energy balance

The overall SEB propagating over a glacier surface is contributed to by a number of factors (Hock, 2005) including:

1. Net radiation (Q_N)
2. Sensible heat flux (Q_H)
3. Latent heat flux (Q_L)
4. Ground heat flux (Q_G)
5. Sensible heat flux from rain (Q_R)
6. Energy consumed by melt (Q_M)

These factors can be represented as part of the overall SEB as:

$$Q_N + Q_H + Q_L + Q_G + Q_R + Q_M = 0 \tag{2.5}$$

Where the factors = 0, there is no surplus or energy deficit. Where the SEB $\neq$ 0, an energy surplus would be represented by a positive value, and a deficit by a negative value. Thus energy then affects the glacier surface by inducing melt or not, hence the close relationship to glacier MB as mentioned at the beginning of section 2.2. Equation 2.5 can be rewritten to show the energy available at the glacier surface (Q) as in (Hock & Holmgren, 1996):

$$Q = Q_N + Q_H + Q_L + Q_G + Q_R + Q_M \tag{2.6}$$

The modeling of the SEB is discussed in section 2.5. A consideration of the effect of changing surface geometry through time on both the SEB and MB is covered in section 2.3.

2.3 Considering surface geometry and topographic effects on SEB and MB

As highlighted in section 2.1, a number of issues exist when considering the quantification of glacier mass change and resultant meltwater contributions. A number of methods are used to assess spatial glacier change over time, a review of which is carried out in the section 2.3.6. This review considers the merits of the different methods as well as their associated limitations, along with possible ways in which mass balance can be assessed considering the SEB distribution using a distributed spatial modelling approach. Such a review is prudent as there is a call for further study of spatial variability of SEB/MB relationships, in particular with reference to the feedbacks and fluctuations related to glacier change as a function of climate (Giesen & Oerlemans, 2010; Oerlemans, 2010a; Carturan *et al.*, 2013). Despite a solid understanding of SEB and MB processes (section 2.2), spatial studies of geometric evolution are required and prove an invaluable tool for decoupling glacier geometric effects from equilibrium conditions (Zemp *et al.*, 2006). To allow for an effective consideration of the methods available (section 2.3.6), an understanding of the effects of geometry on SEB and MB must first be acknowledged and it is these effects that are specifically tested in this thesis. *Geometry* is defined as the slope, aspect and elevation of a given area of a glacier surface. The key effects of geometry changes on the SEB and MB are summarised in table 2.1.

Table 2.1: Geometry effects on SEB and MB

Geometric and assoc. changes	Effects on SEB	Possible effects on MB	Further considerations
Slope	• Modification of shortwave radiation receipt with smaller receipts being associated with steeper slopes • Modification of relationship to surrounding topography which is important when considering diffuse and long-wave radiation receipt. Where slope angles are favorable to radiative receipt from surrounding topography, SEB will be enhanced	• Steeper slope angles will result in more negative specific MB values, as a function of slope alone • Enhanced diffuse radiation receipt will result in more negative specific MB	• Effect of slope on radiation dependent on other factors including elevation, aspect, position relative to surrounding topography and surface elevation • Diffuse radiation dependent on sky view factor (Oke, 1987) and aspect whilst long-wave radiation depends on position relative to surrounding topography • Spatially and temporally variable - this variability must be considered for accurate assessment of effects on SEB and MB

Continued on Next Page...

Table 2.1 – Continued

Geometric and assoc. changes	Effects on SEB	Possible effects on MB	Further considerations
Aspect	• Modification of shortwave radiation receipt with smaller receipts being associated with northerly aspects in the northern hemisphere and southerly aspects in the southern hemisphere • Important when considering the relationship of a given position to surrounding topography which is important when considering diffuse and long-wave radiation receipt. Where aspect angles are favorable to radiative receipt from surrounding topography, SEB will be enhanced. Surface aspects away from surrounding topography will result in less long-wave radiation receipt, but may result in greater diffuse radiation receipt from the sky	• Northerly aspects (in the northern hemisphere) and southerly aspects (in the southern hemisphere) will result in less specific MB change as a function of shortwave radiation receipt alone, as opposed to southerly aspects • Enhanced diffuse or long-wave radiation receipts will result in more negative specific MB	• Effect of aspect on radiation dependent on other factors including elevation, aspect, position relative to surrounding topography and surface elevation. • Spatially and temporally variable and this variability must be considered for accurate assessment of slope effects on radiation receipt, SEB and MB • Diffuse radiation dependent on sky view factor (Oke, 1987) whilst long-wave radiation depends on position relative to surrounding topography

Continued on Next Page...

Table 2.1 – Continued

Geometric and assoc. changes	Effects on SEB	Possible effects on MB	Further considerations
Elevation	• Temperature changes as a function of adiabatic lapse rates, increasing and decreasing sensible heat flux within total SEB • Air pressure associated with elevation is important to consider for calculations of turbulent flux - lowering resulting in increased pressure, increasing turbulent flux contrib. to the SEB • Precipitation gradients vary adiabatically, resulting in increased precipitation values at higher elevations. For an in-situ glacier, reduced elevations will result in reduced precipitation receipt.	• Reduced elevations will result in more negative MB values • Higher air pressures contribute to increasingly negative MB values (as a function of air pressure alone) • Ignoring other environmental factors, reduced elevations resulting in less summer rainfall could result in less negative MB values, as a function of rainfall alone. However, coupled with lower winter accumulation values and a resultant thinner snow pack could enhance negative MB propagation	• Enhancement effects of lower elevations may be dampened by other changes over time (e.g. glacier retreat, changes in hypsometry) • Spatially and temporally variable • Precipitation effects on MB require careful consideration of other factors including glacier relationship to topography, as well as mass movements of snow across the glacier (drifting and avalanching) as precipitation falling in one area is often rerouted to other areas (which themselves may not be susceptible to direct precipitation receipt). Elevation changes on small glaciers not likely to alter precipitation gradients significantly

Continued on Next Page...

Table 2.1 – Continued

Geometric and assoc. changes	Effects on SEB	Possible effects on MB	Further considerations
Hypsometry (area)	• Change in hypsometry affects all of the above factors, limiting or expanding the areas over which they propagate • Where a large % of total area is located around the ELA, an increase in ELA altitude will increase area susceptible to ablation - this infers an increase in SEB surplus	• Where the above factors have a larger area over which to provide conditions for greater SEB values, MB will become more negative • Increasing ELA altitudes where a large % of area exits around the initial ELA position, can result in rapid change in MB, becoming increasingly negative where swaths of former accumulation zone are converted to ablation zone	• Temporally dependent/ ELA change dependent on a variety of different factors within and related to total SEB

Continued on Next Page...

Table 2.1 – Continued

Geometric and assoc. changes	Effects on SEB	Possible effects on MB	Further considerations
Topography	• Shading resulting in reduction of shortwave radiation receipt at the surface - greater shade reduces contribution of shortwave radiation to the SEB • Important for considering the contribution of diffuse radiation - where topography is more restrictive of surface sky view factors, diffuse energy contributions to the SEB will be reduced • A source of long-wave radiation which affects snow and ice near to it. These areas receive more energy in the form of long-wave radiation which enhances the energy available within the SEB	• Greater shade results in reduced specific mass balance (as a function of shortwave radiation alone) • More restricted sky view factors may result in less negative MB (as a function of diffuse radiation alone) • Snow and ice near to topographic features may have more negative MB values than areas further away (as a function of long-wave radiation alone)	• Spatially and temporally variable • Diffuse radiation calculations often used in conjunction with the sky view factor (Oke, 1987) • Effect of long-wave radiation contribution to the surface depends on other topographic factors which limits the amount of direct shortwave radiation reaching certain area of topography. Juxtaposition of the glacier to different topographies affects their susceptibility to long-wave energy contributions from it.

Table 2.1 is not exhaustive of all possible geometric effects on SEB and MB, but has been constructed to identify key elements of importance - most often associated with distributed SEB modelling approaches (section 2.5.3). As can be seen in table 2.1, geometry is important in its effect on different elements of the SEB which in turn affect the specific and total MB of a glacier. These effects are further considered in the following subsections, as well as the importance of spatial and temporal variability (and therefore requirement for their study).

2.3.1 Slope and aspect

Slope and aspect are particularly important when considering the receipt of shortwave radiation on a surface (I). For mid-high latitude surface energy balance studies (see section 2.5), radiation has occasionally been found to contribute as much as 96-99% of the overall balance as in the study of Arendt (1999) on a high Arctic glacier, although lower values more equal to 75% tend to be more common (Arnold *et al.*, 2006b). Not only is incoming radiation of vital importance in terms of its contribution to the SEB, it is also highly susceptible to local environmental variables - namely surface slope, aspect and hillshade values as represented in equations 2.7 and 2.8, adapted from Burrough & McDonnell (1998):

$$I = H \text{ x } cos_i \, S_{in,TOA} \, exp(-\tau / cos\theta_0) \tag{2.7}$$

where H represents the mean % topographic shading for a given time period, i is the solar illumination on the slope, $S_{in,TOA}$ is the exoatmospheric flux, τ is the atmospheric transmissivity, θ_0 is the solar zenith angle. cos_i is calculated using:

$$cos_i = [cos\theta_0 \, cos\beta + sin\theta_0 \, sin\beta \, cos(\phi_0 \, - A)] \, S_{in,TOA} \tag{2.8}$$

where ϕ is the solar azimuth, A is the slope aspect and β is the slope angle. Radiation is often recognised to provide the largest contribution to the overall SEB of a glacier (Benn & Evans, 1998). As a consequence of its importance and sensitivity to surface geometry, distributed surface energy balance modelling approaches pay careful attention to its calculation (e.g. Hock & Noetzli, 1997; Hock & Holmgren, 2005). Due to lower sun angles, for Arctic glaciers, the implications of

slope and aspect variability on shortwave radiation receipt are important, however their effect may be reduced compared to lower latitudinal areas due to the amount of daylight received on a daily basis during polar summers (Arnold *et al.*, 2006b).

2.3.2 Surface geometry and surrounding topography

Equation 2.7 accounts for the effects of surface geometry on incoming direct shortwave radiation, and the limiting effects of topographic shading. Shading is the result of surrounding topography, which is recognised as a key factor in controlling spatial patterns of SEB propagation and mass balance. The amount of shade that propagates across the glacier surface depends on the juxtaposition of the glacier to surrounding topography, as well as consideration of solar azimuth and zenith angles which are time dependent (as well as latitudinally dependent) (Burrough & McDonnell, 1998; Hock & Holmgren, 2005; Arnold *et al.*, 2006b). The effect of changing hillshade patterns relative to solar position are displayed in figure 2.1.

Where an area of a glacier is shaded, it receives no direct radiation (Hock & Holmgren, 2005). Shading effects have the potential to be much more considerable at higher latitudes (such as in the High Arctic) due to lower solar zenith angles (Arnold *et al.*, 2006b). With surface lowering — another geometric change — hillshade values are likely to increase, resulting in a reduction in the amount of radiation reaching the surface and further reductions of sky view values and therefore receipt of diffuse radiation (from the sky). Considering retreat of glaciers, proportional hillshade of the total glacier area is also likely to change and this is discussed further in chapter 4.

Equation 2.7 accounts for hillshade effects but is exclusive of more complex relationships concerning radiation reflection from slopes and surfaces to one another. Such complex relationships have been calculated in some distributed SEB models such as in Hock & Holmgren (2005). This relationship is also a key element of the *Complex terrain module* of the *Alpine 3D* model (Lehning *et al.*, 2006; Michlmayr *et al.*, 2008). The sky view of a given point on a glacier is

Figure 2.1: Hillshade patterns as a function of solar position and topography. Changing solar position is indicated by sun positions A and B. The expected shade patterns occurring as a function of solar position relative to topography is indicated by the shaded areas. Shaded areas labeled A represent shading expected when the sun is in position A. B^+ is used to indicate shading from position B, as it overlaps the areas shaded when the sun is in position A. Where the glacier is completely shaded, no direct shortwave radiation is incident at the surface, with radiation being contributed to the SEB in the form of diffuse and long wave radiation only.

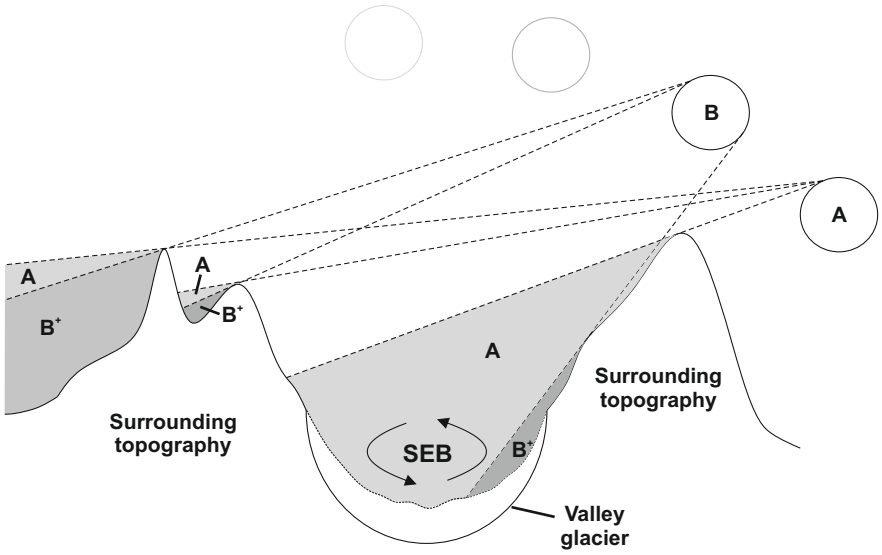

further controlled by topography which is important in its control on the amount of diffuse radiation that can be received at a given point on the glacier surface, which relates to the sky view factor (Oke, 1987). Diffuse radiation is calculated in the distributed model of Hock & Holmgren (2005), considering the sky view factor proposed by Oke (1987). The sky view factor (F) is calculated by Hock & Holmgren (2005) using:

$$F = 1/2\pi \int_0^2 \pi cos^2 \gamma d\varphi \tag{2.9}$$

Where γ is the elevation of the horizon, d and φ is the azimuth, as defined by Oke (1987). This requires a consideration of the elevation angle of the horizon which is directly controlled by the geometry of a given area on the glacier being modelled and which consequently changes as a function of geometric change. Equation 2.9 assumes a horizontal surface, however, as mentioned in Hock & Holmgren (2005), the angle that should be used is that which describes the deviation from the normal to the inclined surface and the direction of radiation.

2.3.3 Elevation

Surface elevation is of great importance for a number of components of the SEB and this is often related to variability in adiabatics, thus change in pressure. As a result of ablation, a glacier thins and consequently the surface elevation at a given point lowers. This forces the surface into a region of greater air temperature, as can be expressed via simple temperature lapse rate relationships. Such changes have been used to explain differences between the reference and conventional surface balance of South Cascade Glacier, Washington, USA (Huss *et al.*, 2012). Elevation changes resulting in such temperature variability have further effects. *Turbulent flux* — the mixing of sensible heat and latent heat — is directly affected by temperature and also by air density (which is affected by pressure). Both of these factors vary with elevation and thus, a change in elevation will result, to some extent, in a change in turbulent flux (although the change may be small) (Cuffey & Paterson, 2010). The effects of changes in these parameters is best illustrated when considering the calculation of sensible (Q_H) and latent heat (Q_L)

flux as components of the aerodynamic approach at calculating turbulent flux (Hock & Holmgren, 2005; Cuffey & Paterson, 2010):

$$Q_H = \rho_a c_a C_H u[T_a - T_s] \tag{2.10}$$

$$Q_L = \rho_a L_{v/s} C_E u[q_a - q_s] \tag{2.11}$$

where ρ_a is air density, c_a is the specific heat capacity of air at a constant pressure, $L_{v/s}$ is the latent heat of vaporization or sublimation, C_H and C_E are coefficients for heat and moisture, u is wind speed, $T_a - T_s$ represents the contrast in temperatures of the lower boundary layer and $q_a - q_s$ represent contrasts in absolute humidity (Cuffey & Paterson, 2010). Giesen & Oerlemans (2012) further account for the dependence of such factors in a simpler consideration of SEB in the form of ψ which is explained further in chapter 5 — the value of ψ being directly affected by air temperature.

Precipitation gradients are also of importance when acknowledging change in elevation over a given glacier, as such gradients are directly dependent on elevation (Nesje, 1992). Precipitation gradients are recognised as being important when considering ELA position variability (e.g. Nesje, 1992; Carrivick & Chase, 2011). As ELA is descriptive of the MB state of a glacier, such gradients should be considered. Some modelling approaches account for such change (e.g. Adalgeirsdottir *et al.*, 2006), whereby precipitation (adiabatically) increases with elevation. Adalgeirsdottir *et al.* (2006) acknowledge 3-dimensional variations in precipitation gradients by calculating precipitation at a point ($p(x, y, z)$) using:

$$p(x, y, z) = (1 + g_z(z - z_0))(1 + g_x(x - x0) + g_y(x - x0))p_c \tag{2.12}$$

where g_x and g_y are site specific horizontal precipitation gradients, g_z is a site specific vertical precipitation gradient, x and y are horizontal coordinates, z is the altitude, x_0, y_0 and z_0 represent the location of a reference position (the meteorological station) in 3-dimensions and p_c is a scaled precipitation value at

a meteorological station. Topography and other factors are also responsible for variations in precipitation with elevation and therefore precipitation gradients — as represented by factors g_x, g_y and g_y — are site specific. Such difficulties as assessing spatial precipitation gradients are an inherent issue of many modelling applications (e.g. Flowers *et al.*, 2005). Where glacier elevation distributions change over time, so will precipitation gradients. Accounting for elevation change — as in this study — is key in modelling approaches reconstructing and predicting future glacier responses to changes in climate as precipitation is key in its contribution to surface mass.

It should be noted that the potential enhancement effects of surface lowering on the SEB may be limited as a proportion of the total glacier when considering changes in hypsometry and accounting for retreat. Considering proportional change, retreat of a glacier to higher elevations may dampen the effect of point specific elevation lowering.

2.3.4 Hypsometry

Glacier MB is extremely susceptible to changes in hypsometry over time. Hypsometry is defined as the relationship between area distribution with elevation. Where large proportions of total glacier area are located around the ELA, changes in hypsometry in this region will result in significant shifts in the position of the ELA, which in turn can result in faster or slower responses to changes in climate (Benn & Evans, 1998). Change in the position of the ELA is particularly effective in changing the balance of a glacier on ice caps, where increase in ELA altitude can turn large parts of the accumulation zone into ablation zone (Nesje, 1992; Brozovic *et al.*, 1997; Carrivick & Brewer, 2004; Nesje *et al.*, 2008; Giesen & Oerlemans, 2010).

2.3.5 Spatial considerations of geometry

The effects of geometry highlighted above — especially with regard to slope, aspect, elevation and position relative to topography — all vary in space. The relationship of geometries between one another results in the presence of a variety

of feedbacks across a glacier surface and analysis of the spatial distribution of such components is key to further understand SEB/MB processes (Oerlemans, 2010a; Carturan *et al.*, 2013). Spatial assessment is further recognised as key in understanding decoupling that is observed between glacier geometries and contemporary warming (Zemp *et al.*, 2006; Carturan *et al.*, 2013). Such study is vital where predictions of future glacier change and contributions to hydrological systems are to be made effectively. Failing to account for spatial variability is misleading in studies of SEB and MB change, as smaller scale variations are not accounted for. Klok & Oerlemans (2002) showed that by neglecting spatial variations in hillshade, clear sky view, reflection from surrounding slopes as well as surface slope and aspect, resulted in a 37% increase in modelled incoming shortwave radiation, resulting in an increase in ablation of 0.34 mm yr^{-1}. The importance of spatial factors are revisited in section 2.5.3.

2.3.6 Geometric evolution: effects and quantification

Geometry is important to consider in the calculation of numerous components of the SEB (as exemplified in equations 2.7, 2.10, 2.11 and 2.12). Many models assume such geometry to be temporally invariant - a number of such models are highlighted in table C.1. However, geometry does not remained fixed and extrapolating calculations of mass balance change into the future using models based on fixed contemporary geometries is incorrect as it fails to acknowledge glacier adjustment to their environments (Le Meur *et al.*, 2007). Thus such calculations should account for geometric change through time (see figure 2.2).

Gerbaux *et al.* (2005) found that by using a constant digital elevation model (DEM) to assess mass balance change for a 23 year period, a considerable source of error in this modelling was attributed to the lack of accounting for elevation changes which were as large as 20 m in some areas of the glacier. Studies of glacier melt also recognise that melt processes are spatially variable — a function of a number of factors of which hillshade is often key (e.g. Hock & Holmgren, 2005; Arnold *et al.*, 2006b) considering its effect on shortwave radiation which is often attributed as the biggest contributor to SEB. Considering elevation change

associated with melting of ice and the variability of such melt processes, this inevitably results in changes in slope and aspect. With further thinning and resultant *retreat* of a glacier, this affects hypsometry. Thus all components of glacier geometry change over time and in response to MB change.

Figure 2.2: Geometric evolution through change in mass balance affects the SEB that acts over it. Such geometric changes should be accounted for when modelling processes occurring at the glacier/climate interface. Ignoring geometric change will provide inaccurate results, especially over longer time periods.

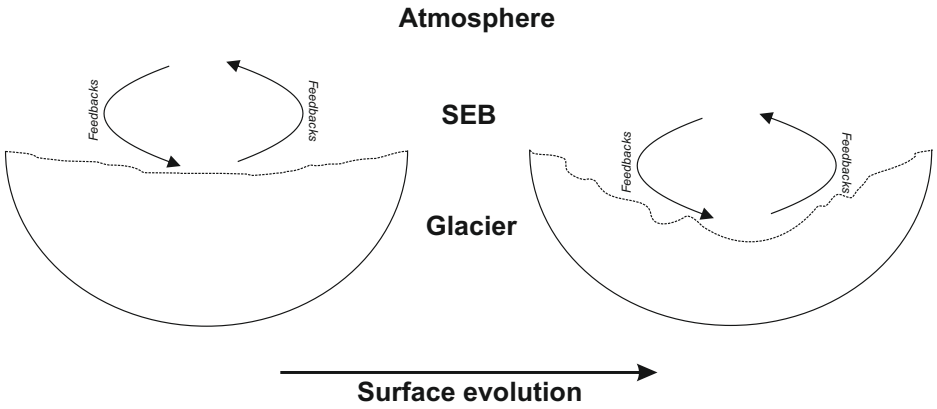

Reference balance modelling — discussed in section 2.2.2 — is an extremely effective way of accounting for the effects of changing glacier geometry on MB, allowing for the identification between climatic forcing and geometric forcing. However, quantification of the effect of geometry on MB has only been carried out in a few studies - namely Paul (2010) and Huss *et al.* (2012). Other studies have also accounted for change according to geometry but preventing DEM updates in distributed model applications (e.g. Arnold *et al.*, 2006b) — differing from the reference balance approach where all geometry is fixed. To quantify the variability between calculated reference and conventional mass balances, thus detailing the proportion of MB change attributed to geometric adjustment as opposed to climate, Huss *et al.* (2012) use a fraction F_i, calculated using:

$$F_i = \Delta B_{c-r,i} / B_{r,i} \tag{2.13}$$

where $\Delta B_{c-r,i}$ is the difference between conventional and reference annual balance, $B_{r,i}$ is the annual reference-surface balance and i represents the year for which the balances represent (Huss *et al.*, 2012).

Despite the importance of geometry in its requirement for the calculation of a number of SEB components, many studies that have not accounted for its evolution have been able to model MB values representative of those observed in the field (e.g. Arnold *et al.*, 1996; Brock *et al.*, 2000a). Such models have usually been operated over short time scales and oppose results of longer time scale model applications such as the aforementioned study of Gerbaux *et al.* (2005). This is explained in results from the 82 year study of Huss *et al.* (2012) where annual variability was found in conventional mass balance values whereas no short-term variability was found to exist in $\Delta B_{c-r,i}$ of equation 2.13, which exhibited instead a steady increase in long term variability. This is implicit of the long-term importance of accounting for varying geometry, indicative that such change over shorter time scales has little effect. Such a conclusion could equally be countered when considering how drastic geometric changes are on a year-by-year basis.

However, considering the more general gradual geometric evolution of the vast majority of glaciers and acknowledging the importance of geometry in terms of the SEB and MB, a key issue that remains which limits further advances in better quantification of geometric modification effects on SEB and MB is the availability of data. Long term studies quantifying topography are required coupled with meteorological records and in-situ MB observations where possible, to be able to assess geometric effects on SEB and MB. Such data are limited, especially in less populated glacierised areas (many more long-term studies exist in the Alps than in the Arctic for example), and furthermore where such data are available, their compilation is thwarted by issues often relating to resolution. These themes of historical study and error are discussed further in section 2.4.1 and are fully addressed by this thesis in chapters 4, 6 and 7.

2.4 Addressing glacier and mass balance change over time

Glacial behavior is controlled by both climate and the physical properties of ice (Paterson, 1994). Due to this close relationship, a better understanding of glacier behaviour and response over time (Oerlemans, 2005) can be sought through the collation of data detailing changing climatic and glaciological conditions. Such data compilation is possible through both glacier/climate monitoring and reconstruction (Bauder *et al.*, 2007; Knoll *et al.*, 2009). Depending on the data available, such data compilations can lead to an improved understanding of variability in both glacier change and processes occurring over both spatial and temporal scales (Carr & Coleman, 2007; Nussbaumer *et al.*, 2011).

A number of different methods exist enabling assessment of glacier response to changes in climate over time. These methods focus on the mass balance of a glacier as discussed in section 2.2. The key approaches include the geodetic, glaciological, flux and hydrological methods, as well as modelling mass balance change from climate records, although this later method excludes all non-climatic related processes (Kaser *et al.*, 2003).

The glaciological method provides in-situ measurements of mass balance change - something that can not be drawn where one of the other methods is applied. This method requires the measurement of both accumulation and ablation at specific points on a glacier, whereby changes are interpolated between measurement points within a network (Østrem & Brugman, 1991; Kaser *et al.*, 2003; Zemp *et al.*, 2013).

The basic methodology requires that changes in ice mass are assessed by changes in surface elevation relative to measured stakes (the number of which is appropriate is discussed in Fountain & Vecchia (1999)) and pits. Observed changes in ice elevation are converted to mass assuming an ice density of 900 kg m^{-3} — this is modified where the materials that change are snow. This requires additional measurements to be carried out, requiring the excavation of glacier-wide representative snow

pits and measurement of snow density (Braithwaite, 2002). A number of critiques comparing the glaciological and the geodetic methods have been carried out (e.g. Østrem & Haakensen, 1999; Hagg *et al.*, 2004). Zemp *et al.* (2013) report that a dozen mass balance studies exist whereby this method has been applied, coupled with decadal geodetic surveys. On comparison of the two, sometimes there is agreement between the MB values calculated and sometimes there is disagreement. The differences between the methods are discussed further in section 2.4.1. The glaciological method is very useful but is only of use for long term studies where past interest in a specific glacier was of a magnitude enough to initiate such a study. Other methods, including the geodetic method, can often be used to draw data from sources that were not necessarily developed for specific glacier study.

The flux method is only useful under steady state conditions as under positive or negative balances which cause an acceleration or slow down of glacier velocity, the method will fail (Kaser *et al.*, 2003). This relates to the principal of mass conservation whereby mass balance should be equally balanced by ice flux divergence and thickness change (Zemp *et al.*, 2010). Application of the method requires consideration of mean glacier velocity as measured at the ELA and ice thickness, from which cross sectional glacier area can be calculated. This method is clearly illustrated and described mathematically in Brown *et al.* (1982).

The hydrological method can be used to assess mass balance as a storage term in a given water balance (Hagg *et al.*, 2004). Such a hydrological balance (B) of an entire area, being calculated for example by:

$$B = P - Q - E \pm \Delta S \tag{2.14}$$

where P is precipitation, Q is runoff, E is evaporation ΔS is variation of other storage elements within a defined catchment (not including glaciers) (Kaser *et al.*, 2003). Such an approach requires a very high level of instrumentation and the maintenance of a high level of both spatial and temporal resolution if useful assessments of mass balance change are to be sought (Hagg *et al.*, 2004).

The use of climate records offers another approach to assess glacier change over time. As glacier MB is affected by both climate and the physical properties of ice (Paterson, 1994), excluding the latter infers that MB can be assessed climatically (Kaser *et al.*, 2003). A number of studies have been conducted whereby the annual balance of glacier has been reconstructed through modelling applications (e.g. Vincent, 2002; Schöner & Böhm, 2007; Nemec *et al.*, 2009). Unlike the other methods, this approach does not account for elements specific to the glacier other than its climatic location.

The geodetic method allows for an indirect assessment of glacier mass change by subtracting successive glacier DEMs from one another. The method requires the availability of accurate elevation surfaces that are then differenced providing the geodetic balance. The method does not provide a true mass balance as this would require the assumptions of static ice density and static bedrock (i.e. no tectonic or isostatic rebound vertical related movement), to be met (Bamber & Rivera, 2007). The methods of DEM acquisition can vary, with data coming from topographic maps, satellite imagery and field surveying methods (ranging from the use of dumpy levels and theodolites to GPS and terrestrial laser scanning) and these are important considerations as the geodetic approach is extremely sensitive to vertical error. As a result of this, surfaces for comparison should be separated by a time step of a magnitude great enough that observed change is greater than associated error (Bamber & Rivera, 2007). Despite the usefulness of this method, where geodetic data have multi-annual time gaps, they cannot be used to obtain accurate mass balance values of annual resolution. This is not an issue where longer time period patterns are being assessed but the method should not replace in situ measurements inherent of the glaciological method where very high resolution data are required over shorter time periods (Fountain *et al.*, 1999b; Bauder, 2001; Bauder *et al.*, 2007). Due to the interest of this project in changing glacier geometry and its effect of the SEB, considering the methods available, the geodetic method is that which is focused on, as it provides a spatial assessment of change (Carturan *et al.*, 2013). This method choice relates partly to the data that are available for the glacier assessed in this study and also to the way in which spatial reconstructions allow for a proper assessment of

changing geometry of a glacier - something that the other methods do not focus on.

The surfaces used in the geodetic method can be derived from topographic maps which also allow for a reconstruction of the pattern of retreat, advance, change in area and hypsometry and changing geometry (slope and aspect) of glaciers through time. It should be highlighted that although glacier terminus position changes can be derived directly from total glacier area maps and imagery (e.g. Leclercq *et al.*, 2012a), there are a number of studies where glacier terminus position alone is recorded, although often this contributes to a larger study (e.g. Zagórski *et al.*, 2008). The specific methods of such characteristic calculations are discussed in chapter 4.

The equilibrium line altitude (ELA) can be derived from a combination of the aforementioned methods and deserves to be addressed briefly here, particularly considering the wide variety of approaches to its calculation. The ELA is a theoretical point where accumulation rates match those of ablation averaged over a balance year (Paterson, 1994; Benn & Lehmkuhl, 2000). Rarely does one altitude across a glacier surface maintain such a property and so the ELA is calculated as a mean altitude across the glacier (Benn & Lehmkuhl, 2000). Such an ELA position is known as the annual ELA. The steady-state ELA, whereby the mass balance at the ELA mean altitude is 0, can only be estimated where multiple annual ELA positions are estimated over a number of years. Where such data are available, ELA mass balance can be plotted against elevation, and through the points a line of best fit can be placed from which the steady state ELA can be deduced (Benn & Lehmkuhl, 2000).

The ELA can be calculated using a variety of methods, many of which require knowledge of the spatial and vertical extent of the glacier and are thus often derived using methods and imagery inherent of the geodetic method (although a single image may be used to derive the ELA where knowledge of mass balance change occurring at positions equal to those represented by the map is available — this links to ideas explored earlier in section 2.2.2). Where glacier geometry is available — whereby geometry relates to area, hypsometry and knowledge of the

altitudinal range — a number of methods can be used to assess ELA position including the specific methodologies discussed in chapter 4:

1. Area x Altitude (AA) method
2. Kinematic method (Hess altitude)
3. Area weighted mean altitude (AWMA)
4. Accumulation Area Ratio (AAR)
5. Toe-to-headwall altitude ratio (THAR)
6. Toe-to-summit altitude method (TSAM)

Where knowledge of the glacier mass balance is known — and assuming positive and negative balance gradients of a generalised balance curve are approximately linear — the Area Altitude Balance Ratio (AABR) method can be used. This was formerly the Balance Ratio (BR) method as in Furbish & Andrews (1984) but later renamed by Osmaston (2005). Assuming the ELA is of an equal position to the transient snow line (TSL), ELA position can be estimated directly from images of the TSL of a given glacier (Kaser *et al.*, 2003). However, such an assumption is rarely true in polar regions due to complications introduced by the presence of superimposed ice (Adams *et al.*, 1998). Many of these methods are very rudimentary and based on wide assumptions, applying only really where a glacier is in steady-state. However, the ELA has been estimated in studies where a glacier is known to not be in steady state, thus using the ELA as a kind of mass balance proxy (e.g. Hawkins, 1985). Furthermore, due to the wide range of values that can be acquired through the application of the different methods of ELA calculation, it is common to approximate its position by taking the average of multiple calculations (Carr & Coleman, 2007; Davies *et al.*, 2012). It should be noted that where the ELA is derived directly from topographic maps (such as via the kinematic routine discussed in Cogley & McIntyre (2003)), the ELA position will be directly related to horizontal and vertical map errors.

2.4.1 The geodetic method: glacier monitoring and previous studies

It is widely recognised that studies assessing the changing characteristics of glaciers in terms of thickness, area, length and volume over various time scales are important for assessing the changing conditions of the cryosphere (Pelto, 2006; Tennant & Menounos, 2013). Direct assessment of glacier change in terms of mass and length did not develop with any particular accuracy until the late 19th century (Nussbaumer *et al.*, 2011). For use of the geodetic method for a specific glacier, data must be sought that can be used to assess spatial change at a specific location over time. Today, a number of methods exist which make this possible — the specific approaches used have been subject to change over time and with technological advances. Today, remote sensing — both satellite and aerial based — provides the only real method of assessing glacier mass change over regional scales (Bamber & Rivera, 2007). A key tool in the development and assessment of change pertained from glacier monitoring and reconstructions are provided by Geographical Information Systems (GIS) (Knoll et al., 2009), providing a simple way to analyse the spatial nature of the data. This allows for simple (geodetic) change analysis between data sets, particularly so relating to the use of raster file types and datasets.

Early glacier studies with the aim of assessing glacier mass balance and change required mass man power and extensive periods of time being spent in the field. Such studies took place in Switzerland (with the initial co-ordination of the Swiss Glacier Inventory (SGI) from 1894), with many studies being focused in Nordic countries by Swedish and Norwegian researchers from the early 20th century (including Ahlmann & Tryselius, 1929; Ahlmann *et al.*, 1933; Ångstrom, 1933; Sverdrup & Ahlmann, 1935; Wallén, 1949). More studies began to develop in the European Alps from the 1930s (Hock, 2005). These studies often made use of the glaciological method but were often associated with the development of glacier scale maps. Map development required the use of manual surveying practices with use later of aerial photography. Aerial photography surveys, as of the 1960s, were taken of glaciers in Switzerland at regular intervals (Bauder *et al.*, 2007). Despite

a wealth of data being available from these studies, accurate position of maps and images is difficult and prone to the errors inherent of pre-GPS methodologies.

The digital age brought the availability of accurate positioning through GPS as well as satellite monitoring from the 1970s onwards, following the launch of Landsat 1, which instigated a number of projects including the development of the United States Geological Surveys (USGS) *Satellite Image Atlas of Glaciers of the World* (Williams & Ferrigno, 2010). A number of tools are now available to glaciologists, providing data in the form of satellite imagery. Examples of the satellites providing imagery include the MSS, TM, ETM+ sensors associated with the Landsat programme and ASTER, aboard the Terra satellite. The spatial resolutions of the data available from the Landsat sensors range from 15-60 m whereas ASTER data has a resolution of 15-30 m. Images used in different studies are sought from a variety of sensors (some of which are no longer operational e.g. those associated with the Corona programme) - knowledge of resolutions is key when searching archives for imagery for a specific location. Glacier imagery can be refined by band processing (bands TM4 and TM5 being used with data from the Landsat TM sensor (Paul, 2002, 2004)) as well as by making use of false colour composites (Paul, 2002). This latter approach can be useful for defining the position of transient snow lines (Krimmel & Meier, 1975; Rott, 1976). The use of satellite imagery is extremely helpful, providing a means of uniform and frequent glacier monitoring (Tennant *et al.*, 2012). Unlike other methods for which their application is planned for a given study (e.g. the glaciological method), it is often possible to make use of satellite imagery from non-specific pass overs to assess glacier change. This means that much more data are now available (of course, this extends to other fields of spatially associated research as well). The methods mentioned above detail passive sensing units which detect naturally available light. These differ to active sensors which provide their own source of illumination (Lillesand *et al.*, 2004). Such active sensing approaches include radar altimetry, airborne laser scanning (ALS), terrestrial laser scanning (TLS) and syntheic aperture radar (SAR).

Today a number of monitoring programmes are in existence and a number of authors are working with remote sensing data enabling high resolution glacier change observations to be made in a number of regions (e.g. Kääb *et al.*, 2002; Ranzi *et al.*, 2004; Raup *et al.*, 2007a,b; Paul, 2008). With the advent of a variety of international remote sensing projects including Global Land Ice Measurements from Space (GLIMS) (Paul, 2002; Bishop *et al.*, 2004; Raup *et al.*, 2007a,b), groups such as the World Glacier Monitoring Service (WGMS, 2013) and missions (e.g. the Gravity Recovery and Climate Experiment (GRACE)), it has become much easier to acquire data and evaluate glacier change over much larger spatial scales compared to the studies of the pre-digital age. Spatially, they provide a pathway by which we can better understand the complex earth surface processes and feedback mechanisms that will both facilitate (and further develop) potential changes in climate (Aniya *et al.*, 1996). However, remote sensing approaches alone are temporally limited and consequently long term reconstructions often require a combination of digital and pre-digital data.

Despite the importance of glacier observations, the ability to maintain long term programmes at a given site has always been thwarted by both funding limitations and (lack of) dedicated researchers (Nussbaumer *et al.*, 2011). To centralise the information on glacier change over time that is available, the World Glacier Monitoring Service (WGMS) was developed in 1986 (Aniya *et al.*, 1997; WGMS, 2013). The WGMS collates information on glacier fluctuations, including mass, area, volume and length which is classed as glacier fluctuation data, as well as on perennial surface ice (glacier inventories) (WGMS, 2013). With the development of the Global Land Ice Measurements from Space (GLIMS) project, for which a global assessment of land ice is the main aim of the project (Paul, 2002; Bishop *et al.*, 2004; Raup *et al.*, 2007a), the WGMS also works in conjunction with the US based National Snow and Ice Data Center (NSIDC), together extending the coverage and increasing the contents of the existing world glacier inventory (WGI) (WGMS, 2013).

A number of monitoring/reconstruction studies are in existence and a sample of these are accounted for in table B.1 in appendix B. The aforementioned geodetic

acquisition methods relate to monitoring of glaciers either where the glacier has been present to work on directly or where images of a glacier are available. Thus the glaciers considered in table B.1 are those still in existence during the 20th century. It is possible to reconstruct former glaciers using a variety of geomorphological indicators including moraines, trim lines, evidence of rock scouring to name but a few (e.g. Derbyshire, 1961; Embleton, 1964; Clapperton, 1971; Russell, 1995; Evans & O Cofaigh, 2003; Evans *et al.*, 2005; Carr & Coleman, 2007). Such methods are not discussed here as they fall out of the remit of this study. Where such methods have been incorporated with studies developed using the techniques mentioned above to estimate uppermost extents for example, they are included and highlighted in table B.1.

The glaciers that have been reconstructed as represented in table B.1 cover regions around the globe including North and South America, the European Alps, India, Tanzania, New Zealand, Russia, Norway and Svalbard. The reconstructions have been possible using a variety of techniques including ground surveys (of varying approaches) and remote sensing. A number of important points can be drawn from the studies selected in table B.1. Issues can be related to the pre-digital and digital methods of data acquisition. The former can be argued to have greater resolution of localised attributes but being limited in terms of spatial resolution and extent whereas the loss of extremely localised resolution is better accounted for in terms of spatial resolution and error quantification by the latter. Such an issue relating to spatial resolution can be exemplified by the data within the SGI for which it is today acknowledged that much of the work carried out barely assessed changes to smaller glaciers (Paul, 2002). This in part links to the sheer number of glaciers within Switzerland. Consequently, the lack of information on smaller glaciers resulted in their behaviour being relatively unknown and therefore unaccounted for (Paul, 2002). The increased assessment of these smaller glaciers was a key objective of SGI 2000 which used remote sensing methods, enabling a more holistic swiss glacier assessment (Paul, 2002), supporting the ability of remote sensing methods to better capture glaciers on a wider scale as addressed by Bayr *et al.* (1994).

Despite the methods that are available today enabling effective spatial glacier change monitoring, a number of issues still exist. Local resolution is one such issue related with the more modern approaches to accounting for individual glacier change. Older aerial photography has been found to provide better resolution, even 10 fold in some studies, compared to the resolution of Landsat TM acquired data (Paul, 2002). This in turn can result in area magnifications that are relics of the method applied as opposed to environmental phenomena. Resolution is also an issue when related to techniques of automatic digitization and digitization at low resolutions. This issue is spatially dependent and is mainly problematic where imagery resolution is poorest.

Developing the point made regarding digitization, a common problem that is clear from the literature is denoting the boundary of a glacier, which is extremely subjective (Hanshaw & Bookhagen, 2013). Multiple methods of glacier outline determination have been suggested (Paul & Kääb, 2005; Racoviteanu *et al.*, 2009). This is an important consideration when compiling multiple maps (assuming they are digitized - i.e. where the original photographs are not available) and is further complicated by poor data resolutions, especially where glacier boundaries are covered with moraine (e.g. Paul, 2002; Carturan *et al.*, 2013). Further considering the resolution of remotely sensed imagery, where resolution is low (ergo pixel size is large), and glacier size is small, the imagery cannot be used to make assessments of change (e.g. Granshaw & Fountain, 2006). Apart from resolution issues, for all remotely sensed images, there is a sensitivity associated with weather conditions, particularly cloud cover, which can prevent useful photographs from being taken (Aniya *et al.*, 1997).

Another issue relates to the locating of and connections of images to ground control points (GCPs). Where studies use more modern imagery, these can be enhanced using different band ratios to uncover GCPs clear on other images (James *et al.*, 2012), reducing errors when georeferencing images. The use of GCPs are also an extremely useful method of planar error assessment. Thus, it is clear that images where clear GCPs cannot be found are at a comparative disadvantage in terms of georeferencing potential and, consequently, associated

horizontal errors. Such issues of error introduction are further magnified where metadata for older images cannot be located. Where such information relates to photography, details may pertain to camera settings. Regarding maps, such metadata may be specific to a datum or projection used (often not displayed on the map itself, especially where not developed for an official body, but as part of a smaller study). Error introduction is further associated with interpolation (where point measurements are available), especially where steeper slopes are concerned (Shahgedanova *et al.*, 2012). Interpolation, and specifically the method of kriging is discussed extensively in Hock (1999).

The different sources of data — despite their limitations — as discussed above are evidence of the spatial data avaialble today that can be used to inform changes in glacier mass balance. Considering the data now available, the geodetic approach — glacier surface comparison — provides both an attractive and convenient method of quantifying such change. However, the method is not without complications. A number of assessments have been carried out considering the merits and pitfalls of the geodetic approach. Many of the errors associated with the method, when considering the use of older analogue photographs, relates to interpretation — an issue less and less related to the imagery that can be collected today such as using radar approaches (Bamber & Rivera, 2007). Differences between the geodetic and traditional glaciological methods when compared directly for the studies identified by Hagg *et al.* (2004), these were found to vary from -0.48 - +0.10 m yr^{-1}. Andreassen (1999) attempted to combine geodetic and glaciological data used to assess Storbreen (Norway) but found that both data sets were prone to large uncertainties, rendering such a comparison void. The geodetic method is extremely sensitive to map error and thus such errors must be considered when interpreting the results of geodetic studies. Østrem & Haakensen (1999) found that errors inherent of the geodetic method were more easily determined than with the glaciological method and that the former is useful for long term studies of changing mass, especially where the maps produced from images are done so using the same approach. Error inherent of surface comparison can be minimised by ensuring the time-step between an image pair allows the surface change component to exceed the error component (Bamber & Rivera, 2007). A

geodetic comparison error is calculated as the root mean square error (RMSE) of the two surfaces and the time interval will always have to be greater than the change in elevation between surfaces divided by the time between the surfaces multiplied by the RMSE. For surfaces derived from poorly constrained data, surface separation time steps of an appropriate length can prove ineffective. With increasingly high resolution data becoming available, such as that derived from interferometry (linking to data as collected by the German TerraSAR-X satellite), data of sufficiently high resolution is becoming more and more easily available.

2.5 Mass balance modelling

Acknowledging the changes that glacier surfaces undergo as identified by many of the authors cited in table B.1 and considering the importance of glacier geometry on surface energy balance (Carturan *et al.*, 2013), attention is now drawn to mass balance modelling approaches that have been used in the past. Of particular importance here is an assessment of models which consider the effects of spatial variation and geometry on the calculation of Q and thus the effect that this has on mass balance. Physical energy balance and temperature index/degree-day models are the main approaches used for calculating glacier melt (Hock, 2003).

2.5.1 Temperature-index/degree-day models

Such models are based on the assumption of an empirical relationship existing between ice melt and air temperature (Hock, 2005) as has been proven by numerous studies (e.g. Braithwaite, 1981). Such models are often applied where data are limited to only temperature, and merits leading to their application, other than limited data input requirements, relate to the ease of forecasting temperature changes, good model performance compared to more complex approaches and their computational simplicity (Hock, 2003). Such models are often based on the use of degree-day factor values (DDF) where the DDF is the factor of proportionality when considering melt relative to the sum of positive temperatures (Hock, 2003). The positive degree notion is important as it differs to a daily temperature which

includes cooler temperatures at night, whereas melt will predominantly have occurred during the day (Hock, 2003). A variety of DDFs have been calculated, varying for both snow and ice, by different authors (e.g. Schytt, 1964; Laumann & Reeh, 1993; Johannesson *et al.*, 1995; Vincent & Vallon, 1997; Hock, 1999) using methods varying from energy balance computation to use of ablation stakes.

Although temperature-index models can be used on limited data sets, a number of models apply much more complex models including other components such as radiation, precipitation and refreezing (e.g. Cazorzi & Fontana, 1996; Hock, 1999; Braithwaite & Zhang, 2000). Such increased complexity leads almost to the development of a physical surface energy balance model approach.

Despite relative model simplicity, there have been some attempts at considering spatial and geometric effects on melt. Where such models are applied to a DEM, simple lapse rate corrections can be applied to consider temperature variations with elevation. Some studies (e.g. Dunn & Colohan, 1999) have considered the effect of aspect on melt, by enhancing melt rates on south facing slopes. Hock (1999) incorporated a radiation component that considered the local effects of surface slope, aspect and clear-sky proportional view (i.e. the effect of hill shading) in an attempt to further incorporate spatial mass balance variation.

2.5.2 Physical energy balance models

Compared to temperature-index/degree-day models, physical SEB models (referred to as SEB models from here) are much more complex and require much larger amounts of input data, which can restrict their application for more remote or inaccessible locations. The approach differs considerably as melt is not a function purely of temperature as in simple temperature-index models, considering contributions to the total SEB from a variety of different factors as discussed in section 2.2.3. SEB models are the most physically justified type of model considering the factors considered in their make-up (MacDougall & Flowers, 2010). A further benefit of this added complexity is being able to run sensitivity analyses to assess contributions of specific components to the SEB and the MB (Le Meur

et al., 2007). From the main components of which the SEB is comprised, the energy for melt (Q) can be defined as in Hock & Noetzli (1997) using:

$$Q = G(1 - \alpha) + L_{net} + Q_H + Q_E + Q_R \tag{2.15}$$

where G is global radiation, α is albedo, L_{net} is net long wave radiation, Q_H is sensible heat flux, Q_E is latent heat flux and Q_R is the energy supplied by rain. This equation can be represented using another approach by (Giesen & Oerlemans, 2012):

$$Q = (1 - \alpha)\tau S_{in,TOA} + \psi \tag{2.16}$$

where $S_{in,TOA}$ is the incoming radiation at the top of the atmosphere. Equation 2.16 is taken from a new model developed to apply more complex considerations of the SEB to glaciers for which data is relatively limited. Consequently, terms Q_H and Q_E (known collectively as "turbulent flux") as well as L_net are considered together, and thus a bulk function (ψ) is applied (Giesen & Oerlemans, 2012). In essence, the resultant model based on equation 2.16 could be seen as a sophisticated temperature-index model (akin to that of Hock (1999) where temperature is coupled with radiation) when considering the limited data input, however its treatment of ψ is very different in terms of its relationship to temperature. The specific calculation of these and other SEB components applied in different models are extensive and variable. Numerous parameterizations have been constructed for the calculation of some parameters of the balance, many of which are reviewed thoroughly in Hock (2005) and consequently they are not discussed here. However, calculations of energy balance components are discussed in the make up of the model developed for this study (see chapter 5), with consideration also being paid to external factors affecting the specific contributions of the different components such as surface albedo.

Point studies applying SEB models are numerous, and entail the calculation of SEB at specific points across a glacier surface (e.g. Hock & Holmgren, 1996; Oerlemans, 2000). Point studies are more easily applied than distributed approaches, resulting in a small number of applications apparent in the literature (Brock *et al.*, 2000a).

The latter model type requires consideration of extrapolation of SEB components across a known extent (Hock, 2005). Distributed SEB models require either the extrapolation or parametrization of SEB components across a grid (MacDougall & Flowers, 2010). Difficulties in extrapolation across a glacier grid are further enhanced as many existing bulk functions for parameter calculations cannot easily be applied to different cells due to issues relating to the assumptions of stationarity, homogeneity and constancy on which many bulk methods are based, these assumptions not being met in a glacier environment (Hock & Noetzli, 1997). Consequently, they allow for incorporation of glacier wide (therefore spatially variant) characteristics in the calculation of SEB and MB and this is discussed in section 2.5.3.

2.5.3 Spatially modelling MB

Many point MB models have been developed (a list of which are presented in table 2 of Hock (2005)) but specifically grid-based SEB approaches are not that common and this is associated with the difficulty in extrapolating input data (often point based) over an entire grid (Hock, 2005). Many studies that have applied sophisticated mass balance models do not consider geometrical surface profile updates in tandem with mass balance change (Giesen & Oerlemans, 2010). However, more and more studies are now apparent (e.g. Giesen & Oerlemans, 2012), trying to assess and incorporate the effects of glacier geometry and mass balance changes in greater detail (Oerlemans, 2010a). A number of grid-based studies are identified and presented in table C.1 in appendix C, selected where applications have been sought to assess spatial variations in SEB and effects on MB. Some of the models included use more simple temperature-index approaches, but these are still relatively advanced, accounting for other processes including radiation. Where such models account for changing geometry throughout the model periods, this is highlighted. Due to the interest of this study on geometrical changes and consequent effects and modifications of the SEB, table C.1 also includes reference balance studies (discussed in section 2.2.2). The key findings of the selected studies are highlighted in all cases.

Of the studies selected and presented in table C.1, many have been facilitated over mountain glaciers and icecaps. The complexity of the studies varies from relatively simple distributed approaches using degree-day models (usually accounting for radiation and precipitation effects) to more advanced approaches using full physical SEB approaches to model mass balance. Depending on the study objectives, some approaches are particularly complex, coupling mass balance methods with models accounting for complex boundary level meteorological processes and glacier/ice cap flow dynamics. Limitations in the more complex physical approaches (equally inherent of more simplistic approaches, albeit indirectly), relate to methods of parameterizing various processes, including albedo and surface roughness (Arnold *et al.*, 1996; Hock & Noetzli, 1997; Brock *et al.*, 2000a). The level of parameterization is dependent on the number (and quality) of measured variables available for different locales, which in turn affects model transferability (MacDougall & Flowers, 2010).

The majority of the models highlighted in table C.1 account for the effects of surface geometry, particularly in relation to its modification of incoming shortwave radiation, but also with regard to multiple reflection and other considerations in some cases, as with the *Alpine 3D* model (Lehning *et al.*, 2006; Michlmayr *et al.*, 2008)). Despite accounting for surface geometry derived from input DEMs, not all models account for geometric evolution in response to mass balance. Of the models accounting for geometric evolution, its effect on SEB and MB is often more profound over longer time scales. This consideration of time-dependence may in part explain its exclusion from models with shorter time-scale objectives, and the time factor may also explain why modelled MB values, calculated exclusive of geometry dynamism, are often still in good agreement with observed values (e.g. Arnold *et al.*, 1996). Outside of glacier surface specific geometry, topographic factors relating to shadows are frequently highlighted as being of total importance, explaining spatial variations in SEB distribution and mass balance change.

Table C.1 is not inclusive of all distributed studies, highlighting only a number of keys studies. It is however clear that many of these studies have been focused in the European Alps (especially more recently) with few being focused north of the

Arctic Circle, especially when considering dynamic surface geometric adjustment. Specifically, no studies using reference balance methods have been facilitated in this area.

2.6 Summary

The key findings of this review are summarised as follows:

1. Small mountain glaciers are excellent indicators of climate change, relating predominantly to the close relationship between MB and climate and their size determined fast response times.

2. Geometry is an important consideration, especially when addressing long term glacier change. The omission of geometric evolution from modelling studies results in unrealistic and erroneous outputs.

3. The specific effects of changing surface geometry on components of the SEB and therefore on MB are complex and inter-related

4. The concept of the *reference balance* is very useful for addressing relationships between glacier change and climate over time (Elsberg *et al.*, 2001; Huss *et al.*, 2012). Few studies have so far used this approach to assess such relationships and none of the examples from the literature have so far been applied to glaciers north of the Arctic Circle.

5. Geodetic methods have been used for the assessment of change at a number of locations for glaciers under a variety of climates. Methods of data assimilation include field based methods coupled with remote sensing approaches (using both aerial photography and satellite imagery). Where relative DEMs of a surface can be produced, mass balance can easily be calculated. However, where relative DEM development is not possible, the acquisition of numerous well established GCPs and a good geodetic network are key to minimizing errors.

6. Distributed SEB models are becoming more widely used which relates to the increasing interest in spatio-temporal variations in the glacier surface and the components of the SEB.

7. Despite many models acknowledging the effect of glacier geometry (slope, aspect and elevation) and that of surrounding topography (e.g. shade) on calculations of SEB components such as shortwave radiation, few acknowledge these relationships temporally, especially geometric variability.

8. No applications considerate of surface geometric adjustment have been applied to small mountain glaciers north of the Arctic Circle.

Chapter 3

Study area and local climate

This project is based on Kårsagalciären, a small mountain glacier in northern Sweden. This glacier has an extensive record of past study which offers a catalogue of data including full topographic maps as well as accounts of retreat and other activity including jökulhlaups (including Ahlmann & Tryselius, 1929; Wallén, 1948, 1949; Wallén, 1959; Karlén, 1973; Holmlund, 1989; Bodin, 1993). Coupled with the nearby research centre - the Abisko naturvetenskapliga station (ANS), meteorological data since the early 20th century are available offering opportunities for comparative analysis and integration of meteorological data as well as with ground based cryospheric observations. The glacier is located 25 km east of the nearby village of Abisko which is well connected to the mining hub of Kiruna from which flights to Stockholm are frequently flown. During the winter, the glacier is accessible by snowmobile or ski. During the summer months, the lack of snow allows for site access by hiking. There is a commercial helipad nearby that can be used where large payloads of equipment are required that cannot be taken out by snowmobile during the winter.

3.1 Study site and description

Kårsagalciären (referred to as Kårsa from this point forwards) is a small mountain glacier located in the Vuoittasrita massif, on the border between northern Sweden and Norway. Small glaciers are defined here as being < 5 km^2 in area. The name Kårsa can be translated from the Sami *Kårså* which means *narrow valley*,

the translated name thus being the *narrow valley glacier*. The contemporary glacier is located at 68.358739°N, 18.323593°E and sits between the peaks of Gorsačohkka (1554 m a.s.l.) and Vássejietnja (1590 m) (see figure 3.1). It is positioned at the head of west-east trending U-shaped Kårsavagge (*Kårsa valley*), along which meltwater and valley drainage is channeled towards Lake Tornetraäsk, approximately 25 km to the east. The valley floor shows evidence of numerous glacifluvial deposits with little evidence of till (Bodin, 1993). Kårsavagge is scarred by past glacial activity with the presence of numerous moraine systems and other landforms discussed in Sjögren (1909), Holdar (1959) and Karlén (1973).

Following repeat visits by a number of observers, the glacier was seen to advance from 1886-1912 with noticeable thickening of the margin. Since around 1912, the glacier has been in a state of near constant retreat, with some isolated areas of minor advance (Karlén, 1973; Bodin, 1993). Earlier studies comparing temperature records from nearby stations acknowledge that a clear temperature change/terminus position relationship was difficult to establish and this in part owes to the varying nature of the bed topography as well as the state of annually variable winter balance conditions (Karlén, 1973). As of 2008 the glacier had an area of approximately 0.89 km^2, with two detached lobes to the immediate SW and SE, the lobe to the SE named in previous studies (see Ahlmann & Tryselius, 1929; Wallén, 1948) as the *Kårsa side glacier* (see figure 3.2). Considering the acknowledged sensitivity of small mountain glaciers, especially in Arctic areas (Dowdeswell *et al.*, 1997; Bingham *et al.*, 2006), the small size of Kårsa places it within a category of 64.2% of all Arctic glaciers, identified in 2009 to have areas of < 2 km^2 (Rippin *et al.*, 2011).

To assist in a basic description of the glacier today, a number of images of the glacier taken in September 2012 are displayed in figure 3.2. During the summer months — when it is possible to see Kårsa uncovered from its winter snow conditions — the glacier displays a relatively clean ice surface and a three tier structure. The lowest part of the glacier ramps up in a southerly direction to an ice plateau which then forms a second ramp up to the highest part of the glacier. Extending from the first and lowest tier of the glacier, there is a steep

Figure 3.1: Study site map. The top panel shows the contemporary glacier outline as derived from aerial photography (taken in July 2008) with the surrounding topography being extracted from the Bodin (1993) map (also created from aerial photography). The Kårsa side glacier is omitted from this image. The middle panel shows the location of the study site, highlighted in red, relative to the rest of Scandinavia and the Arctic Circle. The lower panel shows an excerpt of the 2006 Lantmäteriet BD6 Fjällkartan of the Abisko-Kebnekaise-Narvik region. The area displayed in the top panel is highlighted within the red box extent.

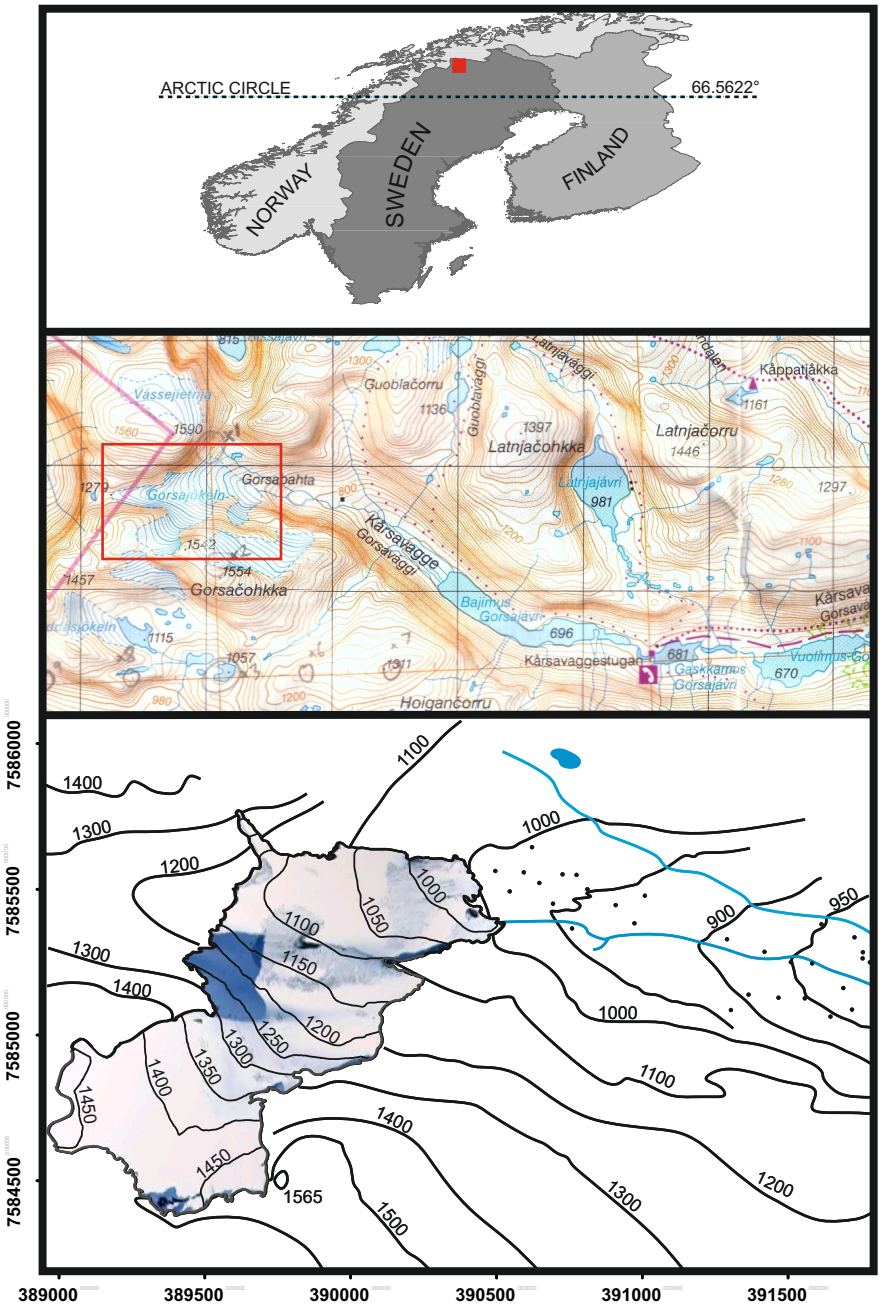

ramp which runs to the north-west. During the summer there is still evidence of the presence of some snow in the highest reaches of the glacier however the depth and structure of the snow in this specific region has not been assessed due to difficulty relating to access. At the centre of the glacier there is a clear extrusion of bed rock protruding through the centre of the glacier from which moraine can be seen entrained in the surface ice down stream from the outcrop. Along the south-eastern terminus margin, melt water from the upper reaches of the glacier falls over the steep terrain and run underneath the glacier. The terminus of the glacier and the area over the central bedrock protrusion are heavily crevassed. In all previous studies of the glacier (discussed below), the glacier has always been land terminating, however following observations in the winter of 2011, there is now the development of a small proglacial lake, implying that the future of the glacier terminus may be affected by buoyancy and calving related mass loss events (see figure 3.2).

3.2 Past investigations of the glacier

Kårsa was selected for this study as opposed to any of the other small sensitive glaciers in northern Sweden due to the wealth of available data and information on the glacier throughout the 20th century as well as its accessibility. The amount of data in part owes to the Swedish national mass balance programme that has been collating data since the early 1940s. The accessibility of the glacier to researchers has always been of great value, particularly following the development of the *Ofotenbanan* railway in 1903 (Bodin, 1993), and the modern infrastructure of roads and nearby Kiruna airport.

The first documentation of study at the glacier was made by Svenious (1910) and Pyk (1914), who accounted for a number of photographs being taken of the terminus from 1884 and into the early 20th century. Early measurements of the terminus were made by Rabot and Mercanton (1914 in Karlén (1973)), where terminus advance was observed of between 10 and 20 m. The first major study that resulted in the development of a full topographic map of the glacier in 1926

Figure 3.2: Glacier photographs September 2012. The top photograph shows the glacier from the north-east whereby the lower, mid and upper glacier are clearly visible. Crevassing towards the terminus is clear as well as a bed rock exposure in the middle of the glacier. The middle photograph is taken from the east of the glacier terminus and displays the proglacial lake formation that appears to be continuing in its development although flotation of the terminus is not yet apparent (Rippin, 2013 (*pers. comm.*)). The bottom image depicts the Kårsa side glacier taken from the north-east.

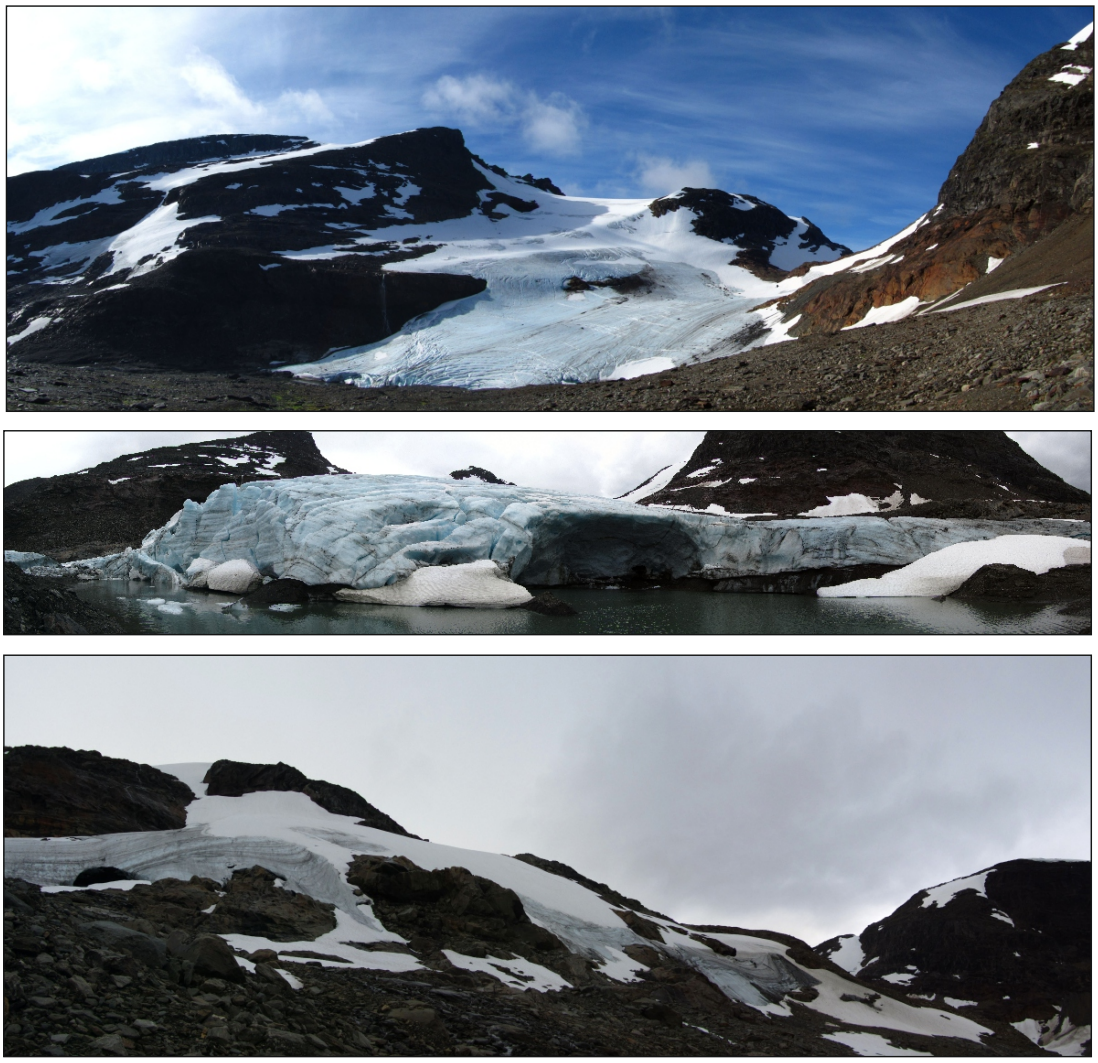

was published by Ahlmann & Tryselius (1929). This paper also included a number of smaller scaled maps regarding terminus positions in the preceding years. Continuous acknowledgment of the terminus position was recorded then in Ahlmann & Lindblad (1940). From 1941-1947, C.C. Wallén, a student of Ahlmann's, began an intensive study of the glacier with regard to its relation to climate (see Wallén, 1948, 1949; Wallén, 1959), resulting in a second full topographical map of the glacier (although only focused on the main glacier lobe and not the side glacier). Due to the close-knit relationship between the glacier and its surrounding topography, the retreat pattern of the glacier was not regarded as representative of glacier retreat throughout Sweden and as a consequence of this, Kårsa was put under less scientific scrutiny. Another of Ahlmann's students, V. Schytt, focused on nearby Störglaciären due to its simple geometry and accessibility - this glacier now having one of the longest mass balance records in the world, running from 1941 to the present, the latter glacier becoming the key study site of the Swedish national mass balance programme.

Following the study of Wallén (Wallén, 1948, 1949), a couple of aerial photographs of the glacier were taken in 1959 and 1978 with a map being constructed following an expedition from Durham university in 1961, however errors were found to exist with the elevations in the latter mapping effort (Schytt, 1963). Mass balance study was not repeated on the glacier until the early 1980s (Eriksson, unpubl.) with the next published study being undertaken by A. Bodin in 1989 (Bodin, 1993). The Bodin (1993) study resulted in the development of a new topographic map as well as radar surveys to assess glacier thickness. This study is the first to revisit the glacier since A. Bodin. Table A.1 in appendix A displays the data available for the glacier including data collected as part of this study. Despite the wealth of information available, accounting for all of the data available requires a multi-lingual approach with some texts being only available in Swedish or German.

3.3 Climatic conditions

The location of the glacier in the mountains west of Abisko is no coincidence, being related both to the favourable topographical and meteorological conditions

Figure 3.3: Abisko climate conditions averaged over the period 1920-2012 as measured at ANS. Total precipitation values are displayed with average monthly temperature values.

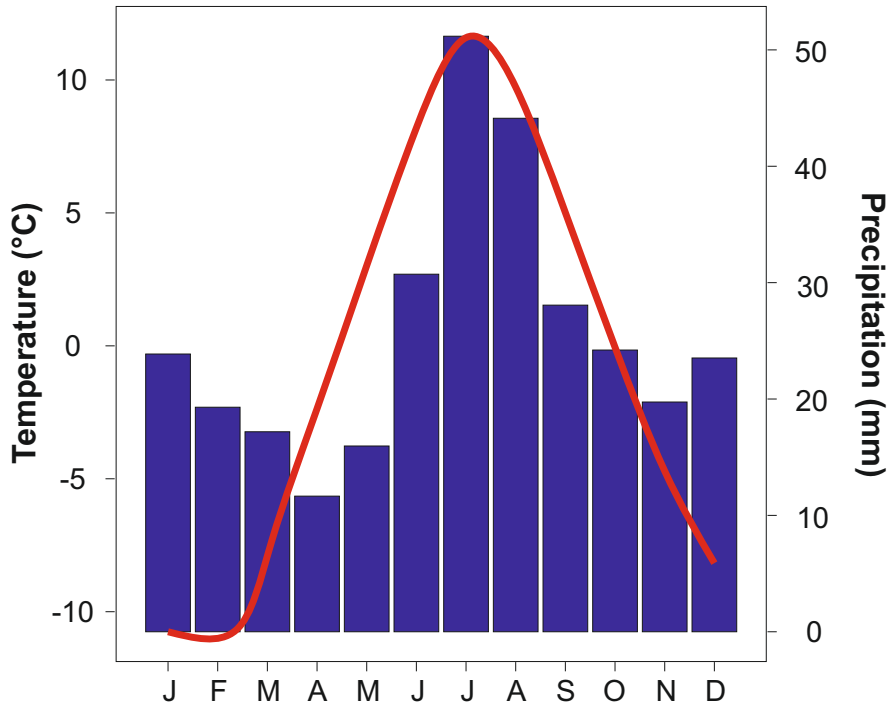

offered and with this small area catching snow-laden south westerly winds (Wallén, 1949). Climatic conditions here are split between maritime and continental, the maritime conditions often prevailing in the winter months, being replaced by more stable continental conditions during the summer months (Wallén, 1948, 1949). A continuous weather station has been maintained at the Abisko naturvetenskapliga station (ANS) since the early 20th century, for which mean climatic conditions are compiled and displayed in figure 3.3.

Mean July temperatures are calculated at 11.7 °C, compared to -10.7 °C in February. July precipitation totals are greatest at 51.2 mm compared to the lowest values in April of 11.7 mm yr^{-1}. Previous studies of the glacier coupled observations with meteorological records from nearby Riksgränsen, however these records are difficult to acquire. To assess more accurate meteorological conditions at the glacier itself (Riksgränsen meteorological conditions are not associated with

Figure 3.4: AWS position and set-up at the glacier. Top left shows the AWS from the east with the glacier terminus in the background. The bottom left shows the set-up during the winter when maintenance and data download were carried out (March 2009-2012). The image to the right shows data download in September 2012. The white tube that is visible contained a Tinytag temperature sensor which acted as a back-up in case of thermometer issues with the main weather station.

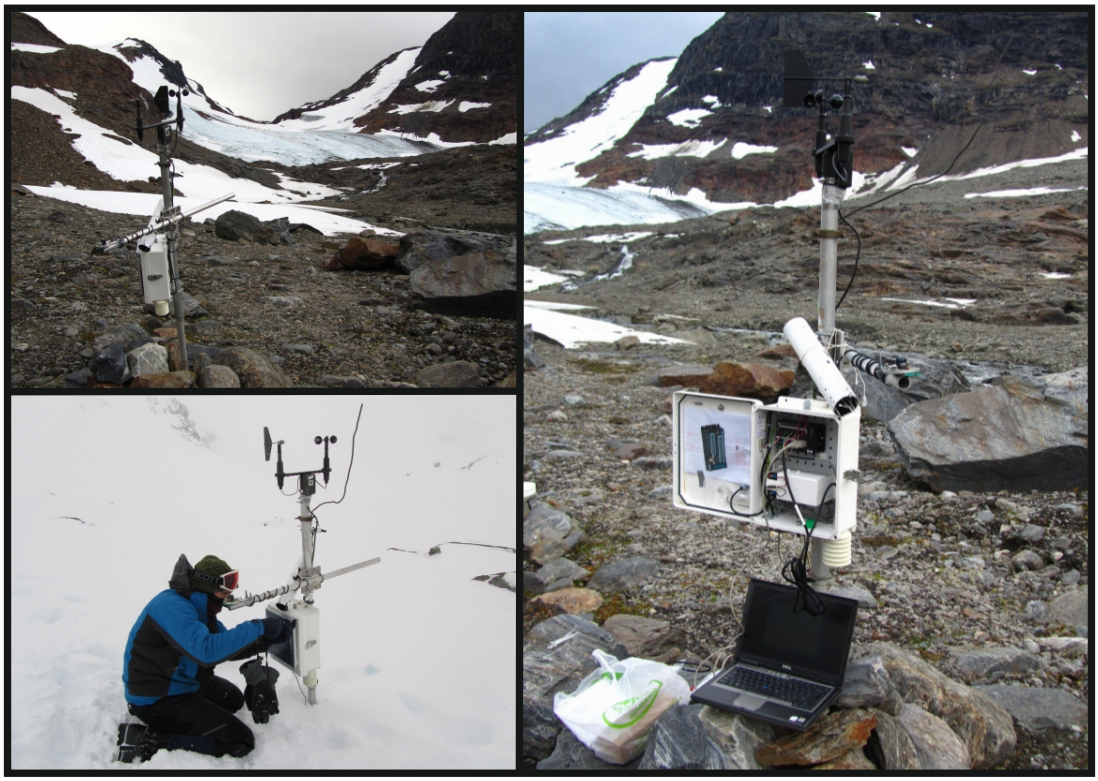

the presence of a nearby glacier), a Campbell Scientific automatic weather station (AWS) (using a Campbell Scientific CR200 datalogger) was used to record a variety of data from 2007, based at the terminus of the glacier. The location and AWS set up are displayed in figure 3.4. This has been downloaded approximately every six months since its installation, when any required maintenance is also carried out.

Mean temperature and wet precipitation records are displayed in figure 3.5. Mean July temperatures were calculated at 8.6°C, compared to -10.6°C in February. July precipitation totals are greatest at 515 mm. Winter accumulation values are not

Figure 3.5: Kårsavagge climate conditions averaged over the period July 2007 - October 2011 as measured at the AWS. Total precipitation values are displayed with average monthly temperature values. The tipping bucket precipitation collection system does not allow for assessment of frozen precipitation and is subject to adverse measurements where snow that accumulates over the measurement equipment melts with increased temperatures. Winter snow accumulation is discussed in chapter 5.

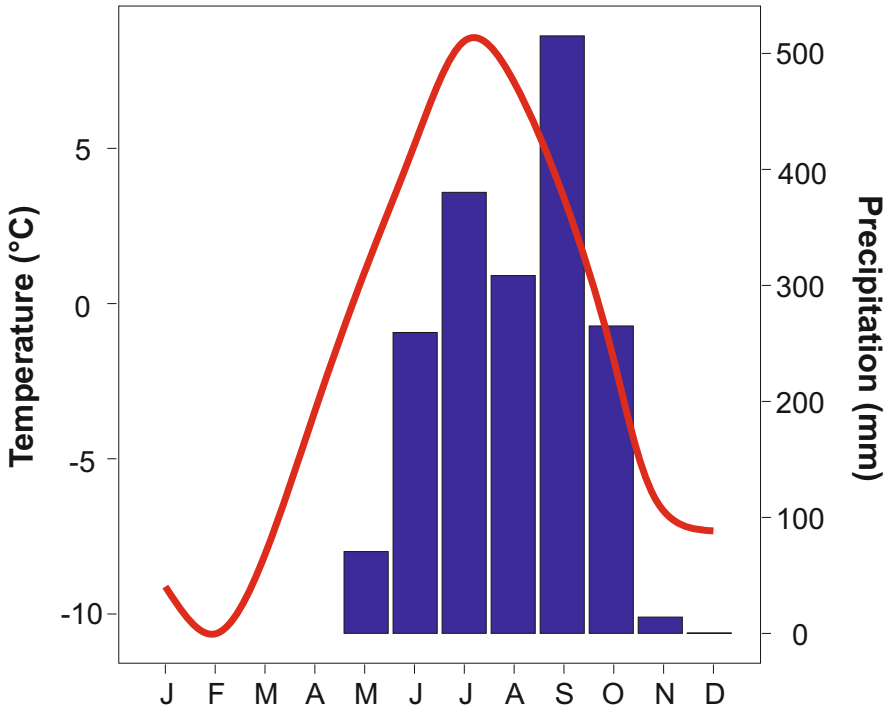

measured at the station due to the limitations of the tipping bucket precipitation collection method used. Snow pack thickness assessment and calculations are discussed in chapters 4 and 5.

To quantify winter snow pack conditions across the glacier, a number of snow pits were excavated during the winter field seasons of 2009, 2010 and 2011. The results of these analyses are discussed further in chapters 4 and 5.

Chapter 4

Geo-spatial and field based methods

The aim of this study is to understand and assess spatio-temporal glaciological change and this requires the construction of a full GIS, encompassing spatial data representative of the glacier for a number of different time steps, ultimately providing information on glacier geometry. With the availability of such geometric data, it is possible to consider the wider effects that change in their values have on SEB and mass balance (MB). These methods require the integration of a variety of different data sets, acquired using both desk and field based approaches. *Contemporary data* is reference to that acquired in the field (by the author) and using aerial photography in the period 2008-2011. *Historical data* refers to data acquired from previous studies in the period 1909-1991 (the 2010 surface falls into this category allowing for 1991-2010 comparison, however the 2010 reconstruction uses the contemporary approach). The terms *contemporary* and *historical* used from this point forward refer to analysis or results of data created using the aforementioned sources. Many of the methods used here are novel and different to those used in prior studies, their development having arisen as a consequence of the data available. In particular, these novel methods attempt to account for change in as wide a spatial context as possible, avoiding errors that can be associated with single point analyses. This chapter addresses the project objectives of:

- Collating historic topographic maps and reports as well as data from the

field to ascertain glacier geometry, meteorological conditions and snow pack characteristics

- Applying geostatistical methods to reconstruct 3D glacier geometry and enable geometry and geometric change analyses (through development of a GIS)

- Accounting for sensitivity of applied geostatistical techniques on reconstructed surface properties

4.1 Co-ordinate systems and geodesy

All data in this study are projected in UTM WGS 1984 zone 34N. All georeferencing (discussed further in section 4.2.2) is relative to the Lantmäteriet BD6 Fjällkarta for the Abisko region. The BD6 map is published using the RT 90 projected co-ordinate system and plots elevation relative to the RH 2000 Swedish National height system - the RT 90 projection was converted to UTM WGS 1984 zone 34N prior to all georeferencing. The RH 2000 Swedish National height system is based on the Normaal Amsterdams Peil (NAP) vertical datum, as with most other European height systems (Lantmäteriet website (Height systems RH 2000, accessed April 2011)). The RH 2000 elevation model referenced here differs to the preceding height models of RH 00 and RH 75 as it has been updated to account for changes due to isostatic adjustment which is significant between revisions with a mean increase in elevation by approximately 1 m between RH 00 (representative of height in 1900) to RH 2000 (representative of height in 2000). These isostatic adjustments are most exaggerated in northern Sweden (Lantmäteriet, 2011). Orthometric elevations on the BD6 map are in 20 m intervals and are all in metres above sea level (m a.s.l.).

All maps used within this study (discussed in section 4.2.1) use orthometric heights. For data collected using dGPS, heights were converted from ellipsoidal heights to orthometric heights using a geoid correction. The geoid, an irregular surface which is an approximation of mean sea level, differs to the ellipsoid which is a

Figure 4.1: The surface, ellipsoid and geoid height (adapted from Lantmäteriet, 2010

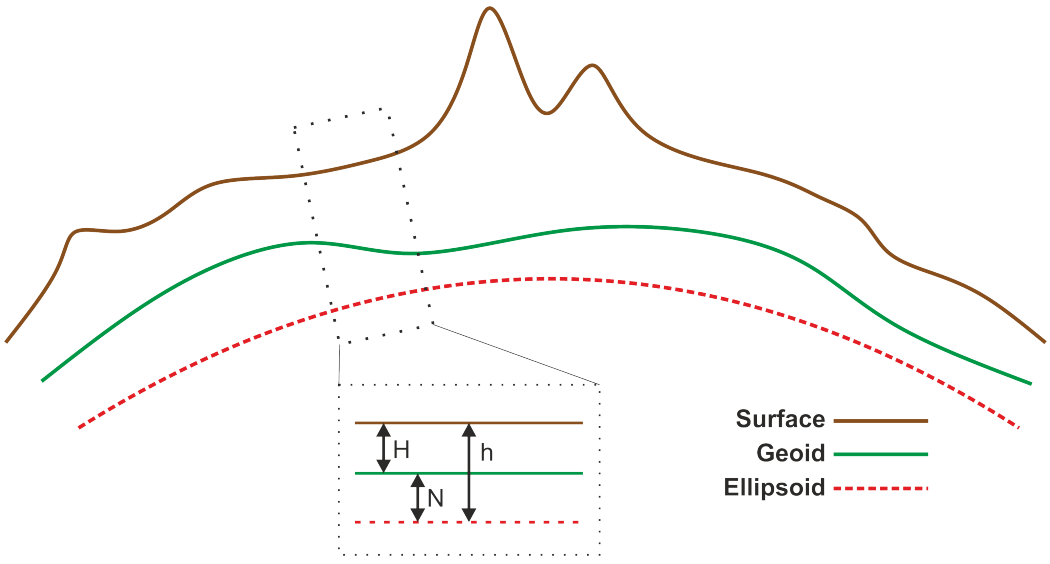

hypothetical equipotential gravitational surface - see figure 4.1 (ESRI, 2009).

The correction of ellipsoidal to orthometric heights requires knowledge of the geoid height (separation between the ellipsoid and the geoid). Where geoid height is N, ellipsoidal height is h and orthometric height is H, ellipsoidal elevations can be corrected to orthometric using the following equation:

$$H = h - N \tag{4.1}$$

The geoid height changes in space and consequently a single value cannot be assumed to represent a total area of interest. Upon investigation of the variability of the geoid height, it was found to be no greater than 0.1 m. To account for a mean geoid height across Kårsa, a number of points were constructed across the glacier (see figure 4.2) with a mean spacing of 200 m.

The geoid height ID points were constructed in UTM WGS 1984 zone 34N and then converted to the geographic SWEREF 99 projection. A geoid model was provided by Lantmäteriet, from which users were able to calculate geoid height using the SWEN08 RH2000 geoid model (Lantmäteriet, 2010). Geoid heights were computed for all geoid ID points and a mean of 32.01 m was calculated.

Figure 4.2: Points (in red) created for the identification of geoid height across the area of interest. The points are displayed in the WGS 1984 34N projected co-ordinate system - analysis required them to be in the SWEREF 99 geographic projection

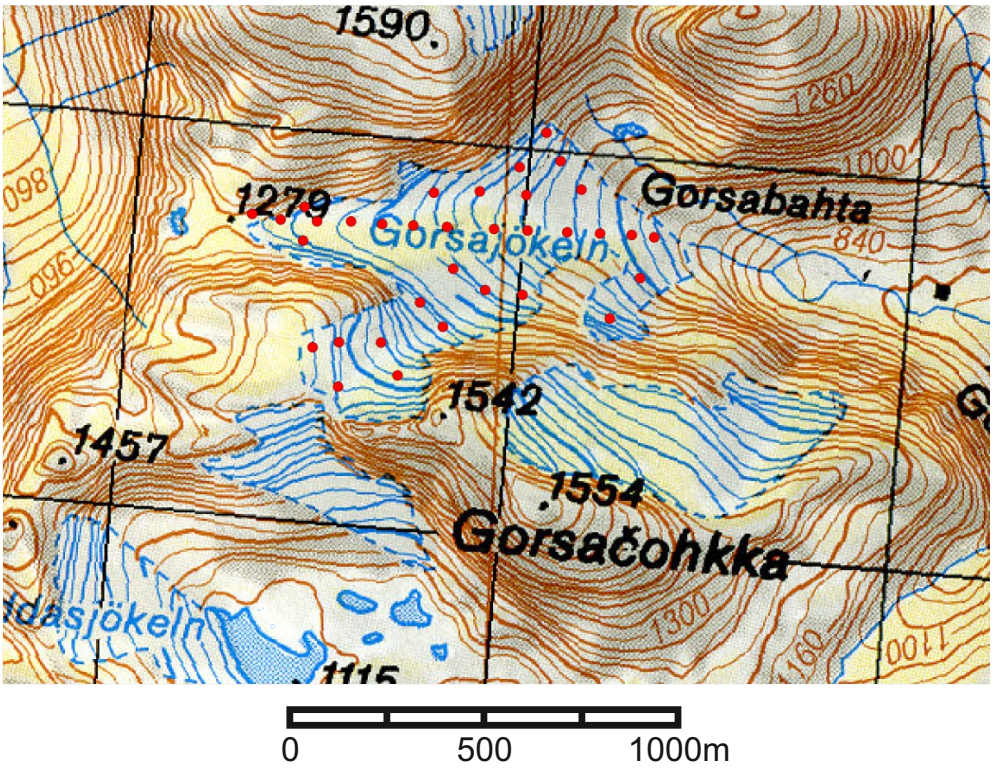

This value satisfies the N portion of equation 4.1 and has been used to correct all dGPS measured ellipsoidal heights to orthometric heights for this study.

4.2 Data acquisition and surface development

This project requires the development of a detailed GIS detailing Kårsa in 3 dimensions for the period of 1926-2010. This has been facilitated using split approach:

1. Reconstruction of the summer surface of the glacier on an approximate 20 year interval for the period 1926-2010

2. Reconstruction of the summer surface of the glacier on a 1 year interval for the period 2007-2010

The first approach was a desk based study requiring the compilation of previously constructed maps and other documents whereas the second approach requires both field and desk based methodologies, so to provide data directly from the field to enable the development of detailed contemporary maps, in combination with data from other sources including aerial photographs where they are available. Integrating point data acquired both in the field and from a variety of available maps requires working up using a number of geostatistical approaches. The overall process required for full GIS development is conceptualised in figure 4.3.

4.2.1 Historical data acquisition and compilation

As described in chapter 3, there is a wealth of data available for Kårsa, which significantly supports the decision to carry out a long term analysis of this particular glacier. Complete topographic maps of the main glacier exist for the years 1926, 1943, 1959, 1963, 1973, 1978 and 1991, of varying quality and scale. These are all derived from aerial photography, however the original photographs could not be sourced. The maps resultant of photogrammetric methods applied by different cartographers were used here for digitization purposes.

Figure 4.3: GIS development conceptualisation. All references to kriging are expanded upon in section 4.2.5. The application of kriging to area and historical surface development is discussed in section 4.2.6 and section 4.2.7 for contemporary surface development. Data acquisition for the historical reconstruction is described in section 4.2.1 and in section 4.2.7 for the contemporary surfaces.

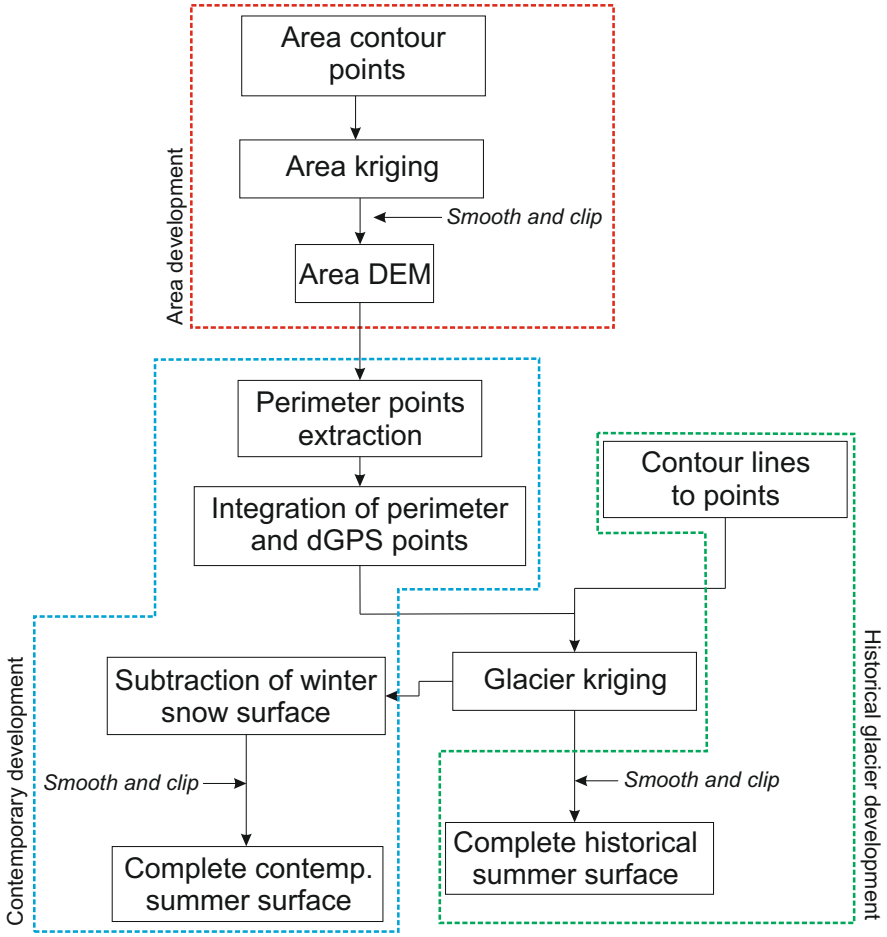

Prior to digitization, maps were georeferenced to a georeferenced aerial photograph of the glacier locale coupled with the 1: 100 000 topographic mountain map of the area, using ArcMap v9.3. Georeferencing was difficult as the available maps vary in resolution compared to the base maps to which they are georeferenced relative to, and furthermore, the focus of the maps in many instances is restricted to the glacier itself with little attention of surrounding topographic (and more stable features) considered. For this reason, the 1963 and 1973 maps were discarded as there were not enough points available by which to adequately position the map. Of the maps remaining, georeference point pairs were selected according to identifiable geological features including constrained streams crossing clear contour lines, contour kinks of the valley side walls and isolated water bodies. Using the more easily georeferenced contemporary aerial photograph of the region, it was also possible to constrain the maps by areas of the glacier that according to the maps had changed little, such as in topographically constrained and sheltered regions. In the absence of other features, few other georeferencing options were available. Spline fits were applied to the maps, with points that distorted the maps significantly being disregarded. Maintaining minimal distortion of the available maps required as wide a point coverage as possible.

Due to the restriction in georeferencing point pair synthesis - a product of both limited identifiable features from topographic maps and disagreements between maps as a function of varying resolution - assessing horizontal errors is extremely difficult. This is further discussed in section 4.2.2.

Once the maps were georeferenced as best as possible, polygons and vectors pertaining to the overall extent and contours were manually digitized within ArcMap. The polygons were used within the area analysis. Contours were converted to points to which elevation, eastings and northings data were attached, allowing for the development of 3D point clouds for each of the maps.

4.2.2 Horizontal error quantification

There are multiple sources of error that can be introduced through the data compilation process, especially considering the nature of the data - maps developed by different authors using different methods over time. Such issues are inherent of other reconstruction studies (e.g. Nuth *et al.*, 2007). The maps used here were all derived form aerial photographs and the process of stereoscopy. Associated with the 1926-1991 photographs, there are few details other than the location of the glacier (lat/long) and a scale bar. There were no details such as with regard to the orthorectification process applied (prone to numerous internal errors itself (Thibert *et al.*, 2008)) or details of the cameras used (which could also be used to indicate distortion). Furthermore, no prior assessment of orthorectification error had been carried out for the images in question. In this study, all surfaces have been georeferenced relative to the 2006 Lantmäteriet BD6 1:100 000 map of the Abisko-Kebnekaise-Narvik area and a georeferenced 2008 photograph of the western end of Kårsavagge in which Kårsa resides. The historical maps from 1926-1991 vary significantly in the level of detail available. The GCPs used to locate the different maps included simple features including the edges of lakes, sharp breaks of slope and stark kinks in contour profiles. However a number of details were found between maps that were in complete disagreement. These are illustrated in figure 4.4.

A further hindrance to georeferencing this area and a further issue relating to the selection of GCPs is associated with the transient nature of the environment, being in a state of deglaciation and with associated erosional processes being active. Events during the study period such as the jökulhlaup mentioned in the literature occurring in the 1980s (see Holmlund, 1989) will also have changed the landscape. This further complicates identifying *stable* GCPs. Another issue is that the maps used here have each been developed for a time specific study of the glacier and this may have contributed to lesser attention being paid to the surrounding topography - an issue when attempting to georeference all of the maps into a single database.

Figure 4.4: Selected feature differences for maps available for the 1926-2010 period. Images displayed together on a single row are presented within the same view window in terms of top-left corner xy coordinates. Horizontal distances are indicated for each row of images.

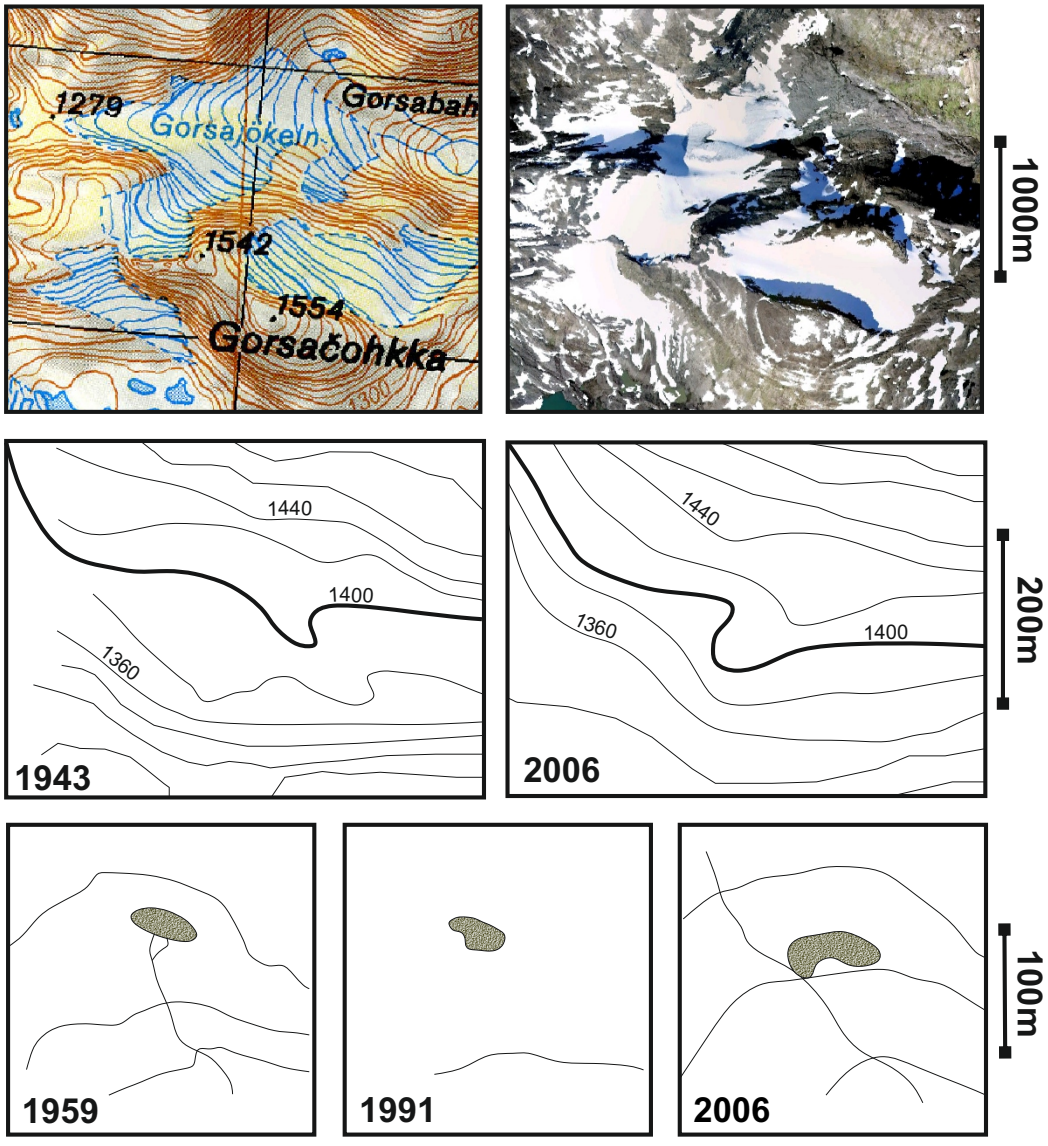

Considering the aforementioned details, it is prudent to quantify horizontal and vertical errors. Knowledge of these errors in turn allows one to consider whether glaciological observations derived from subsequent map analysis, including terminus position change and surface elevation lowering, are a function of environmental conditions or are an artifact/resultant limitation of the data processing method.

Horizontal errors are often calculated by identifying non-glacial (therefore assumed static) points represented by successive maps, the residuals providing the error and allowing for variance in error over a given area (e.g. Nuth *et al.*, 2007). In this instance (and as represented in figure 4.4), it is extremely difficult to fairly represent horizontal errors between the maps here and no clear estimate can be given for the individual maps considering the information available. However, vertical errors are considered without a horizontal component for the development of the glacier bed map, required for analysis of glacier thickness and consequently volume. Considering vertical errors gives an indication of possible mean errors and error ranges associated with the aforementioned glaciological variables for the different mapped years. This is discussed in detail in section 4.3.5. These vertical errors are likely a function of horizontal errors, which can have significant effects in terms of elevation. This is of greater importance in steeper rather than flatter areas, as great changes in elevation over small horizontal distances are associated with the former. Isostatic rebound, which in northern parts of Sweden can be up to 1.0 m yr^{-100}, is not considered explicitly in the error calculation although this is catered for in the errors reported in section 4.3.5 as the area elevation map considers the most up to date elevation map of Sweden (Lantmäteriet, 2010).

4.2.3 Contemporary data acquisition and compilation

Unlike the data required for the historical reconstruction, contemporary data required the collection of data directly from the field as well as integration with an aerial photograph taken in 2008 and sought from Lantmäteriet (*Lantmäteriet, pers.comm.*).

Fieldwork was carried out in March 2008, 2009, 2010 and 2011 on Kårsa. In 2008 and 2009, the lower reaches of the glacier were surveyed using a differential Global Positioning System (dGPS). A Ground Penetrating Radar (GPR) survey was run across the lower reaches of the glacier in 2009. The upper reaches of the glacier were covered with dGPS in 2010 and 2011. For accurate surveying of the glacier surface and also of all GPR traces, real time kinematic (RTK) dGPS data were collected using a Leica GPS500 dGPS receiver (Rippin *et al.*, 2011). The dGPS was used whilst being mounted on a snowmobile (for the lower reaches of the glacier) and in a backpack where terrain was more difficult to access, namely the upper regions of the glacier. Where the mounting was changed, the antenna height was altered to maintain accuracy. The dGPS base station, also a Leica GPS500 receiver unit, was located in front of the glacier at one of two base stations (see figure 4.6). The specific location of the base station was known to extremely high accuracy (<0.005 m) following an 8 hour static occupation and post-processing of data relative to continuous dGPS receivers at Kiruna and Narvik. This was carried out by Dr J. Carrivick in the summer of 2007. The location of data points collected in the field are illustrated in figure 4.5.

The GPR data were collected using a PulseEkko Pro system, trailed both behind a snowmobile and on foot (see figure 4.6). An antenna sledge, also carrying dGPS equipment to precisely locate GPR traces, was towed approximately 6 m behind the snowmobile (Rippin *et al.*, 2011) or 1 m behind a person when being dragged on foot. The antennas were set up parallel to each other and at 90°to the direction of survey (this set up was chosen to minimise offline reflections (Murray *et al.*, 2007)). The GPR data were collected at a 1 m step size with 50 MHz frequency antennas (Rippin *et al.*, 2011) and this was carried out so to obtain a long profile trace of the W-E trending part of Kårsa as well as smaller N-S trending transects across the long profile. Post-processing of the dGPS and GPR data was carried out using Leica GeoOffice and ReflexW respectively (Rippin *et al.*, 2011).

Regarding dGPS readings, the points collected in the field did not extend to the boundaries of the glacier. To obtain point elevation values at the perimeter, an outline of the glacier was digitized from the 2008 aerial photograph sought from

Figure 4.5: Field data collection: dGPS, GPR and snowpack thickness measurement point locations. The points are shown relative to the 2008 glacier outline as identified from aerial photography.

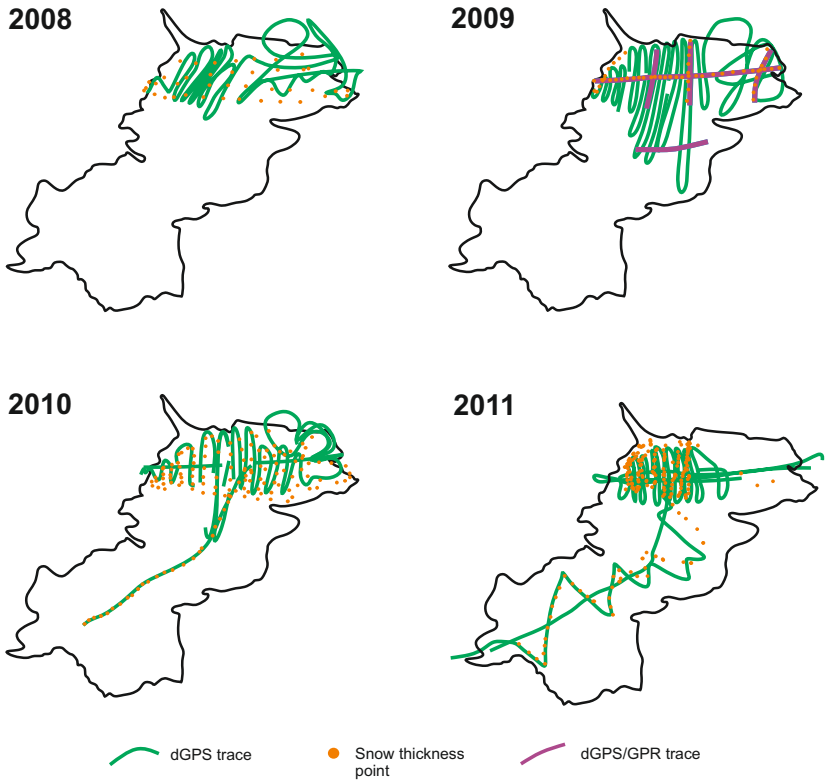

Google Earth (Lantmäteriet, 2010). The glacier outline, as an ArcGIS polygon, was layered over the area DEM and converted to points. The elevations of the underlying DEM were then combined with the lat/long of each point of the glacier outline. These points, now with latitude, longitude and elevation attributes, were combined with the summer surface points, developed as mentioned above.

To approximate the thickness of the winter snowpack covering the glacier, to ultimately enable an assessment of the sumer glacier surface elevation, snow probing across the glacier was also carried out. This method has been applied in other studies to measure winter snow thickness (Østrem & Brugman, 1991). Snow probe surveys were carried out across as much of the glacier surface as was possible considering time constraints, weather conditions and slope stability whilst working in the field (see figure 4.6). These points were collected across the northern portion of the glacier during 2009 with points being collected from all over the glacier in 2010 and 2011. At each point, longitude and latitude was measured using a combination of GPS units including a Leica dGPS 500 and a hand held Garmin GPS device. Snow depth was estimated using a purpose made aluminium snow probe. It was possible to assess when the base of the winter snow pack had been reached as the probe could not be pushed any deeper (the density increase being indicative of a firn layer). To ensure that the tip of the probe was not lying on an ice lens, the snow probe was repeatedly inserted to break through any such obstruction.

Coupled with snow probe assessment of the winter snow pack depth, a number of snow pits were excavated across the glacier. Pits were dug to the ice surface. In some cases, the firn layer was reached from which further excavation was not possible. Following excavation, one face was left uncleaned so as not to smudge layers and deform snow crystal structure. The structure of the snow pack was then described with regard to the presence and thickness of ice lenses and the apparent structure of the snow pack (which was usually found to be structure-less). Following log structure assessment, three density measurements were taken per 50cm from across the uncleaned snow pit wall, using a 250 cc snow sampler (www.snowmetrics.com). Snow samples were then measured using a spring balance

Figure 4.6: Field method photographs (clockwise from top left): dGPS measurements made by snowmobile; Tandem snow thickness and dGPS measurement; dGPS base station at the glacier terminus allowing for increased range between the base station and rover unit to allow surveys of the upper glacier; Snow pit analysis and snow density measurement; Second dGPS base station allowing for surveying of the lower glacier only (drawing of a short straw allowed for a period of monitoring the generator during surveys); GPR survey of the upper glacier.

(see figure 4.6). These were later averaged per 50 cm and per pit, and scaled up giving a density in kg m^{-3}. All snow pits showed evidence of both wind packing and re-freezing processes, accounted for by snow crystal structure and the presence of numerous ice lenses. A log profile of a stereotypical pit that was excavated is shown in figure 4.7. All pits excavated were within the lower portion of the glacier due to accessibility and observed snow stability. The mean density of the winter snow pack derived from all of the snow pits excavated in the 2009-2011 period was 407.13 kg m^{-3} (which qualifies as an average density for wind slab (Paterson, 1994)). More in depth assessment of density is continued in section 5.4.6.

4.2.4 Bed DEM development

The GPR and dGPS data, collected as described in section 4.2.3, were checked for internal data consistency using a cross-over method. This involved selecting locations where the transects crossed over one another. Three cross over locations were observed and at each cross over, the two closest points were assessed and the difference in elevation (both GPR and dGPS) were accounted for (see figure 4.8). A mean GPR and dGPS error was then calculated for each cross-over location. Mean GPR error was found to be ±3.7 m however this was significantly increased by the presence of a single GPR value where the individual error was 10.8 m. Exclusion of this outlier from the dataset rendered mean vertical GPR error to ±1.4 m (Rippin *et al.*, 2011). dGPS mean vertical cross-over error was ±0.07 m.

Post-processing of GPR data gave information on ice thickness and combined with known surface elevations from combined use of both the GPR and dGPS measurements, bed elevations were calculated for each point. A glacier bed DEM was constructed using points from the 2009 radar survey, points of known elevation calculated by Bodin (1993), points from the glacier perimeter extracted from the area DEM model (discussed earlier) and a selection of dGPS points of the pro-glacial area collected in 2008. These thickness points were coupled with points measured in 1991/1992 by Bodin (1993). The need for combining the 2009 data with data from surveys in 1991/1992 (Bodin, 1993) owes to the topographical

Figure 4.7: Log profile of a characteristic snow pit as excavated during the 2010 and 2011 winter field seasons. The displayed snow pit was excavated in March 2011 towards the terminus of the glacier. The density profile is displayed as is a general structure of the snow pack. Ice lenses are evidence of melting and refreezing processes - they are likely more numerous deeper in the snow pack due to increased freezing and thawing of the snow pack early on in the accumulation season.

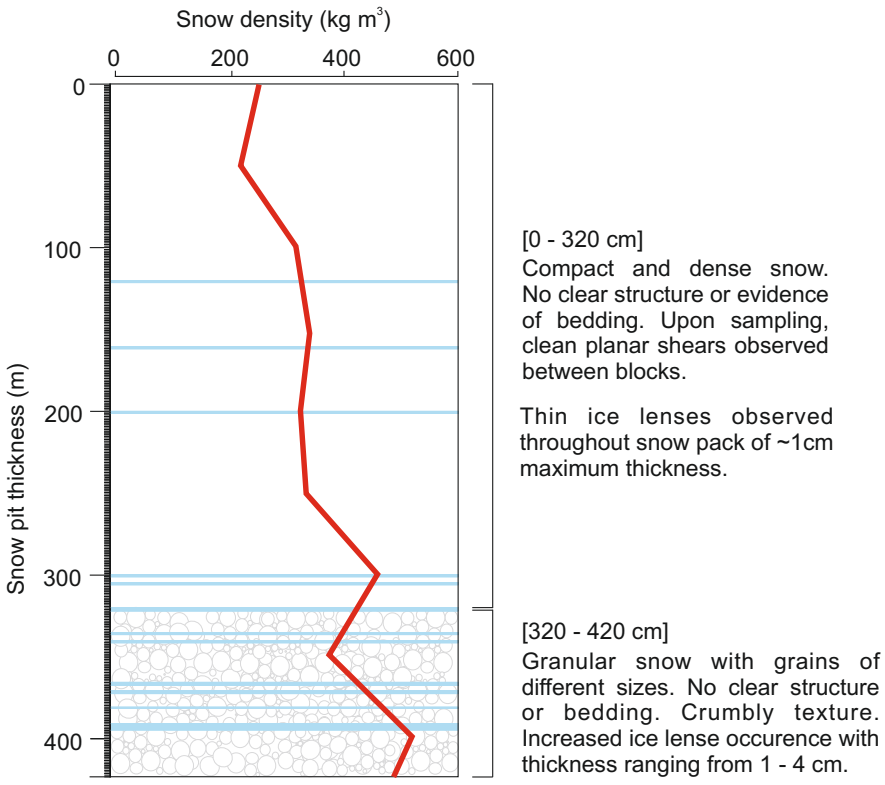

constraints and equipment malfunction experienced during the 2009 and a 2010 field season respectively. Bodin (1993) acquired their points via a radio echo survey which was carried out over the upper portions of the glacier in the spring of 1991 and 1992, extending the coverage of measured ice depth over Kårsa. The surveys carried out in 1991/1992 used a Mark II echo sounder, with a frequency transmission between 2 and 10 MHz, and a pulse width of 0.2 μsec (Bodin, 1993). For each measured point, ice thickness is known. It was possible to create a bed elevation data set from these points by subtracting ice thickness values from the known ice surface elevation at each point at the time, extracted from a surface interpolation of the glacier in 1991 (see below for details on the interpolation routine).

The combination of the two bed elevation data sets (those from Bodin (1993) and from Rippin *et al.* (2011)) raised a number of issues:

1. Positional accuracy

2. Comparative spatial data scarcity of the 1991/1992 data compared with the 2009 data

3. Issues with accuracy of exact measurement sites

These issues were identified by Rippin *et al.* (2011) and consequently a method of cross-over analysis was carried out, comparing the comparative reliability of the two data sets between points within 5 m of one another (see figure 4.8). A $\pm$11.912 m mean cross-over error was found between the 2009 bed and the 1991/1992 bed points. This differs to the $\pm$6.6 m in Rippin *et al.* (2011) which was reduced by the removal of some of the Bodin points. The larger error is maintained as Bodin (1993) also report that the error related to their own points could be $\pm$8 m.

Accepting these errors, these points were integrated with contour points as well as dGPS points collected during the summer of 2008 in the foreground of Kårsa. This compiled point cloud was then used to interpolate a single area-bed DEM using via the kriging model highlighted in section 4.2.5.

Figure 4.8: The location of the Rippin *et al.* (2011) 2009 GPR traces and Bodin (1993) 1991 thickness points are displayed as well as locations of the 2009 point cross-over sites (black circles) and Bodin/Rippin cross-over locations (orange circles).

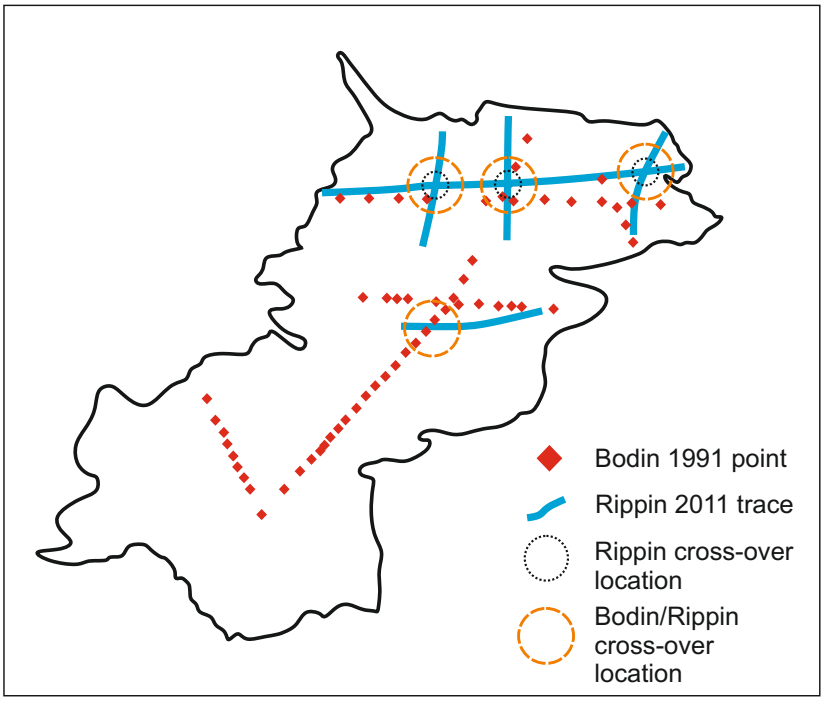

4.2.5 Interpolation: Kriging and other methods

The point clusters collated from historical and contemporary data assimilation were required to interpolate complete surfaces. Here, interpolation refers to the development of a complete surface within a specified area, predicting unknown points from points with known values. The routine applied for this in this study is ordinary kriging which is in line with many other glacier studies (e.g. Hock & Jensen, 1999; Bamber & Layberry, 2001).

Kriging is essentially a form of linear regression but differs from traditional regression as the variables considered are neither believed to be independent nor random (Davis, 2002). It can also be described as an average weighted estimator whereby weights are assigned according to the model that is fitted to the semivariogram (Bamber & Layberry, 2001). Where all points within an input point data set are paired together, the semivariogram is used to compare distance between points (the lag) with the variance between them.

Kriging differs to the many other interpolation methods available as it provides errors associated with each predicted point, which is particularly useful when errors need to be quantified if interpolated surfaces are used as inputs into separate applications (e.g. melt modelling of snow and ice surfaces). There are many types of kriging including ordinary, universal and simple kriging but all can be linked back to the following formula, as it is upon this that the different methods of kriging are based:

$$Z(x) = \mu(x) + \varepsilon(x) \tag{4.2}$$

where Z is a reference to observations at all locations (x), μ represents a deterministic trend and ε is directly associated to autocorrelated (where autocorrelation states that points close to each other will be more similar to one another than points that are further apart) errors within the data (ESRI, 2009). So any value is ultimately the summation of a trend and errors associated with that trend.

Ordinary kriging is the most commonly employed form of kriging and is used within this study, defined as:

$$Z(x) = \mu + \varepsilon(x) \tag{4.3}$$

Here, μ is known to be a constant, but it is unknown by value. By assuming a constant mean, all values of ε can be known (and then changed proportionately with increases/decreases in the pseudo-value of μ) when using simple kriging. This is again a large assumption but useful nonetheless (ESRI, 2009) where the characteristics of a data set are largely understood from prior analysis (e.g. semivariogram analysis). This method of kriging is best applied where data are known to have a trend but where that trend cannot be discerned as to being a product of autocorrelation or an actual trend (ESRI, 2009).

The interpolation routine applied consisted of the following steps:

1. Assessment of trends present within the data (with trend removal if necessary)
2. Semivariogram analysis of the points, comparing different semivariogram models
3. Assessment of semivariogram statistics
4. Running of the best simple kriging model

All data points were analysed for any trend present amongst them by comparing elevation against lat/long position. For each year, the glacier point clusters showed a second order polynomial trend. Other than for the points used for the development of the area DEM for which a clear trend was less discernible, the aforementioned second order trend was removed for all kriging analyses. The removal of the trend ensured that any statistical analysis carried out through the kriging process was focused on short-range component variation between points (ESRI, 2009) which was essential considering that the glacier surfaces being constructed were to analyse changes to surface morphology. Trends were added

back into the data following semivariogram analysis.

With the data points having been assessed for trends, semivariograms (which represent spacing between point pairs against variance) were analysed for each set using the following model types: Circular; Spherical; Tetraspherical; Pentaspherical (pentaspher.); Exponential; Gaussian; Rational Quadratic; Hole Effect; K-Bessel; J-Bessel; and Stable. Each model (a form of regression line) fits the data spread in a slightly different fashion. The best model for the data was chosen, in part using the procedure of Hock & Jensen (1999), according to:

1. *Best* model statistical score
2. Visual fit on the semivariogram (possible using Geostatistical wizard in ArcGIS)
3. Visual assessment of the resultant surface when using the specific model

Following ESRI (2009) guidelines, statistically, the best semivariogram model for a data set should have:

1. Standardised mean closest to 0
2. Smallest RMS prediction error
3. Average standard error closest to the RMS error (cross validation (Hock and Jensen, 1999)
4. Standardised RMS closest to 1

For each model, each of these variables was treated equally and given a rank value, whereby a higher value was explicit of a more favorable statistic. The model with the highest score was then tested visually; both on the semivariogram and with a surface interpolation developed using the specific model in question and viewed in ArcScene. The ranking process applied to the model statistics is exemplified as for the 2011 winter surface (applying a second order trend removal) in table 4.1.

Table 4.1: Example of the ranking method applied to assess the statistical strength of applied semivariogram models to point data. The data used here is based on the 2011 winter point data cloud. In this instance, the stable model was found to be strongest.

Model	$\hat{x}$	RMS	Pst.	Average Std. Error	$\hat{x}$ Std. error	Pst.	Std. RMS	Pst.	RMS - $\bar{x}$ Std.error	Pst.	Pst. totals
Circular	0.012	0.785	10	2.300	0.001	8	0.234	6	1.511	8	32
Spherical	0.012	0.787	9	2.331	0.001	9	0.230	5	1.544	7	30
Tetraspherical	0.012	0.788	8	2.353	0.001	10	0.228	4	1.565	6	28
Pentaspher.	0.012	0.789	7	2.364	0.001	11	0.227	3	1.575	5	26
Exponential	0.014	0.831	6	2.654	0.001	8	0.203	2	1.823	4	20
Gaussian	-0.137	1.937	3	4.978	-0.028	4	0.389	9	3.041	3	19
Rational Quadratic	-0.035	0.986	5	1.199	-0.029	3	0.784	10	0.213	11	29
Hole Effect	-0.159	2.220	2	6.552	-0.025	5	0.338	8	4.332	2	17
K-Bessel	-0.002	1.018	4	0.356	0.092	2	34.750	1	-0.662	9	16
J-Bessel	-0.154	2.528	1	8.380	-0.019	6	0.300	7	5.852	1	15
Stable	0.006	0.694	11	1.016	0.002	7	0.793	11	0.322	10	39

Table 4.2: Trend removal effects on mean surface elevation and standard error statistics. These errors are calculated relative to the initial input data - this is pertinent for the 2008-2011 surfaces which are representative of the winter (w) surface conditions. These surfaces are later converted to summer surfaces with snow layer removal (resulting in the 2007, 2008, 2009 and 2010 summer surfaces).

	No trend removal		Second order trend removal	
	$\hat{x}$ elevation (m)	Std. error (m)	$\hat{x}$ elevation (m)	Std. error (m)
1926	1217.39	17.33	1217.79	22.05
1943	1180.58	22.16	1180.43	14.92
1959	1207.31	18.02	1207.30	12.02
1978	1206.52	6.09	1206.30	3.17
1991	1210.81	20.92	1211.57	15.64
2008 (w)	1251.29	40.42	1250.63	14.43
2009 (w)	1246.69	33.72	1245.73	11.69
2010 (w)	-	-	1240.95	6.93
2011 (w)	1243.65	31.13	1242.57	5.68

To ensure that trend removal was the best option for surface development, a full run through of the aforementioned interpolation procedure was carried out with a trend removal and without a trend removal. The results of the comparison can be seen below in table 4.2.

The mean error was found to be less for the surfaces created following trend removal and due to the objective of assessing morphological change, and therefore short-range component variation, all glacier surface interpolations were treated with complete trend removal.

4.2.6 Area DEM and Historical DEM development

The specific model statistics of the semivariogram models (second order trend removed) used to develop the area DEM and the historical (1926-1991) surfaces are summarised below in table 4.3.

Table 4.3: Statistical report of strongest semivariogram models for area/bed and historical surface DEM development. These results were combined with the overall *best ordinary kriging application* as discussed in section 4.2.5.

DEM	Model type	Mean error (m)	RMS (m)	Avg. Std. error (m)	$\bar{x}$ std error (m)	RMS std. (m)	RMS - average std error (m)
Area/Bed	K-Bessel	0.000	0.300	3.946	0.000	0.074	3.65
1926	Exponential	0.009	5.946	22.810	0.000	0.284	16.86
1943	Pentaspher.	-0.002	0.922	9.860	-0.000	0.100	8.94
1959	Exponential	0.008	2.185	13.490	0.001	0.166	11.31
1978	K-Bessel	0.004	3.691	4.973	-0.003	0.799	1.28
1991	Stable	0.001	0.362	5.942	0.000	0.044	5.58

The model strength assessment, the results of which are visible in table 4.3, was coupled with both a visual assessment of the models and the semivariogram, as well as an assessment of the resultant surface, using the statistically strongest model. Final surfaces were eventually developed using the models as identified in table 4.3 as these models also showed the best visible fit and most realistic final surfaces when considering knowledge of the real glacier surface from photographs or field experience. As can be seen in table 4.3, different models were applied for the different DEMs and this is a function of the varying structure of the different input point clouds. All surface were then smoothed using a low-pass filter in ArcMap v9.3 and v10.0.

4.2.7 Contemporary surface development

The specific model statistics of the semivariogram models (second order trend removed) used to develop the contemporary (2007-2010) winter surfaces are summarised below in table 4.4.

Table 4.4: Statistical report of strongest semivariogram models for area/bed and historical surface DEM development. These results were combined with the overall *best ordinary kriging application* as discussed in section 4.2.5.

DEM	Model type	Mean	RMS	Avg. Std. error	$\bar{x}$ std error	RMS std.	RMS - average std error
		(m)	(m)	(m)	(m)	(m)	(m)
2008 (w)	Stable	0.001	0.967	2.390	0.002	0.691	1.423
2009 (w)	Stable	-0.001	0.844	2.894	0.000	0.390	2.050
2010 (w)	K-Bessel	0.001	0.900	1.209	-0.003	0.800	0.309
2011 (w)	Stable	0.006	0.694	1.016	0.002	0.793	0.322

Table 4.5: Snowpack mean thickness values

Year	x depth (m)
2008	2.36
2009	2.26
2010	2.26
2011	3.28

As mentioned in section 4.2.6, these statistics were taken into consideration along with the other components of best interpolation approach selection as discussed in section 4.2.5. Unlike with the historical surfaces, creating contemporary winter surfaces is only part way through the contemporary surface development process as for comparison with prior years (and to avoid comparing varying winter snow accumulation patterns), all surfaces are normalised to summer conditions - the 2008-2011 winter surfaces being covered by winter snow accumulation. Summer surfaces were created by subtracting winter snow thickness interpolation layers.

Complete winter snow thickness surfaces were developed for 2008-2010 using the snow probe points collected during the winter field seasons (see section 4.2.3). The 2008 and 2009 point data sets were comparatively limited, the 2010 data set has a centre line running up the southern part of the glacier - the area that 2008/2009 lack data. The 2011 point collection was the most encompassing with regard to the steeper southern part of the glacier. To populate the 2008 and 2009 snow thickness point clouds, the 2010 centreline was combined, based on the assumption that the smaller centreline region is less subject to variation than the wider region covered by the 2011 snow thickness points.

The 2010 depths along the centreline were not used in their raw state when joined with the 2008 and 2009 point measurements. To attempt to correct depths to possible 2008/2009 conditions, it is assumed that inter-annual snow accumulation residuals for the glacier as a whole are relatively uniform. Mean depth of all points in the accumulation zone was then calculated, the results of which can be seen in table 4.5.

The difference in mean thickness between 2009 and 2010 was found to be 0 m, and 0.10 m between 2008 and 2010. The centreline points were then merged with the 2008 and 2009 point clouds, the 2010 centreline points to be joined with the 2008 points being corrected by -0.10 m. These points were then used as an input for second order global trend interpolation. The resultant surface was then smoothed using a low pass filter. A simple regression based interpolator was used due to the limited point input and, unlike kriging which honours input point z values, this was not required to the same accuracy due to the dynamic nature of the snow thicknesses measured on a day by day basis. A second order polynomial trend was identified as being most appropriate through comparison of snow thickness values against distance from the terminus. Snow depths were found to be greatest at the centre of the glacier and least at the terminus and the south-western point of the glacier. A first order polynomial did not account for this pattern whereas a second order polynomial did.

Summer surfaces are then calculated by subtracting the snow thickness layers from the winter surfaces.

4.2.8 Interpolation errors and sensitivity

Horizontal errors in terms of georeferencing and vertical errors with regard to the dGPS are considered in the preceding sections. Kriging is a useful interpolator as it provides evidence of the error in the prediction surface developed using a given input data set. This can be acquired as a standard error value from which distributed maps can be developed. It is found that the greatest errors occur with increasing distance from measured points. Mean standard errors for the different surfaces are displayed in table 4.6. The errors increase with distance from points and this relates to the model fit with the semivariogram. With increasing lag between paired input points, variance becomes increasingly noisy. Errors here are found to be largest for the 1926 surface which maintains a relatively shallow gradient resulting in larger lags between contour lines - this increases noise as the semivariogram is less effective at longer lags. Thus, standard error can only be used as an approximate indicator of interpolation accuracy, and not a definite sign

Table 4.6: Trend removal effects on mean surface elevation and standard error statistics. These errors are calculated relative to the initial input data - this is pertinent for the 2008-2011 surfaces which are representative of the winter (w) surface conditions. These surfaces are later converted to summer surfaces with snow layer removal (resulting in the 2007, 2008, 2009 and 2010 summer surfaces).

Year (DEM)	$\hat{x}$ Std. error (m)
1926	22.05
1943	14.92
1959	12.02
1978	3.17
1991	15.64
2008 (w)	14.43
2009 (w)	11.69
2010 (w)	6.93
2011 (w)	5.68

of a surface being more or less accurate, being more related to model efficiency at longer lags.

Whereas standard error alludes to the errors relating to point spacing, a further consideration that must be made is the error associated with the input points themselves. These are identified in this study using a Monte Carlo approach. As with the standard error maps, errors are generally greatest where point concentrations are least.

The application of a Monte Carlo analysis fits the triple approach that should be considered when a user wishes to use the results of a quantitative modelling approach (Burrough & McDonnell, 1998):

1. Input data accuracy (field data/digitization outputs)
2. Model quality (semivariogram model choice)
3. Input data/model interaction

Monte Carlo simulation allowed the assessment of the effect of input data on the interpolation routine by adding random 'noise' to the input data points (Heywood

Figure 4.9: Monte Carlo simulation work flow

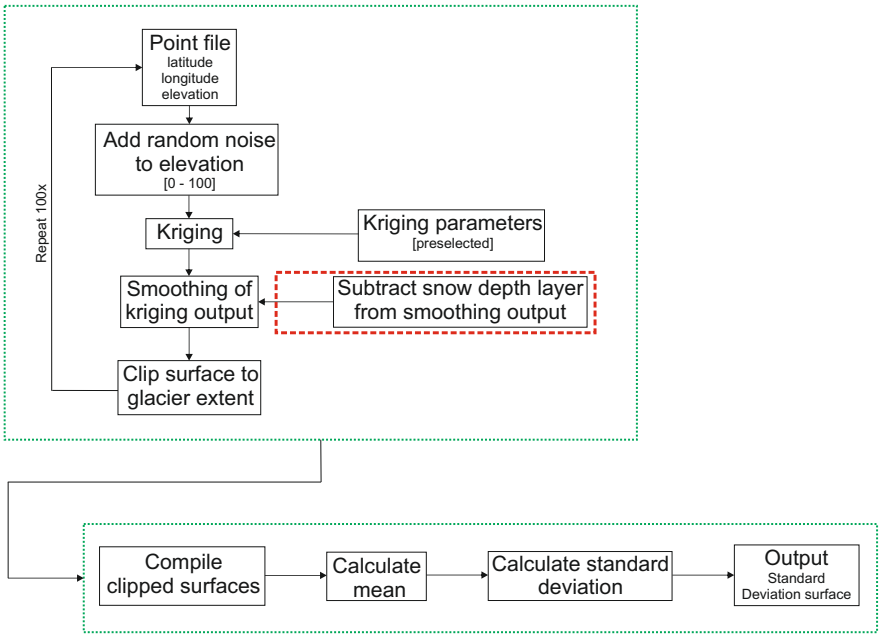

et al., 2006). Such an approach has been used in other GIS studies (e.g. Emmi & Horton, 1995; Zhou *et al.*, 2003). In the model simulations used here, the random noise added to each point elevation of the input data set is between 0 and 100 m. These values were chosen to clearly identify areas that are particularly susceptible to erroneous points (i.e. areas for which few points are available). The maximum value of 100 m is also deemed suitable as it covers potential error values that will have been introduced using point elevation data from the area DEM developed from Lantmäteriet contour point data, used for the contemporary surface reconstructions. It is reported that the 1:100 000 Fjällkarten product series can have horizontal errors up to 20 m (Lantmäteriet, 2012). In mountainous regions, such as those in which Kårsa is located, 20 m horizontal error could result in substantial vertical error (ignoring potential error in vertical elevations).

The Monte Carlo simulations were run separately for both historical and contemporary reconstructions. A combined work flow is illustrated in figure 4.9.

The Monte Carlo simulation used here is described as follows:

1. Simulation initialized by importing a point file that will be used within the interpolation algorithm to develop a continuous surface;
2. Point elevations are modified by the addition of a random number between 0 and 100 to each of the elevation values
3. Modified points passed into the kriging algorithm for which the kriging parameters are specific to each model run, selected according to the different point files for each year of data available (see section 4.2.5);
4. Kriging output is smoothed;
5. For the contemporary surfaces (for which the input points relate to winter surface elevations as opposed to summer elevations, as with the historic point sets), a snow layer is subtracted from the smoothed layer. This provides a summer surface (the extent of which is the rectangular extent of the input points). For the historic surfaces, this subtraction is not required.
6. The surface clipped according to the extent of the glacier;

The entire loop was then repeated 100x, each time adding random noise to a clean input point file. Once all iterations have been carried out, the output surfaces are collated and averaged - the simulation output representing distributed standard deviations across the glacier surface. The simulation is run for the years 1926, 1943, 1959, 1978, 1991, 2008-2011. The years 2008-2011 require the extra stage involving snow surface subtraction - this allows the development of summer surfaces (2007-2010).

The final simulation output was the standard deviation surface. Where standard deviation is high, this was indicative of areas highly susceptible to erroneous point spikes. Low standard deviations indicate areas of lower sensitivity. Standard deviation values should not be treated as absolutes. The values displayed in figures 6.2 and 7.1 (in chapters 6 and 7 respectively) are sensitive to the number of runs used to create them. 100 runs have been carried out for each surface - had 1000

runs been carried out, values would likely be different. The surfaces shown are useful for pattern recognition regarding areas of high and low sensitivity (relating to high and low standard deviations respectively).

The results of the Monte Carlo sensitivity analyses are discussed in chapters 6 and 7. The usefulness of this method is also discussed in chapter 10.

4.3 Calculation of glaciological parameters

4.3.1 Terminus retreat

The retreat of a glacier terminus is a frequently used feature to assess glacier change over time (e.g. Finsterwalder, 1962; Jangpangi & Vohra, 1962; Allison & Keage, 1986; Dobhal *et al.*, 2004; Kaser *et al.*, 2004; Cook *et al.*, 2005; Kulkarni *et al.*, 2007), with increasing rates of retreat being used to exemplify changes in glacier mass balance. They are also often used to imply mass loss although this can be ambiguous as retreat due to increased temperature at lower elevations could result in growth in the accumulation area.

Difficulty in estimating terminus retreat is introduced when assessing the end point of the terminus itself. Retreat rates along a glacier terminus can vary due to the location of the ice near to valley side walls, presence of moraines, undercutting of sections of the terminus by meltwater outlets and subglacial bed form effects (driving crevasse formation). As a result of this, it cannot be assumed that the retreat rate of the most distal terminus point is representative of mean glacier recession.

In an attempt to provide a solution to the problem of defining the terminus extent, here the glacier terminus of Kårsa is defined as being any part of the glacier perimeter falling within a 300 m radius of the point on the glacier that is furthest to the east. This is identified using a simple buffer technique (see figure 4.10). When calculating near distances, the glacier terminus from which distances are measured are represented by a series of points divided by an equal 10 m spacing,

Figure 4.10: Identifying the glacier terminus using a 300 m buffer

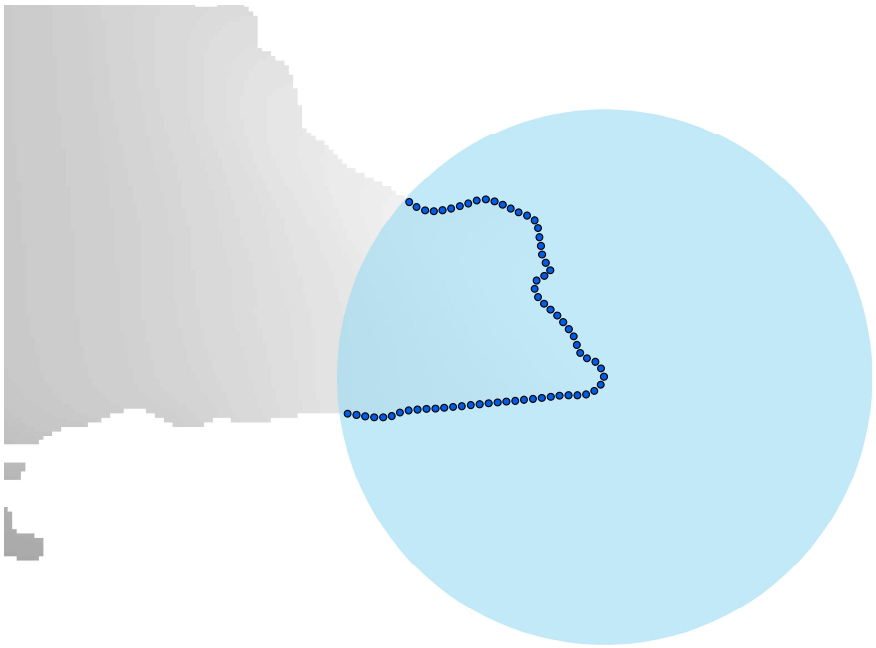

positioned along the terminus boundary.

To assess the retreat of Kårsa, six different methods were considered:

1. A *furthest point* method whereby retreat is inferred by calculating the distance between the furthest eastern points of different glacier terminus stances

2. A *reference terminus to terminus* function whereby the nearest difference is calculated between the 1909 terminus and the 1926 - 2010 termini. A mean value is taken.

3. A *terminus to reference terminus* function whereby the nearest difference is calculated between the 1926 - 2010 termini and the 1909 terminus. A mean value is taken.

4. A *terminus to line* near function whereby points of a 10 m spacing are distributed along a N/S trending line, the centre of which is based on the most eastern point of the 1909 digitized terminus from Ahlmann & Tryselius (1929). The near function is then used to assess the shortest distance between each point along the boundary of the glacier for the years 1926, 1943, 1959, 1978, 1991 and 2008 and the line. Mean values are used. All retreat is relative to the 1909 glacier terminus. This is made possible by first calculating the distance between the 1909 terminus and the line. This value is then subtracted from the mean distances of all other terminus positions (1926 - 2008), essentially treating the 1909 distance as 0.

5. A *line to terminus* near function the same as the previous method except that now the distance from the vertical line to the terminus points is calculated.

6. A *recession by area* as employed during analysis of the retreat of Scott Glacier, Svalbard in Zagórski *et al.* (2008). This utilised the equation:

$$C = \frac{P}{GFa} \tag{4.4}$$

where C is average recession (m), P is the area uncovered due to recession (m^2) and GFa is the length of the glacier front. This method is referred to as the *recession by area method* from this point forward. Using this method for Kårsa, we take GFa to be the length of the average glacier terminus position which falls between the terminus of interest (s_i) and the previous terminus position (s_p). The termini s_i and s_p were derived from the 300 m buffer analysis described above.

Terminus retreat values calculated using the aforementioned methods are reported in table 4.7. These values are reported here as they were instrumental in assessing the *best* approach to retreat assessment.

Table 4.7: Terminus retreat values using different methodological approaches

Year	Furthest point (m)	Reference terminus to terminus (m)	terminus to reference terminus (m)	Terminus to line (m)	Line to terminus (m)	Recession by area (m)
1909	0	0	0	0	0	0
1926	35	28	32	34	24	33
1943	424	330	349	433	322	365
1959	728	618	609	717	596	439
1978	878	764	763	874	736	526
1991	1054	934	931	1048	902	621
2008	1336	1197	1188	1292	1160	785

Limitations vary between the different terminus retreat methods. This is exemplified by the 551 m range between the maximum (1336 m) and minimum (785 m) retreat rates that have been calculated. The *near* method used within ArcMap where terminus retreats in this study are assessed, calculates the shortest distance between two points, where the points can be parts of multiple features. Depending on the positioning of the different features, this can result in isolating features whereby only one point from the feature is nearer to all of the points in another feature class. This provides a significant limitation where a spatially distributed method is required, as the near distance is then calculated using only this single point. The problem is illustrated in figure 4.11.

The *furthest point* method is reliant on single points; one for each terminus position. This differs to all of the other methods (2-5 in the above terminus retreat method experiments list) which invoke a spatially distributed approach to terminus retreat. The *furthest point* is similar to the frequently employed centerline studies (e.g. Dobhal *et al.*, 2004; Shugar *et al.*, 2010) which are more quickly carried out (requiring fewer measurements) but lacking in acknowledgment of spatially distributed variance (Barrand *et al.*, 2010). As such approaches neglect spatial variance, they are less accurate in approximating terminus retreat. Despite the spatial accountability missed by the *furthest point* method, it, as well as methods 2–5, are all susceptible to the limiting characteristics of near analysis in a similar way.

The distance values extracted when using the different methods (1-5) are not necessarily inclusive of all points that make up the feature from which distance is being calculated. Using the example of using the *near* function to measure the *near* distance from the reference terminus to the terminus of interest, points could be neglected from the terminus of interest. If one point within the overall terminus of interest feature is closer to the total reference terminus feature, that point may be the only one used to calculate distances (as can be seen in figure 4.11b). This explains some of the variability between the measured values using this *near* tool. This reasoning also explains the requirement for both feature of interest to reference feature and reference feature to feature of interest measurements. The points utilised in the *near* analyses vary according to the positioning of the

Figure 4.11: Limitations of the use of a *near* function to assess retreat. Figure *(a)* shows a situation where the use of the near function does not result in measurements relative to a single point. Figure *(b)* displays how measurements can be affected by a single point, especially where the reference points (in this case the 1909 perimeter points) are further away from the objective (the 1943 terminus position).

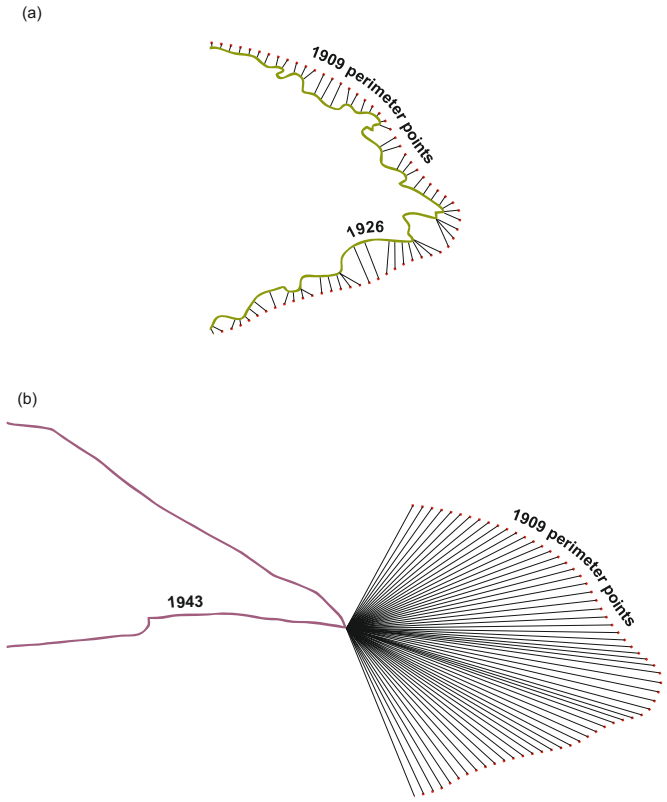

feature of interest relative to the feature from which distance is being measured - this is more difficult when both features have more complex geometries. In some instances, points will be shared i.e. multiple *near* distances will be calculated according to a single point.

The *terminus to line near* approach was used to limit the point sharing effects that can be experienced when using the *terminus of interest to reference terminus* and *reference terminus to terminus of interest* methods. The north-south trending line relative to which the point distances are calculated provides a feature of non-complex geometry. By measuring the distance from each point of the terminus

to this simple geometric line feature (see 4.12 (a and b)), the user ensures that all distance lines between the two features remain equidistant from one another. Consequently, the trigonometrical issues resulting in point sharing experienced when using features of a more complex geometry as a reference to measure distance from, are removed. These distances are therefore truly Euclidean. The retreat rate that is of interest here is that relative to the earliest known terminus position. For Kårsa that is the 1909 frontal extent. The mean distance of the 1909 terminus is measured relative to the north-south line (with the central point distance being zero as it shares the same space as the north-south line). The mean of these distances is then calculated providing an initial mean spatially corrected retreat rate this provides a zero value. Distances are then calculated for all of the other terminus positions (1926 2008), the mean then being calculated. From these values, the mean 1909 distance from the north-south line is subtracted to make all mean retreat values relative to the 1909 terminus position (and not the north-south line itself).

The *line to terminus* approach is used for completeness. With this method, it is still possible to experience point sharing effects, for the same reasons as for the *terminus of interest to reference terminus* and *reference terminus to terminus of interest* methods.

The *recession by area* method (Zagórski *et al.*, 2008), along with a mean terminus position requires a known area of glacier loss (i.e. area that has been uncovered as a consequence of recession), which is located between the terminus of interest (s_i) and the previous extent (s_p). Calculating the area of loss value is simple where the endpoints of s_p and s_i join (see figure 4.13).

This is complicated however when the two do not connect. Where the latter instance occurs, the area of loss due to retreat is calculated by joining the terminus endpoints to one another, accounting for all of the area between the termini constrained by the endpoint joins (see figure 4.14). However, this does not account for all of the area lost by a retreating glacier, a large amount of which does not occur around the terminus alone. This issue will vary between glaciers due to

Figure 4.12: The line to terminus method. As with the *near* method, depending on terminus geometry point sharing is still possible therefore giving inaccurate spatially distributed retreat values. This is best exemplified by figure (b) (although not as exaggerated as in figure 4.11).

(a)

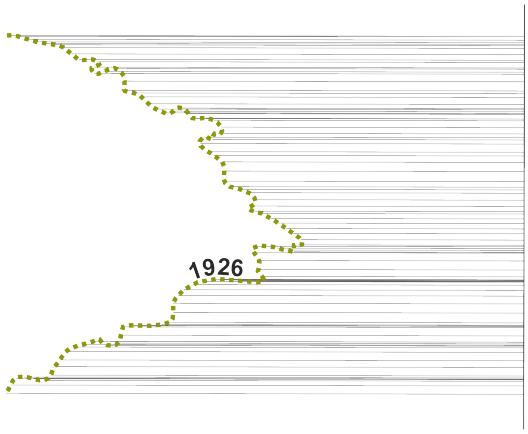

(b)

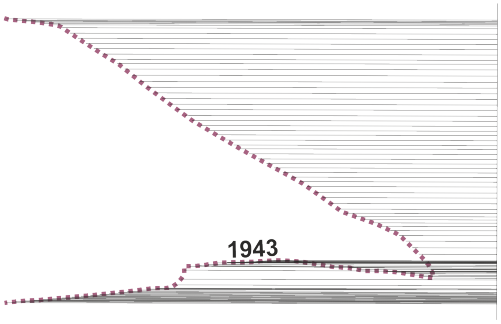

Figure 4.13: Recession by area method whereby a simple area change calculation is possible, the retreating area forming a complete polygon.

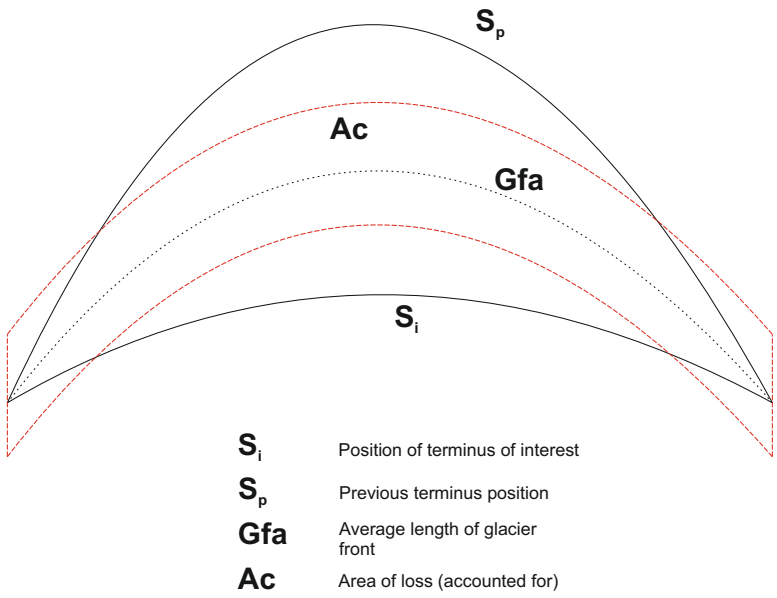

variability in altitudinal distribution as well as juxtaposition to valley side walls positions where increases in melt rates are likely (Hock & Holmgren, 2005; Benn & Evans, 2010).

The *recession by area method* provides the lowest retreat rate value and this is likely to be due to the difficulty in assessing the area of loss that equates to the value P. This will also be affected by the mean length of the terminus, which highlights the importance of defining exactly what part of the glacier is the terminus.

Centreline studies are easily carried out as they are quick, requiring only a single measurement. The *furthest point* method is similar to centreline analysis, involving the measurement of the distance between the furthest down glacier points along the s_p and s_i terminus outlines (which in this case is the most easterly point). This is a simple and crude method which provides the retreat of the furthest point alone. Using this method alone, it is impossible to account for spatial variation of retreat along the glacier terminus. It is included within this assessment for

Figure 4.14: Recession by area method whereby only a complex area change calculation is possible. This is a more realistic scenario whereby the area of retreat does not allow for area loss within a closed polygon area, thus introducing problems of where to limit the assessment of retreat and consequently requiring a careful definition of the position of the terminus.

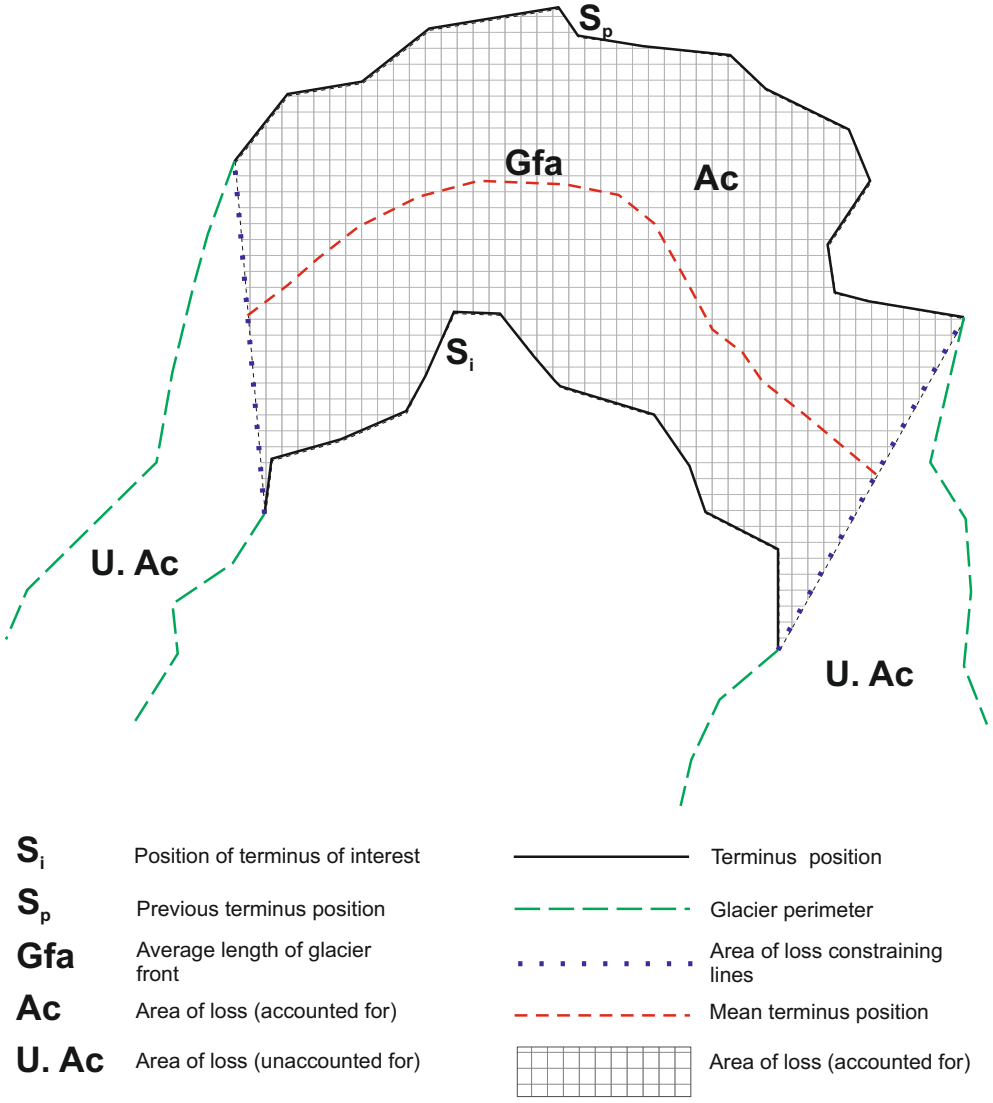

completeness.

Equidistant distance lines are required between the reference object (s_p)and the object of interest (s_i). The only method providing this that is tested here is the *terminus to line method*. The results from retreat analysis are discussed in chapter 6.

4.3.2 Area

The surface area of the glacier for each year was calculated as the area within polygons of the glacier which are used to extract the cells from rasters of the glacier surface, derived from contours and dGPS points (sections 4.2.6 and 4.2.7). This method of area is equal to the Raster Planar Surface Area (RPA) referred to in Jiskoot *et al.* (2009) and is often used in glacier inventories (Jiskoot *et al.*, 2009).

4.3.3 Elevation change and surface slope and aspect

Surface elevation change between input raster was calculated using the raster calculator tool within ArcGIS v9.3 and 10.0. The same functionality is built into the model for which the main components are defined in chapter 5. Slope and aspect are calculated using the interpolated surfaces for the historical and contemporary periods using the inbuilt tools of ArcGIS v9.3 and v10.0. The algorithms applied for both slope and aspect are derived from Burrough & McDonnell (1998) and of a given raster, calculate spatially weighted slope and aspect values using a 9 cell search window. The specific algorithms used within Arc are replicated within the melt model which is discussed in detail in chapter 5.

4.3.4 Hypsometry

Hypsometry is reference to area distribution by elevation. Hypsometry was calculated in this study by accounting for the area distribution both within elevation bands and generalised at specific point elevations (i.e. metre by metre). These data are plotted both in categorised line charts and cumulative area charts in

chapters 6 and 7. It is also possible to quantify and analyse hypsometric change using single values. Those used in this study include elevation-relief (ER) ratio values (Wood & Snell, 1960) and hypsometric index (HI) values (Jiskoot *et al.*, 2009).

ER values (Wood & Snell, 1960) are calculated using:

$$ER = \frac{z_{\hat{x}} - z_{min}}{z_{max} - z_{min}} \tag{4.5}$$

where $z_{\hat{x}}$,z_{min}, and z_{max} are the elevation mean, maximum and minimum values. Where the mean elevation within a range is high, a large ER value is calculated compared to a lower value when mean elevation is low. This method is often used for more geomorphological applications to compare different areas and associated processes. However, it is worth mentioning here as it simply conveys changes in the glacier catchment over time.

The ER value is very similar to the Hypsometric Index (HI) and these values have been reported in other studies (e.g. Davies *et al.*, 2012). HI is calculated using:

$$HI = \frac{H_{max} - H_{med}}{H_{med} - H_{min}} \tag{4.6}$$

where H_{max} and H_{min} are the maximum and minimum glacier elevations and H_{med} is the elevation of the contour that halves the glacier (Jiskoot *et al.*, 2000, 2009). Jiskoot *et al.* (2009) used HI values to place glaciers into different categories, summarising simple area distributions. The Jiskoot *et al.* (2009) study devised five categories but they are summarised in three here:

1. Top heavy (HI < -1.5)

2. Equidimensional (-1.2 < HI < 1.2)

3. Bottom heavy (HI > 1.5)

4.3.5 Glacier thickness and volume

Glacier thickness was calculated by subtracting a raster surface of the glacier bed (see section 4.2.4) from the best surface topography interpolation of the glacier for a given year. Due to the nature of the maps available - a mix of high resolution glacier topographic maps (between 1:5000 and 1:25000) and the lower resolution area contour map (1:100 000 with horizontal errors between 1 m and 100 m (Lantmäteriet, 2010)), as well as the variety of methods used to create them, both from the digital and pre-digital mapping eras, there is a significant level of disagreement. When subtracting the bed raster, constructed mainly using the regional contour map, from the glacier surface rasters (higher resolution maps), this results in negative thickness values occurring due to the bed raster being of a higher elevation than the glacier surface raster. This is an artifact and needed to be dealt with, as observed by Rippin *et al.* (2011).

The 2009 bed DEM exists within the overall Area-Bed DEM which was a combination of the 2009 bed DEM, regional contours and dGPS data collected from the eastern fore-ground of Kårsa. This was based on an assumption that, apart from the area within the extent of the glacier in 2009, the present day surface is representative of the former glacier bed surface. This is unlikely to be accurate as such an assumption neglects the effects of glacial processes during retreats and advances, fluvial reworking across the area, weathering processes and mas movement. For example, under this assumption, the 1926 bed will show evidence of all post-dated push/dump/lateral moraines occurring after the 1926 glacier had long retreated, due to the activity of the glacier in its later stages. Unfortunately, such features cannot be removed from the bed DEM and this increases likely error with glacier thickness estimates.

To account for errors introduced by the overlaying of the glacier surface interpolations over the Area-Bed DEM, the most likely points to share a common value are those on the glacier margin - the point where land cover crosses the non-ice/ice boundary. A point perimeter was constructed around each glacier

Table 4.8: Mean perimeter point agreement (statistical bias). Where value is positive, the glacier surface was at a greater elevation than the Area-Bed DEM on average. Where the value is negative, the glacier surface was lower than the elevation of the Area-Bed DEM on average

Year	$\bar{x}$ error m
1926	+12.87
1943	-15.07
1959	+8.68
1978	-0.04
1991	+4.55

surface interpolation from 1926 - 1991 within ArcGIS. At each point location, elevation values for both the glacier surface in question and the underlying Area-Bed DEM were queried, the difference between them then being calculated. Mean error values were than accounted for for each outline, indicating the overall level of agreement between glacier surface perimeters and the Area-Bed DEM (see table 4.8). This specific routine was not carried out for the contemporary glacier as it was constructed from perimeter points for which elevations were extracted directly from the Area DEM. The values calculated give an indication of vertical error however, the method by which the contours of the actual glacier surface available from the 1926-1991 maps were constructed is unknown and provides unknown error itself. This has been identified as a problem in previous studies (e.g. Nuth *et al.*, 2007) and is extremely difficult to accurately quantify, especially considering the limited information on the original cartographic methodological process that is available.

To account for a maximum likely thickness surface the following conditions are met:

1. If cell value is greater than the minus positive error value, then add the positive error value
2. If cell value is between the most negative value in the data set and the minus positive error value, then make cell value equal to zero

To account for a minimum likely thickness surface the following conditions were met:

1. If cell value is greater than the positive error value, then subtract the positive error value

2. If cell value is less than the positive error value, then make cell value equal to zero

All surfaces incorporate the bed surface created from the 2009 GPR/Bodin glacier thickness points and therefore must account for the ±11.912 m error term associated with it. Where perimeter agreement error values are less than the 2009 GPR/Bodin error term, we apply the latter.

Once surfaces of maximum and minimum error had been created, it was then possible to calculate maximum and minimum mean values. It was then possible to calculate the error boundary either side of these mean values. For the maximum surface mean, this gives us a maximum mean ±error (resulting in a maximum maximum mean (mean + error) and a minimum maximum mean (mean - error). For the minimum surface mean, this gives us a minimum mean (resulting in a maximum minimum mean (mean + error) and a minimum minimum mean (mean - error).

Using these methods, maximum likely glacier thickness was then calculated resulting in two values - one using the maximum error method and the second using a minimum error method. Mean likely maximum thickness can then be assessed as the mid-point of these two values. Mean thickness can also be calculated using the maximum and minimum methods (providing a maximum method mean and a minimum method mean). The mean with ± error is the mid-point of these two values (see table 4.9). Using the maximum, minimum and mean likely surfaces, respective volumes are then calculated (table 4.10).

Table 4.9: Thickness analysis results. The * implies that the perimeter error was less than the contemporary bed error and so the latter, larger error was used. The † implies that this was the contemporary bed error and is therefore from a different source to the historical perimeter errors.

Year	DEM compatability error (m)	Max. thickness (max. error calc.) (m)	Max. thickness (min. error calc.) (m)	Mean max. thickness (m)	Mean thickness (max. error calc.) (m)	Mean thickness (min. error method) (m)	Mean thickness (m)
1926	12.87	150.37	124.63	137.50	40.47	20.14	30.31
1943	15.07	106.03	75.89	90.96	24.19	8.70	16.45
1959	8.68*	116.33	92.50	104.42	38.35	18.83	28.59
1978	0.04*	100.61	76.78	88.70	29.97	14.15	22.06
1991	4.55*	113.62	89.79	101.71	34.60	16.87	25.74
2010	11.91†	67.91	44.09	56.00	24.67	6.13	15.40

Table 4.10: Ice volume analysis results. The $*$ implies that the perimeter error was less than the contemporary bed error and so the latter, larger error was used. The † implies that this was the contemporary bed error and is therefore from a different source to the historical perimeter errors.

Year	Associated error (m)	Max. Volume (x 10^{-3} km^3)	Min. Volume (x 10^{-3} km^3)	$\bar{x}$ Volume (x 10^{-3} km^3)
1926	± 12.87	166.94	83.69	125.31
1943	± 15.07	47.69	17.31	32.50
1959	± 8.68*	69.08	34.38	51.73
1978	± 0.04*	46.58	22.24	34.41
1991	± 4.55*	38.95	19.13	29.04
2010	± 11.91†	21.28	5.39	13.33

4.3.6 Basal shear stress

Shear stress exerted on the bed of the glacier is calculated using the equation:

$$\tau_b = \rho_i \, g \, h \, sin\alpha \tag{4.7}$$

where ρ_i is the density of ice (assumed here to be 900 kg m^{-3}), g is gravitational acceleration (9.81 m s^{-2}), h is ice thickness and α is the surface slope angle (in radians) (Benn & Evans, 1998). Ice thickness and slope values are taken from rasters of the glacier. The slope raster is developed as described in section 4.3.3. τ_b values are calculated directly from ice thickness and slope values and thus, any errors associated with these parameters will be translated into the stress values (Thorp, 1991). Shear stress is calculated in this study for centreline profiles for each year. Stress at a given point is calculated from slope and thickness values averaged from values taken from points of a distance equal to the mean glacier thickness, either side of the point of interest. Slope is calculated for the point of interest by considering the elevations of the points either side of it and the distance between them. This in effect gives values of a moving average equal to 2x the glacier mean thickness and reduces the effects of longitudinal and lateral variations that would be expected in stress values along the glacier (Raymond, 1980).

4.3.7 Annual mass balance values

There are many ways of accounting for mass balance change as mentioned in section 2.4 of chapter 2. Here, the geodetic method to assess change was used and an approximation of annual mass balance values is calculated using the data calculated using the methods described in section 4.3.3. Annual balance values are also shown for the model runs although the change is observed using a geodetic approach again (output surface DEM subtracted from the input surface DEM). Mass balance was calculated by firstly accounting for the specific balance (equation 2.1), calculating the annual balance of the entire glacier (equation 2.2) and then calculating the mean annual balance (equation 2.3) (Cuffey & Paterson, 2010). Where b_n has been calculated for a surface where data on surface change is only available over large time steps, the value calculated for b_n using equation 2.1 is then divided by the number of years in the interval between $t1$ and $t2$. To convert changes in mass to m w.e. (melt water equivalent) values, changes in terms of ice thickness are considered. Glacier ice density is assumed to be 900 kg m^{-3} compared to water at 1000 kg m^{-3}. Where B_n or $\bar{b_n}$ are in m (ice), m w.e. is calculated using equation 2.4.

4.3.8 ELA

As described in chapter 2, the ELA is a theoretical point at which ablation is equal to accumulation over a year, thus giving a zero annual mass balance value. The annual ELA is unlikely to occur along a single contour line due to a number of topographic and morphological factors and consequently, the ELA is merely the mean elevation contour at which zero mass balance values are calculated (Benn & Lehmkuhl, 2000). Furthermore, the annual ELA differs to the steady state ELA which is calculated from datasets accounting for glacier change over a number of years (Benn & Lehmkuhl, 2000).

There are a number of different methods available to approximate the ELA and these are discussed briefly in section 2.4 of chapter 2. Within this study the glacier ELA was calculated using the following methods:

1. Hess altitude
2. Median elevation (H_{med})
3. Accumulation Area Ratio (AAR)
4. Accumulation Area (AA)
5. Area Altitude Balance Ratio (AABR)

The Hess altitude is defined as the point at which convex contour lines become convex lines, as identified when considering the contour map of a given glacier. The Hess altitude, also known as the "Kinematic ELA (Leonard & Fountain, 2003) was introduced as a means of estimating firn-line elevation by Hess (1904 cited in Leonard & Fountain, 2003). The transition from concave contour lines, on which the method is based, develop in the accumulation area and convert to convex contour lines in the ablation area. The convex profile is caused by snow being blown from the glacier margins to the centre of the glacier whereas concavity is caused by the reverse process (Leonard & Fountain, 2003). Use of the method is limited (Cogley & McIntyre, 2003), although examples of its use include studies by Zverkova *et al.* (1982), Fountain *et al.* (1999a) and Miller *et al.* (1975). The method is alluded to in Davies *et al.* (2012) but is not used in the final results of the study due to the scatter of ELA elevations it produced and its limited application due to contour line profiles. The method is not discussed in Sugden & John (1976) or Benn & Evans (2010). It is included within this study as a point of interest and to see how well it correlates with the other ELA methods used.

The H_{med} simply takes the median altitude from the elevation range of a given glacier. This method was developed at the end of the 19th century by Höfer (1879) and Kurowski (1891). It has been used in a few studies including (Carrivick & Brewer, 2004) and (Davies *et al.*, 2012). However its use is limited to glaciers with more regular geometries from which calculations are most reliable (Porter, 1975).

A frequently used method is the AAR. It is based on the broad assumption that under steady-state conditions, the ratio of the accumulation area to the ablation area is fixed. It can be represented mathematically using:

$$AAR = \frac{A_c}{A_c + A_b} \tag{4.8}$$

A wide range of AAR values exist from 0.2 - 0.8, with values representing the portion of the total glacier area representing the accumulation zone (i.e. an AAR of 0.8 means the accumulation area is equal to 80% of the total glacier area) (Benn & Evans, 2010). For glaciers located in high latitudes, common AAR values representing steady state conditions are often between 0.5-0.8 (Meier & Post, 1962). Using the AAR ratio, the elevation of the ELA is equal to that of the contour which lies beneath the area of the accumulation zone as given by the AAR value. A limitation of the AAR is that it does not account for glacier specific hypsometry or the mass balance curve (Osmaston, 2005). These limitations increase the error uncertainty around the value predicted.

Selecting the most applicable AAR is difficult and some studies have used multiple AAR values to calculate ELA positions for a range of glaciers, selecting the most appropriate AAR as being the one producing the smallest variance between predicted ELAs (see Kaser & Osmaston, 2002). In this study, the AAR ratio is approximated from the mass balance curve which is created between each mapping interval as discussed above in section 4.3.7.

The AA method is similar to the AAR in that it assumes a fixed ratio to exist between the accumulation and ablation zones. It differs however to the AAR method as it requires information on the areas between contour bands, thus taking into account glacier hypsometry. As with the AAR method, it still does not account for the glacier mass balance, which is represented by the Balance Ratio (BR) value (Osmaston, 2005). As with the other methods, it was devised at the end of the 19th century by Kurowski (1891). Prior to automation of calculations, the method had fallen out of use due to the number of calculations required (Osmaston, 2005). However, Sissons (1974, 1980) simplified the calculations required and

to calculate the ELA using this method, where A_i is the area between a given contour interval and h_i is the mid-elevation of the contour interval, the following equation is used:

$$ELA = \frac{\sum A_i h_i}{\sum A_i} \tag{4.9}$$

The method was originally based on using the mid-altitude of the glacier and the simplification introduced by Sissons (1974, 1980) was that the mid altitude of any given contour band for which the area was known, could be used (as in equation 4.9).

It is possible to work the equation to use different ratios, thus changing equation 4.9 which is akin to using an AAR of 0.5. For example, to calculate the ELA using an assumed AAR ratio of 0.6 (therefore a larger accumulation area), the following equation could be used:

$$ELA = \frac{\sum A_i \left(h_i \left(h_i - \left(h_i/5\right)\right)\right)}{\sum A_i} \tag{4.10}$$

Equally, to calculate the ELA using an assumed AAR ratio of 0.4 (therefore a smaller accumulation area), the following equation could be used:

$$ELA = \frac{\sum A_i \left(h_i \left(h_i + \left(h_i/5\right)\right)\right)}{\sum A_i} \tag{4.11}$$

The BR is calculated from the ratio of the accumulation and ablation gradients of a mass balance curve. BR values were calculated in this study by the use of simple linear regression of the appropriate portions of the mass balance curves and taking the gradients. None of the aforementioned methods account for hypsometry and the BR. The AABR method, developed by Furbish & Andrews (1984), originally named the BR method and renamed by Osmaston (2005) was developed to provide such a method thus it accounts for both the glacier geometry and the mass balance curve as opposed to geometry alone. AABR is based on two assumptions (Benn & Lehmkuhl, 2000):

Figure 4.15: AABR methodology diagram (modified from (Furbish & Andrews, 1984) and (Benn & Gemmell, 1997))

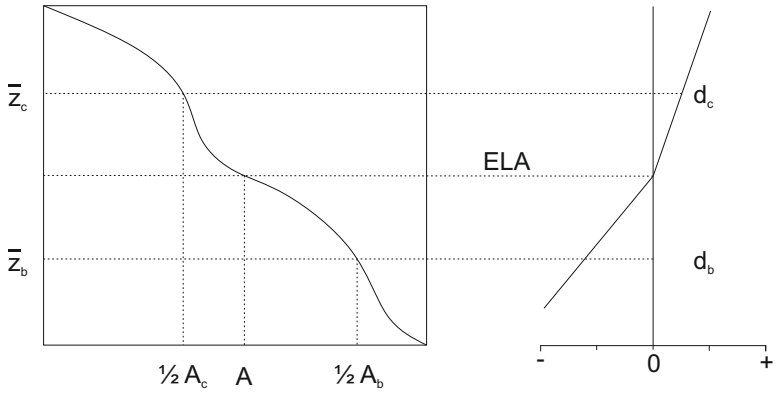

1. Ablation and accumulation gradients are approximately linear
2. The ratio between the two is known (this is the balance ratio of BR - the ratio of the slopes of the mass balance/altitude curve below and above the ELA (Osmaston, 2005))

The AABR method calculates the ELA by using linear ablation and accumulation gradients and area-weighted mean altitudes (i.e. the AA method based on a median value which is similar to using an AAR of 0.5). This results in the introduction of a number of factors. Respectively, d_b and d_c represent the ablation and accumulation measured at the mean altitudes of the ablation (z_b) and accumulation (z_b) areas (Furbish & Andrews, 1984; Benn & Gemmell, 1997). The ELA is located at the position on the glacier where the values of these factors are equal to the balance ratio, as in equation 4.12 (illustrated in figure 4.15):

$$BR = \frac{z_c.A_c}{z_b.A_b} \tag{4.12}$$

The AABR method, as defined above, is applied in this study using the spreadsheet created by Osmaston (2005). The spreadsheet and its application are also discussed in Osmaston (2005). At the time of publication of Osmaston (2005), it was possible to download a version of the spreadsheet. Unfortunately as the author is now deceased, this is no longer possible and the spreadsheet must be built by the user using the instructions in Osmaston (2005). It should be noted that

these instructions require some modification, specifically for step 12 of appendix A where the formula required should be [=$ E2 ($ D2-$ H$ 2)]. It is also useful to disregard the pasting of individual cells I and J and to simply copy and paste the IJK blocks using the aforementioned equation fix.

It is common to use 2 or more methods of ELA estimation to approximate the ELA of a given glacier (Benn *et al.*, 2005). To create a best estimate of the ELA, an average value (ELA_{mean}) was calculated as in Davies *et al.* (2012). ELA_{mean} is calculated using:

$$ELA_{\text{mean}} = \frac{ELA_1 + ELA_2 + ELA_n}{n} \tag{4.13}$$

where the ELA_1 - ELA_n represent the ELA estimates using different methods and n is the total number of ELA methods used.

Chapter 5

Model methods

A bespoke computer based distributed SEB model has been developed specifically to meet the aims of this study. The model has a graphical user interface (GUI) and provides a platform that has been developed for a typical small Arctic mountain glacier. The code for the model can be accessed from `https://github.com/Chris35Wills/SEB_model_java_files`. This chapter discusses the methods used in the development of the SEB model, the geometric inputs of which are derived using many of the methods discussed in chapter 4. The combined application of these methods allows for an understanding of SEB effects as a consequence of changing geometry on glacier MB. Treatment of the model input data (predominantly with regard to meteorological inputs), the different algorithms used and model set up are all discussed here as well as the consideration of different approaches by which to implement certain parameters. Although this chapter is principally methodological, the model for which the methods apply is in itself a major outcome of this study and this is discussed further in chapter 10. This chapter provides the basis for addressing the project objectives of:

- Developing a user friendly grid based distributed surface energy balance model which uses reconstructed surfaces as an input, combined with meteorological data from the field
- Conducting model scenarios with the developed model to assess the effects of meteorological and topographic forcing as well as geometry change on surface energy balance and mass balance change

5.1 Contemporary data: Automatic Weather Station (AWS) data integration

Meteorological data are available for Kårsa from June 2007 - the present, collected from an AWS installed by the University of Leeds. Automated observations include surface measurements of incoming shortwave radiation (W m^{-2}), air temperature (°C) (from approximately 2 m above the surface) and wet precipitation (mm)(rainfall). AWS location is discussed in chapter 3 and the data are discussed in section 9.2.1 of chapter 9. Due to AWS issues, relating partly to component malfunctions but mainly problems due to data storage capacity and battery power (a result of constant low temperatures), these records are not continuous, with gaps of varying sizes occurring. The melt modelling carried out in this project required a continuous stream of temperature and precipitation values. To enable model run facilitation, gap filling methods were applied to the temperature and precipitation data. The radiation data were treated separately (see section 5.3.2).

5.1.1 Temperature data: Gap filling and the use of multiple imputation

The temperature data set collated by the AWS is 90% complete with some months missing values due to AWS issues (see figure 5.1). Due to the requirement of a continuous stream of temperature data for the model to run, these gaps needed to be filled and a simple linear function was found not to be suitable as it failed to account for the varying temporal frequencies inherent of the data that was collected successfully.

Gaps in the temperature dataset were populated using a multiple imputation method, implemented using the Amelia II package in R. Unlike mean missing data imputation methods, MI allows avoidance of biases that become associated with variances and covariances inherent of these methods (Honaker *et al.*, 2012). This method has been shown to perform well in a number of different missing data situations (Wayman, 2003).

Figure 5.1: Temperature line plot displaying the raw data collected by the AWS. The clear gaps could not easily be filled using simple techniques as these failed to account for the varying temporal frequencies inherent of the collected data values.

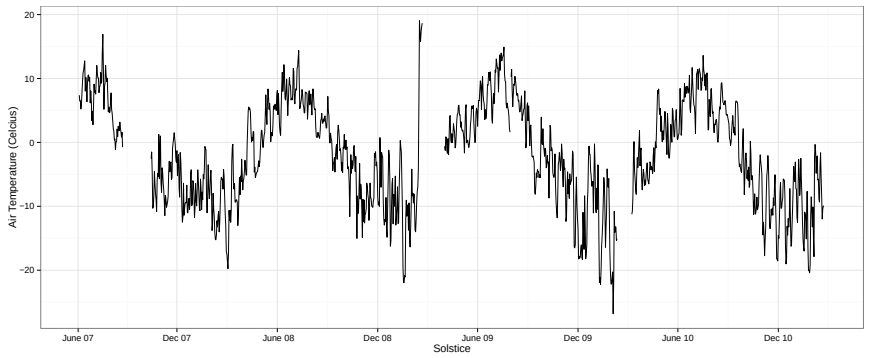

Where K is the number of imputation runs carried out, the Amelia II programme imputes K number of values for each gap within a given dataset, resulting in K filled data sets. These filled data sets maintain known observations, providing imputed values for all gaps. In this sense, MI is similar to other exact interpolations (such as kriging in spatial statistics). The resulting K number of imputed (and thus *complete*) data sets can then be averaged to provide a final complete data set. The method is summarised in figure 5.2. Using MI, missing values are predicted from the existing values in the original dataset. These predicted values then replace any missing values in the data set which results in an imputed data set (Wayman, 2003).

Use of Amelia II requires the assumptions that the data have a multivariate normal distribution and that missing values are *missing at random* (MAR). The Kårsa AWS temperature data set used here has been shown to be approximately normally distributed prior to performing the MI. The data set has thus been used without subsequent transformations. The assumption of multivariate normal distribution has been found to work well with the applied MI, even when compared to more complex models (Honaker *et al.*, 2012). The MAR assumption on the other hand relates to the fact that missing values occur at random in relation to

Figure 5.2: Multiple imputation work flow

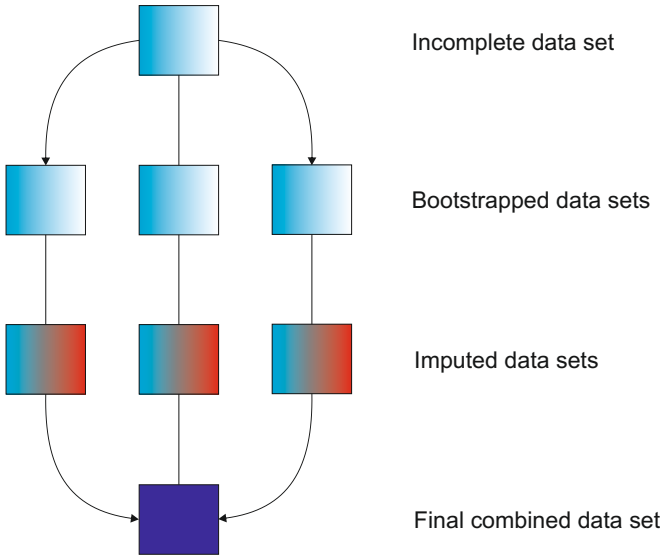

the observed data. This assumption could be met in the present data set as given any month between 2007 and 2011, *missingness* did not depend directly on the observed temperature measurements.

Two MI runs (each of 20 imputations) were carried out. The results of the first run can be seen in figure 5.3. The spike that can be seen occurring during the spring of 2009 occurs prior to a period of thermometer malfunction. Thermometer malfunction is likely to have begun prior to cessation of data recording, and this spike, which exceeds the range of temperatures exhibited by the rest of the data set, is likely to be evidence of this. The data points causing the spiking were removed and a second full MI run was carried out - the removed values being imputed as if they had been missing. The output of the second run can be seen in figure 5.4. This temperature data set is that which is used fr the contemporary model runs. The temperature data starts on the third day of AWS data collection, allowing for a day of instrumentation equilibration.

A standard error of 2.78 was calculated for the imputations. The calculation of

Figure 5.3: Temperature line plot (result of MI 1)

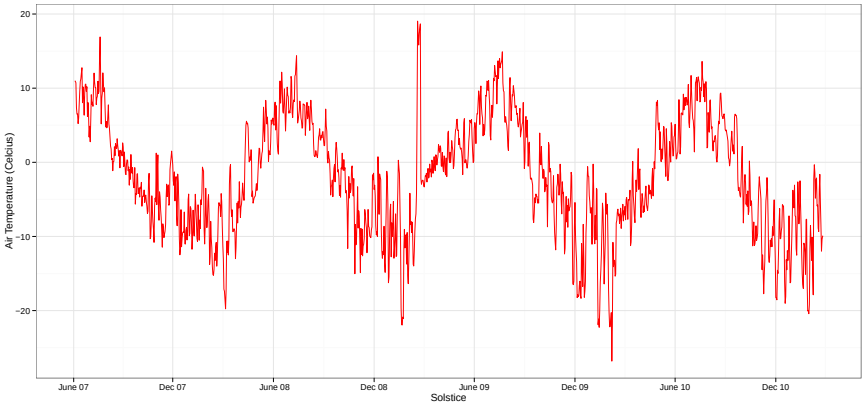

Figure 5.4: Temperature line plot (result of MI 2)

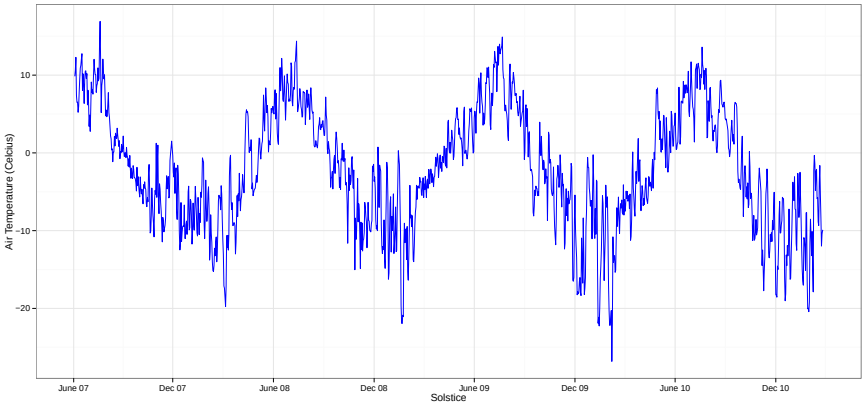

standard error in this instance requires evaluation of the mean of all imputed data sets ($\bar{\theta}$) using $\bar{\theta} = K^{-1} \sum_{k=1}^{K} \hat{\theta}_k$ where $\hat{\theta}_k$ is the mean of an individual imputed data set (Honaker *et al.*, 2012). Total variance (T) of $\bar{\theta}$ is then calculated for k imputed data sets using:

$$T = \overline{W} \; + \; (1 \; + K^{-1}) \, B \tag{5.1}$$

where:

$$\overline{W} = K^{-1} \sum_{k=1}^{K} W_k \tag{5.2}$$

Figure 5.5 displays histograms of the original temperature data distribution as well as the first, fifth, tenth, fifteenth and twentieth imputation outputs.

From the histograms, it is apparent that imputations are more limited towards the extremes of the data, deviating from the input data most apparently for the 0 - 10 °C bin. This is further supported by figure 5.6 where it is clear that the majority of predictions fall between -10 - ˜3°C, there is a low prediction frequency between 3 - 10°C and then there is an increase in prediction density from ˜10 - 12°C. Due to the nature of this method coupled with the available data, extreme temperature events, both peaks and troughs, are likely to be under- and overestimated respectively.

Figure 5.7 displays charts for the years 2007 - 2011 with imputations highlighted along with associated error bars for each estimation. The 2008 and 2011 charts show no imputations as there were no data gaps. They are included here for completeness. The largest data gaps occur during the autumn of 2007 and the springs of 2009 and 2010. These events are random relative to the temperature trends and a function of temperature sensor malfunction.

Figure 5.5: Histograms of the original and the first, fifth, tenth, fifteenth and twentieth imputed temperature data sets

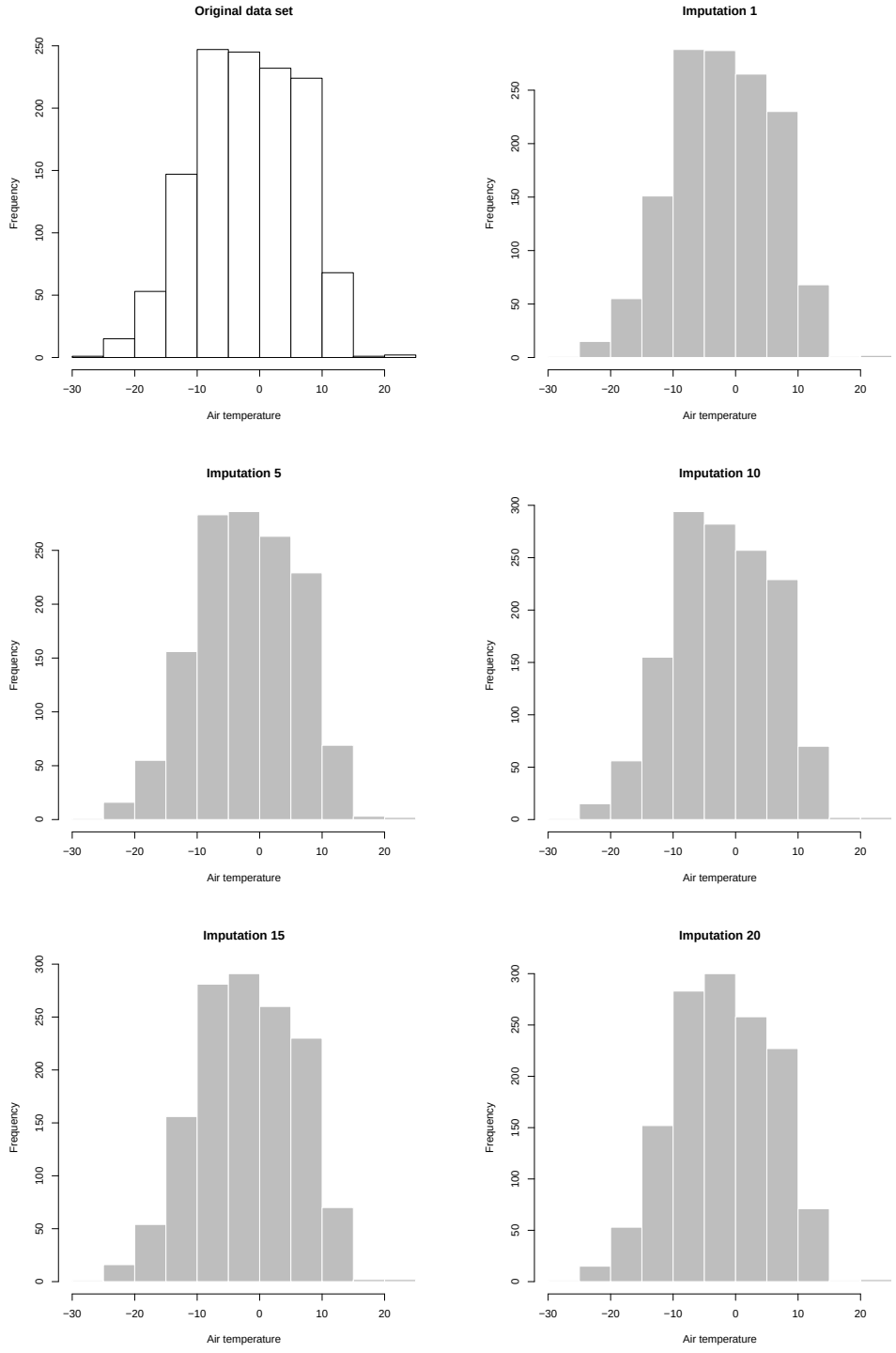

Figure 5.6: Multiple imputation prediction density. Predictions are concentrated between -10 - ˜3°C with fewer predictions in the 3 - 10°C range. There is a small increase in prediction density between ˜10 - 12°C

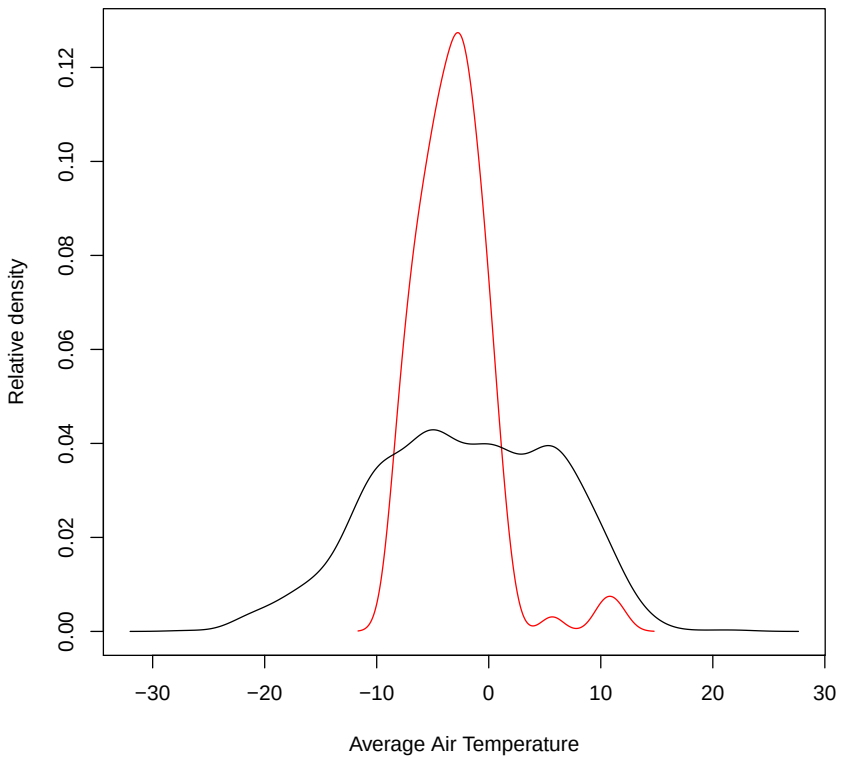

Figure 5.7: Annual temperature data sets with associated error of imputation estimates

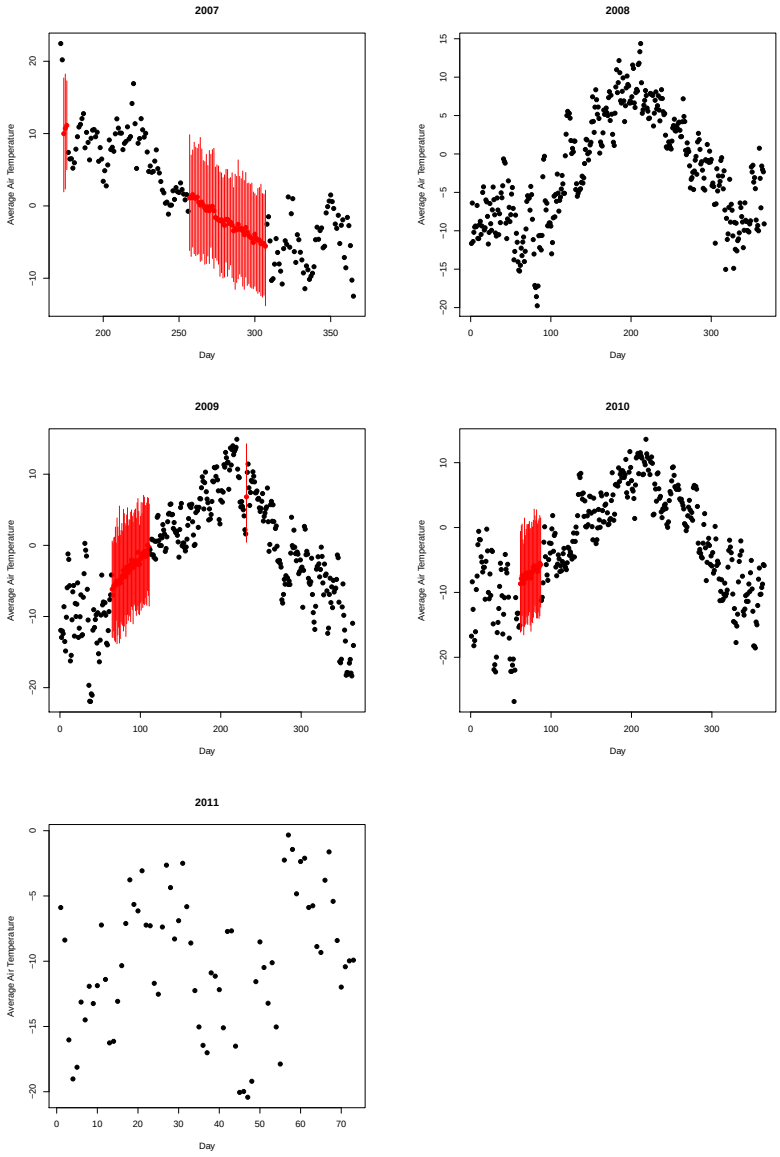

5.1.2 Contemporary precipitation data

The contemporary model is driven by precipitation data collected at the AWS over the 2007-2011 period. Due to the relative sparsity of values, no attempt is made to gap fill as such a process would be purely academic with too few observations available for accurate reconstructions.

5.2 Historical data: Adjusting distal data (ANS) to local conditions (AWS)

5.2.1 Historical temperature data

Temperature data are available from ANS from 1920 to September 2012 (data collection at ANS is on-going, extending outside of the remit of this study). The temperature data are available as daily means, with no gaps throughout the record. ANS is located ˜25 km east of Kårsa,and is located on the western shoreline of Lake Torneträsk at an elevation of ˜370 m a.s.l.

To correct the temperature data available to be equivalent to the AWS, a lapse rate was required. Data from the AWS that crossed over with data available from the ANS provides a cross over data set from 2007 - 2011. The AWS data was averaged over the month to allow it to be compared with the ANS data. The completed AWS dataset developed using multiple imputation was not used during this analysis, with any gaps in the record being ignored. The ANS and AWS components of the cross-over dataset are plotted together and are displayed in figure 5.8.

As can be seen in figure 5.8, there are differences between the two temperature regimes. The mean difference between the two data sets was 1.96°C, with a range of 7.94 °C and a maximum difference of 4.29°C. Temperature at ANS was generally greater than at the AWS from March to November, with the differences being lesser between approximately December and February. Temperature as measured at ANS was lower than that measured at the AWS for some winter months as

Figure 5.8: ANS/AWS temperature cross-over data: July 2007 - February 2011

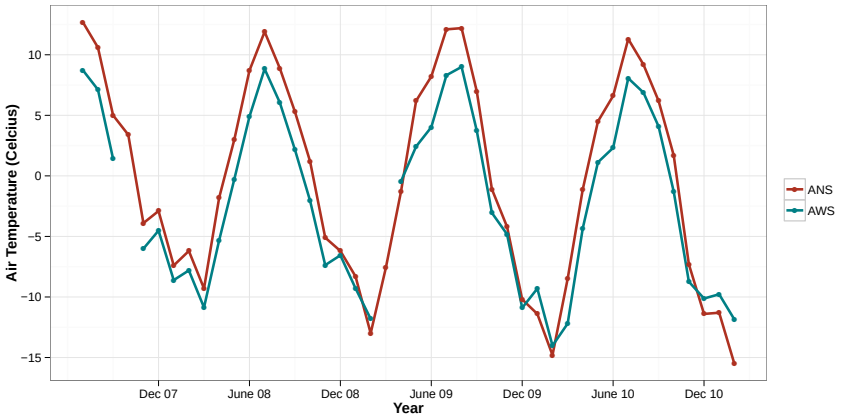

can be seen for February 2009 and January and February 2010 and 2011. These differences can be explained in part by the differing levels of interplay between the continental and continental/maritime regimes manifest over Abisko compared to over Kårsa, difference in elevation (in terms of adiabatic variations) as well as the relative juxtaposition of ANS to Lake Torneträsk which will also have an effect. A number of other effects including differences in the overall surface albedo of the area, surface aspect and wind patterns will also be instrumental in the differences in measured temperature (see Petersen & Pellicciotti, 2011).

To apply a single fixed lapse rate to correct the ANS data to the area around the AWS was inappropriate in this situation. Furthermore, lapse rates are known to vary temporally. Temperature from the cross over data set was first analysed on a monthly basis, where tests were carried out for the validity of applying 1st, second or third order polynomial models to assist in temperature lapsing. Only to the months of May, August and December could significant 1st order polynomials be applied. For all other months and models, results were insignificant (see table 5.1). This is largely a function of the restricted crossover dataset (a maximum of 4 ANS/AWS point pairs per month).

To acquire a stronger and more applicable prediction model, the crossover data

Table 5.1: Monthly ANS/AWS temperature regression analysis results (NS refers to a non-significant test and NA refers to a non-applicable test)

	Polynomial		
Month	1st order	2nd order	3rd order
J	NS	NS	NS
F	NS	NS	NS
M	NA	NA	NA
A	NS	NA	NA
M	Sig.	NA	NA
J	NS	NA	NA
J	NS	NS	NA
A	Sig.	NS	NA
S	NS	NS	NA
O	NS	NA	NA
N	NS	NS	NA
D	Sig.	NS	NA

Table 5.2: Seasonal ANS/AWS temperature regression analysis results

	Polynomial			
Month	1st order	2nd order	3rd order	Best model
Summer	Sig.	Sig.	Sig.	1st order
Winter	Sig.	Sig.	Sig.	1st order

were then split into two seasonal groups - summer and winter. Where mean monthly temperatures within the crossover dataset were greater than 0°C, the season was set as summer, otherwise winter. For all years, the months of May, June, July, August and September were classed as summer with the remaining months being winter. The split dataset was then assessed on an individual basis for regression model significance (see table 5.2).

Significant 1st, 2nd and 3rd order polynomial regressions were found for both the summer and winter data sets. ANOVA tests were run to test improvements in model fit between the 1st, 2nd and 3rd order equations, resulting in the first order being the most suitable. The seasonal data point distributions can be seen in

figure 5.9, both with a smooth line applied and the chosen linear regression model of the summer regression equation ($p = 5.886 \times 10^{-13}$, $r^2 = 0.9638$):

$$y = -3.26257 + 0.98692x \tag{5.3}$$

and the winter regression equation ($p = 2.288 \times 10^{-11}$, $r^2 = 0.8739$):

$$y = -2.84141 + 0.70835x \tag{5.4}$$

Considering the strength of the seasonal model results, the equations 5.3 and 5.4 are used to alter the ANS monthly mean temperature dataset. The adapted ANS dataset is compared next to the raw ANS temperatures below in figure 5.10.

Considering the application of regressions 5.3 and 5.4, peak temperatures measured at ANS were capped, as is to be expected when considering figure 5.8. Equally, the ANS minimum temperatures on average have been reduced. The regression method applied here provides results as would be expected, with regard to generally lower temperatures in summer and similar temperatures during the winter. However, as the regressions were calculated for the 2007 - 2011 cross-over period, two assumptions had to be made. The first is that of homogeneity of variance - variation and patterns within the cross-over data set are assumed to be valid for the full 1920 - 2011 ANS dataset. The second assumption is based on the stability of the regressions as they are extrapolated outside of the range of values upon which the equations were derived through the monthly analysis of the cross-over data.

The adjusted ANS data is used within the historical model runs.

5.2.2 Historical winter precipitation

Snow depth has been recorded at ANS since 1920 based on both a fixed point and a transect of points from which is derived a daily average. For effective modelling, winter precipitation was required to be distributed across a grid within the model. This has been effected within the contemporary model by integrating

Figure 5.9: Winter and summer temperature seasonal point distributions for ANS against AWS. The upper charts have a smooth line superimposed to give an idea of the general trend. The lower charts display the applied linear regressions of 5.3 and 5.4 for the summer and winter months respectively.

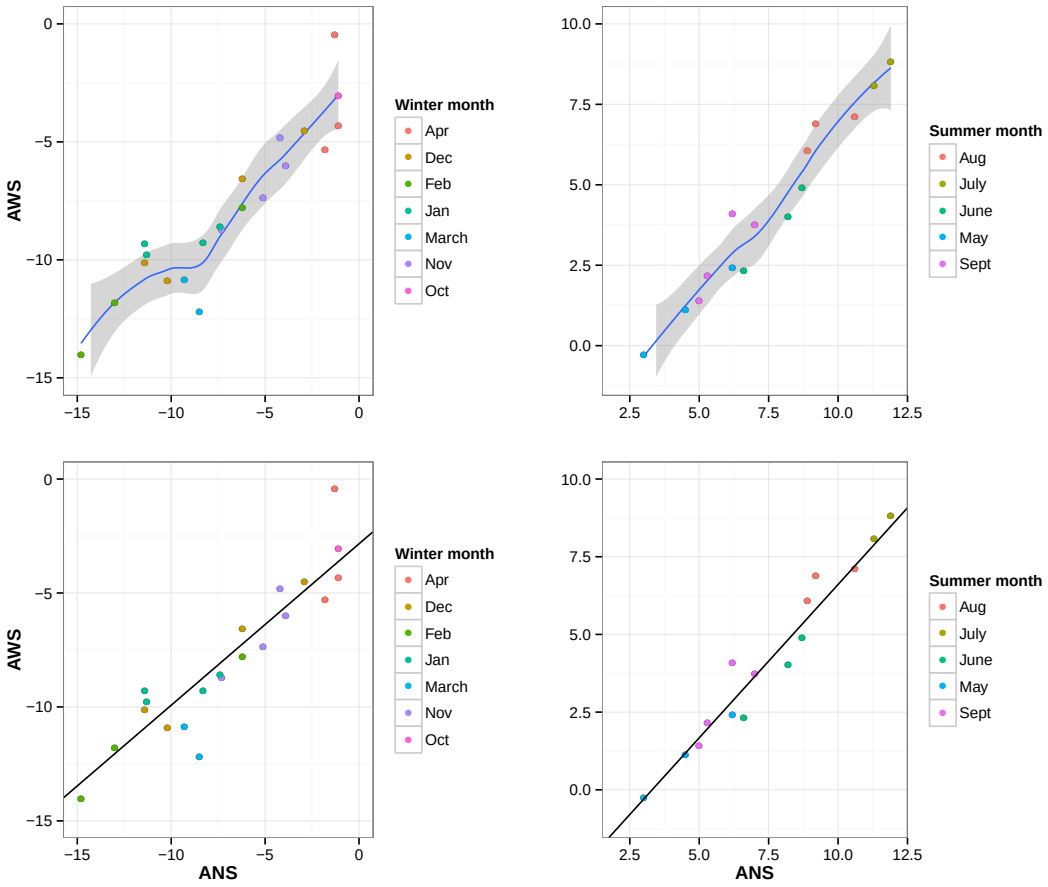

Figure 5.10: Raw and adjusted ANS temperature data 1920 - 2011. The top and lower charts display the raw and adjusted data respectively.

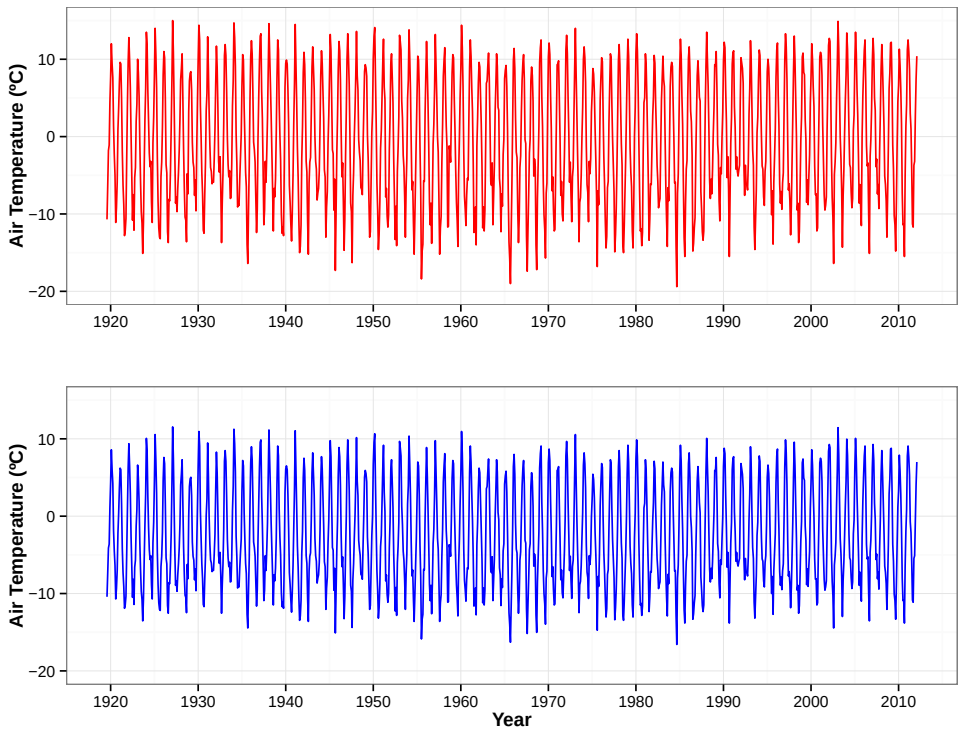

data collected from the field on end of winter season snow depths, distributed across the glacier (this is described in section 4.2.7 of chapter 4). Distributed snow depth across the glacier at the end of the winter season is unknown prior to the first snow probe assessment carried out in 2008. The following approach to approximate distribution was applied:

1. Compare mean contemporary end of winter season snow accumulation from the glacier with the accumulation as measured at ANS, for the years 2008 - 2011 (cross-over) and approximate a lapse correction

2. Approximate the distribution of end of winter season snow thickness as a function of elevation across the glacier by means of polynomial regression

3. Using the "lapse" corrected end of winter season snow depth from ANS, calculate snow thickness distribution across the glacier (for which the elevation map is specific to the year in question) using the statistically most appropriate regression model

The following assumptions were made in this analysis:

1. Homogeneity of variance between contemporary snow patterns (2008 - 2011) and patterns that existed prior to data collection

2. Validity of applied corrections and regression equations is maintained through extrapolation (important in terms of meteorological trends propagating outside of the 2008-2011 ANS/AWS cross over period and with regard to the glacier elevation range prior to snow thickness data assessment which differs to the present, especially below approximately 900 m)

Records of daily snow depth measurements are available from ANS from 1st January 1920 to the present day, with few gaps. The method of snow depth assessment has been a combination of a transect of stakes from which a mean snow thickness was derived and also the use of a single stake. The measurements accumulate through the season, thus equating to total amount of snow as opposed to daily snowfall amount. An end of winter season snow thickness for ANS, comparable with that measured at the glacier using the snow probe technique

through the 2008 - 2011 winter field seasons, always facilitated in March, has been derived. The winter total thickness value is estimated by calculating the maximum thickness recorded during the month of March for each year at ANS. This provides a raw ANS dataset illustrated in figure 5.11. There were some gaps in the ANS snow thickness data set. These gaps were filled, due to the model requiring a continuous data input set, with the following considerations. Where there is:

(a) only a transect measurement, this value is used

(b) only a single stake measurement, this value is used

(c) both stake type measurements, average of the two is used

(d) neither value but one the year before and after, an average of the before and after values is used

(e) only a value before, use this value

(f) only a value after, use this value

(g) no value before or after, correct before and after and calc. the middle value as the average of the two fixed values (a combination of methods e, f and d)

Due to the different geographic locations of ANS and Kårsa, it was prudent to consider variation in snow depth measurements between the two sites. Consequently, the data cannot be used in its raw format. To estimate the difference in mean snowfall between the two sites, the data was compared where it crossed over, which was for the years 2008 - 2011. The mean measured snow depth values from the glacier were compared with the March maximum values at ANS (an assumption being made that the measurement of snow thickness during the field work campaigns was a near as possible to the maximum winter snow thickness) - see table 5.3. The difference between the two sites was calculated each year and then averaged - the resultant value of 2.00 being an estimate of how much more snow could be expected at the glacier, given a specific snow thickness measurement at ANS.

Figure 5.11: Raw and adjusted snow thickness measured at ANS 1920 - 2012

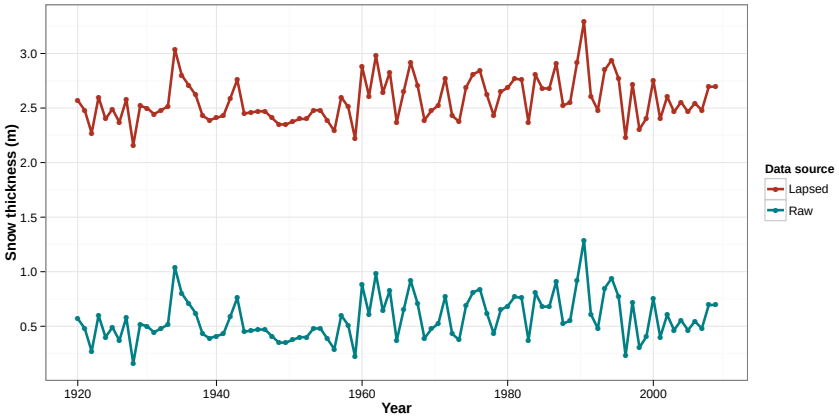

Table 5.3: Mean end of winter season snow depth comparison: Kårsa vs. ANS

Year	Kårsa thickness (m)	ANS thickness (m)	Difference (m)
2008	2.36	0.47	1.90
2009	2.26	0.55	1.71
2010	2.31	0.48	1.83
2011	3.24	0.70	2.55
Mean			2.00

The resultant mean difference was applied to lapse all ANS winter thickness values, *correcting* them to the glacier locale. The results of the lapse can be seen in figure 5.11.

Snow thickness distribution as a function of elevation was approximated using the data collected for the contemporary glacier analysis (winter snow depths for 2008 - 2011). Through analysis of the data, regression equations were drawn to best estimate the distribution. The most appropriate equation was then used to distribute winter snow as a function of elevation for the years where actual end of winter season snow depth is unknown.

Snow thickness was plotted against glacier elevation (figure 5.12) to which lines of best fit were applied to give an impression of the general trend. The data available for the different years varies with regard to spatial extent (see chapter 4). During the 2008 and 2009 field seasons, few snow thickness points were collected in the upper reaches of the glacier, being isolated to the more easily accessible ablation zone. Data collection in the 2010 and 2011 seasons was comparatively much more extended, with points being taken up into the accumulation zone, thus allowing for accountability of snow thickness at higher elevations.

With regard to regression analysis, the difference in spatial coverage of snow thickness points between 2008 - 2011 results in interesting variance, with 3rd order polynomials being most significant in 2008 and 2009 and 2nd order polynomials being most significant in 2010 and 2011. 1st, 2nd and 3rd order polynomial regression were tested on the snow thickness data for individual years (2008, 2009, 2010 and 2011), all of the years, and 2010 and 2011 together. Analysis of the 2010 and 2011 thickness data together was deemed appropriate as these two years shared a similar spatial data coverage, in both the lower and upper reaches of the glacier. The exemplified analysis for 2010 and 2011 diverts analytical focus from the lower elevations alone (as with the 2008 and 2009 data), enabling proportionally greater inclusion of snow thickness distribution at higher elevations. Basic test results can be seen below in figure 5.4.

Figure 5.12: Winter snow thickness as a function of elevation: 2008 - 2011

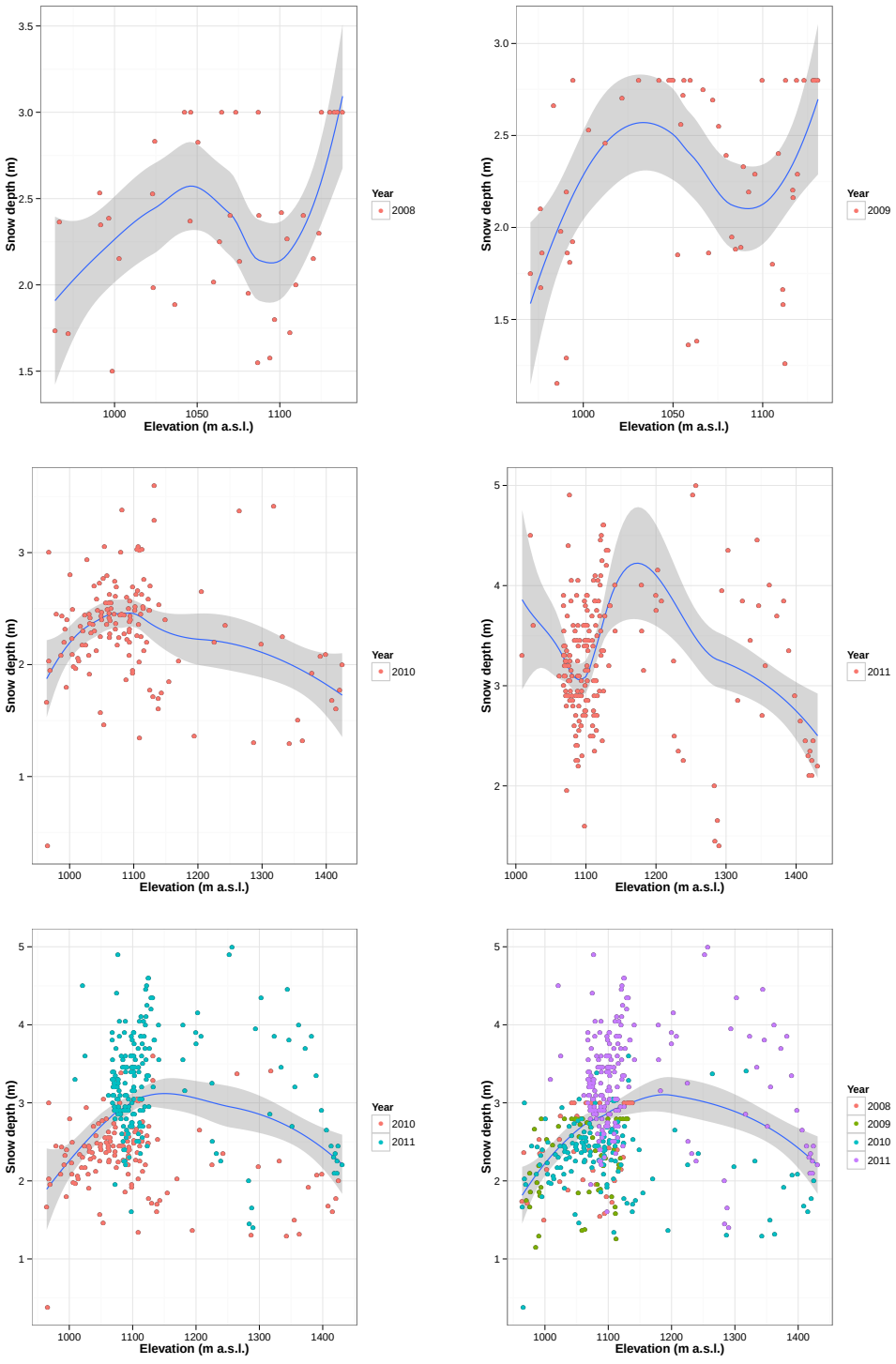

Table 5.4: 1st, 2nd and 3rd order polynomial regression analysis results for contemporary snow thickness vs. elevation

Year	1st order polynomial		2nd order polynomial		3rd order polynomial	
	multiple r^2	p	multiple r^2	p	multiple r^2	p
2008	0.07	0.09	0.08	0.24	0.24	0.02
2009	0.05	0.09	0.08	0.10	0.23	0.00
2010	0.04	0.02	0.13	0.00	0.14	0.00
2011	0.02	0.04	0.07	0.00	0.08	0.00
2010/2011	0.00	0.85	0.13	0.00	0.13	0.00
All	0.01	0.05	0.14	0.00	0.14	0.00

For the 2008 and 2009 data sets, 3rd order polynomial regressions were found to be most significant. For the individual 2010 and 2011 analyses, both 1st and 2nd order polynomial fits were significant. Despite the regressions being significant, they were all found to be very weak. Following ANOVA analysis, where the null hypothesis was that a 2nd order polynomial would not be a significant improvement on a 1st order polynomial, in both instances, the null hypothesis was proved incorrect (with p values of 0.0002 in both instances). For the 2010/2011 combined distribution, 1st and 2nd order polynomials were found to be significant. An ANOVA test was used to assess whether 2nd order provided a significant improvement, whereby the null hypothesis; a second order polynomial will not be a significant improvement on a 1st order polynomial; was proved incorrect ($p = 0.3059$). Analysis of all of the data available together resulted in 1st, 2nd and 3rd order polynomials being significant, although the individual coefficients of the 3rd order were themselves not significant. Nonetheless, ANOVA tests was carried out for all polynomials. The 2nd and 3rd order polynomials were found to be significant improvements on the 1st order polynomial ($p = 0.00$ in both cases). However, the 3rd order was not found to be significantly stronger than the 2nd order polynomial ($p = 0.6173$).

The winter snow thickness data for Kårsa was all that was available for the glacier. The data was collected once each year and therefore was essentially a snap shot of the overall snow distribution pattern. It is likely that the spatial pattern of snow depth is subject to wind re-distribution which will provide daily variations in depth

distribution. However, the general pattern is captured by the data available. To estimate thickness distribution as best as possible prior to the records illustrated here (therefore predicting from 1920 onwards), the best data to base an estimation on is that with the greatest elevation coverage, which was here attributed to the combined 2010/2011 data. The data when combined with 2008 and 2009 which has a data bias to lower elevations distorts the regression model, to satisfying lower elevations, unlike the 2010/2011 data. The most significant regression from the combined 2010/2011 analysis was used to distribute snow as a function of elevation prior to the contemporary analysis, using a second order polynomial regression equation of:

$$y = -28.39 + 0.05252x - 0.00002181x^2 \pm difference\ in\ mean \qquad (5.5)$$

By adding/subtracting the difference in the mean snow values (between the mean for the year in question and the mean from which the regression equation was derived), the curve was adjusted to suit different snow conditions. Using equation 5.5, its effectiveness was tested by predicting the measured 2010 and 2011 snow depths according to elevation. The $\bar{x}$ difference between the modelled and predicted values was 0.55 m with a range of 2.02 m. Experimentation with equation 5.5 showed that for elevations less than 820 m a.s.l., predicted snow depths were negative - this is a function of the extrapolation of the regression equation beyond its original constraints. The negative values and the stark reduction in snow thickness are artifacts of the applied method. However, there are no other data available for this region. In order to account for the aforementioned limitations, where snow thickness values fall below predicted snow depth as calculated for the minimum elevation from which the regression curve was created (with the addition/subtraction of the difference in means), snow thickness will be set to this calculated value. In implementing this method, snow thickness values will have a finite limit.

Snow depth at a given elevation will therefore be calculated by multiplying the mean (adjusted) end of season snow depth for a given year by equation 5.5 (where

x is the elevation (m a.s.l.)).

5.2.3 Historical summer precipitation

Summer months within the ANS/AWS crossover dataset were identified as in section 5.2.2 as a function of mean monthly temperature between the ANS and AWS sites. Total precipitation was compared for the two sites for these summer months, regardless of year (thus ignoring any annual trends). In doing so it is possible to assess any relationship that exists between precipitation amounts at the two sites as a function of the precipitation magnitude. To assist in correcting ANS precipitation values to the glacier locale, regression models were tested with the data. The only significant regression equation was a first order polynomial (p = 0.04, $r^2 = 0.24$) (see figure 5.13) of:

$$y = 0.02777 + 1.20866x \tag{5.6}$$

Polynomials of 2nd and 3rd order were insignificant (with respective p values of 0.13 and 0.26).

The r^2 of equation 5.6 is low. There was a weak positive correlation between AWS and ANS datasets (Kendall's τ: p = 0.03, $\tau = 0.39$ and Spearman's ρ: p = 0.03 and $\rho = 0.51$). Considering the weak correlation and regression coefficients, there was no correction of the ANS precipitation data to the glacier locale.

5.3 Solar radiation

5.3.1 Calculating $S_{in,TOA}$

$S_{in,TOA}$ was calculated as a daily mean using solar geometries acquired from the NOAA (2012), using the equation (taken from Sellers (1965)):

$$S_{in,TOA} = I_0(\frac{Rm}{R})^2 \, (cos\eta \, cos\delta \, cos\omega + sin\eta \, sin\delta) \tag{5.7}$$

where $I_0 = 1368$ Wm^{-2} (the solar constant taken from (Fröhlich, 1993)), Rm and R are the mean and instantaneous sun-earth distances, η is latitude, δ is the solar

Figure 5.13: ANS/AWS monthly precipitation totals point scatter. The equation of the line is equal to 5.6.

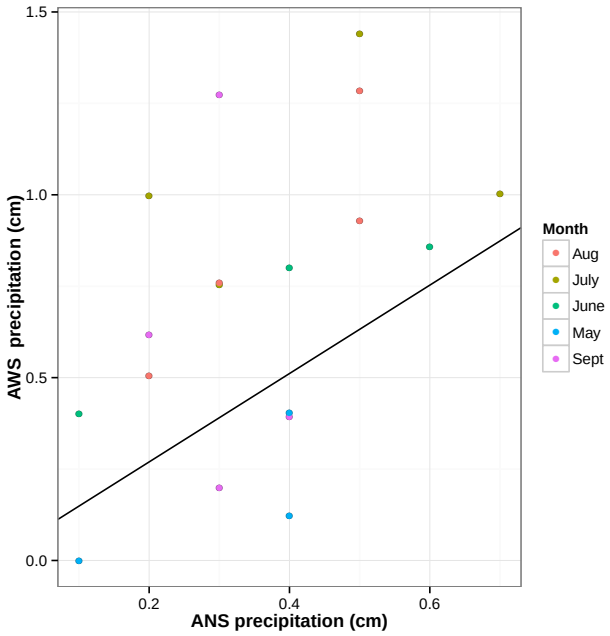

Table 5.5: Calculating mean daily $S_{in,TOA}$: comparing 6 hour intervals with 6 minute intervals

Date	6 hour interval mean Wm^{-2}	6 minute interval mean Wm^{-2}
15/1/10	3.22	0.65
15/2/10	53.56	43.41
15/3/10	114.46	137.99
15/4/10	286.58	281.82
15/5/10	427.90	419.14
15/6/10	503.17	503.31
15/7/10	466.84	466.18
15/8/10	353.03	341.62
15/9/10	174.94	194.73
15/10/10	76.48	75.74
15/11/10	17.72	8.93
15/12/10	0	0

declination and ω is the solar hour angle (Hock & Holmgren, 2005). Here we treat Rm as equal to R (1 A.U. (IAU, 2012)) which is a reasonable assumption as the variance between Rm and R never exceeds more than 3.5% (Sellers, 1965). To calculate mean daily $S_{in,TOA}$ using this method, $S_{in,TOA}$ was calculated for each day using time specific geometries at midnight, 6am, noon and 6pm - the average $S_{in,TOA}$ is then calculated in Wm^{-2}. When using $S_{in,TOA}$ to drive the model, negative values for $S_{in,TOA}$ (occurring during the Arctic winter) are set to 0 Wm^{-2}. Otherwise values were not adjusted. The use of midnight, 6am, noon and 6pm values was compared to calculating mean daily $S_{in,TOA}$ from geometries assessed every 6 minutes (providing greater coverage of changing geometrical relationships throughout the day) for the 15th of each month in 2010 (table 5.5).

Compared to the 6 minute interval method, the 6 hour method underestimates in March, June and September with a tendency to overestimate in the other months. The overall mean error from the above assessment is ± 0.365.As other approximations are made for processes including transmissivity, it was prudent to approximate $S_{in,TOA}$ in a relatively simple way. To calculate it at much smaller time steps would have resulted in unnecessarily high resolution.

Figure 5.14: Daily mean interval calculated $S_{in,TOA}$ (figure (i)) and daily mean $S_{in,TOA}$ integrated with expected $S_{in,TOA}$ at other northern latitudes figure (ii). Figure (ii) is adapted from Oerlemans (2010b)

.

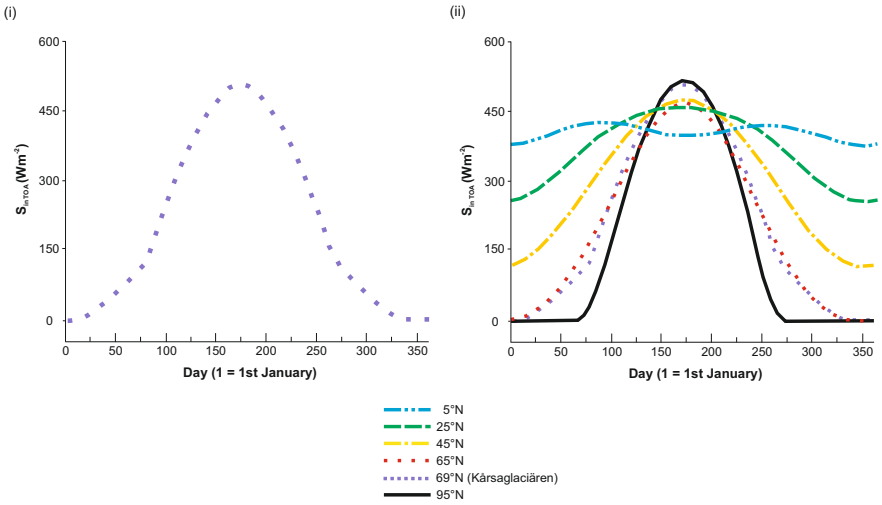

To compare this interval method of $S_{in,TOA}$ calculation, a comparison was made with expected daily mean values at a number of other northern latitudes taken from Oerlemans (2010a)(figure 5.14).

The interval calculations appear more stepped which owes to the calculation being derived from the times specified. This will lead to underestimations at certain times of the year (particularly when $S_{in,TOA}$ is low) - using a smaller time step would result in fewer 0 $S_{in,TOA}$ values being incorporated in the calculation of mean daily $S_{in,TOA}$. As this effect was most exaggerated when $S_{in,TOA}$ was small, it was not expected to significantly affect melt modelling assessments.

Mean values for the intervals over the 1926 - 2011 period are displayed in figure 5.15. During the summer months, values were greatest and especially so at noon as would be expected.

$S_{in,TOA}$ was greater than zero for most of the year at noon, except at the very

Figure 5.15: Average daily $S_{in,TOA}$ values for the 1926 - 2011 period at Kårsa at midnight, 6am, noon and 6pm

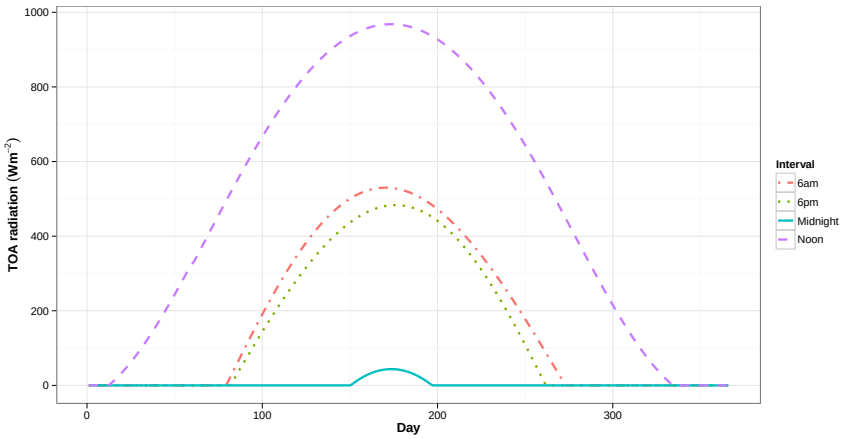

beginning and end of the year (day numbers 1-11 and 335-366). $S_{in,TOA}$ zero values occur for days 1-150 and 198-366 at midnight. The occurrence of values for day numbers 151-197 is indicative of longer Arctic daylight conditions during which high latitude regions experience the *midnight sun*. Zero $S_{in,TOA}$ values occur for day numbers 1-78 and 273-366 at 6am and for 1-82 and 263-366 at 6pm. $S_{in,TOA}$ values were greater than 0 at 6am 4 days earlier than at 6pm and remained so 10 days after values at 6pm return to 0.

5.3.2 Accounting for radiation at the surface: Atmospheric transmissivity (τ) estimation using a global/$S_{in,TOA}$ radiation ratio analysis

Atmospheric transmissivity (τ) is a vital component when calculating the amount of incoming shortwave radiation incident to a surface from exoatmospheric flux (top of atmosphere radiation ($S_{in,TOA}$)). Klok & Oerlemans (2002) calculated incoming radiation at the surface using:

$$I = S_{in,TOA} cos(z) T_R T_g T_w T_{as} T_{cl} \tag{5.8}$$

where I is surface shortwave radiation, T_R and T_g are transmission coefficients for Rayleigh scattering and gas absorption respectively, T_w is water-vapor absorption, $T_a s$ is the transmission coefficient for aerosol attenuation and $T_c l$ is a cloud factor (Klok & Oerlemans, 2002). The AWS installed at the terminus of Kårsa was used to collect global radiation for the period 1/7/2007 - 14/3/2011. Cloud observations were not carried out for Kårsa and so such a calculation as 5.8 could not be applied. Global radiation data were also available from ANS in nearby Abisko (˜25 km east). To estimate transmissivity, a method is employed that does not require cloud observations directly, as in Hock & Noetzli (1997), which requires the multiplication of $S_{in,TOA}$ by the ratio of measured global radiation over $S_{in,TOA}$.

To emulate the effect of transmissivity, the ratio of measured global radiation over $S_{in,TOA}$ is represented by τ (Hock & Noetzli, 1997; Hock & Holmgren, 2005):

$$\tau = \frac{I}{S_{in,TOA}} \tag{5.9}$$

To calculate τ, values for I were those measured at the AWS.

A mean value for τ was used throughout the model runs. Values for τ were originally calculated using $S_{in,TOA}$ and measured global radiation at the surface data from ANS and the AWS for the periods 1/7/1984 - 21/8/2011 and 1/7/2007 - 14/2/2011 respectively. As discussed in Hock & Holmgren (2005), estimates of τ are expected to decrease in accuracy as radiation amounts decrease. As suggested by (Hock & Holmgren, 1996), τ estimates calculated where zenith angles are greater than 85 (at 6am, noon and 6pm) and/or $S_{in,TOA}$ estimates are < 20 Wm^{-2} were ignored. Mean values of τ are calculated only from complete years. Where there were instances of τ estimation values > 1 (i.e. measured surface global radiation $> S_{in,TOA}$), these were treated as no data values so as not to affect mean values for τ. This is acceptable as such instances are caused by other radiation sources whereas here the concern is only with direct solar radiation.

Despite varying climatic conditions, estimates for τ for both ANS and the AWS were compared. As the two sites are relatively close to one another (approx. 25 km),

analysis of τ in both instances was completed to assess the best methods by which to calculate the value and also to provide information for its variability over time. Single mean values for τ were estimated at 0.44 and 0.44 from the ANS and AWS datasets respectively. The mean values reported here were calculated by averaging daily τ estimates. Separate τ values were calculated for ANS and AWS at 0.44 and 0.45 respectively whereby τ was estimated using the ratio of annual mean global radiation at the surface/annual mean $S_{in,TOA}$. The methodology leading to the calculation of a mean value of τ is important. By calculating a mean τ using daily values, all daily τ values will have the same weight in the end result. As τ estimate accuracy is expected to decrease with reduced radiation amounts, this could result in a more erroneous value. By using a mean τ calculated from using the ratio of mean annual measured global radiation/mean annual $S_{in,TOA}$, the larger radiation values will have more weight when calculating the mean, thus providing more robust τ estimations (Giesen, 2012 (pers. comm.)). Both sets of values correlate well with τ estimates approximated for other sites across the globe including Midtalsbreen (Norway), Storbreen (Norway) and Kongsvegen (Svalbard) where values of 0.54, 0.48 and 0.55 were approximated respectively (Giesen & Oerlemans, 2012).

The effectiveness of the estimated τ values were assessed by comparing mean annual measured global radiation at the surface values against estimated global radiation at the surface values. Estimated and measured global radiation values and estimation errors can be seen in table 5.6.

The daily average method for estimation of τ was most effective in both instances, with the least error being associated with global radiation at the surface estimates. The largest errors using both daily and annual means are associated with the AWS data. This was likely to be a function of the juxtaposition of the AWS near to valley side walls which will be a constant source of radiation which will interfere with the equipment. During the mid-winter months when $S_{in,TOA}$ was equal to zero, the AWS still records radiation values (although small). This is not the case with the ANS data which does not have this juxtaposition issue - zero values of measured global radiation also exist during the winter months when $S_{in,TOA}$ is

Table 5.6: Estimated surface global radiation vs. measured global radiation at ANS and AWS using mean daily and mean annual τ estimations. Estimate errors are considered only where $S_{in,TOA}$ is > measured global radiation at the surface, otherwise the resultant estimate it disregarded.

	Daily mean			
Site	Estimated Wm^{-2}	Measured Wm^{-2}	Diff. Wm^{-2}	Error %
ANS	97.16	97.18	0.02	0.02
AWS	114.30	111.21	-3.09	-2.78

	Annual mean			
Site	Estimated Wm^{-2}	Measured Wm^{-2}	Diff. Wm^{-2}	Error %
ANS	96.33	97.18	0.85	0.88
AWS	117.17	111.21	-5.96	-5.36

equal to zero as would be expected.

The ANS dataset goes back much further in time than the data available from the AWS and this is useful for estimating a value for τ that can be used with confidence when predicting radiation receipt at the surface prior to the records available. The mean τ values mentioned above are no more than $\pm$ 0.01 apart at most. Annual variability in τ is assessed for the 1985-2011 ANS data to quantify its stability overtime and thus deduce the validity of applying a single mean value over the time period that is modelled. The 1985-2010 τ estimates conformed to non-parametric correlation testing. Using a Spearmans R correlation test, values of p = 0.703 and $\rho = 0.08$ were calculated. A Kendall tau test was also run giving p = 0.631 and $Kendall\ \tau = 0.07$. Both of these tests are indicative of the presence of a weak and insignificant correlation between mean annual τ and time (years) (see figure 5.16).

As τ is extrapolated back to 1926 for the model runs, the low r^2 value and insignificance of the correlations provides no basis on which to make the assumption that the apparent trends observed extend back further than 1985. Therefore, due

Figure 5.16: Correlogram for annual mean τ estimations vs. time (year) for the AWS 1985 - 2010 dataset

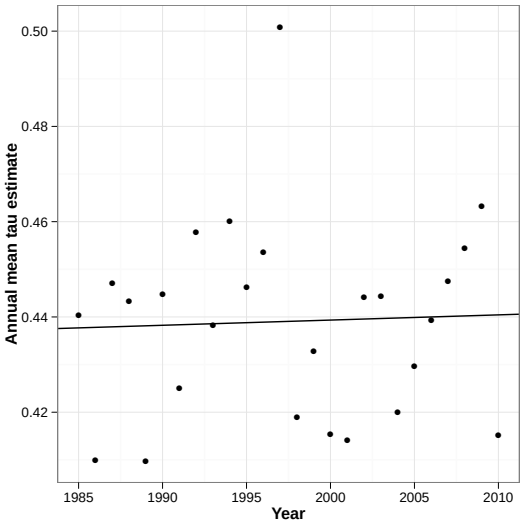

to the temporal limits of the data, a single mean value for τ will be used for all historical model runs.

To assess the variability in τ between the two sites, annual values were calculated and compared using both daily and annual mean ratios (table 5.7). This was carried out for the years 2008-2010 as these are the only complete years that overlap between the two sites.

Table 5.7: Comparison of annual values for τ at ANS and the AWS calculated using daily and annual mean ratios

	Daily means		Annual means	
Year	ANS	AWS	ANS	AWS
2008	0.46	0.46	0.45	0.46
2009	0.46	0.45	0.46	0.46
2010	0.43	0.43	0.42	0.42
Mean	0.45	0.45	0.44	0.45

Table 5.8: Estimation error of monthly global radiation at the surface (Wm^{-2}) where $\tau = 0.45$. Positive errors indicate overestimates whereas negative values indicate underestimates.

Month	Error (%)
Jan	114.1
Feb	77.9
Mar	9.7
Apr	-18.0
May	-13.7
Jun	-1.0
Jul	13.0
Aug	21.8
Sep	39.2
Oct	61.8
Nov	131.4
Dec	-

Using the global/$S_{in,TOA}$ ratio method, the daily average calculated values displayed a similar pattern in τ at both sites with little variation in mean values (a joint mean τ estimate of 0.45). Similar variability is observed when using the annual average method with similar mean estimates. Annual methods of averaging are likely to be more reliable as they are more weighted to large $S_{in,TOA}$ amounts Hock & Holmgren (2005). ANS is subject to different meteorological conditions to Kårsa due to its proximity to Lake Torneträsk. Despite these climatic differences, there is little noticeable difference in τ between the two sites.

As a result of this analysis, the annual mean value of 0.45 as calculated using the AWS dataset was used for τ which is fixed for all model runs (in accordance with the aforementioned ANS tau vs. time correlation analysis). Error as a function of month using the AWS dataset was analysed to assess the months in which τ estimates were most effective (see table 5.8).
The largest underestimates (%) occur for the months October - February when radiation values are smallest. The results displayed in table 5.8 account only for when $S_{in,TOA}$ is greater than measured global radiation at the surface. As

reported earlier, use of the 0.45 values of τ results in a mean error of ca. -5% (underestimate). If accounting for instances where $S_{in,TOA}$ < measured global radiation at the surface, this increases the error to ca. 8%. The occurrence of such incidents is indicative that the radiation received by the sensors at that time was not from direct incoming solar radiation. Global radiation at the surface is best estimated at the AWS during June which follows with better predictions for τ being made using the global/$S_{in,TOA}$ ratio method when radiation values are greatest.

A τ value of 0.45 is used in all model runs.

5.4 Model algorithms and considerations

5.4.1 Calculating radiation incident at the surface (I)

I is defined here as:

$$I = H \text{ x } [cos\theta_0\, cos\beta + sin\theta_0\, sin\beta\, cos(\phi_0 - A)]\, S_{in,TOA} \text{ x } exp(-T_0/cos\theta_0) \quad (5.10)$$

where H is hillshade (mean % topographic shading for a given time period), τ is the atmospheric transmissivity, θ_0 is the solar zenith angle, ϕ is the solar azimuth, A is the slope aspect and β is the slope angle. All of these factors are calculated dynamically, changing over time thus enabling quantification of both solar seasonality ($S_{in,TOA}$ θ_0 ϕ) and glacier surface adjustments(A and β) (modified from Burrough & McDonnell (1998)). I is calculated with all angles in radians.

Equation 5.10 operates well however its validity was compromised when the sun was positioned low on the horizon. Where θ_0 approaches $\pi/2$, the cosine of θ_0 becomes asymptotic with 0. In the term $exp(-T_0/cos\theta_0)$, with θ_0 as the denominator, a value asymptotic to infinity is calculated. Consequently, the use of equation 5.10 is truncated for θ_0 angles > 84°. θ_0 values greater than this result in values with errors of an order of magnitude greater than 1 to occur. For instances affected by this truncation, I is automatically set to 0. Given the potential order

of magnitude errors associated with this range of the function, setting I to 0 introduces a trivial error, and is unlikely to be problematic in mountainous regions, such as with the location of Kårsa. In flatter areas where the sky view of a given position is not so limited by surrounding topography, I would be set to the value of that calculated for 84°.

5.4.2 Albedo (α)

α refers to the reflectivity of a surface over the shortwave spectrum (0.35-2.8m) (Jonsell *et al.*, 2003; Hock, 2005). The effect of snow albedo on incoming radiation has been quite well studied, however little has been done with regard to ice albedo (Cutler & Munro, 1996; Jonsell *et al.*, 2003) which is often treated as a spatial and temporal constant (Hock, 2005).

Physical characteristics that may affect a surface include: grain size; water and impurity content; surface roughness; ice crystal orientation and structure; surface radiative properties (Hock, 2005). It is possible for these different characteristics to interact with each other. For example, where water content is high, its presence increases between individual ice increases grain size, reducing the potential albedo of a surface (Hock, 2005). As grain size decreases, single scattering (as opposed to multiple scattering) increases which results in an increase in surface albedo (Carroll & Fitch, 1981). Increasing grain size leads to decreases in snow albedo due to changes to the air-ice interface pathway within a snow mass (Warren, 1982). A photon can only be scattered when it is between ice crystals (travelling along the air-ice pathway) once within an ice crystal, absorption as opposed to scattering takes place. The increase in grain size reduces the air-ice pathway, reducing scattering and increasing absorption (Warren, 1982).

Rock debris, sediments and atmospheric particles contribute to the modification of glacier albedo (Warren & Wiscombe, 1980; Warren, 1982; Hock, 2005). Studies comparing dirty, clean, smooth and hummocky ice revealed significant spatial variations as a function of impurity content which proved more effective than surface roughness (Cutler & Munro, 1996). The effect of impurities has more

affect on the visible than the near-infrared spectrum if one considers hemispherical reflectivity (Cutler & Munro, 1996). Small amounts of atmospheric particles have been found to affect reflectivity significantly. 10 ppmw of desert dust or 0.1 ppmw of carbon soot were found to reduce albedo by a few percent (Warren & Wiscombe, 1980), the effect of which is greater for coarse-grained than fine-grained snow (Warren, 1982).

Where debris has been present over ice, ablation has been affected accordingly. There appears to be two types of effect that can be induced by a debris layer depending on its thickness. This is named its *critical thickness*. This has been studied in particular for glaciers in the Himalaya (see for example Nakawo & Takahashi, 1982; Nakawo & Young, 1982; Nakawo & Rana, 1999), for which different threshold values have been identified for different glaciers ranging from 1-2 cm (Nakawo & Rana, 1999) to approximately 5 cm (Nakawo & Young, 1982).

Many parameterizations have been devised to deal with snow and ice albedo to different levels of complexity (e.g. Escher-Vetter, 1980; Tangborn, 1984; Oerlemans & Hoogendoorn, 1989; Oerlemans & Knapp, 1998; Arnold *et al.*, 1996). These are discussed in more detail in Brock *et al.* (2000b). To deal with morphological changes to the snow pack over time, the methods devised in Brock *et al.* (2000b) have resulted in good agreement with albedo observations in the field (Brock *et al.*, 2000b).

In some studies, remote sensing techniques have been used to identify changing glacier albedo (e.g. Giesen & Oerlemans, 2010) however images of an appropriate resolution are not readily available for Kårsa.

Due to limited observations with regard to snow events, to use a parameterization that accounts for such factors is not appropriate. Consequently, standard fixed values are used for albedo to estimate attenuation of I. The values used are taken from Paterson (1994) and can be seen in table D.1. A value of 0.70 is chosen for snow to account for both fresh snow and developing firn. 0.70 falls between α approximations made for firn to dry snow in Paterson (1994). A value of 0.39, a

mid-value between 0.26 and 0.51 as approximated for slightly dirty ice to clean ice in Paterson (1994), is used for ice as the surface of Kårsa is relatively clean, as observed both in the field and from summer photographs. These are approximations as quantitative measurements have not been possible as part of this study (the sensitivity of the overall model to these assumptions is discussed in chapter 8).

Further to the aforementioned effect of debris on surface albedo, the thickness of the overlying snow surface over ice has also been considered with regard to adopting the reflective properties of the underlying surface (Ohata *et al.*, 1980; Kayastha, 1994). Ohata *et al.* (1980) found that where snow was of a thickness $\leq$ 0.25 mm, the snow surface α was affected by the underlying surface. Giesen & Oerlemans (2010) affected the albedo of snow once snow reached a small thickness, according to a depth scale value (d_* equal to 0.001 m w.e.), whereby the α instance was then treated as a mix of α_{snow} and α_{ice}. This method was also employed in the melt model of Leclercq *et al.* (2011). In the model of Giesen & Oerlemans (2010), snow albedo was also altered as a function of temperature whereby snow α_snow was equal to 0.90 when temperatures were $\leq$268.5 K and α_snow was equal to 0.69 for temperatures >274.6 K. This increased level of α complexity was coupled with a time dependent α function for snow regarding the number of days since the last snow fall.

This value has been used as a threshold whereby when snow surface thickness at a given point falls below this value, the albedo that is then used to modify the calculation of Q is taken to be that of the surface beneath - the ice. Equally, when the snow thickness is greater than this threshold value, an albedo value specific for the snow surface is adopted.

5.4.3 Bulk flux (ψ)

To account for other fluxes that are not explicitly calculated here including turbulent flux and the effect of long wave radiation, a bulk parameterization was used, estimated using ψ (see equation 5.13). This bulk method parameterisation

was based on observations carried out at 11 glaciers (Giesen & Oerlemans, 2012), situated in environments governed by differing climatic regimes. ψ depends upon:

$$\psi = \begin{cases} \psi_{min} + cT_a \text{ for } T_a \geq T_{tip}; \\ \psi_{min} \qquad\quad \text{for } T_a < T_{tip}. \end{cases} \tag{5.11}$$

whereby, under a threshold temp (T_{tip}), ψ maintains a constant value (ψ_{min}) and where air temperature (T_a) is $\geq$ to the threshold temperature, the value of ψ increases in a linear fashion according to c multiplied by T_a. The values of factors c, ψ_{min} and T_{tip} are provided in Giesen & Oerlemans (2012). The factor values vary according to the different climatic settings.

5.4.4 Lapse rate functions

Air temperature is an important variable to consider as it drives many processes affecting energy fluxes which drive the energy balance (Petersen & Pellicciotti, 2011). Its importance is such that simpler models have been wholly reliant upon temperature as an input, such as temperature index and degree day models (e.g. Braithwaite & Zhang, 2000; Raper & Braithwaite, 2006). Knowledge of the temperature distribution across an area of interest is limited by the number of measurement points available. Consequently, to approximate temperatures at unknown locations as a function of elevation, a lapse rate (LR) must be used.

A temperature LR can be defined as a change in temperature as a function of height, where the change is positive if temperature increases, or negative if temperature decreases, as a function of elevation (Glickman, 2000; Minder *et al.*, 2010). The LR that is usually employed is equal to the *standard moist adiabatic lapse rate (MALR)* or *standard environmental lapse rate* which is to a value of -0.0065°K (Ballantyne, 2002; Michlmayr *et al.*, 2008; Gardner *et al.*, 2009). A range of other LRs have been used by a number of authors, applied both as constant LRs (CLR) and variable LRs (VLR), varying both spatially and temporally. CLR examples include those of MacDougall & Flowers (2010), based on Kluane and Kaskawusch Glacier, Canada where LRs of -0.006 and -0.0053 ($\bar{x}$) were calculated respectively. A CLR was also used in the generic alpine mass balance model developed by

Oerlemans (1993). An example of a VLR application is that by Hock & Holmgren (2005), from Storglaciären, Sweden, where a LR of -0.0055 ($\bar{x}$) was calculated.

Surface temperature is variable as a function of multiple factors including: surface albedo, roughness and aspect; wind patterns; relative humidity; cloud cover and the presence of a melting surface (Petersen & Pellicciotti, 2011). As a consequence of the number of contributing factors affecting surface temperature, it is little surprise that modelling applications prove to be highly sensitive to the LRs that are employed (e.g. Hodgkins *et al.*, 2012). Thus whenever possible, for small scale studies it is prudent to consider small scale spatial and temporal variations with regard to the calculation of LRs, and to then consider the most appropriate method of employment of the LR within the model in question.

Within the model, a CLR is used as there is no knowledge of spatially variability of temperature across Kårsa due to limitations in the monitoring equipment installed and available. A number of different LRs are experimented with and these are discussed in section 8.4.6 of chapter 8.

5.4.5 Precipitation

Contemporary algorithm A seasonal component was calculated for the input data as a function of air temperature. Where there are five consecutive days of temperatures below 0°C according to measurements recorded at the AWS, it was assumed that the climate governing the area around the glacier had entered a winter phase. Equally, following five consecutive days of temperatures greater than 0°C, it was assumed that the summer season had begun. This relatively simplistic approach was a consequence of the data available. When the air temperature is above freezing, a tipping bucket rainfall gauge is operational at the AWS, for which read outs are acquired at the programmed time step. However, once temperatures shift to below freezing, the gauge becomes inoperable. Thus, in circumstances where precipitation at the AWS was frozen, such events will have been missed. By splitting the precipitation seasons between summer and winter, it was possible to simulate precipitation using rainfall data in the summer and using knowledge

of the end of season winter snow pack depth to simulate precipitation during the winter.

When the season on a given day is equal to summer, temperatures are calculated using a lapse rate function across the glacier surface as a function of elevation. Where air temperature is greater than a given snowfall threshold factor (T_{Thresh}), it is assumed that wet precipitation measured at the AWS will fall to an equal amount at the cell in question. This precipitation is not stored within the model, being assumed to run off the glacier surface. Where the air temperature is less than or equal to T_{Thresh}, it is assumed that precipitation at the cell in question falls as snow. The amount of snow that falls on the cell is calculated by dividing the wet precipitation amount measured at the AWS by the density of summer snow (see table D.1). This calculation uses the density in kg m^{-3} divided by 100 (e.g. where fresh snow density is 200 kg m^{-3} and temperature at a cell is below the snow threshold, snowfall is equal to the wet precipitation amount divided by 0.2). This snow is then accumulated within a summer snow layer. Any future summer snowfall events occurring within the model will add to the overall summer snow depth at the cell in question. The presence of summer snow has multiple effects which propagate throughout the model, resulting in changes in albedo and density, which affect the solar radiation and melting algorithms.

During the winter season, there is no precipitation data available from the AWS. In this instance, a pre-calculated end of winter season snow depth layer is required (discussed in section 4.2.7 of chapter 4). At the beginning of the winter season, the summer snow thickness is set to 0.0 m at each cell as it is assumed that any summer snow still present at the end of the summer season adds to the total snow measured in the field at the end of the winter. At the start of the main model loop (see figure 5.18, considering the input meteorological data (which specifies day, month, year and "season"), the number of winter days occurring within a winter season are counted. These are counted according to the month and the year so that the number of winter days within a specific winter season are totaled (e.g. winter 2007/2008). For example, assuming that the model was to be run from 1/6/07 until 1/6/08, to calculate the number of winter days occurring in the

2007/2008 winter season, winter days are counted where they occur in September, October, November or December of 2007 and in January, February, March, April and May of 2008. With the winter day total calculated, the amount of snow that falls on each day within the winter season is equal to the end of winter season snow depth at a given cell / by the number of winter days within the winter season. This accumulates throughout the winter season until the total amount of winter snow at a given cell is equal to that in the uploaded, pre-calculated end of winter season snow depth surface for the winter season in question. The amount of snow that accumulates at a specific cell position cannot exceed the value dictated by the pre-calculated surface. This forms the winter snow thickness surface which affects albedo and density, within the solar radiation and melting algorithms.

From field observations and snow pit analysis (see section 4.2.3 of chapter 4), it was apparent that wind as a mode of snow redistribution and mass loss is an active process. The average snow density from winter snowpack analysis for the 2008 - 2011 season revealed a value of 407.13 kg m^{-3} which is a typical density associated with wind slab (Paterson, 1994). The model does not directly account for wind. To cater for this, a wind factor is introduced to modify the winter snow melt (see table D.1).

Historical algorithm As with the summer precipitation algorithm, seasonal values were calculated for the input data as a function of air temperature. Where monthly mean temperature < 0°C, the season was set to winter. Conversely, where temperature > 0°C, the season was set to summer.

During the summer months, precipitation was calculated as for the summer precipitation algorithm. However, unlike for the contemporary model, the historical model used monthly mean precipitation totals from the ANS field station. This is discussed in detail in section 5.2.2. Using the same lapse rate method as in the contemporary model, but using a monthly mean temperature, where a cell temperature $\leq T_{Thresh}$, precipitation falls as snow. Where cell temperature $> T_{Thresh}$, precipitation falls as rain and was assumed to run off the glacier surface.

Table 5.9: Mean winter snowpack density (kg m^{-3}) from snow pit analysis. The density headers refer to different snow pits assessed in the same field season.

Year	Pit 1	Pit 2	Pit 3	Pit 4	$\bar{x}$
2008	328.02	354.32	373.41	-	351.92
2009	349.63	361.86	-	-	355.75
2010	514.40	508.80	520.40	-	514.53
2011	366.33	413.33	408.33	437.33	406.33
Overall	-	-	-	-	407.13

For the winter season, ANS snow thickness values for the end of the winter season were scaled up to the glacier location. This is discussed in detail in section 5.2.2. Winter snow was distributed across the glacier surface as a function of elevation using equation 5.5 which was adjusted according to the mean snow value of the given model run (see section 5.2.2). Considering the year and month of the model time step, the number of winter months occurring in the given winter season are calculated. The total winter accumulation at a given cell was then calculated using equation 5.5, considering the elevation of the cell in question. This was then recalculated as a monthly accumulation value by dividing the total winter accumulation at the given cell by the total number of winter months occurring within the given winter season. The total amount of accumulation in a winter season cannot exceed the expected snow thickness at a given cell according to 5.5 considering the season specific total snow accumulation value. The wind factor as described above is also considered here.

5.4.6 Snow and ice density

Ice density is fixed at 900 kg m^{-3} and the use of this is further discussed in chapter 4. Summer snow density was set at 200 kg m^{-3} which falls between typical densities expected for damp new snow and settled snow, which range from 100 - 300 kg m^{-3} as taken from Paterson (1994). The winter snow density is fixed at 407.13 kg m^{-3} which is the average winter snowpack density as calculated from snow pit analysis data collated through the 2008 - 2011 winter field seasons as discussed in section 4.2.3 of chapter 4, the results of which analysis can be seen below in table 5.9.

5.4.7 Calculating ice melt

The energy available (Q in $Wm^{-}2$) at the surface of the glacier was calculated simply as:

$$Q = (1 - \alpha)\tau S_{in,TOA} + \psi \tag{5.12}$$

where the first term refers to net short-wave radiation and the latter refers to and the latter to all other fluxes as a function of air temperature (Leclercq *et al.*, 2011; Giesen & Oerlemans, 2012). In this equation, α is albedo, τ is atmospheric transmissivity and $S_{in,TOA}$ is incoming radiation at the top of the atmosphere.

Equation 5.12 was modified here to capture daily/monthly changes in solar relationships and surface geometry:

$$Q = (1 - \alpha)I + \psi \tag{5.13}$$

The value used for α depends on the medium (snow or ice) over which Q is being calculated (for more details see section 5.4.2). When Q is > 0, this positive energy is used to facilitate surface melt. The model that is used in this study works across a grid where cells have fixed dimensions of 5 m x 5 m, providing a total grid of 25 m^2 cells. When Q is calculated within the model as in equation 5.13, this provides the energy for a second for a m^2. This value is scaled up to give the total amount of energy in one second (*Joules* (J)) for the 25 m^2 cell (Q x 25) which here is called "Available energy". This is scaled up according to the time-step of the model by multiplying it by the number of seconds within the time-step.

The amount of energy required to completely melt (here called *Total energy*) a cell of snow or ice, was initially calculated whereby the cell type (snow/ice) and volume was considered, as well as the respective associated density (see table D.1). The mass was then calculated and then multiplied by the latent heat of fusion (L_f - see table D.1). Ergo, *Total energy* is in J. In terms of order of melting, this was dictated by the model architecture. The model is layered whereby a snow layer, which accumulates according to the precipitation

algorithm (see section 5.4.5), is above the glacier thickness layer (uploaded by the user - see table D.2). Mass loss first affects the snow layer at a position [i, j], only affecting the glacier thickness layer at position [i, j] when the snow layer is 0.

How much melt actually occurred at a given snow/ice cell was calculated in terms of thickness is given by:

$$\frac{Available\ energy}{Total\ energy} \text{ x } Cell\ Thickness \tag{5.14}$$

and in terms of volume:

$$\frac{Available\ energy}{Total\ energy} \text{ x } Cell\ Volume \tag{5.15}$$

5.5 Slope and aspect routines

Slope was calculated according to the slope line which is defined here as "[a] line of locally greatest rate of change of altitude, along which a frictionless ball starting from rest would roll" (pp. 316 Jones, 1998). Aspect is defined here as "[t] he horizontal direction of movement down a slope line. The compass direction (measured in degrees from a reference) in which the plane tangent to the surface at a point faces, measured outward from the surface at right angles to the contours" (pg. 315 of Jones, 1998). The algorithms defined below were calculated for each cell of the input glacier surface at the beginning of each model run. Consequently, where a given cell loses elevation through melting, slope and aspect values were updated.

The slope algorithm implemented within the model was a third order finite distance estimator taken from Horn (1981). Assuming a 9 square grid with the cell of interest located at the centre, uses all eight surrounding cells. The algorithm enabled assessment of variation in slope along the north-south and west-east gradients, the estimated slope value being a product of these difference

calculations (Burrough & McDonnell, 1998). Slope (in degrees) was calculated using the following:

$$slope = ATAN(\sqrt{[dz/dx]^2 + [dz/dy]^2}) * 180/\pi \tag{5.16}$$

where $[dz/dx]$ and $[dz/dy]$ are the rates of change of the gradients along the north-south and east-west planes respectively (Horn, 1981; Burrough & McDonnell, 1998; ESRI, 2011b). Assuming the cell for which slope was calculated takes position $[i, j]$:

$$[dz/dx] = [(z_{i-1,j+1} + 2z_{i,j+1} + z_{i+1,j+1})] \tag{5.17}$$

$$- (z_{i-1,j-1} + 2z_{i,j-1} + z_{i+1,j-1})/8\delta x \tag{5.18}$$

and:

$$[dz/dy] = [(z_{i+1,j-1} + 2z_{i+1,j} + z_{i+1,j+1})] \tag{5.19}$$

$$- (z_{i-1,j-1} + 2z_{i-1,j} + z_{i-1,j+1})/8\delta x \tag{5.20}$$

This algorithm is the same as that used in ArcGIS and is an example of one of many slope algorithms that have been developed (e.g. Sharpnack & Akin, 1969; Fleming & Hoffer, 1979; Zevenbergen & Thorne, 1987). A selection of these algorithms were ranked in Jones (1998) in which the Horn (1981) method described above was found to perform well in both slope and aspect calculations. Aspect was calculated here using:

$$aspect = 57.29578 * ATAN2([dz/dy], -[dz/dx]) \tag{5.21}$$

This used the same surrounding cells as the Horn (1981) method and is equal to that used in ArcGIS (ESRI, 2011a).

5.5.1 "Ice melts.... *and so does rock*" and other possible scenarios

The total amount of mass loss was limited by the total mass that is available i.e. that which exists at a given point in time in the snow or glacier thickness layers active within the model. Where these layers already have a value of 0, no melt occurs. Where *Available energy* > *Total energy*, it was possible that the ratio methods (equations 5.14 and 5.15) would result in mass loss greater than possible. To prevent these impossible mass loss occurrences, in such instances where *Available energy* > *Total energy*, the cell thickness was reduced to 0 m and then held at 0 m. When calculating surface change, the ratio of *Available energy* to *Total energy* could not be used alone - only together with knowledge of the thickness of ice that is available.

Where a snow cell at a given position was reduced to 0 during a single time step, without exhausting the *Available energy*, the remaining energy was then used to calculate the amount of melt experienced by the same cell position of the ice thickness layer, which was then updated. If there was still energy once both the snow and ice thickness layers had been zeroed, no more melt could occur and the energy surplus was ignored.

5.6 Historical and contemporary model structures and descriptions

The historical model was based on data with a monthly time step, but considers radiation data on a daily interval. The contemporary model differed to the historical model as it was based on all data having a daily time step. The specific data inputs used for the historical and contemporary models are described in the aforementioned sections. Flow diagrams of the historical and contemporary models are displayed in figures 5.17 and 5.18 respectively.

Figure 5.17: Historical model flow diagram (monthly time step)

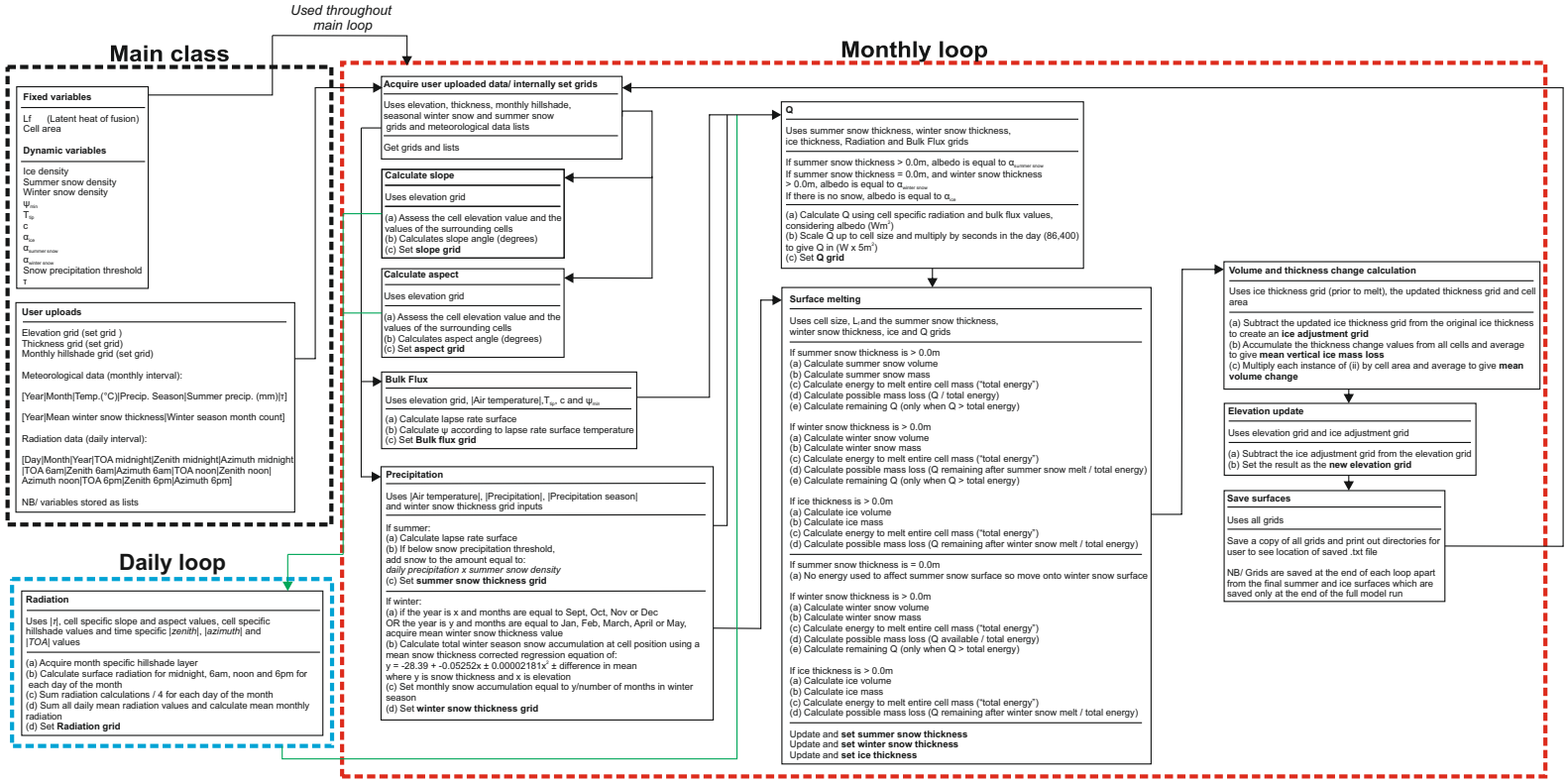

Figure 5.18: Contemporary model flow diagram (daily time step)

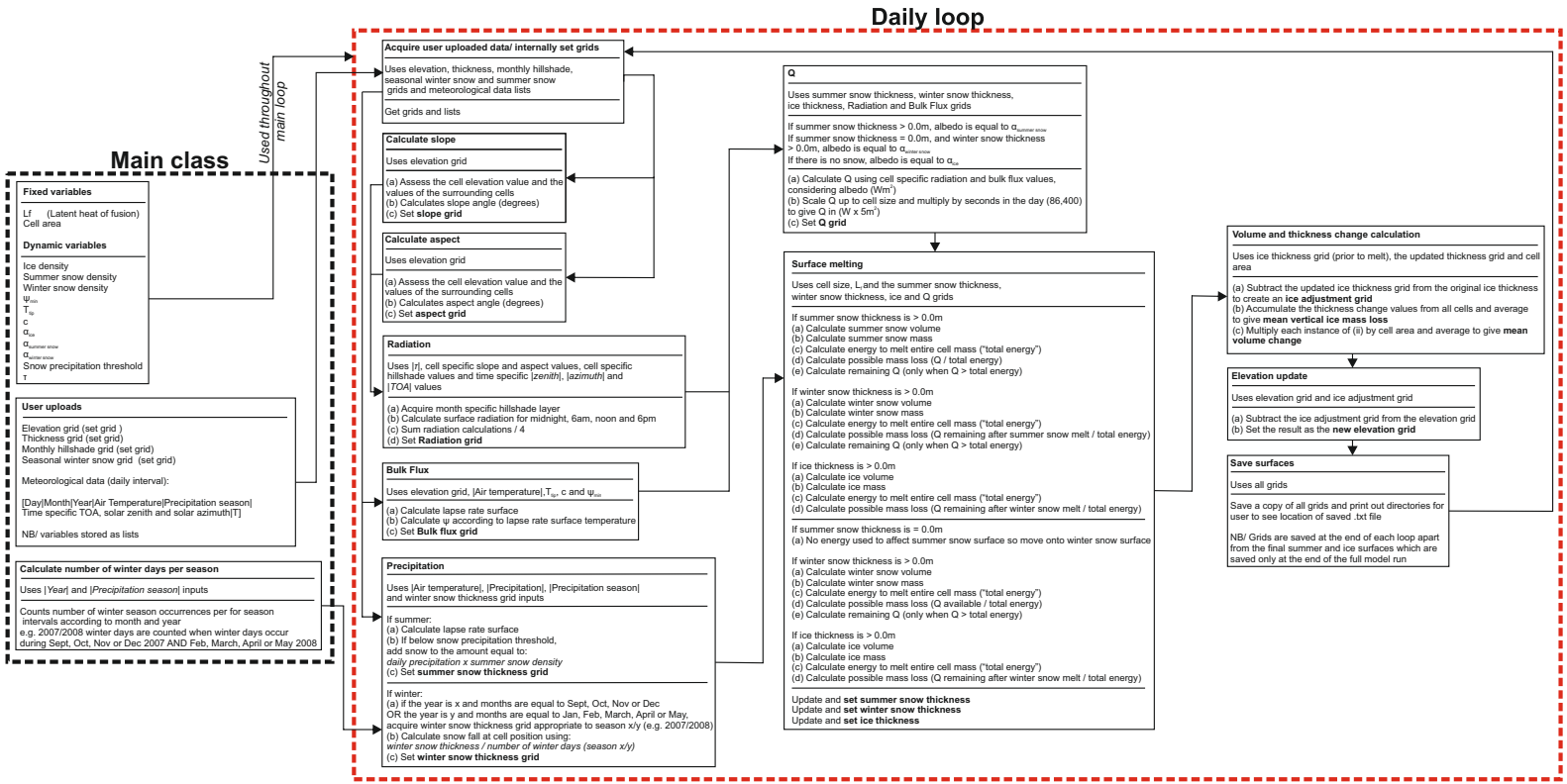

5.7 Programming considerations: floating point precision

All of the aforementioned algorithms are coded in Java (the source code can be downloaded from `https://github.com/Chris35Wills/SEB_model_java_files`). Different programmes deal with the rounding of numbers using different protocols. Differences in calculations involving decimal values can be computed to give one value in one programme and a slightly different value in another. These rounding issues essentially concern floating point precision. Two programmes that have been used in this study include Microsoft Excel and ArcGIS which contain maths functions of their own. The energy balance model has been developed in Java. The aforementioned programmes and the Java language all deal with decimalisation slightly differently. Repeating the same calculation in each programme can result in slightly different results. To test this, ASCII grids of I and ψ were calculated within the energy balance model. Using equation 5.13 and as described in section 5.4.7, a grid of Q was calculated. This was then compared to a grid of Q calculated in ArcGIS, using exported grids directly from the model of I and ψ. The difference of the two separately calculated Q grids was then explored. It was found that there were small differences across the surface in the number of Watts available. The approximate maximum error calculated from these differences was $\pm 1.867 \times 10^{-4}$ %. In this instance the error was found to be extremely small (much less than 1 order of magnitude) but different none the less.

5.8 Transferable and user-friendly SEB model development

The aforementioned algorithms and input data treatment allow for careful analysis of complex distributed glacier surface geometrical effects on the SEB, in turn affecting MB. This is enhanced by the ability to alter the level of geometry update within the model. For the aim of understanding geometry effects on MB, such numerical analysis suffices and this is often the case with scientific modelling applications to complex problems. However, the ability for another user to come

and simply *use a model* is hindered by the requirement to integrate all of the appropriate algorithms within a frame work, which requires a level of programming skill and large investment of time. On many occasions, models are outlined in terms of their construction (e.g. Giesen & Oerlemans, 2010), however are rarely made openly available. This is unlike some of the open source ice sheet models including GLIMMER which invites users to work and integrate on versions of the model directly (Rutt *et al.*, 2009). There are some examples of mass balance models that have been made available to allow researchers and students to manipulate data and test changes in melt and mass balance, including that of Brock & Arnold (2000). The Brock & Arnold (2000) model allows for SEB modelling at the point scale through the manipulation of a Microsoft Excel spreadsheet. However, this is still limited in terms of graphical user interface (GUI) of its own, relying on the installation of Microsoft Excel on a user's computer. Distributed modelling is outside of the remit of the model exemplified. The *Alpine 3D* model described by Lehning *et al.* (2006) and as used by Michlmayr *et al.* (2008), despite its advancements and considerations of distributed SEB modelling does not provide visualisation in an easy, complete and simple package. Furthermore, it has extremely large data requirements.

The model designed in this study, using all of the aforementioned algorithms, allows simple distributed SEB modelling in the form of a stand alone programme, offering the user the ability to visualize model inputs and resultant processed and modelled surfaces in the forms of standard planar maps. Use of the model on a user's computer requires only the installation of the freely available Java Runtime Environment (Version 7). All data inputs are easily uploaded using a windows style navigation pane, requiring data input in ASCII/ESRI GRID file format (for surfaces) and CSV files (for meteorological inputs). On data upload, surfaces are visible within the main programme viewing pane. When one of the processing tools is selected and run, statements are constantly updated informing the user of job progress. Upon the completion of processing, a number of calculations can be carried out through the GUI directly including calculations of mean change in thickness, elevation change and area change. It is also possible to export all surfaces - such as glacier ice surface and thickness layers - as an ASCII file. This

functionality enables further statistical analysis which can be preformed through a wide range of open source GIS packages (including QGIS and GRASS) as well as the open source R statistical package. ASCII file import is also possible where a user has access to an ArcGIS license. A series of images of the model's GUI can be found in appendix E.

Chapter 6

Results: Historical reconstruction of Kårsa

This chapter addresses changes that have occurred to Kårsa over the 1926 - 2010 period, as identified from a reconstruction of the glacier facilitated using a variety of topographic maps covering the glacier available for 1926, 1943, 1959, 1978, 1991 as well as a high resolution field study carried out in the winter of 2011 from which a map of the glacier for the summer of 2010 was derived. All maps available prior to that created for 2010 were derived from aerial photographs taken during the summer months of the years stated (July or August). This is discussed in detail in chapter 4. This 84 year reconstruction allows for an assessment of the changing geometry of the glacier through time and is thus fundamental in its contribution to the overall thesis aim of understanding the effect that changing surface geometry has had on the glacier over the past century, discussed further in chapter 10. The key changes in length, elevation, area, volume and thickness are summarised in figure 6.1. This chapter meets the objective of

- Accounting for sensitivity of applied geostatistical techniques on reconstructed surface properties

therefore addressing the project aim of:

- Providing a full 3D glacier geometry reconstruction and assessment of a small mountain glacier, since the beginning of the 20th century, over decadal time scales

Figure 6.1: Geometry change summary. Short dashes, a solid line and long dashes represent maximum, mean and minimum expected values respectively. Calculation of these parameters is considered in chapter 4. Further description of these parameter changes are discussed in sections 6.2 - 6.6.

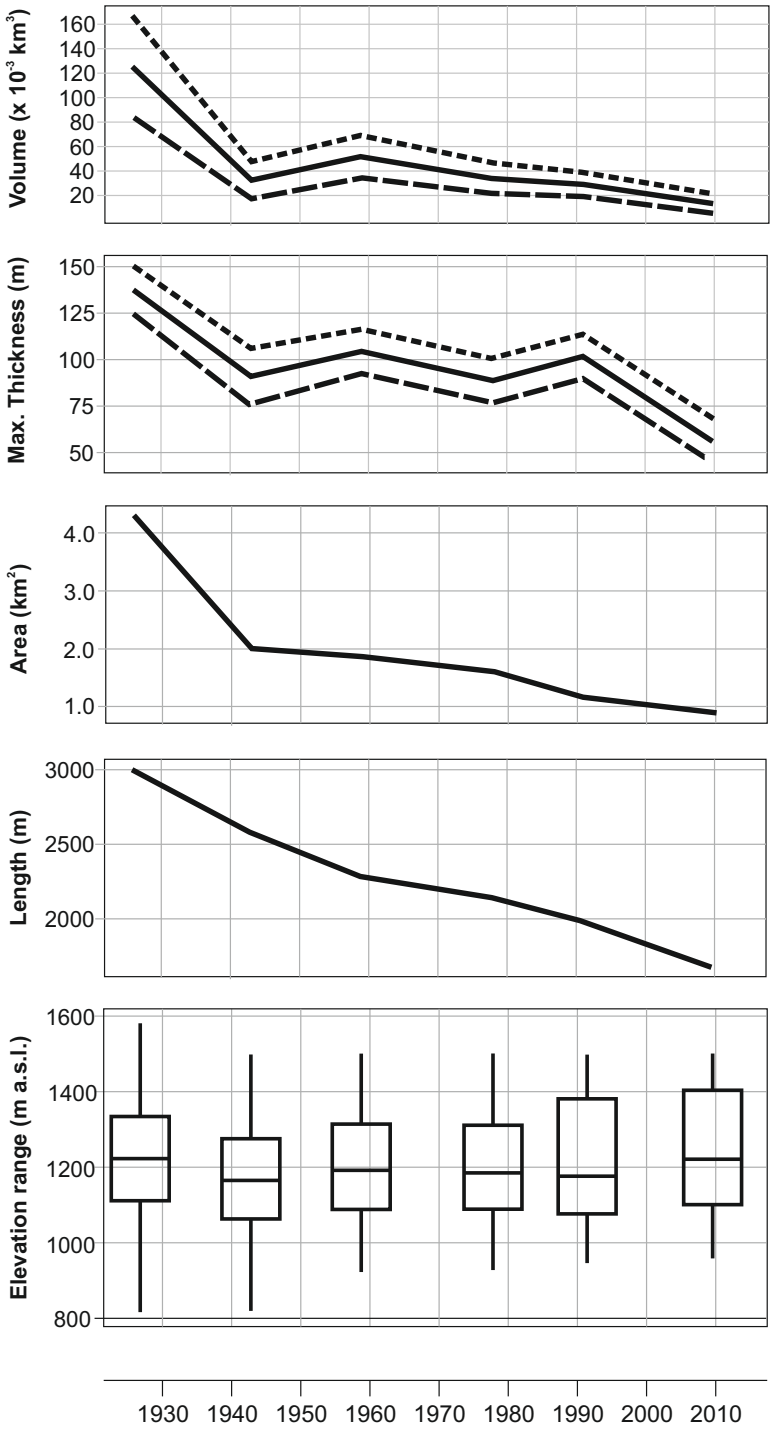

Table 6.1: Absolute mean surface interpolation perimeter errors (vertical plane). The 2010 perimeter shows 0.0 m error as the perimeter elevations are taken directly from the area DEM to which all other perimeter elevations are compared.

Year	Absolute $\bar{x}$ error m
1926	±25.0
1943	±18.6
1959	±15.8
1978	±16.4
1991	±19.6
2010	0.0

6.1 Surface reconstruction sensitivity analysis

To properly assess the results of surface change analysis, the methods and sensitivity of reconstructed surfaces is summarised here. The process of reconstructing any dynamic landform over a long period using data from a variety of different sources, each using different methods, is prone to numerous sources of error. Difficulties in the quantification of error in the horizontal plane and a discussion of the method of acquiring values for errors in the vertical plane are discussed in sections 4.2.2 and 4.3.5 of chapter 4 respectively. Absolute mean vertical errors associated with the perimeter points of the different reconstructions, calculated where the elevation of a perimeter point from a given reconstruction base map is compared with the elevation at the same point from the Lantmäteriet BD6 contemporary 1: 100 000 scale DEM of the Abisko-Kebnekaise-Narvik mountain region, are displayed in table 6.1.

The historical glacier surface reconstructions have been developed using a number of digitized points, derived for each year by digitising contour lines present on georeferenced topographic maps, the digitised lines then being converted to point clouds, containing xyz data (see section 4.2.1 of chapter 4). The maps and digitized contours for most of the reconstructed years only provide information for the glacier itself, with little information of the surrounding topography. As the glacier surface is dynamic, the glacier itself cannot be used to quantify vertical plane agreement between maps of different years. By assuming that where contour lines end at the perimeter of the glacier the elevation matches non-glacial elevation,

this offers the only real measure of agreement between maps according to the aforementioned 1: 100 000 area DEM. The values in table 6.1 only act as a rough indicator of vertical error as the only real comparison achieved by calculating errors in this way is between higher resolution historic base maps (approx. 1: 5000) and a lower resolution area DEM (1: 100 000). Separate to this error analysis, to assess the sensitivity of the interpolated surfaces for the different years as a function of incorrect data points, should they be present on the maps or be introduced through the data compilation stage, results of a Monte Carlo simulation are presented. The specific methodology for this simulation is discussed in section 4.2.8. Standard deviation maps of the glacier for the 1926 - 2010 intervals are displayed in figure 6.2. High standard deviations are indicative of areas of high sensitivity to rogue data points.

The standard deviation patterns (figure 6.2) vary significantly and this appears to link to the variability in the contour data and points available for each reconstruction. The 1926 surface shows areas of greatest sensitivity (between 20 - 30 m) surrounding points along the contour lines. Points that are closer to areas of unknown values have the most weight in affecting the interpolation value - points further away have less of an impact on the final calculation. This is why for 1926, areas further away from known points have smaller standard deviation values. These areas are predicted from a set of points (which fall within a specified search window) that are more equally weighted. Consequently, an erroneous value in one point will be less influential as it will be evened out by the other known values. The variance in standard deviation is relatively uniform across the surface. The northern centre portion of the glacier displays areas of least sensitivity. These areas occur specifically where the overall contour pattern alters from a convex to concave pattern. As a consequence of this pattern change, the distance between the contour lines available is increased (increasing the mean distance of points being used to predict values between the contour lines). This convex/concave pattern transition is discussed in section 4.3.8 of chapter 4.

A similar pattern to 1926 is observed again in 1943 and 1959. There is a noticeable reduction in sensitivity in the 1943 surface which relates to the number of digitized

Figure 6.2: Historical surface (1926-1991) standard deviations following Monte Carlo analysis

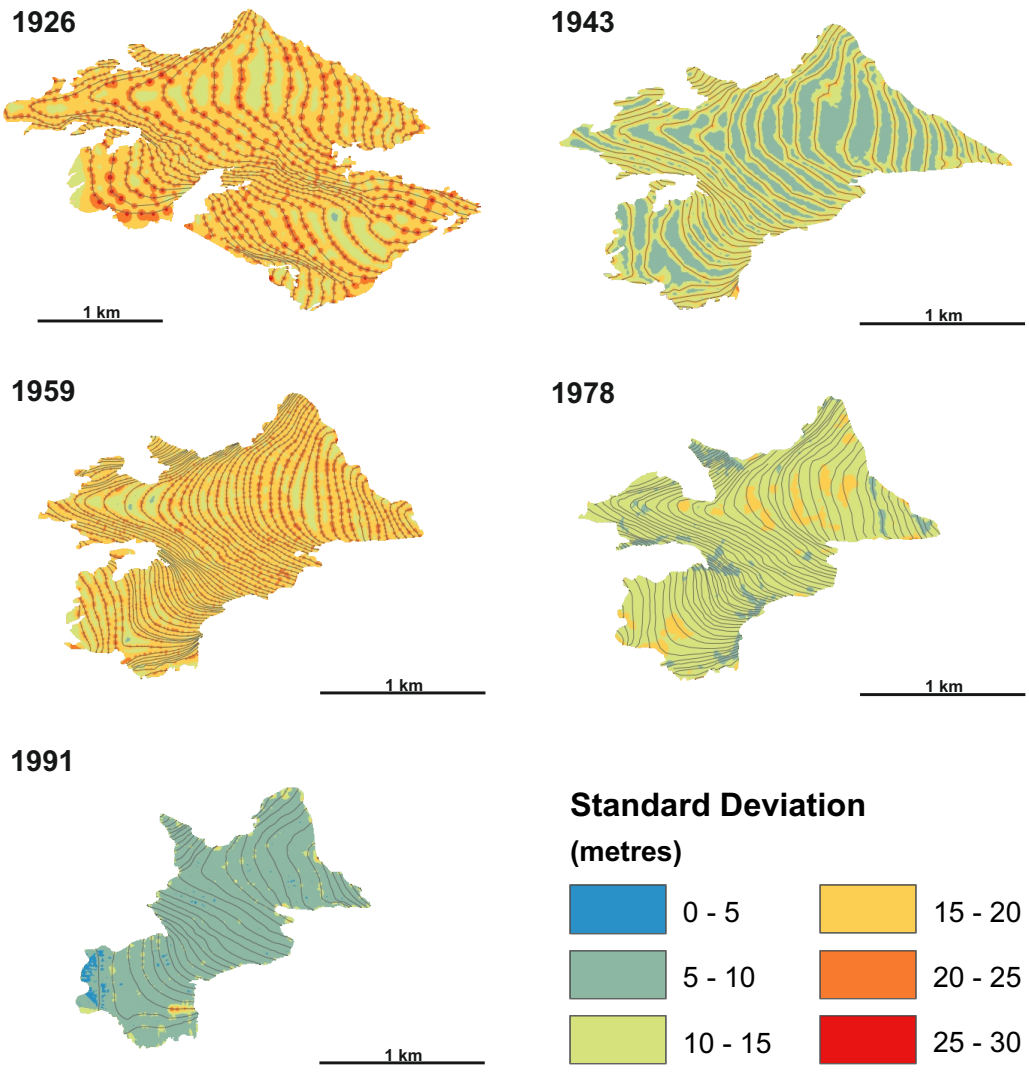

Table 6.2: Point file populations and contour spacings used for 1926 - 1991 surface interpolations (Point numbers are referred to as within the perimeter as these are the points most likely to affect the glacier interior as a function of the search window value employed)

Year	Contour spacing (m)	Total Points	Points within glacier perimeter
1926	25	1504	1050
1943	20	7693	3078
1959	10	3442	2367
1978	10	1691	1239
1991	20	39089	16631

points available along each contour line (3078 points fall within the glacier perimeter compared to 1050 in 1926 - see table 6.2). 1959 shows an increase in sensitivity along the contour lines for the same reasons as in 1926. Compared to 1943, the 1959 surface also has fewer points within the glacier perimeter. Both 1943 and 1959 display similar reductions in sensitivity most clearly where contour lines alter from convex to concave - where mean available contour spacing is greatest.

The 1978 and 1991 surfaces appear to have quite different standard deviation spatial distributions compared to those observed for 1926-1959. Compared to 1926 and 1943, the 1978 surface has a smaller contour spacing (see table 6.2). This however does not explain the shift in spatial variance as the 1959 surface is also constructed from 10 m contours. Upon closer inspection, the 1978 contour lines are considerably more convex and closer together than those that are present for 1926-1959. Consequently, the points constructed from these contour lines have a much less linear appearance. This will then affect the kriging search window as more points that are closer to an area of unknown value will be available. This further reduces the effect of an erroneous point on unknown point prediction. The same occurs for the 1991 surface although this can also be attributed to a much greater point availability (16631 points compared to 1239 in 1978 - this is a function of the method of line to point extraction employed within ArcGIS).

The 1978-1991 standard deviation distribution forms a paradox with the 1926-1959 surfaces. Whereas the latter surfaces show reduced sensitivity with increased distance from points (due to reduced weight of any single point on a prediction), the 1978 and 1991 surfaces show the inverse of this. The 1978 surface shows this more than the 1991 surface, with areas along the centre of the glacier with standard deviations between 15 – 20 m between contour line positions. This compares to standard deviations between 5 – 15 m occurring for the surfaces 1926-1959. For 1978, these areas of increased uncertainty are possibly linked to large spacings between contours - this will have a lessened effect on reducing known point errors than if the known point values were closer together and more similar.

6.2 Area change and terminus retreat

Glacier areas are derived from glacier extents digitized from available topographic maps and aerial photography as discussed in chapter 4. The change in area is illustrated in figure 6.3, which also shows the position of the Kårsa side glacier for completeness.

Area change is illustrated in figure 6.1 with values displayed in table 6.3. There has been a total area change of 3.41 km^2 over the 84 year study period, with the largest changes being attributed to the 1926-1943 period which is associated with the disintegration of the glacier in to two distinct parts - the main glacier and the side glacier. The area of the side glacier is only accounted for in the assessment of the 1926 glacier, when all parts were joined.

Associated with the change in area is the retreat of the glacier terminus. The terminus is identified as the area to the north east of the main glacier body. A number of methods have been trialled to assess the retreat of the terminus relative to the known terminus position of 1909 (see section 4.3.1). Only terminus position is known for this year with no full area map being available. Figure 6.4 shows the change in terminus position for years 1909 - 2008.

Figure 6.3: The area of Kårsa reconstructed for the years 1926 - 2008. Outlines are digitized from available topographic maps and aerial photography. The side glacier is also displayed for completeness.

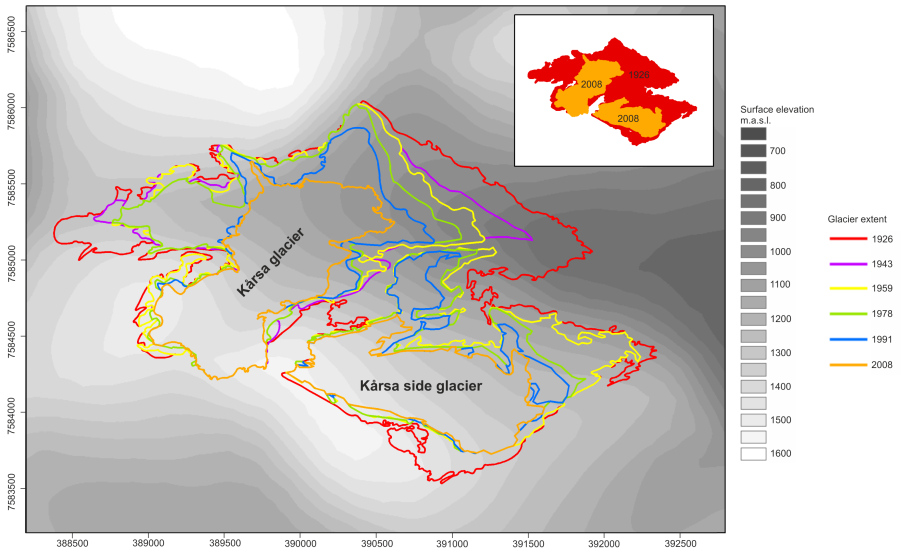

Table 6.3: Surface area change 1926 - 2010

Year	Area (km^2)	Mean change per year since last measured area (km^2 yr^{-1})	Total change since last measured area (km^2)
1926	4.30	-	-
1943	2.00	0.135	2.30
1959	1.86	0.008	0.14
1978	1.60	0.014	0.26
1991	1.16	0.034	0.44
2008	0.89	0.016	0.27

Figure 6.4: The changing terminus position of Kårsa. The 1909 terminus is highlighted within the inset box where it is also displayed as a string of points.

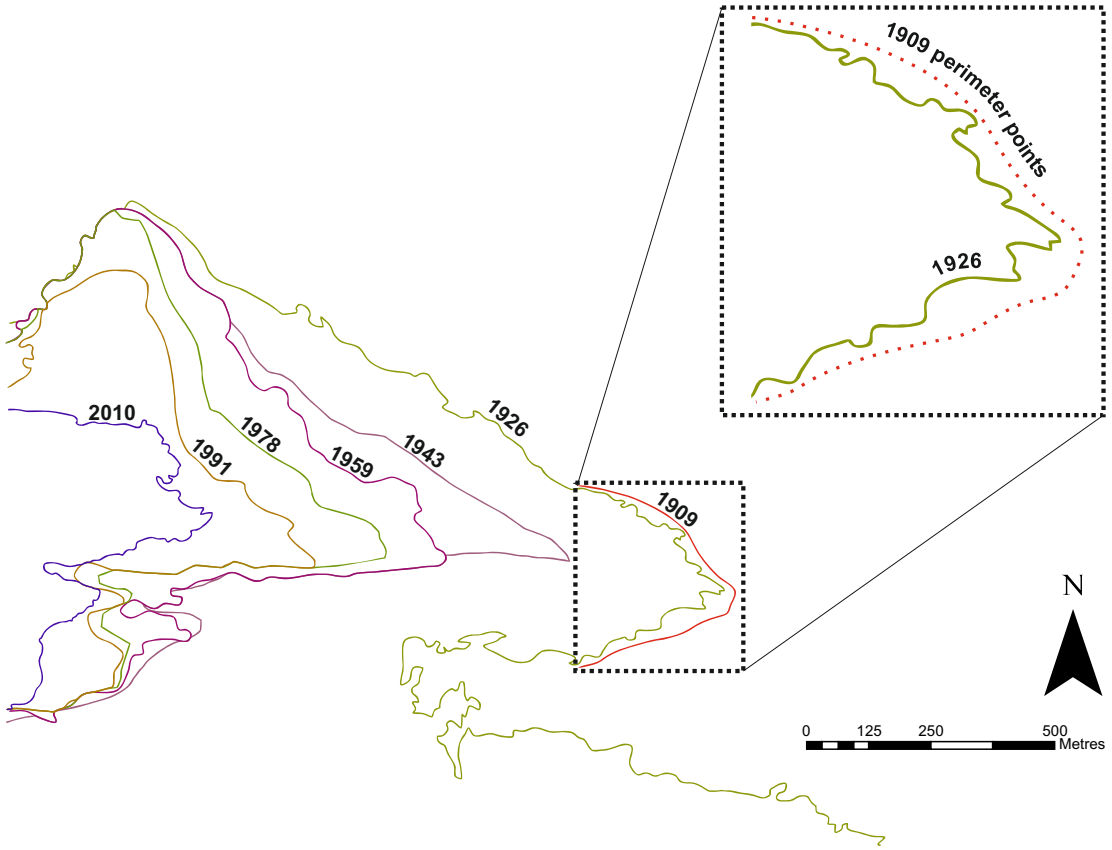

Table 6.4: Glacier terminus retreat for the 1909 - 2008 period using a *terminus to line* method. Cumulative retreat rates, as well as total retreat between mapping intervals and annual retreat rates between mapping intervals are displayed. Inter-annual variation of terminus retreat rates is not available due to the temporal resolution of the data.

Year	Cumulative retreat (m)	Retreat since last measured position (m)	Annual terminus retreat since last mapped position (m)
1909	0.0	-	-
1926	34.0	34.0	2.0
1943	433.0	399.0	23.5
1959	717.0	284.0	17.8
1978	874.0	157.0	8.3
1991	1048.0	174.0	13.4
2008	1292.0	244.0	14.4

A number of methods were identified for calculating terminus retreat, including both point specific and spatially distributed approaches. The methods applied are detailed in section 4.3.1 of chapter 4 and the results of the different methods are displayed in table 6.4. Retreat rate is reported here using the *terminus to line* method. This method is used as it is the only method of those considered, that does not have associated point sharing issues or problems linking to area definition. The *terminus to line* method removes such limitations, allowing for true euclidean retreat distances, not possible due to geometric interplay and difficulties with the other methods. The terminus is defined as the perimeter of the glacier falling within a 300 m buffer of the most eastern point of the glacier. The most eastern point is chosen in line with definitions of flowline locations as in Giesen & Oerlemans (2010), where the flowline extends from the flow start point to the lowest point in the ice. The easter point is constantly the lowest point of ice for Kårsa.

The most significant retreat is accounted for between 1926-1943, with the least retreat from 1909-1926. From 1926-1943, annual retreat rates decrease to a second minimum in 1959-1978 of 8.3 m yr^{-1}, following which annual retreat rates increase again.

6.3 Elevation change

Glacier elevation maps are summarised in figure 6.5 and hypsometry charts are displayed in figure 6.6. Elevation range change is illustrated in figure 6.1. There are some very large changes with regard to the elevation bands represented by the glacier. The 800-900 m band is represented at the terminus in 1926 and 1943 but is no longer present by 1959 when the lowest band represented is the 900-1000 m.

With the loss of the side glacier between 1926 and 1943 and the loss of the western lobe of the glacier between 1978 and 1991, the proportion of the glacier represented by the different elevation bands changes dramatically. Hypsometric changes, displayed in charts 6.6 help to better describe the changes that have taken place.

For the 1926 surface, 47% of the total glacier area is within the 1100-1300 m elevation band, peaking in the 1250-1300 m band. This is clearly discernible in the 1926 chart (6.6). A secondary smaller peak can be identified for the 1400-1450 m band. Compared to the more subtle area peaks that can be identified from the 1926 surface, hypsometry charts for the other years show much clearer peaks in area. These vary in altitude over time. In 1943, the majority of the surface area (60%) is in the 1100-1250 m band with a secondary area bulge at 1400-1450 m (10%). The 1943 pattern is closely replicated in 1959 where 60% of the surface is at 1100-1250 m. However, the 1959 surface shows a secondary bulge stretching over both the 1400-1450 and 1450-1500 elevation bands, indicative of a proportional increase in glacier area at higher altitudes between the 1943/1959 map intervals. The major area bulge in 1978 is between 1000-1250 m (61%) - this peak begins at an elevation 100 m less than in 1943 and 1959. The same proportional area is present at 1400-1450 m as in 1943. The 1991 surface shows peaks between 1000-1200 m (50%) and 1400-1450 m (13%). The reduction in the lower bulge elevation range may be attributed to the loss of the western lobe of the glacier which in 1978 represented a large portion of area within the 1200-1300 m band. By 2010, the double area bulge pattern is still clear as for all previous years, especially from 1943 onwards, with 25% of the surface area within the 1050-1150 m band and 20% in the 1400-1450 m

Figure 6.5: Historical glacier elevation maps (Summer 1926 - 2010). The 1926 map is shown at a different scale to the 1943- 2010 maps, which maintain the same scale as shown in the legend to the bottom right of the figure. The 1943 - 2010 maps also hold the same spatial position so that changes in area through time can be distinguished. Errors per year according to glacier perimeter/area DEM agreement are as 1926: ±25.0 m, 1943: ±18.6 m, 1959: ±15.8 m, 1978: ±16.4 m, 1991: ±19.6 m and 2010: ±0.0 m

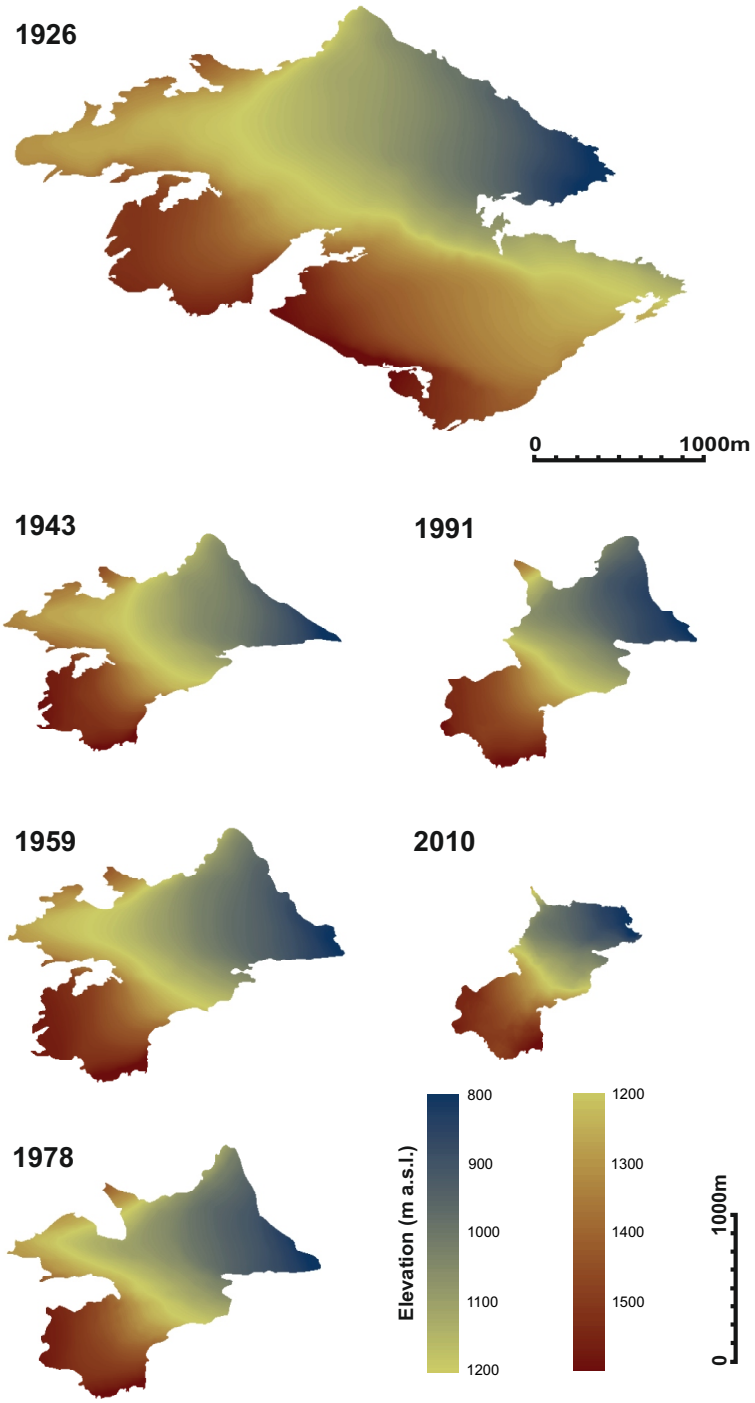

Figure 6.6: Historical glacier hypsometry charts (Summer 1926 - 2010)

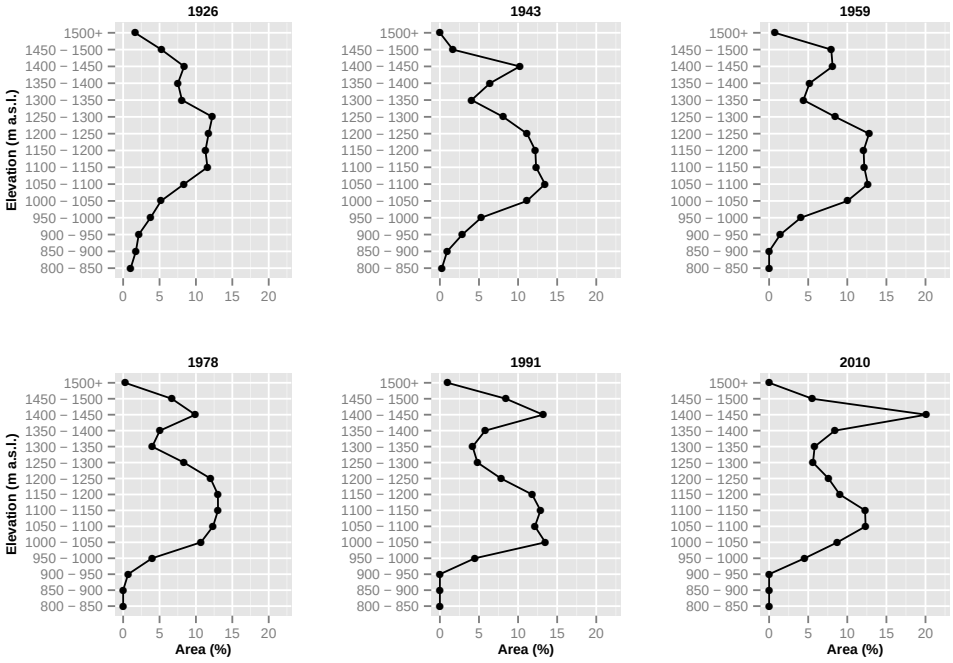

band. The proportion of the 2010 surface within the 1400-1450 m band is greater than for any other year. As with other years, increases in certain categories do not necessarily imply growth, being equally a function of reduction in elevation area at lower altitudes. For all years, there is a trough around the 1300-1350 m band. For all years, this elevation band is present within a topographic constriction which relative to the glacier today, divides the upper and lower catchments almost in half.

To compare hypsometry of the glacier for different years as succinctly as possible, curves for all years are displayed against cumulative area (%), displayed in figure 6.7. To enable a numeric comparison, ER values over the period of interest here are 0.53, 0.53, 0.50, 0.49, 0.48 and 0.51 for 1926, 1943, 1959, 1978, 1991 and 2010 respectively. There is a clear reduction from 1926 to 1991 in ER values increasing again in 2010. Similar to the ER values, HI is calculated giving values of -0.89, -0.95, -1.17, -1.27, -1.53 and -1.06 are calculated for Kårsa. Considering the Jiskoot *et al.* (2009) characterisation of glaciers when using HI (discussed in section 4), the values derived here for Kårsa from 1926 to 1959 place it within the

Figure 6.7: Glacier hypsometry curves against cumulative area (%) 1926 - 2010

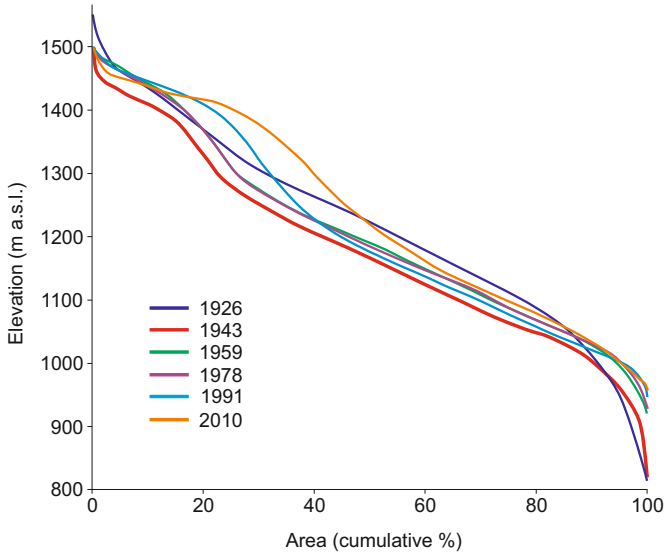

equidimensional category. The glacier in 1978-1991 is categorised as being top heavy and then in 2010 it is once again within the equidimensional category. These changes are closely linked to the disintegration process of the glacier including loss of the side glacier and the western lobe. The HI values are displayed over time in figure 6.8.

6.4 Glacier profile change

Glacier elevation change is illustrated in both long profile and cross profiles in figures 6.9 and 6.10. The long profile follows the centerline which satisfies all years (i.e. running from the southern accumulation area to the terminus in the east). The change in length linked with the long profile change is illustrated in figure 6.1. Figure 6.9 clearly displays the retreat of the glacier terminus and an incremental lowering of the glacier surface, especially when considering the profile from a distance >900 m from transect point "A" at an approximate altitude of 1200 m a.s.l. Changes in the mid and upper sections are not clearly discernible for most years although the 2010 surface is clearly the lowest relative to all other mapped surface elevations. The long profile clearly shows the retreat of the glacier terminus to higher elevations, as discussed in detail in section 6.2. There are some

Figure 6.8: Hypsometry Index (HI) values over time 1926 - 2010

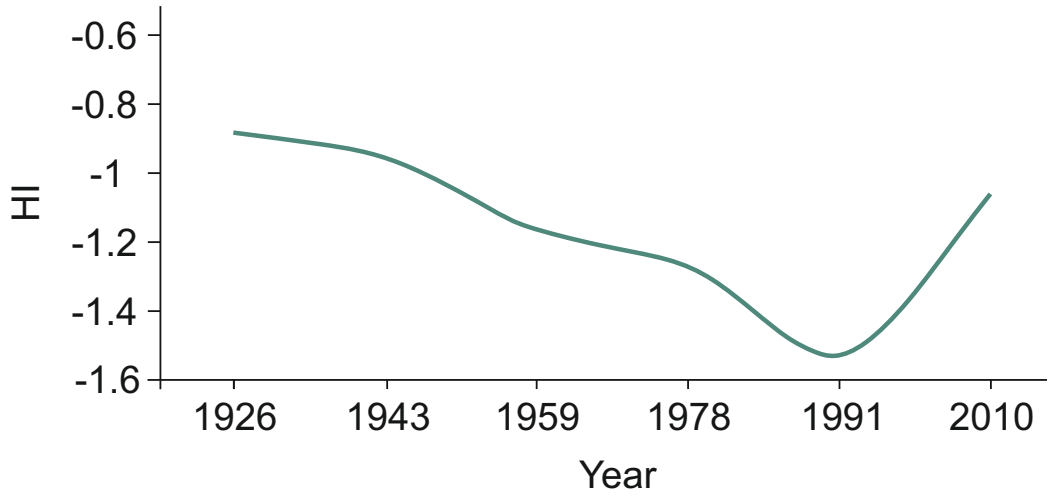

changes in glacier slope apparent in figure 6.9 but these are better illustrated and described in section 6.7.

Figure 6.9: Long profile of the glacier for the years 1926 (±25.0 m), 1943 (±18.6 m), 1959 (±15.8 m), 1978 (±16.4 m), 1991 (±19.6 m) and 2010 (±0.0 m). The profile is constructed along the mean centerline position, discussed in the above text, between points 'A' and 'B' as illustrated on the inset map.

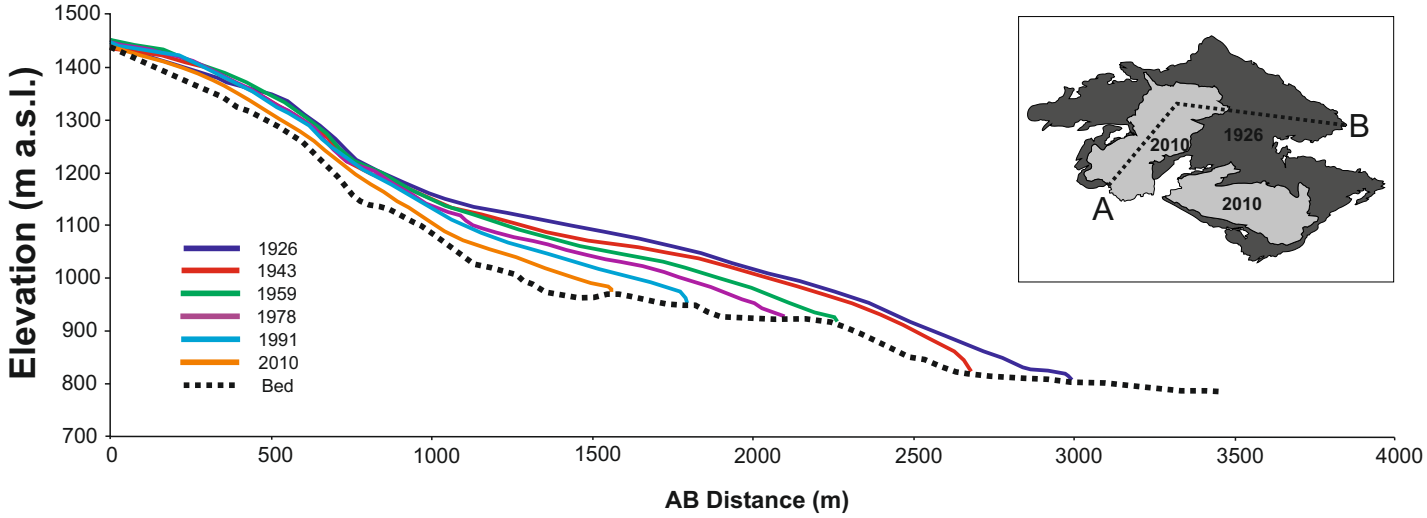

The cross profiles displayed in figure 6.10 account for all years from 1926-2010. To be able to consider an 84 year comparative transect, the transects illustrated are those constructed across an area of the glacier present for all years. The transects are constructed within the boundaries of the contemporary glacier. A general trend of lowering is observed in the lower, middle and upper transects displayed in figure 6.10 with each year tending to be lower on average than the year mapped previously. The only year that does not fit this trend in any of these regions is the 1943 surface.

The lower section transect shows a smooth glacier surface in 1926 which becomes increasingly concave towards 2010, with the most concavity in 2010 being approximately 350 m from (L)A where the ice begins to thin when considering the rise in elevation of the bed profile. The 1943 profile falls below the 1959 surface as well as below the 1978 and 1991 surfaces for distances >270 m from (L)A. This may be indicative of either an increase in glacier mass or a result of glacier dynamic change between 1943 and 1959, resulting in more mass being present in this area. Considering vertical errors (see section 6.1), this may also be an error associated with the mapped data (discussed in section 4). The 1943 was a particularly difficult map to integrate into the overall GIS database (see chapter 4) and is associated with the largest vertical error, having a mean vertical error of -7.55 m.

The middle glacier transect shows a pattern similar to the lower glacier with each profiles being lower than that mapped for the year previously. The 1926 surface is relatively convex compared to later surfaces becoming increasingly convex. This increase in convexity is particularly apparent for the 1978 surface, approximately 180-190 m from transect point (M)A at an altitude of 1300 m a.s.l. and for the 2010 surface 150 m from (M)A at an altitude of 1280 m a.s.l. The 1943 surface is lower than all surfaces apart from the 2010 surface, possibly for reasons as discussed above.

The upper glacier surface does not show as clear a pattern as for the other transects. The 1959 surface has the greatest mean altitude, with the 1943 surface having the lowest mean altitude. The 1926 surface remains below the mean elevations of 1959, 1978, 1991 as well as large portions of 2010. The pattern of increasing

Figure 6.10: Cross profiles of the lower, mid and upper sections of the glacier 1926 (±25.0 m), 1943 (±18.6 m), 1959 (±15.8 m), 1978 (±16.4 m), 1991 (±19.6 m) and 2010 (±0.0 m). The profiles are constructed for sections of the lower, mid and upper contemporary glacier and also consider the glacier surface at the same points for 1926 - 1991 to allow for comparisons to be drawn as discussed in the text. Transect positions are between 'A' and 'B' for the lower (L), mid (M) and upper (U) areas as illustrated on the inset map.

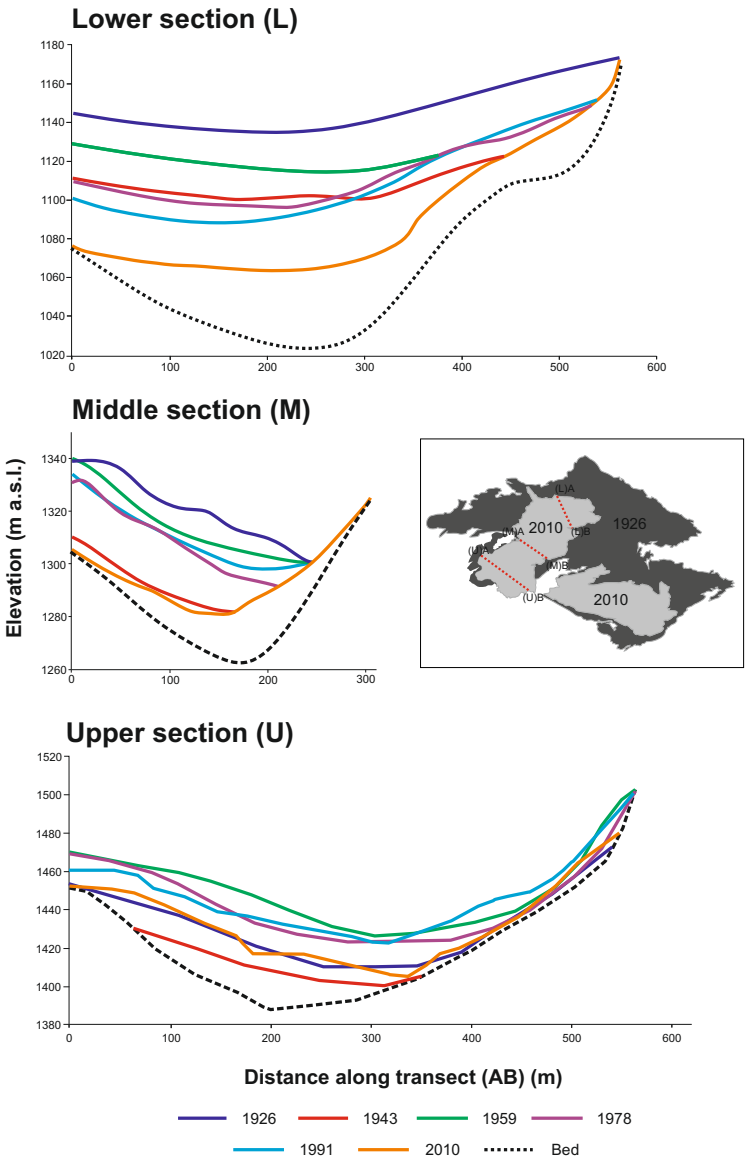

concavity is not apparent for the upper transect.

Change in the geometry of Kårsa is clearly displayed in figures 6.9 and 6.10. These changes in geometry are expected to affect the components of the SEB and therefore the MB. This is assessed further through SEB experiments, the results of which are presented in chapter 9.

6.5 Map interval elevation change

Elevation change has been calculated for each interval between the complete glacier surfaces that are available for Kårsa. Resultant difference maps can be seen in figure 6.12. Proportions of melt according to total melt categories can be seen in figure 6.11.

The difference surface between 1943 and 1926 shows a general pattern of elevation reduction (see figures 6.12 and 6.13), implicit of a negative mass state. The mean elevation lowering total is -29 m. There is some elevation increase (mean value of +0.39 m yr^{-1}) at the extreme west of the glacier, at the edges of the upper and lower accumulation zones (most clear on figures 6.12 and 6.13). This should be treated with caution however as most uncertainty in the vertical plane is associated with the glacier boundary. Between 1926 and 1943, there was the detachment of the Kårsa side glacier (Ahlmann & Tryselius, 1929). Its associated elevation loss is not accounted for here where elevation change is relative only to the most recent surface (in this case, 1943).

Glacier elevation increased between 1943 and 1959, with a mean positive elevation change of 19.90 m. These increases occur across 97% of the glacier surface and are most concentrated in the upper accumulation area. There is also calculated surface lowering which occurs around the glacier terminus to the east. The mean calculated lowering is -0.12 m and accounts for only 3% of the 1959 glacier surface area.

Figure 6.11: Proportional elevation change categories for periods between 1926-2010. These categories are displayed spatially in figures 6.12 and 6.13 with associated errors.

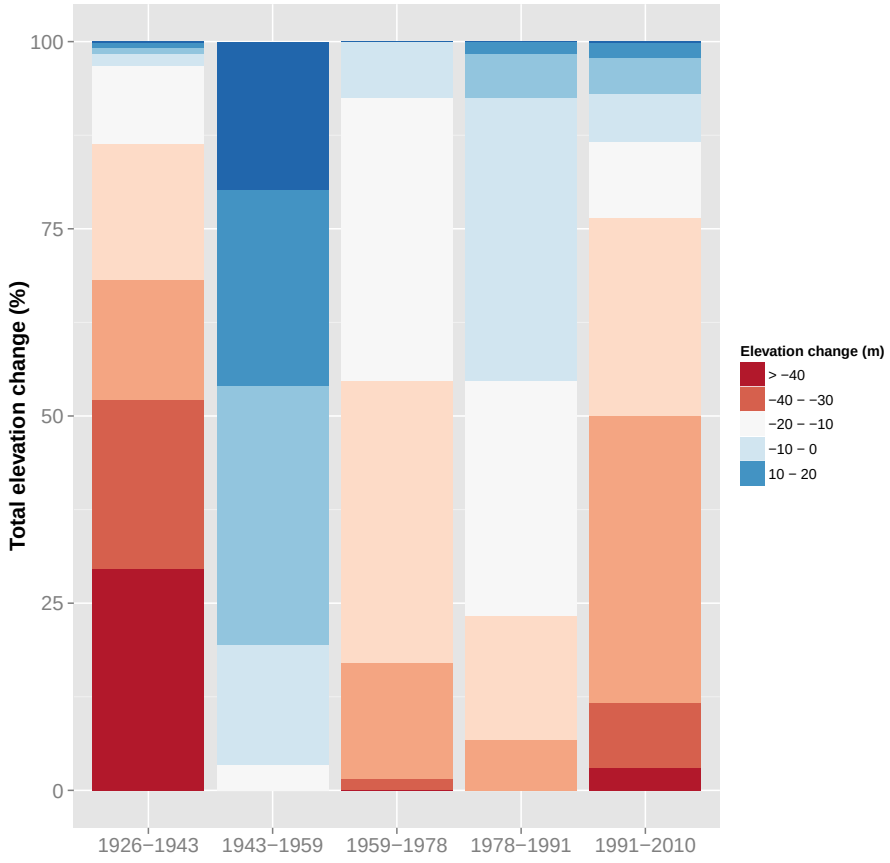

Figure 6.12: Total elevation change between mapping intervals where (a) 1926-1943 (±43.6 m)(b) 1943-1959 (±34.4 m) (c) 1959-1978 (±32.2 m) (d) 1978 - 1991 (±36.0 m) (e) 1991-2010 (±19.6 m). Errors are calculated according to glacier/area DEM perimeter point agreement.

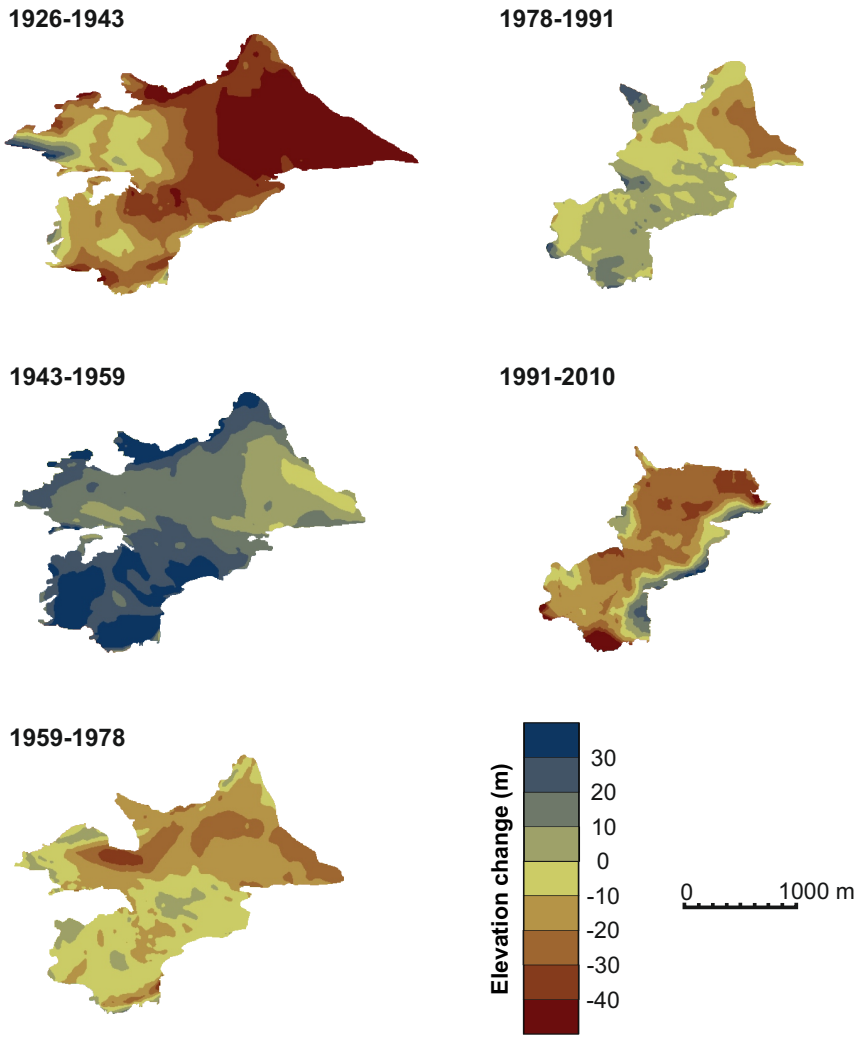

Figure 6.13: Mean elevation change per year between mapping intervals with change in m per year where (i) 1926-1943 (±2.56 m) (ii) 1943-1959 (±2.15 m) (iii) 1959-1978 (±1.69 m) (iv) 1978 - 1991 (±2.77 m) (v) 1991-2010 (±1.03 m)

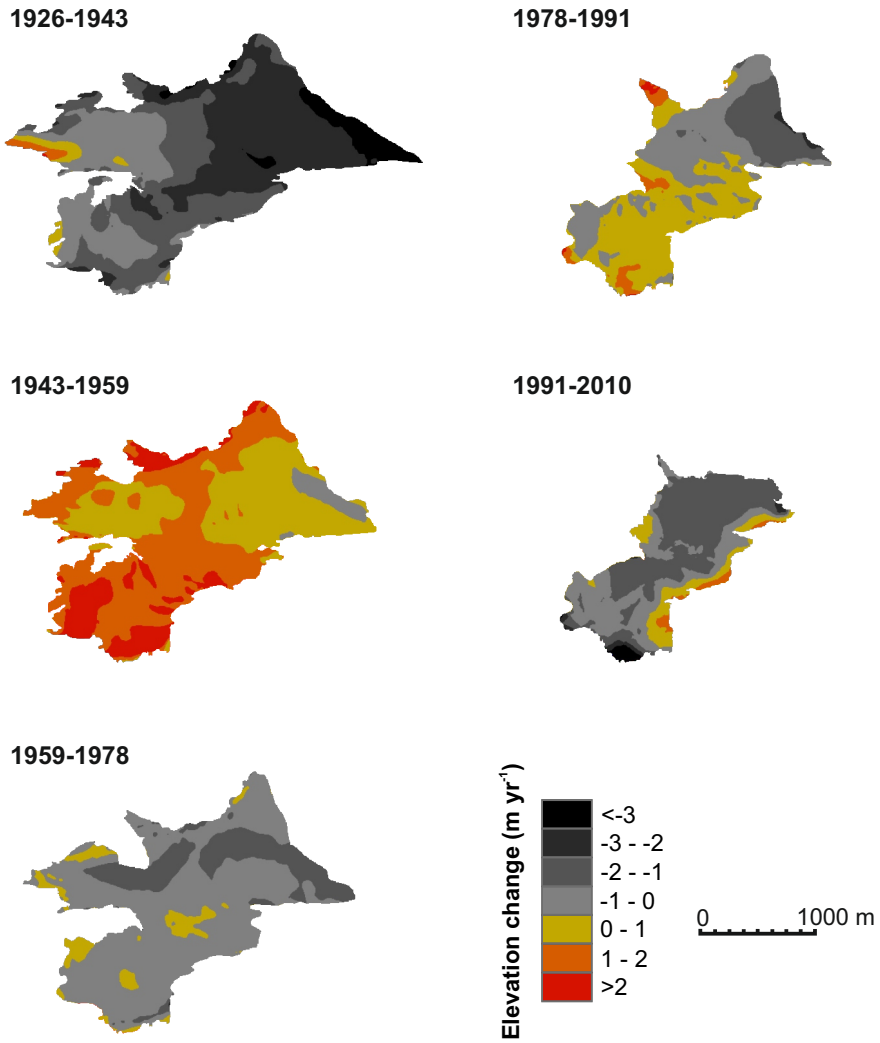

The elevation lowering trend reappears following the elevation increase of 1943 - 1959. Elevation lowering accounts for 92% of the 1978/1959 difference surface, with a mean value of -11.80 m. The pattern of lowering is interesting, showing a concentration of reductions following a line from west to east across the northern portion of the glacier. This shows lowering in the middle of the glacier body, following a centre line, for which Kårsa arguably has two with one running from the terminus to the extreme west of the glacier and the second running from the centre of the northern glacier area to the south west. With the loss of the western lobe between 1978 and 1991, the second centre line is all that remains. There is a small amount of elevation increase, occurring in the west and south-west, as well as in the centre of the upper accumulation area.

The first two cases of elevation increase are possibly erroneous and should be treated with caution. This caution relates to their proximity to the glacier boundary which is the area of greatest uncertainty with regard to the initial summer surface interpolations. The third case however, regarding elevation increase in the centre of the accumulation zone can not be sufficiently explained with this alone. There are three possible reasons why such an increase has been observed:

1. Interpolation error
2. Presence of snow from a summer snowfall event or snow drifts at the time of mapping
3. Indication towards currently unaccounted for dynamic processes

The mean elevation increase is +0.15 m across the surface with a maximum increase of +13.74 m. Accounting for only the central zone of elevation increase, a mean of approximately +0.70 m and a maximum of +5.08 m are observed.

The centre-line lowering trend of 1959-1978 is continued between 1978-1991. The mean observed lowering in elevation is -5.33 m. Lowering occurs over 55% of the 1991 glacier area. The remaining 45% is accounted for by surface elevation increases which occur across the majority of the southern portion of the glacier, as

well as the tongue located to the north-west. Mean elevation increase is calculated to be +2.74 m. The observed elevation increases to the north-east should be treated cautiously. The mean value for this portion is +13.90 m with a maximum value of +29.96 m. This point is highlighted as from work in the field, it is known that this area is prone to avalanching and the likelihood of there being a thick ice presence there is very small, especially one that would have increased by nearly 30 m.

Between 1978 and 1991, there was the detachment of the western accumulation area. Its associated elevation loss is not accounted for here where elevation change is relative only to the most recent surface (in this case, 1991).

Since 1991, there has been overall surface lowering with a mean value of -19.00 m. As seen in figure 6.12, there is some extreme lowering on the southern tip of the glacier but this is most likely attributed to interpolation error. This has not been removed from the surface used to calculate the aforementioned mean lowering. 16% of the 2011 area is accounted for by positive elevation increase (mean value of +1.53 m). These areas are focused around the glacier boundary to the east and for a small region to the west (see figures 6.12 and 6.13). Again, these must be treated with caution as they are located in regions that during the development of the 2010 summer surface, were constructed only from points extracted from a 50 m DEM. As identified from the Monte Carlo analysis, these areas are sensitive to rogue data points.

6.6 Glacier thickness change

Glacier thickness maps are represented in figure 6.14. The pattern shared by all thickness maps is for a thick area to be located in the central north, thinning to the glacier terminus in the east as well as towards the southern accumulation area.

In terms of proportional area within different 20 m thickness categories, the most populated category for all years is 0 - 10 m. This category is smallest in 1959 (28%) and largest in 1943 (56%) followed by 1978 (46%) and 2010 (40%). The majority

Figure 6.14: Historical mean thickness maps 1926 (±12.87 m), 1943 (±15.07 m), 1959 (±11.91 m), 1978 (±11.91 m), 1991 (±11.91 m) and 2010 (±11.91 m). Errors here are based on the statistical mean bias of the glacier/area DEM perimeter point elevation comparisons. The 1926 map is displayed using a different scale to those for 1943-2010 and this is specified by the two scale bars on the figure.

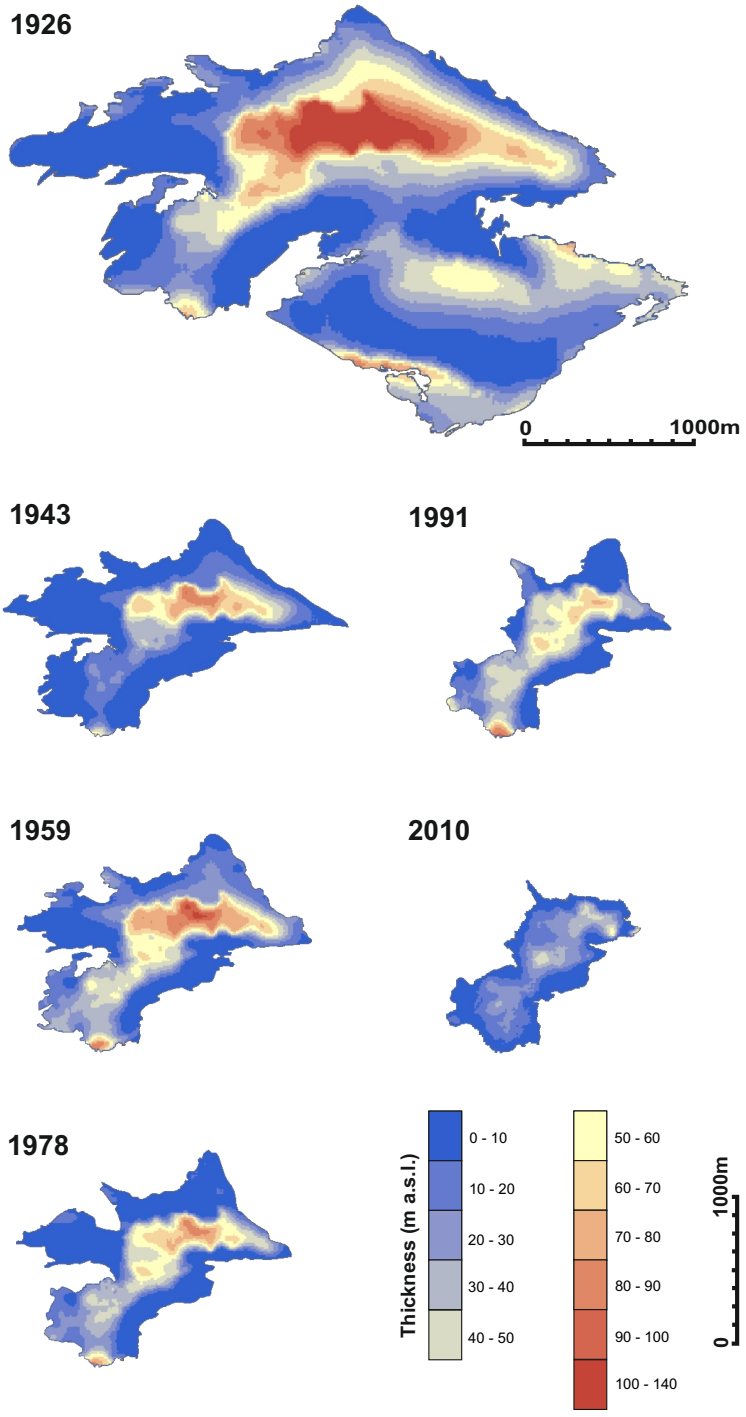

of the glacier thickness for all years is <50 m with 100% of the glacier in 2010 being <50 m. Thicknesses >50 m, account for 20% of the 1926 and 1959 glacier with increasingly smaller values for 1978 and 1991 (15% and 14% respectively). 12% of the 1943 is within the >50 m which potentially implies great mass loss for 1926-1943 followed by great mass increase from 1943-1959. The mapped surfaces show some areas of thick ice to along the south western periphery of the main glacier lobe as well as along the side glacier in 1926. This is likely erroneous and is associated with discrepancies between the glacier surfaces and the bed DEM. Consequently thickness in these areas should be ignored.

The general trend is for a reduction in mean thickness whereby the trend falls within the error margins (see figure 6.1). The 1943 surface has the most associated vertical error (see section 6.1) and these errors may explain the greater proportion values of the glacier being represented in the smaller thickness categories, as well as the break in the general negative trend observed when considering change in mean glacier thickness (figure 6.1). The large errors associated here with the thickness surfaces are associated with the development of the bed DEM and this is discussed along with the error limits applied to the thickness chart in figure 6.1, in section 4. The glacier thickness here is a best estimate and the spatial patterns are thus more useful than specific values such as the mean when assessing changes over time.

Glacier volume change is summarised in figure 6.1 . The mean volume change from 1926 - 2010 is estimated at 111.97 x 10^{-3} km^3. Maximum and minimum volume estimates for the different years are displayed in table 6.5. The pattern of change is much stronger for volume than for thickness with a clear reduction over time. The trend is also largely outside of the error margins of the individual volume estimates. The 1943 surface still breaks the overall reduction trend and this may be either a product of error or mass wasting followed by growth as mentioned above.

Table 6.5: Glacier volume: mean, maximum and minimum estimates (1926 - 2010)

Year	Max. Vol. (km^3 x 10^{-3})	Min. Vol. (km^3 x 10^{-3})	$\bar{x}$ Vol. (km^3 x 10^{-3})
1926	166.94	83.69	125.31
1943	47.69	17.31	32.50
1959	69.08	34.38	51.73
1978	46.58	22.24	34.41
1991	38.95	19.13	29.04
2010	21.28	5.39	13.33

6.7 Slope change

The slope of a glacier surface is extremely important when considering the receipt of radiation. This is discussed in section 2.3.1. Considering equation 2.7, changes in slope angles will change values of I and therefore contributions of I to Q (see equation 5.13). Surface slope maps are displayed in figure 6.15. The general pattern maintained throughout the period of investigation is of: more gentle slopes within the central northern section of the glacier, with slope increasing towards the terminus in the east; steep slopes along the perimeter to the north west, along the southern edge of the glacier's western flank (apparent in 1991 an 2010 following loss of the flank) and to the south east; slopes between 20-30°at the mid section between the area to the north/north east and the south west; gentle slopes to the south west.

The 1926 surface shows steep slopes present along the northern and southern flanks of the side glacier. Concerning the lower glacier to the north, from 1943 - 2010 it takes on a steeper profile, with increasing large areas being represented more by the 10-20°category than the 0-5°. The mid section between the area to the north/north east and that to the south west also becomes increasingly steeper with more area being represented by the 20-25°category in 2010 than in 1926. There appears to have been little change in glacier slope to the south west. To quantify categorical changes in slope over time, the appropriate data are presented in the charts in figure 6.16.

Figure 6.15: Glacier surface slope maps 1926 - 2010. The 1926 map is drawn at a different scale to the 1943-2010 maps. The appropriate scale is indicated next to the 1926 map. Slope is calculated from elevation and therefore elevation errors as indicated in figures 6.12 and 6.13 are acknowledged.

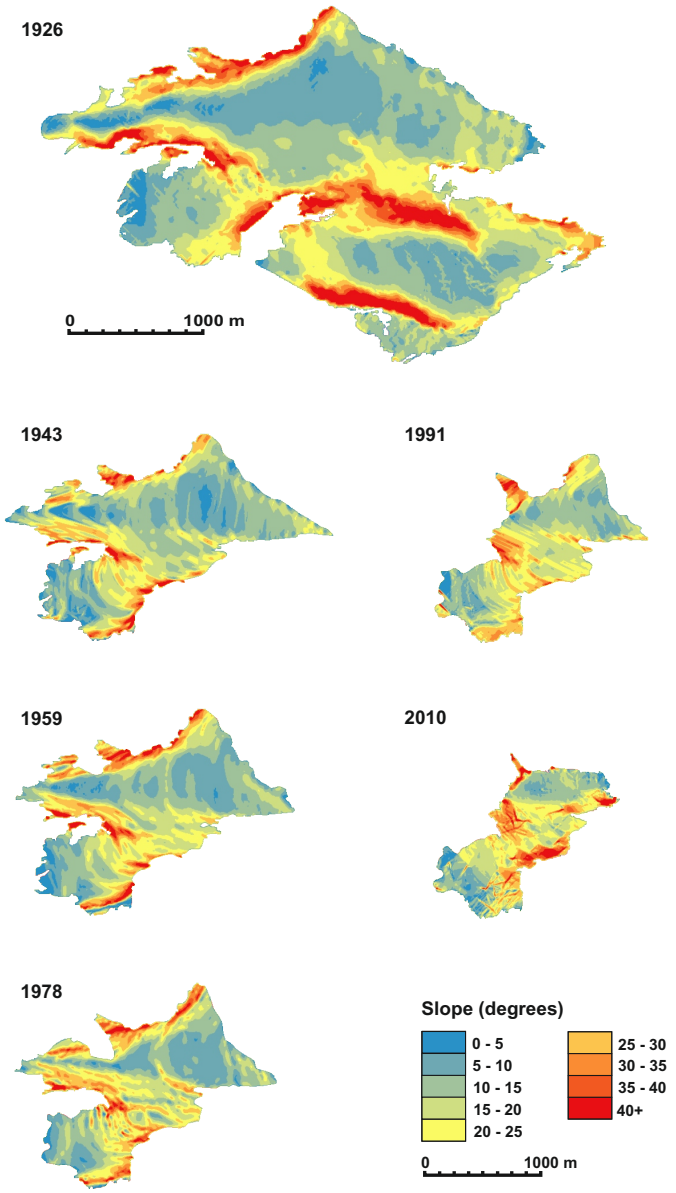

Figure 6.16: Glacier surface slope histograms 1926 - 2010.

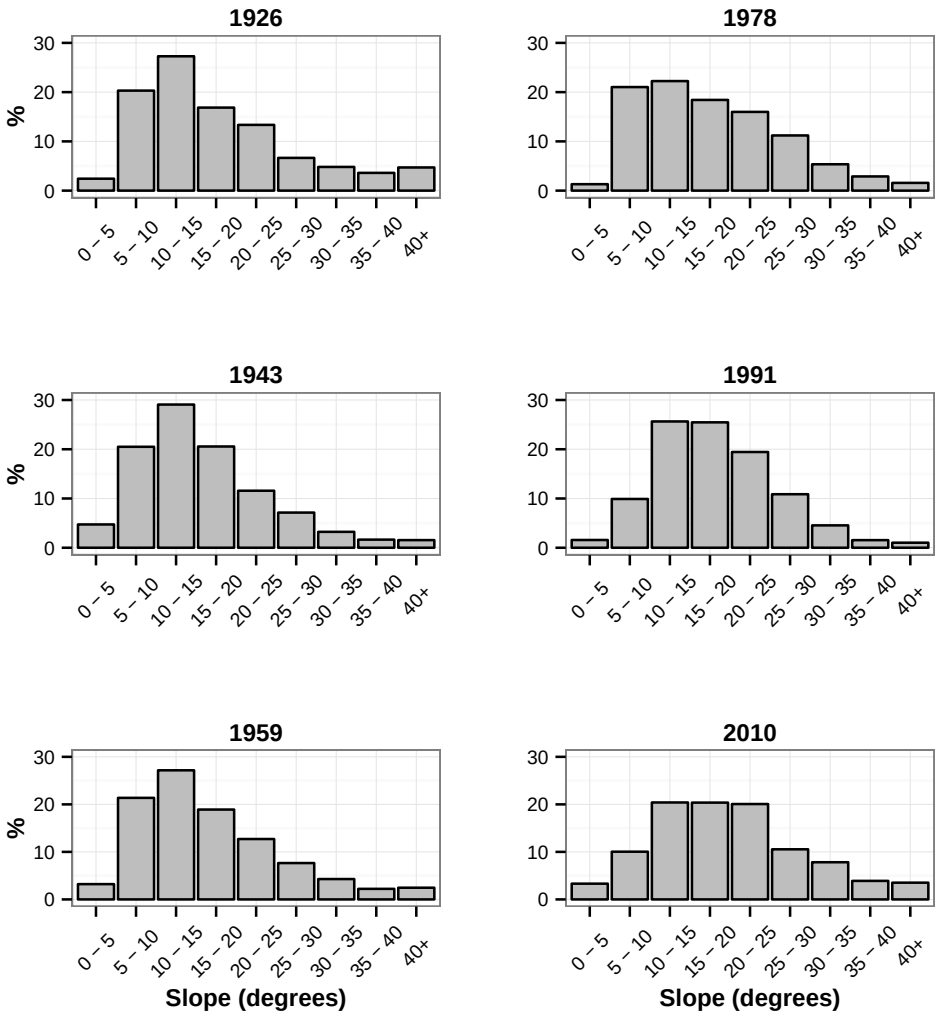

An assessment of the proportions of the glacier surface area represented by the charts in figure 6.16 shows an increase in the larger slope categories through time. 27% of the glacier surface in 1926 is between 10 - 15°, with a further 20% falling between 5- 10°. 13% of the glacier surface is of an angle >30°which is largely accounted for by the presence of the Kårsa side glacier where over 1/3 of the surface is of an angle >20%. These relatively steep angles are related to the ridge over which the side glacier was located, which is east trending from the peak of Gorsačohkka . The main lobe (to the north and trending from east to west) generally maintains a slope angle of 5-15°, which follows a relatively steep terminus to the east (15-20°). Stepping up to the accumulation area in the south-west, there is a marked increase in slope angle (approx. 20-25°) before the surface flattens out to between 0-15°to the extreme south-west. The steep slope angles apparent around the glacier margins exemplify the interaction between the glacier and the steep surrounding topography from which the glacier hangs.

By 1943, 29% of the glacier surface was between 10-15°with only 5% of the surface being than 30°. The reduction in slope 30°compared to 1926 relates to the loss of the Kårsa side glacier and also retreat around the glacier perimeter. Retreat around the perimeter will have had quite a significant effect on the overall proportions of the glacier's slope distribution, with the main lobe retreating back from the steep surrounding mountain slopes, moving into the gentler angle of the main valley basin.

27% of the glacier in 1959 had slope angles between 10-15°, the mean slope of the glacier being approximately 17°. The area of the glacier with an angle of 30% increased from the 1943 value by 3% to 8%. This is most noticeable on the northern margins of the glacier perimeter. This may relate to increased melting away from the margins, with differential melting and therefore surface lowering occurring. Of interest is an increase in slope angles to the middle south-east portion of the glacier where an increase in zones falling between 10-25°becomes more apparent. This is likely to be indicative of an increase in the stepped nature of the glacier that is observed by 2010.

The increase in mean slope angle from 1943 continues, with a mean of 18°, in 1978. A noticeable reduction in the proportion of the surface falling between 10-15°is observed with 22% by 1978 compared to 27% in 1959 and 29% in 1943. A trend also begins to emerge with regard to the increasing area of the glacier exhibiting slope angles >30°, for which 10% of the 1978 surface represents. This is an increase from the 6% value in 1943. Comparing the distribution maps of 1978 and 1959, the centre of the east-west trending northern portion of the glacier appears to have become increasingly steep with a significant reduction in the area of the glacier with slope angles between 0-15°. There is a clear shift in the slope proportions between 0-15°, moving from 52% of the surface in 1959 to 45% in 1978. This proportional loss of 7% is made up by an increase in the proportion of the surface with slope angles between 15-30°, moving from 39% in 1959 to 46% in 1978.

Mean slope in 1991 matched that of 1978 at 18°however this is not a good representation of the surface slope angle distribution. The matching mean values can be explained by slightly steeper slopes at the northern glacier perimeter in 1978 compared to 1991 (with 10% of the 1978 surface being accounted for by slopes 30°compared to 7% in 1991). There is a significant shift in the portion of the surface with slope values between 5-10°, with these slope angles representing only 10% of the surface in 1991 compared to 21% in 1978 which is attributed both to retreat from the terminus in the east as well as loss of the western accumulation zone. There is a slight increase in the area of the surface represented in the 10-15°category from 22% in 1978 to 26% in 1991. These changes are further reflected between 1978 and 1991 by changes in the area with a slopes 0-15°(45% to 37% respectively) and between 15-30°(46% to 56% respectively). Consequently, the majority of the surface by from 1978 to 1991 has steepened noticeably.

The mean slope in 2010 is 20°. Compared to the 1991 surface, the most significant increases occur in the proportion of the surface with slope values greater 30°where a 8% shift is observed from 7% (1991) to 15% (2010). The area for the 0-15°category reduces from 37% in 1991 to 34% in 2010. A reduction is also observed for the 15-20°category from 56% (1991) to 51% (2010). The areas where the steep slopes are observed, particularly on the southern portion of the terminus (to the east)

and the middle south-east section of the glacier are accounted for by few measured points and should be treated cautiously. The stepped glacier profile of the glacier is apparent as in 1991 (but the first plateau is not so well defined.

6.8 Aspect change

Surface aspect, as with slope is extremely important when considering the receipt of radiation at the glacier surface. This is discussed in section 2.3.1. Considering equation 2.7, changes in surface aspect changes the value of I and therefore contributions of I to Q (see equation 5.13). Surface aspect maps are displayed in figure 6.17. For the northern section of the glacier is for a reduction in E facing slopes, with increases in slopes facing SE and NE through to 1991, and then a reduction in SE slopes with loss of mass in the north. The central glacier area as well as to the SW appear to have undergone few changes over time (as with slope discussed in section 6.7). For the 1926-1978 surfaces, the western lobe appears to have acquired an increasingly NE aspect from being more N in 1926. The E periphery of the glacier has become increasingly N in aspect, although for the 2010 surface this should be treated with caution as considering this occurs in the area of greatest sensitivity as highlighted in section 6.1.

To further investigate changes in aspect, data are presented using radar plots in figure 6.18. Compared to the more N 1926 plot, those for 1943-1991 maintain increasingly E aspects. The 2010 plot is much more akin to that of 1926 than the 1943-1991 plots. This transition is related to the large areas of the side glacier in 1926 which maintained N aspects. Following the detachment of the side glacier between the 1926 and 1943 mapping intervals, the main lobe of the glacier then maintains a more E aspect as is clear in the plots. Thus, despite similar proportional representations between 1926 and 2010 as displayed in figure 6.18, spatially the patterns are quite different.

Quantification of some of the major aspect changes reveals overall decreases in easterly aspects (NE-SE) from 74% in 1926 to 67% in 2010, with increases in easterly aspects for 1943-1991 being particularly associated with detachment

Figure 6.17: Glacier surface aspect maps 1926 - 2010. The 1926 map is drawn at a different scale to the 1943-2010 maps. The appropriate scale is indicated next to the 1926 map. Glacier aspect is predominantly N-E, with the majority of the surface for all years holding a NE aspect

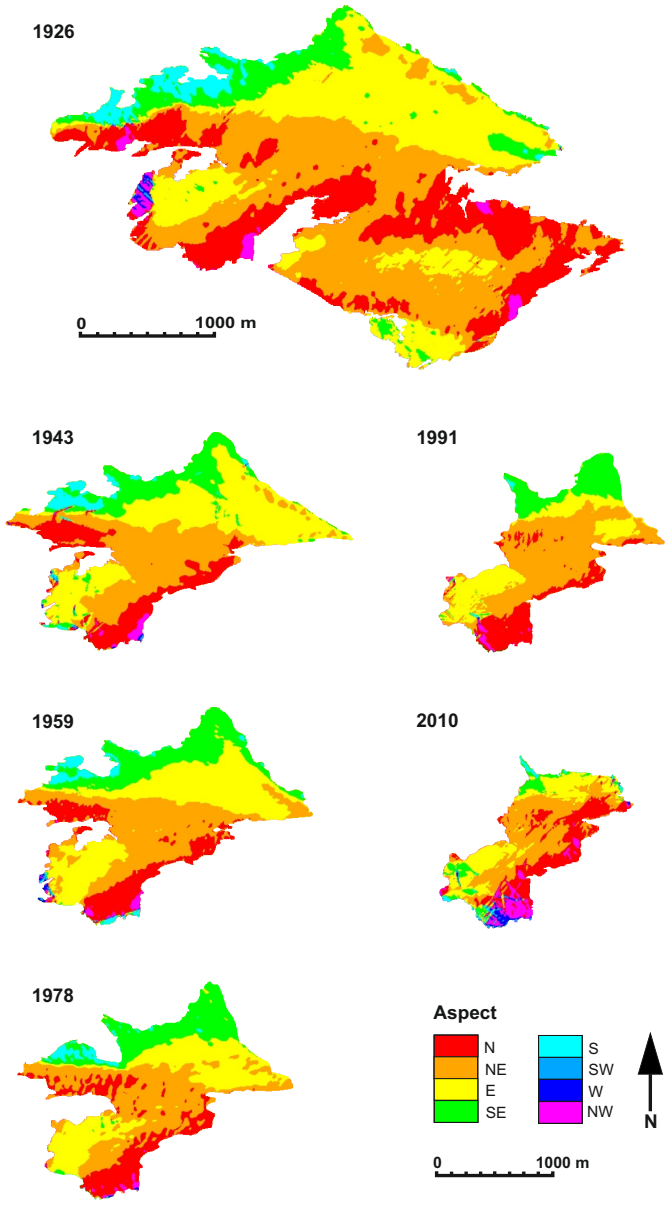

Figure 6.18: Glacier surface aspect radar charts 1926 - 2010.

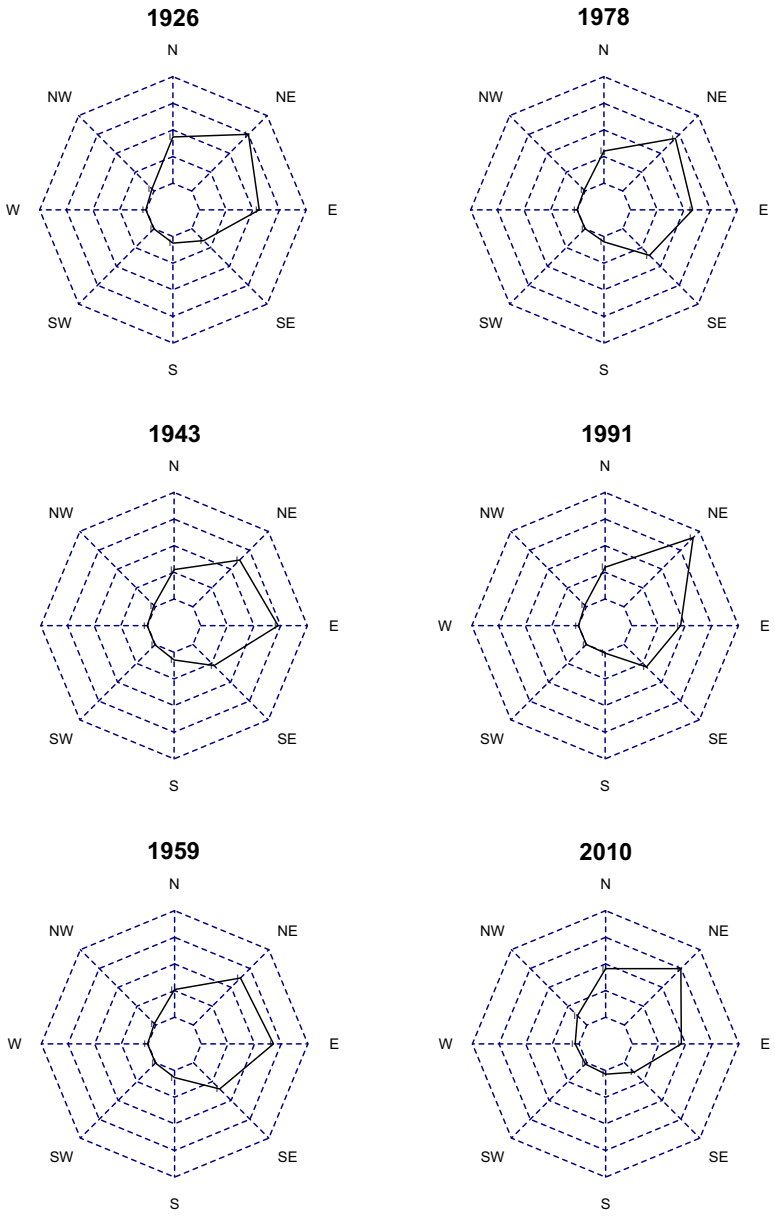

of the side glacier.Overall, the proportion of the 2010 surface with a N aspect almost matches that of 1926 (23% compared to 22%) despite decreasing between 1943-1991. There is also a noticeable increase in area with a westerly aspect (SW-W) from 1926 to 2010, the former with a 2% coverage compared to 9% in 2010.

6.9 Glaciological parameters

The glacier is assessed here for different glaciological parameters, specifically mass balance change, the position of the ELA, basal shear stress and annual estimated sliding potential as a function of glacier morphology and an estimation of likely temperatures at the glacier bed, as a function of thickness. The Methods by which the results displayed here are calculated are discussed in section 4.3 of chapter 4.

6.9.1 Glacier mass balance change

Using the difference surfaces discussed in section 6.5 and displayed in figure 6.13, it is possible to calculate changes in glacier mass balance for the different mapping intervals. Mass balance changes (m w.e) are displayed against elevation for the different mapping intervals in figure 6.19. Glacier mass balance change is calculated using a fixed ice density of 900 kg m^{-3} and this is discussed in section 4.3.7. The values displayed are generalised for elevations on a 1 m interval. Where multiple b_n values exist for a single elevation, a mean value is calculated. For this reason, the mass balance curves in figure 6.19 give a different surface change profile than is represented when considering the glacier long profile (figure 6.9). This is mentioned as the more negative change displayed for the terminus area of the 1943 long profile is not well represented in figure 6.19, as the values are raised by averaging with positive growth in other areas of the glacier at the same altitude.

$\bar{b_n}$ values are calculated for each of the mapping intervals, displayed below in table 6.6. Both figure 6.19 and table 6.6 clearly show that for the majority of the period of interest, the glacier was in a state of negative balance. From using the geodetic approach, only for the 1943-1959 interval is the glacier identified as being

Figure 6.19: Annual mass balance curves for map intervals 1926 - 2010

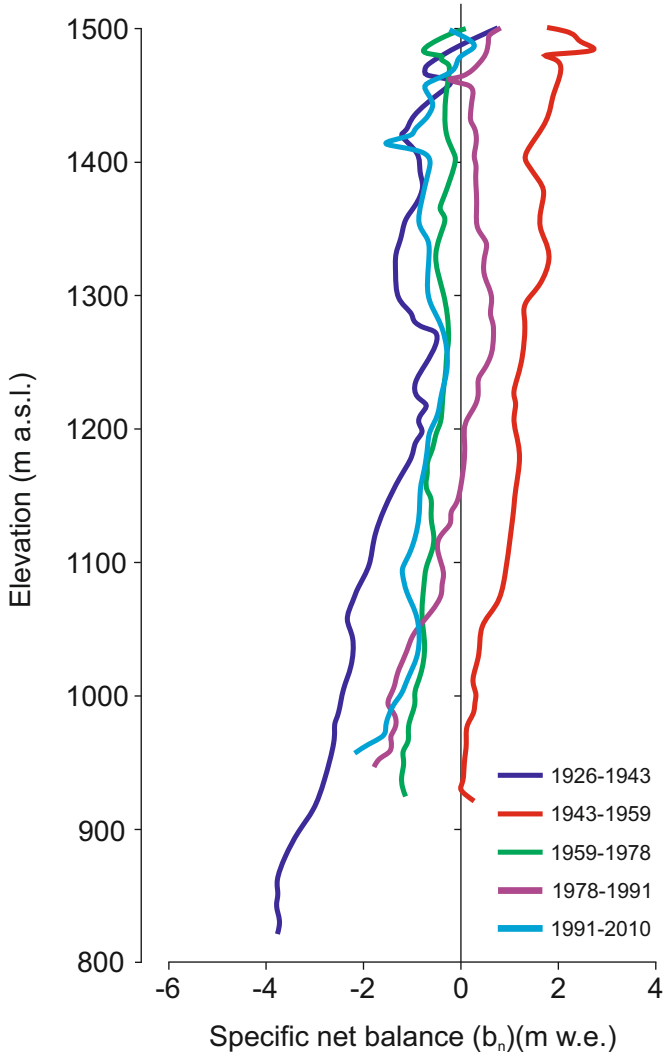

Table 6.6: $\bar{b_n}$ calculated for mapping intervals 1926 - 2010

Year	$\bar{b_n}$
1926-1943	-1.53
1943-1959	+1.11
1959-1978	-0.55
1978-1991	-0.18
1991-2010	-0.84

in a state of positive balance. Indeed, for the 1943-1959 interval, the majority of the glacier surface appears to have been in a state of positive balance despite terminus retreat still occurring. This apparent inconsistency may be related to the snapshot nature of the methodology applied which may hide any re-advances that may have occurred throughout the 1943-1959 period, which results in only retreat being identified. The 1926-1943 period is identified as having the most negative balance and considering the pattern of change in b_n as a function of generalised elevation, this is most accentuated at elevations below 1200 m a.s.l. The 1959-1978 and 1991-2010 surface appear to be mainly in states of negative balance across the generalised altitudinal range with positive balance changes being identified only at the most elevated portions of the glacier (>1490 m a.s.l.). Considering b_n as a function of elevation, the 1978 surface shows a different trend to any of the other intervals which are either predominantly in states of negative or positive balance. The 1978-1991 surface is negative below 1150 m a.s.l. and positive above the same elevation, with negative balance being identified only for a small range around 1460 m a.s.l.

6.9.2 ELA

Over the 1926-2010 period, considering overall surface lowering and thickness change patterns as well as dramatic terminus retreat, on average Kårsa has been in a state of negative balance. As in Hawkins (1985), despite these negative balance conditions, snapshots of the ELA are acquired for each map available by assuming steady state conditions. Consequently, the ELA values unlikely represent actual 0 balance conditions as would be required for true steady-state conditions. ELA methods are discussed throughout chapter 2 and the methods applied here are

detailed in section 4.3.8 of chapter 4. As was previously discussed, for each of the different methods, here specifically concerning the AAR and AA, a number of factors can be used by which to calculate the ELA altitude. A brief sensitivity analysis was carried out to assess the effect of using different AAR values from 0.4-0.8 and ratios of 0.5, 0.6 and 0.7 in the AA equations (the equations for which are highlighted in section 4.3.8 of chapter 4). The values derived for the different methods are displayed below in table 6.7. Between the different methods, the mean range between the maximum and minimum elevations calculated is 485 m which is evidence for the existence of large discrepancies between the methods. The AA method using different ratios was particularly sensitive to 10% changes in the accumulation area within the ratio applied.

Table 6.7: ELA elevations 1926 - 2010 using different approaches

		AA		Hmed	Hess			AAR			AABR	Range
Year	0.4	0.5	0.6			0.4	0.5	0.6	0.7	0.8		
1926	1470	1225	980	1222	1070	1263	1221	1177	1132	1088	-	490
1943	1417	1181	945	1167	1030	1206	1166	1123	1082	1048	-	472
1959	1450	1208	966	1191	1040	1225	1189	1146	1106	1066	-	483
1978	1449	1208	966	1184	1060	1222	1183	1146	1111	1066	-	483
1991	1460	1217	973	1178	1040	1227	1176	1137	1098	1057	1201	487
2010	1488	1240	992	1220	-	1298	1220	1160	1116	1078	-	496

Figure 6.20: ELA positions for 1943 - 2010 with mass balance at each position indicated. Mass balance values are taken from the generalised mass balance curves constructed in section 6.9.1

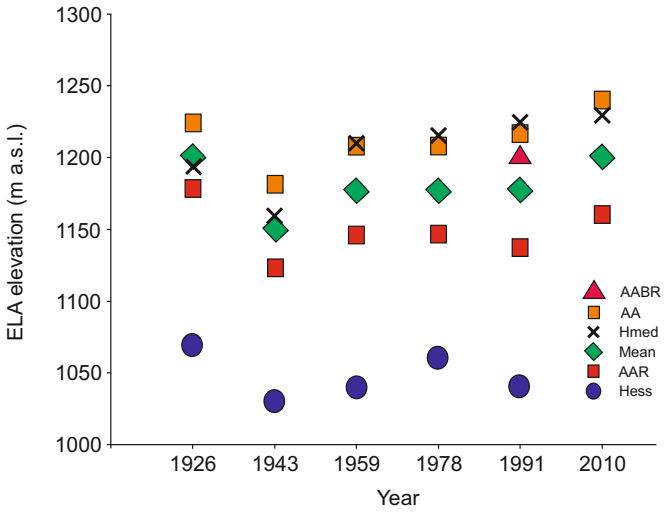

To assess variations in elevation using the different methods over time, positions using AABR, AA (0.5 ratio), H_{med} and AAR (0.6 value) methods were plotted as displayed in figure 6.20. The mean value is calculated by combining the AA and AAR methods. Hess altitudes are also calculated although this was not possible for all years with the 2010 surface not showing an apparent transition form concave to convex contour lines. A 0.6 AAR value is used for AAR ELA estimates as this is a common value used to assess steady state conditions (Torsnes *et al.*, 1993; Davies *et al.*, 2012). A mean ELA position is calculated from the AAR, AA and H_{med} values for each year. The AABR was only calculated for 1991 as the 1978-1991 mass balance data (section 6.9.1) provided the only curve indicating a split between positive and negative mass balance generalised across the surface. To ensure the same treatment is paid to each data set, the AABR value is not included in the calculation of the mean ELA position. The mean variation in predicted ELA between all of these methods (excluding the AABR elevation) is 146 m.

Using the same methods as used in figure 6.20, the changing ELA position against mass balance values for 1943-2010 are displayed in figure 6.21. From the figure, it is clear that 0 or positive mass balance values were at the ELA only in 1959

Figure 6.21: ELA positions for 1943 - 2010 with mass balance at each position indicated. Mass balance values are taken from the generalised mass balance curves constructed in section 6.9.1. No Hess altitude is calculated for 2010.

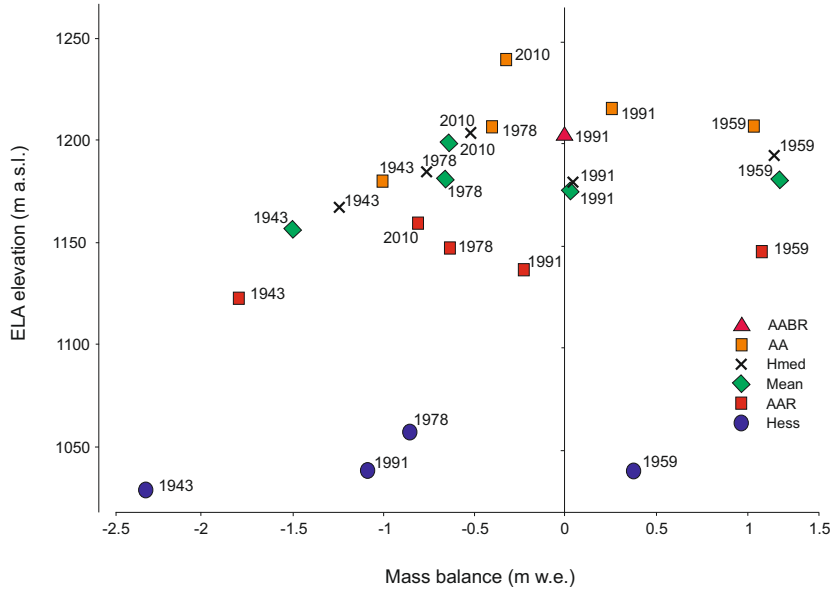

(1943-1959 mass balance data) and 1991 (1978-1991 data). It must be reiterated that the ELA values here assume steady state conditions, as in Hawkins (1985) even though over the 1926-2010 period the glacier was on average in a negative state of balance. A very general trend that can be drawn using the mean ELA position is that it is higher in 2010 than it was in 1943 although of a similar position to that in 1926 which is a function of the changing spatial distribution of glacier mass, altering with the removal of the Kårsa side-glacier and the western lobe.

6.9.3 Basal shear stress (τ_b) 1926 - 2010

A calculation of stress exertion by the glacier over time is indicative of the effect that changing morphology is likely to have had on glacier dynamics. This is useful to consider despite dynamics not having being directly measured within this study, providing a dataset that can be directly integrated with the study of the thermal regime of Kårsa carried out by Rippin *et al.* (2011), where it was proposed that an

earlier glacier configuration (with different dynamics) may have been the reason for the smaller glacier of 2010 having a thermal structure reminiscent of a much large glacier. Basal shear stress is calculated using equation 4.7 described in section 4.3.6 of chapter 4, where slope and thickness values are calculated for a given point from elevation and thickness values taken at a distance equal to the mean thickness of the glacier from either side of the point in question. This method is used to minimize the effects that lateral and longitudinal variations in both ice thickness and stress, associated with extensional and compressional ice flow, may have on basal sheer stress calculations (Thorp, 1991). Raymond (1980) proposed that elevation and thickness values should be calculated for a given point from values of a distance equal to 10-20 times the ice thickness. Considering the small nature of the glacier and still quite large thickness values, following this method would result in very few basal stress estimates. Consequently a spacing equal to mean ice thickness is deemed sufficient to estimate a trend in basal shear stress change over time. Stress profiles are displayed in figure 6.22.

For all years except 1943, figure 6.22 illustrates that maximum τ_b occurs at approximately 700 m from the back of the glacier which is the region of greatest ice thickness as displayed in figure 6.14 and of steeper slopes, as displayed in figure 6.15. This was to be expected as ice thickness is closely linked to τ_b (Thorp, 1991). With the exception of 1943, from 1926 to 1978, τ_b reduces with time from a maximum of 345 kPa in 1926 to 176 kPa in 1978 (averages of 119 and 69 kPa respectively). However, τ_b increases in 1991 which relates to increasing slope angles in the region of thickest ice as illustrated clearly in figures 6.15 and 6.16 - maximum τ_b in 1991 increases to 221 kPa (with a mean τ_b of 86 kPa). The profile by 2010 displays much lower stress values with an average τ_b of 31 kPa. There is still a spike approximately 700 m from the back of the glacier with a maximum τ_b of 102 kPa. The stark reduction of τ_b displayed by the 2010 profile compared to the 1991 profile is predominantly a function of reduced ice thickness as illustrated earlier in figures 6.10, 6.12 and 6.13.

Considering the close relationship between τ_b and thickness and surface slope values (Thorp, 1991; Benn & Evans, 1998), the errors associated with these

Figure 6.22: Centreline basal stress profiles 1926 - 2010. Profiles are constructed along the A-B centreline as used in figure 6.9. The uppermost chart displays all profiles together with the subsequent charts displaying the stress profiles for individual years.

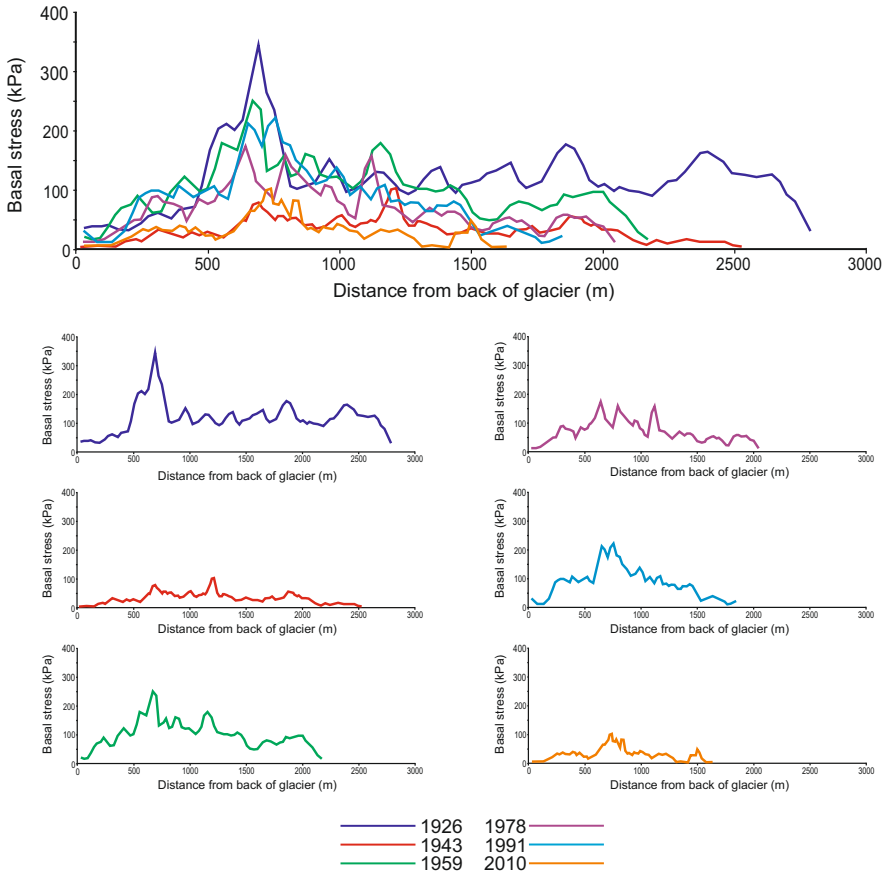

components must be considered. For the 1926-2010 surfaces, errors related to the actual glacier surface and therefore calculation of slope are relatively small with few areas of great sensitivity identified through the Monte Carlo surface sensitivity analysis (section 6.1). The greatest errors are associated with the calculation of ice thickness and thus the agreement between the glacier surface DEMs and the area bed DEM (the development of which is discussed in chapter 4).

Of all years, the 1943 surface appears to exhibit the least stress. The τ_b spike at approximately 700 m from the back of the glacier is not represented in 1943 either. The low values are likely the result of data errors, the 1943 surface being identified as having the largest vertical error (sections 6.1 and 4.3.5 of chapter 4) of all the historical surfaces, which relates to poor glacier surface/ area bed DEM agreement.

6.10 Summary

Using geodetic observation techniques, the methods of which are defined in chapter 4, it has been possible to assess the change Kårsa has undergone for the period of 1909–2010. The glacier has reduced in area from 4.30 - 0.89 km^2. The rate of area loss increased from 1943–1991 (0.008–0.034 km^2 yr^{-1}) and slowed down between 1991–2010 (0.016 km^2 yr^{-1}). Quantifying hypsometry change using the HI categorisation of Jiskoot *et al.* (2009), the glacier has changed from being equidimensional for the years 1926, 1943 and 1959; top heavy in 1978 and 1991; equidimensional in 2010. The terminus of the glacier has retreated a total of 1292 m in the period of observation. The rate of retreat decreased between 1943–1978 (23.5–8.3 m yr^{-1}) and increased from 1978-2008 (8.3–14.4 m yr^{-1}). The glacier has thinned by a rate of 0.35 m w.e. yr^{-1} which has resulted in an annual reduction in the maximum thickness of 0.85 m w.e. yr^{-1} (from 137 m in 1926 to 56 m in 2010). Thinning has been most focused along the glacier centre-line, especially in the lower reaches of the glacier area to the north/north-east. The trend of thinning has yielded a volume loss of 1.33 x 10^{-3} km^3 yr^{-1}. Glacier slope has increased with the surface being represented by slope angles in the range 10–25°in 2010 compared to 5–20°in 1926. The overall glacier aspect has varied between north-east and

east, being primarily north-east in 2010. Coupling glacier thinning and changes in slope, the basal stress exerted by the glacier along its centreline has reduced from a mean of 119 kPa (1926) to 31 kPa (2010). These changes have been considered in terms of mass balance change directly. Geodetic mass balance varies between positive and negative between 1926 and 1959. From 1959-1991, mass balance became increasingly less negative (-0.55 – -0.18 m w.e. yr^{-1}), becoming more negative from 1991–2010 (-0.18 – -0.84 m w.e. yr^{-1}).

The results of this chapter address the objective of *accounting for sensitivity of applied geostatistical techniques on reconstructed surface properties* which assists in meeting the project aim of *providing a full 3D glacier geometry reconstruction and assessment of a small mountain glacier, since the beginning of the 20th century, over decadal time scales*. The resultant surfaces developed act as an input to chapters 8 and 9. Changes in geometry are discussed in chapter 10.

Chapter 7

Results: Reconstruction of Kårsa 2007 - 2010

The key aim of this section is to address the changes that have occurred to Kårsa over the 2007-2010 (contemporary) period on an annual time scale as opposed to the longer time scale changes discussed in chapter 6. This is made possible using a combination of aerial photography, ground based surveying and geodetic analysis methods. Consequently, the geometry of the glacier has been reconstructed using a different approach to that applied in chapter 6. The data required here was sourced from both the field and from colour aerial photography. Data from the field are collected using a variety of techniques which are described extensively in section 4.2.3 of chapter 4. Fieldwork was carried out each March/April of 2008, 2009, 2010 and 2011 providing data for the glacier at the end of the winter season. The reconstruction here is for the summer season and is the result of processing of the winter glacier reconstructions by subtracting snow cover interpolation surfaces. Throughout the 2007-2011 study period, only one high resolution aerial photograph was available, taken in June 2008 (Lantmäteriet, 2010). This photograph has been the source of the glacier outline throughout this period. Due to the lack of temporal data with regard to the glacier outline, it has not been possible to consider change in the horizontal plane with regard to terminus retreat and area change. This chapter meets the objective of:

- Accounting for sensitivity of applied geostatistical techniques on recon-

structed surface properties

therefore addressing the project aim of:

- Providing a full 3D glacier geometry reconstruction and assessment of a small mountain glacier, since the beginning of the 20th century, over annual time scales

7.1 Surface reconstruction sensitivity analysis

The contemporary surface reconstruction process (section 4.2.3 of chapter 4) was driven by dGPS points collected in the field. These varied in number and distribution with each field excursion, limited by a number of factors including accessibility to steeper slopes and snow depth with the associated ease of maneuverability across the surface. Consequently in some years points have been acquired whereas in other years they have not. The presence/absence of points within the interpolation process has a very large effect on the final surface that will be calculated (much like removing the central pole of a tent). To address the issue of surface interpolation sensitivity, Monte Carlo simulations were carried out for the contemporary surfaces, the results of which can be seen in figure 7.1. The specific method of implementing the simulation is discussed in section 4.2.8 of chapter 4. The results displayed in figure 7.1 are the winter surfaces from which summer surfaces were constructed following the subtraction of year specific winter snowpack layers.

The contemporary surface (2007-2010) standard deviation patterns displayed in figure 7.1 have a very different spatial distribution compared to those observed for 1926-1991 described in section 6.1 of chapter 6. This is particularly apparent for 2007-2009 where there is a clear split between lower standard deviations in the northern part of the glacier and higher values in the southern glacier. These patterns appear to be highly susceptible to construction point (i.e. from dGPS and contour data) distribution.

Figure 7.1: Contemporary Monte Carlo surface sensitivity analysis results. The Monte Carlo surfaces shown are the winter surfaces from which summer surfaces were calculated following the subtraction of year specific winter snowpack thickness layers. Areas of highest standard deviation (Std.Dev.) show locations across the glacier of greatest sensitivity in the interpolation process. This is a function of the points available from which to create the surface. The input elevation points used to create the different surfaces are also displayed.

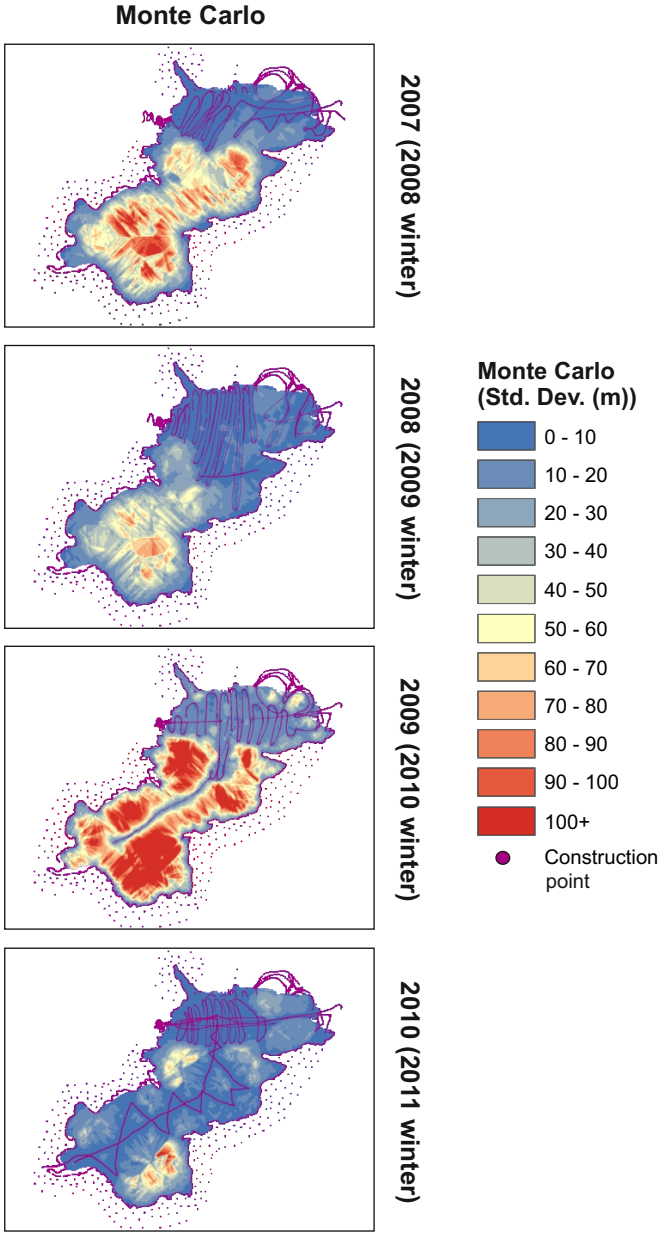

Table 7.1: Point file populations and contour spacings used for the 2007 - 2010 surface interpolations (Point numbers are referred to as within the perimeter as these are the points most likely to affect the glacier interior as a function of the search window value employed)

Year	Total Points	Points within glacier perimeter
2008	7122	3798
2009	9453	6690
2010	5714	4270
2011	14919	13110

The 2007 surface is constructed from a total of 7122 points of which approximately 50% fall within the glacier perimeter extent. Of this 50%, the majority of points are located within the northern glacier area. Within this northern area, standard deviation variance due to the effect of spurious point values are kept relatively low (generally between 0-30 m). These lower standard deviations are maintained around the glacier perimeter where there are also known points. The southern and central portions show significantly greater standard deviation values, ranging from 40 m+. This is attributed to the lack of known points in these areas. Standard deviations are likely to be particularly high in some regions rather than others as a function of the points selected to calculate unknown values, selected according to the kriging search neighborhood parameters. Where there are significant differences in the values of known points, noise will have a much greater influence than if the known points are generally of a similar value.

The same pattern for 2007 is observed for 2008 however the central region shows comparatively lower mean standard deviations. The points available for the 2008 surface construction extend much further from the northern glacier area than in 2007 (see also table 7.1). Consequently, there is a greater concentration of points available from which to predict unknown values. This reduces the impact of spikes in the known point data set on unknown point predictions. The southern area maintains a similar pattern to 2007 where standard deviations are greatest where there are fewest points available.

The glacier in 2009 has a greater spatial point coverage than 2007-2008, however

the number of points available is only 60% of those used for the 2008 surface. This reduction in point availability helps explain some of the variance observed with regard to standard deviations in the central portion of the glacier. The point coverage in this region is not as extensive as for 2007-2008, leaving larger gaps. This results in more distant, and therefore potentially less similar, points being used to predict unknown values within these gaps. In such cases, erroneous data spikes can have significant weight in affecting predicted values.

Moving from the central zone to the southern zone, large standard deviations (50 m+) are apparent - the pattern similar to that of 2007. There are points available in this region forming a centre line. Within the immediate vicinity of these points, standard deviation is reduced. This differs to the patterns observed around points for the 1926-1959 surfaces discussed above and may be explained by the higher point concentration along the centerline in 2009. The higher point concentration, resulting in greater weighting of all points, will reduce the effect of erroneous points - this not being the case for the more sparse point data used for 1926-1959, whereby the point closest to an unknown value will have a significantly greater weight compared to other points falling within the kriging search neighborhood.

The large standard deviations occurring in the central and southern regions, despite the availability of centerline points can still be explained by sparse data availability. It is possible that apparent sensitivity is further increased by the presence of the centerline points. The points that will be used to predict unknown values between the centerline and the glacier perimeter will come from both of these regions, specific points being selected that are closest to a prediction at a given time. The distance between the points used to aid the predictions within these areas could be within the order of 250 m and given the nature of the topography in which these points exist, they are likely to be significantly dissimilar - the presence of spikes in such a point selection will therefore affect predictions greatly, thus explaining both high standard deviations and sensitivity. Without the centerline points, the perimeter points alone would be used to predict values across the center of the glacier - although resultant predictions would likely be inaccurate (again linking to the concept of increased distance/reduced similarity), the points

used would potentially be more similar - a scenario in which data spikes affect predictions to a lesser degree. The centerline points provide too much dissimilarity as described above. Ultimately, this sensitivity is a relic of the interpolation method itself as opposed to a realistic measure of true surface values, highlighting the inadequacy of this interpolation method in regions of sparse known data points.

The 2010 surface shows the smallest standard deviation values of the 2007-2010 surfaces. This is the result of a greater spatial point distribution across the entire glacier. There are still some zone of higher sensitivity in the western central zone and the south eastern southern zone which relate to point gaps and therefore result in greater distances between points (potentially being more dissimilar) used for prediction.

7.2 Elevation change

The glacier surface in terms of elevation and hypsometry is summarised in figure 7.2. There are few discernible changes in elevation distribution through the 2007-2010 period. This is better observed when considering the hypsometry curves and acknowledging elevation-area ratio values.

Regarding hypsometry, the smallest areas are associated with the extremes of the glacier elevation range, with a trough in terms of area around the mid-glacier elevation bands. The main area peak for all years is within the 1400-1450 m a.s.l. range, accounting for approximately 20% of the total glacier area in 2007, 2008, 2009 and 2010. There is a smaller peak occurring within the 1050-1100 and the 1100-1150 m a.s.l. bands which account for approximately 11% and 12% of the overall glacier area for all years respectively. Between years, in terms of the overall distribution patterns identified in figure 7.3 there are no significant changes. There is evidence of some small shifts in the 1100-1300 m a.s.l. range between the years 2007–2010, but these are likely to be the function of data availability for each year; consequently such changes are likely artifacts of the reconstruction process.

Figure 7.2: Contemporary glacier elevation maps and hypsometry charts (Summer 2007 - 2010). There is little noticeable change between the surface elevation maps. The most significant changes are displayed by the hypsometry curves in the range 1100-1300 m a.s.l. and this is discussed in the text.

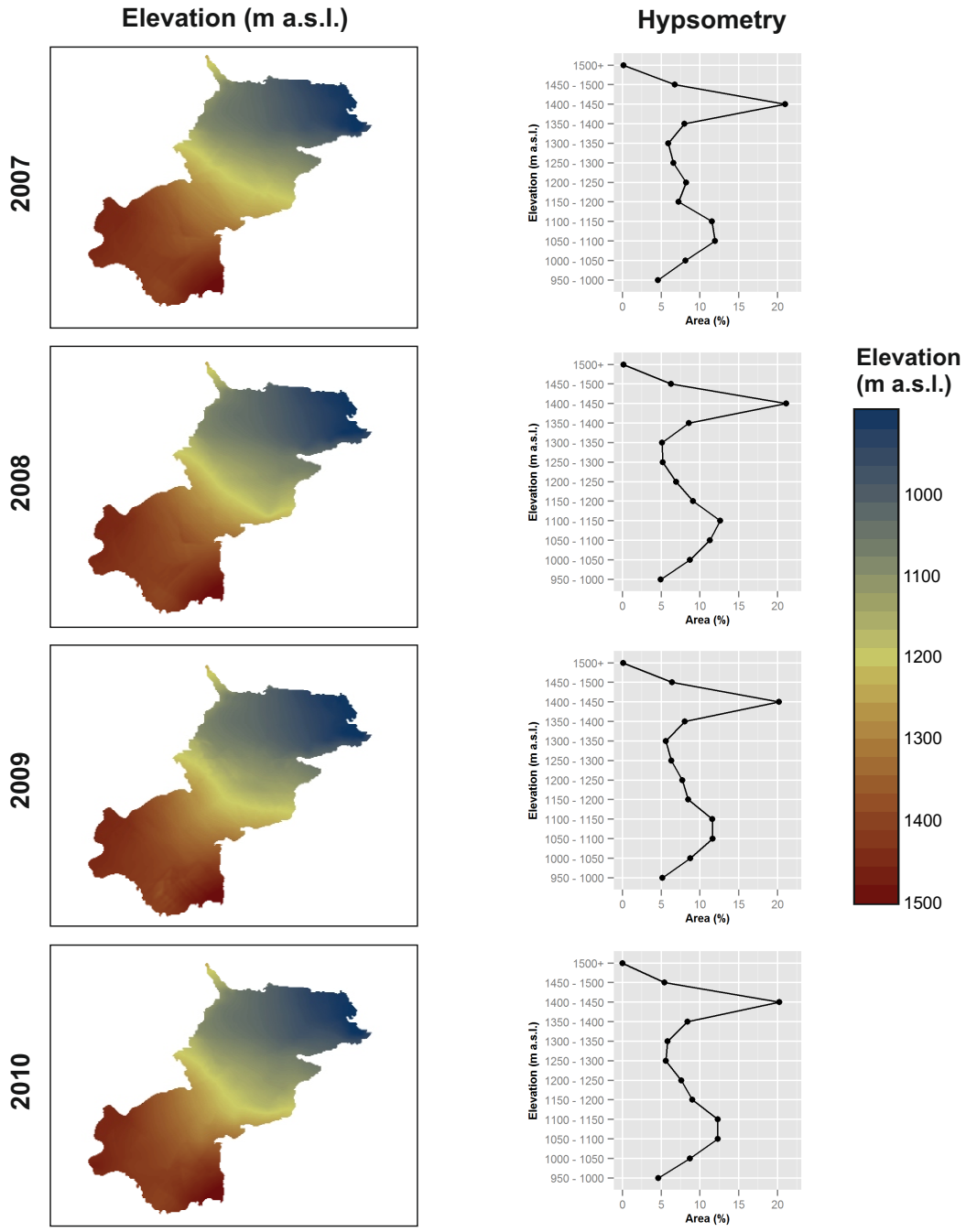

Figure 7.3: Glacier hypsometry curves against cumulative area (%) 2007 - 2010

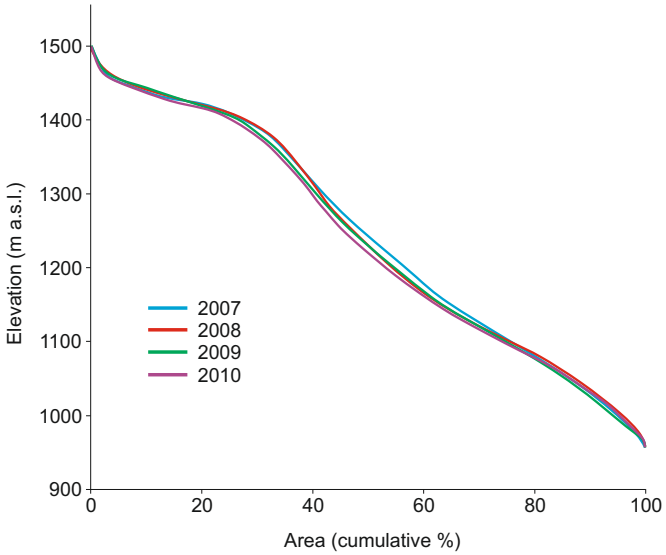

To compare the hypsometry distributions as succinctly as possible, cumulative area curves are displayed in figure 7.3. These are best described numerically and as with the historical hypsometry results discussed in section 6.3 of chapter 6, ER values are reported. Values of 0.52, 0.51, 0.52 and 0.51 are calculated for 2007, 2008, 2009 and 2010 respectively. This gives a mean ER for the 2007-2010 period of 0.52. HI values of -0.93, -1.07, -1.01 and -1.06 are calculated for 2007-2010 respectively and are displayed in figure 7.4. The lack of variance in ER and HI values further supports the minimal variation in hypsometry altitudinal distribution during the 2007-2010 period.

To account for the change in the elevation between years, the surface prior to a given year is subtracted from that of the given year. The results of these calculations are displayed in figure 7.5. The figures for the total glacier area have a lot of associated noise, with some areas being represented by large ± differences in elevation, many of which are deemed as unrealistic annual changes. The positive changes and large negative changes are most likely artifacts of the reconstruction process and are not thought to be natural/observable phenomena. This is discussed further in section 7.1. The least noise is associated with the area to the north of the glacier. This area of all of the reconstructions is the least

Figure 7.4: Hypsometry Index (HI) values over time 2007 - 2010

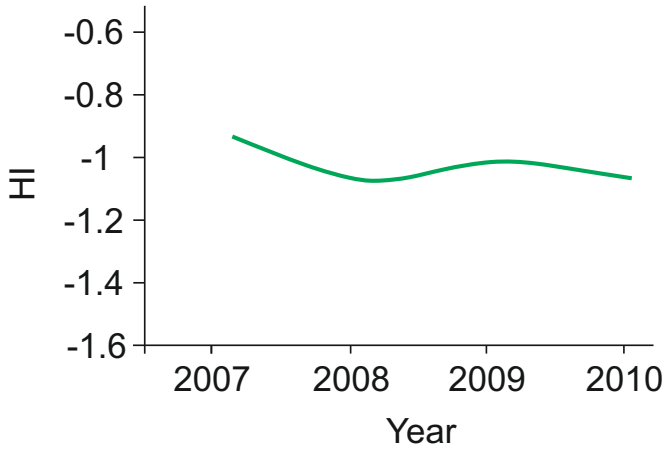

sensitive in terms of the effect of data on surface interpolations and thus is the most reliable in terms of changes which are environmentally controlled as opposed to being the function of data availability or interpolation processes. To further investigate this specific region, the second column of figure 7.5 is dedicated to this region.

For all surfaces, the majority of surface change occurs within the 0 - -2 category. There are areas of increase identified in the presented maps but these are located in areas least represented by data points collected in the field and thus in areas of the glacier reconstructions most sensitive to error. These regions are predominantly towards the glacier periphery and along the centre of the upper glacier to the south where points where well distributed points were only collected in 2011, making them available only for the 2010 summer surface interpolation. Considering the total glacier area, 39%, 29% and 27% of the calculated elevation change occurred in the 0 - -2 m change category for 2007/2008, 2008/2009 and 2009/2010 respectively.

Considering where collected field data point density was greatest, in the lower portion of the glacier located to the north, this area is focused on specifically in terms of annual elevation change. This area is considered in the second column of figure 7.5. The specific location of the lower glacier is illustrated in figure 7.6.

Figure 7.5: Contemporary annual difference surfaces for 2007 - 2008, 2008 - 2009 and 2009 - 2010 for the total glacier and specifically the northern portion of the glacier. Areas of large ± changes are discussed further in the text. The specific location of the northern portion of the glacier which is focused on is indicated in figure 7.6.

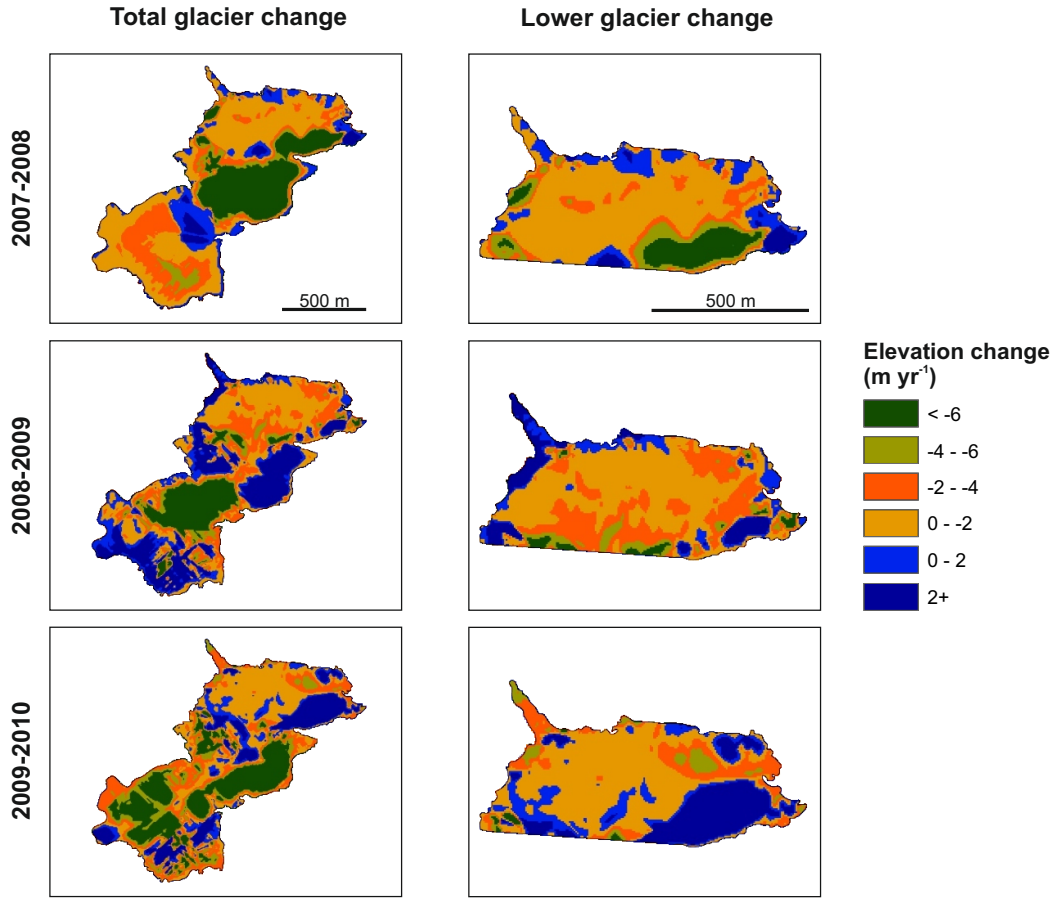

Figure 7.6: Photograph of Kårsa in September 2012 highlighting the split between the lower and upper portions of the glacier (defined by ease of accessibility during the winter months). The lower part of the glacier which had the highest density of elevation measurement points in all winter seasons is located beneath the dashed red line. Due to the increased point concentration in this region, geodetic assessment of change is most reliable here, unlike in the upper glacier above the red line where point density varied much more between different field seasons. The inset map highlights the lower glacier in dark grey as opposed to the upper catchment depicted in light grey. The lower glacier highlighted here represents 0.33% of the total glacier area.

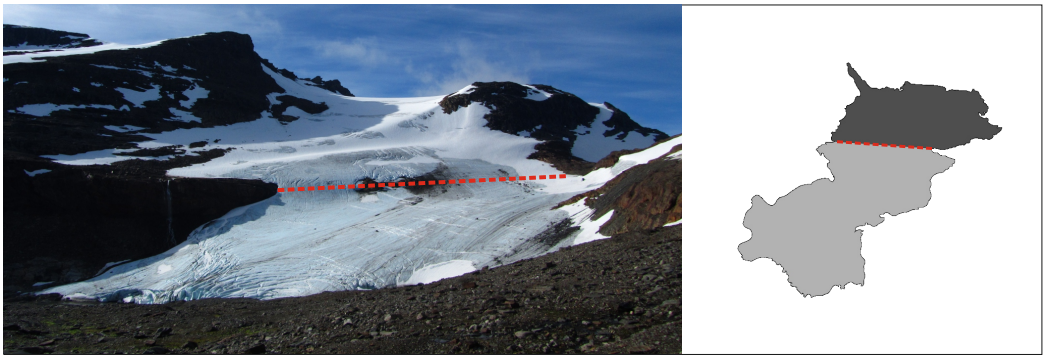

Across the lower glacier, there are still areas of very large ± changes which is also associated with the absence/presence of data points in intermittent years, resulting in unequal surface interpolations. However, the vast majority of change for all years falls within the 0 - -2 m change category with values of 55%, 48% and 47% for 2007/2008, 2008/2009 and 2009/2010 respectively. The -2 - -4 m change category is not well represented in the 2007/2008 and 2009/2010 assessments however there is a large increase in change within this range for 2008/2009 where it accounts for 27% of all change compared to 11% and 14% for 2007/2008 and 2009/2010 respectively. Change in this range is reasonable within a year and thus this can be taken as an indication of increased melt activity in 2008/2009 relative to 2007/2008 and 2009/2010.

7.3 Long profile change

Change occurrences across the lower glacier are illustrated in both long profile and cross profile in figure 7.7. The long profile follows the centerline of the lower glacier running from the western end of the accumulation area to the terminus in the east (AB).

Considering the AB long profile, there is a clear trend of surface lowering with each year being present below the last. There are no apparent changes in slope (these are investigated in more detail in plan form in section 7.5). The A'B'transect should only be considered between 0 m and 300 m (indicated by the vertical line) from A' as within this area, all surfaces have a high point density. Limited points are available for 2007 and 2010 past the 300 m mark (see figure 7.1 compared to the inset map of figure 7.7) and this distorts the transect as is apparent in the surface profile illustrated for distances along the transect >300 m. Between 0 - 300 m, the pattern of lowering is again clear with no obvious changes in slope. Patterns of increased convexity through time, identified for the historical transects (section 6.4 of chapter 6) are not apparent here.

7.4 Thickness and volume change

The glacier in terms of thickness is summarised in figure 7.8. Generalizing the 2007-2010 pattern, the thickest ice is located in the glacier centre and to the centre of the north-east area, indicating two apparent troughs of thick ice. The largest thickness values trend along the central line of the glacier from north-east to south-west.

Considering spatial thickness distribution on an annual basis, it is clear from figure 7.8 that the greatest thickness is account for in 2007, the least so being in 2010. The 0-20 thickness category represents 49%, 58%, 62% and 68% of the 2007, 2008, 2009 and 2010 thickness surfaces respectively. This 20 m category therefore represents the majority of the ice thickness of each of the surfaces. Considering areas of greatest thickness, the 40-50 category represents 11%, 6%, 3% and 2% of the 2007, 2008, 2009 and 2010 surfaces respectively. The 50+ thickness category represents 6% of the glacier in 2007 compared to 2% of the 2008 surface and 0% of the 2009 and 2010 surfaces.

There are clear reductions in thickness over the 2007-2010 scale and these are presented in figure 7.9. Mean annual thickness change for 2007-2008, 2008-2009 and 2009-2010 were 4.14, 1.61, 1.93 m yr^{-1} respectively. The general trend of reduced

Figure 7.7: Contemporary glacier long profile and transect (Summer 2007 - 2010). The long profile (AB) and the transect (A'B') are constructed only for the lower glacier as this is where all years have the highest density of elevation data points, therefore providing the most information on surface change over time. The area between 0 m and 300 m along A'B' is discussed in the text.

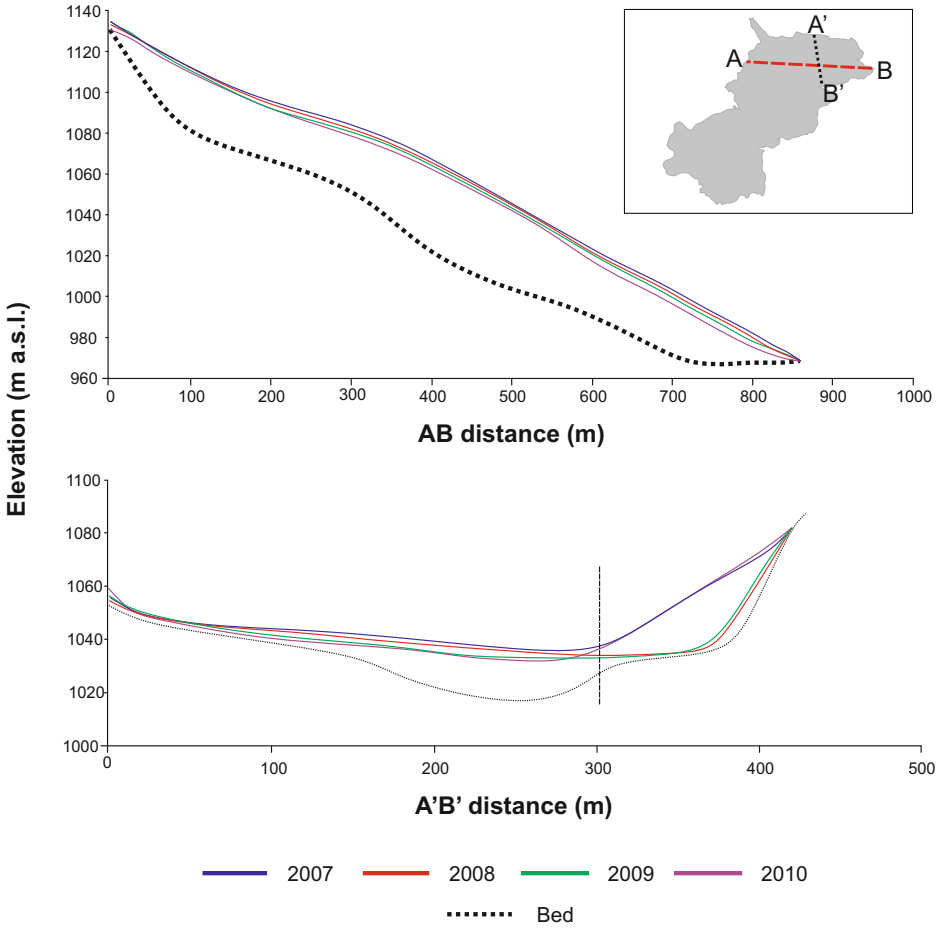

Figure 7.8: Contemporary glacier mean thickness maps (Summer 2007 - 2010)

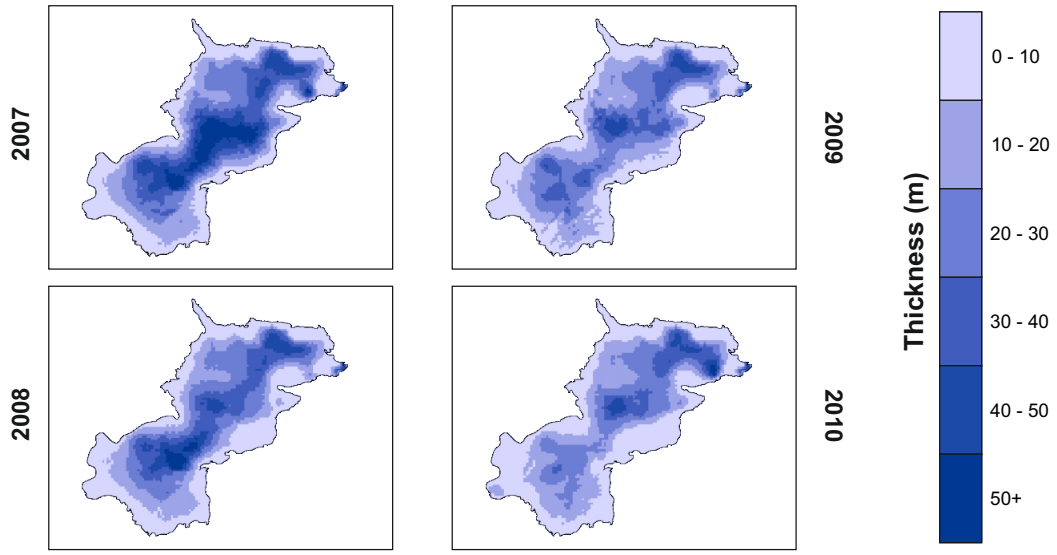

thickness is clearly illustrated with changes in the mean thickness from 22.97 m to 15.29 m from 2007-2010, giving a total change of 7.68±9.61 m. Considering that the change is within the error margin, these changes are not reliable. The errors used here are calculated from maximum, mean and minimum expected thickness surfaces for the 2007-2010 created as per the methodology discussed in section 4.3.5 of chapter 4. Glacier volume change is also summarised in figure 7.9. Over the contemporary period, volume reduced from 5.74 x 10^{-2} km^3 to 3.82 x 10^{-2} km^3. Mean annual volume change for 2007-2008, 2008-2009 and 2009-2010 were 0.10, 0.04 and 0.05 x 10^{-3} km^3 respectively. This gives an overall change of 1.92±2.30 x 10^{-3} km^3. As with the thickness change pattern, the change is within the error margin, these changes are not reliable.

7.5 Change in slope and aspect during 2007 - 2010

Slope and aspect of a glacier surface is extremely important when considering the receipt of radiation. This is discussed in section 2.3.1 of chapter 2. Considering

Figure 7.9: Contemporary mean glacier thickness and volume charts (Summer 2007 - 2010). Short dashes, a solid line and long dashes represent maximum, mean and minimum expected values respectively.

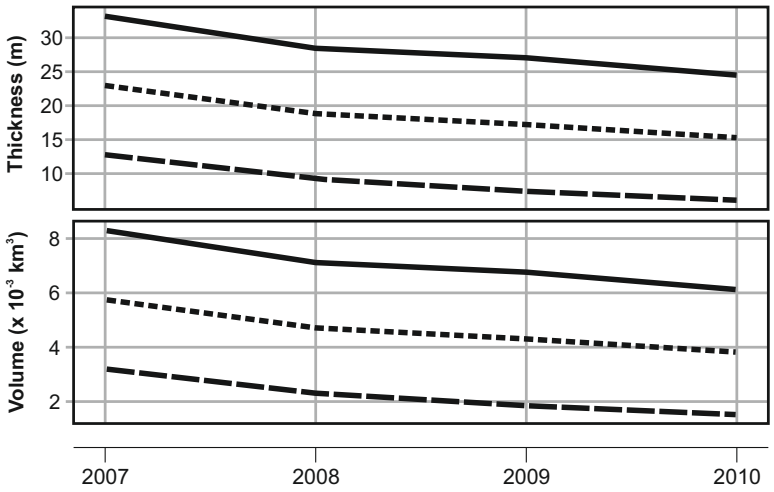

equation 2.7, changes in slope and aspect angles will change values of I and therefore contributions of I to Q (see equation 5.13). The glacier surface in terms of slope is summarised in figure 7.10. Firstly, the entire glacier surface is described in terms of slope distribution. Throughout the contemporary period the glacier is steepest along the north-west tongue, along the southern edge of the glacier terminus to the east and along the edges of the central glacier body. The flattest areas are in the areas of highest and lowest glacier elevation, to the south-west and north of the glacier centre respectively.

Considering slope distribution on a year by year basis, from 2008-2009 slope values are particularly accentuated along the southern edge of the glacier terminus to the east. In 2008 and 2010, the surface is particularly steep along the eastern flank of the glacier centre. The 2008 surface appears steepest in the glacier centre compared to all other years. The majority of the glacier area is represented by the 10-20 and 20-30°categories. Of the 2007, 2008, 2009 and 2010 surfaces respectively, 34%, 38%, 38% and 41% of the area falls within the 10-20°category and 37%, 29%, 30% and 31% falls within the 20-30°category. These descriptives are likely a function of data point distribution as opposed to any natural phenomena.

Figure 7.10: Contemporary glacier slope maps and categorised histograms (Summer 2007 - 2010)

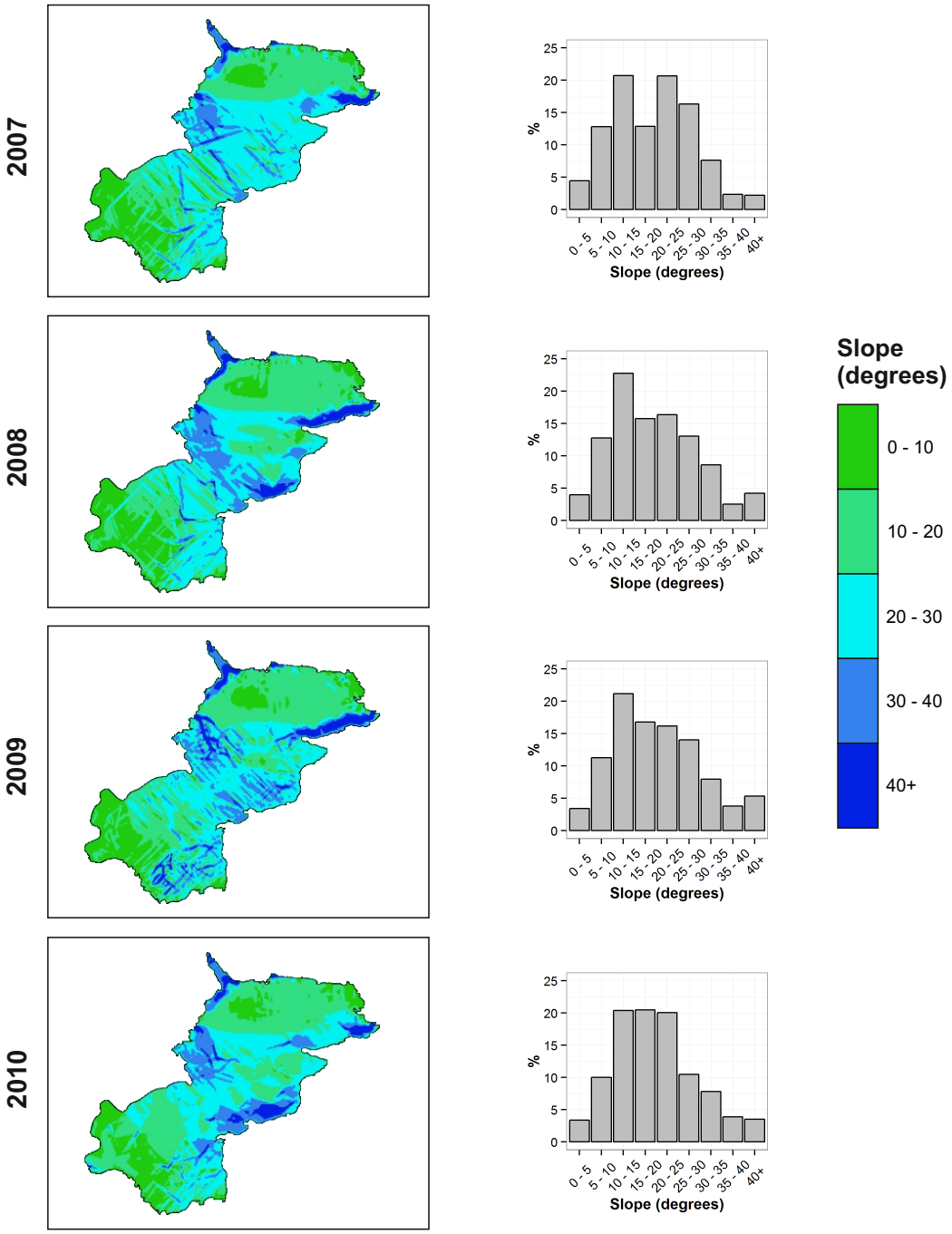

The lower northern glacier area (defined in figure 7.6) is considered in terms of slope distribution specifically as it is assumed to be representative of greatest data consistency due to the highest collection of data points being available in this locale for all years. In the lower glacier area, the majority of the glacier slope area for all years falls within the 10-20°category (more specifically within 10-15°). There are no strong patterns of change between the years, however, some subtle changes can be drawn from the surfaces displayed in figure 7.10 and this in itself provides an opportunity to test how sensitive the SEB is to these changes in slope in terms of how it affects MB. Results of geometry effects on SEB for the contemporary surface are described in section 9.2 of chapter 9. Even if changes in slope are a function of data input and resultant interpolation, the effect of geometry change on SEB is still an important consideration to make as it provides an indication as to how important surface input surfaces are for simple SEB modelling applications.

The glacier surface in terms of aspect is summarised in figure 7.11. Considering the glacier as a whole, the majority of the surface holds a NE aspect, the areas meeting this condition being accounted for from the middle reaches of the glacier. The northern reaches of the glacier as well as the area to the south west, associated with least slopes and lowest and highest elevation respectively hold predominantly easterly aspects. The south-east flank of the glacier has a N aspect (this area is also associated with high hillshade values discussed in section 8.3.2). The only areas with southerly aspects are the steep tongue to the far north-west and the south-eastern tip.

On a year by year basis, no particularly strong trends become apparent. For all years, the majority of the surface is represented by NE aspects with percentage area values of 40%, 43%, 32% and 38% for 2007, 2008, 2009 and 2010 respectively. Compared to all other years, 2008 has the least area represented by N aspects with a slight increase in area in the NE category.

For the northern lower glacier (see figure 7.6) all years, the majority of the surface is represented by NE/E aspects with percentage area values of 23%, 24%, 23% and 23% for 2007, 2008, 2009 and 2010 respectively. There are no apparent strong

Figure 7.11: Contemporary glacier aspect maps (Summer 2007 - 2010). Glacier aspect is predominantly N-E, with the majority of the surface for all years holding a NE aspect.

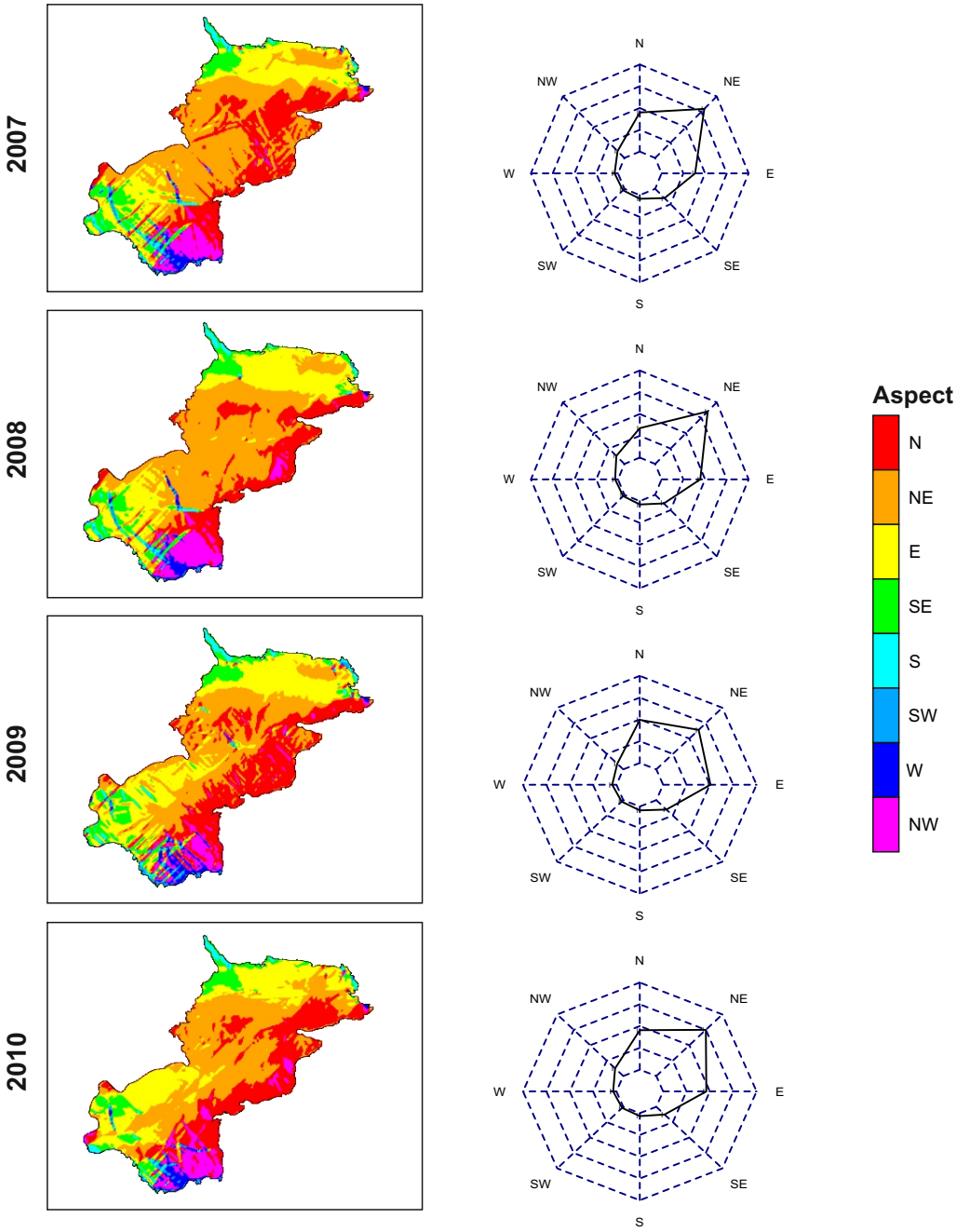

Table 7.2: Mean $\bar{b_n}$ values calculated for annual periods 2007 - 2010.

Year	$\bar{b_n}$
2007-2008	-4.38
2008-2009	-1.16
2009-2010	-2.33

changes in aspect across this part of the glacier throughout the 2007-2010 period.

As with the slope analysis, for the glacier as a whole there are no strong patterns of change in aspect between 2007-2010, however, some subtle changes can be drawn from the surfaces displayed in figure 7.11 and this in itself provides an opportunity to test how sensitive the SEB is to these changes in slope in terms of how it affects MB. As with the slope changes, results of geometry effects on SEB for the contemporary surface are described in section 9.2 of chapter 9.

7.6 Change in glaciological parameters

The glacier is assessed here for different glaciological parameters, specifically mass balance change and basal shear stress. The methods by which the results displayed here are calculated are discussed in section 4.3 of chapter 4.

7.6.1 Glacier mass balance change

Using the glacier difference surfaces discussed in section 7.2, glacier mass balance curves are calculated for 2007-2008, 2008-2009 and 2009-2010. Mass balance change (m w.e) is calculated using a fixed ice density of 900 kg m^{-3} and this is discussed in section 4.3.7 of chapter 4. The values displayed are generalised for elevations on a 1 m interval. Where multiple b_n values exist for a single elevation, a mean value is calculated. Mass balance changes are displayed against elevation for the different mapping intervals in figure 7.12. $\bar{b_n}$ values are calculated for each of the mapping intervals, displayed in table 7.2

The mass balance curves displayed in figure 7.12 are for the entire glacier surfaces and are thus extremely sensitive to data point availability as required to produce

Figure 7.12: Mass balance curves for map intervals 2007 - 2010

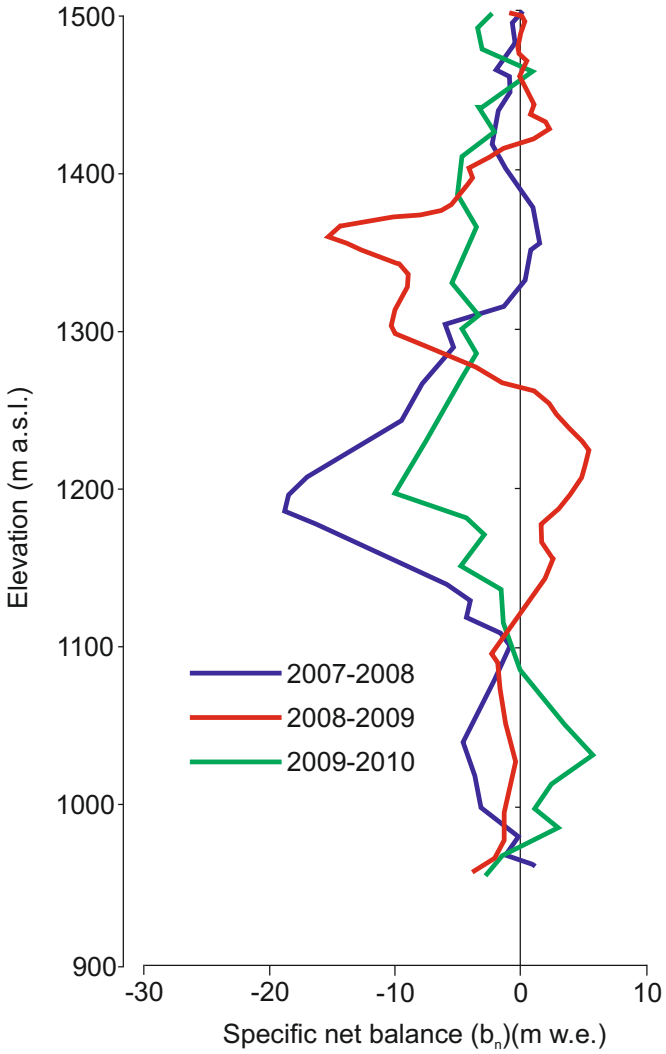

the interpolations. Table 7.2 clearly shows that for the entire contemporary period, the glacier has been in a state of negative balance with with 2008-2009 having the least negative balance and 2007-2008 having the most negative balance. The extreme variation in the patterns and the extremely high rates of change are not environmental signals but a product of the methodology applied. It is useful to compare figure 7.12 with figure 7.5 as the spikes and troughs can easily be related and this relates directly to point gaps and areas of the interpolations with the highest sensitivity discussed in section 7.1. Consequently, these curves are displayed for completeness but are not reliable representations of mass balance with many of the increases/decreases being directly related to data point presence and absence between the different surfaces. It is extremely difficult to assess which changes are real and which are artificial. The data set available for the contemporary glacier (2007-2010) is appropriate for broad pattern changes but not for statistical analysis as here.

7.6.2 Basal stress (τ_b) 2007 - 2010

As in section 6.9.3 of chapter 6, basal stress is useful to consider despite dynamics not having being directly measured within this study. Basal shear stress is calculated using equation 4.7 described in section 4.3.6 of chapter 4, along the glacier centre-line as illustrated by the A-B line in figure 6.9. Slope and thickness values are calculated for a given point from elevation and thickness values taken at a distance equal to the mean thickness of the glacier from either side of the point in question. Stress profiles are displayed in figure 7.13. For all years, figure 7.13 illustrates that maximum τ_b occurs at approximately 700 m from the back of the glacier which is the region of greatest ice thickness as displayed in figure 7.8 and of steeper slopes, as displayed in figure 7.10. This was to be expected as ice thickness is closely linked to τ_b (Thorp, 1991).

Of all of the surfaces, that of 2007 displays the greatest τ_b values (median = 56 kPa) compared to 2010 (median = 30 kPa). These differences are related to point availability from which the elevation surfaces were constructed affecting calculations of surface slope and ice thickness. The 2009-2010 stress profiles

Figure 7.13: Centreline basal stress profiles 2007 - 2010. Profiles are constructed along the A-B centreline as used in figure 6.9. The uppermost chart displays all profiles together with the subsequent charts displaying the stress profiles for individual years.

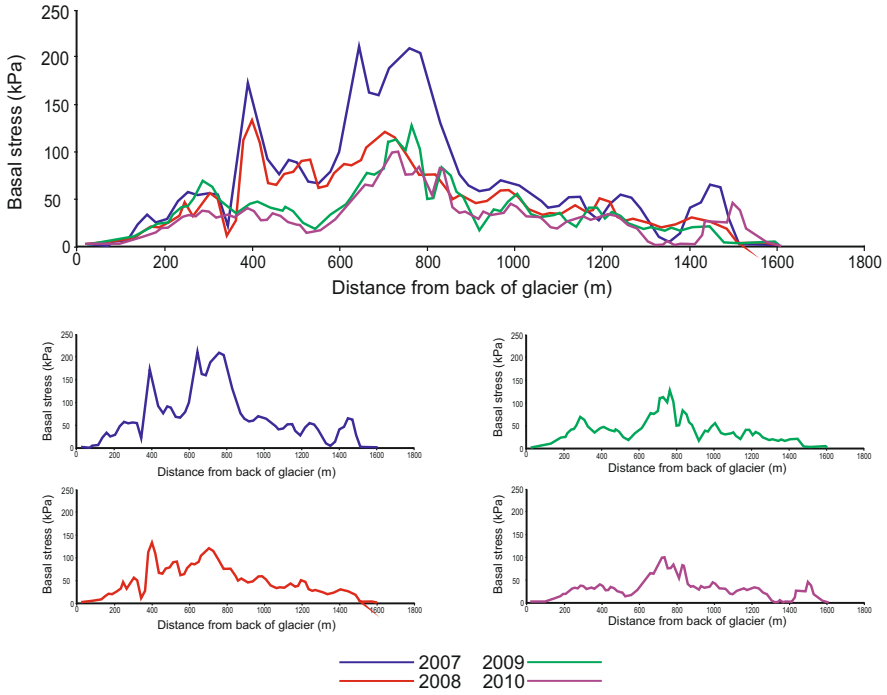

display a much smaller range in values when compared to the 2007-2008 profiles, particularly closer to the back of the glacier. Centreline points were available for surface interpolation for the 2009-2010 surfaces and this will have reduced the surface slope profile. This does not however alter the general stress pattern observed for all years. Caution is paid to making overly specific comments on inter-annual τ_b values, considering the varying reliability of the input elevation surfaces from which surface slope and ice thickness are directly derived.

7.7 Summary

Accounting for glacier change using the geodetic approach (the methods of which are described in chapter 4) is less easily quantified than for chapter 6. This is primarily a function of surface sensitivity to varying input data point cloud density for the different years, as addressed in section 7.1. Nonetheless, acknowledgment of glacier change for the 2007-2010 using an annual time step has been possible. With regard to elevation change, for all years, the glacier shows the majority of change to be within the 0–2 m elevation loss category. This is particularly clear for the lower glacier (to the north as displayed in figure 7.6). Lowering of the lower portion of the glacier is exemplified in long profiles (figure 7.7), although cross profiles are more difficult to interpret (as a function of point cloud density issues). In terms of thickness change, mean thickness has decreased from ˜23 m (2007) to ˜15 m (2010). Greatest thickness values are consistently found to the north/north-east of the glacier. Change in thickness is quantified as an overall mean reduction of 7.68 m ± 9.61 m and is coupled with a volume change of 1.92±2.30 x 10^{-3} km^3. Both of these changes fall within the error margins and this is directly a function of the aforementioned point cloud density issues. No significant changes in slope and aspect are reported. The lack of reported change in slope can be used to infer that changes in τ_b are purely a function of change in thickness. Median τ_b values reduced from 48 kPa (2007) to 33 kPa (2010). As thickness is likely the key driver in τ_b changes, the associated error with thickness change questions how large the real changes in τ_b will have been, however a decrease in stress is believable when considering elevation lowering of the lower glacier, where

input point clouds were most dense and the greatest ice thickness values were found.

Neither area change or terminus retreat are considered for the period 2007-2010 as only one map of the glacier outline was available (for 2008). This is not to say that it is not possible that area change or retreat may have occurred. It is possible however to consider changes in hypsometry as a function of elevation change. Quantifying hypsometric dynamism using the Jiskoot *et al.* (2009) classification system, for 2007-2010, Kårsa was found not to change from its equidimensional status.

This chapter addresses the objective of *accounting for sensitivity of applied geostatistical techniques on reconstructed surface properties* which assists in meeting the project aim of *providing a full 3D glacier geometry reconstruction and assessment of a small mountain glacier, since the beginning of the 20th century, over annual time scales*. The surfaces developed for this chapter are used as inputs for modelling experiments for which the results are presented in chapters 8 and 9. The geometric changes that have been considered here are discussed further with the results of chapter 6 in chapter 10. Considering the associated issues with point cloud density for the 2007-2010 glacier geometry analysis, alternative approaches to point cloud acquisition of glacier surfaces are discussed in section 10.6 of chapter 10.

Chapter 8

Results: Model sensitivity analysis

Le Meur *et al.* (2007) acknowledge the usefulness of more physical SEB model approaches in that they allow for sensitivity analyses to easily be carried out, enabling assessment of the contribution and effects of different parameters within, and associated with, the SEB. This ultimately leads to a better understanding of spatial processes and their effects at the local scale. A grid based distributed SEB model has been developed (see chapter 5) specifically for this study to test the effects of changes in glacier surface geometry over time, in part using a reference balance approach (as discussed in section 2.2.2 and further in chapter 9). This chapter first addresses the set up of model parameters, sensitivity of the model to the method of hillshade calculation and overall confidence in the model output (sections 8.1 - 8.3.2). Following proof of model confidence, the results of scenario model runs are described (section 8.4). The scenarios that are tested provide information of the sensitivity of the model to varying parameter values relative to the default values that are set up in priming the model as described in section 8.1, the methods behind which are explained in chapter 5.

Sensitivity of model parameters is considered separately to the sensitivity of surface DEM development. The latter sensitivity assessment is with regard to variability of input point cloud density to interpolation algorithms required for historical and contemporary surface reconstruction - considered in sections 6.1

and 7.1 of chapters 6 and 7 respectively. Due to the relatively simple approach to calculating SEB applied here, it is prudent to carry out an in depth sensitivity analysis of the different components and factors considered, especially where large changes are found to be the functions of parameter adjustments. Model sensitivity in itself provides information on the different conditions governing SEB and MB change across Kårsa.

This chapter meets the objectives of:

- Developing a user friendly grid based distributed surface energy balance model which uses reconstructed surfaces as an input, combined with meteorological data from the field
- Conducting model scenarios with the developed model to assess the effects of meteorological and topographic forcing on surface energy balance and mass balance change

therefore addressing the project aim of:

- Assessing the sensitivity of the surface energy balance and mass balance change to meteorological and topographical forcing

8.1 Model set up and confidence testing: priming of c, ψ_{min}, and T_{tip} variables

The mass balance model developed by Giesen & Oerlemans (2012) and further developed in this study, requires the setting of a number of variables (see chapter 5). Some of these variables are set using measurements from data available from the field (e.g. τ) whereas others are known or assumed constants (e.g. lapse rate and Lf). Some variables, specifically those required for the calculation of ψ, could not be derived from site specific measurements and are not constants. A selection of values for these variables are provided for a number of different glaciers in different climatic settings, following meteorological analysis by Giesen & Oerlemans (2012). Considering the location to which the model is applied here, of

Table 8.1: Variations in the variables used for the calculation of ψ

Variable	Variable set 1	Variable set 2
c	8.7	8.4
T_{tip}	-25	-19
ψ_{min}	-1.5	+0.2

the variables available, two sites best represent the climate specific to Kårsa. These are Midtdalsbreen and Storbreen, both located in Norway at 60.57°N, 7.47°E and 61.60°N and 8.13°E respectively. These positions compare with 68.35°N, 18.29°E for Kårsa. These two glaciers are the closest climatically to Kårsa, therefore variables from these sites are the most appropriate to tune the model with. Values for τ and α_{ice} are also available for these sites but with data available from Kårsa, site specific values can be used.

Midtdalsbreen and Storbreen represent different glacier types. Midtdalsbreen is an outlet glacier of the Hardangerjøkulen icecap and Storbreen is a valley glacier located to in the Jotunheimen mountain massif (Giesen *et al.*, 2009). In terms of area, Storbreen is smaller at 5.4 km^2 compared to Midtdalsbreen at 6.7 km^2. Both glaciers have a mean NE aspect. In terms of energy contributions to the overall SEB, Midtdalsbreen has a higher portion attributed to turbulent flux due to a strong katabatic regime, associated with the Hardangerjøkulen icecap. Storbreen does not have such a significant turbulent flux contribution to the SEB, but receives more in terms of net radiation (Giesen *et al.*, 2009). In terms of retreat, for the period 1982-2006, Midtdalsbreen retreated 25 m whilst Storbreen retreated 80 m (Giesen *et al.*, 2009).

The Midtdalsbreen and Storbreen variables are referred to as variable set 1 and 2 respectively. With regard to the variations in c, ψ_{min}, and T_{tip} between the two variable sets, see table 8.1.

To test the variability in modelled melt using the two variable sets, experiments were carried out using both the contemporary and historical models for the periods of winter 2009 - winter 2010 and winter 1959 - winter 1978 respectively. These

Figure 8.1: Contemporary and historical modelled melt using different variables for the calculation of ψ, taken from analysis of meteorological data collected at Midtdalsbreen and Storbreen (Giesen & Oerlemans, 2012). Surface lowering is displayed as total surface lowering for the map interval periods of 1959 - 1978 and 2009 - 2010.

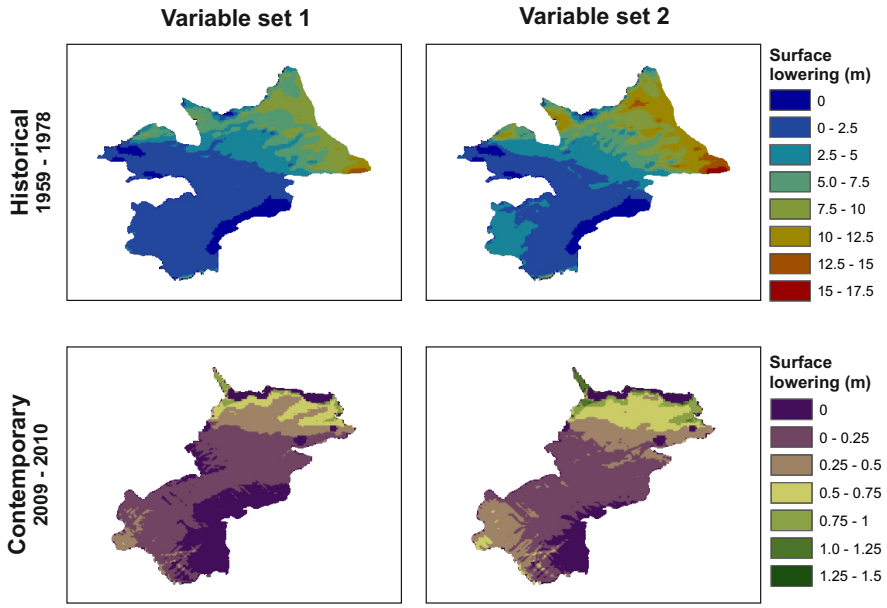

periods were chosen for the contemporary and historical models respectively as they are regarded as the *best* mapped surfaces available. For the contemporary model, this selection is supported as the 2009 and 2010 surfaces have the greatest point coverages in terms of the 2007 - 2010 surface range. The historical model is tested for the 1959 - 1978 period as of all the maps available for the 1926 - 2010 period, these are both created from aerial photographs providing the widest glacier coverage and drafted by the same cartographer using the same process (facilitated at Stockholm University in 1984), which further reduces error. Other surface pairs for periods appropriate for integration with the application of the historical model utilize surfaces derived from base maps developed by different users using different methods and are therefore prone to greater error. Modelled annual surface melt for the aforementioned periods can be seen below in figure 8.1.

Table 8.2: Proportional surface elevation change for the 1959 - 1978 period. Positive and negative values indicate growth and lowering respectively

Category	Geodetic %	Variable set 1 %	Variable set 2 %
-40 - -30	2	0	0
-30 - -20	15	0	0
-20 - -10	38	1	13
-10 - 0	38	99	87
0 - 10	7	0	0

The *best* variable set up is chosen in accordance to the proximity of the proportions of melt occurring within each elevation change band between modelled and mapped surfaces. The proportions of melt for the contemporary and historical periods, derived from geodetic and modelled assessments can be seen in tables 8.2 and 8.3.

For the 1959 - 1978 period, 64% of mapped surface lowering (see chapter 6) occurred within the 0-10 m and 10-20 m ranges, with 32% of melt occurring within each range. For the variable set 1 historical run, 99% of the surface lowering occurred within the 0-10 m range. For the variable set 2 contemporary run, 87% of the surface lowering occurred within the 0-10 m range, with 13% of change within the 10-20 m range. Geodetic analysis of the 1959-1978 surface resulted in the identification of changes greater than 20 m which were not accounted for within the model runs.

For the 2009 - 2010 period, mapped surface lowering (discussed in chapter 7) was greatest in the 0-1 m range, within which 32% of melt occurred, with 26% of change occurring within the 1-2 m range. For the variable set 1 contemporary run, 100% of the surface lowering occurred within the 0-1 m range. For the variable set 2 contemporary run, 99% of the surface lowering occurred within the 0-1 m range, with 1% of change within the 1-2 m range. Geodetic analysis of the 2009-2010 surface resulted in the identification of change within the 2-3 m range which was not accounted for within the model runs.

Table 8.3: Proportional surface elevation change for the 2009 - 2010 period. Positive and negative values indicate growth and lowering respectively

Category	Geodetic %	Variable set 1 %	Variable set 2 %
-3 - -2	22	0	0
-2 - -1	26	0	1
-1 - 0	32	100	99
0 - 1	13	0	0
1 - 2	7	0	0

When considering the difference between the variable 1 and variable 2 surfaces (figure 8.2) similar patterns can be identified for both the historical and contemporary surfaces. More melt was accounted for using variable set 2 and consequently, when considering the difference between variable set output 1 and variable set output 2, most differences are negative. The least change for both surfaces (falling within the 0 and 0 - -1 m and 0 - -0.01 m change ranges for historical and contemporary runs respectively) occurring at overall proportions of 43% and 35% for the historical and contemporary surfaces respectively can be attributed to areas subject to the greatest portions of hillshade throughout the melt season. Conversely, the areas where change was greatest were confined to the southwest, central and north/north eastern parts of the glacier with proportions of 57% and 65% in the -1 - -5 and -0.1 - -0.4 ranges for the historical and contemporary runs respectively. These areas are those least affected by monthly mean hillshade during the summer months. This is implicit that variable set 2 favours radiative processes over variable set 1 which is not surprising when considering variable set 2 is derived from a valley glacier unlike variable set 1 which is derived from an icecap outlet glacier.

Both the historical and contemporary model runs do not account for any increases in surface elevation. Elevation changes have been highlighted in sections 6.3 and 7.2 of chapters 6 and 7 respectively. Such increases accounted for in the geodetic assessment may be the result of mapping errors between the surfaces used to derive the elevation change maps. Some of these changes may of course be real. Glacier growth is not accounted for in the model runs. Regarding melt and assuming that some elevation increases are erroneous, benefits associated with the models are

Figure 8.2: Difference surfaces for the contemporary and historical modelled melt using different variables for the calculation of ψ, taken from analysis of meteorological data collected at Midtdalsbreen and Storbreen (Giesen & Oerlemans, 2012). Surface lowering is displayed as total surface lowering for the map interval periods of 1959 - 1978 and 2009 - 2010.

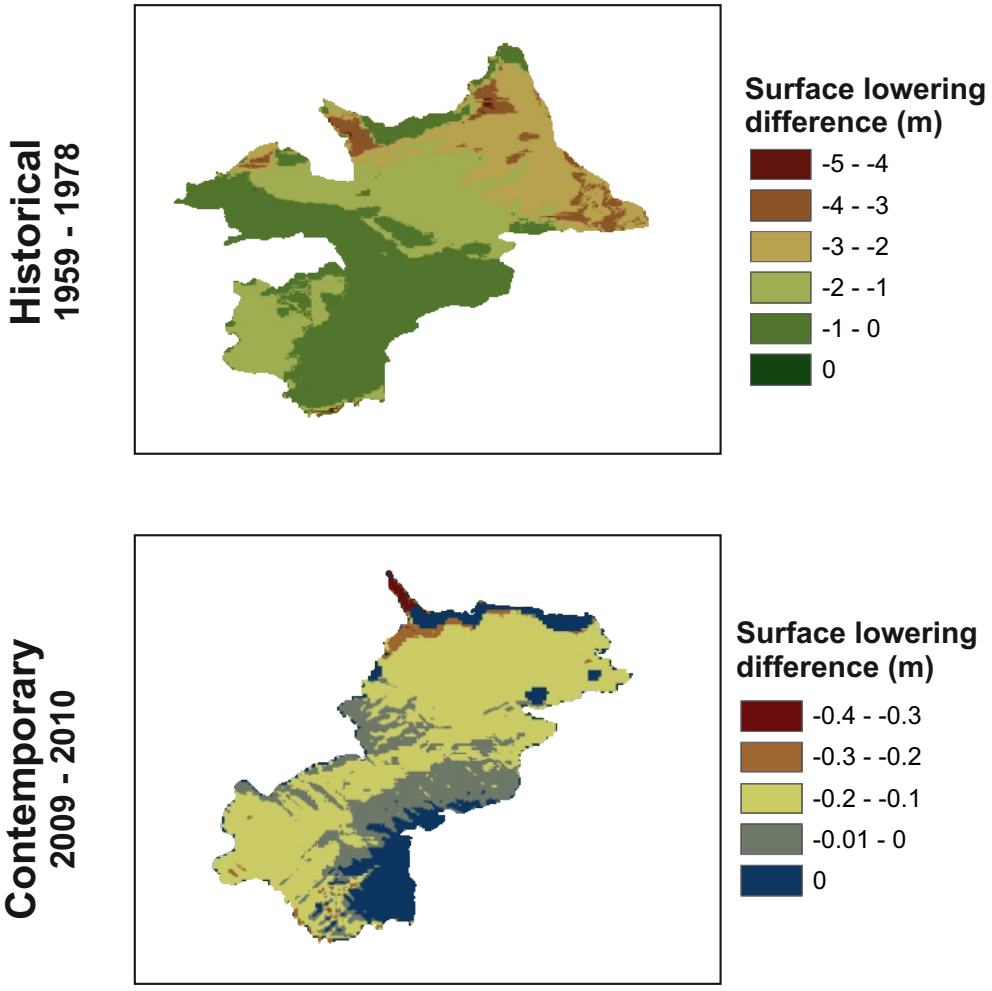

that they are not restricted by errors between the start and end surfaces in the same way as the geodetic analysis, only ever considering the initial input surface and the SEB that propagates across it.

In summary, from this assessment, the set 2 variables are most suitable for the modelling of both contemporary and historical surface lowering as a function of SEB energy surplus, driving glacier surface melt. In terms of the proportions of melt occurring within specific ranges, both models replicate patterns of surface lowering identified by geodetic analysis.

8.2 Model error quantification

Section 8.4 considers the sensitivity of the contemporary and historical models to changes in the values of fixed factors and these results are ultimately summarised in section 8.4.8. Assessing model error as a function of these different factors would require a sub-factor Monte Carlo type sampling strategy whereby all factors would have to be tested, within the range of reasonable distribution of the different factors, whilst considering all factor combinations possible. This would amount to a very large number of model runs and this approach is too intensive with regard to computing power.

Error is thus considered by subtracting modelled change (using the set 2 variable values) from geodetically calculated change for the 1959-1978 and 2009-2010 periods for the historical and contemporary models respectively. Maps representing the spatial variability in model error is displayed in figure 8.3. Negative values indicate model overestimates. The following median error values are calculated - the lower glacier region is defined in figure 7.6 in section 7.2 of chapter 7:

1. Historical model (total glacier): -0.36 m (-0.33 m w.e.)
2. Contemporary model (total glacier): -1.96 m (-1.76 m w.e.)
3. Contemporary model (lower glacier): -0.08 m (-0.08 m w.e.)

Figure 8.3: Model error analysis: historical and contemporary geodetic-model elevation change differences. Negative values indicate model overestimates.

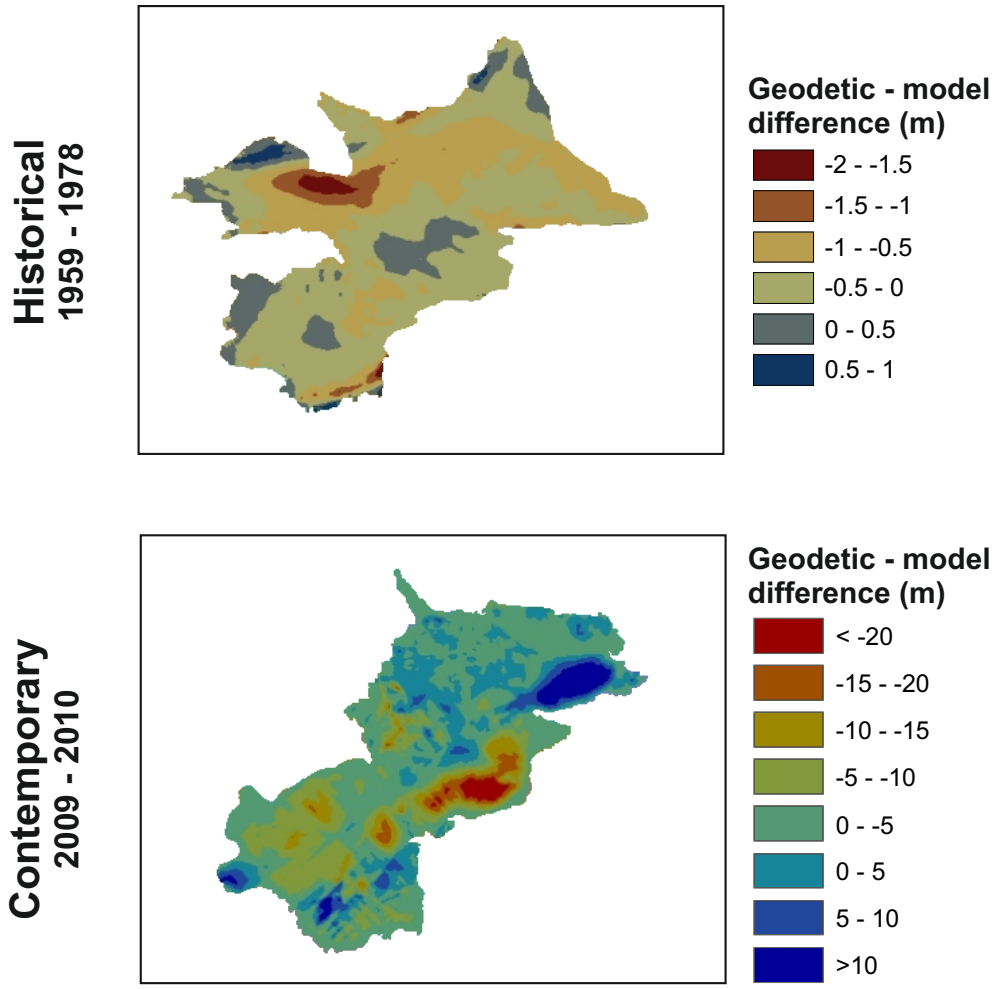

8.3 Topographic shading and consequential hillshade effects

Prior to running a full sensitivity analysis on the different components of the model, the spatial distribution of hillshade is considered first. The effect of hillshade has been found to be extremely important in controlling spatial patterns of SEB and resultant MB (e.g. Arnold *et al.*, 2006b). Thus, by assessing hillshade patterns, resultant coverage (and therefore potential controls on SEB and MB) can be considered when assessing the spatial variability in the effects of other components.

8.3.1 Direct solar radiation at the surface: 1926-2010

To account for the effect that hillshade has over the glacier surface during the summer months when melt and therefore surface change is at its peak, topographic hillshade maps are considered. Hillshade is representative of the effect of topographic shading across the surface, changing over time as a function of solar position relative to surrounding topography and the relationship between a given point on the surface and its relative position to the surrounding topography - hillshade and topographic shade, where referred to, describe the same process. These are displayed in figure 8.4 for all years addressed through the historical reconstruction of the glacier (see chapter 6) at noon for the months of June, July and August. For the 1926 hillshade maps, the Kårsa side glacier is still visible, not being detached until the mid-1930s. Following its detachment, during the 1930s, it is not accounted for in the maps of the glacier from 1943 onwards here, in line with Wallén (1948) who disregarded this portion of the glacier for further study due to it no longer contributing to the main body of the glacier. This rationale is further extended to the minor side lobe accounted for in the Wallén (1948) study divided by the moraine ridge which existed along the southern flank of the glacier. Consequently, considering the aforementioned details, change in hillshade when considering the side-glacier is not considered post-1926. It is included in the consideration of overall hillshade cover of the glacier as a whole how-

ever (figure 8.5) as at the time, the side-glacier was a part of the main glacier body.

For all years, there is a clear increase in the hillshade across the glacier from June to July which is due to increasingly lower sun angles relative to increasing time following the summer solstice (mid-June). The June/July patterns show relatively little change when compared to the August pattern. During these two months, for the years 1926-1959, the ablation area to the north and north east, as well as the south west of the glacier fall mainly within the 0-20% and 20-40 % hillshade categories, the former category being represent of areas least affected by hillshade. The centre of the glacier during these months falls within the categories 40 - 100% although predominantly in the 40-60% category. From 1978-1991 for the June/July period, the ablation area, mainly focused in the east falls increasingly into the 40-60% category more so than for the glacier prior to 1978. This is a function of the glacier retreating back to the former position of the more sheltered areas of the ablation zone where it existed (albeit at a higher elevation) prior to 1978. Spatially, the 1978 and 1991 surfaces show less surface area within the 20-40% categories compared to the glacier prior to 1978. By 2010, during June and July, there are still some areas of the glacier within the 20-40% and 80-100% categories - these areas are equal to those represented in all of the surfaces prior to 2010, being the areas that have showed least change - predominantly the area to the south west and the northern flank. The ablation zone is largely within the 40-60% category with a larger portion of the glacier within the 60-80% category.

Hillshade is much greater across the glacier during August. The area of greatest shade falls at the join between the apparent glacier lobe to the south west (the accumulation zone which is both at the highest elevation and where the slope is steepest). As the glacier reduces in size from 1926-2010, the south western lobe changes little in area when compared to the glacier area to the west and east/north-east. Consequently, the pattern of retreat has resulted in the glacier by 2010 being located in the area of greatest shade. A much larger portion of the glacier appears to be represented by the 60-80% category by 2010 when compared to all years previously, although this pattern propagates for the main glacier body

Figure 8.4: Hillshade across the glacier surface at noon for June, July and August: 1926-2010

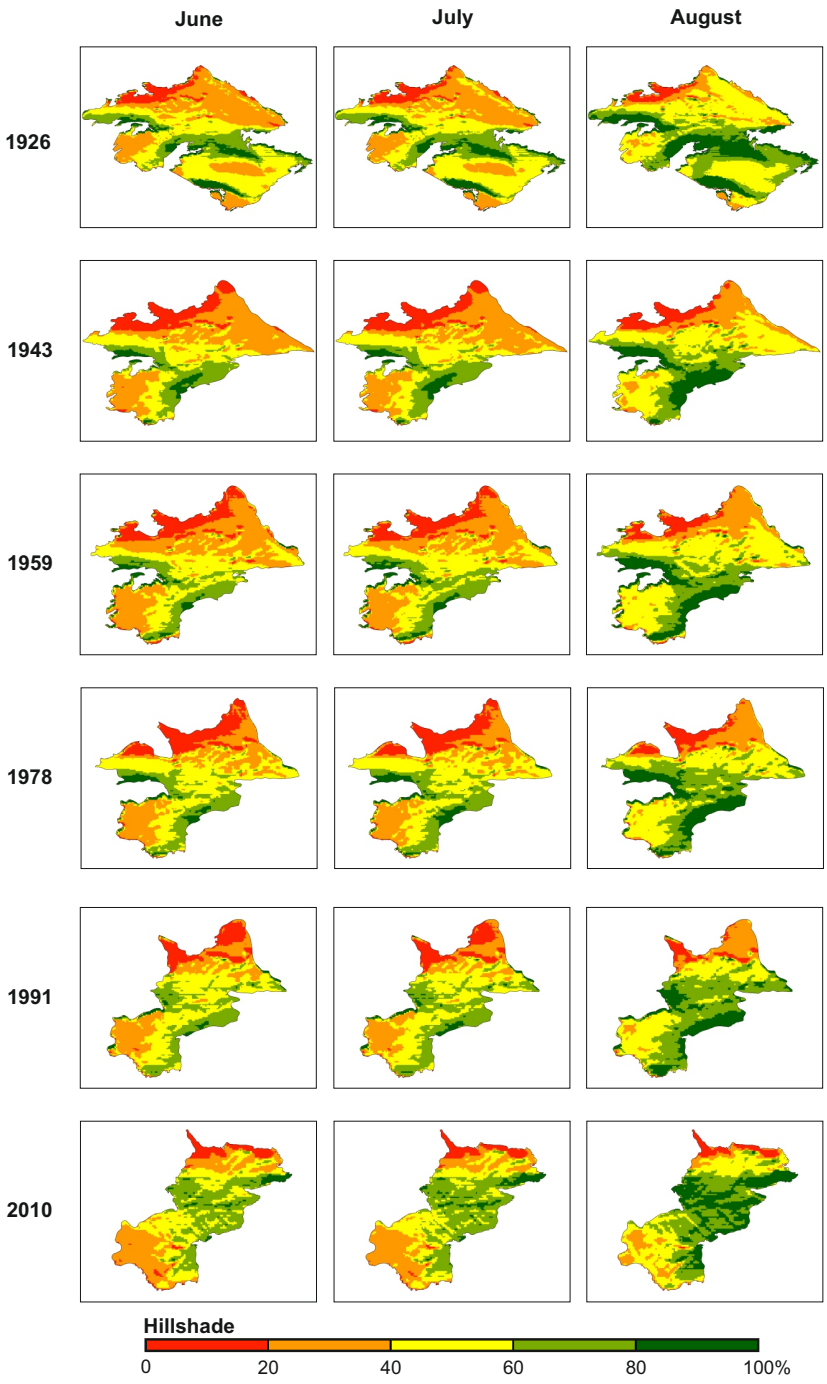

Figure 8.5: Portion of hillshade across the glacier surface at noon for June, July and August: 1926-2010

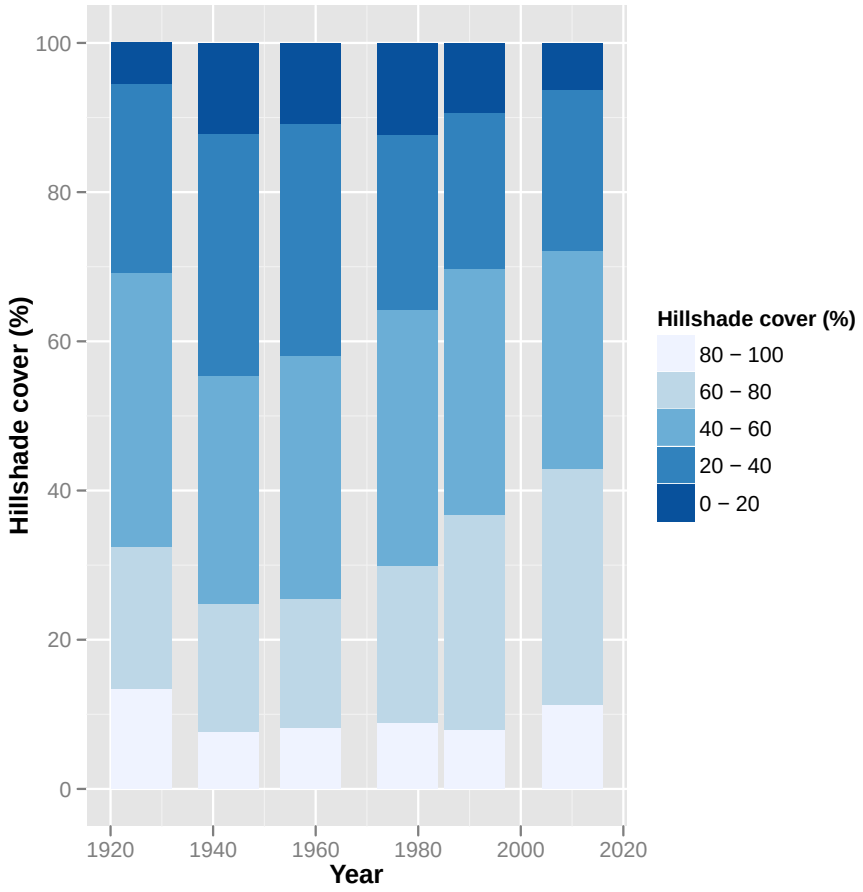

for all years from 1926.

The changing hillshade cover across the glacier during the melt season for the years is quantified in figure 8.5. From 1926-1943, there is a reduction in the area of the glacier represented by the 60-100% hillshade categories. This is attributed to the detachment of the side glacier of which a large portion was in the shade during the months of June-August. From 1943-2010, there is a clear increase in the portion of the overall glacier area represented within the greater hillshade categories. The portion of the glacier within the 60-100% hillshade category increases from 25% to 43% for the 1943 and 2010 surfaces respectively. The areas of least shade reduce from 45% to 28% for the same years. This shows a clear increase in the effect that shade has had over the glacier over time. The increasing hillshade cover of the main lobe of Kårsa from 1926 - 2010 is a function of the glacier retreating to areas of increased shade. The most shaded portion of the glacier represented by the glacier in 1926, making up only a small area of the glaciers then total area, largely accommodates the glacier extent by 2010.

8.3.2 Direct solar radiation at the surface: 2007-2010

Two sets of experiments with regard to radiation incident at the surface as a function of topographic hillshade effects were facilitated for the glacier surface between 2007-2010. Experiments were run for the summer solstice of each year. The first experiment accounts for incoming shortwave radiation at the surface where topographic hillshade is accounted for. This differs to the second experiment where clear-sky conditions are assumed and topographic hillshade is not accounted for. The spatial variability of these experimental results are displayed in figure 8.6. Experimental runs were also carried out for the spring and autumnal equinoxes. Due to low sun angles associated with the shorter daylight hours at the latitude in question, mean daily $S_{in,TOA}$ are small and this results in very small values for I (see equations 5.10 and 5.7). For this reason, the resultant surfaces are not displayed.

Figure 8.6: Surface radiation at the glacier surface: clear sky vs. shaded conditions (Summer solstice). Maps of variability are display only for the solstice as this is when energy from radiation is greatest and is most important for melt. Shade increases through July and August (as identified in figure 8.4) but the spatial variation between 2007-2010 is negligible.

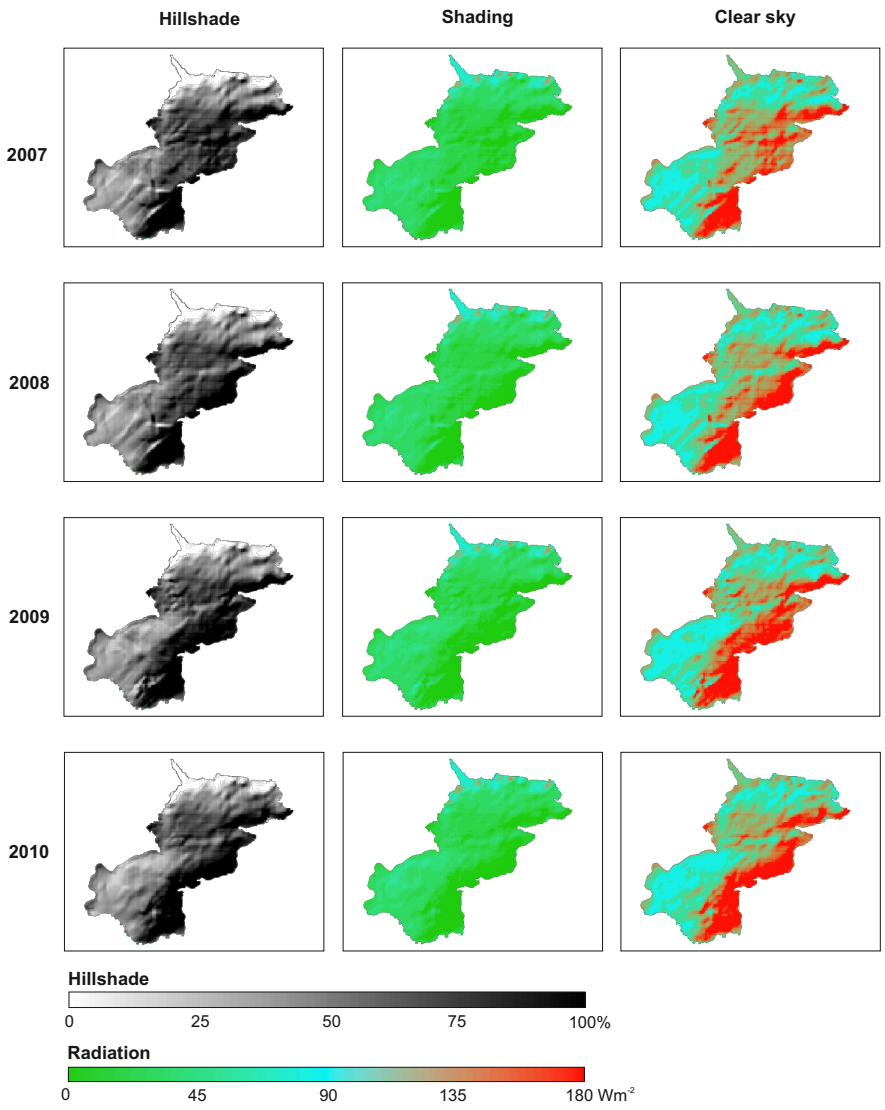

Shading is greatest along the south eastern edge of the glacier with areas of least shade occurring along the northern portion of the glacier towards the perimeter. The south west portion of the glacier also receives little shade. This general shading pattern is apparent for 2007-2010 although there are some very subtle variations. The 2007 appears to receive more shade along the centre of the glacier than 2008-2010. The 2009 and 2010 surfaces have less shade across the south west lobe than 2007-2008.

Considering the surface measured shortwave radiation distribution, whilst accounting for the effects of topographic hillshade, the highest values occur along the northern glacier edge and to the north west where shade is most limited. This is where the glacier ablation zone occurs. The south west of the glacier also shows a slightly higher radiation receipt than any areas to the south east where hillshade is greatest.

Under clear sky conditions, the spatial distribution of surface radiation at the glacier surface is inverse to that which occurs under shaded conditions. Generally, areas receiving the most radiation occur along the south western edge whereas those receiving the least occur to the north east. The extreme south western edges show high levels of radiation receipt but this is likely a relic from the surface interpolation process and thus should be disregarded. The 2008-2010 surfaces are relatively uniform compared to one another. The 2007 surface, whilst still displaying the same general pattern, shows some areas of increased radiation receipt across the centre of the glacier - this may be due to micro-topographical effects relating to the 2007 DEM.

8.4 Model sensitivity analysis

In this section, the sensitivity of the models to different parameters, in terms of surface elevation change and mean summer Q (calculated from energy surfaces for June, July and August) for test periods of August 1959- June 1978 (using the historical model) and October 2009 - December 2010 (using the contemporary model), are tested. These surfaces are considered the *best* available for the historic

and contemporary periods respectively as described in section 8.3.1. The factors to which model sensitivity is tested are:

1. Atmospheric transmissivity (proxy) (τ)
2. Snow albedo ($\alpha_s now$)
3. Ice albedo ($\alpha_i ce$)
4. Wind factor value
5. Snowfall temperature threshold
6. Temperature lapse rate value
7. Winter snowpack thickness

8.4.1 Sensitivity Analysis: τ

Values of τ in the range of 0.35 - 0.55 with 0.05 increments were experimented with, using both the contemporary and historical models for the 2009-2010 and 1959-1978 time periods respectively, for reasons discussed in section 8.1. The results of these experiments are discussed within the context of the separate models.

Smaller values for τ resulted in a greater value being attributed to radiation component I which results in a greater value for Q. This instigates a greater instance of elevation change at a given cell, the effect of which is however dampened as values for τ increase through to 0.55, reducing the value of I and therefore Q. The spatial distribution for the effect of changing τ can be seen in figures 8.7 and 8.8.

For both model runs, the increases in melt and surface Q are most apparent in the northern and south western portions of the glacier - the ablation zone and the upper accumulation area respectively. The areas of the glacier where these changes are most pronounced are affected less by hillshade than the more central portions of the glacier where variations in spatial distribution of elevation change and Q are more limited. Both Q and surface elevation change have similar spatial patterns

Figure 8.7: Contemporary model response in terms of surface elevation change and June/July/August mean summer Q, to changing values of τ from 0.35 - 0.55 for the period of October 2009 - December 2010. Mean summer surface Q is calculated as the mean of Q values extracted for the middle of June, July and August 2010.

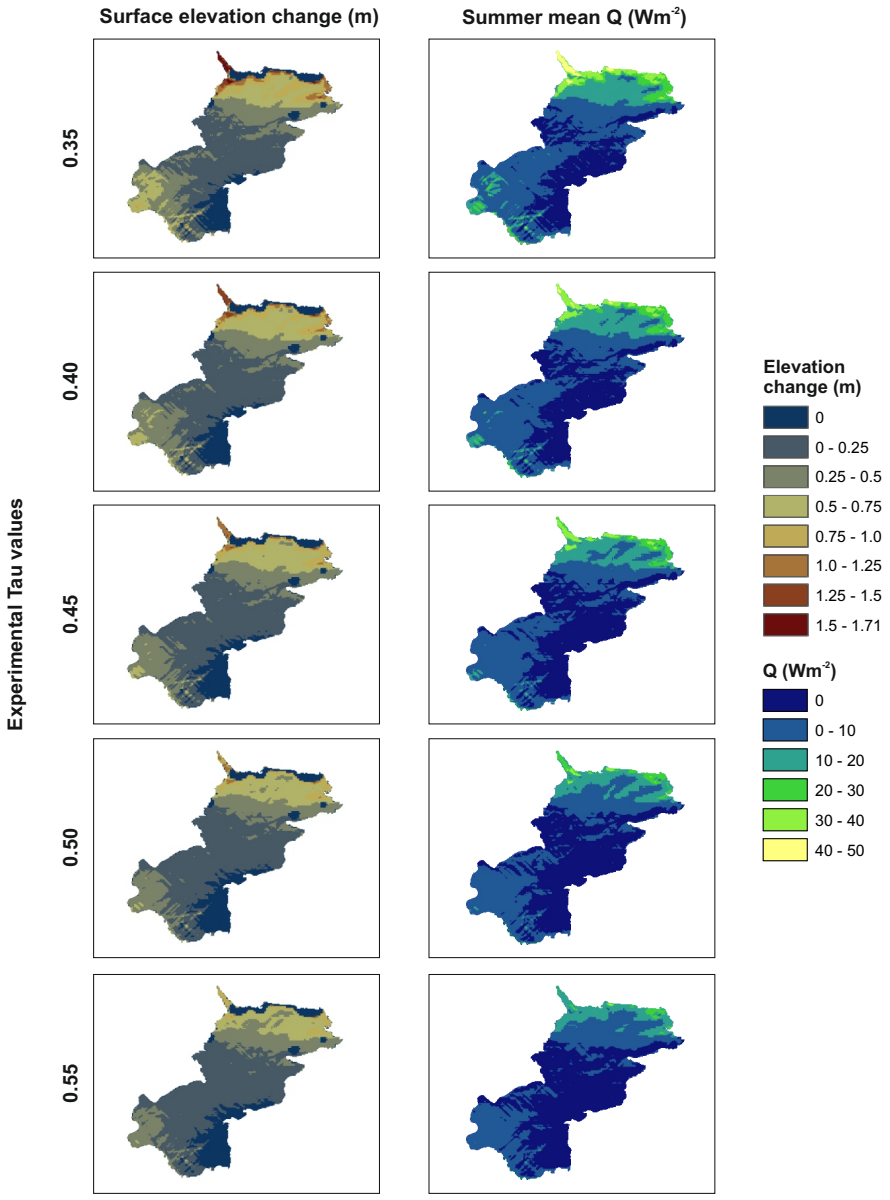

Figure 8.8: Historical model response in terms of surface elevation change and June/July/August mean summer Q, to changing values of τ from 0.35 - 0.55 for the period of August 1959 - July 1978. Mean summer surface Q is calculated as the mean of Q values for June, July and August of 1969 (randomly selected from the year test range)

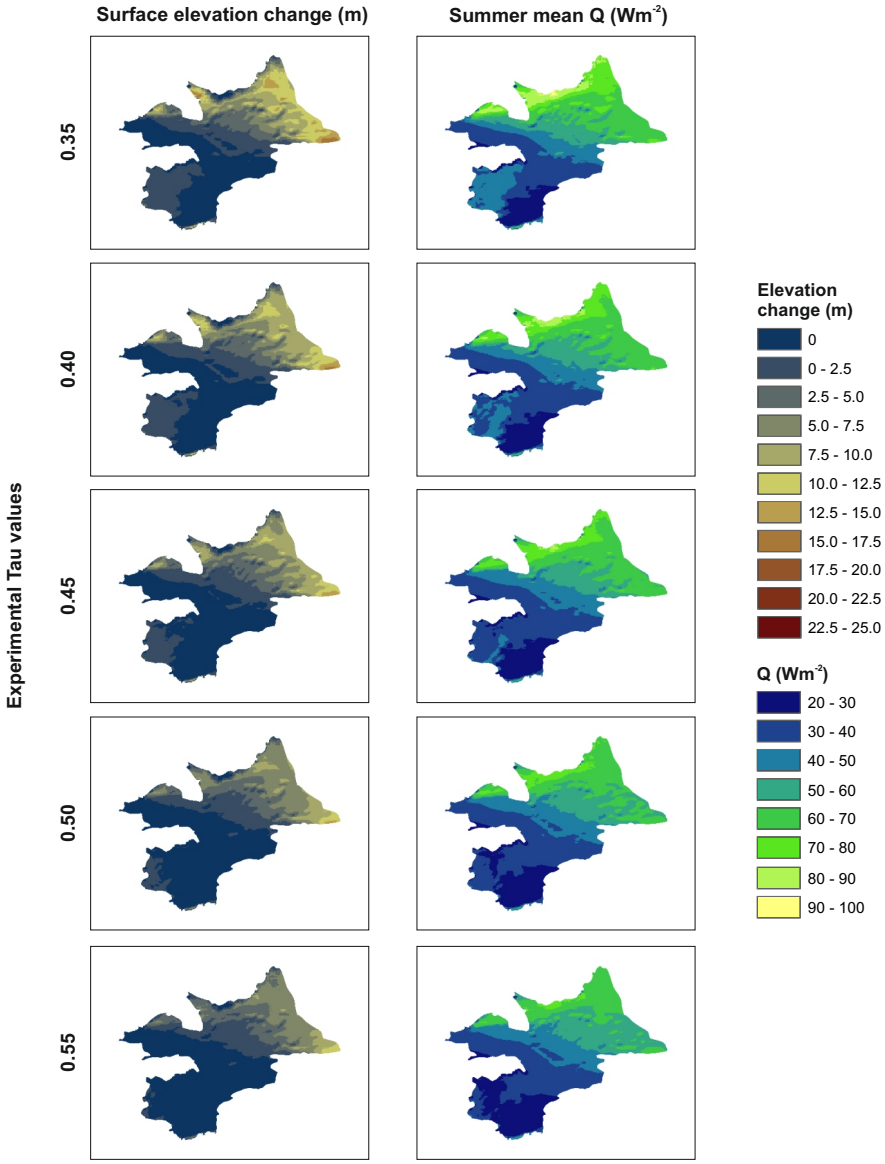

as would be expected, with Q driving surface elevation change. Differences in the patterns of Q and elevation change are more apparent in figure 8.7 than figure 8.8 which is in part attributable to the method of calculating the mean Q surfaces using mid values for June, July and August - this method is likely to miss of the most significant melt events, a signature of which will be left on the total elevation change surfaces. For both figures 8.7 and 8.8, the surface change and Q surfaces will inevitably show some disagreement as the former are totals whereas the latter are averages. Also, throughout the model run time frames, snow melt occurs. Whilst there is snow present, elevation change will not occur and thus further disagreements between the surface change and Q surfaces may occur.

Considering changes in proportional elevation change following changes in τ (see table 8.4), within the 0 - 0.25 m change category proportional surface melt reduced for all experiments as τ was reduced from 0.55 to 0.35. For all experiment outputs, proportional changes greater than 0.25 m increased as τ decreased. In terms of the extreme values, within the 0 - 0.75 m change category, 97% and 90% of the change occurred for τ values of 0.55 and 0.35 respectively, indicating greater surface elevation change with lower τ values. For the historical experiment outputs (table 8.5), the proportion of melt occurring within the 0 change category decreased as τ decreased. for change between 0 - 2.5 m, the melt proportion increased with decreasing values for τ which is balanced by the increase in the 0 m change category. For all surfaces, the proportion of elevation change greater than 2.5 m collectively increased as τ decreased, as would be expected for greater elevation change with smaller values for τ. In terms of the extremes, within the 0 - 7.5 m change category, 97% and 78% of the change occurred for τ values of 0.55 and 0.35 respectively.

The pattern of change in terms of the extreme values used to test τ sensitivity can be seen in figure 8.9. For the historical surface, between the two τ values, the greatest differences are to the north/ north east. This is where elevation (in terms of m a.s.l.) is lowest and hillshade is least affecting. Consequently, where Q is greater as a function of lower τ values, snow melt will be more efficient, revealing the ice surface earlier during the ablation season and resulting in more significant elevation change. Where changes are less pronounced, and thus sensitivity to

Table 8.4: Contemporary surface categorical elevation change following changes in τ

Elevation change (m)	Experimental Tau values				
	0.35 %	0.4 %	0.45 %	0.5 %	0.55 %
0.00	12.18	13.05	14.16	15.25	16.31
0.0 - 0.25	38.03	41.83	44.54	47.13	49.73
0.25 - 0.50	25.42	25.18	23.62	21.92	21.11
0.50 - 0.75	14.22	12.79	12.31	11.55	10.09
0.75 - 1.0	6.35	4.81	3.98	3.52	2.69
1.0 - 1.25	2.38	1.49	1.32	0.63	0.07
1.25 - 1.50	0.83	0.84	0.08	0.01	0.00
1.50 - 1.71	0.59	0.01	0.00	0.00	0.00

Table 8.5: Historical surface categorical elevation change following changes in τ

Elevation change (m)	Experimental Tau values				
	0.35 %	0.4 %	0.45 %	0.5 %	0.55 %
0	35.06	38.21	42.72	48.37	52.79
0 - 2.5	25.26	24.06	21.88	18.35	16.47
2.5 - 5.0	9.74	10.25	10.61	11.63	13.56
5 - 7.5	8.29	9.35	11.98	15.78	14.24
7.5 - 10.0	9.77	12.60	10.58	4.81	2.23
10 - 12.5	8.90	4.66	1.79	0.87	0.70
12.5 - 15.0	2.38	0.70	0.44	0.20	0.00
15 - 17.5	0.59	0.17	0.00	0.00	0.00

Figure 8.9: Historical and contemporary difference surfaces according to extremes in τ value settings

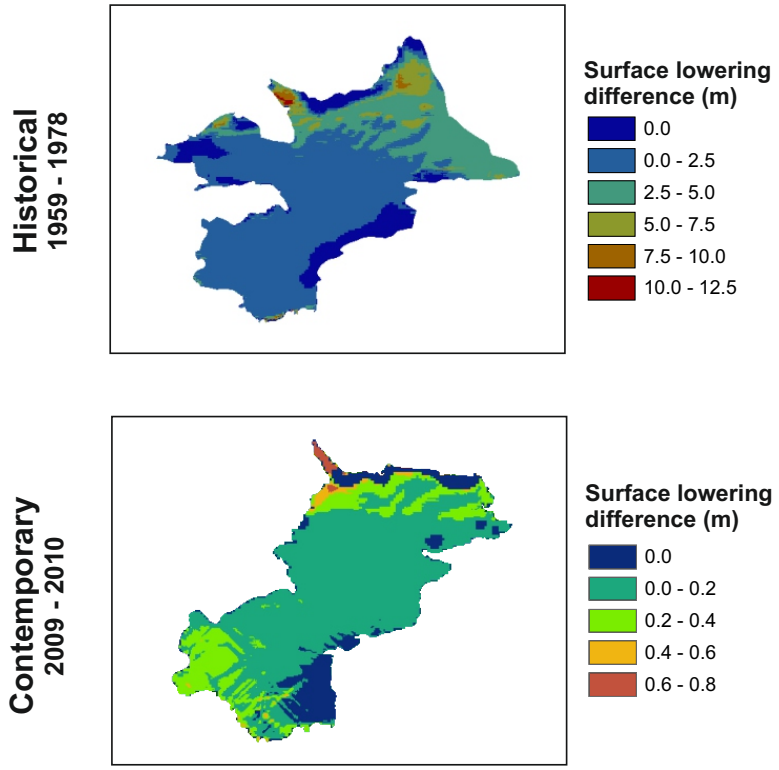

changes in τ is reduced, elevation (m a.s.l.) is greater resulting in lower temperatures (therefore input of ψ to Q) and hillshade is greater. As a consequence of this, snow melt rates will be reduced, therefore protecting the ice surface from exposure and thus hindering elevation change. For the contemporary difference surface, changes and therefore sensitivity to changes in τ are most pronounced in the north and to the south west. There is much less relative change when compared to the historical difference surface, changes for the contemporary surface being limited to where hillshade is least affecting.

Considering the spatial variations of elevation change identified from the difference surfaces created from the historical and contemporary model runs from the testing of the extreme values of τ, hillshade appears to be quite important. Sensitivity to

τ tends to be much greater where hillshade has less presence.

8.4.2 Sensitivity Analysis: α_{snow}

α_{snow} is tested for values in the range of 0.60 0.80 with 0.05 increments, using both the contemporary and historical models for the 2009-2010 and 1959-1978 time periods respectively to test the sensitivity of the model in terms of the distribution of melt and the calculation of Q. These intervals are selected as they fall within an established range of generic snow albedo values (Paterson, 1994). A default value of 0.70 is used for α_{snow} as discussed in section 5.4.2 of chapter 5. The results of these experiments are discussed within the context of the separate models.

Where α_{snow} was smaller than the 0.70 default setting, increased melt was observed — converse to where α_{snow} was greater than the default. The spatial distribution for the effect of changing α_{snow} can be seen in figures 8.10 and 8.11.

For all contemporary sensitivity tests, melt is consistently focused to the north of the glacier in the presumed ablation zone. As the value of α_{snow} reduces, the amount of modelled surface elevation changes also increases to the south west. The melt pattern changes are also replicated by the distribution of Q across the surface. The south west portion of the glacier is the most elevated and thus, as a function of the applied lapse rate will be susceptible to the lowest air temperatures which will in turn result in smaller contributions from ψ to the overall surface energy Q and therefore ice melt. The areas of greatest melt are also located where hillshade is of the lowest values.

The observed pattern for the contemporary tests also exists throughout the historical suite of experiment results. Obvious differences exist in the area of (relatively) most melt which is more focused to the north east than the north in general as for the contemporary results. This can be explained in part to the change in hillshade distribution with the old glacier terminus being relatively more exposed to the east than to the north alone, resulting in a relative increase in melt as a function of location. As α_{snow} is reduced, glacier surface elevation increases from the north

east to the west as well as in the south west region (as for the contemporary experiments).

In terms of the proportions of melt occurring within the categories defined in figures 8.10 and 8.11, for the contemporary model output (see table 8.6), surface elevation change in the 0 - 0.25 m category decreased as α_{snow} decreased from 0.80 - 0.60. Conversely, melt occurring in categories between 0.25 - 1.66 m increased as α_{snow} decreased. The decrease in the 0 - 0.25 m category with decreasing values for α_{snow} can be explained as elevation changes migrate into the larger (> 0.25 m) elevation change categories. Comparing the extreme values for the contemporary experiments, for the 0 - 0.75 m elevation change category, 98% and 89% of melt occurred for α_{snow} values of 0.8 and 0.6 respectively.

For the historical model outputs (see table 8.7), there is no change within the 0 m elevation change category (with all instances being attributable to positions where ice thickness is at 0 m from the beginning of the model run and therefore elevation change is not possible). For the 0 - 2.5 m elevation change category, there is less proportional melt modelled as α_{snow} decreases from 0.80 - 0.60. Collectively for categories indicative of elevation change greater than 0.5 m, the proportion of modelled melt increases with reductions in the value of α_{snow}. Comparing the extreme values for the historical experiments, for the 0 - 7.5 m elevation change category, 89% and 69% of melt occurred for α_{snow} values of 0.8 and 0.6 respectively.

To assess the main differences between using α_{snow} values of 0.60 and 0.80, difference surfaces are displayed in figure 8.12 for both the contemporary and historical models. These surfaces are calculated by subtracting the 0.80 experimental surfaces from the 0.60 experimental surfaces. For the historical experiments, relative changes are most pronounced across the northern area of the glacier with some increases to the south west. Relative changes area least from the south east perimeter to the west north west - this is where hillshade is greatest. Coupled with a large value of 0.80 for α_{snow}, this appears to hinder snow melt, by limiting the exposure of the ice surface, required for elevation change to be recorded. The most noticeable changes are where the glacier elevation (m a.s.l.) is lowest and therefore

Figure 8.10: Contemporary model response in terms of surface elevation change and June/July/August mean summer Q, to changing values of α_{snow} from 0.60 - 0.80 for the period of October 2009 - December 2010. Mean summer surface Q is calculated as the mean of Q values extracted for the middle of June, July and August 2010.

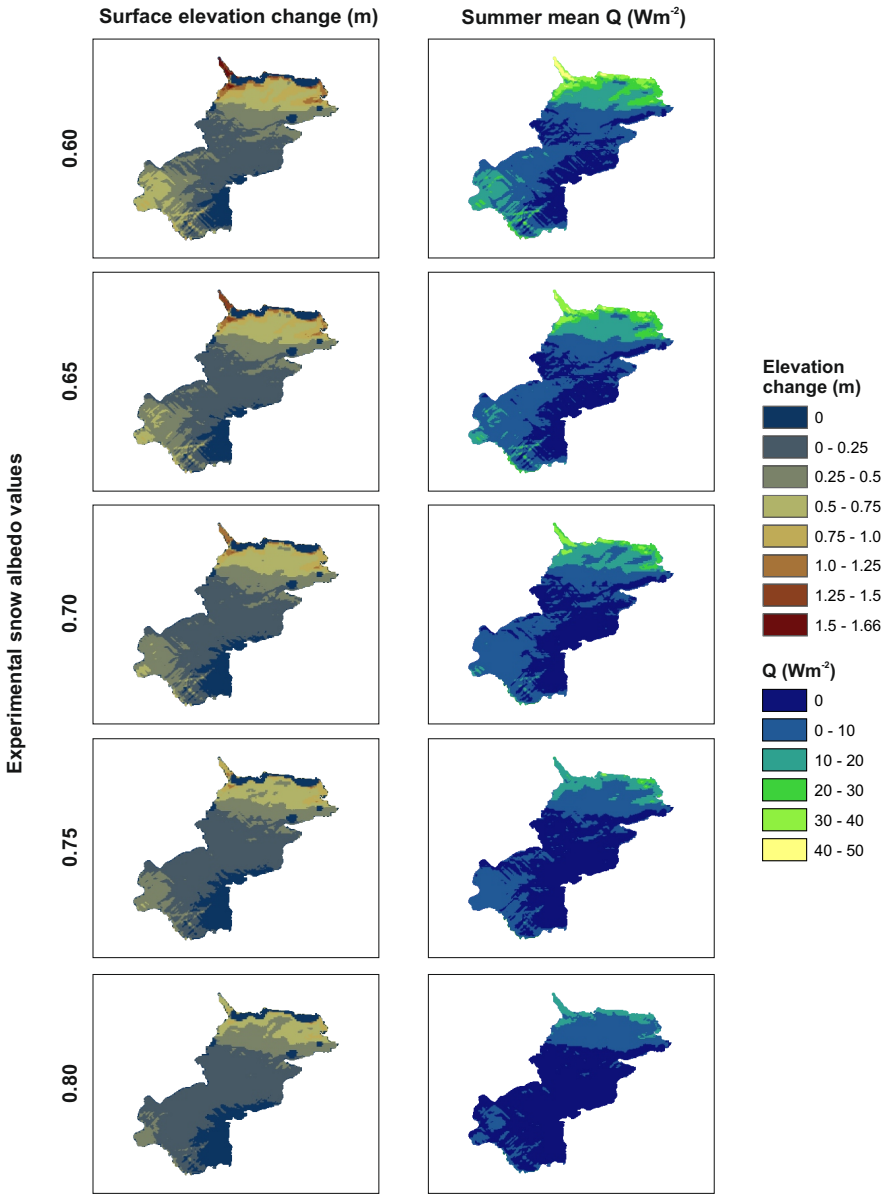

Figure 8.11: Historical model response in terms of surface elevation change and June/July/August mean summer Q, to changing values of α_{snow} from 0.60 - 0.80 for the period of August 1959 - July 1978. Mean summer surface Q is calculated as the mean of Q values for June, July and August of 1969 (randomly selected from the year test range)

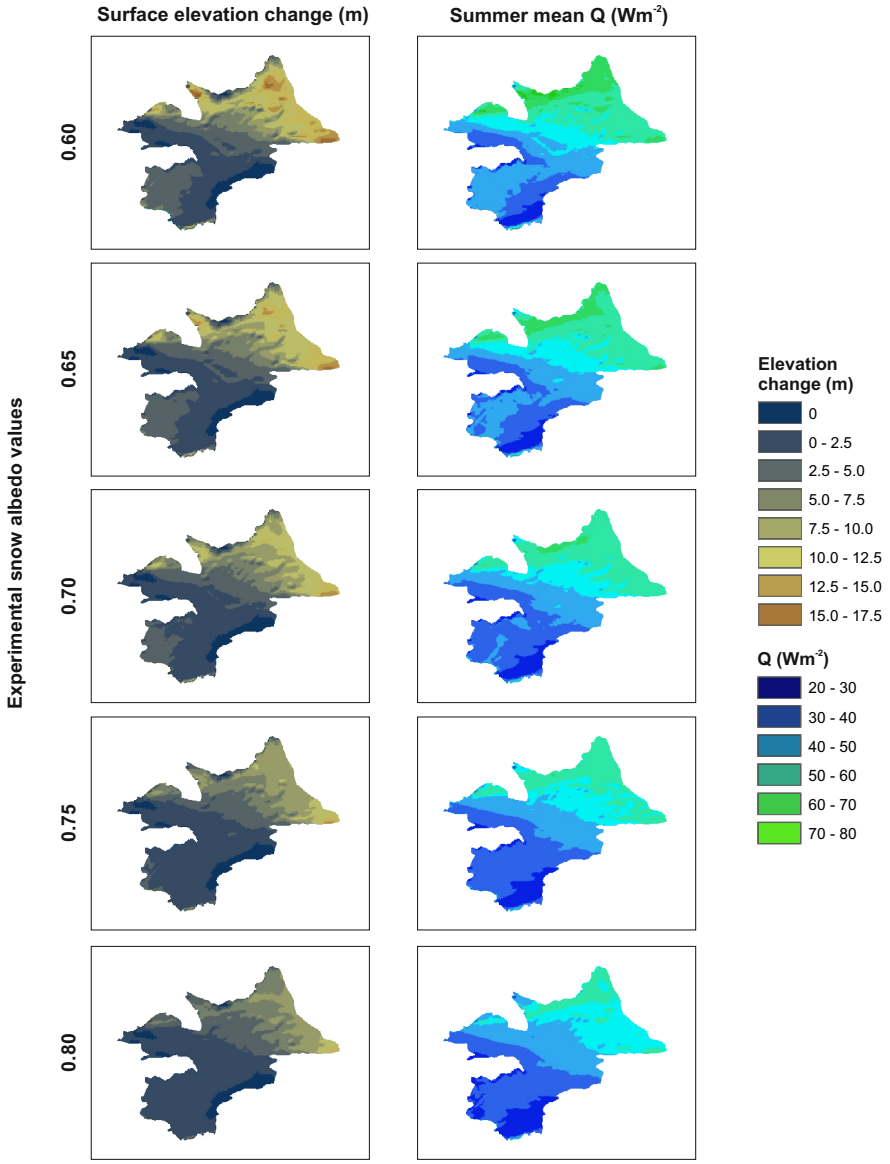

Table 8.6: Snow albedo sensitivity results: contemporary results

	Experimental snow albedo values				
	0.6	0.65	0.7	0.75	0.8
Elevation change (m)	%	%	%	%	%
0	11.48	12.61	14.16	16.11	18.41
0 - 0.25	36.20	40.67	44.54	48.28	53.16
0.25 - 0.5	25.96	25.72	23.62	20.96	17.76
0.5 - 0.75	15.65	13.42	12.31	10.96	8.98
0.75 - 1	6.90	5.13	3.98	3.32	1.67
1 - 1.25	2.50	1.58	1.32	0.36	0.03
1.25 - 1.5	0.82	0.87	0.08	0.00	0.00
1.5 - 1.66	0.50	0.01	0.00	0.00	0.00

Table 8.7: Snow albedo sensitivity results: historical results

	Experimental snow albedo values				
	0.6	0.65	0.7	0.75	0.8
Elevation change (m)	%	%	%	%	%
0	6.63	6.63	6.63	6.63	6.63
0 - 2.5	26.93	30.17	36.09	45.30	50.93
2.5 - 5	24.80	24.76	21.88	16.08	16.55
5 - 7.5	10.17	9.94	10.61	12.63	15.57
7.5 - 10	7.42	8.62	11.98	15.91	8.89
10 - 12.5	9.14	12.36	10.58	2.55	0.97
12.5 - 15	10.46	6.05	1.79	0.78	0.47
15 - 17.5	3.43	1.29	0.44	0.14	0.00
17.5 - 20	0.95	0.19	0.00	0.00	0.00
20 - 22.5	0.08	0.00	0.00	0.00	0.00

Figure 8.12: Difference surfaces of model outputs for α_{snow} values between 0.60 and 0.80. The surfaces are calculated by subtracting the 0.80 surfaces from those calculated with a value of 0.60. Therefore, values indicate where surface change was greater under conditions where α_{snow} was set to 0.60.

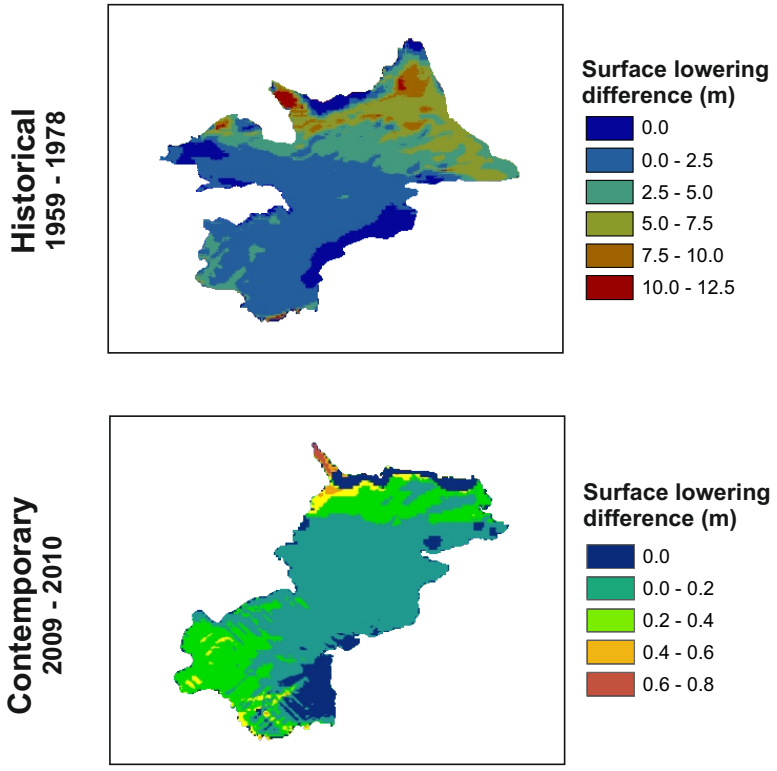

air temperatures are highest (which directly influences ψ and its contribution to Q). Where α_{snow} is of a lesser value, snow will melt faster exposing the ice surface and allowing energy surplus to drive elevation change. For the contemporary experiment difference surfaces, a α_{snow} of 0.60 results in greatest change in the northern and south western areas of the glacier with little change across the centre of the glacier. These areas are those least affected by hillshade and consequently the rate of snow melt will increased, allowing exposure of the ice surface. The difference between the two values of α_{snow} is not as apparent as for the historical model as the change in glacier size by 2009/2010 results in a much larger portion of the glacier being affected by hillshade which retards snow melt rates to a great extent.

8.4.3 Sensitivity Analysis: α_{ice}

To test the sensitivity of the model in terms of the distribution of melt and the calculation of Q, experiments are run using values of 0.29, 0.34, 0.39, 0.44 and 0.49 for α_{ice}. These intervals are selected as they fall within an established range of generic ice albedo values (Paterson, 1994). A default value of 0.39 is used for α_{ice} as discussed in section 5.4.2 of chapter 5. The results of these experiments are discussed within the context of the separate models.

Where α_{ice} was smaller than the 0.39 default setting, small areas of increased melt were observed. Decreases in the amount of total melt resulted from increasing the value of α_{ice} relative to the default. The spatial distribution for the effect of changing α_{ice} can be seen in figures 8.13 and 8.14.

The contemporary model outputs do not appear to be particularly sensitive to changes in α_{ice}. There is some more melt associated with smaller values for α_{ice} which can be identified to the far north east and the upper north west. There are some very slight increases to the south west. Mean melt values of 0.28 m and 0.25 m are recorded for models using α_{ice} values of 0.29 and 0.49 respectively.

As with the contemporary model, the historical model is not particularly sensitive to changes in α_{ice}. Observable change appears to be along the north east perimeter of the glacier, which is associated with low hillshade values, lower elevations and thinner winter snow pack. The enhancement of Q can be seen clearly in figure 8.13, with the greatest changes being focused to the north of the glacier. Mean melt values of 4.54 m and 4.19 m are recorded for models using α_{ice} values of 0.29 and 0.49 respectively.

Considering proportional melt across the surface (table 8.8), for the contemporary model run, within the 0 - 0.25 m category, values decreased as α_{ice} decreased. This would be expected as for all categories greater than 0.25 m change, values increased as α_{ice} decreased. In the range 0 - 0.75 m, 94% and 95% of elevation change occurred for model runs using α_{ice} values of 0.29 and 0.49 respectively. In terms of elevation change relative to these model experiments, a significant negative correlation exists between melt and increasing values of α_{ice} ($p = 0.00$, Pearsons correlation coefficient = -0.99).

For the historical model runs, the proportion of melt (table 8.9) occurring within the 0 - 2.5 m category decreased as α_{ice} decreased. Between 2.5 - 10 m change the patterns of change between the different experiment runs is unclear. This can be explained as the changes modelled filtered through to the larger elevation change categories. Categories representing elevation change greater than 10 m then increased with decreasing values for α_{ice}. In the range 0 - 7.5 m, 74% and 76% of elevation change occurred for model runs using α_{ice} values of 0.29 and 0.49 respectively. In terms of elevation change relative to these model experiments, a significant negative correlation exists between melt and increasing values of α_{ice} ($p = 0.00$, Pearsons correlation coefficient = -0.99).

To assess the main differences between using α_{ice} values of 0.29 and 0.49, difference surfaces are displayed in figure 8.12 for both the contemporary and historical models. These surfaces are calculated by subtracting the 0.49 experimental surfaces from the 0.29 experimental surfaces.

Figure 8.13: Contemporary model response in terms of surface elevation change and June/July/August mean summer Q, to changing values of α_{ice} from 0.29 - 0.49 for the period of October 2009 - December 2010. Mean summer surface Q is calculated as the mean of Q values extracted for the middle of June, July and August 2010.

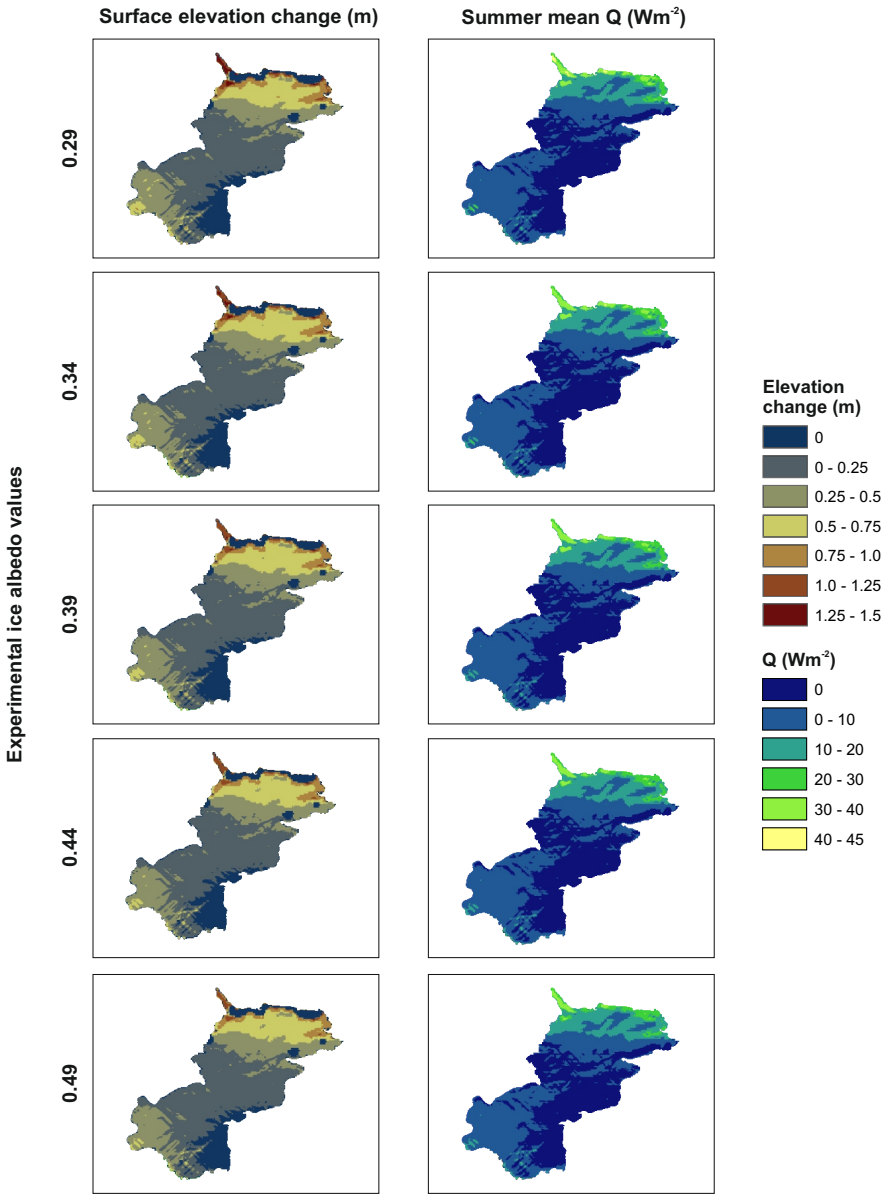

Figure 8.14: Historical model response in terms of surface elevation change and June/July/August mean summer Q, to changing values of α_{ice} from 0.29 - 0.49 for the period of August 1959 - July 1978. Mean summer surface Q is calculated as the mean of Q values for June, July and August of 1969 (randomly selected from the year test range)

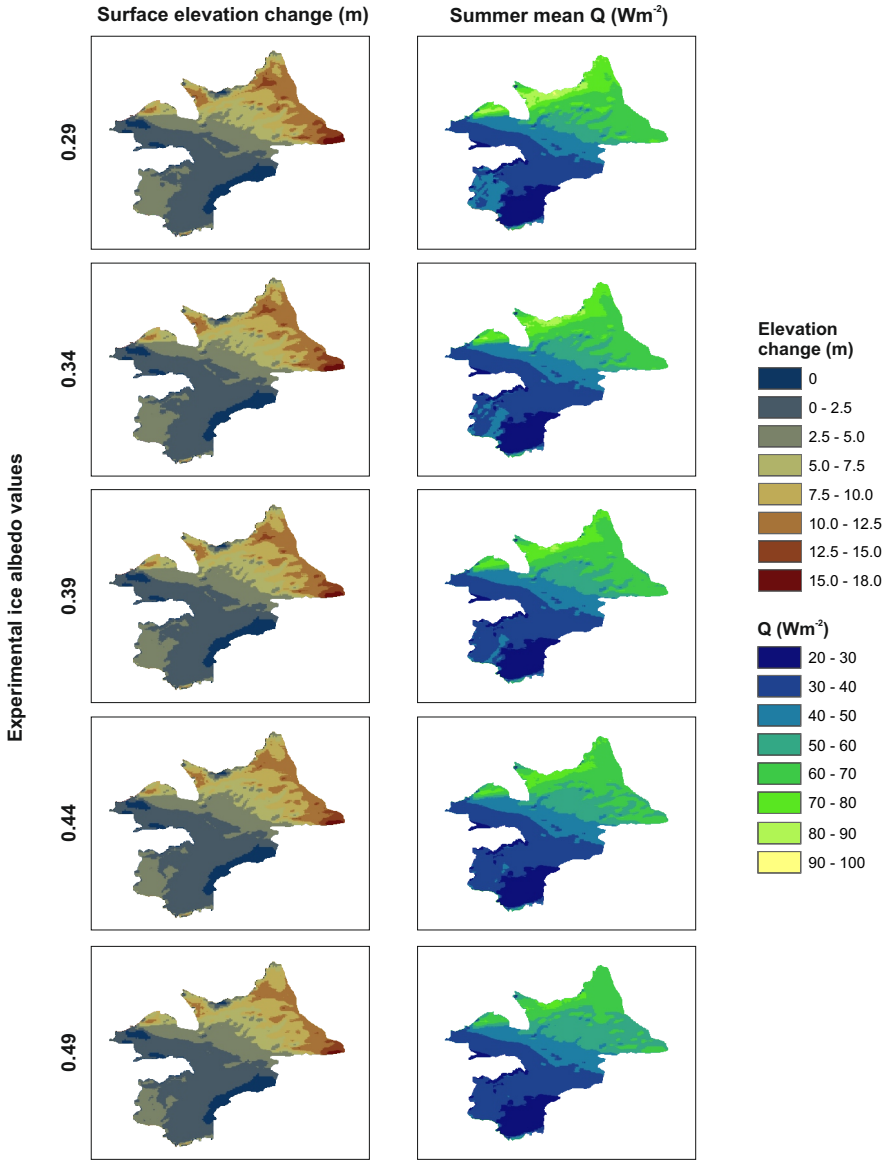

Table 8.8: Ice albedo sensitivity results: contemporary results

	Experimental ice albedo values				
	0.29	0.34	0.39	0.44	0.49
Elevation change (m)	%	%	%	%	%
0	14.16	14.16	14.16	14.16	14.16
0 - 0.25	43.49	44.00	44.54	45.16	45.81
0.25 - 0.5	23.70	23.68	23.62	23.53	23.42
0.5 - 0.75	12.41	12.35	12.31	12.14	12.10
0.75 - 1	4.16	4.10	3.98	3.85	3.68
1 - 1.25	1.42	1.38	1.32	1.14	0.83
1.25 - 1.5	0.65	0.33	0.08	0.01	0.01

Table 8.9: Ice albedo sensitivity results: historical results

	Experimental ice albedo values				
	0.29	0.34	0.39	0.44	0.49
Elevation change (m)	%	%	%	%	%
0	6.63	6.63	6.63	6.63	6.63
0 - 2.5	34.51	35.33	36.09	36.95	37.95
2.5 - 5	22.42	22.09	21.88	21.57	21.02
5 - 7.5	10.68	10.68	10.61	10.67	10.87
7.5 - 10	10.72	11.23	11.98	12.54	13.28
10 - 12.5	11.80	11.34	10.58	10.04	8.94
12.5 - 15	2.52	2.10	1.79	1.26	1.08
15 - 18.0	0.72	0.60	0.44	0.34	0.24

Figure 8.15: Difference surfaces of model outputs for α_{ice} values between 0.29 and 0.49. The surfaces are calculated by subtracting the 0.49 surfaces from those calculated with a value of 0.29. Therefore, values indicate where surface change was greater under conditions where α_{ice} was set to 0.49.

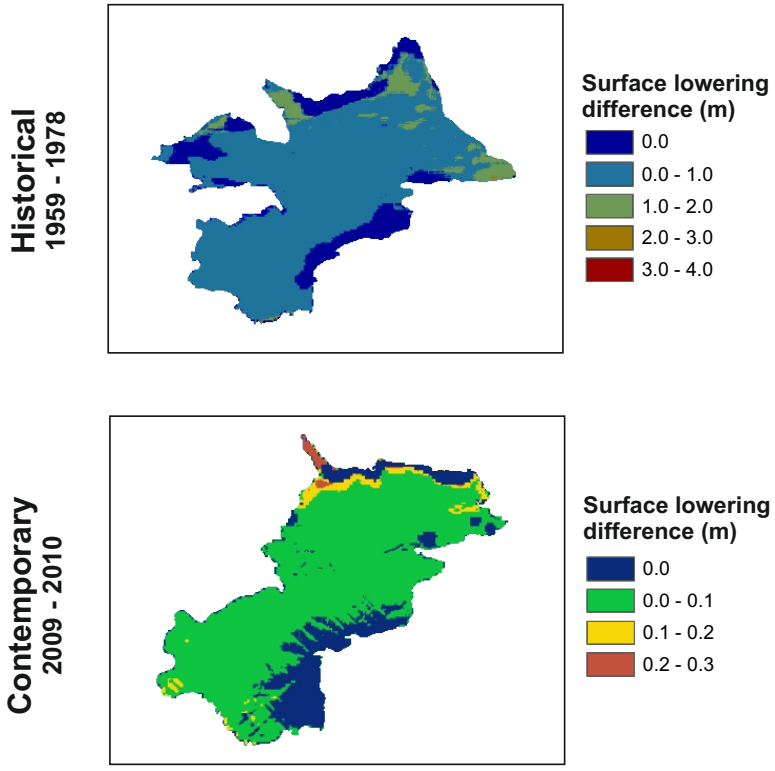

8.4.4 Sensitivity Analysis: Wind factor

The wind factor is used to simply emulate the effect that wind would be expected to have on stripping snow off the glacier surface. Wind patterns are not calculated specifically within the model. From field observations, melt is not the only factor leading to mass loss with wind being important. This has not been specifically quantified by measurements however. The wind factor value is implemented within the model by modifying the rate of snow melt. The factor is a value between 1 and 0. The closer the value is to 0, the greater the effect that the factor has on snow mass loss; the inverse being true for a factor value closer to 1. References to elevation change as a function of melt throughout this chapter and chapter 9, although altered by the value of the wind factor (see below), represent ice surface change as calculated using equation 5.13. This is separate to the elevation of the top of the snowpack that sits on the glacier surface which is affected by the wind factor (through varying snowpack thickness).

To test the sensitivity of the model in terms of the distribution of melt and the calculation of Q, experiments are run using values of 0.3, 0.4, 0.5, 0.6 and 0.7 for the wind factor, using both the contemporary and historical models for the 2009-2010 and 1959-1978 time periods respectively, for reasons discussed in section 8.1. A default value of 0.5 is used within the normal model set up. The results of these experiments are discussed within the context of the separate models. The spatial distribution for the effect of changing wind factor values can be seen in figures 8.16 and 8.17.

Spatially for the contemporary experiments, smaller wind factor values result in melt extent occurring within the 0.5 - 1.0 m category to extend from the more northern region, increasingly south. This migration is uphill, in terms of glacier elevation (m a.s.l.). To the south west of the glacier, there is also an increase in elevation change. Relative to the center of the glacier, snow thickness is less in this region. Conversely, as the wind factor increases towards 0.70, melt within the 0.5-1.0 migrates north. The melt patterns are matched by the Q surface patterns.

As with the contemporary experimental surface outputs, smaller wind factor values result in greater elevation change. As the wind factor reduces from 0.70 to 0.30, elevation change initially focused at the terminus to the east spreads increasingly west. There is also increasing elevation change propagating from the south west and then to the centre of the glacier. There is little change to the west using different wind factors which may relate to hillshade.

Considering the proportion of melt occurring within different elevation change categories, for the contemporary sensitivity experiments (see table 8.10), elevation change within the 0 - 0.25 m category reduced as the wind factor size decreased from 0.70 to 0.3. For elevation changes of 2.5 m or greater, the proportion of melt increased as the wind factor decreased in size. Assessing the proportion of melt occurring within the 0 - 0.75 m elevation change category, values of 83% and 99% are recorded for wind factor values of 0.3 and 0.7 respectively. These results support the enhanced elevation change effect that a smaller wind factor value has on the model.

For the historical wind factor sensitivity experiments (see table 8.11), the proportion of melt occurring within the 0 - 2.5 m elevation change category decreased with the application of smaller wind factor values. The general overall trend was for an increase in melt occurring in the larger elevation change categories (7.5 - 22.5 m) as smaller wind factor values were applied. The pattern of change based on individual categories is not as clear as for some of the aforementioned proportional change descriptions for other sensitivity experiments discussed here. This may be explained in part due to local effects relating to the spatial variability in snow thickness across the surface as well as other factors including hillshade. Despite potentially localised effects, the overall trend of increased elevation change with reduced wind factor values still stands. This is further supported when considering the proportion of melt in the 0 - 7.5 m category for the extreme values tested. Proportions in this category of 61% and 97% for wind factor values of 0.3 and 0.7 being recorded respectively.

Figure 8.16: Contemporary model response in terms of surface elevation change and June/July/August mean summer Q, to changing wind factor values from 0.3 - 0.7 for the period of October 2009 - December 2010. Mean summer surface Q is calculated as the mean of Q values extracted for the middle of June, July and August 2010.

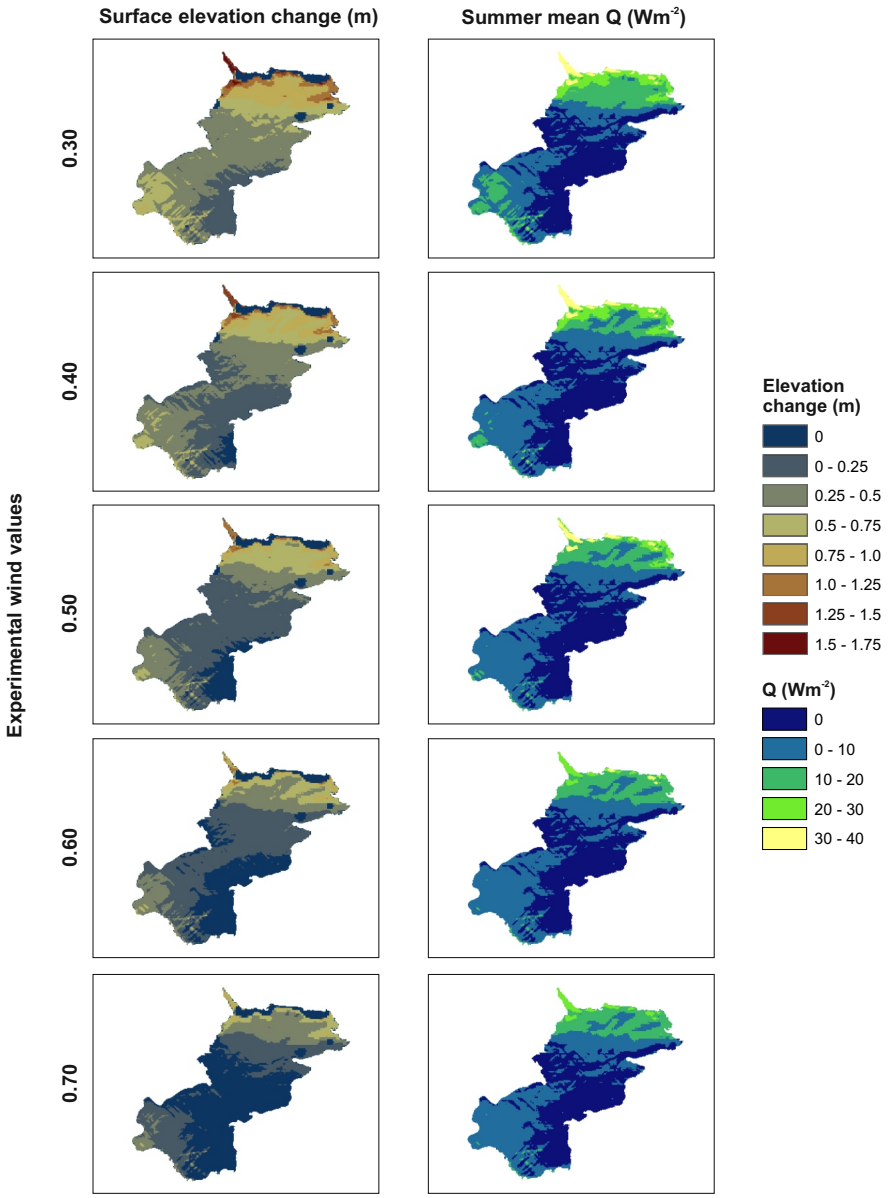

Figure 8.17: Historical model response in terms of surface elevation change and June/July/August mean summer Q, to changing wind factor values from 0.3 - 0.7 for the period of August 1959 - July 1978. Mean summer surface Q is calculated as the mean of Q values for June, July and August of 1969 (randomly selected from the year test range)

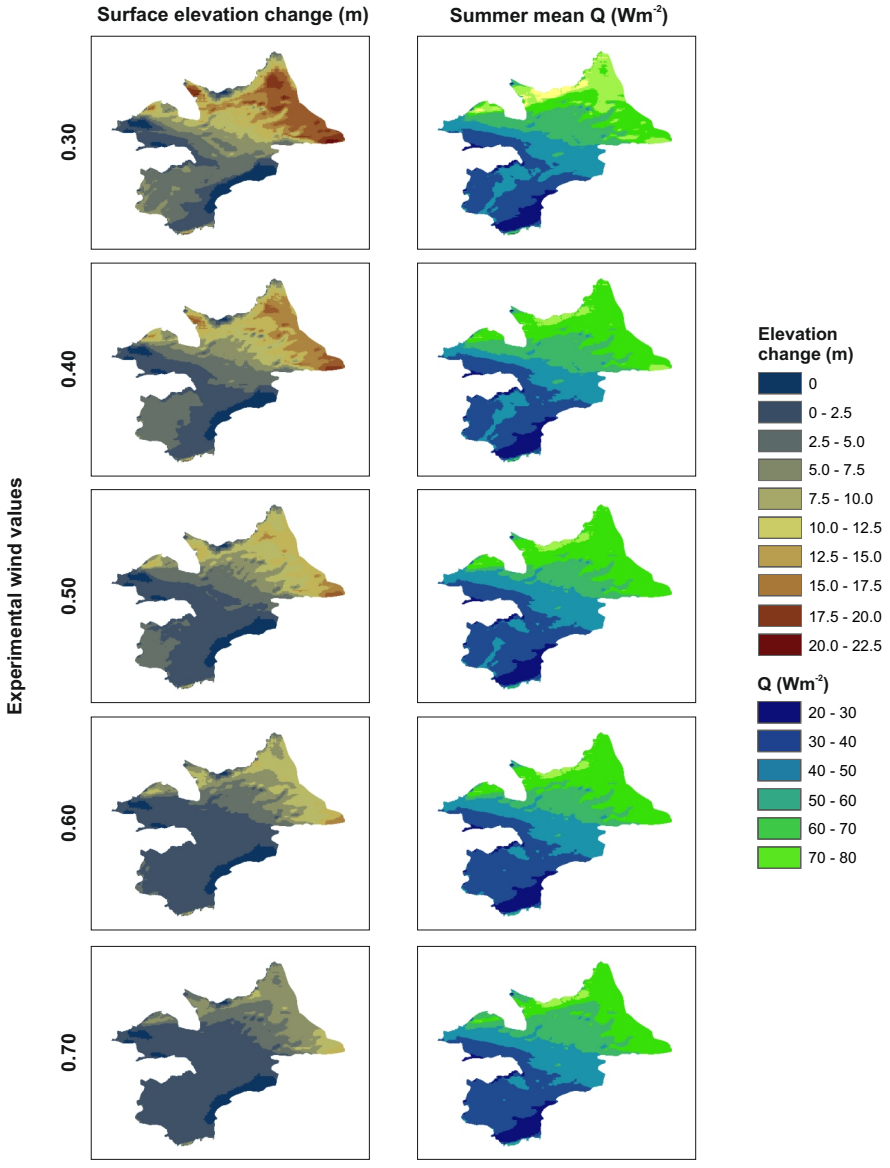

Table 8.10: Wind factor sensitivity results: contemporary results

	Experimental wind values				
	0.3	0.4	0.5	0.6	0.7
Elevation change (m)	%	%	%	%	%
0	5.13	7.75	14.16	28.38	51.62
0 - 0.25	14.29	31.15	44.54	42.60	28.22
0.25 - 0.5	44.42	37.93	23.62	19.09	14.79
0.5 - 0.75	18.66	12.78	12.31	7.17	4.32
0.75 - 1	11.47	7.18	3.98	2.33	1.04
1 - 1.25	4.23	2.27	1.32	0.42	0.01
1.25 - 1.5	1.21	0.93	0.08	0.00	0.00
1.5 - 1.75	0.60	0.01	0.00	0.00	0.00

Table 8.11: Wind factor sensitivity results: historical results

	Experimental wind values				
	0.3	0.4	0.5	0.6	0.7
Elevation change (m)	%	%	%	%	%
0	6.63	6.63	6.63	5.77	5.77
0 - 2.5	14.48	24.27	36.09	28.89	29.05
2.5 - 5	26.03	26.58	21.88	21.93	21.83
5 - 7.5	13.50	10.67	10.61	15.61	21.12
7.5 - 10	8.75	9.10	11.98	26.05	20.56
10 - 12.5	8.88	9.52	10.58	1.76	1.67
12.5 - 15	7.22	10.43	1.79	0.00	0.00
15 - 17.5	11.15	2.45	0.44	0.00	0.00
17.5 - 20	3.06	0.35	0.00	0.00	0.00
20 - 22.5	0.31	0.00	0.00	0.00	0.00

Figure 8.18: Difference surfaces of model outputs for wind factor values between 0.3 and 0.7. The surfaces are calculated by subtracting the 0.7 surfaces from those calculated with a value of 0.3. Therefore, values indicate where surface change was greater under conditions where the wind factor value was set to 0.3.

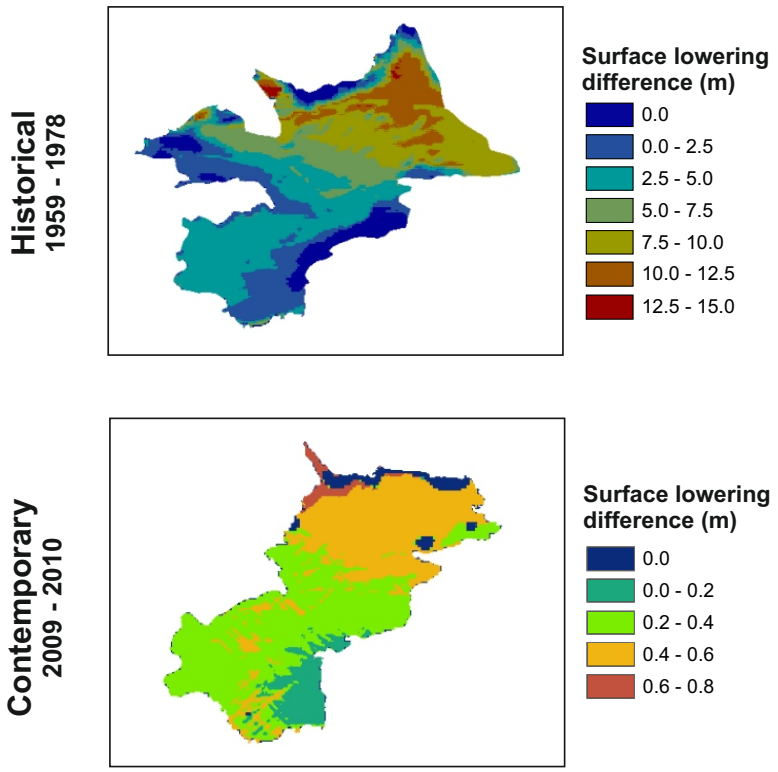

To assess the main differences between using different wind factor values of 0.3 and 0.7, difference surfaces are displayed in figure 8.18 for both the contemporary and historical models. These surfaces are calculated by subtracting the 0.7 experimental surfaces from the 0.3 experimental surfaces.

8.4.5 Sensitivity Analysis: Snowfall threshold

The default snowfall factor employed within the model is 1.5°C. When a cell is at or below this temperature during the summer months and there is recorded precipitation, the precipitation will fall at the cell in question as snow (the specifics of this are discussed in section 5.4.5 of chapter 5). A value of 1.5°C is used here as

Table 8.12: Proportional melt resultant of the snowfall threshold sensitivity analysis for values in the range of 0.5 - 2.5°C using the contemporary model (2009 - 2010)

	Experimental snow threshold values				
	0.5	1.0	1.5	2.0	2.5
Elevation change (m)	%	%	%	%	%
0	13.78	13.91	14.16	14.42	14.71
0 - 0.25	44.46	44.55	44.54	44.74	44.78
0.25 - 0.5	23.82	23.69	23.62	23.35	23.09
0.5 - 0.75	12.39	12.42	12.31	12.16	12.14
0.75 - 1	4.07	4.00	3.98	3.96	3.93
1 - 1.25	1.38	1.34	1.32	1.30	1.30
1.25 - 1.45	0.11	0.09	0.08	0.07	0.04

Table 8.13: Proportional melt resultant of the snowfall threshold sensitivity analysis for values in the range of 0.5 - 2.5°C using the historical model (1959 - 1978)

	Experimental snow threshold values				
	0.5	1.0	1.5	2.0	2.5
Elevation change (m)	%	%	%	%	%
0	6.63	6.63	6.63	6.63	6.63
0 - 2.5	35.32	35.50	36.09	36.10	36.38
2.5 - 5	22.62	22.45	21.88	21.91	21.79
5 - 7.5	10.59	10.58	10.61	10.69	10.75
7.5 - 10	11.91	11.97	11.98	11.98	12.19
10 - 12.5	10.66	10.61	10.58	10.53	10.20
12.5 - 15	1.82	1.82	1.79	1.73	1.64
15 - 17	0.44	0.44	0.44	0.43	0.42

taken from Giesen & Oerlemans (2012). To test model sensitivity to this factor, five experiments were run, with values deviating either side of the default by 0.5°C, giving an experimental range of 0.5 - 2.5°C.

Despite the variability of the values applied, there was very little spatial variation in surface elevation change and Q propagation for both the contemporary and historical model runs. Consequently maps are not displayed. Proportional melt values are presented in tables 8.12 and 8.13.

For the contemporary results, it is clear that there is little change between the

categories with regard to changing snowfall threshold values. Taking the 0 - 0.75 m elevation change for example, 94% and 95% of total melt occurred within this range for threshold values of 0.5 and 2.5 respectively. Where there are changes between categories, the maximum difference is <1% of proportional melt. Similar trends are apparent within the historical results. Within the 0 - 7.5 m range, 75% and 76% of proportional melt was modelled for threshold values of 0.5 and 2.5 respectively. This is indicative of little change. There are some very small increases in melt with threshold values closer to 0.5 identified within elevation change categories >2.5 m but no changes are >1%.

8.4.6 Sensitivity Analysis: Temperature lapse rate

A default lapse rate of 0.0065°K m^{-1} is set within the model, adopted from Giesen & Oerlemans (2012) and discussed in section 5.4.4 of chapter 5. Sensitivity experiments are reported here where lapse rates in the range of 0.0050 - 0.0070°K m^{-1} were tested. Where the lapse rate was closer to 0.0050°K m^{-1}, far greater melt was observed for both the contemporary and historical model runs compared to using a lapse rate closer to 0.0070°K m^{-1}. The results of these experiments are discussed within the context of the separate models and model run output maps are displayed in figures 8.19 and 8.20.

A strong pattern is apparent for elevation change and change in Q in response to different lapse rate values for the contemporary model run. Using a lapse rate of 0.0070°K m^{-1}, melt within the 0.25 m+ elevation change category is restricted to the south west and northern portions of the glacier with the centre of the glacier being represented by elevation change within the 0 - 2.5 m elevation change category. As the lapse rate reduces towards 0.0050, elevation change increases from the south west to the centre of the glacier along a north east trajectory. Elevation change in the far south west increases from being within the 0.25 - 0.5 m range to mainly the 0.5 - 0.75 m range. The centre of the glacier becomes increasingly represented by the 0.25 - 0.5 category as the lapse rate reduces to 0.0050. In the northern area of the glacier, with lapse rate values closer to 0.0050, areas within the 0.75 - 1.0 m elevation change category increase in size and elevation change

Figure 8.19: Contemporary model response in terms of surface elevation change and June/July/August mean summer Q, to changing lapse rate values from 0.0050 - 0.0070°K m^{-1} for the period October 2009 - December 2010. Mean summer surface Q is calculated as the mean of Q values extracted for the middle of June, July and August 2010.

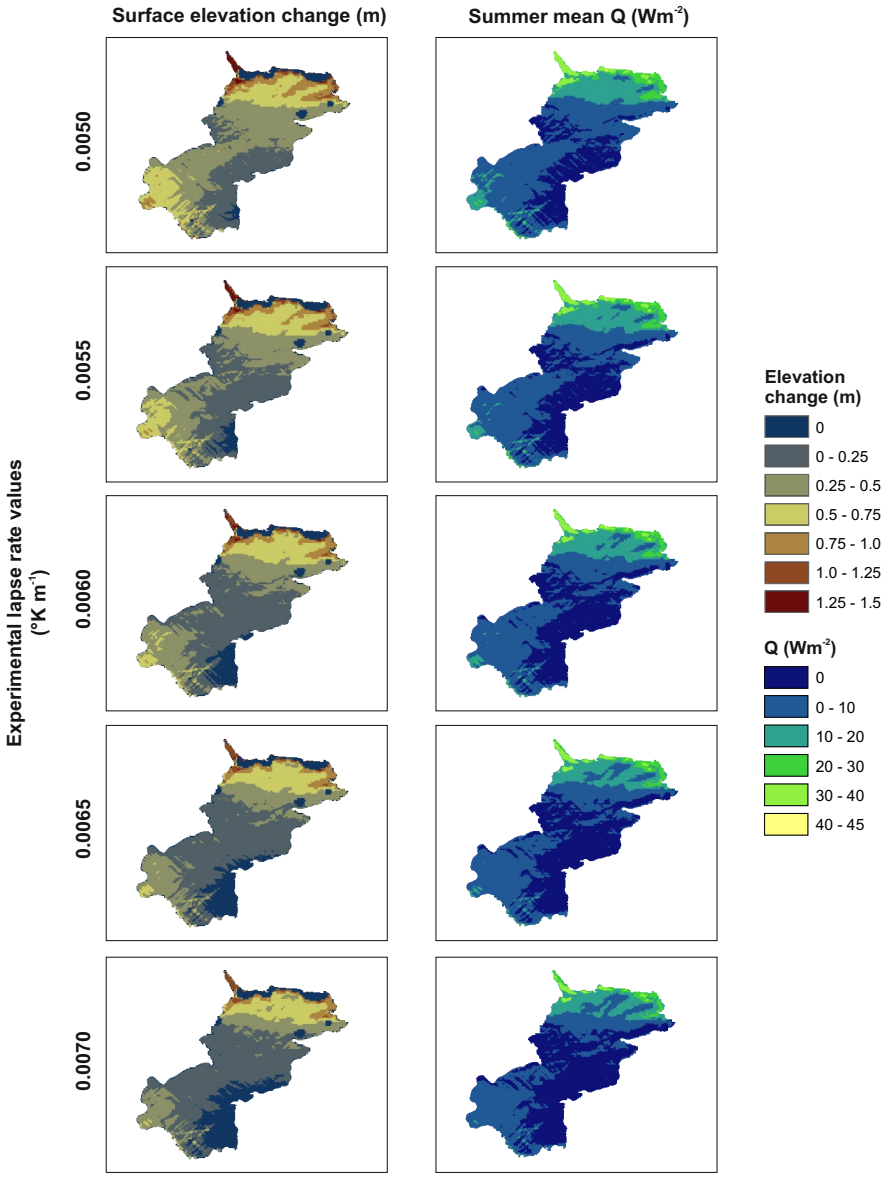

Figure 8.20: Historical model response in terms of surface elevation change and June/July/August mean summer Q, to changing lapse rate values from 0.0050 - 0.0070°K m^{-1} for the period August 1959 - June 1978. Mean summer surface Q is calculated as the mean of Q values for the June, July and August 1969 (randomly selected).

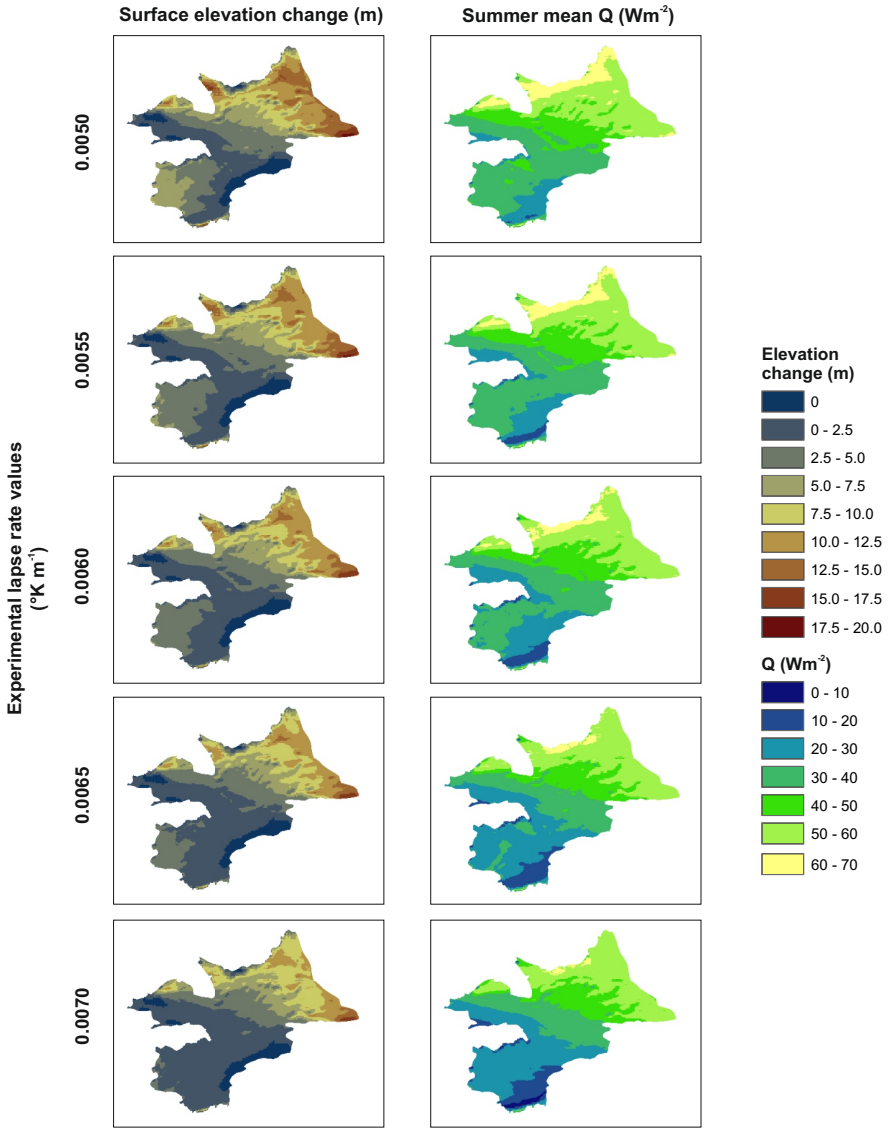

Table 8.14: Proportional melt (contemporary) resultant of temperature lapse rate variation for values in the range of 0.0050 - 0.0070°K m^{-1}

	Experimental lapse rate values				
	0.005	0.0055	0.006	0.0065	0.007
Elevation change (m)	%	%	%	%	%
0	5.92	7.72	10.67	14.16	19.50
0 - 0.25	23.35	32.44	40.51	44.54	46.11
0.25 - 0.5	41.02	34.78	28.54	23.62	18.68
0.5 - 0.75	19.77	17.25	14.05	12.31	10.95
0.75 - 1	7.24	5.66	4.47	3.98	3.61
1 - 1.25	1.84	1.55	1.48	1.32	1.13
1.25 - 1.5	0.86	0.61	0.28	0.08	0.01

increases south towards the glacier centre. These changes in elevation change are matched by changes represented by the summer Q maps.

A very similar response pattern is displayed by the historical model results with increasing elevation change rates encroaching to the centre of the glacier from the south west and the north/north east. These patterns are equally expressed by the Q surfaces. Relative increases in elevation change in the northern portion of the glacier advance on a more east-west/east-south west trajectory than for the contemporary surfaces which matches the relatively different hillshade coverage manifested over the glacier for these years.

For both models, even at 0.0050, the lowest lapse rate experimented with here, elevation change is still most limited at the centre of the glacier. This region is the most affected by hillshade and is also associated with the thickest winter snow cover (see sections 8.3.1, 8.3.2 as well as 5.1.2 and 5.2.2 in chapter 5). Considering the temperature forcing induced, these are identified as limiting factors to surface elevation change.

For the contemporary model run, with regard to proportional elevation change (see table 8.14) there is a large reduction in change occurring within the 0 m category, reducing by 14% as the lapse rate shifts from 0.0070 - 0.0050. A small percentage of the 0 category is fixed as it is associated with parts of the glacier

Table 8.15: Proportional melt (historical) resultant of temperature lapse rate variation for values in the range of 0.0050 - 0.0070°K m^{-1}

	Experimental lapse rate values				
	0.005	0.0055	0.006	0.0065	0.007
Elevation change (m)	%	%	%	%	%
0	6.63	6.63	6.63	6.63	6.63
0 - 2.5	20.99	24.83	29.45	36.09	45.02
2.5 - 5	23.73	28.04	26.20	21.88	14.95
5 - 7.5	17.63	11.58	10.93	10.61	10.90
7.5 - 10	9.65	9.75	10.24	11.98	14.32
10 - 12.5	12.00	13.41	12.97	10.58	6.83
12.5 - 15	7.99	4.91	2.94	1.79	1.02
15 - 17.5	1.14	0.75	0.65	0.44	0.33
17.5 - 20	0.24	0.10	0.00	0.00	0.00

where ice thickness is unknown and consequently set to 0. However, a large portion of this category is not defined in this way and a reduction in this category for increasingly smaller lapse rate values is because of increased surface melt relating to an increase in Q. Within the 0 - 0.25 m category there is a reduction in the proportion of melt occurring as lapse rate value reduces. This can be explained as more melt is attributed to the larger categories. Overall, there is an increase in the proportion of elevation change occurring between 0.5 - 1.5 m as lapse rate values reduce towards 0.0050. The most noticeable increase occurs within the 0.25 - 0.75 m category where there is an increase from 30% to 61% of melt occurring when using lapse rate values of 0.0070 and 0.0050 respectively. The drivers for these changes are described above.

For the historical model, proportional melt (see table 8.15) decreases in the 0 - 2.5 m category as the lapse rate moves from 0.0070 to 0.0050. There is then an overall increase in the proportion of melt between 2.5 - 20.0 m as the lapse rate value decreases, with 75% and 48% of melt occurring within this category for lapse rate values of 0.0050 and 0.0070 respectively. In the 0-7.5 m category, more melt occurs using a greater lapse rate - model outputs being 69% and 78% for lapse rates of 0.0050 and 0.0070 respectively. To assess the main differences between using different lapse rates of 0.0050 and 0.0070, difference surfaces are

Figure 8.21: Difference surfaces of model outputs for lapse rate values between 0.0050 and 0.0070°K m^{-1}. The surfaces are calculated by subtracting the 0.0070 surfaces from those calculated with a lapse rate of 0.0050°K m^{-1}. Therefore, values indicate where surface change was greater under conditions where the lapse rate was at 0.0050°K m^{-1}.

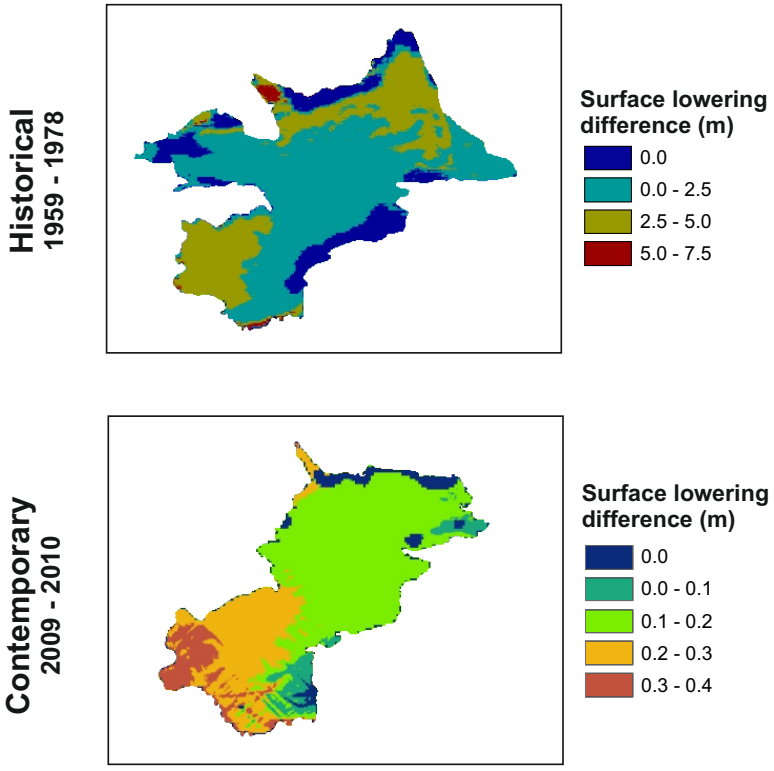

displayed in figure 8.21 for both the contemporary and historical models. These surfaces are calculated by subtracting the 0.0070 experimental surfaces from the 0.0050 experimental surfaces.

8.4.7 Sensitivity Analysis: Winter snowpack thickness

Snow thickness during the winter months is based on snow probe measurements taken at the end of the accumulation season. It is assumed that depths measured are representative of the total accumulation throughout the winter season at a given point. The probe measurements are then used to interpolate a winter snow surface. To assess the density of the winter snow pack, snow pits were excavated and densities measured. It is possible that the method applied by which to approximate winter snow thickness is either an over or underestimate - largely due to the effects of wind. The snow surface once day can be very different the next due to drifting. The snow density analysis (see section 5.4.6 in chapter 5) alludes to the density profile being similar to that associated with wind slab. Consequently, to test model sensitivity to under or overestimates of winter snow pack thickness, experiments were run testing overestimates of +0.5 m and +1.0 m and underestimates of -0.5 m and -1.0 m. The default is tested for completeness. For the contemporary model, this involved the addition/subtraction of the value being tested to the input winter snow surfaces. For the historical model, it required an alteration to the winter snow distribution algorithm, with specific regard to the factor used to alter ANS analysis to the glacier mean snow thickness (see section 5.2.2 in chapter 5).

Forcing the model with a variable winter snowpack thickness has a very striking result in the pattern of elevation change identified from the model outputs. Where the snowpack is greatest (the +1.0 scenario), surface change is limited to the north and south west of the glacier. As the snowpack forcing lessens, surface change alters most noticeably in the glacier centre with the most limited surface change being focused along the south east perimeter of the glacier (this is an area affected largely by topographic shading) when using the default snowpack thickness setting (±0.0 modification). With reduced snowpack thickness forced with a

-0.5 modification, change affects the entire glacier with parts of the central glacier contributing to change within the 0.25 - 0.5 m category (limited in all previous runs to the 0 - 0.25 m change category). With -0.5 m forcing, the south-west of the glacier has noticeable increases in the 0.5 - 0.75 m change category. With -1.0 m forcing, across the glacier, change is limited within the 0 - 0.25 m change category, with most change occurring at higher rates. The most limited melt is at the glacier perimeter (where ice thickness is limited and therefore results in 0 change once depleted) and within the centre of the glacier - where the winter snowpack is remains thickest (despite a change in overall snow thickness) and topographic shading is greatest. These changes are replicated by the Q surfaces although to a lesser extent, especially within the centre of the glacier where the snowpack is thicker. A thicker snowpack will remain through the ablation season longer than a thinner pack, largely due to its modification of I as a function of α_{snow} (see equations 5.10 and 5.13).

Snow thickness forcing has an equally striking impact on the historical model outputs. A modification of -1.0 drastically increases overall melt with mean melt being 7.8 m compared to 2.6 m for when a +1.0 m modification is applied. The area least affected by the change in snow thickness is the centre of the glacier (which represents the middle of the overall elevation range) where the snow is thickest relative to the rest of the surface (see section 5.2.2 of chapter 5) and hillshade is most affecting (see sections 8.3.1 and 8.3.2). The areas of greatest increase in melt with the -0.5 m and -1.0 m modifications are most notably the north-east regions with significant change also to the south west. Q patterns match the elevation change patterns, both of which are displayed in figure 8.23. It should be noted that -1.0 m and +1.0 m scenarios are unrealistic during the winter season, especially where the snowpack is already known/predicted to be at its thinnest (i.e. $\leq$1.0 m) but these experiments are still useful in discerning overall factors driving change over the glacier surface and for the identification of the most sensitive regions.

Considering the elevation change resultant of the contemporary model runs (see table 8.16), in all cases, as snow thickness reduced, the proportion of change

Figure 8.22: Contemporary model response in terms of surface elevation change and June/July/August mean summer Q, to winter snow thickness, modified by values in the range +1.0 - -1.0 m for the period October 2009 - December 2010. Mean summer surface Q is calculated as the mean of Q values extracted for the middle of June, July and August 2010.

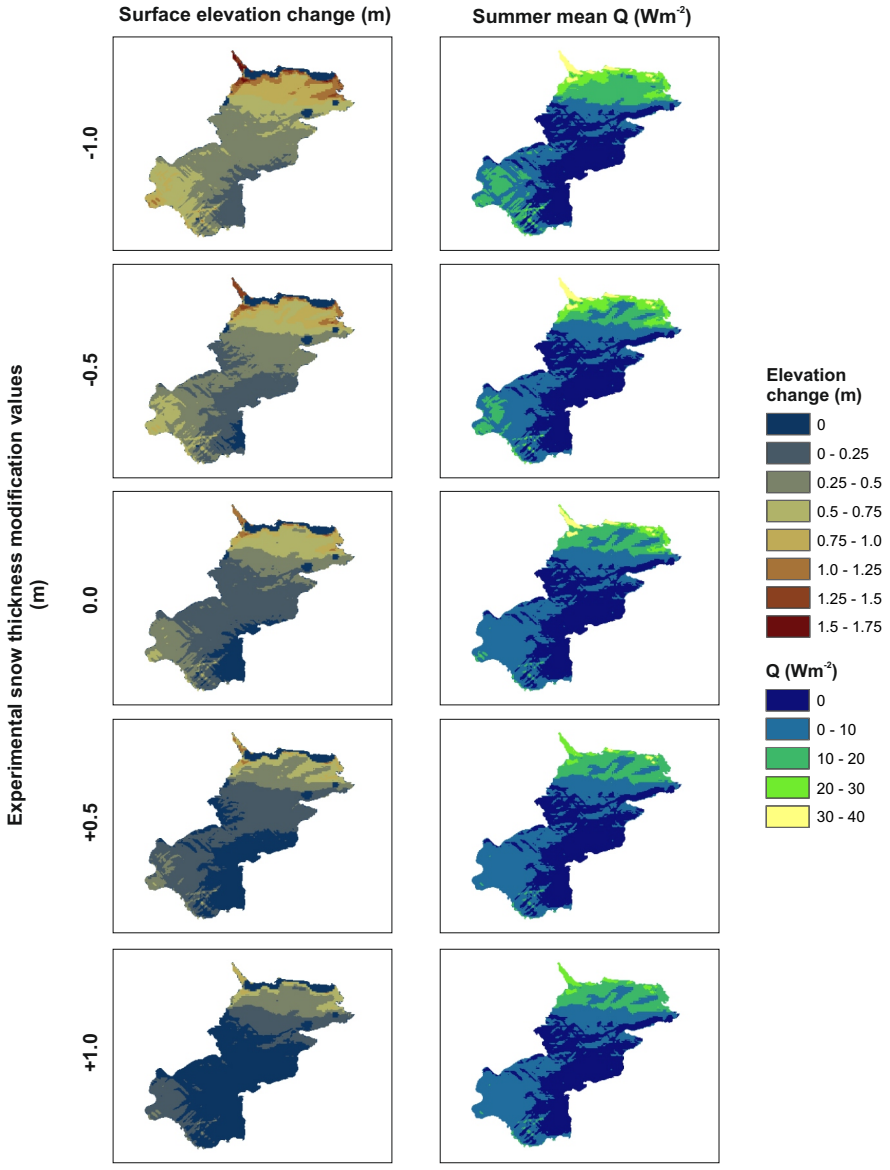

Figure 8.23: Historical model response in terms of surface elevation change and June/July/August mean summer Q, to winter snow thickness, modified by values in the range +1.0 - -1.0 m for the period October 2009 - December 2010. Mean summer surface Q is calculated as the mean of Q values extracted for the middle of June, July and August 2010.

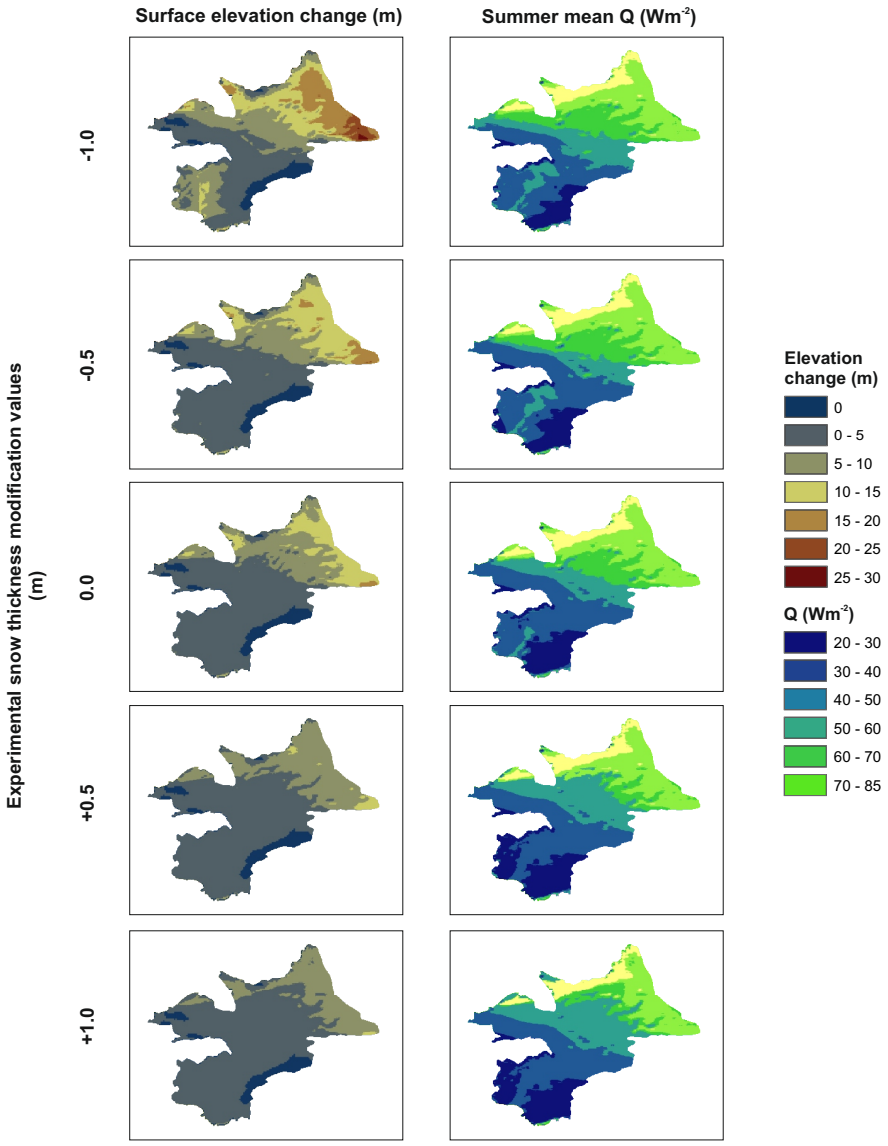

falling within the 0 category reduced, in total by 53% between the greatest and least snow thickness conditions. For the 0 - 0.25 m change category, the amount of melt increased when moving from the greatest snow thickness to the lesser default, however, values then decreased for greater snow thicknesses set by the addition of +0.5 and +1.0 m. This can be explained as change associated with these conditions were in the larger categories. For categories 0.25 - 1.75 m, in all cases, as snow thickness reduced, elevation change increased. The proportion of change occurring within this category for the most extreme settings of +1.0 m and -1.0 m were 17% and 84% respectively. For the 0 - 0.75 m category, portions of 79% and 99% elevation change are associated with the -1.0 and +1.0 settings respectively. Less snow across the glacier surface resulted in vastly increased surface change.

For the historical model outputs (see table 8.17), there is a decrease in the amount of elevation change within the 0 - 5.0 m category as the amount of snow decreases (from +1.0 m to -1.0 m). This is explained as where there is less snow, a larger proportion of melt falls into the larger elevation change categories. For the 15.0 - 30.0 m category, there is a clear increase in the amount of elevation change occurring for each modification towards a thinner snowpack. For model runs with +0.5 m and +1.0 m modifications, no elevation change occurs within the 15.0 - 30.0 m category. The pattern of increasing elevation change with reduced snow is not as clearly represented by the 5.0 - 10.0 m and 10.0 - 15.0 m categories individually, but treated together, the increase is clear. To compare the extremes, with a modification of +1.0 m, 21% of melt occurs within this collective category. The portion of elevation change is increased to 44% with a -1.0 m modification.

To assess the main differences between the snowpack thickness forcing model results, when using +1.0 m and -1.0 m, difference surfaces are displayed in figure 8.24 for both the contemporary and historical models. These surfaces are calculated by subtracting the +1.0 experimental surfaces from the -1.0 m experimental surfaces.

Table 8.16: Proportional melt (contemporary) resultant of experimental winter snow thickness values

	Experimental snow thickness values				
	-1.0	-0.5	0.0	0.5	1.0
Elevation change (m)	%	%	%	%	%
0	5.13	7.25	14.16	32.27	58.27
0 - 0.25	11.06	27.34	44.54	42.93	24.42
0.25 - 0.5	40.78	38.08	23.62	15.54	12.38
0.5 - 0.75	22.44	16.19	12.31	6.72	3.90
0.75 - 1	13.82	7.76	3.98	2.07	1.02
1 - 1.25	4.75	2.43	1.32	0.47	0.01
1.25 - 1.5	1.49	0.94	0.08	0.00	0.00
1.5 - 1.75	0.53	0.01	0.00	0.00	0.00

Table 8.17: Proportional melt (historical) resultant of experimental winter snow thickness values

	Experimental snow thickness values				
	-1.0	-0.5	0.0	0.5	1.0
Elevation change (m)	%	%	%	%	%
0	6.63	6.63	6.63	6.63	6.63
0 - 5.0	34.40	52.1	58.00	64.60	72.70
5.0 - 10.0	28.70	19.1	22.60	27.10	20.50
10.0 - 15.0	15.70	18.7	12.40	1.70	0.20
15.0 - 20.0	12.0	3.50	0.40	0.00	0.00
20.0 - 25.0	2.40	0.03	0.00	0.00	0.00
25.0 - 30.0	0.20	0.00	0.00	0.00	0.00

Figure 8.24: Difference surfaces of model outputs for winter conditions forced with +1.0 m and -1.0 m modifications. The surfaces are calculated by subtracting the +1.0 m surfaces from those calculated with a modification of -1.0 m. Therefore, values indicate where surface change was greater under conditions with a -1.0 m modification

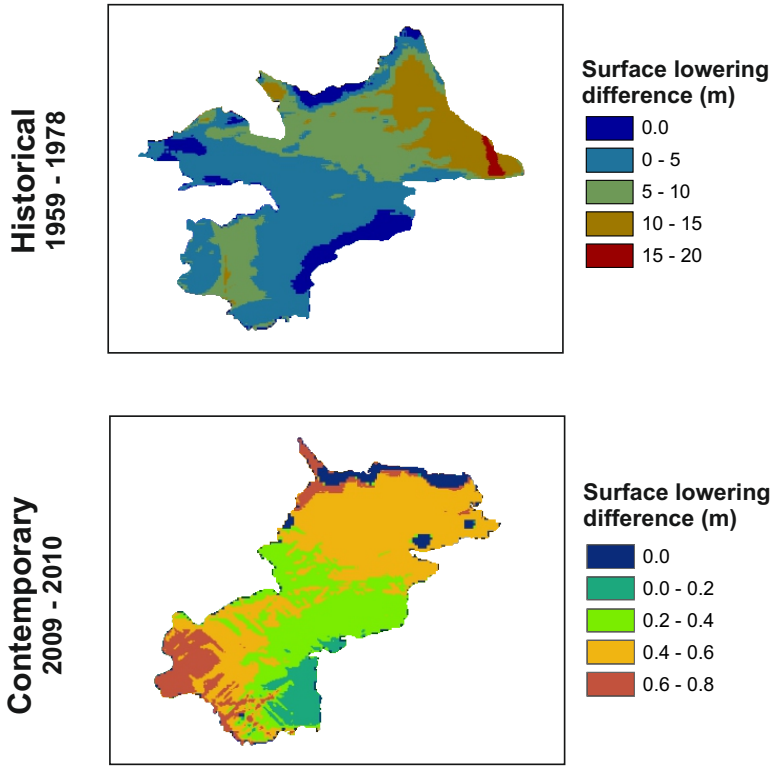

8.4.8 Summary

This chapter has provided an error analysis comparing the performance of a bespoke designed SEB model against observed geodetically derived glacier change for which model surface error values have been calculated. Annual errors (of model overestimation) of -0.33 and -1.76 m w.e yr^{-1} were found for the historical and contemporary models respectively. Considering the lower glacier alone, contemporary model error was reduced to -0.08 m w.e yr^{-1}.

To summarise the sensitivity experiments of analysed in sections 8.4.1 through to 8.4.7, the main changes are displayed in table 8.18. Both the contemporary and historical models were most sensitive firstly to decreases in the winter snowpack, increases in the effect of wind (a value closer to 0), thirdly equally sensitive to decreases in the applied temperature lapse rate (rates closer to 0.0050°K m^{-1}) and reductions in α_{snow} values, and then τ. Comparatively, the models were least sensitive when associated with reductions to the snowfall threshold and α_{ice}. The nature of the experiments has resulted in the isolation of individual factors and consequently does not account for co-linear relationships between them. Such relationships are both likely to exist and also be important in terms of mass loss sensitivity. Furthermore, as ice dynamics are not accounted for by the modelling/sensitivity analysis approach, this may further influence the effect of a given factor on the glacier's sensitivity in terms of mass loss. Essentially, by excluding the effects of dynamics, this results in the sensitivity experiments being based on "reference" type dynamics. The dynamics are fixed as of the date and time of the glacier at the beginning of any given model run and do not change.

Table 8.18: Model sensitivity to factors discussed in sections 8.4.1 to 8.4.7. Increases and decreases are in reference to the % change in surface elevation change relevant to the default factor setting

	Contemporary model		Historical model	
Experiment	Increase	Decrease	Increase	Decrease
	%	%	%	%
τ (0.35)	25.12	0.00	20.63	0.00
τ (0.40)	11.37	0.00	9.82	0.00
τ (0.45)	-	-	-	-
τ (0.50)	0.00	-9.51	0.00	-8.91
τ (0.55)	0.00	-17.45	0.00	-16.79
α_{snow} (0.60)	29.86	0.00	31.16	0.00
α_{snow} (0.65)	14.77	0.00	15.60	0.00
α_{snow} (0.70)	-	-	-	-
α_{snow} (0.75)	0.00	-13.68	0.00	-15.37
α_{snow} (0.80)	0.00	-25.92	0.00	-29.29
α_{ice} (0.29)	4.76	0.00	3.96	0.00
α_{ice} (0.34)	2.38	0.00	1.99	0.00
α_{ice} (0.39)	-	-	-	-
α_{ice} (0.44)	0.00	-2.37	0.00	-2.01
α_{ice} (0.49)	0.00	-4.72	0.00	-4.05
Wind (0.30)	77.23	0.00	65.66	0.00
Wind (0.40)	36.82	0.00	30.34	0.00
Wind (0.50)	-	-	-	-
Wind (0.60)	0.00	-31.89	0.00	-25.64
Wind (0.70)	0.00	-55.65	0.00	-46.38
Snowfall thresh. (0.5)	1.39	0.00	0.45	0.00
Snowfall thresh. (1.0)	0.68	0.00	0.33	0.00
Snowfall thresh. (1.5)	-	-	-	-
Snowfall thresh. (2.0)	0.00	-1.00	0.00	-0.27
Snowfall thresh. (2.5)	0.00	-1.79	0.00	-0.96
TLR (0.0050)	30.10	0.00	20.45	0.00

Continued on Next Page...

Table 8.18 - Continued

Experiment	Contemporary model		Historical model	
	Increase %	Decrease %	Increase %	Decrease %
TLR (0.0055)	14.54	0.00	9.92	0.00
TLR (0.0060)	-	-	-	-
TLR (0.0065)	0.00	-13.67	0.00	-9.33
TLR (0.0070)	0.00	-26.19	0.00	-18.01
Winter snow thick. (-1.0)	93.03	0.00	72.30	0.00
Winter snow thick. (-0.5)	44.04	0.00	29.94	0.00
Winter snow thick. (0.0)	-	-	-	-
Winter snow thick. (+0.5)	0.00	-37.37	0.00	-25.87
Winter snow thick. (+1.0)	0.00	-62.96	0.00	-46.92

These experiments in themselves provide a lot of information to the melt pattern of the glacier and the controls upon it and this is discussed in chapter 10. To further address the change that the test parameters had on the model, the mean summer energy available at the surface (Q), as calculated using equation 5.13, is considered for which the results are displayed in figures 8.25 and 8.26. The box-plots are constructed for the contemporary model outputs using mean daily Q calculated for all days in June, July and August. The plots for the historical model are constructed using the June, July and August monthly Q means.

The change in mean Q measured across the glacier surface for the different sensitivity runs (figures 8.25 and 8.26) holds a very similar trend to the maps used to illustrate surface elevation change under the same conditions in sections 8.4.1 to 8.4.7 as would be expected. For the historical model runs and with reference to figure 8.25), with increasing distance from the origin along the x axis there is a clear reduction in Q for the τ, α_{snow}, α_{ice}, and lapse rate experiments. The same pattern is displayed by the wind and snow thickness modification charts also, albeit much more subtly. There is no particular change for the summer snowfall threshold experiment. For the contemporary experiments, clear reductions in Q

Figure 8.25: Boxplots displaying sensitivity analysis results using the historical model for the period of 1959 - 1978 (June, July and August)

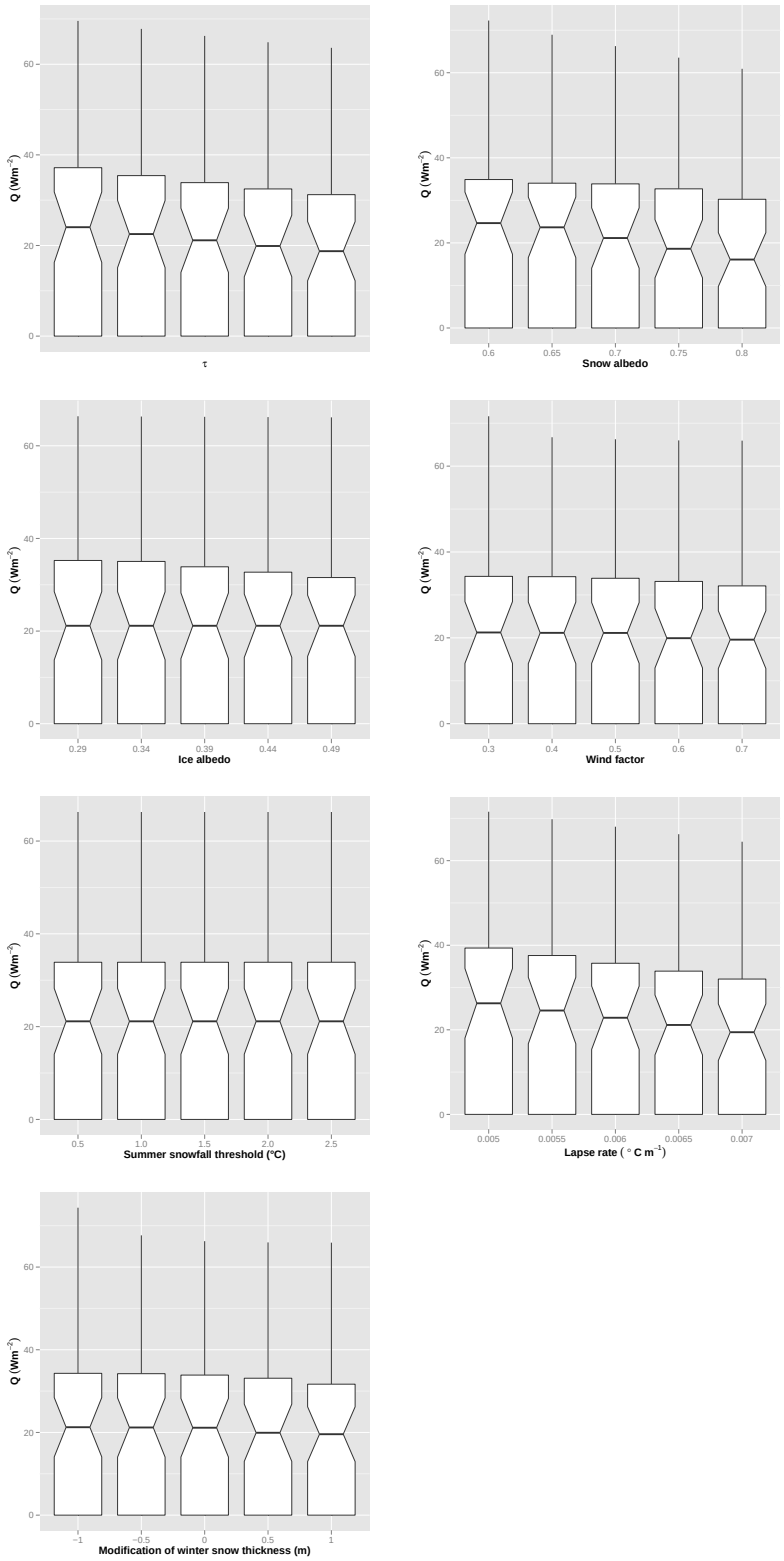

Figure 8.26: Boxplots displaying sensitivity analysis results using the contemporary model for the period of 2009-2010 (June, July and August)

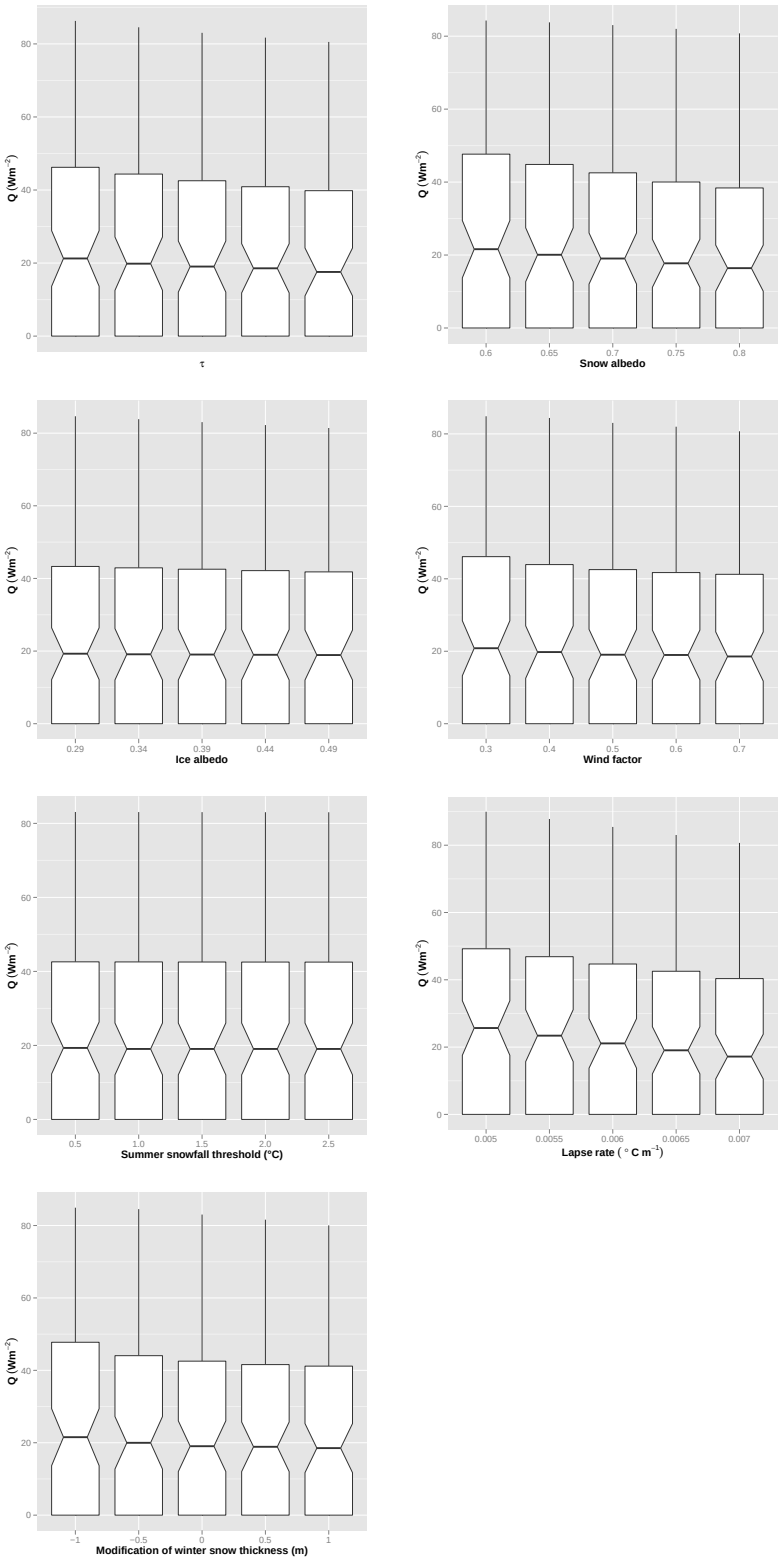

can be observed for the τ, α_{snow}, lapse rate experiments and thickness modification experiments. There is a subtle reduction in Q with increases in α_{ice} and no real change when considering summer snowfall threshold temperature.

The differences between the two models in terms of sensitivity are that the contemporary model shows a stronger sensitivity to winter snow thickness modification when compared to the historical model and the historical model shows a greater sensitivity to α_{ice}. The increased sensitivity of the historical model to ice albedo is possibly associated with the presence of a shallower snowpack at lower altitudes which is more rapidly removed during the ablation period (due to enhanced bulk flux contribution relating to higher temperatures as a function of adiabatic change), exposing the ice and enabling modification of surface Q. Importantly, this will couple with lower hillshade cover which further enhances surface Q, further increasing the rate of winter snowpack removal during the ablation period. The increased sensitivity of the contemporary model to increases in the winter snowpack thickness is interesting. Due to increased hillshade cover of the 2009-2010 glacier extent compared to that during the 1959-1978 period, the surface of which is used in the historical sensitivity analysis,a thicker snowpack will take considerably longer to remove during the ablation season, due both the increased volume and the change in α that this brings, further reducing Q at the surface. The reduced effect of hillshade across the 1959-1978 glacier surface is likely to be a key factor in the relatively reduced sensitivity of the historical model, which will result in relatively enhanced snow melt compared to a more shaded surface. This is discussed in chapter 10.

Comparing the default settings for the different sensitivity experiments represented in the individual plots of figures 8.25 and 8.26, mean Q is lower when using the contemporary model relative to the historical model, where mean Q is approximately 18 Wm^{-2} and 21 Wm^{-2} respectively. As discussed in section 8.3, the glacier by 2010 is much more shaded than it was in 1959, and it is to this which the reduction of mean Q is attributed. A true difference in Q between the two models may in fact be greater than that calculated here as the mean value of Q for the historical model may be underestimated when compared to

the contemporary model as the former is driven by mean monthly temperatures compared to the latter which is driven by daily temperatures. Monthly averaging may result in the calculation of lower temperatures — which are then used as the model input — as the mean will be sensitive to extremely low temperature values, despite lower temperatures perhaps existing for fewer hours when melt is not actually occurring.

This chapter, coupled with chapter 5 meets the aim of *developing a user friendly grid based distributed surface energy balance model which uses reconstructed surfaces as an input, combined with meteorological data from the field* and addresses the objective of *conducting model scenarios with the developed model to assess the effects of meteorological and topographic forcing on surface energy balance and mass balance change*. Considering the model performance compared to observed glacier change, model sensitivity can be used to infer glacier sensitivity. The model sensitivity results that have been considered here are coupled with the results of glacier change assessment (chapters 6 and 7) and further discussed in chapter 10 to derive an understanding of the effects of sensitivity on glacier mass change for the period 1926-2010.

Chapter 9

Results: Conventional and reference mass balance modelling

Two models — the *historical* and the *contemporary* (the definitions of which are outlined at the beginning of chapter 4) — are used to test the effect that changes in surface geometry have on ice melt on Kårsa over time. For each experimental period (discussed in sections 9.1 and 9.2.1), four experiments were carried out. Each experiment alters how the glacier surface changes through time in terms of slope and aspect as a function of elevation. To look at the effect of these properties, the experiments are defined as:

1. **Dynamic**: As the ice surface of the glacier melts, the elevation of a given cell within the model reduces. As the elevation changes the relationship with the surrounding cells is considered, resulting in changes in surface slope and aspect angles.

2. **Slope fixed** [referred to as the *Slope* model]: As the ice surface of the glacier melts, the elevation of a given cell within the model reduces. As the elevation changes the relationship with the surrounding cells is considered, resulting in changes in surface aspect angles. The surface slope angle does not change, being calculated only once for the surface at the beginning of the model run.

3. **Aspect fixed** [referred to as the *Aspect* model]: As the ice surface of the glacier melts, the elevation of a given cell within the model reduces. As the elevation changes the relationship with the surrounding cells is considered, resulting in changes in surface slope angles. The surface aspect angle does not change, being calculated only once for the surface at the beginning of the model run.

4. **Slope and aspect fixed** [referred to as the *Slope and Aspect* model]: As the ice surface of the glacier melts, the elevation of a given cell within the model reduces. Despite the elevation changes the surface slope and aspect angles do not change, being calculated only once for the surface at the beginning of the model run.

This chapter meets the objective of:

- Conducting model scenarios with the developed model to assess the effects of geometry change on surface energy balance and mass balance change

therefore addressing the project aim of:

- Assess the effect of changing glacier geometry on the surface energy balance and mass balance of a small mountain glacier throughout the 20th and early 21st century with focus on solar radiation contributions and glacier-topography relationships

9.1 Historical melt modelling experiment results

9.1.1 Meteorological inputs for model runs: 1926-2010

The historical melt model runs were carried out for the periods 1926-1943, 1943-1959, 1959-1978, 1978-1991 and 1991-2010. These intervals are defined in conjunction with the maps of the glacier available and that have been used for the geodetic assessment of glacier change in chapter 6. As discussed at the beginning of this chapter, four model runs were implemented for the different time periods. Of interest in this study is the effect that changing glacier surface geometry has

on ice melt. To assess the effect that the conditions of each different model had on overall ice melt, results are addressed in terms of mean annual melt. There is also consideration of any changes in the energy mix - specifically the contribution of the separate components of I and ψ to Q and acknowledgment of changing meteorological conditions.

The meteorological conditions — compiled using methods described in section 5.2 of chapter 5 — that are used as the model input are summarised in figure 9.1. The mean end of winter season snow thickness and the temperatures displayed are averaged from across the glacier surface (temperature as a function of elevation through time is discussed in detail in chapter 5). Summer (June, July and August) and winter (November, December, January and February) temperatures are displayed over time to further emphasise any trends observable from the data available.

A visual assessment of the annual temperature data across the glacier from 1926 to 2010 reveals that there are no particularly discernible trends, especially when considering the moving average. Considering mean annual temperatures, the warmest years were 1990 and 1938 with average temperatures of -3.7 and -3.8°C respectively. The coolest years were 1955 and 1966 with average temperatures of -7.1 and -6.9°C respectively. The warmest decades were the 2000s and 1930s with temperatures of -4.2 and -4.7°C respectively. The coolest decades were the 1950s and 60s with temperatures of -5.6 and -5.4°C respectively.

Spring temperatures over the 1926-2010 period appear to be relatively stable. Upon closer inspection there are some quite large changes. The warmest springs were in 2003 and 2004, both with mean temperatures of 5.0°C. The coldest springs were in 1966 and 1955 with temperatures of -9.5 and -9.1°C respectively. This is indicative of a range in mean spring temperatures of approximately 4°C.

The summer temperatures show more variation with peaks and troughs being more apparent. Using a 10 point moving average, there are periodical peaks

Figure 9.1: Meteorological data (as model input) for the 1926 - 2010 period (Air temperature and mean winter snowpack thickness)

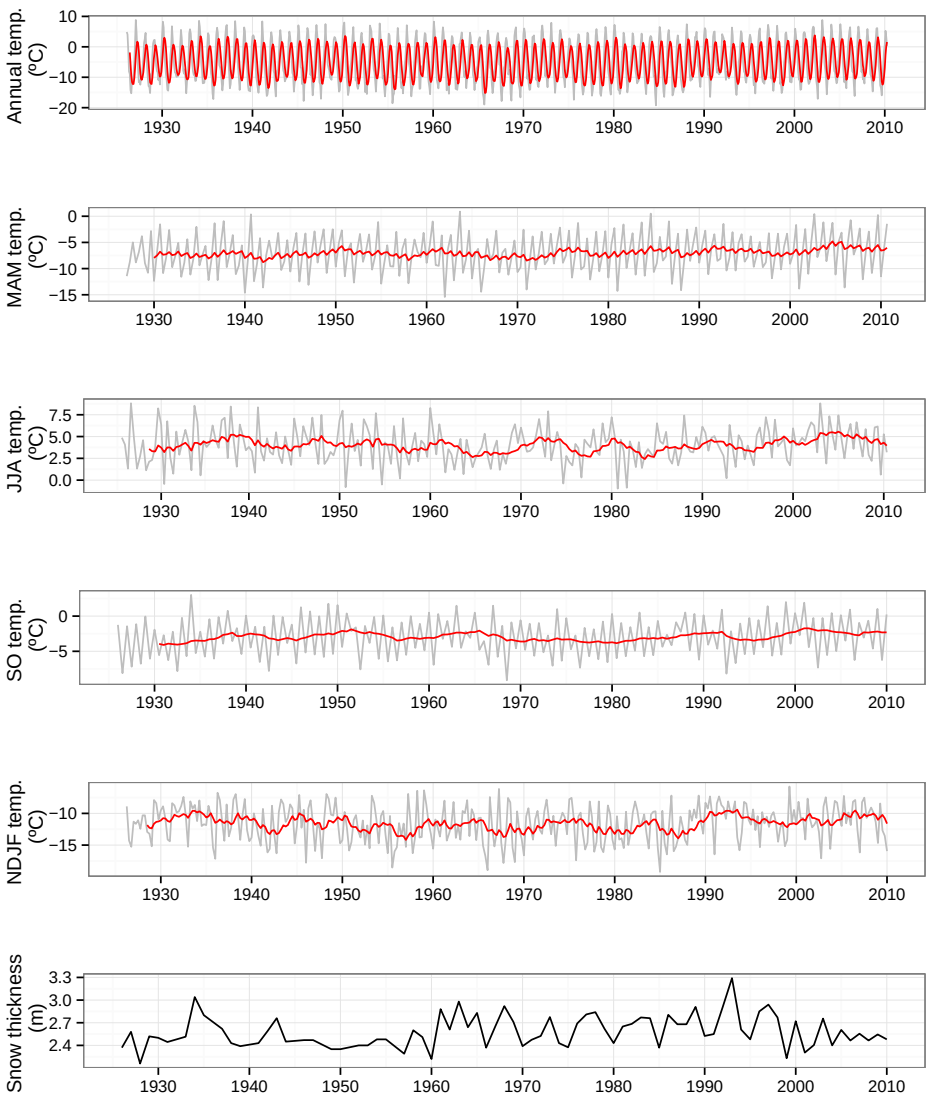

approximately every 10-12 years and an approximate 10 year periodicity for temperature troughs. The warmest summer decades were the 1930s and the 2000s with means of 4.6 and 4.7°C respectively. The coolest summer decades were the 1920s and 1960s, both with a mean temperature of 3.5°C. The warmest summers were in 1950 and 2002 with mean temperatures of 6.3 and 6.2°C respectively. The coolest summers were in 1975 and 1929 with mean temperatures of 1.5 and 1.9°C respectively.

The coolest autumn temperatures are recorded for 1968 and 1966 both with temperatures of -5.2°C. The warmest Autumn temperatures were in 2010 and 1951 with respective temperatures of 0.2 and -0.9°C.

The winter temperatures show a slightly different periodicity compared to the summer temperatures. Up to 1970, temperature troughs have an approximate 5 year periodicity. From the 1970s, the spacing increases to approximately every 10 years. A return to a shorter trough spacing appears to redevelop at the beginning of the 2000s. The trough periodicity is approximately matched by the spacing between winter temperature peaks. The coldest winter decades were the 1950s and the 1960s with means of -12.4 and -12.3°C respectively. The warmest winter decades were the 1930s and 1990s/2000s, with mean temperatures of -10.8 and -10.9°C respectively. The coldest winters were in 1965/1966 and 1955/1956 with mean temperatures of -15.1 and -15.4°C respectively. The warmest winters were in 1991/1992 and 1948/1949 with mean temperatures of -8.4 and -8.8°C respectively.

9.1.2 Surface melting under different experimental conditions: 1926-2010

Considering mean glacier melt in terms of quartiles (figure 9.2) there appears to be no significant change when considering the median, upper and lower quartiles in annual melt for all experiments in the period 1943-2010. The only clear changes are in the outliers and such variability is most apparent when considering the results for experiments conducted for the 1959-1978 period, with there being more outliers for the dynamic model than for the slope, aspect and slope & aspect

models. This general lack of trend is not however followed by the results of experiments conducted for the 1926-1943 period. In this instance, there is a stark contrast between the dynamic model results and those for the slope, aspect and slope & aspect models. There is a difference in mean melt from 0.31 m yr^{-1}, for the dynamic output, compared to 0.74 m yr^{-1} for the remaining three models. Considering the other models relative to the dynamic model run in terms of the lower and upper quartiles, these are 0.1 m and 0.6 m greater respectively. Considering these quartiles, it can be deduced that there is an increase in the interquartile range from 0.36 m to 0.86 m for the dynamic and other runs respectively indicating a greater dispersion of melt values. When considering the outliers, these are not thought to be anomalous but are special cases, explained as being caused by the positioning of areas of the glacier in particularly favorable conditions to melt. Clearly from this, for the 1926-1943 period, surface melt was enhanced where slope, aspect or both slope and aspect together were fixed, compared to a dynamic model run where slope and aspect change through time in line with surface elevation lowering occurring in response to ice melt.

Considering the limited changes between the model outputs for the 1946-2010 period following the assessment of figure 9.2, as to be expected, there is little difference between the categorized melt patterns for the same period as can be seen in figure 9.3. There are some subtle changes that can be identified but these are most apparent as changes over time as opposed to changes between model outputs and this will be discussed further below in relation to figure 9.4. Some very subtle shifts in the proportional melt can be deduced between some model runs, for example during the 1991-2010 test period, a slight increase in the 0 - 0.25 m category can be seen between the dynamic and aspect runs which then reduces again for the slope and slope and aspect runs. Such changes are within the order of <1% and consequently are not treated as being significant.

The most clear changes in proportional melt can be drawn from the 1926-1943 test period where there is a very clear shift in the pattern of change when considering the dynamic compared to the other model runs. Fixing geometry either in terms of slope, aspect or both slope and aspect together results in a decrease from 77%

Figure 9.2: Box plots of annual surface melting for experiments within the 1926 - 2010 period

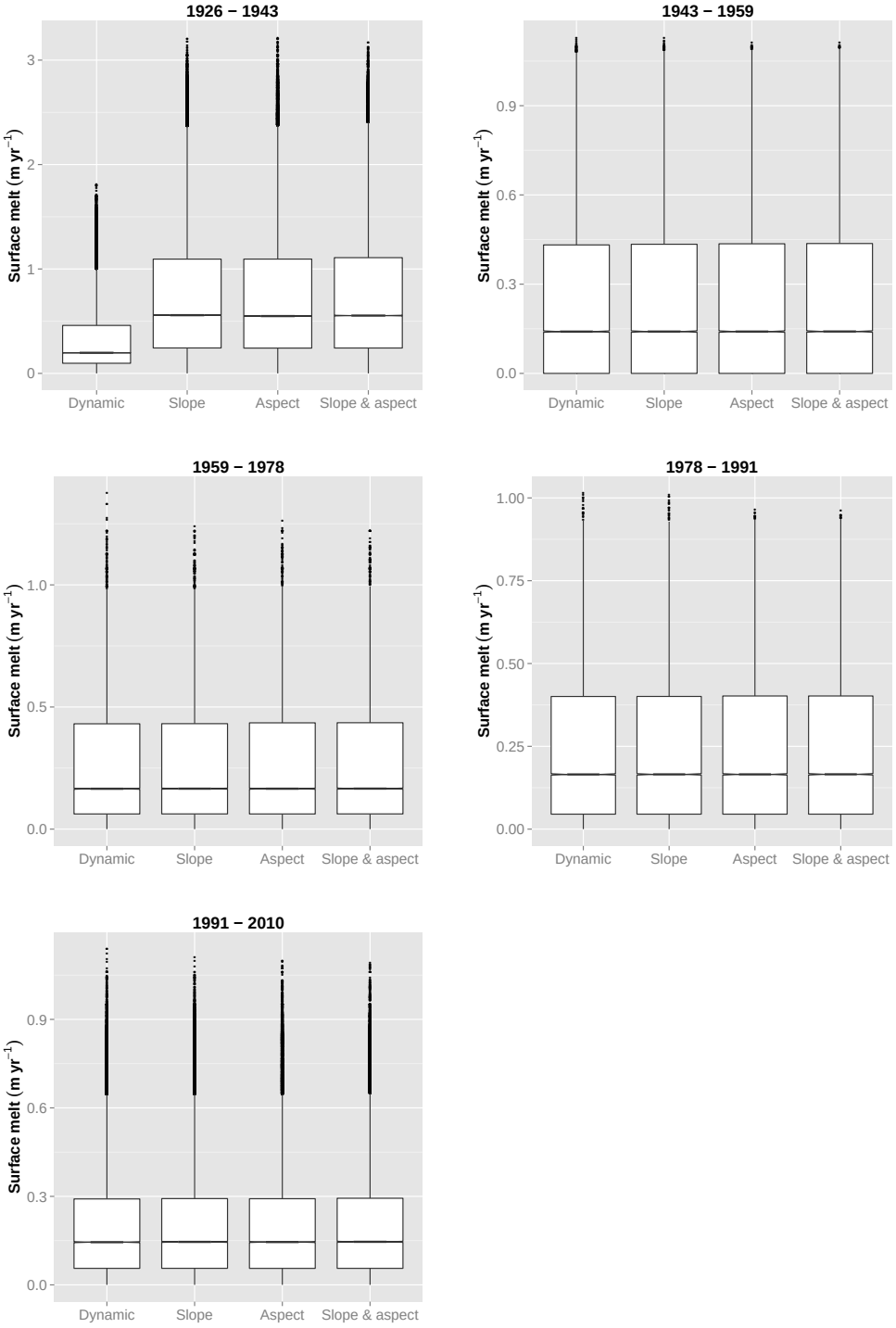

to 46% of melt occurring within the 0-0.5 melt category. For all other categories, the dynamic model run proportions are exceeded by those of the other runs with an increase in total glacier melt proportions of 7%, 8%, 10% in the 0.5-1, 1-1.5 and 1.5-2 m categories. For the slope, aspect and slope and aspect runs, there is also melt accounted for in categories of melt >2 m which are not reached when using the dynamic model. This further addresses the sensitivity of the glacier to geometry change during the 1926 - 1943 period and the lack of sensitivity to it from 1943 onwards, there being little or no change between dynamic and fixed geometry model runs in this period.

So far, the model outputs have been considered in terms of the effects that geometry specifically has on melt rates. It is also both interesting and prudent to consider the changes in melt patterns over time *as well* as considering the effects of geometry change. Change over time, relative to the models used, are displayed in figure 9.4. Irrespective of the models used and considering median annual melt values, thus avoiding any skew that mean values will be susceptible to considering some areas of comparatively high melt, annual melt rates were greatest during 1926-1943 jointly followed by 1959-1978 and 1978-1991, with the least melt jointly for the 1943-1959 and 1991-2010 periods. The change in melt rate is displayed for the dynamic model runs for all periods in figure 9.5. Specifically considering annual melt rates >0.75 m yr^{-1} and again irrespective of the models used, the most melt occurred during 1926-1943, followed by 1943-1959, 1991-2010, 1978-1991 and 1959-1978. Considering annual melt rates <0.75 m yr^{-1}, the most melt occurred during 1959-1978 followed by 1978-1991, 1991-2010, 1943-1959 and 1926-1943 which matches the pattern represented when using the median as a measure of overall melt.

For all runs within the 1943-1959, 1959-1978, 1978-1991 and 1991-2010 periods, the aforementioned patterns hold true and do not vary. The general patterns mentioned above also hold for all model runs within the 1926-1943 time frame however the specific proportions vary significantly. Using the median as a measure of annual melt for dynamic and fixed geometry runs (treated together here), values of 0.2 m yr^{-1} and 0.6 m yr^{-1} are found respectively. This still indicates that the

Figure 9.3: Cumulative histograms of annual surface melt for experiments within the 1926 - 2010 period. Plots are displayed here to emphasize the changes within a set time frame as a function of model type.

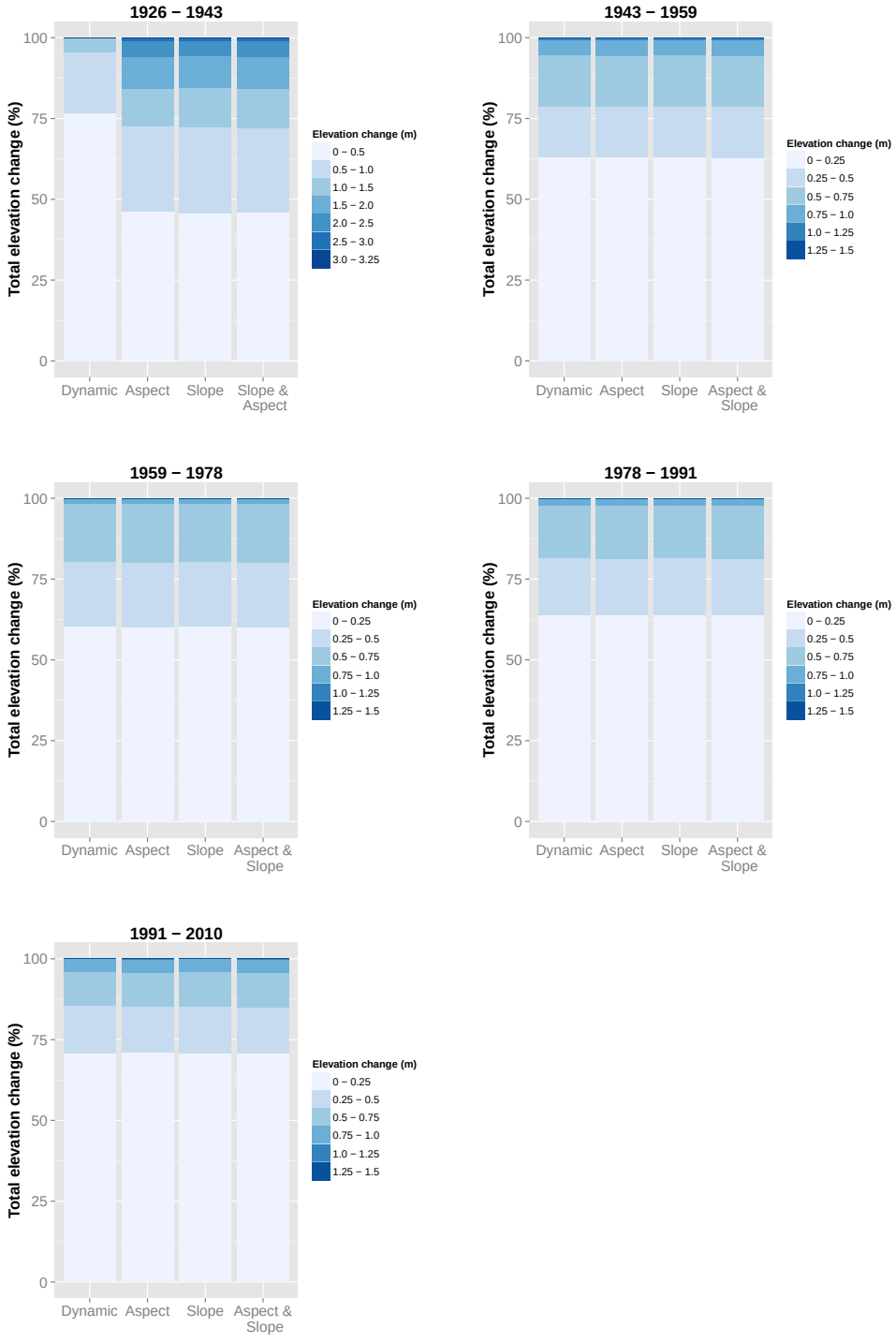

Figure 9.4: Cumulative histograms of annual surface melt for experiments within the 1926 - 2010 period. Plots are displayed here to emphasize the change in melt patterns over time as a function of Model type.

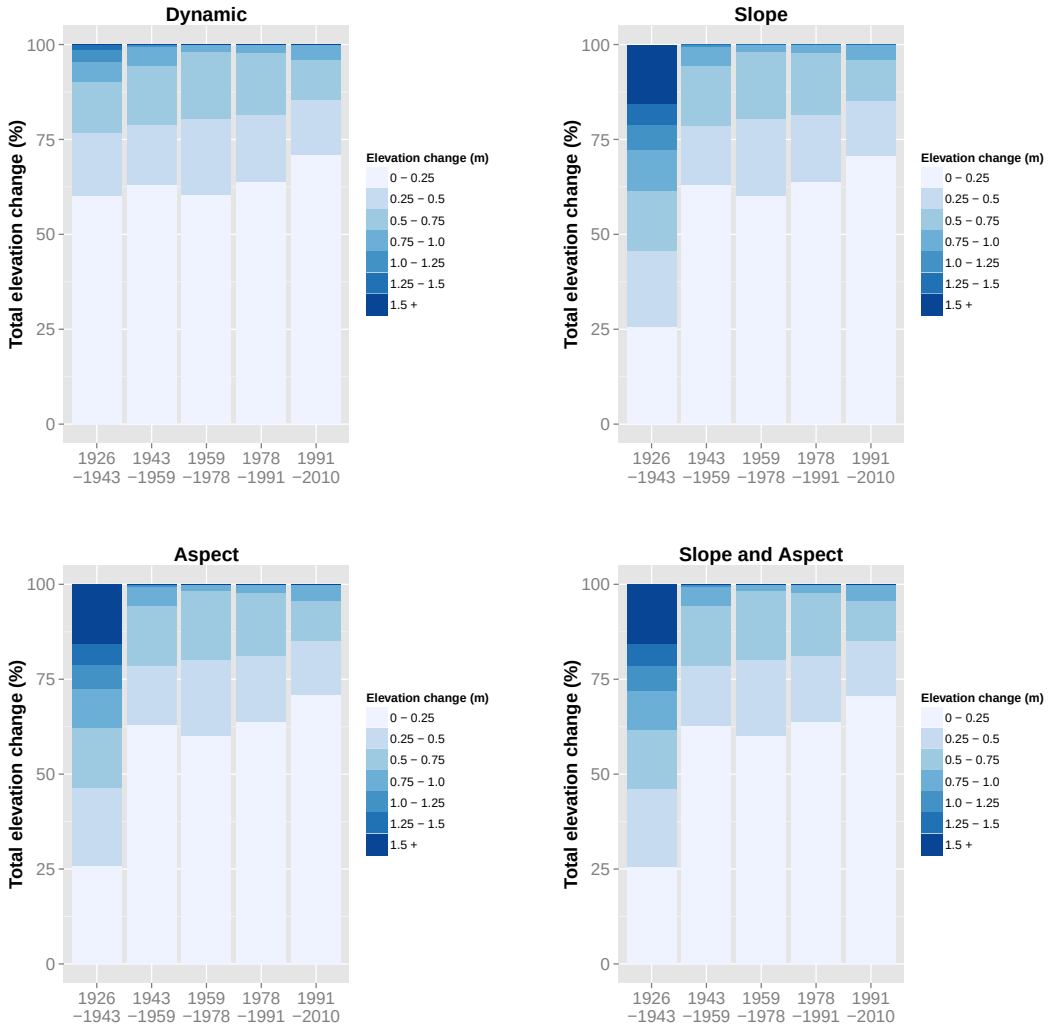

Figure 9.5: Historical model experiment results: Change in melt rate over the 1926 - 2010 period (results from the dynamic model experiments)

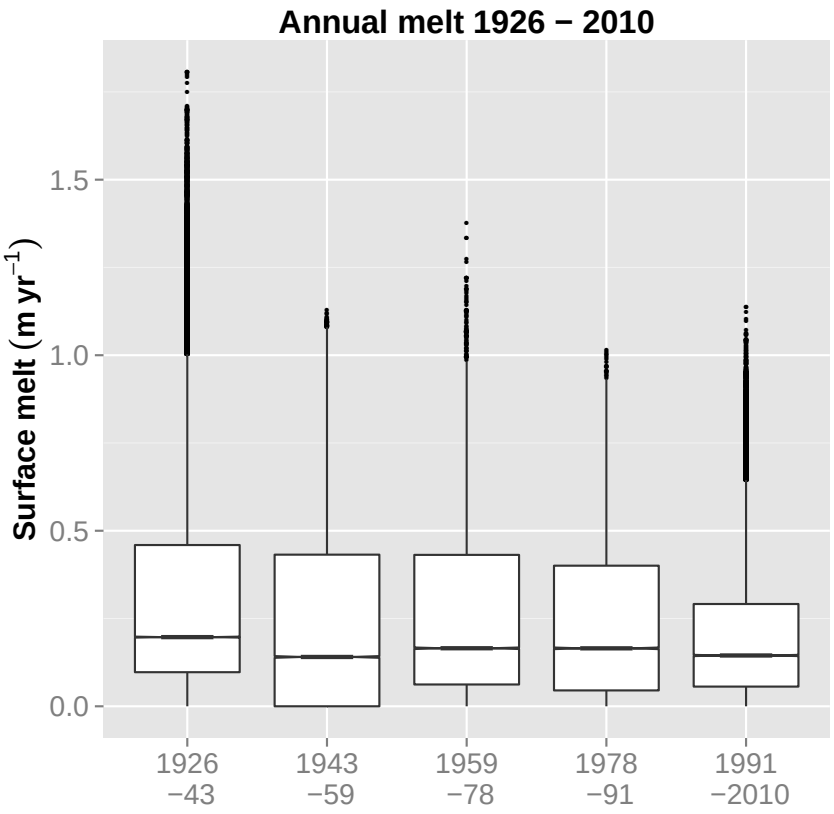

highest annual melt, based on the median, was during 1926-1943, but to a much greater extent when considering fixed geometry. With regard to melt rates >0.75 m yr^{-1}, 10% and 38% of melt occurred for the dynamic and fixed runs respectively. The increased levels of melt for the fixed model runs in the 1926-1943 period are matched by a reduction in the total glacier melt occurring within the 0.75 m yr^{-1} category with a 62% representation compared to 90% for the dynamic run.

9.1.3 Historical mass balance change

Mass balance curves for the individual model runs and map interval time periods are displayed in figure 9.6. For all runs there is a general trend for reduced mass balance change with elevation. The separate model runs appear to have had little effect on mass balance patterns across the glacier elevation range following 1943. Prior to 1943, the slope fixed, aspect fixed and both slope and aspect fixed model runs have a strong effect on the 1926-1943 mass balance profile, dramatically increasing melt, particularly at elevations below approximately 1200 m a.s.l. The maximum modelled melt for the 1926-1943 increases from -1.25 m w.e for the dynamic run to approximately -2.4 m w.e. Reductions in mass balance change are clearly illustrated by the 1926-1943 curve under fixed model conditions between the 1190 - 1300 m a.s.l. elevation range. Such changes are not easily discernible for the other map intervals.

Figure 9.7 presents mass balance curves average from the results of the full length historical model run, from 1926-2010, and represented according to the 2010 elevation range. The curves in figure 9.7 indicate enhanced melting conditions under all fixed model runs, the most suppressed values being calculated for the dynamic run. The fixed runs all have a maximum mass balance change value of approximately -1.25 m w.e. compared to -0.5 m w.e. for the dynamic run. All runs show mass balance changes to be most suppressed in the 1190 - 1300 m a.s.l. elevation range and then above 1400 m a.s.l. but again, this is enhanced for the fixed runs.

Figure 9.6: Map interval mass balance curves for the aspect fixed, slope fixed, both fixed and dynamic model runs. Curves are displayed in m w.e. and are generalised for elevation bands on a 1 m interval across the different glacier ranges.

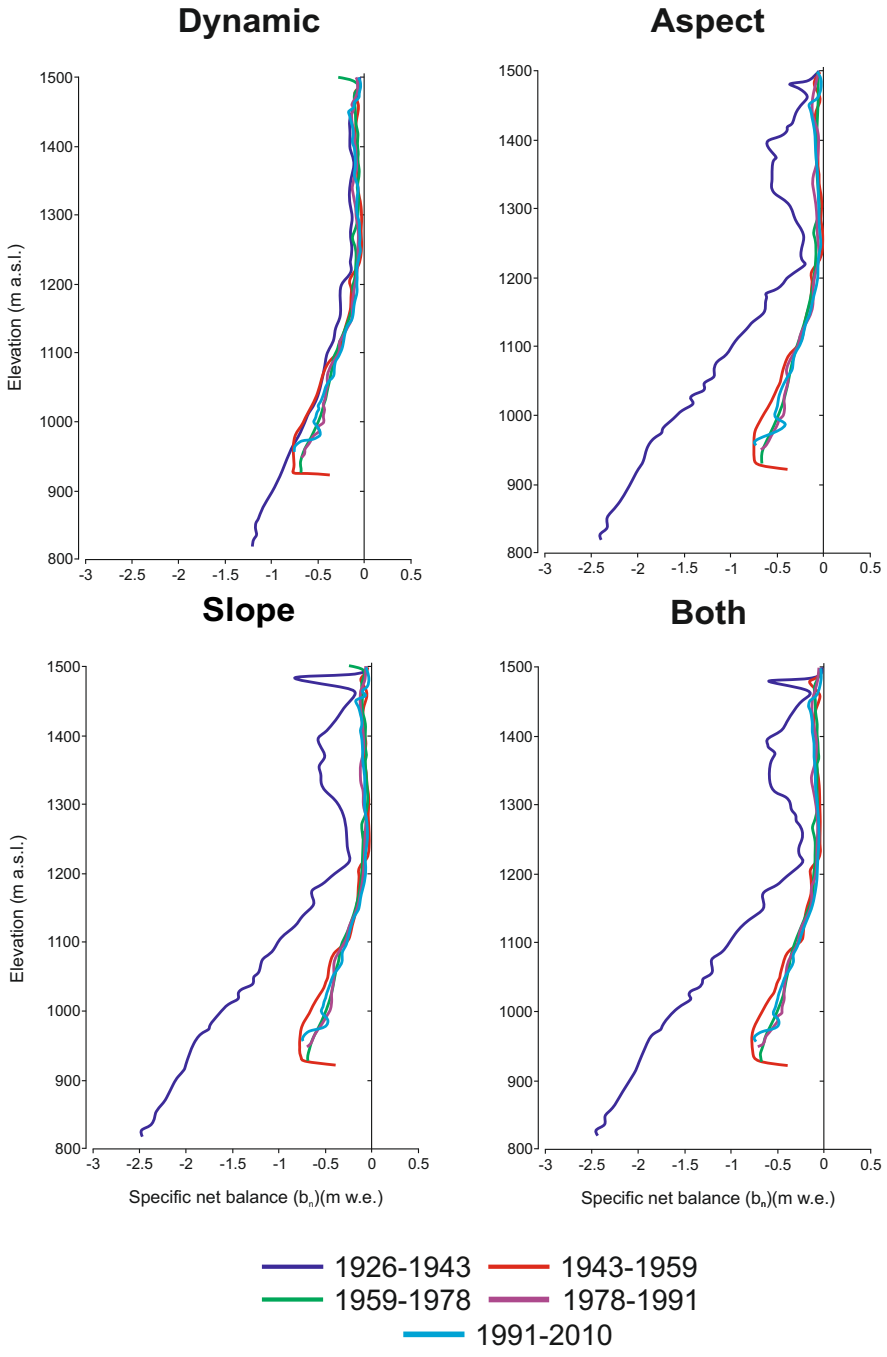

Figure 9.7: Mass balance curves for the aspect fixed, slope fixed, both fixed and dynamic model runs over the full 1926-2010 time period. Curves are displayed in m w.e. and are generalised for elevation bands on a 1 m interval across the different glacier ranges.

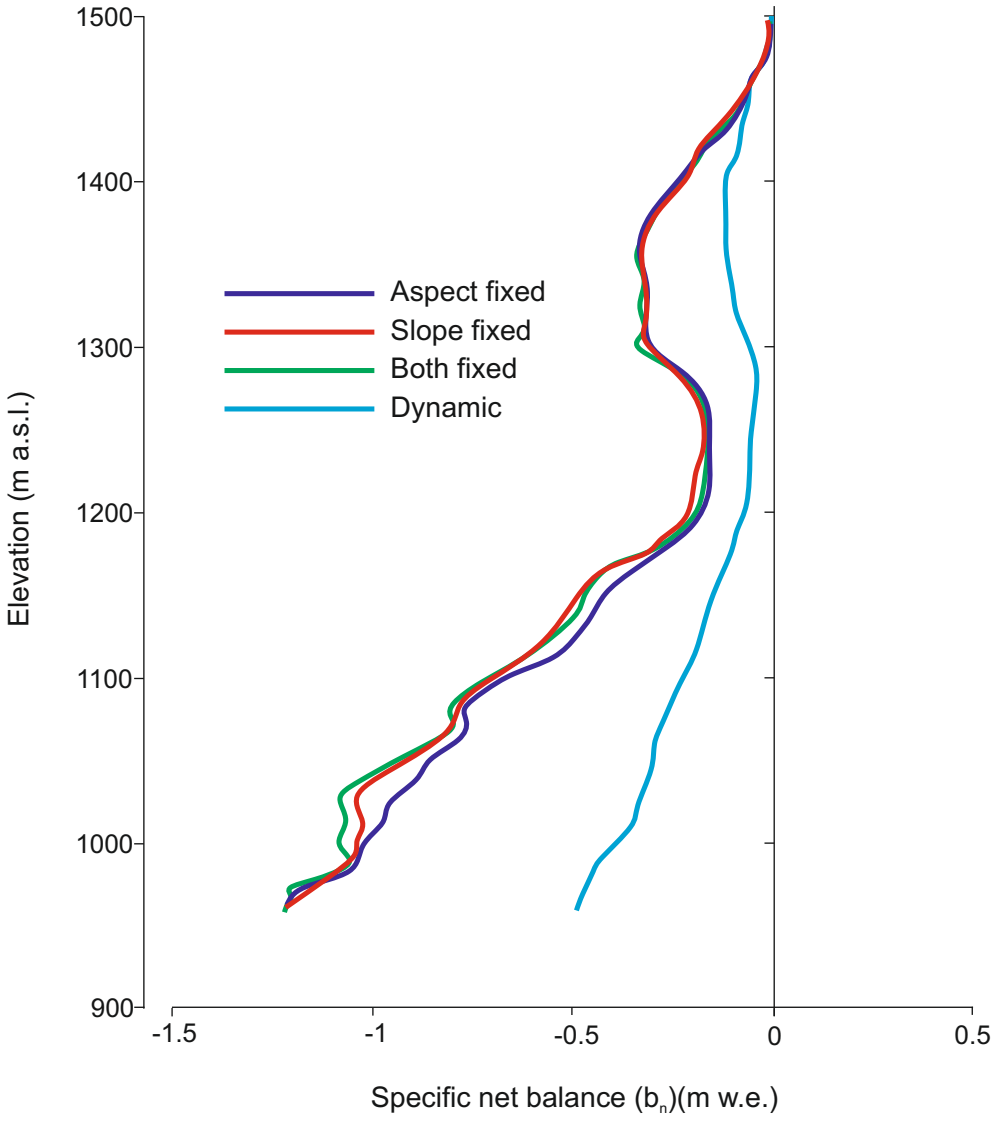

Table 9.1: F_i statistics representing melt differences between dynamic and non-dynamic experimental model runs: 1926 - 2010

Model interval	Aspect F_i	Slope F_i	Both F_i
1926-1943	-0.58	-0.58	-0.58
1943-1959	0.00	0.00	0.00
1959-1978	0.00	0.00	-0.01
1978-1991	0.00	0.00	0.00
1991-2010	-0.01	0.00	-0.01
1926-2010	-0.39	-0.41	-0.40

9.1.4 F_i statistics: 1926-2010

As discussed in section 2.3.6, Huss *et al.* (2012) proposed the use of the F_i statistic to quantify the difference between conventional and reference balance calculations (see equation 2.13). As few studies have acknowledged the specific variability between conventional and reference mass balance, the use of this analytical approach is prudent in this study in an attempt to further integrate usage of the method in future research. To further quantify change in the melt that propagates under the different experimental conditions forced in this study, a modified version of the F_i statistic is used, whereby the value of F_i is calculated using conventional and reference mean elevation changes as opposed to mass balance values. The results for the 1926-2010 runs are presented in table 9.1 - negative F_i values occur where the reference balance is less than the conventional balance and *vice versa*. For the individual periods between 1943-2010, there is no real difference between the dynamic and experimental runs. The 1926-1943 period shows the strongest sensitivity to all experimental runs with approximately equal differences between the fixed (reference) surface runs and conventional (dynamic) runs. Similar variation between the reference and conventional runs is also found for 1926-2010 period, although the degree of variability is reduced and may be explained by the limited variability identified between conventional and reference balances for the interim periods of 1943-2010.

Huss *et al.* (2012) caution against generalising with the F_i statistic, which is ultimately the % difference between conventional and reference balance surfaces,

as it is only relevant to the specific year or period - and the associated conditions - for which it is calculated. Comparing F_i between periods is made more difficult if one considers the varying relationships that can exist between mass balance change (with potential annual variability) and conventional/reference balance differences (which can vary over longer time frames). These topics are discussed thoroughly in Huss *et al.* (2012) with examples from a number of Swiss glaciers. What can be drawn from this is that the F_i alone is limited outside of considering a specific glacier in a specific period, yet provides a useful approach for considering specific geometric effects within the given time frames.

9.1.5 Change in component contributions to Q: 1926-2010

The change in the proportional contributions of I and ψ to total Q across the glacier surface during the summer months are displayed in figure 9.8. Other than for the 1926-1943 period, there is no observable change in the energy mix, which is implicit that the energy mix is not sensitive to changing surface geometry in the period 1943-2010. Considering dynamic geometric changes in association with a melting glacier surface compared to a surface with fixed geometry, there is a clear difference in the component contributions to the energy mix through the 1926-1943 period. With a fully dynamic geometry, the importance of ψ is far greater than compared to when geometry is fixed when I is a much larger component of Q. The contribution of ψ for the dynamic and fixed runs is 42% and 23% respectively and this compares to contributions of I which are 58% and 77% respectively.

It is interesting to consider the change in energy mix contributions over time (figure 9.9). There is a distinct reduction in the contribution of ψ to Q from 42% to 30% over the 1926-1978 period, which then increases back to 42% by the 1991-2010 period. Conversely, the contribution of I to Q increases from 58% to 69% from 1926-1978 and then reduces to 58% by 1991-2010. Considering the changing size of the glacier in the 1926-1943 and 1991-2010 periods, it is interesting that the proportional contributions are so similar.

Figure 9.8: Surface energy balance (Q) composition change between model run types for experiments during the 1926 - 2010 period.

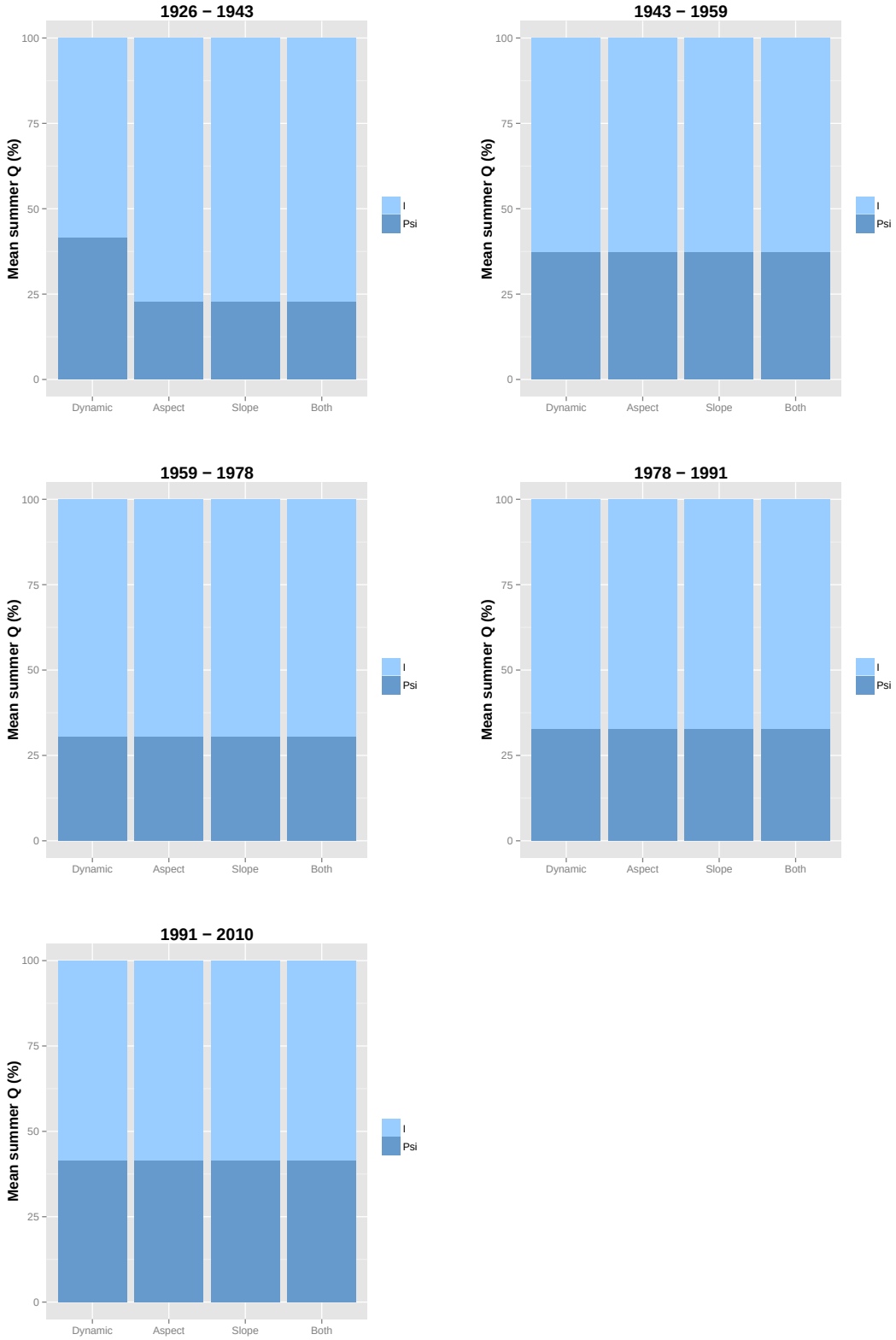

Figure 9.9: Surface energy balance (Q) composition change over the 1926 - 2010 period.

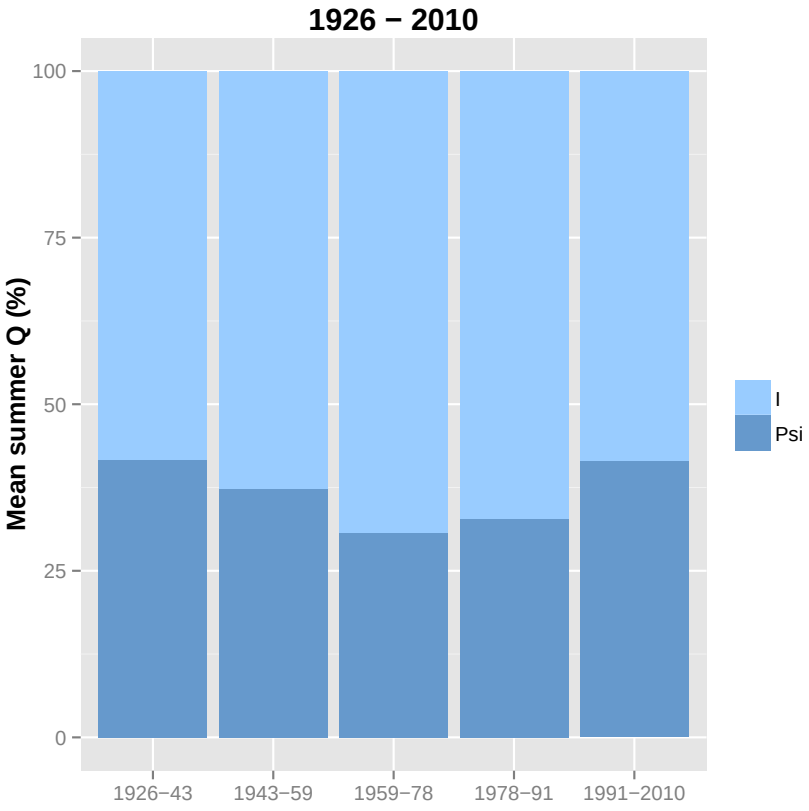

9.2 Contemporary model results

9.2.1 Meteorological inputs for model runs: 2007-2010

The contemporary melt model runs were carried out for the periods 2007-2008, 2008-2009, 2009-2010 and 2007-2010. These intervals are defined in conjunction with the maps of the glacier available and that have been used for the geodetic assessment of glacier change (see chapter 6). As for section 9.1, the same four model runs were used for the defined time periods. As in section 9.1, to assess the effect that the conditions of each different model had on overall ice melt, results are addressed in terms of mean annual melt and any changes in the contribution of components I and ψ to Q and acknowledgment of changing meteorological conditions.

Figure 9.10 illustrates the mean temperature and snow depth data used within the contemporary model runs. This data was compiled using methods described in section 5.1 of chapter 5. Both the temperature and mean end of winter season snow thickness values displayed represent the mean as calculated from across the glacier surface over time. There is an observable temperature fluctuation each January-March where temperature rises and then drops again. This pattern appears strongest in 2010. Spring temperatures were greatest in 2009 with temperatures of -4.1°C compared to the lowest temperature in 2010 at -6.5°C, giving a range of 2.4°C. With regard to the summer temperatures, the warmest year was in 2009 with a mean temperature of 4.2°C. This was opposed by the coolest summer in 2010 with a mean temperature if 2.9°C. Autumn temperatures were lowest in 2007 with temperatures of -6.7°C compared to the warmest temperature of -1.5°C recorded in 2010, giving a 2007-2010 autumn temperature range of 5.2°C. In terms of winter temperatures, the warmest winter was during 2007/2008 with a mean temperature of -9.6°C. The coldest winter was during 2009/2010 with a mean temperature of -12.6°C.

Figure 9.10: Meteorological data (as model input) for the 2007 - 2010 period (Air temperature and mean winter snowpack thickness)

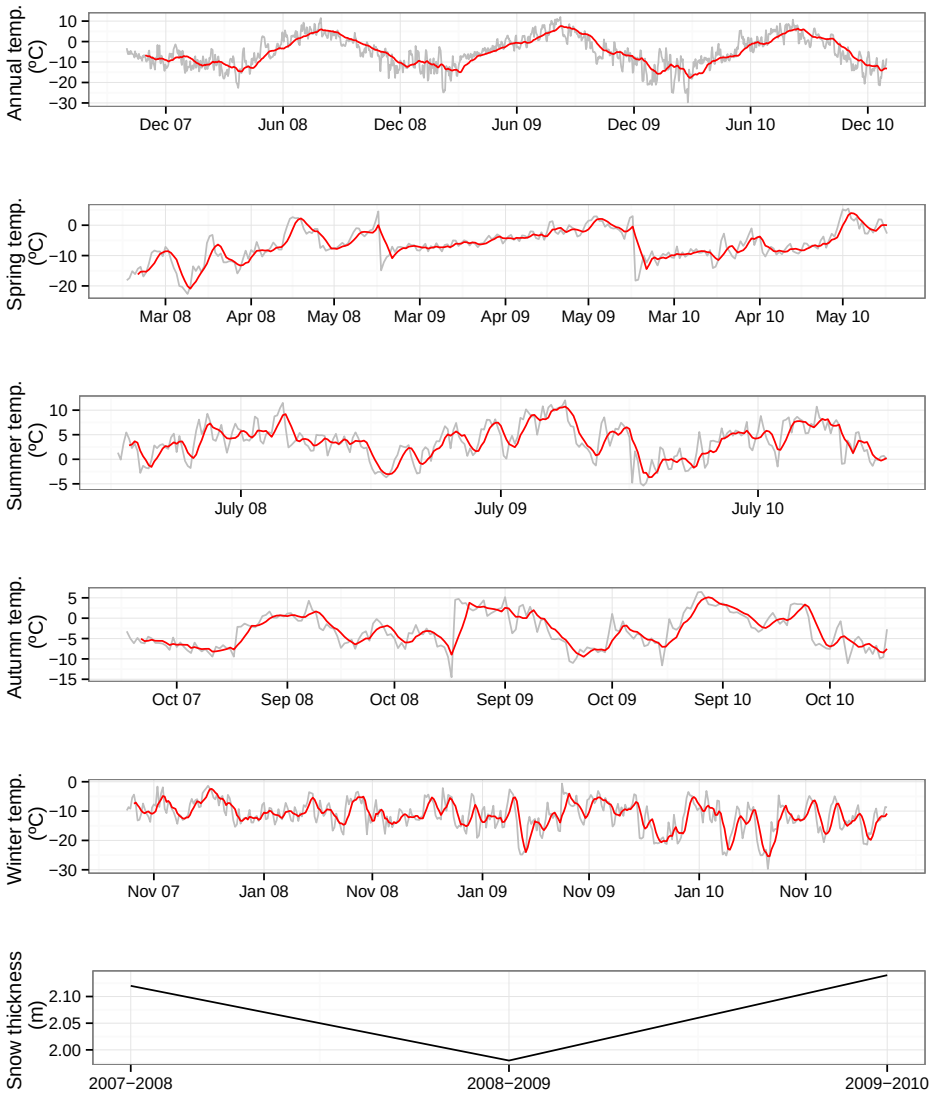

9.2.2 Surface melting under different experimental conditions: 2007-2010

Considering mean glacier melt in terms of quartiles (figure 9.11) there appears to be no significant change when considering the median, upper and lower quartiles in annual melt for all experiments in the period 2007 - 2010. The mean values hold at 0.24 m yr^{-1}, 0.47 m yr^{-1} and 0.27 m yr^{-1} for all model tests within the 2007-2008, 2008-2009, 2009-2010 experimental periods respectively. From this it is apparent that for the 2007-2010 period, the glacier is insensitive to surface geometry change. There are some very subtle changes between the upper and lower quartiles for the models but these are <0.01 m yr^{-1} and consequently are not discussed any further.

Following on from the limited changes between the model outputs discussed above in relation to figure 9.11, there is no real difference between the categorized melt patterns for all test periods as can be seen in figure 9.12.

The most clear changes occurring as a result of the contemporary melt model experiments can be considered when assessing the changes in melt patterns over time. Irrespective of the models used and considering both the mean and median annual melt values, annual melt rates were greatest during 2008-2009 ($\hat{x}$ = -0.47 m; median = -0.41 m), followed by 2009-2010 ($\hat{x}$ = -0.27 m; median = -0.20 m) and then 2007-2008 ($\hat{x}$ = -0.24 m; median = -0.16 m). Specifically considering annual melt rates >0.75 m yr^{-1} and again irrespective of the models used, the most melt occurred during 2008-2009 (18%)), followed jointly by 2009-2010 and 2007-2008 (5%). Considering annual melt rates <0.75 m yr^{-1}, the most melt occurred during 2007-2008 and 2009-2010 jointly (95%) followed by 2008-2009 (82%). The general patterns mentioned hold regardless of the models used, further emphasising the apparent lack of sensitivity of the glacier surface to changes in geometry within the time period tested.

Figure 9.11: Box plots of annual surface melting for experiments within the 2007 - 2010 period

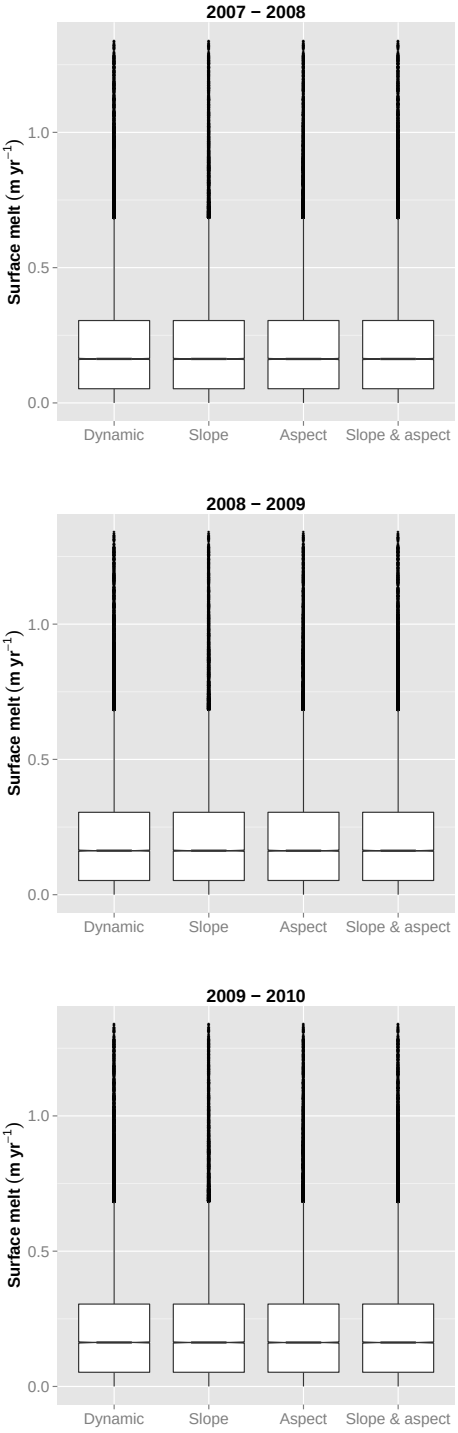

Figure 9.12: Cumulative histograms of annual surface melt for experiments within the 2007 - 2010 period. Plots are displayed here to emphasize the changes within a set time frame as a function of model type.

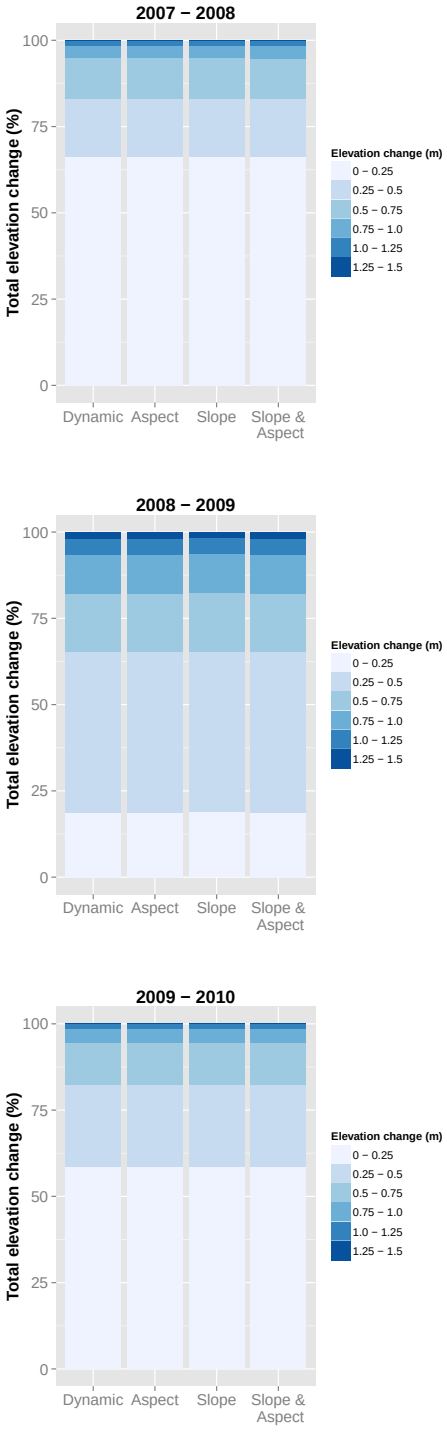

Figure 9.13: Cumulative histograms of annual surface melt for experiments within the 2007 - 2010 period. Plots are displayed here to emphasize the change in melt patterns over time as a function of model type.

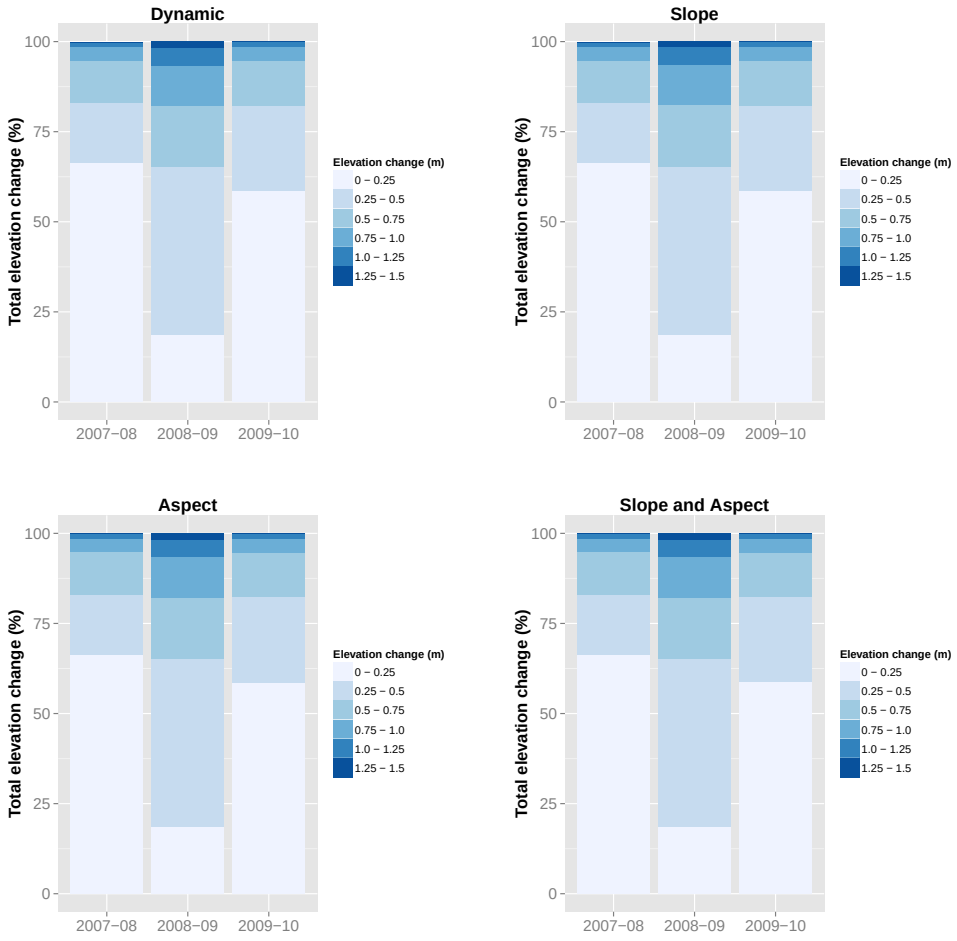

Table 9.2: F_i statistics representing melt differences between dynamic and non-dynamic experimental model runs: 2007 - 2010

Model interval	Aspect F_i	Slope F_i	Both F_i
2007-2008	0.00	0.00	0.00
2008-2009	0.00	0.00	0.00
2009-2010	0.00	0.00	0.00
2007-2010	0.00	0.00	0.00

9.2.3 Contemporary mass balance change

Mass balance curves for the individual model runs and time periods are displayed in figure 9.14. A general reduction in mass balance change with increasing elevation is clear for all model runs, with a trough in this trend appearing for all runs between 1250-1350 m a.s.l. These charts display curves that appear to show mass balance profiles which exhibit no change for the map interval model runs. Changes in mass balance between years are clear, with the most change being attributed to 2008-2009, but between model runs there appears to be little change.

Considering mass balance profile change for the long term model experiments (figure 9.15), thus removing inter-annual variability, the minimal difference between the different model runs is clear.

9.2.4 F_i statistics: 2007-2010

As for the 1926-2010 model runs, change in the melt that propagates under the different experimental conditions is represented here using the modified version of the F_i statistic proposed by Huss *et al.* (2012). The results for the 2007-2010 runs are presented in table 9.2. As is clear, there is no difference between the different runs.

9.2.5 Change in component contributions to Q: 2007-2010

The change in the proportional contributions of I and ψ to total Q across the glacier surface during the summer months are displayed in fugure 9.16. There are no observable changes in the energy mix between the models for all intervals

Figure 9.14: Mass balance curves for the aspect fixed, slope fixed, both fixed and dynamic model runs. Curves are displayed in m w.e. and are generalised for elevation bands on a 1 m interval across the different glacier ranges.

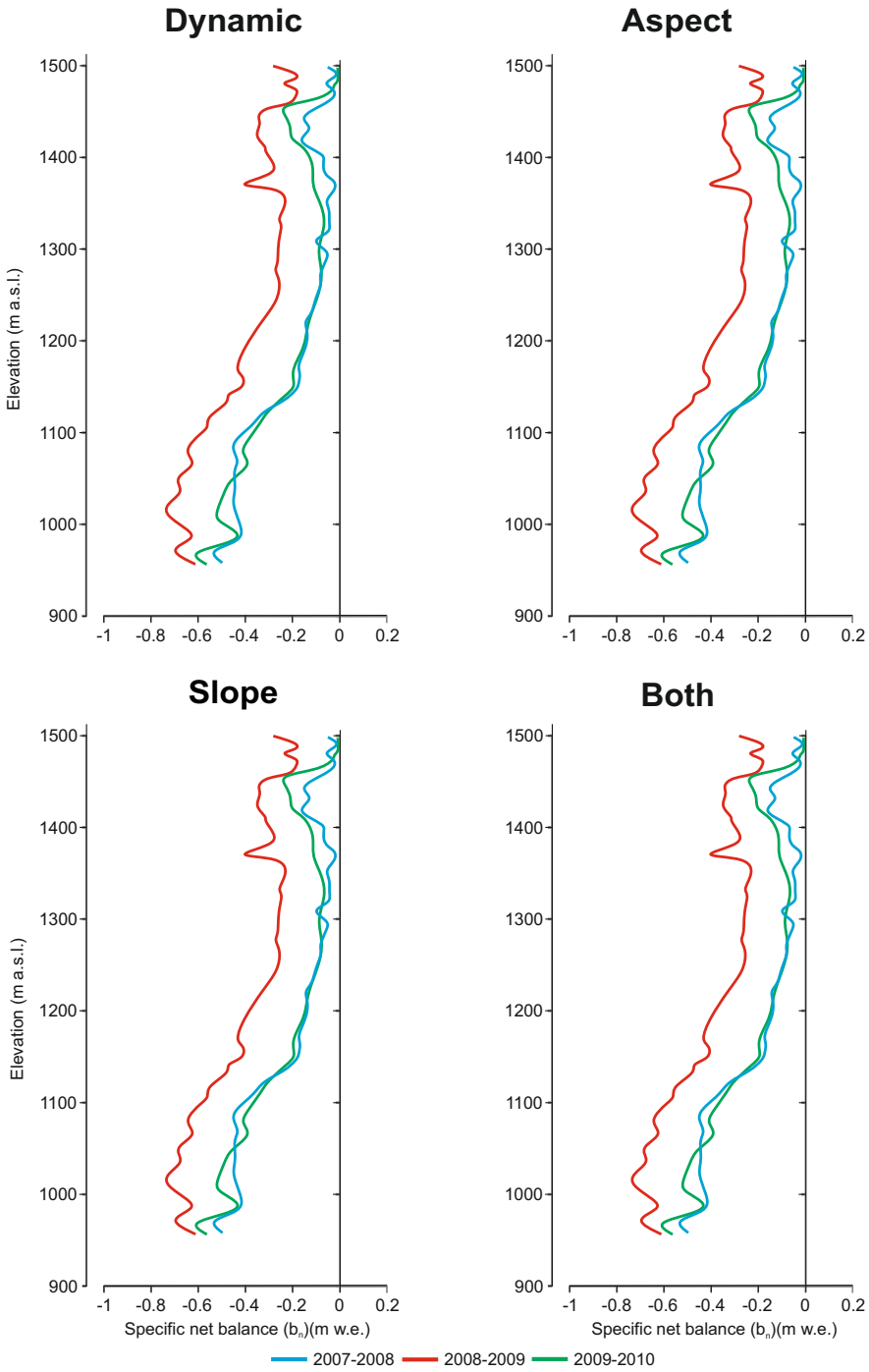

Figure 9.15: Mass balance curves for the aspect fixed, slope fixed, both fixed and dynamic model runs over the full 2007-2010 time period. Curves are displayed in m w.e. and are generalised for elevation bands on a 1 m interval across the different glacier ranges. The lack of difference between the different runs is clear and differs significantly to the pattern shown between model runs for the 1926-2010 period displayed in figure 9.7

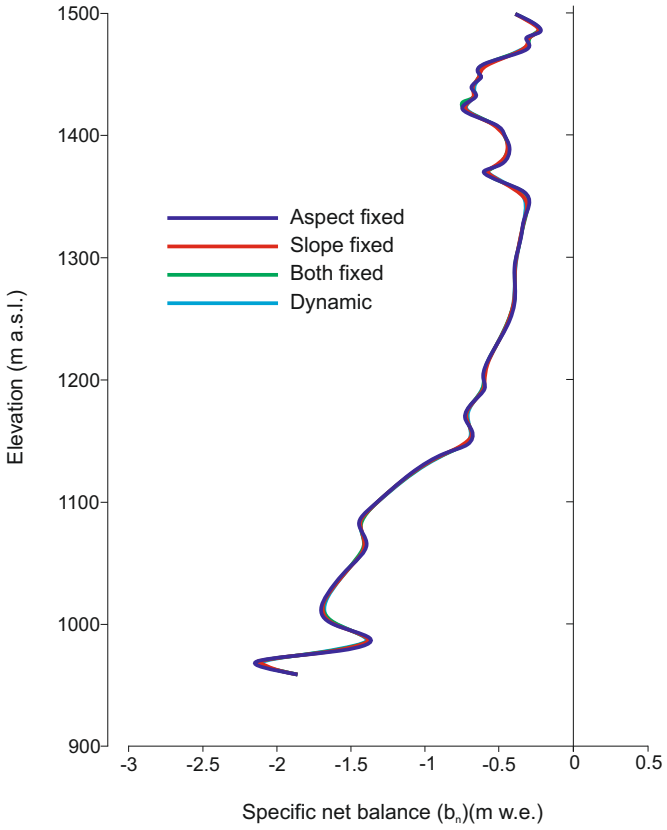

within the 2007-2010 period.

There is some observable change in the contribution of the energy mix components from 2007 to 2010 as displayed in figure 9.17. From 2007-08 to 2008-09, there is an increase in the contribution of ψ from 41% to 52% respectively and a comparative decrease in I from 59% to 48%. From 2008-09 to 2009-10, ψ reduces from 52% to 47% whilst I increases from 48% to 53%.

Figure 9.16: Surface energy balance (Q) composition change between model run types for experiments during the 2007 - 2010 period.

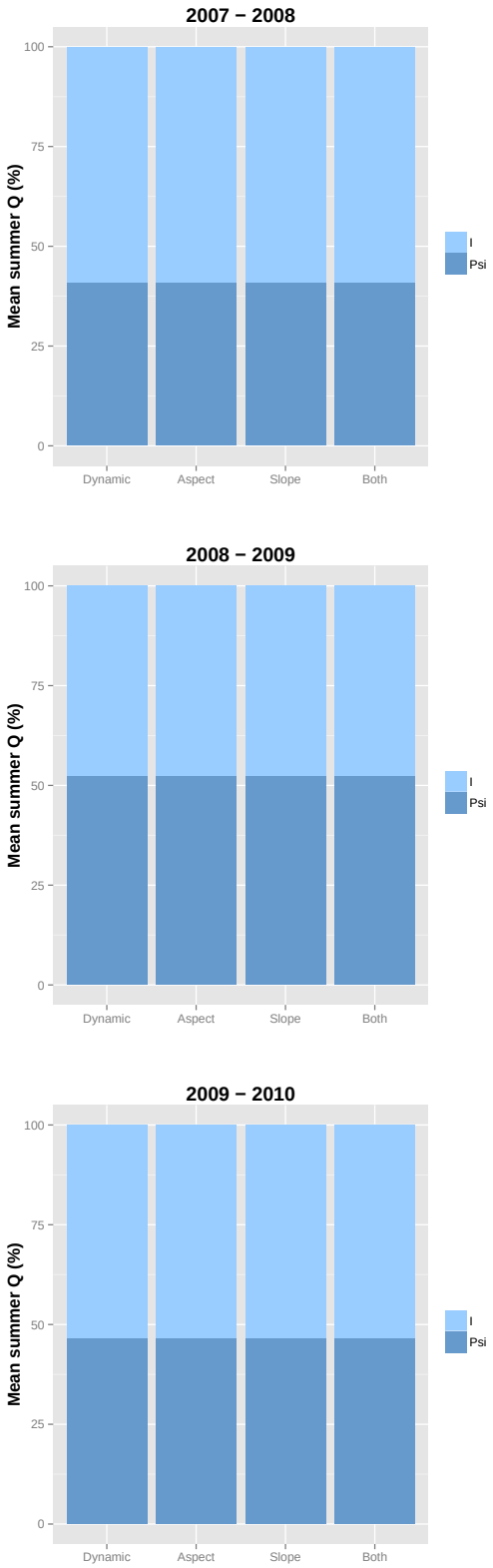

Figure 9.17: Surface energy balance (Q) composition change over the 2007 - 2010 period.

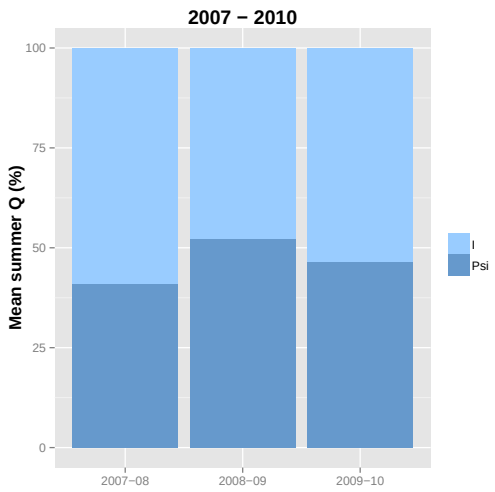

9.3 Modelling experiments summary

Using two versions of the model developed specifically for this study — the *historical* and the *contemporary* (the definitions of which are outlined at the beginning of chapter 4) — dynamic, slope fixed, aspect fixed and slope and aspect fixed scenarios have been facilitated for the periods of: 1926-1943, 1943-1959, 1959-1978, 1978-1991, 1991-2010 and 1926-2010 (using the *historical model*) and 2007-2008, 2008-2009, 2009-2010 and 2007-2010 (using the *contemporary model*). As the model accounts for changing glacier geometry over time as well as the relationship between the glacier and surrounding topography (through hillshade), it has been possible to meet the aim of assessing the effect of changing glacier geometry on the surface energy balance and mass balance. Under fixed conditions (all model runs other than the dynamic), for the period 1926-1943 (and then the 1926-2010 overall change), more negative mass balance conditions were observed. For the period 1926-1943, modelled annual maximum MB under dynamic conditions was calculated at -1.25 m w.e. compared to -2.40 m w.e. under fully fixed conditions. For the period 1926-2010, modelled annual maximum MB under dynamic conditions was calculated at -0.5 m w.e. compared to -1.25 m w.e. under fully fixed conditions. This is implicit of the importance of changing surface geometry values when considering SEB conditions and mass balance change over time. For other periods however, little change was found in mass balance whether geometry was fixed or not.

This chapter meets the objective of *conducting model scenarios with the developed model to assess the effects of geometry change on surface energy balance and mass balance change* which assists in meeting the project aim of *assessing the effect of changing glacier geometry on the surface energy balance and mass balance of a small mountain glacier throughout the 20th and early 21st century with focus on solar radiation contributions and glacier-topography relationships*. The results of this chapter are further considered along with the results of chapters 6, 7 and 8 in chapter 10.

Chapter 10

Discussion

The aims of this study established in chapter 1 were to provide a full 3D glacier geometry reconstruction and assessment of a small mountain glacier, since the beginning of the 20th century, over decadal and annual time scales; assess the sensitivity of the surface energy balance and mass balance change to meteorological and topographical forcing and to assess the effect of changing glacier geometry on the surface energy balance and mass balance of a small mountain glacier throughout the 20th and early 21st century with focus on solar radiation contributions and glacier-topography relationships. In meeting the objectives outlined in chapter 1, it has been possible to address these aims, as well as to qualify field and desk-based requirements for future studies of glacier mass balance change. The results presented in chapters 6 to 9 depict a shrinking glacier throughout the 1909-2010 study period over which there has been a complex suite of glacier-climate feedbacks which have altered over time.

10.1 Glacier change since the early 20th century

Warming and cooling temperature trends in the Swedish sub-Arctic have been identified to hold similar patterns to European and global temperature trends, with average annual temperatures for the region now being greater than 0°C (Callaghan *et al.*, 2010). Mountain glaciers have been identified to be sensitive to changes in climate by a variety of authors (e.g. Granshaw & Fountain, 2006; DeBeer & Sharp, 2009) and the resultant melting reaction of many glaciers is

expected to continue into the 21st century (Dyurgerov & Meier, 2000; Lenaerts *et al.*, 2013). In line with these warmer temperatures and considering sensitivity of mountain glaciers, there are numerous acknowledgments of glacier retreat in regions including Scandinavia, central Europe and North America (e.g. Holmlund *et al.*, 1996; Paul, 2004; Bauder *et al.*, 2007; DeBeer & Sharp, 2007; Zemp *et al.*, 2008; Gardner *et al.*, 2011; Lenaerts *et al.*, 2013).

Holmlund *et al.* (1996) provide a succinct review of a number of longer term studies of glaciers for the period 1915-1994, present within the Kebnekaise massif, northern Sweden, which is within a short distance from the Vuoittasrita massif in which Kårsa is located. The general trend for these glaciers is one of retreat and thus negative balance, for which the same pattern is found for Kårsa as acknowledged in this study. The pattern of change associated with Kårsa is discussed in a larger spatial context, particularly relative to other nearby glaciers in Sweden and Norway (including Svalbard) in sections 10.1.1 to 10.1.7.

10.1.1 Retreat

In this study, Kårsa is found to have retreated a total of 1292 m over the period of 1909-2008. Annual retreat rates (as calculated between available maps) of the whole glacier terminus were calculated as being greatest between 1926-1943 at 23.5 m yr $^{-1}$, reducing to 8.3 m yr $^{-1}$ between 1959-1978 and then increasing to 14.4 m yr $^{-1}$ for 1991-2008. Karlén (1973) proposed that retreat rates of the glacier would vary as a function of change in the slope angle of the underlying bed. Many of the assessments made of terminus position in earlier studies of the glacier were based on single points (Ahlmann & Tryselius, 1929; Wallén, 1948; Karlén, 1973) unlike the more distributed approach used here. Wallén (1949) states that the total retreat of the glacier from 1909-1943 was 200 m. This compares to the calculation of 433 m using the distributed terminus to line approach (see section 6.2 of chapter 6). The difference between these values is either a product of different terminus retreat distance calculation methodologies (whereby the method employed in this study assesses a wider portion of the terminus that displays more recessive traits) or/and may be related to errors in georeferencing of the topographic maps used (this is

discussed in more detail in section 10.4.1). Despite some issues potentially relating to methodologies, the general pattern observed for the total period is one of retreat.

Holmlund *et al.* (1996) reported retreat rates for Storglaciären, Isfallsglaciären, Rabots Glaciär, Riukojietna, Mårmaglaciären and SÖ Kaskasatjåkkoglaciären. Retreat values for the period of 1915-1994 range from 121 m (Mårmaglaciären) to 905 m (Riukojietna). No particular correlation can be drawn between total glacier retreat range and glacier, with the glaciers at either end of the total retreat distance scale having relatively large areas (3.92 km^2 and 4.68 km^2 for the least and most retreat respectively). Based on area, of the glaciers with known retreat rates as addressed in Holmlund *et al.* (1996), Isfallsglaciären is the most similar to Kårsa. Considering the 442 m of measured retreat of Isfallsglaciären, the retreat of Kårsa identified in this study, of 1028 m between 1906-1991, is comparatively great, implicit of varying conditions in some capacity. Considering more distant glaciers, the total retreat of Kårsa, as assessed for the 1906-2008 period, of 1292 m is similar to that of the larger Scott glacier located in Spitsebergen (1230 m), albeit the retreat of the latter is for a slightly longer period (1880-2006) (Zagórski *et al.*, 2008).

The total and annual retreat calculated for Kårsa in this study is considered relative to the numerous glaciers throughout (political) Sweden and Norway in figures 10.1 (total retreat) and 10.2 (annual retreat), for which data have been collected over a similar time period. The data presented are not associated with full geodetic studies for all of these glaciers (examples of full geodetic studies being discussed in section 2.4.1 of chapter 2). The glaciers include those from mainland Sweden and Norway as well as Svalbard. Relative to these other glaciers, the total retreat of Kårsa falls in the middle of the ranges of measured retreat, although is noticeably greater than the values derived for Swedish glaciers. The same pattern is then represented when considering annual retreat rates (the results of which vary slightly to the totals due to some glaciers having longer/shorter periods of observation).

Figure 10.1: Terminus retreat totals for glaciers in the political zones of Sweden and Norway. Data are taken from the WGMS (2013) database. Bars in grey represent Norwegian glaciers, bars in light red represent glaciers in Sweden and the bar in dark red represents Kårsa. Only glaciers with records >90 years are presented - time scales are labeled on the figure.

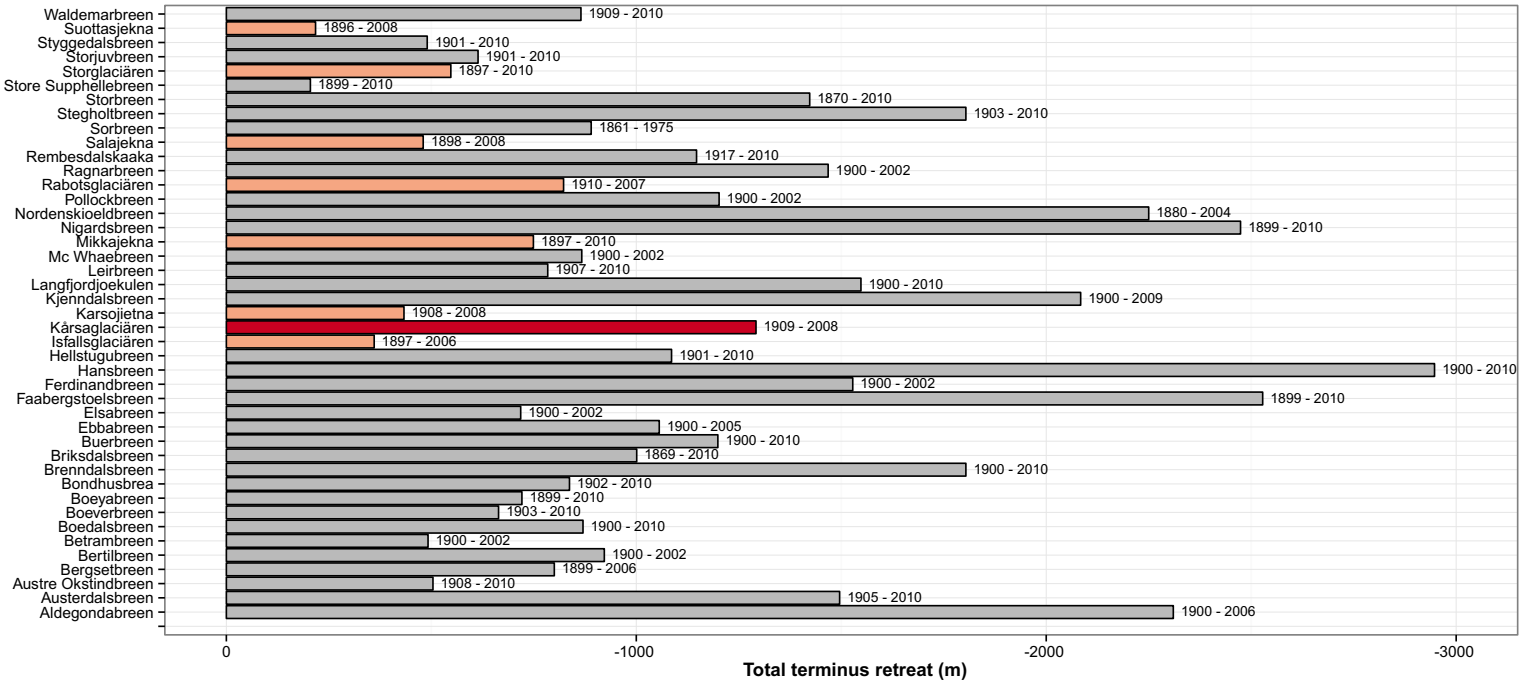

Figure 10.2: Terminus retreat totals for glaciers in the political zones of Sweden and Norway. Data are taken from the WGMS (2013) database. Bars in grey represent Norwegian glaciers, bars in light red represent glaciers in Sweden and the bar in dark red represents Kårsa. Only glaciers with records >90 years are presented - time scales are labeled on the figure.

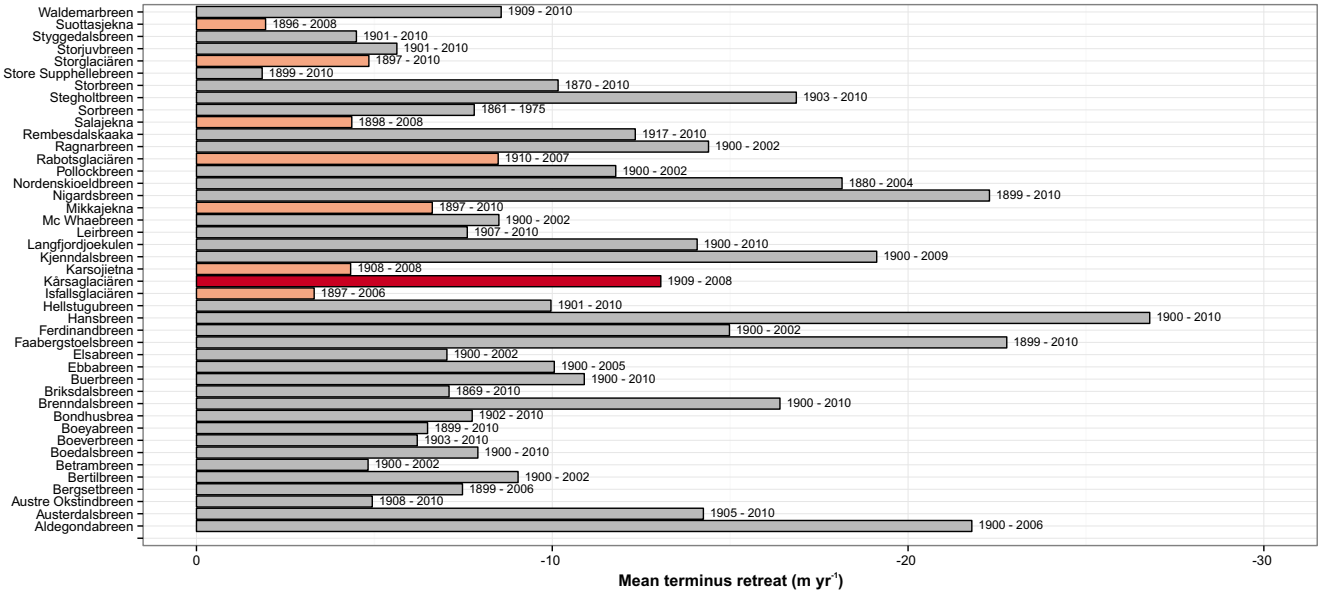

Retreat of mountain glaciers is a common attribute of mountain glaciers in a number of other areas globally, including the European Alps (e.g. Paul, 2002; Zemp *et al.*, 2008). Thus, the pattern exhibited by Kårsa and the glaciers identified in figures 10.1 and 10.2 is not unusual. The size of glaciers has often been found to be important with regard to retreat with studies identifying with single catchments smaller glaciers (<1.0 km^2) to retreat more than larger glaciers (>10 km^2) (Tennant *et al.*, 2012). Considering the larger glaciers of Sweden represented in figures 10.1 and 10.2, a similar pattern of smaller glacier/faster retreat is exhibited when considering nearby Storglaciären. Over the 1908-2008 observation period, the retreat of the glacier has coupled with drastic area changes and this is considered in section 10.1.2.

A limit of the geodetic method employed in this study is that it provides only snapshots through time. As with the geodetic method for assessing mass balance change, a reason that it should not be used to derive accurate annual MB conditions where the intervals between observations are greater than 1 year (Bauder *et al.*, 2007) is that it misses out inter-annual variability. It is this lack of inter-annual variability and thus the observation that the retreat trend is only general, that temporal resolution must be considered. A number of authors have acknowledged general retreat of glaciers in western Europe (e.g. Paul, 2004; Zemp *et al.*, 2006; Diolaiuti *et al.*, 2012) over the 20th century. This pattern has been observed in other areas including Scandinavia (e.g. Holmlund *et al.*, 1996), the Arctic Archipelagos (e.g. Nuth *et al.*, 2007; Zagórski *et al.*, 2008), Canada (e.g. DeBeer & Sharp, 2009; Jiskoot *et al.*, 2009; Gardner *et al.*, 2012; Tennant *et al.*, 2012), South America (e.g. Baraer *et al.*, 2012), North America (e.g. Arendt *et al.*, 2002; Berthier *et al.*, 2010) and the Himalaya (Dobhal *et al.*, 2004).

Inter-annual change combined with inter-catchment variability is important to acknowledge when considering wider glacier change. Such catchment changes may be a function of topography or of climate - acknowledging such variability can help explain why some areas are in retreat whereas others experience glacier advance and growth (Dyurgerov & Meier, 2000). For many regions, the 20th century is not defined completely by retreat with many glaciers in the European Alps having

been observed to have been in balance or to have advanced during the 1970s, with negative balances becoming more characteristic from the 1980s onwards (Hoelzle *et al.*, 2007; Zemp *et al.*, 2008). The balance of nearby Störglaciären was stable for about 15 years from the mid-1970s (Holmlund *et al.*, 1996). Considering these observations from the 1970s, if such a trend occurred during the period of assessment for in this study for Kårsa, as maps were only available in 1959, 1978 and 1991, such advances would be missed. This equally applies to observations of other variability including elevation change and terminus retreat. Thus in a period of retreat, sporadic snap shot assessments which miss possible periods of advance, likely create a more negative reconstruction than may be true.

10.1.2 Area change and disintegration

Following an assessment of records from the WGI (WGMS, 2013), the area of Kårsa today at 0.89 km^2 places it between median area values representative of Scandinavia (0.3 km^2) and the Arctic Archipelagos (1.3 km^2). Median values are used here as a few very large glaciers within the records heavily distort mean values (being 5.74 and 18.8 km^2 for Scandinavia and the Arctic Archipelagos respectively). Compared to the median value for western European glaciers (0.14 km^2), the contemporary area of Kårsa is comparatively large. Although useful to compare with the records of the WGMS (2013), an issue is that the values recorded are often derived from single maps. Consequently this provides only a glimpse of glaciological conditions. These maps range across the second half of the 20th century and thus the above cited regional area values are only employed here to provide a rough comparison. Through this study, the area of Kårsa has decreased significantly from 4.30 to 0.89 km^2 in only 82 years (1926-2008). This general reduction is akin to many other glaciers as identified in other studies (Paul, 2004; Tennant *et al.*, 2012).

Tennant *et al.* (2012) studied 523 mountain glaciers in the Canadian Rocky Mountains over a similar time frame to this study (1919-2006). They found that over the time period, proportional area loss decreased as a function of glacier size with the greatest proportional loss being for glaciers within the 0.5 - 1.0 km^2 area category, losing 67.8% of their total area. For the same period, glaciers in the

1.0 - 5.0 km^2 category lost 53.3% of their area. Similar to Tennant *et al.* (2012), Abermann *et al.* (2009) found in a study of 81 mountain glaciers in the Austrian Ötztal Alps that area changes between 1969 and 2006 decreased proportionally as a function of initial glacier size. Between 1969-1997, the greatest area loss in their study was associated with glaciers <0.1 km^2 (-52.2%), decreasing to -11.8 % for 1997-2006. They also found that glaciers <5.0 km^2 lost 11% of their area in the 1969-1997 period, and -8.9% for 1997-2006, the change in area loss rate being more exaggerated for smaller glaciers. The large contribution of smaller glaciers to overall proportions of melt as identified in the aforementioned studies is also identified in Paul (2002) where glaciers <1 km^2 were found to contribute 59% of overall area loss despite covering 1/3 of the glacier area of the Austrian Glacier Inventory. This sensitivity of small glaciers is further observed in the Italian Alps by both Knoll & Kerschner (2009) and Citterio *et al.* (2007). Both Abermann *et al.* (2009) and Tennant *et al.* (2012) found that in more recent times, smaller glaciers were contributing less to overall area loss changes compared to larger glaciers. This is discussed in Abermann *et al.* (2009) who link this slow down to the faster reaching of equilibrium of smaller glaciers, resulting in a less dramatic response in terms of mass loss.

In this study, mean annual % area loss rates overall vary little over the time periods studied. Considering two periods similar to the Abermann *et al.* (2009) and Tennant *et al.* (2012) studies, in terms of absolute percentages, Kårsa lost 73% of its initial area in 1926-1991 and 23% of its area from 1991-2008. The difference in absolutes is not surprising considering the difference in length of the two periods. Estimating annual retreat rates for the same periods, there is a 1.12% yr^{-1} loss for 1926-1991 compared to 1.37% yr^{-1} for 1991-2008. The difference between these values is small and this is indicative of little variation in the area change rate for Kårsa over the period studied. The area change rates fund here compare to a rate of -1.1% yr^{-1} as found for glaciers in the E. Italian Alps for the 1980s and 2000s (Carturan *et al.*, 2013). Tennant *et al.* (2012) found that area loss rates increased through 2001-2006 compared to 1985-2001 (-2±0.2% compared to -0.5±0.2% respectively). An increase in area loss was also found by Diolaiuti *et al.* (2011) in the Italian Alps, with a loss of 1.74 km^2 and 0.67 km^2 for 1991-2003

and 1981-1991 respectively. Although there appears to be a slight increase in annual area loss with Kårsa in the latter part of the 20th century and early 21st century as in Diolaiuti *et al.* (2011) and Tennant *et al.* (2012), the increase is relatively subtle. Such area loss is common of mountain glaciers in many regions other than those identified here, and this is often coupled with surface lowering and disintegration (Paul, 2004).

Paul (2004) identified rapid disintegration — which here is used to refer to the breakdown of one main lobe into numerous separate smaller lobes — of alpine glaciers through a study of the Swiss Glacier Inventory. Such disintegration has been observed in a number of other inventory based studies (e.g. Citterio *et al.*, 2007; Diolaiuti *et al.*, 2011, 2012; Tennant *et al.*, 2012). The process of disintegration, linking directly to spatial variations in mass loss processes, in many areas has led to an increase in the number of glaciers (although a decrease in mean glacier area) (e.g. Diolaiuti *et al.*, 2011) and is directly associated with increases in mass loss due to relationships with surrounding topography which alters the energy contribution to the glacier (Diolaiuti *et al.*, 2011, 2012).

According to UNESCO, a glacier must be of an area > 0.01 km^2 to be classed as a glacier (UNESCO, 1970). This has been used as a cut-off in other studies (e.g. Abermann *et al.*, 2009) when discussing *glacier* change. The term *glacieret* is used in some studies. UNESCO (1970) define a glacieret as being a small ice mass that exists for two consecutive summers, often being present in hollows or river beds and the result of snow drifting, avalanching or particularly heavy accumulation. Carturan *et al.* (2013) define glacierets as being "distinguished from glaciers based on the absence of evidence of motion and/or lack of a clear distinction between accumulation and ablation areas on aerial photos" (pp275 of Carturan *et al.*, 2013).

Some studies account for glacierets (e.g. Carturan *et al.*, 2013) whereas others do not (e.g. Diolaiuti *et al.*, 2012) (although the latter reference also considers size). This is an important consideration in terms of Kårsa with regard to the Kårsa side-glacier. Kårsa too has undergone the process of disintegration following the separation of the main lobe and the side-glacier between 1926-1943. This

disintegration matches observations of glaciers in similar negative balance states such as in the European Alps (Diolaiuti *et al.*, 2011, 2012) as well as in nearby Spitsbergen (Ziaja, 2005). Following this separation, in the early study of Kårsa by Wallén (1948, 1949), the side-glacier was disregarded as it was not considered of importance regarding mass transfer to the main glacier lobe. Consequently, aerial photographs, resultant maps and details of mass balance change were focused only on the main lobe (as in this study). Little is known of the side-glacier despite it still being relatively large. It would likely be classed as a glacieret (especially when considering the second component of the Carturan *et al.* (2013) definition) although this is conjecture. This portion of ice (depicted in figure 3.2) is another water store that will ultimately contribute meltwater to its local catchment within Kårsavagge and will therefore provide water that will contribute to future SLR. However, its contribution is unknown due to limited glaciological study. The GLIMS entry for Kårsa includes this lobe (as well as the western lobe - also detached from the main lobe) as a part of the overall glacier, albeit as separate components. This better fits the UNESCO definition of a mountain glacier which includes the main glacier body and any other smaller unit groups (UNESCO, 1970). Future studies should therefore acknowledge all components where possible.

10.1.3 Glacier surface lowering

Lowering of the long profile of Kårsa is clear for successive years of analysis (figure 6.9). Coupled with the area loss and disintegration associated with glacier retreat, glacier thinning has been widely observed (Thomson *et al.*, 2000; Rignot *et al.*, 2003; Nuth *et al.*, 2007; Shugar *et al.*, 2010; Rasmussen *et al.*, 2011; Zhang *et al.*, 2012). This is an important consideration regarding glacial contributions to SLR, as it directly relates to reduced glacier volume which also has implications for glacial dynamics (Thorp, 1991).

Through cross-profiling of Kårsa in this study, it has been possible to consider the lowering of the glacier relative to the present day surface. This lowering is generally continuous, especially around the mid-glacier with each successive

surface being generally lower than the last. The only surface against the trend is that for 1943 which may be due to map error which is discussed in section 10.4.1. As glacial dynamics are not considered here, it is possible that there is an issue in considering elevation change as a function of mass flux over a given point. However the cross profiles show the 1943 surface to be considerably lower than the other years - this may be due to extreme surface lowering or may be a direct product of map error. Considering the profiles related to all other years for the lower and mid glacier regions, the most lowering is associated to the north (LA and MA in figure 6.10) - the area associated with the lowest hillshade values across the glacier. This is implicit of the influence of hillshade on surface changes and will be discussed further in section 10.2. For the upper section of the glacier, there is no clear pattern of lowering with the 1926 and 2010 surfaces maintaining a similar profile below the profiles of the glacier in 1959-1991. As this is in the accumulation area of the glacier, this may be related to varying snow conditions which may have further caused issues during the map development process, especially if drifting had occurred.

Repeat assessments of the glacier centreline have been used in many studies to account for glacier surface change in a number of studies, sometimes altimetry based (Arendt *et al.*, 2008; Johnson *et al.*, 2013) but are also inherent of GPS profiling and as a means of assessment of change from topographic maps (e.g. Hagen *et al.*, 1999; Hodgkins *et al.*, 2007; Davies *et al.*, 2012). They are extremely useful measures of changing surface conditions, even more so when there is a good understanding of varying accumulation conditions (Hagen *et al.*, 1999). However, where used alone to assess change, there is a potential to miss out on spatial variability in MB change. Thus, appropriate extrapolation is required to consider glacier-wide change (Berthier *et al.*, 2010). In this sense, cross profiling and transect assessment is helpful for accounting for glacier evolution, highlighting the spatial variability in mass change across the glacier.

The ability to account for spatial change over long time periods, as a function of the spatial data available, is a key merit of this study. The opportunities that the wealth of spatial data available for Kårsa has afforded has been taken

full advantage of, enabling assessments of spatial patterns in elevation change, thickness change, as well as slope and aspect patterns (see chapters 6 and 7). With regard to elevation change, although there is evidence of some elevation increase, the overall trend derived is one of glacier surface lowering with a mean total lowering of 32.6 m between 1926-2010, giving a mean annual lowering of 0.38 m yr^{-1}. This is equivalent to a surface lowering of 0.34 m w.e. yr^{-1}. This value is extremely similar (although this does not mean the spatial pattern of change is identical) to that calculated for nearby Rabots Glaciär for the period of 1910-2003 at -0.38 m w.e. yr^{-1} (as in Brugger *et al.* (2005) and assuming a fixed ice density of 0.9 kg m^{-3} as in this study). An equivalent surface lowering value of -0.35 m w.e. yr^{-1} is calculated for Storglaciären for the period 1910-2001 (Brugger *et al.*, 2005). Further consideration of the changes between Kårsa, Rabots Glaciär and Storglaciären are considered in section 10.1.5.

In the case of Kårsa, the elevation change patterns observed are closely related to areas of greatest hillshade during the summer months as identified in section 8.3.1 of chapter 8, to which the glacier was found to be sensitive (as found in other studies including Arnold *et al.* (e.g. 2006b)). Winter snow pack distribution was also important and tended to be thicker in the areas of greatest hillshade (although not necessarily a direct function of hillshade but more of topography). This resulted in melt being most concentrated to the north and north east of the glacier, which included the terminus region. This area was also the lowest and therefore exposed to warmer temperature as a function of adiabatic processes. Elevation change maps have been constructed also for Rabots Glaciär for 1959-1980, 1980-1989 and 1989-2003. The majority of melt is consistently focused to the west of the glacier which covers the glacier terminus with most melt being observed for the 1959-1980 period during which geometry change for the glacier is considered to be greatest (Brugger *et al.*, 2005). This differs slightly to Kårsa where, if we remove the likely erroneous 1943 surface, the most change occurred between 1926 and 1959, especially with the associated disintegration of the glacier into the main lobe and the side-glacier. Relative to 1978-1991, the 1959-1978 period for Kårsa was one of increased surface lowering, so in this regard there is

some agreement relative to the maps available (and thus the analysis possible) for Rabots Glaciär.

10.1.4 Thickness and volume change: implications for change in glacier thermal regime

As identified in section 10.1.3, glacier elevation change and therefore thinning is directly related to a change in thickness and thus volume. Values of glacier volume can be derived via scaling relationships (e.g. Bahr *et al.*, 1997; Van de Wal & Wild, 2001) but can be more specifically calculated from in-situ measurements of thickness, often using GPR approaches. Such GPR methods have been applied in Sweden (e.g. Björnsson, 1981; Petterson *et al.*, 2003; Petterson & Jansson, 2004) as well as in other regions (e.g. Moran *et al.*, 2003; Irvine-Fynn *et al.*, 2006; Machguth *et al.*, 2006). Limits relating to the assumption of fixed density values in the conversion of volumes to mass changes were recently discussed in Huss (2013), where variations in density between different sites were acknowledged to be significant.

A useful component of this study is that knowledge of the glacier bed, from which thickness can be calculated, is available following GPR surveys in 2009 (Rippin *et al.*, 2011). With the compilation of GPR and dGPS points and the resultant glacier bed construction — in combination with the area DEM — it has been possible to consider glacier thickness both in the past and present. The general trend, as with elevation change, has been of thickness reduction, with the thickest ice being focused along the centreline of the glacier. This pattern of generally continued thickness reduction is the same as has been identified for nearby Rabots Glaciär (Brugger *et al.*, 2005) mentioned in section 10.1.3 with regard to elevation change. Relative to the glacier in 1926, the thickest ice was found at the middle of the glacier. The greatest depths today are to the north of the glacier. Mean thickness in 2010 is half (15 m) of that in 1926 (30 m). Consequently these thickness changes have resulted in large changes in volume, with total volume change being estimated at 111.97 x 10^{-3} km^3 for the 1926-2010 period (the mean

value is reported here, discussed in section 4.3.5 of chapter 4).

This change in volume can be compared to that of Rabots Glaciär which for the 1910-2003 period is reported to have lost 153.2 x 10^{-3} km^3 (Brugger *et al.*, 2005). Annual rates of volume loss for Kårsa and Rabots Glaciär of 1.33 and 1.65 x 10^{-3} km^3 yr^{-1} respectively can thus be calculated. Kårsa and Rabots Glaciär have contemporary areas of 0.89 and 3.70 km^2 respectively. As Rabots Glaciär is considerably larger, considering the similar thickness/elevation change to Kårsa (as reported in section 10.1.2), this larger value would be expected. If these values are normalised according to the contemporary area ratios of Kårsa : Rabots Glaciär (0.89 : 3.70), then a respective annual volume change ratio of 1.33 x 10^{-3} km^3 yr^{-1}: 0.40 x 10^{-3} km^3 yr^{-1} can be constructed. It is clear from this that for its size, Kårsa has lost considerably more in terms of volume.

Change in thickness and volume has significant effects on the stress exerted by the glacier and this changes the dynamics of the glacier which in-turn can affect glacier thermal regime. Rippin *et al.* (2011) proposed that Kårsa exhibited signs of a thermal lag, with its contemporary polythermal state being out-of-sync with its contemporary geometry. It is discussed that polythermal conditions would most likely have developed under thicker ice conditions, enabling greater strain related heating as well as greater insulation against the penetration of colder winter temperatures (Murray *et al.*, 2000; Rippin *et al.*, 2011). Assessing surface geometry (slope) and thickness prior to the conditions of the glacier examined in Rippin *et al.* (2011), it is clear that the glacier was once thicker, with maximum values of 137 m and 55 m for 1926 and 2010 respectively, occurring in the centre of the 1926 glacier which is makes up the northern portion of the contemporary glacier area. Coupling thickness and slope values together allowed for a consideration of changes in basal shear stress, revealing mean values of 119 kPa and 31 kPa for 1926 and 2010 respectively. Maximum values for both years were associated with the thickest ice which is in polythermal identified region in Rippin *et al.* (2011). In this study, maximum stress values of 345 kPa and 102 kPa were found in the area of thickest ice for 1926 and 2010 respectively, showing a decrease in more than double the amount of stress. These findings strongly support the hypothesis that

the contemporary thermal structure is a consequence of prior glacio-geometric conditions.

10.1.5 Area, thickness and volume changes: glacier response within a local context

In the aforementioned sections, comparisons are drawn between Kårsa, Storglaciären and Rabots Glaciär - all of which are located in Swedish Lapland albeit with different areas (0.89, 3.10 and 3.70 km^2 respectively (Brugger *et al.*, 2005)). An interesting pattern has been found previously regarding the varying response of Storglaciären and Rabots Glaciär. Over the period 1959-1999, Storglaciären lost -0.11 km^2 of its area, -5.69 m in thickness and -18.95 x 10^6 m^3 of its volume (Koblet *et al.*, 2010). Despite these negative summary statistics, negative change only dominated the period 1959-1969 and 1969-1980, with 1980-1990 and 1990-1999 being periods of increased thickness and volume (Koblet *et al.*, 2010). These latter periods of growth and stability are seen to be a stabilisation of the glacier following a response to climate warming earlier in the century (Brugger *et al.*, 2005). This differs to the response of Rabots Glaciär which has not stabilised and has continued to thin. Between 1910 and 2003, Rabots Glaciär continuously retreated and lost 153.2 x 10^6 m^3 in volume (Brugger *et al.*, 2005) with no apparent periods of growth as with Storglaciären. Modelling enabled the disentanglement of the response of the two glaciers, revealing Rabots Glaciär to have a response time 1.5 x longer than Storglaciären (Brugger, 2007).

Despite similar annual thickness change values, the response of Kårsa has not been one of thickening and increased volume, especially in the 1980s-2000s, losing 111.98 x 10^{-3} km^3 from 1926-2008. Thus the glacier exhibits a similar pattern of mass change to Rabots Glaciär as opposed to Storglaciären. As the two glaciers are much larger than Kårsa, and considering smaller glaciers are known to exhibit faster response times than those that are larger, the similar conditions of Kårsa and Rabots Glaciär, with specific regard to their shared continued volume reduction and terminus retreat cannot simply be attributed to a shared response time to a

specific shared event. This may be indicative that Kårsa is already responding to changes that Storglaciären and Rabots Glaciär are yet to react to.

10.1.6 Slope and aspect change

Considering World Glacier Inventory (WGI) statistics, the predominantly north easterly (NE) aspect exhibited by Kårsa is typical of many glaciers in western Europe, the Arctic Archipelagos and Scandinavia, where on average 57% of glaciers exhibited north-west (NW) - NE orientations, with other aspects accounting relatively equally for the remaining glaciers. More specifically, from a sample of 510 glaciers in Scandinavia, Carrivick & Brewer (2004), easterly (E) aspects, along with south-easterly (SE) were found to represent a large portion of glaciers. As Kårsa has retreated, its aspect has maintained a predominantly NE aspect, with N aspect increasing by 2010 to the same % as in 1926. As the % aspect is relative to the whole glacier, the loss of the side glacier which maintained a N aspect resulted in significant aspect change for the glacier from 1926-1943. As the glacier has receded up valley (in a W direction), areas of the glacier with mainly NE aspects have gradually disappeared, reducing the % of glacier representing NE aspects. The remaining parts of the glacier located on the more northerly slopes which are also the most shaded. The change in aspect is thus closely related to the elevation profile and aspect of the valley floor, which increases in altitude from E Kårsavagge to the W.

Coupled with the retreat of the glacier to the W to higher and more shaded altitudes, the slope angle has also changed, with a larger portion of the glacier falling within the 15-25°category by 2010 than in any other year. Although steep slopes were also associated with the side-glacier in 1926, which fell predominantly within the 10-15°category, the steepest slopes for all years have been focused mainly about the centre of the 2010 glacier extent. This area of the glacier has become steeper over time but more importantly, this steep area now accounts for a far larger portion of the glacier (over 1/3) than at any point in the past. Thus, considering proportional mean slope, the glacier surface in 2010 is the steepest for the period 1926-2010. This steeper central area is associated with both the

greatest amount of hillshade and snow thickness, the implications of which are discussed in section 10.2.

10.1.7 MB and ELA position

Coupled with other glacier change assessments, negative mass balance over the 20th/21st century has been associated with many mountain glacier studies across the globe and has been shown to be a precursor to area reduction, thinning and retreat. MB cannot accurately be estimated using a geodetic approach, especially where maps are not available on an annual basis, as such a calculation does not allow for an assessment of inter-annual MB variation (Hagg *et al.*, 2004). Thus, to approximate the pattern of change in MB over the study period, generalised long term mass balance curves were calculated between maps intervals (chapters 6 and 7) in this study.

The curves derived for the 1926-2010 period (not including the individual curves form 2007-2010 show general trends of increasingly negative balance with decreasing elevation which can be directly related to temperature gradients. Slightly less negative MB conditions exhibited by some curves around 1280 m are likely associated with increased hillshading, which may also assist in an explanation for more negative MB conditions at lower elevations (as well as increased temperature) for the 1926-1943 map (described below in section 10.2). Only the 1978-1991 curve shows evidence of a +/- MB value split. This might indicate a transition between accumulation and ablation zone conditions with all other surfaces being completely within the negative MB zone apart from the very highest altitudes. The 1943-1959 period is counter to this trend, explained by observed surface elevation increases in the geodetic study - this is likely to be largely erroneous and related to issues with the 1943 glacier map as discussed in section 10.4.1.

Unlike the generally negative MB profiles with elevation characteristic of the 1926-2010 MB curves, the 2007-2010 curves do not show such apparent trends. Compared to the historic MB curves, calculated over longer time periods, the 2007-2010 curves should provide a better assessment of changing MB conditions

as they are derived from annually updated glacier surface maps. However, this is limited by data availability (point coverage) to an almost unusable level as highlighted from the standard error and Monte Carlo sensitivity analyses, with extremely large changes in MB being attributed to point gaps in coverages used to derive surfaces.

Considering the ELA, its position calculated using AABR, AA, H_{med}, Mean, AAR and Hess approaches appeared to decrease between 1926 and 1943, then gradually increasing in elevation to 2010 (following a slight dip in 1991). Of the methods applied, AA, Hess and H_{med} are dependent on topographic maps of the surface and therefore glacier geometry; AAR is irrespective of glacier geometry and AABR is the only method that accounts for MB and hypsometry for the calculation of ELA. Although similar patterns were exhibited by the different methods, very different altitudes were calculated. The source of this variability is directly related to the differences in the methods used described above.

The observed patterns of increasing ELA for Kårsa, especially from 1943-2010, are to be expected considering the negative MB, area reduction and thinning of many other long-term glacier studies. Despite assessed surface, area and volume reductions (which would be indicative of an increasing ELA), the ELA lowered between 1926-1943. The detachment of the side glacier between 1926-1943 adjusted the hypsometry significantly and the related changes in area and elevation range will of affected ELAs calculated using the different methods described above. Geometry does not change as dramatically from 1943-2010, and the observed changes continue to be negative. Using hypsometric dependent methods, it is easier to assess changes in ELA using the same methods. Dramatic changes in geometry must therefore be considered when using hypsometric methods for ELA calculation , and comparing values directly.

The AABR method, used in this study to calculate ELA whilst accounting for MB, is only applied to the 1991 surface using MB data extracted from the 78/91 difference surface. In contrast, Bodin (1993) estimated ELA for Kårsa for 1989/1990, 1990/1991 and 1991/1992 using AAR values estimated from a MB stake network.

Bodin (1993) estimated AAR values of 0.70, 0.55 and 0.91 respectively. Using the AABR method as in the present study, an ELA of 1201 m a.s.l. is calculated, relating well to the geodetically derived MB curve, but being considerably higher than that derived by Bodin (1993). The AABR values are calculated using mean MB curve conditions for the 1978-1991 period, so such a deviation is not unexpected. Assuming the Bodin (1993) value to be more accurate (as based on in-situ measurements - although this will also be prone to error), this highlights the issue of calculating MB values from geodetic assessments of glacier change (Hagg *et al.*, 2004).

The *best* ELA method can only really be assessed when considering in-situ measurements. Of all the methods applied in this study, the AABR method (Furbish & Andrews, 1984; Osmaston, 2005) appears to be the most robust as it accounts for the varying balance ratio curves above and below the ELA, varying with distance from the ELA for a given glacier. As this method is based on actual mass loss information and not purely on the length or shape of the glacier, the AABR approach appears to be able to provide the most accurate (and glacier specific) estimate of the ELA. However, there is not enough data available in this study to quantify this. Here, using a steady state AAR of 0.6 provides similar results to the ELA as calculated by an in-situ measurement derived AAR of 0.55 (Bodin, 1993) for the glacier in 1990/1991.

The main issue relating to ELA estimation is the wide range of elevations between different methods. Due to the large difference in values calculated using different methods, mean values have often been applied (Benn & Gemmell, 1997). This approach is often used but should be done with caution when the range in elevation between methods is large. In the absence of stake networks, if possible, repeat annual centre line assessments could be used for a make shift method of estimating AARs. Using a *standard* AAR seems too presumptuous, especially on an inter-annual basis, although it does work well in some instances such as in the present study of the glacier in 1991.

10.2 Glacier sensitivity to components of the SEB and surrounding topography

A distributed SEB driven melt model has been developed specifically for this study, calculating the SEB whilst utilising a simple bulk flux approach developed by Giesen & Oerlemans (2012) and applied by others (e.g. Leclercq *et al.*, 2012b). Validation is completed by comparing change in the ablation area of the 2009-2010 model run with field measurements, and comparing the results of a dynamic 1959-1978 run with geodetic results. In terms of proportional melt, comparison between modelled and geodetically acquired different surfaces are presented in tables 8.3 and 8.2. Mean surface errors of the historical and contemporary models are discussed in section 8.2 of chapter 8.

Considering annual MB curves (see the dynamic charts in figures 9.6), the model is also found to operate well compared to in-situ MB measurements. Wallén (1948) calculated MB values of -0.42 m w.e. for the period of 1941-48 which compares to an annual MB value of -0.20 m w.e. for the 1943-1959 period modelled in this study. In-situ MB measurements are available from Bodin (1993) but only for the period of 1989-1992, for which model MB values are only available for 1978-1991 and 1991-2010, proving less comparable than the time period cross overs between the model and the Wallén (1948) study.

To assess the sensitivity of Kårsa to different components of the SEB, a grid based model, the details of which were outlined in chapter 5, was designed specifically to provide a platform upon which to preform a variety of experiments. This ultimately enabled an assessment of spatial variability in response to different SEB components across the glacier surface. This is a benefit of such physical approaches at modelling SEB and its effect on glacier MB (Le Meur *et al.*, 2007). For the test periods of 1959-1978 and 2009-2010, a sensitivity analysis of different contributors to the SEB were tested (see chapter 8). Unlike the other factors whose contribution was altered to assess their relative effect on melt, the effect of hillshade was accounted for by taking a binary approach of presence or absence. Testing hillshade and radiation receipt for summer solstice conditions 2007-2010,

ignoring the effect of topographic hillshade was found to increase overall receipt of the glacier by ˜40 Wm^{-2}, inverting the pattern of high-low radiation receipt on the glacier and resulting in increases in some regions in energy of up to 100 Wm^{-2}. Considering topographic shading through the months of June-August for 1959-1978 and 2009-2010, the increasing amount of shade with increasingly lower solar zenith angles was also acknowledged. Greatest shade was continuously found to be in the area shared by the middle of the contemporary glacier outline (between approximately 1150 - 1400 m a.s.l. according to the 2010 elevation map). This region is continuously identified as being related to the lowest melt rates considering default component settings. The changing contribution of I to Q as calculated in equations 5.10 and 5.12 respectively, considering the hillshade patterns observed in figures 8.4 and 8.6, are attributed to the propagation of this pattern as a function of hillshade. This relationship changes over time because as the glacier has retreated from 1926-2010, total area hillshade cover has increased (see figure 8.5) and this has resulted in a general reduction in the contribution of I to the overall energy mix Q from 1959 (see figure 9.9). The increase in contribution of I to Q from 1926-1943 relates to spatially variant hypsometric changes, particularly in relation to the loss of the Kårsa side glacier. No change in area was accounted for between 2007-2010 and the relationship between glacier elevation and surrounding topography did not alter surface-topography relationships enough to increase hillshade cover.

In terms of other factors, the model used in this study was found to be most sensitive to the thickness of the winter snow pack, wind stripping, temperature lapse rate, α_{snow}, and τ. With the arrival of greater temperatures and increased radiation receipt at the surface, the winter snow layer insulates the underlying ice from melt - the longer the snow pack lasts, the longer the more sensitive ice that lies beneath can survive (in terms of the effect of its lower albedo and the effect this has on radiation). The wind factor introduced here replicates (very simply) the effect that wind would have on snow mass movements (i.e. drifting), in effect thinning the snow pack in certain areas. A thinner snowpack under favorable melt conditions will last a more limited period of time than a thicker snow pack. The wind factor introduced here only strips snow, assuming this

snow to be removed from the glacier. Whereas the aforementioned factors affect the presence of the snow pack initially, the temperature lapse rate and α_{snow} affect the way in which the SEB melts the snow. By introducing smaller lapse rate functions (0.0050 rather than 0.0060°K m^{-1} for example), there will be less temperature decline to more negative temperatures with increased elevation. This is important when considering the effect this has on ψ (equation 5.11) which affects Q directly (equation 5.12), decreasing the energy available with a lower temperature. Changes in α_{snow} directly affect the contribution of I (equation 5.10) to Q, with greater albedo values reducing both I and Q and smaller values increasing energy contributions.

Similar sensitivities to the aforementioned factors have been found for other mountain glaciers which supports the conditions and sensitivities found to exist at Kårsa. Arnold *et al.* (2006b) considered the spatial effect of hillshade on SEB of Midre Lovénbreen and found it to play a key role, along with surface aspect and slope, on melt change. Hillshade directly affects shortwave radiation incident at the surface. By disregarding hillshade, total glacier melt was found to increase by 5.30%. Relative to assumed clear sky conditions, hillshade, as a function of surrounding topography, reduced incident radiation by 10% at Morteratschgletscher (Klok & Oerlemans, 2002), 5.2% at Haut Glacier d'Arolla (Arnold *et al.*, 1996) and 6.44% for Midre Lovénbreen (Arnold *et al.*, 2006b).

The importance of temperature lapse rate is of little surprise across the glacier surface, considering the gradient of the slope due to the glaciers large vertical range over a short distance. The spatial variability of lapse rates is considered in Petersen & Pellicciotti (2011) and is found to be particularly important when considering the development of katabatic wind regimes. Testing a range of lapse rates is reasonable as these have been found to vary for different sites as discussed in section 5.4.4 of chapter 5. Temporal variation in lapse rates were not considered here due to limited spatio-temporal meteorological data available.

Atmospheric transmissivity values for 9 glaciers located in different regions around the globe are calculated in Giesen & Oerlemans (2012). Values for atmospheric

transmissivity (τ) range from 0.32 (Chile) - 0.63 (Greenland). The testing of τ using 0.05 increments is reasonable as 0.05 displacements around the default model value used in this study can be expected as a function of varying cloudiness (related to annual variation) and global dimming and brightening (to a larger extent related to decadal variation) (Ohmura, 2009; Wild, 2009; Giesen & Oerlemans, 2012). Air pollution is key in the changing levels of true atmospheric transmissivity of the lower atmosphere, and is also related to cloud development (Huss *et al.*, 2009). Increases in high altitude cloudiness coupled with low global radiation and resulting in lower temperatures in the European Alps has been linked to a period of more balanced glacier mass flux globally (Huss *et al.*, 2009). As of the 1980s, enhanced greenhouse effects and brightening of solar radiation has resulted in warmer temperatures and this is associated with more negative glacier mass balance (Huss *et al.*, 2009).

The snowpack - in terms of both thickness and redistribution - has been found to be extremely important for a number of glaciers. This is primarily as a function of its insulation of a glacier surface and resultant modification of surface albedo (Mernild *et al.*, 2008). Mölg & Hardy (2004) related the mountain glaciers of Kilimanjaro to be extremely sensitive to precipitation for these reasons. As radiation was the key contributor to overall SEB, this modification resulted in significant changes in glacier melt. Where precipitation reduced as a function of changing climate in the study of future climate change over Hardangerjøkulen in Southern Norway, thinner winter snow packs resulted in surface shortwave radiation receipt occurring earlier in the year (Giesen & Oerlemans, 2010), ultimately lengthening the melt season. Model results following the application of the *Alpine 3D* model over Goldbergkees in Austria, were found to deviate primarily as a function of snow thickness variation, largely driven by mass movements including avalanching and wind drifting. Neglection of initial snow values and snow redistribution was associated with mass balance model underestimates in the study of Paul *et al.* (2005).

Albedo of the surface is often cited as a key factor in studies of SEB and MB modelling. Low albedo values are normally associated with the ablation area, and then decrease with altitude (Paul *et al.*, 2005) - primarily as a function of melt

and the presence of snow/ice (of varying levels of degradedness). The importance of albedo is known from a number of glaciers. Variation in melt at the terminus of Hintereisferner, Austria, was associated almost entirely with variations in albedo (Van de Wal *et al.*, 1992). Coupled with spatio-temporal patterns of glacier surface albedo (e.g. Brock *et al.*, 2000a; Jonsell *et al.*, 2003; Klok *et al.*, 2003; Strasser *et al.*, 2004), it has been found that albedo on Arctic glaciers is also sensitive to temporal variations in solar geometry, with albedo effects having been observed to be higher at lower sun angles (Jonsell *et al.*, 2003). Temporal geometry change is considered in all model runs in this study. Arendt (1999) found that for John Evans glacier, Canada, neglecting diurnal variations in solar geometry coupled with albedo resulted in a variance in received shortwave radiation by 16%.

The model was found to be least sensitive to changes in summer snowfall threshold temperatures and α_{ice}. Summer precipitation is low at the glacier (see chapter 3) and thus a lack of sensitivity to the summer snowfall threshold as fund in this study is to be expected. This would be much more important on other glaciers where summer time precipitation is an important contributor to overall mass change. The relative lack of α_{ice} is surprising as this directly affects the rate of ice melt due to modification of the I contributions to Q. Low sensitivity is explained here due to the way in which snow is modelled - α_{ice} only having an effect when the snow layer is removed. The low sensitivity is further explained as sensitivity tests were run for a full year, of which only approximately 25% of the year is associated with melt. Testing model sensitivity specifically over the summer months would possibly have revealed different results.

The acknowledgment of the aforementioned sensitivities provide a large amount of information that is instrumental in understanding the melt pattern of Kårsa, revealing a complex relationship between snow thickness patterns and hillshade, coupled with changes in temperature. Integrating these modelled sensitivities, it is possible to reason why the patterns of retreat presented and discussed in chapters 6, 7 and 10.1 are observed.

The snow pack is identified as a key control. Considering winter snowpack distribution, greatest thicknesses as identified for the 2010/2011 season (when the most measurements were carried out across the glacier), snow thickness was greatest from the middle glacier trending north-east to the terminus, with least thickness being identified to the south-east. A thinner snow pack in the south-east is unusual as this is at the highest elevation, however this is likely due to the effect of wind re-distribution, shifting the snow to lower elevations. This hypothesis is supported by the snow pit analyses that were carried out in which the calculated densities related closely to those found for wind slab see section 5.4.6 of chapter 4). Although thicker snow is associated with the terminus, this is within the region of least hillshade. In this study it was found that coupling the effects of the winter snowpack on ice melt rates with the considerable effect of hillshade on surface radiation receipt, snow at the terminus nevertheless melts faster during the ablation season than the more shaded snow in the middle of the glacier. This results in earlier exposure of the ice surface at the terminus than the mid-glacier. Coupled with lower temperatures in the more elevated and shaded area of the mid-glacier (relative to the 2010 glacier shape), where thicker snow remains, melt rates are lower. This is supported by the results of the dynamic model runs carried out (illustrated throughout chapter 8 by melt surface images for the 1978 and 2010 surfaces under default conditions), where lowest melt rates are continuously identified between ˜1170-1400 m a.s.l. for the 1978 surface and ˜1150-1400 m a.s.l. for the 2010 surface. Snow modelling for model runs prior to the 2008-2011 field data collection period are more limited due to little knowledge of glacier specific winter snow thickness patterns and thus results for these earlier periods are to be treated tentatively.

Whereas thicker snow, increased hillshade and lower temperatures are associated with the continued presence of the glacier in its contemporary position, the converse is associated with the retreat of its mass prior to 2010. Hillshade of the main lobe has continuously increased since 1926, allowing for larger contributions of I to Q. This has been coupled with steadily increasing temperature characteristic of the region over the 20th century (Callaghan *et al.*, 2010) and as identified from temperature records collected at ANS mentioned in chapter 3. Thus, had hillshade

been greater, the rate of retreat may also have been slower. Further contributors to retreat are also associated with the bed slope as discussed in (Karlén, 1973) which relates more to valley geometry than to topographic effects on SEB directly.

Considering the importance of the snow pack existing over Kårsa, more complex treatment of snow needs to be considered. Drifting and avalanching is not considered here, as in other models (e.g. Klok & Oerlemans, 2002), however, a more complex consideration of snow processes would allow for better estimation/replication of redistribution processes and snowpack evolution (density change, albedo change etc.) Snow modelling has been considered by many authors (e.g. Essery *et al.*, 1999; Bartlet & Lehning, 2002; Strasser *et al.*, 2002; Bernhardt *et al.*, 2009, 2010) but has not been employed in this study due to the volume of data required to force and quantify the results of such modelling efforts.

In this study, hillshade patterns are calculated using a topographic DEM derived from a 1: 100 000 map, which provides limited resolution, especially considering the resolutions of the maps from which glacier geometry was derived (˜1: 5,000). In other studies (e.g. Arnold *et al.*, 2006b), LiDAR has been used to provide the area base map. Equally, other methods could include the merging of ASTER data (e.g. Quincey & Glasser, 2009) or derivement of a DEM using TLS methods (e.g. Heritage *et al.*, 2009). Higher resolution DEMs from which to calculate geometries to assess hillshade effects on a surface will enable the calculation of more realistic hillshade modelling. This could have large implications when calculating the energy from incoming radiation - particularly at the transition zones between more and less shaded areas. Therefore, where possible, the highest resolution maps should be sought.

To consider how these varying factor sensitivities fit into to the SEB as a whole, based on equation 5.4.7, a conceptual diagram is presented in figure 10.3. This highlights the complexity of the system that has been considered in this study. Snowpack thickness (represented in figure 10.3 without an associated seasonality which varies as a function of temperature and precipitation), which has been identified as a key control on the energy available at the surface, strongly controls

the albedo of the glacier surface. Based on the treatment of albedo in this study, where snow is present albedo is significantly higher than where there is no snow and therefore bare ice. The importance of the wind factor is clear from its direct effect on snow thickness. Radiation (component I) has been consistently found to provide the majority of the energy to the overall SEB (see sections 9.1.5 and 9.2.5 of chapter 9). Whereby snow presence or absence can reduce the contribution of I to Q by 30-65%, the importance of snowpack thickness as a control is clear. Hillshade has also been found to relate to variations in elevation change through time and this again is as a function of its modification of I - also clearly identified in figure 10.3.

10.3 Conventional mass balance, the reference balance and effects of surface geometry

The distributed SEB model developed in this study has been used dynamically to assess changes in contributions of different SEB components to *conventional* MB change and has also provided an opportunity to compare these changes to *reference balance* conditions as described by Elsberg *et al.* (2001). Few studies have made use of the reference mass balance approach with no such studies having been taken on small mountain glaciers within sub-polar - polar areas, making the present study unique. The model as applied in this study does not account for mass gain over multiple years and nor does it account for dynamics. It is assumed that under positive balance conditions, there will be zero net melt. This is likely to be a source of error, although quantification is impossible due to a lack of inter-annual data. For the dynamic model, the general trend of negative MB matches that of the overall geodetic assessment for 1926-2010. However the period of 1943-1959 is not represented by zero growth which is expected considering the geodetic results for the same period. Coupled with 1991-2010, 1943-1959 melt rates yield the least negative total glacier MB value. This again brings in to question the reliability (and associated issues) with the 1943 glacier reconstruction and therefore implications for change assessment with results related to it.

Figure 10.3: Conceptual diagram of the different contributions to the overall SEB. The factors considered include those which are glacier, topographic and climate related. This is based on the simple calculation of SEB (and therefore factor Q) as defined by equation 5.13 in section 5.4.7 of chapter 5. Solid lines indicate processes considered through the modelling preformed in this study. Dashed lines highlight relationships that are not directly considered.

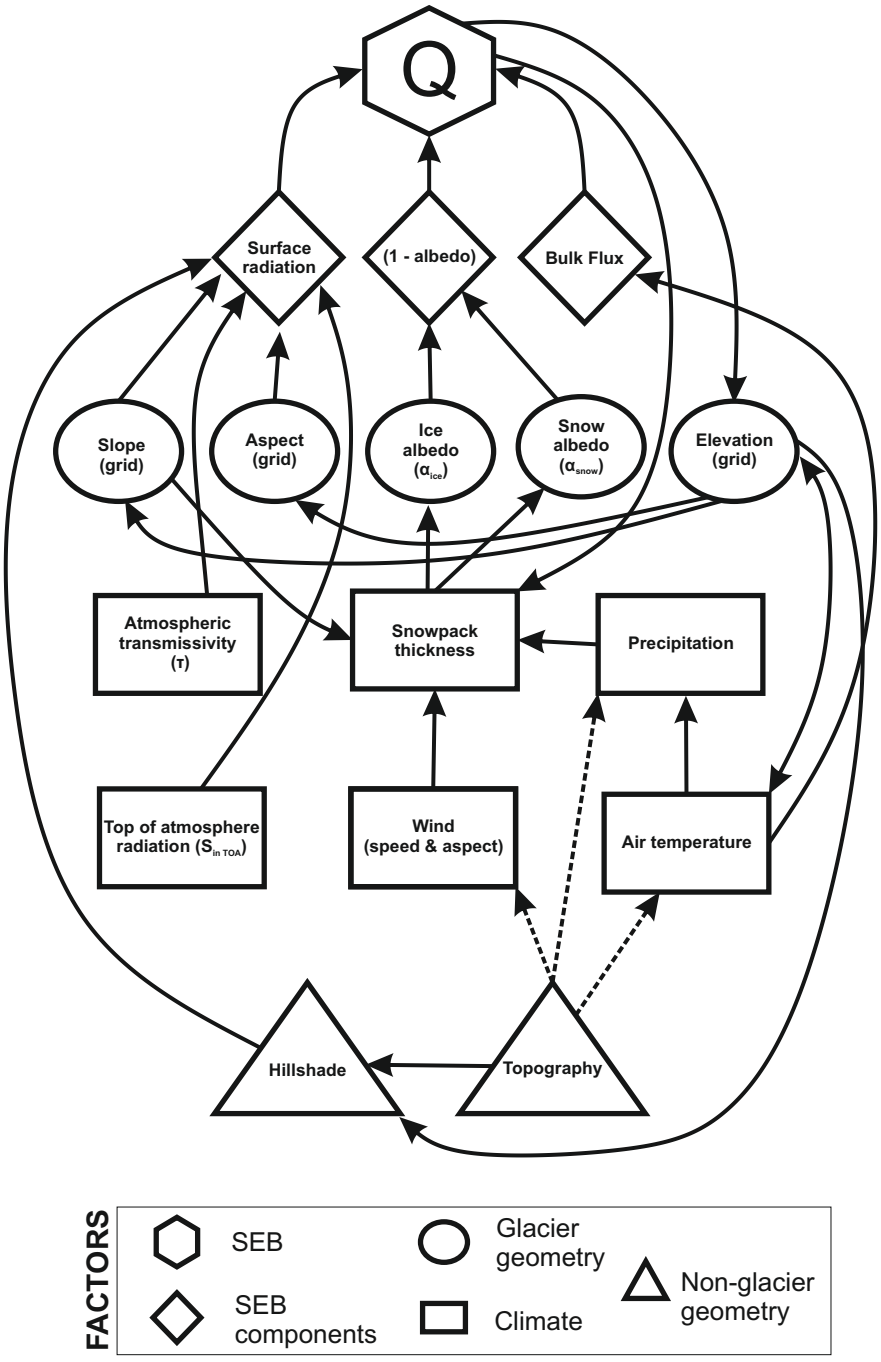

Harrison *et al.* (2009) applied the reference-conventional balance comparison techniques to assess the dynamic health of the Gulkana and Wolverine glaciers in Alaska, USA. The differences between the two mass balance approaches varied for the glaciers relative to response times. A reference-conventional balance comparison was carried out by Paul (2010) to assess changes in MB for a large sample of glaciers in the Swiss Alps where the reference surfaces (and extents) used were for 1850 and 1973. 50-70% of the total change between the two derived mass balance methods for the glacier overall was attributed to changes in geometry, although the specific elements of geometry are not discussed. A key element derived from the Huss *et al.* (2012) study was the spatial variations associated with differences between conventional and reference mass balance values and temporal dependence, with trends only being identified over longer time periods. This ties in particularly well with the observations made by Harrison *et al.* (2009), all of which supports the importance of taking into account glacier response time.

The results found in the present study, comparing conventional and reference balance conditions for Kårsa from 1926-2010 under the same meteorological forcing, yield similar results to the study of Huss *et al.* (2012) carried out for 36 Swiss glaciers for the period 1926-2008. Conventional and reference MB values of -0.31 m w.e. yr^{-1} and -0.74 m w.e. yr^{-1} are calculated respectively, comparing to values of -0.36 m w.e. yr^{-1} and -0.45 m w.e. yr^{-1} from the Huss *et al.* (2012) study. F_i statistics are calculated as in Huss *et al.* (2012) (see chapters 4 and 9) to allow for a inter-comparison, with fixed aspect, slope and both aspect and slope having similar effects relative to conventional balances (all with and F_i of -0.58). However, over longer time periods, slope appeared to have the largest effect (-0.41), although only by a measure of 0.01 more compared to aspect change (-0.39). Unlike the Huss *et al.* (2012) study, here, only slope and aspect are held to account for a reference surface - elevation is not fixed. Thus, deviations between comparable reference and conventional MB values are not only related to different environments and climatic settings but also to the effect that changes in elevation have.

F_i in this case is an average value over specific time-periods and is thus not representative of inter-annual contributions of geometric effects to MB change. No short-term variability was found between conventional and reference balances over short time scales in (Huss *et al.*, 2012) and this is replicated by the data here (e.g. see figure 9.15). Over longer time scales, difference in mass balance is clear, as for 1926-2010. However, these changes do not appear to be fixed to a specific time interval. The period of 1926-1943 is shown to have a significant difference between conventional and reference MB values, whereas other ˜20 year intervals for 1943-1959, 1959-1978, 1978-1991 and 1991-2010 do not show such MB variability. The F_i values for 1926-2010 are mainly evidence of the large effects experienced following the 1926-1943 period, with very little change occurring afterwards. Thus it appears here that the difference between conventional and reference MB is not always temporally related, depending on initial glacier geometric configurations and climatic conditions.

The acknowledged importance of geometric evolution is explained here in terms of radiative forcing, affecting radiation receipt on a slope as defined by equation 5.10 (Hock, 2003), with fixed geometry strongly enhancing negative MB conditions and resulting in a much steeper overall MB gradient. Considering the slope and aspect charts in sections 6.7 and 6.8 of chapter 6, 1926 displays the most NE aspects and lowest slope angles, both of which provide much more optimal radiative receipt conditions than the increasingly steep and more northerly profiles of the glacier in later years. By fixing geometry according to the 1926 configuration, thinning and retreat of the terminus, normally resulting in steeper slopes under dynamic conditions, does not have the dampening effect on MB change that the dynamic model and glacier has. This enhancement of radiation is important considering the contribution of I to Q identified from the dynamic glacier runs (see figure 9.9). Although slope and aspect are frequently acknowledged to be an important control on glacier mass balance (e.g. Klok & Oerlemans, 2002; Hock & Holmgren, 2005; Arnold *et al.*, 2006b), long term temporal evolution has been tested for only a few glaciers (e.g. Harrison *et al.*, 2009; Huss *et al.*, 2012). No examples of slope and aspect evolution are available for the Arctic, which makes these specific results from the modelling carried out in this study unique. In the MB curves

displayed in figures 9.14 and 9.15, the effect of topography is expressed within the regions of greatest hillshade and thickest winter snow locations. The effect of these factors is more enhanced than under dynamic conditions, resulting in much steeper MB gradients to and from the zone most affected (˜1200-1300 m a.s.l.). This emphasises how this region of the glacier changes much less over the total assessed periods and therefore provides further evidence for the dampening effect that topographic and snow insulating effects have on MB (Arnold *et al.*, 2006b). An overall steeper gradient would be expected if this were not the case.

Lowering of the glacier elevation also has large effects although these are not assessed individually, contributing collectively to the dynamic and fixed model responses. With lower elevations, higher temperatures will be experienced (adiabatically) but equally potential hillshade will increase, therefore reducing surface radiation receipt (Paul, 2010). This is considered in section 10.1 but is not tested within the model and thus cannot be compared with other studies in terms of reference balance.

Considering the results here and those of Paul (2010) and Huss *et al.* (2010), the importance of dynamic glacio-geometric configuration in terms of reduced MB response to changes in climate is clear as addressed in Harrison *et al.* (2009). The difference between conventional and reference balance per year is variable, with trends in differences tending to develop over longer time scales (Huss *et al.*, 2012). Trends in these differences will vary from glacier to glacier as a result of topography, for which a clear example is drawn here considering the topographic dampening on MB change around the middle of the glacier. Harrison *et al.* (2009) found that the varying response of different glaciers can enhance or reduce susceptibility to mass loss under less favorable climatic conditions (Harrison *et al.*, 2009), with some glaciers updating rapidly enough to counter adverse effects of climate on mass loss whilst others do not. Thus it is vital that such geometric changes are accounted for when considering longer term analysis of glacier change and addressing expected responses in the future.

10.4 Long term assessment and modelling related limitations

The complex nature of this project, considering the variety of data available and the modelling carried out results in the application of a variety of different methods. The methods that can be used and the results that can be derived are of course directly affected by the data available. Data availability in turn affects the methods that can be applied. This is considered in the following sections with regard to limitations associated with different elements of long term assessment (section 10.4.1) and limitations associated with the modelling approach taken (section 10.4.2).

10.4.1 Issues related to long term assessment

Geodetic methods provide an alternative method of assessing glacier mass change, other than by the more traditional glaciological approach of taking in-situ measurements. The geodetic route should not replace the making of such in-situ measurements however as the two approaches vary in resolution (Hagg *et al.*, 2004) and neither approach is error free (e.g. Østrem & Haakensen, 1999).

Focusing on the geodetic approach, this is most effective where there is a well established geodetic network including accurately located and known GCPs (Andreassen, 1999; Østrem & Haakensen, 1999). The quality of results is completely dependent on the combination of geodetic details of an area and, where maps are used (as opposed to GPS for example - discussed below) and map resolution, the former affecting the positioning of the latter, with the resolution being intrinsic to accurate assessment of conditions between maps.

A number of GCPs were created in the foreground of Kårsa, used for past aerial photography campaigns and for early measures of glacier terminus recession (Ahlmann & Tryselius, 1929). However, although these positions do exist, they are only useful for georeferencing if they are depicted on the majority of maps available, which is not the case here. Furthermore, where a selection of GCPs are

available but are focused in one area, this is of little use for georeferencing other more distant areas as georeferencing transformations require a spread of points for best accuracy. Of the maps available in this study, the original terminus retreat markers from the early studies of the glacier were marked on two of the maps available. However, these points could only be referenced to one another, not being visible on either the topographic base map or the contemporary aerial photograph. Furthermore, they did not match particularly well with GPS measurements of the markers which questions their mapped accuracy (or that of the GPS unit used). Georeferencing and the identification of ad-hoc GCPs was further hindered by the extremely varied resolution between the maps available with glacier maps to a resolution of 1:5000 and the base map (the spatially most accurate nap due to its coupling with an actual coordinate system as opposed to being just a picture) to a resolution of 1:100 000.

Assuming a good geodetic network is available, georeferencing issues should be minimal and accuracy assessments should be straight forward by simply comparing GCP location details of different layers between one another (e.g. Brugger *et al.*, 2005; Nuth *et al.*, 2007). Where aerial photographs are available, errors can also be calculated by considering non-dynamic landforms surrounding the glacier (e.g. mountains and ridges - often related to GCP locations) (Hagg *et al.*, 2004; Shahgedanova *et al.*, 2012). The relatively limited surroundings accounted for in the available maps, and the differing degrees to which they were accounted for, resulted in a number of issues, many of which are identified in section 4.2.2 of chapter 4, resulting in difficulties in both georeferencing and quantifying spatial errors.

Of all the analyses carried out in this study, the most unexpected results are for the geodetically calculated elevation change between 1943 and 1959, where the glacier appears to have been in positive balance. These results were not replicated in the modelling carried out as part of this study and the conditions accounted for in the study of Wallén (1948) (running from 1942 - 1948) are not indicative of extremely positive balance conditions. It is thus possible that the geodetic assessment results for this map are indeed erroneous, relating to an underestimate

of overall glacier elevation. This may be a function of the georeferencing issues (relating to poor GCP identification) but may also be a function of map quality which could be due to a number of reasons including the quality of the original drafting and of the original aerial photograph (Andreassen, 1999; Hagg *et al.*, 2004). If these results are indeed erroneous, counter to the over-estimate in glacier growth for 1943-1959, this implies the identification of overly negative conditions between 1926-1943.

Much in the way that map resolution is key, the same can be said of GPS trace resolution - the higher the resolution, the easier and more accurate any comparisons that are made between data sets. For inter-survey comparison, the same resolutions should be maintained as best as possible, as this allows limitation of spatial errors and thus reasonable assessments of change. To address the effect of changing point resolutions using a GPS approach, as well as accounting for any errors in the point clouds, Monte Carlo experiments were carried out (see section 7.1 of chapter 7). From analysis of the Monte Carlo simulation outputs the following points can be drawn out:

1. Erroneous data points (spikes) are influential on unknown point prediction where data are sparse and the search neighborhood window consist only of distant points

2. Good spatial point distributions are required for more accurate interpolations(especially where the environment results in large similarity changes between points over short distances i.e. there is a steep semivariogram/covariogram)

3. The southern region of Kårsa should be treated with caution for the years 2007-2009 as there is a very poor spatial point distribution and consequently it is highly susceptible to the presence of erroneous points

Generally, higher point density resulted in less error when using the points as an input into interpolation algorithms (discussed below). Due to the varying density of GPS points collected between the different surveys, comparing surfaces spatially is difficult due to the noise. This furthermore complicates interpolations,

especially when considering point changes. Although GPS is extremely useful for positioning, especially considering its accuracy, its employment should be limited to transect studies unless high resolution point clouds can be created. However, this is difficult to achieve considering the often challenging nature of the environments in which points are collected. This issue of point resolution is significant where the objective of the employment of the method is for assessment of (potentially small) surface changes, with the high accuracy of individual points being of little importance when compared to the much larger potential errors of interpolated surfaces which are being compared. The method of surface comparison has still allowed for relatively good mapping of the lower glacier where point density was greatest. It also proved to be useful in so far as planning for other assessments/field campaigns where similar methods are to be used (discussed in section 10.6). As mentioned above, the point density directly affects resultant surface interpolations with greater numbers and distributions of points better constraining interpolation methods employed. The kriging method used in this study was used as it qualifies as the optimum interpolator due to its consideration of variance with distance and thus of variations in auto-correlation. The system by which the best semivariogram model was chosen, as discussed in section 4.2.5 of chapter 4, highlights the differences between the various models available and thus the careful consideration that must be paid to model selection, varying directly as a function of the distribution of the input point cloud data. This notion of susceptibility to varying point distribution can be extended to other kriging methods (see Hock & Jensen, 1999) and interpolation methods in general.

A further consideration is the effectiveness of deriving summer glacier surface profiles from winter field approaches. In this study, the 2007-2010 summer surfaces were derived from dGPS and snow probe assessment in the winters of 2008-2011. The key assumption made being that the summer surface is simply the winter snow surface minus the winter snow pack depth. As has been identified in chapter 3 and with specific reference to figure 3.2, the summer surface of Kårsa shows evidence of large bed rock protrusions. These are not accounted for in the summer surfaces constructed here and thus call for a requirement to quantify summer surfaces derived using the method in this thesis with information from the ground

- ideally aerial imagery. This is important as such bedrock outcrops will increase long-wave radiation contributions to the SEB due to their different α values which in turn strongly influences surface melt and MB (Diolaiuti *et al.*, 2011).

These methodological issues are important and the consideration of the issues relating to the geodetic method, including map resolution, GCP identification, data point cloud density and distribution , as well as the interpolation routines relate to a recent acknowledgment of stark differences in global glacier change assessments between combined geodetic and field based glacier studies, with remote sensing methods. For a number of regions around the globe, glaciological methods have been found to account for MB change much more negatively when compared to results from GRACE (Gardner *et al.*, 2013). A number of reasons including logistical constraints and the issues of in-situ measurements (such as stakes melting in) are suggested for this more negative MB acknowledgment using glaciological and geodetic approaches (Gardner *et al.*, 2013; Kerr, 2013). However, this also brings into question the accuracy of other geodetic studies which is controlled by the maps available and the interpolation tools applied, as acknowledged throughout this study.

10.4.2 Modelling related limitations

The simple model applied here is effective in that it operates according to field observations (where points are of the highest resolution), provides a means to test model sensitivity to different controls and allows for a consideration of geometric effects on MB. The user friendly interface, distributed approach to SEB calculation, site specific considerations of glacier geometry and effects on incident radiation, as well as the ability for reference based modelling runs, make the model developed in this study an advancement on past simple model approaches (e.g. Arnold *et al.*, 1996; Brock & Arnold, 2000; Leclercq *et al.*, 2011; Giesen & Oerlemans, 2012). However, a number of limitations relate to the application of such a simple model. These are related to the omission of glacier dynamics processes, lack of mass accumulation and simple modelling of snow and turbulent fluxes. These limitations cannot be avoided in this instance as the data to validate

more complex approaches are simply not available. Furthermore, considering the validation carried out, for the purposes of this study, the advantages of such enhanced complexity would likely be lost when one considers also input data reliability. There are examples of simple dynamics models that have been applied to longer term studies (e.g. Leclercq *et al.*, 2011) however these often assume the presence of a fixed thermal regime. For example, the Leclercq *et al.* (2011) study assumes temperate conditions. This becomes difficult when a regime cannot be assumed fixed as with Kårsa for which the thermal regime is believed to have changed over time (Rippin *et al.*, 2011). Considering these issues with dynamics, this leads to further issues relating to snow accumulation and how mass distribution is treated within the model. Without sufficient data, it could be argued that the integration of further complexity does not necessarily improve accuracy and may even introduce a false sense of detail.

Snow mass movement modelling, especially by wind, is required to better understand the processes occurring at Kårsa, the evidence of wind redistribution processes being highlighted in the snow pit analysis discussed in section 4.2.3 of chapter 4. Taking refreezing into account, also identified to be of importance from snow pit analysis, would be a further consideration and relatively easily constrained as in Leclercq *et al.* (2011).

10.5 A simple transferable grid based model designed for Arctic glaciers: adaptability and availability

The model developed specifically for this study has provided an effective platform to consider changes in SEB and MB over time as a function of dynamic and fixed geometry with changing meteorological conditions. The model allows runs at varying time steps (days and months) and can easily be developed to consider higher temporal resolutions (this being a function primarily of the meteorological input data). There are some limitations (see section 10.4.2) however these are generally related to much higher resolution processes for which data would rarely

be expected to be available, especially with regard to the simple modelling applications that the model was designed to be used for. The model has been tested against the best available historical DEMs and change maps (see section 8.1 of chapter 8) and is found to reproduce the general patterns of observed elevation and thickness change. The model also operates within the constraints of in-situ mass balance measurements as calculated by Wallén (1948) and Bodin (1993), despite these mass balance values being calculated over daily time steps and the only input surfaces being available throughout model development being calculated on >10 year time steps, with meteorological data being available up to 2007 on monthly time steps (this then being corrected from the location of ANS to the glacier - see chapter 5).

The area of Kårsa as calculated from its 2008 extent was 0.89 km^2, placing it within a category of 64.2% of all Arctic glaciers which in 2009 were reported to have an area of <2 km^2 (Rippin *et al.*, 2011). A larger portion, 77.9% of Arctic glaciers, were found to have an area of <5 km^2 (Rippin *et al.*, 2011). By developing and testing the model specifically for Kårsa, and acknowledging that the results of processing fall within geodetic and in-situ mass balance observations, this study has provided a grid based physical SEB model for a glacier representative of other glaciers in the Arctic. As the model is grid based, it models change whilst considering spatial variability which is a big advance on more common point based models which are limited primarily by spatial coverage (Hock, 2005).

The model source code is freely available as mentioned in section 5.7 of chapter 5. This code will be continuously updated. Under the *GNU General Public License (Version 2)*, users are free to download the code and manipulate it at will, so long as future developments made available to other users include the same rights as stated within the aforementioned license (see appendix F). The hope is that other researchers will take advantage of the existing model structure developed for this study and apply it to other glaciers to enable further SEB experimentation. With the code itself being available, then further development is encouraged.

10.6 Outlook: Considerations for future studies

This study has addressed a number of different elements of glaciological science - in particular:

- Historical glacier reconstruction (3D) over decadal time scales
- Contemporary glacier reconstruction (3D) over annual time scales
- Distributed SEB modelling.

Relating to these different components, a number of suggestions are made with regard to considerations for future studies. Historical surface reconstruction constituted chapter 6 and provided the inputs for historical SEB modelling addressed in chapters 8 and 9. A key issue relating to the integration of historical maps as outlined in chapter 4 related to error analysis. Horizontal and vertical errors are usually carried out through the identification of GCPs (e.g. Brugger *et al.*, 2005; Nuth *et al.*, 2007). However, this is not possible where GCPs cannot be identified. Furthermore, errors are invariably introduced where map development is facilitated by different cartographers using different methods (the methods of which are unknown for all of the glacier topographic maps used in this study, other than that they are based on aerial photographs). To attempt to quantify and therefore make known the accuracy of subsequent analyses, where possible, the following suggestions should be considered:

- Acquire original aerial photographs (this should enable easier GCP identification - many potential GCPs may be disregarded by cartographers depending on the objective underlying map development)
- Identify details of the cameras used (for indication of possible distortion)
- If aerial photographs are available for successive years, develop maps and therefore DEMs using a fixed and consistent method (therefore possible to quantify methodological error introduction)

Contemporary glacier reconstruction constituted chapter 7 and provided the inputs for contemporary SEB modelling addressed in chapters 8 and 9. The methods for contemporary glacier surface reconstruction are discussed in depth in chapter 4. The main issues relating to these reconstructions were a consequence of the pseudo-random point clouds developed as a consequence of the employed snowmobile/dGPS method. The nature of the resultant point clouds, and their effects on surface interpolations are analysed in section 7.1 of chapter 7. Clear problems arise where gaps in the point clouds exist. This leads to a number of suggestions for alternative methods for data collection, focused primarily on accuracy:

- Drone, blimp, kite and UAV (Unmanned aerial vehicle) surveys - coupled with high resolution cameras and a dGPS unit, it is possible to collect numerous georeferenced photographs of the study site. Such approaches has been used for other terrain analysis studies (e.g. Smith *et al.*, 2009; Niethammer *et al.*, 2012). Photographs can then be used to create a point cloud from which DEMs can be developed as described below.

- Static cameras networks placed around the object (in this case the glacier) of interest taking photographs on a set interval (enables multiple time frames to be accounted for following a single equipment set up procedure) (e.g. James & Robson, 2012). Photographs can then be used to create a point cloud from which DEMs can be developed as described below.

- TLS methods (e.g. Avian & Bauer, 2006; Heritage *et al.*, 2009; Kociuba *et al.*, (in press)) - provide an automatic point cloud of the surveyed area (LiDAR technique).

- ALS methods (e.g. Arnold *et al.*, 2006b,a; Hopkinson & Demuth, 2006; Kohler *et al.*, 2007) - provide an automatic point cloud of the surveyed area (LiDAR technique).

The UAV and static camera methods differ to the use of TLS and LiDAR studies in both terms of affordability and the nature of the data collected in the first instance. The latter two methods are considerably more expensive (and cumbersome) - with

laser scanners costing between £50 - 100, 000 (Carrivick *et al.*, 2013) and LiDAR units normally being mounted on aircraft for which flight time is expensive. These methods do allow for a large spatial coverage of data to be acquired but, especially with regard to the laser scanning data, processing of data is not simple and is thus time consuming. These methods ultimately provide data in the form of point clouds from which DEMs can be constructed. Comparatively, the use of Drone, blimp, kite and UAV surveys, as well as fixed camera networks are much lower in cost and considerably less cumbersome which increases their ease of use in the field. Unlike the laser methods, these depend on optical imagery. By collating numerous photographs of an object, methods such as *Structure from Motion* (SfM) (James & Robson, 2012; Westoby *et al.*, 2012) can be used to extract 3D structure from overlapping images (Westoby *et al.*, 2012), and these can then be converted to point clouds which can be used to develop DEMs. This method is discussed extensively in Westoby *et al.* (2012). A variety of freely available software is available to facilitate this procedure including Microsoft Photosynth and Bundler (Carrivick *et al.*, 2013). An issue that will remain and that cannot be addressed by optical image analysis, especially during the winter months at higher elevations where there is no sunlight for many months, is an accurate assessment of winter snow pack thickness. Microwave remote sensing imagery would be an option but is limited in coverage, spatial and temporal resolution.

SEB modelling has been instrumental throughout this study (chapters 5, 8 and 9), especially when considering the sensitivity of the glacier to different SEB components and geometric change and its effect on these SEB components. Following sensitivity analyses addressed in chapter 8 and the varying results addressed in chapter 9, the following suggestions are made for future modelling studies:

- For modelling approaches over short time scales (months to a few years), continuously updated DEMs are not of great importance with regard to estimations of melt as geometry changes (slope and aspect) are found to only propagate over longer time scales thus a better investment of time would be in acquiring a single high resolution DEM of the glacier and surroundings at the beginning of a given study

- Meteorological data collection, especially with regard to τ and its associated variability
- The snowpack is extremely important in its suppression of surface melt as a function of thickness which results in surface insulation and control of surface albedo - for improved modelling results, the spatial variability in the snow pack thickness needs to be mapped as accurately as possible
- Where higher resolution and more complex considerations of SEB and MB are to be carried out, the inclusion of wind and resultant snow redistribution is found to be important, especially in complex mountain environments

Chapter 11

Conclusions

To conclude this study, a summary is first presented, followed by a consideration of areas for further study and then a presentation of the key findings.

11.1 Summary

The aims of this study are outlined in chapter 1. These aims have been achieved through the completion of the set objectives also outlined in chapter 1.

The first, second and third objectives: ***Collate historic topographic maps and reports as well as data from the field to ascertain glacier geometry, meteorological conditions and snow pack characteristics***, ***Apply geostatistical methods to reconstruct 3D glacier geometry and enable geometry and geometric change analyses (through development of a GIS)*** and ***Account for sensitivity of applied geostatistical techniques on reconstructed surface properties***, are addressed fully in chapters 4, 6 and 7. Topographic maps of the glacier were acquired and compiled for the years 1926, 1943, 1959, 1978, 1991. Following field data collection, maps of the glacier under summer conditions were developed for the years 2007, 2008, 2009, 2010. Meteorological data was compiled from different sources (ANS and the installed AWS) for the periods 1920-present (ANS) and 2007-2011 (AWS). Winter snow accumulation was collated at AWS for the period 1920-present and measured at the glacier following field data collection for the winters of 2007-2008, 2008-2009,

2009-2010, 2010-2011.

The collated maps were digitized enabling the development of DEMs using a carefully analysed ordinary kriging approach. DEM sensitivity was analysed as a function of the interpolation process using statistics reported from the kriging algorithm (trend removal results displayed in table 4.2 in section 4.2.5 of chapter 4). DEM sensitivity to the effects of point cloud density was considered using a Monte Carlo sensitivity analysis approach, which involved the addition of random noise to point clusters and acknowledgment of the effect of such noise on resultant interpolations, highlighting the most sensitive regions to point noise. DEMs were then analysed which revealed that the glacier has undergone large changes in terms of its geometric characteristics. For the 1926-2010 period, elevation is acknowledged to have lowered by 33 m on average, giving a mean rate of elevation loss of 0.35 m w.e. yr^{-1}. Thickness is assessed to have reduced from a maximum of 137 m to 56 m — which equates to an annual change in maximum thickness of 0.85 m w.e. yr^{-1}. Volume has reduced by 111.97 x 10^{-3} km^3 from 125.31 to 13.33 x 10^{-3} km^3 — a rate of loss of 1.33 x 10^{-3} km^3 yr^{-1}.

The fourth objective: ***Develop a user friendly grid based distributed surface energy balance model which uses reconstructed surfaces as an input, combined with meteorological data from the field***, is detailed in its construction in chapter 5. Examples of the model are displayed in appendix E and the computer code is available under open source licensing from `https://github.com/Chris35Wills/SEB_model_java_files`. A model was developed with a user friendly interface enabling dynamic and fixed geometry (reference surface) model simulations. The model platform uses uploaded GRID/ASCII surfaces as an input (as developed using the methods outlined in chapter 4 and analysed in chapters 6 and 7). Distributed SEB energy was calculated using equation 5.13 based on meteorological data collected in the field, and this was achieved for monthly and daily time steps (for the historical and contemporary models respectively). Radiation was calculated on a 6 hourly time step, regardless of lower resolution time step input meteorological data (temperature etc.). By altering the input GRID/ASCII surfaces as a function of energy availability, the

model allowed for dynamic surface geometry updates every time step.

Compared to geodetic observations of MB and in-situ measurements as collated by Wallén (1948), the model works extremely well. Annual errors based on the geodetic surface/model surface analysis for the historic model were calculated at -0.33 m w.e. and -1.76 m w.e. for the contemporary model. Considering the lower glacier alone when using the contemporary model, mean annual error is reduced to -0.08 m w.e. Difficulties in error analysis were a function of unquantifiable mapped data errors addressed in sections 4.2.2 and 4.3.5 of chapter 4.

The fifth objective: ***Conduct model scenarios with the developed model to assess the effects of meteorological and topographic forcing as well as geometry change on surface energy balance and mass balance change***, is addressed in chapters 8 and 9. Sensitivity tests were carried out to see the effect of small changes in key factors (namely atmospheric transmissivity, snow albedo, ice albedo, wind, summer snowfall threshold, lapse rate and winter snow thickness) and these are summarised in table 8.18 in section 8.4.8 of chapter 8. The glacier was found to be highly sensitive to hillshade (and its modification of radiation receipt at the surface) and snow thickness (as affected by wind, which in turn affects surface albedo and then surface radiation receipt).

Dynamic, aspect fixed, slope fixed and slope and aspect fixed scenarios were modelled for the following time steps:

- 1926-1943, 1943-1959, 1959-1978, 1978-1991, 1991-2010 and 1926-2010 (historical model)
- 2007-2008, 2008-2009, 2009-2010 and 2007-2010 (contemporary model)

With regard to 1926-1943 (and then the 1926-2010 overall change), the fixed geometry surfaces (i.e. all apart from the dynamic scenario) resulted in much more negative mass balance conditions. For the period 1926-1943, modelled annual maximum MB under dynamic conditions was calculated at -1.25 m w.e. compared to -2.40 m w.e. under fully fixed conditions. For the period 1926-2010, modelled

annual maximum MB under dynamic conditions was calculated at -0.5 m w.e. compared to -1.25 m w.e. under fully fixed conditions. Changing values in terms of slope and aspect angles were therefore found to be key in reducing melt - this being directly related to the calculation of incident radiation (I) as calculated using equation 5.10. This relates to the large changes in geometry during the 1926-1943 period as acknowledged through the geodetic assessment. This result is important as the effect of changing geometry has often been neglected by SEB/MB models in the past. Very little change was found in mass balance for other model time steps inter-surface - particularly with regard to the contemporary surface.

11.2 Suggestions for further study

There are a number of exciting elements highlighted in this study that provide impetus for future development and analysis. The increasing availability of low-cost, low-bulk techniques for terrain analysis and point acquisition (e.g. Westoby *et al.*, 2012; Carrivick *et al.*, 2013) offers new ways to develop DEMs as discussed in section 10.6 of chapter 10. Such methods should be considered for multi-annual survey programmes, such as carried out for Kårsa in this study for the period 2007-2010. Coupled with error analyses (including the Monte Carlo simulations implemented in this study), these surfaces could be used to assess terrain change over time. It would be interesting to use resultant DEMs as inputs in the SEB model developed here to assess model reliability and derive new error values. A further area for development would be the assessment of snow mass movement processes over small Arctic glaciers. Many of the existing snow models that have been developed are specific to alpine catchments (e.g. Bartlet & Lehning, 2002; Michlmayr *et al.*, 2008). This would provide further insight into controls on SEB and MB in mountainous Arctic regions, although such work would be highly data intensive and inevitably site specific.

An important element that was not considered in this study was that of glacier dynamics. In terms of glacier mass balance change and surface sensitivity to different elements of the surface energy balance, this should in future be considered to a greater extent. Although the geodetic method — applied throughout this

study — is a useful method of assessing mass balance change over time, it gives little or no insight as to why certain changes occur (Bamber & Rivera, 2007). This is where other approaches including the mass conservation method and the flux-divergence approach would be effective as they would allow dynamics and mass balance components to be more effectively separated (Rott *et al.*, 1998; Bamber & Rivera, 2007; Seroussi *et al.*, 2011; Morlighem *et al.*, 2013).

During the final visits to the glacier, there was clear development of a proglacial lake along the glacier terminus. The question of calving is key in glaciology today and yet a fully comprehensive understanding remains elusive (Benn *et al.*, 2007a,b). This is primarily associated with tidewater glaciers linking to ice sheets thus also relating to saline water conditions and tidal effects. However, should the lake continue to grow at Kårsa and should the margin begin to float, the effect of calving would be interesting to consider, especially with regard to the effect that it could have on enhanced glacier terminus retreat rates. This could be an exciting avenue to pursue as should such an effect be found to occur, the consequences could be significant.

11.3 Key findings

The key methodological findings can be summarised as follows:

- When mapping areas using point cloud approaches, high spatial resolution and coverage is key in enabling accurate interpolation and therefore DEM development
  - Pseudo-random point collection does not allow for accurate surface change assessments
  - There are now a variety of low cost, low bulk methods available to acquire point clouds of glaciers from which accurate DEMs can be derived
  - Monte Carlo simulations involving the introduction of randomly distributed point error values provide an extremely useful means to assess

DEM interpolation sensitivity to varying point cloud densities. The results of such analyses provide means of surface quality control when considering spatial change.

  - When integrating topographic maps or aerial photographs into such analyses, a good geodetic network (with regard to identification of shared GCPs between maps) is vital to ensure accurate error assessment

- Careful consideration needs to be taken as to the approaches used to derive changes in glaciological parameters including ELA terminus retreat values as these can vary significantly across the glacier terminus

  - Differences in retreat of up to 551 m were found using different methods of assessment
  - The best assessment of terminus retreat considers retreat on a spatial scale as opposed to the consideration of a single point
  - Differences in ELA estimation of up to 496 m were calculated
  - Multiple ELA methods must be considered as opposed to one - where mass balance data are available, these will be significantly improved (e.g. AABR)

- Simple SEB modelling approaches can be used to simulate mass balance change processes with high accuracy, especially when considering variability in spatial conditions so long as topographic conditions (namely hillshade) are considered

  - Available meteorological records and analyses for other glaciers provide a database from which basic constants (varying as a function of location) can be derived (see Giesen & Oerlemans, 2012)
  - Coupled with available DEMs of a glacier and its surroundings (which can be derived from relatively low resolution area maps), accurate ice melt simulations are possible for a small mountain glacier by combining the use of the now available aforementioned constants with basic site specific meteorological data (air temperature, precipitation, incident

radiation) which can be collected by the means of low cost, simple, AWS set-ups

- Considering the limited input variables for the developed model and the lack of site specific scaling factors, the model can easily be applied to other glaciers - the code for the model can be freely downloaded from `https://github.com/Chris35Wills/SEB_model_java_files` and offers a user friendly GUI.

The key findings of this study are as follows:

- Kårsa glacier, as with many other glaciers in Scandinavia and Europe, has reduced in area, retreated and thinned extensively throughout the 20th century, in line with climatic warming in the region as acknowledge by Callaghan *et al.* (2010)
  - Areas has reduced by 3.41 km^2 for the period 1926-2008 coupled with a retreat of 1292 m - the rate of retreat has increased since 1978 (8.3–14.4 m yr^{-1}). Total and annual retreat values are similar to those observed for other glaciers in Scandinavia.
  - Surface lowering for the 1926-2010 period has been at a rate of 0.35 m w.e. yr^{-1} which has resulted in an annual reduction in the maximum thickness of 0.85 m w.e. yr^{-1}. This gives a volume change of 1.33 x 10^{-3} km^3 yr^{-1}. The thinning of Kårsa is found to be at a rate similar to the much larger nearby Rabots Glciär, the rate of which for both is continuing unlike for nearby Storglaciären which is evidence for differences in glacier response times.
  - Change on an annual basis for the period 2007-2010 is less clear with changes in thickness being quantified as an overall mean reduction of 7.68 m $\pm$9.61 m, coupled with a volume change of 1.92 $\pm$2.30 x 10^{-3} km^3.
  - Coupled with retreat and thinning, the glacier has undergone disintegration as observed of other glaciers in Scandinavia and the European Alps.

- Knowledge of glacier thinning aids in a better understanding of changes in the thermal regime of the glacier
  - Rippin *et al.* (2011) found Kårsa to exhibit a thermal lag - proving to have a polythermal core whereas it was expected the glacier would be frozen to its bed
  - This study has highlighted how the previous thickness and surface slope distribution of the glacier resulted in increased basal stress which may have resulted in increased ice temperature and the development of the thermal regime discovered by Rippin *et al.* (2011)
- Topographic factors (hillshade) and the thickness of the snow pack are key in the control of mass balance change at Kårsa
  - The effect of hillshade on the incident radiation budget of Kårsa has increased dramatically as the glacier has retreated.
  - The thickness of the winter snow pack is found to have a significant effect on the melt of the glacier, greatly affecting the length of the melt season experienced by the glacier in a given year.
- Over very short time periods changes in slope and aspect have no significant effect on MB change of Kårsa.
  - No significant changes in SEB and MB were found between dynamic and fixed geometry melt simulations for the 2007-2010 period. These results relate directly to the geodetic analysis of glacier change for the same period, where geometry was found to change very little.
- Over longer time periods, specifically for the period 1926-1943, geometry was found to have a significant effect on MB and SEB
  - Fixed geometry runs results in much more negative mass balance for the period 1926-1943 compared to any other map interval experiments. This effect then propagates when considering the full 1926-2010 period.

– This relates to the observed change through geodetic analysis - the main lobe of the glacier in 1943 surface being steeper than in 1926. This is important as lesser slope angles relate to increase radiation receipt at the surface.

– Effect of geometry on SEB and MB cannot be simply related to time as other modelling experiments for similar time periods (based on the map intervals) do not replicate the results of the 1926-1943 period.

– As glacier geometry effects cannot be simply linked to time, it is imperative that future studies consider changes in glacier geometry on SEB and MB for accurate assessments of glacier response to climate.

11.4 The fate of Kårsaglaciären

The final field season conducted by Leeds University at the glacier was completed during the summer of 2013. This resulted in the retrieval of the AWS and also the removal of a network of cameras that were being used by Dr David Rippin for a photogrammetry study and that had been collecting images on a daily basis for the past year. The final visit also saw the use of a TLS which enabled the acquisition of a very high resolution DEM of the glacier and surrounding area. Photography of the surface was also carried out. The TLS and surface photography outputs were both in aid of a study into surface roughness upscaling — carried out by Dr Mark Smith and Dr Duncan Quincey. Considering the trends identified in the study presented here, the glacier will likely continue to retreat, however, the rate at which it does so will likely be strongly influenced by the increasing proportion of the glacier that is shaded by the surrounding mountains. The effect that the developing proglacial lake will have on the terminus will also be of interest in terms of potential calving and the effect that this may have on the rate of retreat and disintegration of the glacier. This will prompt an interesting return to research of the glacier in the future.

References

Abermann, J., Lambrecht, A., Fischer, A., & Kuhn, M. 2009. Quantifying changes and trends in glacier area and volume in the Austrian Ötztal Alps (1969-1997-2006). *The Cryosphere Discussions*, **3**, 415–441. 329, 330

Adalgeirsdottir, G., Jóhannesson, T., Björnsson, H., Pálsson, F., & Sigurdsson, O. 2006. Response of Hofjökull and southern Vatnajökull, Iceland, to climate change. *J. Geophys. Res.,*, **111**, F03001. 25

Adams, W. P., Cogley, J. G., Ecclestone, M. A., & Demuth, M. N. 1998. A Small Glacier as an Index of Regional Mass Balance: Baby Glacier, Axel Heiberg Island, 1959-1992. *Geografiska Annaler. Series A, Physical Geography*, **80**(1), 37–50. 34

Ahlmann, H. W:Son, & Tryselius, O. 1929. Der Kårsa-Gletscher in Schwedisch-Lappland. *Geografiska Annaler*, **11**, 1 – 32. 35, 48, 49, 53, 90, 179, 323, 353

Ahlmann, H.W., & Lindblad, T. 1940. Die Grössenveränderungen des Karsajökels in Schwedisch-Lappland während der Jahre 19091939. *Geografiska Annaler*, **22**(12), 80–94. 53

Ahlmann, H.W., Ångström, A., & Fjeldstad, Jonas Ekman. 1933. Scientific results of the Swedish-Norwegian Arctic Expedition in the summer of 1931, Part IX-X. *Geografiska Annaler*, **15**, 261–348. 35

Allison, I.F., & Keage, P.L. 1986. Recent changes in the glaciers of Heard Island. *Polar Record*, **23**(144), 255–271. 88

Andreassen, L. M. 1999. Comparing Traditional Mass Balance Measurements with Long-Term Volume Change Extracted from Topographical Maps: A Case Study of Storbreen Glacier in Jotunheimen, Norway, for the Period 1940-1997. *Geografiska Annaler*, **81A**(4), 467–476. 40, 353, 355

Ångstrom, A. 1933. Scientific results of the Swedish Norwegian arctic expedition in the summer of 1931. VII. On the total radiation from sun and sky at Sveanor. *Geografiska Annaler*, **16**, 151–160. 2, 35

Aniya, M., Sato, H., Naruse, R., Skvarca, P., & Casassa, G. 1996. The use of staellite and airborne imagery to inventory outlet glaciers of the southern Patagonia Icefield, South America. *Photogrammetric Engineering and Remote Sensing*, **62**(12), 1361–1369. 37

Aniya, Masamu, Sato, Hiroaki, Naruse, Renji, Skvarca, Pedro, & Casassa, Gino. 1997. Recent Glacier Variations in the Southern Patagonia Icefield, South America. *Arctic and Alpine Research*, **29**(1), 1–12. 37, 39

Arendt, A. 1999. Approaches to modelling the surface albedo of a high Arctic glacier. *Geografiska Annaler*, **81A**(4), 477–487. 21, 345

Arendt, A.A., Luthcke, S.B., Larsen, C.F., Abdalati, W., Krabill, W.B., & Beedle, M.J. 2008. Validation of high-resolution GRACE mascon estimates of glacier mass changes in the St Elias Mountains, Alaska, USA, using aircraft laser altimetry. *Journal of Glaciology*, **54**(188), 778–787. 332

Arendt, Anthony A., Echelmeyer, Keith A., Harrison, William D., Lingle, Craig S., & Valentine, Virginia B. 2002. Rapid Wastage of Alaska Glaciers and Their Contribution to Rising Sea Level. *Science*, **297**(5580), 382–386. 7, 327

Arnold, N. S., Willis, I. C., Sharp, M.J., Richards, K.S., & Lawson, W.J. 1996. A distributed surface energy-balance model for a small valley glacier. I. Development and testing for Haut Glacier d'Arolla, Valais, Switzerland. *Journal of Glaciology*, **42**(140), 77–89. 29, 45, 145, 343, 357, 425

Arnold, N. S., Rees, W. G., Devereux, B. J., & Amable, G. S. 2006a. Evaluating the potential of high-resolution airborne LiDAR data in glaciology. *International Journal of Remote Sensing*, **27**(6), 1233–1251. 361

Arnold, N.S., Rees, W.G., Hodson, A.J., & Kohler, J. 2006b. Topographic controls on the surface energy balance of a high Arctic valley glacier. *Journal of Geophysical Research*, **111**, 649–658. 21, 22, 27, 28, 239, 333, 343, 347, 351, 352, 361

Avian, M., & Bauer, A. 2006. First Results on Monitoring Glacier Dynamics with the Aid of Terrestrial Laser Scanning on Pasterze Glacier (Hohe Tauern, Austria). *Grazer Schriften der Geographie und Raumforschung*, **41**, 27–36. 361

Bahr, D. B., M.F., Meier, & S.D., Peckham. 1997. The physical basis of glacier volume-area scaling. *Journal of Geophysical Research*, **102**(B9), 20355–20362. 334

Bahr, David B., Dyurgerov, Mark, & Meier, Mark F. 2009. Sea-level rise from glaciers and ice caps: A lower bound. *Geophys. Res. Lett.*, **36**(3), L03501. 7

Ballantyne, C.K. 2002. The Loch Lomond advance on the Isle of Mull, Scotland: glacier reconstruction and palaeoclimatic implications. *Journal of Quaternary Science*, **17**, 759–771. 147

Bamber, J.L., & Layberry, R.L. 2001. A new ice thickness and bed data set for the Greenland ice sheet 1. Measurement, data reduction, and errors. *Journal of Geophysical Research*, **106**(D24), 33,773–33,780. 75

Bamber, J.L., & Rivera, A. 2007. A review of remote sensing methods for glacier mass balance determination. *Global and Planetary Change*, **59**, 138–148. 32, 35, 40, 368

Baraer, Michel, Mark, Bryan G., McKenzie, Jeffrey M., Condom, Thomas, Bury, Jeffrey, Huh, Kyung-In, Portocarrero, Cesar, Gómez, Jesús, & Rathay, Sarah. 2012. Glacier recession and water resources in Peru's Cordillera Blanca. *Journal of Glaciology*, **58**(207), 134–150. 327

Barrand, N. E., James, T. D., & Murray, T. 2010. Spatio-temporal variability in elevation changes of two high-Arctic valley glaciers. *Journal of Glaciology*, **56**(199), 771–780. 8, 9, 92

Barry, R.G. 1992. *Mountain weather and climate*. 2nd ed edn. London: Routledge Physical Environment Series. 6

Barry, R.G. 2008. *Mountain weather and climate*. 3rd edition edn. Cambridge: Cambridge University Press. 6

Bartlet, P., & Lehning, M. 2002. A physical SNOWPACK model for the Swiss avalanche warning Part I: numerical model. *Cold Regions Science and Technology*, **35**, 123–145. 347, 367

Bates, B., Kundzewicz, Z.W., Wu, S., & Palutikof, J. 2008. *Climate change and water*. Vol. Technical Paper 6. IPCC. 7

Bauder, A. 2001. Bestimmung der Massenbilanz von Gletschern mit Fernerkundungsmethoden und Fliessmodellierungen: eine Sensitivitätsstudie auf dem Unteraargletscher. *Mitt. VAW/ETH*, **169**. 32

Bauder, A., Funk, M., & Huss, M. 2007. Ice-volume changes of selected glaciers in the Swiss Alps since the end of the 19th century. *Annals of Glaciology*, **46**(1), 145–149. 30, 32, 35, 323, 327

Bayr, K. J., Hall, D. K., & Kovalick, W. M. 1994. Observations on glaciers in the eastern Austrian Alps using satellite data. *International Journal of Remote Sensing*, **15**(9), 1733–1742. 38

Benn, D.I., & Evans, D.J.A. 1998. *Glaciers and Glaciation*. 1st ed. edn. London: Arnold. 11, 21, 26, 104, 202

Benn, D.I., & Evans, D.J.A. 2010. *Glaciers and Glaciation*. 2nd ed. edn. London: Hodder Education. 10, 96, 106, 107

Benn, D.I., & Gemmell, A.M.D. 1997. Calculating equilibrium-line altitudes of former glaciers: a new computer spreadsheet. *Glacial Geology and Geomorphology Web Site http://ggg.qub.ac.uk/ggg [website no longer working].* 109, 340

Benn, D.I., Owen, L.A., Osmaston, H.A., Seltzer, G.O., Porter, S.C., & Mark, B. 2005. Reconstruction of equilibrium-line altitudes for tropical and sub-tropical glaciers. *Quaternary International*, **138**, 8–21. 110

Benn, D.I., Hulton, N.R.J., & Mottram, R.H. 2007a. 'Calving laws', 'sliding laws' and the stability of tidewater glaciers. *Annals of Glaciology*, **46**, 123–130. 368

Benn, D.I., Warren, C.R., & Mottram, R.H. 2007b. Calving processes and the dynamics of calving glaciers. *Earth-Science Reviews*, **82**, 143–179. 368

Benn, Douglas I., & Lehmkuhl, Frank. 2000. Mass balance and equilibrium-line altitudes of glaciers in high-mountain environments. *Quaternary International*, **65-66**, 15–29. 33, 105, 108

Bernhardt, M., Zängl, G., Liston, G. E., Strasser, U., & Mauser, W. 2009. Using wind fields from a high-resolution atmospheric model for simulating snow dynamics in mountainous terrain. *Hydrological Processes*, **23**(7), 1064–1075. 347

Bernhardt, M., Liston, G. E., Strasser, U., Zängl, G., & Schulz, K. 2010. High resolution modelling of snow transport in complex terrain using downscaled MM5 wind fields. *The Cryosphere*, **4**, 99–113. 347

Berthier, E., Schiefer, E., Clarke, G. K. C., Menounos, B., & Remy, F. 2010. Contribution of Alaskan glaciers to sea-level rise derived from satellite imagery. *Nature Geosci*, **3**(2), 92–95. 9, 327, 332

BFE. 2013. http://www.bfe.admin.ch/themen/00490/00491/index.html?lang=en. [**Accessed 6th May 2013**]. 6

Bingham, R.G., Nienow, P.W., Sharp, M.J., & Copland, L. 2006. Hydrology and dynamics of a polythermal (mostly cold) High Arctic glacier. *Earth Surface Processes and Landforms*, **31**(12), 1463–1479. 49

Bishop, Michael P.and Olsenholler, Jeffrey A., Shroder, John F., Barry, Roger G., Raup, Bruce H., Bush, Andrew B. G., Copland, Luke, Dwyer, John L., Fountain, Andrew G., Haeberli, Wilfried, Kääb, Andreas, Paul, Frank Hall, Dorothy K., Kargel, Jeffrey S., Molnia, Bruce F., Trabant, Dennis C., & Wessels, Rick. 2004. Global Land Ice Measurements from Space (GLIMS): Remote Sensing and GIS Investigations of the Earth's Cryosphere. *Geocarto International*, **19**(2), 57–84. 37

Björnsson, Helgi. 1981. Radio-Echo Sounding Maps of Storglaciären, Isfallsglaciären and Rabots Glaciär, Northern Sweden. *Geografiska Annaler. Series A, Physical Geography*, **63**(3/4), 225–231. 334

Bodin, A. 1993. *Physical properties of the Kårsa glacier, Swedish Lapland.* 48, 49, 50, 51, 53, 71, 73, 74, 339, 340, 341, 359

Braithwaite, R., & Zhang, Y. 2000. Sensitivity of mass balance of five Swiss glaciers to temperature changes assessed by tuning a degree-day model. *Journal of Glaciology*, **46**, 7 – 14. 2, 42, 147

Braithwaite, R. J. 2002. Glacier mass balance: the first 50 years of international monitoring. *Progress in Physical Geography*, **26**(1), 76–95. 12, 31

Braithwaite, R.J. 1981. On glacier energy balance, ablation, and air temperature. *Journal of Glaciology*, **27**(97), 381–391. 41

Brock, B. W., & Arnold, N. S. 2000. A spreadsheet-based (Microsoft Excel) point surface energy balance model for glacier and snow melt studies. *Earth Surface Processes and Landforms*, **25**, 649–658. 159, 357

Brock, Ben W., Willis, Ian C., Sharp, Martin J., & Arnold, Neil S. 2000a. Modelling seasonal and spatial variations in the surface energy balance of Haut Glacier d'Arolla, Switzerland. *Annals of Glaciology*, **31**(1), 53–62. 29, 43, 45, 345, 424

Brock, B.W., Willis, I.C., & Sharp, M.J. 2000b. Measurement and parameterization of albedo variations at Haut Glacier d'Arolla, Switzerland. *Journal of Glaciology*, **46**, 675 – 688. 145

Brown, C. S., Meier, M. F., & Post, A. 1982. *Calving Speed of Alaska Tidewater Glaciers, With Application to Columbia Glacier.* Tech. rept. US Geological Survey. 31

Brozovic, Nicholas, Burbank, Douglas W., & Meigs, Andrew J. 1997. Climatic Limits on Landscape Development in the Northwestern Himalaya. *Science*, **276**(5312), 571–574. 26

Brugger, K. A. 2007. The non-synchronous response of Rabots Glaciär and Storglaciären, northern Sweden, to recent climate change: a comparative study. *Annals of Glaciology*, **46**, 275–282. 336

Brugger, K. A., Refsnider, Kurt A., & Whitehill, M. F. 2005. Variation in glacier length and ice volume of Rabots Glaciär, Sweden, in response to climate change, 19102003. *Annals of Glaciology*, **42**, 180–188. 333, 334, 335, 336, 354, 360

Burrough, P.A., & McDonnell, R.A. 1998. *Principles of Geographical Information Systems.* Oxford: Oxford University Press. 21, 22, 85, 98, 143, 154

Callaghan, Terry V., Bergholm, Fredrik, Christensen, Torben R., Jonasson, Christer, Kokfelt, Ulla, & Johansson, Margareta. 2010. A new climate era in the sub-Arctic: Accelerating climate changes and multiple impacts. *Geophys. Res. Lett.*, **37**(14), L14705. 322, 346, 370

Carr, S., & Coleman, C. 2007. An improved technique for the reconstruction of former glacier mass-balance and dynamics. *Geomorphology*, **92**, 76–90. 30, 34, 38

Carrivick, J.L., & Brewer, T.R. 2004. Improving Local Estimations and Regional Trends of Glacier Equilibrium Line Altitudes. *Geografiska Annaler. Series A, Physical Geography*, **86**(1), 67–79. 26, 106, 337

Carrivick, J.L., & Chase, S.E. 2011. Spatial and temporal variability of annual glacier equilibrium line altitudes in the Southern Alps, New Zealand. *New Zealand Journal of Geology and Geophysics*, **54**(4), 415–429. 8, 9, 25

Carrivick, Jonathan, & Rushmer, E. 2009. Inter- and Intra-catchment Variations in Proglacial Geomorphology: An Example from Franz Josef Glacier and Fox Glacier, New Zealand. *Arctic, Antarctic, and Alpine Research*, **41**(1), 18–36. 9

Carrivick, Jonathan L., Smith, Mark W., Quincey, Duncan J., & Carver, Steve J. 2013. Developments in budget remote sensing for the geosciences. *Geology Today*, **29**(4), 138–143. 362, 367

Carroll, J.J., & Fitch, B.W. 1981. Effects of Solar Elevation and Cloudiness on Snow Albedo at the South Pole. *Journal of Geophysical Research*, **86**, 5271–5276. 144

Carturan, L., R., Filippi, Seppi, R., Gabrielli, P., Notarnicola, C., Bertoldi, L., Paul, F., Rastner, P., Cazorzi, F., Dinale, R., & Dalla Fontana, G. 2013. Area and volume loss of the glaciers in the Ortles-Cevedale group (Eastern Italian Alps): controls and imbalance of the remaining glaciers. *The Cryosphere Discuss.*, **7**, 267–319. 15, 27, 32, 39, 41, 329, 330, 331

Cazorzi, F., & Fontana, G.D. 1996. Snowmelt modelling by combining air temperature and a distributed radiation index. *Journal of Hydrology*, **181**, 169–187. 42

Chen, J., & Ohmura, A. 1990. Estimation of Alpine glacier water resources and their change since the 1870s. *Hydrology in Mountainous Regions: IAHS Publications*, **193**, pp127–135. 6

Church, J.A., et al. 2001. Changes in sea level. *Climate Change 2001: The Scientific Basis — Contribution of Working Group I to the Third Assessment Report of the Intergovernmental Panel on Climate Change*, 639693. 5, 7

Citterio, M., Diolaiuti, G., Smiraglia, C., D'Agata, C., Carnielli, T., Stella, G., & Siletto, G. B. 2007. The fluctuations of Italian Glaciers during the last century: a contribution to knowledge about alpine glacier changes. *Geografiska Annaler: Series A, Physical Geography*, **89**(3), 167–184. 6, 7, 329, 330

Clapperton, C.M. 1971. The location and origin of glacial meltwater phenomena in the eastern Cheviot Hills. *Proceedings of the Yorkshire Geological Society*, **38**, 361–380. 38

Cogley, J., & McIntyre, M. 2003. Hess Altitudes and Other Morphological Estimators of Glacier Equilibrium Lines. *Arctic, Antarctic, and Alpine Research*, **35**(4), 482–488. 34, 106

Cogley, J. G. 2009. Geodetic and direct mass-balance measurements: comparison andjoint analysis. *Annals of Glaciology*, **50**, 96–100. 7

Cogley, J. G. 2011. Present and future states of Himalaya and Karakoram glaciers. *Annals of Glaciology*, **52**, 69–73. 7

Cook, A. J., Fox, A. J., Vaughan, D. G., & Ferrigno, J. G. 2005. Retreating Glacier Fronts on the Antarctic Peninsula over the Past Half-Century. *Science*, **308**, 541–544. 88

Cuffey, K.M., & Paterson, W. S. B. 2010. *The Physics of Glaciers*. 4th edn. Oxford: Butterworth-Heinemann. 11, 24, 25, 105

Cutler, P.M., & Munro, D.S. 1996. Visible and near-infrared reflectivity during the ablation period on Peyto Glacier, Alberta, Canada. *Journal of Glaciology*, **42**, 333–340. 144, 145

Davies, B.J., Carrivick, J.L., Glasser, N. F., Hambrey, M.J., & Smellie, J.L. 2012. Variable glacier response to atmospheric warming, northern Antarctic Peninsula, 19882009. *The Cryosphere*, **6**, 1031–1048. 34, 99, 106, 110, 200, 332

Davis, J.C. 2002. *Statistics and Data Analyses in Geology*. Third edition edn. Chichester: John Wiley and Sons. 75

De Woul, M. 2008. Response of glaciers to climate change: Mass balance sensitivity, sea level rise and runoff. *Dissertations from the Department of Physical Geography and Quaternary Geology*, **13**. 5

DeBeer, C.M., & Sharp, M.J. 2007. Recent changes in glacier area and volume within the southern Canadian Cordillera. *Annals of Glaciology*, **46**, 215–221. 323

DeBeer, C.M., & Sharp, M.J. 2009. Topographic influences on recent changes of very small glaciers in the Monashee Mountains, British Columbia, Canada. *Journal of Glaciology*, **55**, 691–700. 7, 322, 327

Derbyshire, E. 1961. Subglacial col gullies and the deglaciation of the north-east Cheviots. *Transactions of the Institute of British Geographers*, **29**, 31 46. 38

Diolaiuti, G., Bocchiola, D., Vagliasindi, M., D'Agata, C., & Smiraglia, C. 2012. The 19752005 glacier changes in Aosta Valley (Italy) and the relations with climate evolution. *Progress in Physical Geography*, **36**(6), 764–785. 327, 330, 331

Diolaiuti, Guglielmina Adele, Maragno, Davide, D'Agata, Carlo, Smiraglia, Claudio, & Bocchiola, Daniele. 2011. Glacier retreat and climate change: Documenting the last 50 years of Alpine glacier history from area and geometry changes of Dosdè Piazzi glaciers (Lombardy Alps, Italy). *Progress in Physical Geography*, **35**(2), 161–182. 5, 6, 7, 329, 330, 331, 357

Dobhal, D.P., Gergan, J.T., & Thayyen, R.J. 2004. Recession and morphogeometrical changes of Dokriani glacier (1962–1995) Garhwal Himalaya, India. *Current Science*, **86**(5). 88, 92, 327

Dowdeswell, J. A., Hagen, J. O., Björnsson, H., Glazovsky, A. F., Harrison, W.D., Holmlund, P., Jania, J., Koerner, R. M., Lefauconnier, B., Ommanney, C., Simon, L., & Thomas, R.H. 1997. The Mass Balance of Circum-Arctic Glaciers and Recent Climate Change. *Quaternary Research*, **48**(1), 1–14. 49

Dunn, S.M., & Colohan, R.J.E. 1999. Developing the snow component of a distributed hydrological model: a step-wise approach based on multi-objective analysis. *Journal of Hydrology*, **223**(116). 42

Dyurgerov, M. 2003. Mountain and subpolar glaciers show an increase in sensitivity to climate warming and intensification of the water cycle. *Journal of Hydrology*, **282**(1-4), 164–176. 1

Dyurgerov, M. B., & Meier, M.F. 1997. Mass Balance of Mountain and Subpolar Glaciers: A New Global Assessment for 1961-1990. *Arctic and Alpine Research*, **29**(4), 379–391. 1

Dyurgerov, Mark B., & Meier, Mark F. 2000. Twentieth century climate change: Evidence from small glaciers. *Proceedings of the National Academy of Sciences*, **97**(4), 1406–1411. 1, 5, 323, 327

Elsberg, D.H., Harrison, W.D., Echelmeyer, K.A., & Krimmel, R.M. 2001. Quantifying the effects of climate and surface change on glacier mass balance. *Journal of Glaciology*, **47**(159), 649–658. 12, 13, 46, 348

Embleton, C. 1964. The deglaciation of Arfon and southern Anglesey and the origin of the Menai Straits. *Proceedings of the Geologists Association*, **75**, 407–430. 38

Emmi, Philip C., & Horton, Carl A. 1995. A Monte Carlo simulation of error propagation in a GIS-based assessment of seismic risk. *International Journal of Geographical Information Systems*, **9**(4), 447–461. 86

Escher-Vetter, H. 1980. Der Strahlungshaushalt des Vernagtferners als Basis der Energiehaushaltsberechnung zur Bestimmung der Schmeltzwasserproduktion eines Alpengletschers. *Universistät München Meteorologisches Institute Wissenschaftliche Mitteilungen*. 145

ESRI. 2009. ArcGIS 9.3 Desktop Help. *http:// webhelp.esri.com/ arcgisdesktop/ 9.3/*, [**Accessed 6th January 2010**]. 59, 75, 76, 77

ESRI. 2011a. ArcGIS 10.0 Desktop Help: How Aspect works. *http:// help.arcgis.com/ en/ arcgisdesktop/ 10.0/ help/ index.html*, [**Accessed 3rd November 2011**]. 154

ESRI. 2011b. ArcGIS 10.0 Desktop Help: How Slope works. *http:// help.arcgis.com/ en/ arcgisdesktop/ 10.0/ help/ index.html*, [**Accessed 3rd November 2011**]. 154

Essery, R., Li, L., & Pomeroy, J. 1999. A distributed model of blowing snow over complex terrain. *Hydrological Processes*, **13**, 2423–2438. 347

Evans, D.J.A., & O Cofaigh, C. 2003. Depositional evidence for marginal oscillations of the Irish Sea Ice Stream in southeast Ireland during the last glaciation. *Boreas*, **32**, 76101. 38

Evans, D.J.A., Clark, C.D., & Mitchell, W.A. 2005. The last British Ice Sheet: A review of the evidence utilised in the compilation of the Glacial Map of Britain. *Earth-Science Reviews*, **70**, 253–312. 38

Finsterwalder, R. 1962. Measurement of glacier variations in the Eastern Alps, particularly in the Gurgl area. *In:* Ward, W. (ed), *Variations of the regime of existing glaciers*, vol. 58. The Symposium of Obergurgl: IAHS. 88

Finsterwalder, S., & Schunk, H. 1887. Der Suldenferner. *Zeitschrift des Deutschen und Oesterreichischen Alpenvereins*, **18**, 72–89. 2

Fleming, K. M., Dowdeswell, J. A., & Oerlemans, J. 1997. Modelling the mass balance of northwest Spitsbergen glaciers and responses to climate change. *Annals of Glaciology*, **24**, 203210. 7

Fleming, M.D., & Hoffer, R.M. 1979. Machine Processing of Landsat MSS Data and DMA Topographic Data for Forest CoverType Mapping. *LARS Technical Reports*, **80**, 377–390. 154

Flowers, G. E., Marshall, S. J., Björnsson, H., & Clarke, G. K. C. 2005. Sensitivity of Vatnajokull ice cap hydrology and dynamics to climate warming over the next 2 centuries. *Journal of Geophysical Research*, **110**, F02011. 26, 428

Folland, C.K. et al. 2001. Observed Climate Variability and Change. *Climate Change 2001: The Scientific Basis*, **Contribution of Working Group I to the Third Assessment Report of the Intergovernmental Panel on Climate Change**, 881. 7

Førland, E.J., & Hanssen-Bauer, I. 2003. Past and future climate variations in the Norwegian Arctic: overview and novel analyses. *Polar Research*, **22**(2), 113–124. 9

Fountain, A.G., Lewis, K. J., & Doran, P. T. 1999a. Spatial climatic variation and its control on glacier equilibrium line altitude in Taylor Valley, Antarctica. *Global and Planetary Change*, **22**, 1–10. 106

Fountain, A.G., Jansson, P., Kaser, G., & Dyurgerov, M. B. 1999b. Summary of the Workshop on Methods of Mass Balance Measurements and Modelling, Tarfala, Sweden August 1012, 1998. *Geografiska Annaler*, **81A**(4), 461–465. 32

Fountain, Andrew G., & Vecchia, Aldo. 1999. How many Stakes are Required to Measure the Mass Balance of a Glacier? *Geografiska Annaler: Series A, Physical Geography*, **81**(4), 563–573. 30

Fröhlich, C. 1993. *Changes of total solar irradiance*. Geophys. Monogr. Ser., vol. 75. Washington, DC: AGU. 133

Furbish, D.J., & Andrews, J.T. 1984. The use of hypsometry to indicate long term stability and response of valleys glaciers to changes in mass transfer. *Journal Glaciology*, **30**, 199–211. 34, 108, 109, 340

Gardner, A., Moholdt, G., Arendt, A., & Wouters, B. 2012. Accelerated contributions of Canadas Baffin and Bylot Island glaciers to sea level rise over the past half century. *The Cryosphere*, **6**, 11031125. 327

Gardner, A. S., Sharp, M. J., Koerner, R. M., Labine, C., Boon, S., Marshall, S. J., Burgess, D.O., & Lewis, D. 2009. Near-surface temperature lapse rates over Arctic glaciers and their implications for temperature downscaling. *Journal of Climate*, **22**(16), 4281–4298. 147

Gardner, Alex S., Moholdt, Geir, Wouters, Bert, Wolken, Gabriel J., Burgess, David O., Sharp, Martin J., Cogley, J. Graham, Braun, Carsten, & Labine, Claude. 2011. Sharply increased mass loss from glaciers and ice caps in the Canadian Arctic Archipelago. *Nature*, **473**(7347), 357–360. 5, 323

Gardner, Alex S., Moholdt, Geir, Cogley, J. Graham, Wouters, Bert, Arendt, Anthony A., Wahr, John, Berthier, Etienne, Hock, Regine, Pfeffer, W. Tad, Kaser, Georg, Ligtenberg, Stefan R. M., Bolch, Tobias, Sharp, Martin J., Hagen, Jon Ove, van den Broeke, Michiel R., & Paul, Frank. 2013. A Reconciled Estimate of Glacier Contributions to Sea Level Rise: 2003 to 2009. *Science*, **340**(6134), 852–857. 8, 357

Gerbaux, M., Genthon, C., Etchevers, P., Vincent, C., & Dedieu, J. P. 2005. Surface mass balance of glaciers in the French Alps: distributed modeling and sensitivity to climate change. *Journal of Glaciology*, **51**, 561–572. 2, 27, 29, 430

Giesen, R. H., & Oerlemans, J. 2010. Response of the ice cap Hardangerjøkulen in southern Norway to the 20th and 21st century climates. *The Cryosphere*, **4**(2), 191–213. 15, 26, 44, 145, 146, 159, 170, 344

Giesen, R. H., & Oerlemans, J. 2012. Global application of a surface mass balance model using gridded climate data. *The Cryosphere Discuss.*, **6**(2), 1445–1490. xvii, 25, 43, 44, 139, 147, 152, 231, 233, 236, 270, 271, 341, 343, 344, 357, 369, 437

Giesen, R. H., Andreassen, L. M., van den Broeke, M. R., & Oerlemans, J. 2009. Comparison of the meteorology and surface energy balance at Storbreen and Midtdalsbreen, two glaciers in southern Norway. *The Cryosphere*, **3**(1), 57–74. 232

Glasser, N., Harrison, S., Jansson, K.N., Anderson, K., & Cowley, A. 2011. Global sea-level contribution from the Patagonian Icefields since the Little Ice Age maximum. *Nature Geoscience*, **4**, 303–307. 8

Glickman, T. 2000. *Glossary of Meteorology*. American Meteorological Society. 147

Granshaw, F.D., & Fountain, A. G. 2006. Glacier change (1958-1998) in the North Cascades National Park Complex, Washington, USA. *Journal of Glaciology*, **52**, 251–256. 6, 7, 9, 39, 322

Grudd, H. 1990. Small glaciers as sensitive indicators of climatic fluctuations. *Geografiska Annaler*, **72A**, 119–128. 6

Haeberli, W., & Beniston, M. 1998. Climate Change and Its Impacts on Glaciers and Permafrost in the Alps. *Ambio*, **27**(4), 258–265. 6

Haeberli, W., Frauenfelder, R., Hoelzle, M., & Maisch, M. 1999. On rates and acceleration trends of global glacier mass changes. *Geografiska Annaler Series a-Physical Geography*, **81A**(4), 585–591. 5

Haeberli, W., Hoelzle, M., Paul, F., & Zemp, M. 2007. Integrated monitoring of mountain glaciers as key indicators of global climate change: the European Alps. *Annals of Glaciology*, **46**(1), 150–160. 1

Hagen, J.O., Melvold, K., Eiken, T., Isaksson, E., & Lefauconnier, B. 1999. Mass balance methods on Kongsvegen, Svalbard. *Geografiska Annaler*, **81A**, 593–601. 332

Hagg, W.J., Braun, L.N., Uvarov, N., & Makarevich, K.G. 2004. A comparison of three methods of mass-balance determination in the Tuyuksu glacier region, Tien Shan, Central Asia. *Journal of Glaciology*, **50**(171), 505–510. 31, 40, 338, 340, 353, 354, 355

Hanshaw, M.N., & Bookhagen, B. 2013. Glacial areas, lake areas, and snowlines from 1975 to 2012: status of the Cordillera Vilcanota, including the Quelccaya Ice Cap, northern central Andes, Peru. *The Cryosphere Discussions*, **7**, 573–634. 39

Harrison, William D., Cox, L.H., Hock, R., March, R.S., & Pettit, E.C. 2009. Implications for the dynamic health of a glacier from comparison of conventional and reference-surface balances. *Annal of Glaciology*, **50**, 25–30. 2, 13, 14, 350, 351, 352

Hawkins, F. 1985. Equilibrium-line altitudes and palaeoenvironments in the Merchants Bay area, Baffin Island, NWT, Canada. *Journal of Glaciology*, **31**, 205–213. 34, 197, 201

Heritage, George L., Milan, David J., Large, Andrew R. G., & Fuller, Ian C. 2009. Influence of survey strategy and interpolation model on DEM quality. *Geomorphology*, **112**(34), 334–344. 347, 361

Heywood, D.I., Cornelius, S., & Carver, S. 2006. *An introduction to Geographical Information Systems*. Pearson Prentice Hall. 85

Hock, R. 1999. A distributed temperature-index ice- and snowmelt model including potential direct solar radiation. *Journal of Glaciology*, **45**(149), 101–111. 40, 42, 43, 430, 434

Hock, R. 2003. Temperature index melt modelling in mountain areas. *Journal of Hydrology*, **282**, 104–115. 41, 42, 351

Hock, R. 2005. Glacier melt: a review of processes and their modelling. *Progress in Physical Geography*, **29**, 362–391. 2, 10, 14, 41, 43, 44, 144, 359

Hock, R., & Holmgren, B. 1996. Some aspects of energy balance and ablation of Storglaciren, northern Sweden. *Geografiska Annaler*, **78A**(2-3), 121–131. 14, 43, 138

Hock, R., & Noetzli, C. 1997. Areal melt and discharge modelling of Storglaciären, Sweden. *Annals of Glaciology*, **24**, 211 – 216. 2, 21, 43, 44, 45, 138

Hock, Regine, & Holmgren, B. 2005. A distributed surface energy-balance model for complex topography and its application to Storglaciären, Sweden. *Journal of Glaciology*, **51**, 25–36. 21, 22, 24, 25, 27, 96, 135, 138, 142, 148, 351

Hock, Regine, & Jensen, Holger. 1999. Application of Kriging Interpolation for Glacier Mass Balance Computations. *Geografiska Annaler: Series A, Physical Geography*, **81**(4), 611–619. 75, 77, 356

Hock, Regine, de Woul, Mattias, Radi, Valentina, & Dyurgerov, Mark. 2009. Mountain glaciers and ice caps around Antarctica make a large sea-level rise contribution. *Geophys. Res. Lett.*, **36**(7), L07501. 7, 8

Hodgkins, R., Carr, S., Pálsson, F., Gudmundsson, S., & Björnsson, H. 2012. Sensitivity analysis of temperature-index melt simulations to near-surface lapse rates and degree-day factors at Vestari-Hagafellsjökull, Langjökull, Iceland. *Hydrological Processes*. 148

Hodgkins, Richard, Fox, Adrian, & Nuttall, Anne-Marie. 2007. Geometry change between 1990 and 2003 at Finsterwalderbreen, a Svalbard surge-type glacier, from GPS profiling. *Annals of Glaciology*, **46**(1), 131–135. 332

Hoelzle, M., Chinn, T., Stumm, D., Paul, F., Zemp, M., & Haeberli, W. 2007. The application of glacier inventory data for estimating past climate change effects on mountain glaciers: A comparison between the European Alps and the Southern Alps of New Zealand. *Global and Planetary Change*, **56**(1-2), 69–82. 328

Höfer, H. 1879. Gletscher- und Eiszeit-Studien. *Abhandlungen der Mathematisch-Physikalische Klasse der Königlich Bayerischen Akademie der Wissenschaften*, **79**, 331–367. 106

Holdar, C.G. 1959. The Inland Ice in the Abisko Area. *Geografiska Annaler*, **41**(4), 231–235. 49

Holmlund, P. 1989. Kårsaglaciären. *Fjällklubbsnyth*, **4**, 13–15. 48, 64

Holmlund, P., Karlen, W., & Grudd, H. 1996. Fifty Years of Mass Balance and Glacier Front Observations at the Tarfala Research Station. *Geografiska Annaler. Series A, Physical Geography*, **78**(2/3), 105–114. 323, 324, 327, 328

Honaker, J., King, G., & Blackwell, M. 2012 (May). *AMELIA II: A Program for Missing Data*. R manual. 112, 113, 116

Hopkinson, C., & Demuth, M. N. 2006. Using airborne lidar to assess the influence of glacier downwasting on water resources in the Canadian Rocky Mountains. *Canadian Journal of Remote Sensing*, **32**(2), 212–222. 361

Horn, B. K. P. 1981. Hill shading and the reflectance map. *Proceedings of the IEEE*, **69**(1), 14–47. 153, 154

Huss, M. 2013. Density assumptions for converting geodetic glacier volume change to mass change. *The Cryosphere*, **7**, 877–887. 9, 334

Huss, M., Farinotti, D., Bauder, A., & Funk, M. 2008. Modelling runoff from highly glacierized alpine drainage basins in a changing climate. *Hydrological Processes*, **22**, 3888–3902. 13

Huss, M., Funk, M., & Ohmura, A. 2009. Strong Alpine glacier melt in the 1940s due to enhanced solar radiation. *Geophysical Research Letters*, **36**, L23501. 344

Huss, M., Hock, R., Bauder, A., & Funk, M. 2010. 100-year mass changes in the Swiss Alps linked to the Atlantic Multidecadal Oscillation. *Geophys. Res. Lett.*, **37**(10), L10501. 13, 352

Huss, M., Hock, R., Bauder, A., & Funk, M. 2012. Conventional versus reference-surface mass balance. *Journal of Glaciology*, **38**(208), 278–286. 2, 6, 12, 13, 24, 28, 29, 46, 305, 306, 315, 350, 351, 352

IAU. 2012. Resolutions B1, B2, B3 and B4. *In: The XXVIII General Assembly of the International Astronomical Union*. 135

Irvine-Fynn, T.D.L., Moorman, B.J., Williams, J.L.M., & Walter, F.S.A. 2006. Seasonal changes in ground-penetrating radar signature observed at a polythermal glacier, Bylot Island, Canada. *Earth Surface Processes and Landforms*, **31**, 892–909. 334

Jacob, Thomas, Wahr, John, Pfeffer, W. Tad, & Swenson, Sean. 2012. Recent contributions of glaciers and ice caps to sea level rise. *Nature*, **Advance online publication**. 6, 7

James, M. R., & Robson, S. 2012. Straightforward reconstruction of 3D surfaces and topography with a camera: Accuracy and geoscience application. *Journal of Geophysical Research: Earth Surface*, **117**(F3), F03017. 361, 362

James, T. D., Murray, T., Barrand, N. E., Sykes, H. J., Fox, A. J., & King, M. A. 2012. Observations of enhanced thinning in the upper reaches of Svalbard glaciers. *The Cryosphere*, **6**(6), 1369–1381. 1, 7, 39

Jangpangi, B.S., & Vohra, C.P. 1962. The retreat of the Shunkalpa (Ralam) glacier in Central Himalaya, Pithoragarh District, Uttar Pradesh, India. *Geological Survey of India*, 234–238. 88

Jiskoot, H., Murray, T., & Boyle, P. 2000. Controls on the distribution of surge-type glaciers in Svalbard. *Journal of Glaciology*, **46**(154), 412–422. 99

Jiskoot, H., Curran, C.J., Tessler, D.L., & Shenton, L.R. 2009. Changes in Clemenceau Icefield and Chaba Group glaciers, Canada, related to hypsometry, tributary detachment, lengthslope and areaaspect relations. *Annals of Glaciology*, **50**(53), 133–143. 98, 99, 173, 204, 229, 327

Johannesson, T., Sigurdsson, O., Laumann, T., & Kennett, M. 1995. Degree-day glacier mass-balance modelling with applications to glaciers in Iceland, Norway and Greenland. *Journal of Glaciology*, **41**(138), 345–358. 42

Johnson, A. J., Larsen, C.F., Murphy, N., Arendt, A.A., & Zirnheld, S.L. 2013. Mass balance in the Glacier Bay area of Alaska, USA, and British Columbia, Canada, 19952011, using airborne laser altimetry. *Journal of Glaciology*, **59**(216). 332

Jones, Kevin H. 1998. A comparison of algorithms used to compute hill slope as a property of the DEM. *Computers and Geosciences*, **24**(4), 315–323. 153, 154

Jonsell, U., Hock, R., & Holmgren, B. 2003. Spatial and temporal variations in albedo on Storglaciären, Sweden. *Journal of Glaciology*, **49**, 59–68. 144, 345

Kääb, A., Huggel, C., Paul, F., Wessels, R., Raup, B., Kieffer, H., & Kargel, J. 2002. Glacier monitoring from ASTER imagery: accuracy and applications. *Proceedings of the ARSeL-LISSIG-Workshop Observing our Cryosphere from Space, Bern, March 11 13*, 43–53. 37

Karlén, W. 1973. Holocene glacier and climatic variations, Kebnekaise Mountains, Swedish Lapland. *Geografiska Annaler*, **55A**, 29–63. 48, 49, 51, 323, 347

Kaser, G., & Osmaston, H. 2002. *Tropical Glaciers*. International Hydrology Series. Cambridge: Cambridge University Press. 107

Kaser, G., Fountain, A., & Jansson, P. 2003. A manual for monitoring the mass balance of mountain glaciers with particular attention to low latitude characteristics. A contribution from the International Commission on Snow and Ice (ICSI) to the UNESCO HKH-Friend programme. *IHP-VI, Technical Documents in Hydrology*, **59**. 30, 31, 32, 34

Kaser, G., Cogley, J. Graham, Dyurgerov, M. B., Meier, F., & Ohmura, A. 2006. Mass balance of glaciers and ice caps: Consensus estimates for 19612004. *Geophysical Research Letters*, **33**, L19501. 7, 8

Kaser, Georg, Hardy, Douglas R., Mlg, Thomas, Bradley, Raymond S., & Hyera, Tharsis M. 2004. Modern glacier retreat on Kilimanjaro as evidence of climate change: observations and facts. *International Journal of Climatology*, **24**(3), 329–339. 88

Kayastha, R. B. 1994. *Sensitivity of glacier mass balance to meteorological conditions in the Himalaya*. M.Phil. thesis, Institute for Hyrdospheric-Atmospheric Sciences, Nagoya University. 146

Kerr, R.A. 2013. Melting Glaciers, Not Just Ice Sheets, Stoking Sea-Level Rise. *Science*, **340**(6134), 798. 8, 357

Klok, E. J., & Oerlemans, J. 2002. Model study of the spatial distribution of the energy and mass balance of Morteratschgletscher, Switzerland. *Journal of Glaciology*, **48**(163), 505–518. 27, 137, 138, 343, 347, 351, 432

Klok, E. J. Lisette, Greuell, Wouter, & Oerlemans, Johannes. 2003. Temporal and spatial variation of the surface albedo of Morteratschgletscher, Switzerland, as derived from 12 Landsat images. *Journal of Glaciology*, **49**(167), 491–502. 345

Knoll, Christoph, & Kerschner, Hanns. 2009. A glacier inventory for South Tyrol, Italy, based on airborne laser-scanner data. *Annals of Glaciology*, **50**(53), 46–52. 329

Knoll, Christoph, Heller, Armin, Kerschner, Hanns, & Rastner, Philipp. 2009. A GIS-based Reconstruction of Little Ice Age Glacier Maximum Extents for South Tyrol, Italy. *Transactions in GIS*, **13**(5/6), 449–463. 30

Koblet, T., Gärtner-Roer, I., Zemp, M., Jansson, P., Thee, P., Haeberli, W., & Holmlund, P. 2010. Reanalysis of multi-temporal aerial images of Storglaciären, Sweden (1959 - 99)Part 1: Determination of length, area, and volume changes. *The Cryosphere*, **4**(3), 333–343. 336

Kociuba, W., Kubisz, W., & Zagórski, P. (in press). Use of terrestrial laser scanning (TLS) for monitoring and modelling of geomorphic processes and phenomena at a small and medium spatial scale in Polar environment (Scott River Spitsbergen). *Geomorphology*. 361

Kohler, J., James, T. D., Murray, T., Nuth, C., Brandt, O., Barrand, N. E., Aas, H. F., & Luckman, A. 2007. Acceleration in thinning rate on western Svalbard glaciers. *Geophysical Research Letters*, **34**, L18502. 361

Krimmel, R. M., & Meier, M. F. 1975. Glacier applications of ERTS-1 images. *Journal of Glaciology*, **15**, 391–402. 36

Kuhn, M. 1981. Climate and Glaciers. *International Association of Hydrological Sciences*, **Publication no. 131**, 320. 5

Kulkarni, A.V., Bahuguna, I.M., Rathore, B.P., Singh, S.K., Randhawa, S.S., Sood, R.K., & Dhar, S. 2007. Glacial retreat in Himalaya using Indian Remote Sensing satellite data. *Current Science*, **92**(1). 88

Kurowski, L. 1891. *Die Höhe der Schneegrenze mit besonderer Berucksochtigung der Finsteraarhorngruppe*. Vol. Bd 5. Heft I. 106, 107

Lantmäteriet. 2010. Lantmäteriet Homepage. *http://www.lantmateriet.se/*, [**Accessed January 2010 - April 2013**]. 59, 66, 69, 100, 206

Lantmäteriet. 2012. *GSD-Mountain Map - Presentation*. 86

Laumann, T., & Reeh, N. 1993. Sensitivity to climate change of the mass balance of glaciers in southern Norway. *Journal of Glaciology*, **39**(133), 656–665. 42

Le Meur, E., Gerbaux, M., Schäfer, M., & Vincent, C. 2007. Disappearance of an Alpine glacier over the 21st Century simulated from modeling its future surface

mass balance. *Earth and Planetary Science Letters*, **261**, 367–374. 27, 42, 230, 341

Leclercq, P. W., Weidick, A., Paul, F., Bolch, T., Citterio, M., & Oerlemans, J. 2012a. Brief communication "Historical glacier length changes in West Greenland". *The Cryosphere*, **6**, 1339–1343. 33

Leclercq, P.W., Pitte, P., Giesen, R.H., Masiokas, M.H., & Oerlemans, J. 2011. Climatic interpretation of the length fluctuations of Glaciar Frías, North Patagonia, Argentina. *Clim. Past Discuss.*, **7**, 3653 – 3697. 146, 152, 357, 358

Leclercq, P.W., Pitte, P., Giesen, R. H., Masiokas, M.H., & Oerlemans, J. 2012b. Modelling and climatic interpretation of the length fluctuations of Glaciar Frías (north Patagonian Andes, Argentina) 1639-2009 AD. *Clim. Past*, **8**, 1385–1402. 341

Lee, H., Shum, C.K., Tseng, K-H., Huang, Z., & Sohn, H-G. 2013. Elevation changes of Bering Glacier System, Alaska, from 1992 to 2010, observed by satellite radar altimetry. *Remote Sensing of Environment*, **132**, 40–48. 7

Lefauconnier, B., Hagen, J. O., Ørbæk, J. B., Melvold, K., & Isaksson, E. 1999. Glacier balance trends in the Kongsfjorden area, western Spitsbergen, Svalbard, in relation to climate. *Polar Research*, **18**, 307–313. 7

Lehning, M., Völksch, I., Gustafsson, D., Nguyen, T. A., Stähli, M., & Zappa, M. 2006. ALPINE3D: a detailed model of mountain surface processes and its application to snow hydrology. *Hydrological Processes*, **20**(10), 2111–2128. 22, 45, 159, 431

Lemke, P. et al. 2007. Observations: changes in snow, ice and frozen ground. *Climate Change 2007: The Physical Science Basis — Contribution of Working Group I to the Fourth Assessment Report of the Intergovernmental Panel on Climate Change*, 996. 5

Lenaerts, J. T. M., van Angelen, J. H., van den Broeke, M. R., Gardner, A. S., Wouters, B., & van Meijgaard, E. 2013. Irreversible mass loss of Canadian Arctic Archipelago glaciers. *Geophysical Research Letters*, **40**, 1–5. 5, 323

Leonard, Katherine C., & Fountain, Andrew G. 2003. Map-based methods for estimating glacier equilibrium-line altitudes. *Journal of Glaciology*, **49**(166), 329–336. 106

Lillesand, T.M., Kiefer, R.W., & Chipman, J.W. 2004. *Remote Sensing and Image Interpretation*. 5th ed edn. Hoboken: John Wiley and Sons. 36

MacDougall, A.H., & Flowers, G.E. 2010. Spatial and Temporal Transferability of a Distributed Energy-Balance Glacier Melt Model. *Journal of Climate*, **24**(5), 1480–1498. 2, 42, 44, 45, 147

Machguth, H., Eisen, O., Paul, F., & Hoelzle, M. 2006. Strong spatial variability of snow accumulation observed with helicopter-borne GPR on two adjacent Alpine glaciers. *Geophys. Res. Lett.*, **33**(L13503). 334

Meier, M. F., & Post, A.S. 1962. Recent variations in mass net budgets of glaciers in western North America. *IASH*, **58**, 63–77. 107

Meier, M. F., Dyurgerov, M.B., Rick, U. K., O'Neel, S., Pfeffer, W.T., Anderson, R.S., Anderson, S.P., & Glazovsky, A.F. 2007. Glaciers dominate eustatic sea-level rise in the 21st century. *Science*, **317**, 1064–1067. 1, 7, 8

Mernild, S.H., Liston, G.E., Kane, D.L., Knudsen, N.T., & Hasholt, B. 2008. Snow, runoff, and mass balance modeling for the entire Mittivakkat Glacier (19982006), Ammassalik Island, SE Greenland. *Geografisk Tidsskrift-Danish Journal of Geography*, **108**(1), 121–136. 344

Michlmayr, G., Lehning, M., Koboltschnig, G., Holzmann, H., Zappa, M., Mott, R., & Schöner, W. 2008. Application of the Alpine 3D model for glacier mass balance and glacier runoff studies at Goldbergkees, Austria. *Hydrological Processes*, **22**(19), 3941–3949. 2, 22, 45, 147, 159, 367

Miller, G. H., Bradley, R. S., & Andrews, J. T. 1975. The glaciation level and lowest equilibrium line altitude in the high Canadian Arctic: maps and climatic interpretation. *Arctic and Alpine Research*, **7**, 155–168. 106

Minder, J.R., Mote, P.W., & Lundquist, J.D. 2010. Surface temperature lapse rates over complex terrain: Lessons from the Cascade Mountains. *Journal of Geophysical Research*, **115**, D14122. 147

Mölg, T., & Hardy, D. R. 2004. Ablation and associated energy balance of a horizontal glacier surface on Kilimanjaro. *Journal of Geophysical Research*, **109**, D16104. 344

Moran, M.L., Greenfield, R.J., & Arcone, S.A. 2003. Modeling GPR radiation and reflection characteristics for a complex temperate glacier bed. *Geophysics*, **68**(2), 559–565. 334

Morlighem, M., Rignot, E., Moughinot, J., Wu, X., Seroussi, H., Larour, E., & Paden, J. 2013. High-resolution bed topography mapping of Russell Glacier, Greenland, inferred from Operation IceBridge data. *Journal of Glaciology*, **59**, 1015–1023. 368

Murray, T., Stuart, G. W., Miller, P. J., Woodward, J., Smith, A. M., Porter, P.R., & Jiskoot, H. 2000. Glacier surge propagation by thermal evolution at the bed. *Journal of Geophysical Research: Solid Earth*, **105**(B6), 13491–13507. 335

Murray, T., Booth, A., & Rippin, D.M. 2007. Water-content of glacier-ice: limitations on estimates from velocity analysis of surface ground-penetrating radar surveys. *Journal of Environmental and Engineering Geophysics*, **12**, 87–99. 67

Nakawo, M., & Rana, B. 1999. Estimate of Ablation Rate of Glacier Ice under a Supraglacial Debris Layer. *Geografiska Annaler*, **81**, 695–701. 145

Nakawo, M., & Takahashi, S. 1982. A simplified model for estimating glacier ablation under a debris layer. *Pages 137–145 of: IAHS Publ. No. 138.* Hydrological Aspects of Alpine and High Mountain Areas: Proceedings of the Exeter Symposium, July 1982. 145

Nakawo, M., & Young, G.J. 1982. Estimate of glacier ablation under a debris layer from surface temperature and meteorological variables. *Journal of Glaciology*, **28**, 29–34. 145

Nemec, J., Huybrechts, P., Rybak, O., & Oerlemans, J. 2009. Reconstruction of the annual balance of Vadret da Morteratsch, Switzerland, since 1865. *Annals of Glaciology*, **50**, 126–134. 32

Nesje, A. 1992. Topographical effects on the equilibrium-line altitude on glaciers. *GeoJournal*, **27**(4), 383–391. 25, 26

Nesje, A., Bakke, J., Dahl, S.O., Lie, Ø., & Matthews, J.A. 2008. Norwegian mountain glaciers in the past, present and future. *Global and Planetary Change*, **60**, 10–27. 26

Niethammer, U., James, M. R., Rothmund, S., Travelletti, J., & Joswig, M. 2012. UAV-based remote sensing of the Super-Sauze landslide : evaluation and results. *Engineering Geology*, **128**(1), 2–11. 361

NOAA. 2012 (oct). *NOAA Solar Calculator*. 133

Nussbaumer, S. U., Nesje, A., & Zumbühl, H. J. 2011. Historical glacier fluctuations of Jostedalsbreen and Folgefonna (southern Norway) reassessed by new pictorial and written evidence. *The Holocene*, **21**(3), 455–471. 30, 35, 37

Nuth, C., Kohler, J., Aas, H. F., Brandt, O., & Hagen, J. O. 2007. Glacier geometry and elevation changes on Svalbard (1936-90): a baseline dataset. *Annals of Glaciology*, **46**(1), 106–116. 64, 66, 101, 327, 331, 354, 360

Oerlemans, J. 1987. The heat budget of the Ross drainage basin. *Pages 287–292 of:* van der Veen, C. J., & Oerlemans, J. (eds), *Dynamics of the West Antarctic Ice Sheet*. Reidel. 9

Oerlemans, J. 1993. A model for the surface balance of ice masses: part I. Alpine Glaciers. *Zeitschrift für Gletscherkunde und Glazialgeolgie*, **27/28**, 63–83. 148

Oerlemans, J. 2000. Analysis of a 3 year meteorological record from the ablation zone of Morteratschgletscher, Switzerland: energy and mass balance. *Journal of Glaciology*, **46**, 571–579. 43

Oerlemans, J. 2005. Extracting a Climate Signal from 169 Glacier Records. *Science*, **308**(5722), 675–677. 6, 30

Oerlemans, J. 2010a. *The Microclimates of Valley Glaciers*. Universiteitsbibliotheek Utrecht: Utrecht Publishing and Archiving Services. 15, 27, 44, 136

Oerlemans, J.]. 2010b. *The Microclimate of Valley Glaciers*. Igitur (Utrecht Publishing and Archiving Services). 136

Oerlemans, J., & Hoogendoorn, N.C. 1989. Mass-balance gradients and climatic change. *Journal of Glaciology*, **35**, 399–405. 145

Oerlemans, J., & Knapp, W.H. 1998. A 1 year record of global radiation and albedo in the ablation zone of Morteratschgletscher, Switzerland. *Journal of Glaciology*, **44**, 231–238. 145

Oerlemans, J., Anderson, B., Hubbard, A., Huybrechts, P., Jóhannesson, T., Knap, W. H., Schmeits, M., Stroeven, A. P., van de Wal, R. S. W., Wallinga, J., & Zuo, Z. 1998. Modelling the response of glaciers to climate warming. *Climate Dynamics*, **14**(4), 267–274. 5

Ohata, Tetsuo, Ikegami, Koichi, & Higuchi, Keiji. 1980. Albedo of Glacier AX 010 during the Summer Season in Shorong Himalaya, East Nepal : Glaciological Expedition of Nepal, Contribution No. 68. *Journal of the Japanese Society of Snow and Ice*, **41**, 48–54. 146

Ohmura, A. 2009. Observed decadal variations in surface solar radiation and their causes. *J. Geophys. Res.*, **114**, D00D05. 344

Oke, T. 1987. *Boundary Layer Climates*. London: Routledge. 16, 17, 20, 24

Osmaston, H. 2005. Estimates of glacier equilibrium line altitudes by the AreaAltitude, the AreaAltitude Balance Ratio and the AreaAltitude Balance Index methods and their validation. *Quaternary International*, **138-139**(0), 22–31. 34, 107, 108, 109, 340

Østrem, G., & Brugman, M. 1991. Glacier Mass-Balance Measurements: A Manual for Field and Office Work. *NHRI Science Report*, 224. 30, 69

Østrem, G., & Haakensen, N. 1999. Map Comparison or Traditional Mass-Balance Measurements: Which Method Is Better? *Geografiska Annaler*, **81A**(4), 703–711. 31, 40, 353

Paterson, W.S.B. 1994. *The Physics of Glaciers*. Oxford: Butterworth-Heinemann. 5, 30, 32, 33, 71, 145, 146, 150, 151, 252, 258

Paul, F. 2002. Changes in glacier area in Tyrol, Austria, between 1969 and 1992 derived from Landsat 5 Thematic Mapper and Austrian Glacier Inventory data. *International Journal of Remote Sensing*, **23**(4), 787–799. 36, 37, 38, 39, 327, 329

Paul, F. 2004. Rapid disintegration of Alpine glaciers observed with satellite data. *Geophys. Res. Lett.*, **31**(21), L21402. 2, 36, 323, 327, 328, 330

Paul, F. 2008. Calculation of glacier elevation changes with SRTM: Is there an elevation dependent bias? *Journal of Glaciology*, **55**(188), 945–946. 37

Paul, F. 2010. The influence of changes in glacier extent and surface elevation on modeled mass balance. *The Cryosphere Discussions*, **4**, 737–766. 2, 13, 28, 350, 352

Paul, F. 2011. Sea-level rise: Melting glaciers and ice caps. *Nature Geoscience*, **4**(2), 71–72. 8

Paul, F., & Kääb, A. 2005. Perspectives on the production of a glacier inventory from multispectral satellite data in Arctic Canada: Cumberland Peninsula, Baffin Island. *Annals of Glaciology*, **42**, 59–66. 39

Paul, F., Machguth, H., & Kääb, A. 2005. On the impact of glacier albedo under conditions of extreme glacier melt: the summer of 2003 in the Alps. *EARSeL eProceedings*, **4**, 139–149. 344

Pelto, M. S. 2006. The current disequilibrium of North Cascade glaciers. *Hydrological Processes*, **20**(4), 769–779. 35

Petersen, L., & Pellicciotti, F. 2011. Spatial and temporal variability of air temperature on a melting glacier: Atmospheric controls, extrapolation methods and their effect on melt modeling, Juncal Norte Glacier, Chile. *Journal of Geophysical Research*, **116**. 121, 147, 148, 343

Petterson, R., & Jansson, P. 2004. Spatial variability in water content at the cold-temperate transition surface of the polythermal Storglaciären, Sweden. *Journal of Geophysical Research*, **109**(F02009). 334

Petterson, R., Jansson, P., & Holmlund, P. 2003. Cold surface layer thinning on Storglaciären, Sweden, observed by repeated ground penetrating radar surveys. *Journal of Geophysical Research*, **108**(F1). 334

Porter, Stephen C. 1975. Glaciation Limit in New Zealand's Southern Alps. *Arctic and Alpine Research*, **7**(1), 33–37. 106

Quincey, D. J., & Glasser, N. F. 2009. Morphological and ice-dynamical changes on the Tasman Glacier, New Zealand, 19902007. *Global and Planetary Change*, **68**(3), 185–197. 347

Racoviteanu, A. E., Paul, F., Raup, B., Khalsa, S. J. S., & Armstrong, R. 2009. Challenges and recommendations in mapping of glacier parameters from space: results of the 2008 Global Land Ice Measurements from Space (GLIMS) workshop, Boulder, Colorado, USA. *Annal of Glaciology*, **50**(53), 53–69. 39

Radić, V., & Hock, R. 2011. Regionally differentiated contribution of mountain glaciers and ice caps to future sea-level rise. *Nature Geoscience*, **4**, 90–94. 7, 8

Rangwala, I., & Miller, J. 2012. Climate change in mountains: a review of elevation-dependent warming and its possible causes. *Climatic Change*, **114**(3), 527–547. 6

Ranzi, R., Grossi, G., Iacovelli, L., & Taschner, S. 2004. Use of multispectral ASTER images for mapping debris-covered glaciers within the GLIMS project. *Geoscience and Remote Sensing Symposium, 2004. IGARSS '04. Proceedings. 2004 IEEE International*, **2**, 1144–1147. 37

Raper, S.C.B., & Braithwaite, R.J. 2006. Low sea level rise projections from mountain glaciers and icecaps under global warming. *Nature*, **439**, 311–313. 1, 5, 7, 8, 9, 147

Rasmussen, L. A., Conway, H., Krimmel, R. M., & Hock, R. 2011. Surface mass balance, thinning and iceberg production, Columbia Glacier, Alaska, 1948–2007. *Journal of Glaciology*, **57**(203), 431–440. 331

Raup, B., Racoviteanu, A., Khalsa, S. J. S., Helm, C., Armstrong, R., & Arnaud, Y. 2007a. The GLIMS geospatial glacier database: A new tool for studying glacier change. *Global and Planetary Change*, **56**(1-2), 101–110. 37

Raup, B., Kääb, A., Kargel, J. S., Bishop, M. P., Hamilton, G., Lee, E., Paul, F., Rau, F., Soltesz, D., Khalsa, S. J. S., Beedle, M., & Helm, C. 2007b. Remote sensing and GIS technology in the Global Land Ice Measurements from Space (GLIMS) Project. *Computers and Geosciences*, **33**(1), 104–125. 37

Raymond, C.F. 1980. Temperate valley glaciers. *In:* Colbeck, S.C. (ed), *Dynamics of snow and ice masses*. New York: Academic Press. 104, 202

Rignot, E., Rivera, A., & Casassa, G. 2003. Contribution of the Patagonia Icefields of South America to sea level rise. *Science*, **302**, 434–437. 331

Rippin, D.M., Carrivick, J.L., & Williams, C. 2011. Evidence towards a thermal lag in the response of Kårsaglaciären, northern Sweden, to climate change. *Journal of Glaciology*, **57**(205), 895–903. ii, 7, 49, 67, 71, 73, 74, 100, 201, 334, 335, 358, 359, 371

Rott, H. 1976. Analyse der Schneeflächen auf Gletschern der Tiroler Zentralalpen aus Landsat Bildern. *Zeitschrift für Gletscherkunde und Glazialgeologie*, **12**, 128. 36

Rott, H., Stuefer, M., Siegel, A., Skvarca, P., & Eckstaller, A. 1998. Mass fluxes and dynamics of Moreno Glacier, Southern Patagonia Icefield. *Geophysical Research Letters*, **25**, 1407–1410. 368

Russell, A.J. 1995. Late Devensian meltwater movement and storage within the Ochil hills, central Scotland. *Scottish Journal of Geology*, **31**, 65–78. 38

Rutt, I.C., Hagdorn, M., Hulton, N.R.J., & Payne, A.J . 2009. The Glimmer community ice sheet model. *J. Geophys. Res.*, **114**, F02004. 159

Salinger, J., Chinn, T., Willsman, A., & Fitzharris, B. 2008. Glacier response to climate change. *Water and Atmosphere*, **16**(3), 16–17. 9

Schöner, W., & Böhm, R. 2007. A statistical mass-balance model for reconstruction of LIA ice mass for glaciers in the European Alps. *Annals of Glaciology*, **46**, 161–169. 32

Schytt, V. 1963. Glaciärernas Liv. *Svenska Turistföreningen Årsskrift Norrbotten*, 144–158. 53

Schytt, V. 1964. Scientifc results of the Swedish Glaciological Expedition to Nordaustlandet, Spitsbergen, 1957 and 1958. *Geografiska Annaler*, **46**(3), 243–281. 42

Sellers, W.D. 1965. *Physical Climatology.* Chicago: The University of Chicago Press. 133, 135

Seroussi, H., Morlighem, M., Rignot, E., Larour, E., Aubry, D., Ben Dhia, H., & Kristensen, Steen Savstrup. 2011. Ice flux divergence anomalies on 79north Glacier, Greenland. *Geophysical Research Letters*, **38**, L09501. 368

Shahgedanova, M., Nosenko, G., Bushueva, I., & Ivanov, M. 2012. Changes in area and geodetic mass balance of small glaciers, Polar Urals, Russia, 1950–2008. *Journal of Glaciology*, **58**(211), 953–964. 40, 354

Sharpnack, D.A., & Akin, G. 1969. An algorithm for computing slope and aspect from elevations. *Photogrammetric Engineering*, **35**(3), 247–248. 154

Shepherd, A., & Wingham, D. 2007. Recent Sea-Level Contributions of the Antarctic and Greenland Ice Sheets. *Science*, **315**, 1529–1532. 7

Shugar, D. H., Rabus, B. T., & Clague, J. J. 2010. Elevation changes (1949–1995) of Black Rapids Glacier, Alaska, derived from a multi-baseline InSAR DEM and historical maps. *Journal of Glaciology*, **56**(198), 625–634. 9, 92, 331

Sissons, J. B. 1974. A Late-Glacial Ice Cap in the Central Grampians, Scotland. *Transactions of the Institute of British Geographers*, 95–114. 107, 108

Sissons, J.B. 1980. The Loch Lomond advance in the Lake District, northern England. *Transactions Royal Society Edinburgh: Earth Sciences*, **71**, 1327. 107, 108

Sjögren, O. 1909. Geografiska och glacialgeografiska studier vid Torneträsk. *Sveriges Geologiska Undersökning*, **Serie C 219**, 210. 49

Smith, M. J., Chandler, J., & Rose, J. 2009. High spatial resolution data acquisition for the geosciences: kite aerial photography. *Earth Surface Processes and Landforms*, **34**(1), 155–161. 361

Solomon, S., Qin, D., Manning, M., Chen, Z., Marquis, M., Averyt, K.B., Tignor, M., & Miller, H.L. [eds.]. 2007. *Climate change 2007: the physical science basis. Contribution of Working Group I tothe Fourth Assessment Report of the Intergovernmental Panel on Climate Change.* Cambridge: Cambridge University Press. 5, 7

Strasser, U., Etchevers, P., & Lejeune, Y. 2002. Inter-Comparison of two Snow Models with Different Complexity using Data from an Alpine Site. *Nordic Hydrology*, **33**(1), 15–26. 347

Strasser, U., Corripio, J., Pellicciotti, F., Burlando, P., Brock, B., & Funk, M. 2004. Spatial and temporal variability of meteorological variables at Haut Glacier dArolla (Switzerland) during the ablation season 2001: Measurements and simulations. *Journal of Geophysical Research*, **109**, D03103. 345

Sugden, D. E., & John, B. S. 1976. *Glaciers and Landscape.* London: Arnold. 106

Svenious, F.V. 1910. Die Gletscher Schwedens im Jahre 1908. *Sveriges Geologiska Undersökning*, **Serie Ca 5 part I**, 1–53. 51

Sverdrup, H. U., & Ahlmann, H.W. 1935. Scientific Results of the Norwegian-Swedish Spitsbergen Expedition in 1934. Part IV-V. *Geografiska Annaler*, **17**, 145–218. 35

Tangborn, W.V. 1984. Prediction of glacier derived runoff for hydroelectric development. *Geografiska Annaler*, **66A**, 257–265. 145

Tennant, C., & Menounos, B. 2013. Glacier Change of the Canadian Rocky Mountains, 1919-2009. *Journal of Glaciology*, **59**, 671–686. 35

Tennant, C., Menounos, B., Wheate, R., & Clague, J. J. 2012. Area change of glaciers in the Canadian Rocky Mountains, 1919 to 2006. *The Cryosphere*, **6**, 1541–1552. 36, 327, 328, 329, 330

Thibert, E., Vincent, C., Blanc, R., & Eckert, N. 2008. Glaciological and Volumetric Mass Balance Measurements: An error analysis over 51 years, Sarennes Glacier, French Alps. *Journal of Glaciology*, **54**, 522–532. 12, 64

Thomson, M. H., Kirkbride, M. P., & Brock, B. W. 2000. Twentieth century surface elevation change of the Miage Glacier, Italian Alps. *Pages 219–225 of:* Nakawo, M., Raymond, C. F., & Fountain, A. (eds), *Debris-Covered Glaciers*. Iahs Publication. Wallingford: Int Assoc Hydrological Sciences. 331

Thorp, P.W. 1991. Surface profiles and basal shear stresses of outlet glaciers from a Late-glacial mountain ice field in western Scotland. *Journal of Glaciology*, **37**(125), 77–88. 104, 202, 226, 331

Torsnes, I., Rye, N., & Nesje, A. 1993. Modern and Little Ice Age Equilibrium-Line Altitudes on Outlet Valley Glaciers from Jostedalsbreen, western Norway: An Evaluation of Different Approaches to Their Calculation. *Arctic and Alpine Research*, **25**(2), 106–116. 200

UNESCO. 1970. Perennial Snow and Ice Masses. *Technical Papers in Hydrology*, **1**. 330, 331

Van de Wal, R. S. W., & Wild, M. 2001. Modelling the response of glaciers to climate change by applying volume-area scaling in combination with a high resolution GCM. *Climate Dynamics*, **18**(3), 359–366. 334

Van de Wal, R. S.W., Oerlemans, J., & van der Hage, J.C. 1992. A study of ablation variations on the tongue of Hintereisferner, Austrian Alps. *Journal of Glaciology*, **38**(130), 319–324. 345

Vincent, C. 2002. Influence of climate change over the 20th Century on four French glacier mass balances. *J. Geophys. Res.*, **107**(D19), 4375. 32

Vincent, C., & Vallon, M. 1997. Meteorological controls on glacier mass balance: empirical relations suggested by measurements on glacier de Sarennes, France. *Journal of Glaciology*, **43**(143), 131–137. 42

Wallén, C. C. 1948. Glacial-meteorological investigations on the Kårsa glacier in Swedish Lappland. *Geografiska Annaler*, **30**(3-4), 451–672. 48, 49, 53, 54, 239, 323, 331, 341, 354, 359, 366

Wallén, C. C. 1949. The Shrinkage of the Kårsa Glacier and Its Probable Meteorological Causes. *Geografiska Annaler*, **31**, 275–291. 35, 48, 53, 54, 323, 331

Wallén, C. C. 1959. The Kårsa Glacier and its relation to the climate of the Torne Träsk region. *Geografiska Annaler*, **41**(4), 236–244. 48, 53

Warren, S.G. 1982. Optical Properties of Snow. *Reviews of Geophysics*, **20**, 67–89. 144, 145

Warren, S.G., & Wiscombe, W.J. 1980. A Model for the Spectral Albedo of Snow. II: Snow containing Atmospheric Aerosols. *Journal of the Atmospheric Sciences*, **37**, 2734–2745. 144, 145

Wayman, J.C. 2003. *Multiple Imputation For Missing Data: What Is It And How Can I Use It?* Annual Meeting of the American Educational Research Association. 112, 113

Westoby, M. J., Brasington, J., Glasser, N. F., Hambrey, M. J., & Reynolds, J. M. 2012. Structure-from-Motion photogrammetry: A low-cost, effective tool for geoscience applications. *Geomorphology*, **179**, 300–314. 362, 367

WGMS. 2013. World Glacier Monitoring Service Homepage. *http://www.geo.uzh.ch/microsite/wgms/about.html*, [**Accessed 5th May 2013**]. 37, 325, 326, 328

Wild, M. 2009. Global dimming and brightening: A review. *J. Geophys. Res.*, **114**, D00D16. 344

Williams, R. S., & Ferrigno, J. G. 2010. Satellite Image Atlas of Glaciers of the World. *http://pubs.usgs.gov/fs/2005/3056*, [**Accessed 13th September 2011**]. 36

Wood, W.F., & Snell, J.B. 1960. *A Quantitative System for Classifying Landforms.* Quartermaster Research and Engineering Command, US Army. 99

Xu, J., Grumbine, R. E., Shrestha, A., Eriksson, M., Yang, X., Wang, Y. U. N., & Wilkes, A. 2009. The Melting Himalayas: Cascading Effects of Climate Change on Water, Biodiversity, and Livelihoods. *Conservation Biology*, **23**(3), 520–530. 7

Zagórski, P., Siwek, K., Gluza, A., & Bartoszewski, S.A. 2008. Changes in the extent and geometry of the Scott Glacier, Spitsbergen. *Polish Polar Research*, **29**(2), 163–185. 33, 90, 94, 324, 327

Zemp, M., Haeberli, W., Hoelzle, M., & Paul, F. 2006. Alpine glaciers to disappear within decades? *Geophys. Res. Lett.*, **33**(13), L13504. 5, 6, 15, 27, 327

Zemp, M., Paul, F., Hoelze, M., & Haeberli, W. 2008. *Glacier Fluctuations in the European Alps 1850 - 2000.* University of California Press, Ltd. 323, 327, 328

Zemp, M., Jansson, P., Holmlund, P., Gärtner-Roer, I., Koblet, T., Thee, P., & Haeberli, W. 2010. Reanalysis of multi-temporal aerial images of Storglaciären, Sweden (1959 - 99) — Part 2: Comparison of glaciological and volumetric mass balances. *The Cryosphere*, **4**, 345–357. 31

Zemp, M., Thibert, E., Huss, M., Stumm, D., Rolstad Denby, C., Nuth, C., Nussbaumer, S. U., Moholdt, G., Mercer, A., Mayer, C., Joerg, P. C., Jansson, P., Hynek, B., Fischer, A., Escher-Vetter, H., Elvehy, H., & Andreassen, L. M.

2013. Uncertainties and re-analysis of glacier mass balance measurements. *The Cryosphere Discussions*, **7**, 789–839. 8, 30, 31

Zevenbergen, L. W., & Thorne, C. R. 1987. Quantitative analysis of land surface topography. *Earth Surface Processes and Landforms*, **12**(1), 47–56. 154

Zhang, Y., Liu, S., Shangguan, D., Li, J., & Zhao, J. 2012. Thinning and shrinkage of Laohugou No. 12 glacier in the Western Qilian Mountains, China, from 1957 to 2007. *Journal of Mountain Science*, **9**(3), 343–350. 331

Zhou, G., Esaki, T., Mitani, Y., Xie, M., & Mori, J. 2003. Spatial probabilistic modeling of slope failure using an integrated GIS Monte Carlo simulation approach. *Engineering Geology*, **68**(34), 373–386. 86

Ziaja, W. 2005. Response of the Nordenskiöld Land (Spitsbergen) glaciers Grumantbreen, Håbergbreen and Dryadbreen to the climate warming after the Little Ice Age. *Annals of Glaciology*, **42**, 189–194. 331

Zverkova, N.M., Krenke, A.N., & Chemova, L.P. 1982. Osposobakh opredeleniya granitsii pitaniya lednika [On methods of determining the equilibrium line of glaciers. In Russian with English summary.]. *Materialy Glyatsiologicheskikh Issledovaniya*, **43**, 199–207. 106

Zwally, H.J., Giovinetto, M.B., Li, J., Cornejo, H.G., Beckley, M.A., Brenner, A.C., Saba, J.L., & Yi, D. 2005. Mass changes of the Greenland and Antarctic ice sheets and shelves and contributions to sea-level rise: 1992-2002. *Journal of Glaciology*, **51**(175), 509–527. 8

Appendix A

Kårsaglaciären data availability

Table A.1: Data available for Kårsa. Data highlighted in bold is directly used in this study. Where map data is omitted, this relates to an inability for effective georeferencing (see section 4.2.1).

Year	Data	Source	Other details
1884	Terminus photograph	Svenious, 1890	-
1886	Terminus photograph	Svenious, 1890 and 1910	-
1886	Map of the terminus	Svenious, 1910	-
1903-08	Various photographs	Sjögren, 1909	-
1908	Various photographs	Svenious, 1910	-
1909	**Terminus position map**	**Svenious, 1910; Ahlmann and Tryselius, 1929**	**Swedish/German**
1917	Terminus measurements	Ahlmann and Lindbald, 1940	German
1919	Terminus measurements	Ahlmann and Lindbald, 1940	German
1920	Map of the terminus	Ahlmann and Tryselius, 1929	German
1924	Terminus measurements	Ahlmann and Lindbald, 1940	German
1925	Map of the terminus	Ahlmann and Lindbald, 1940	German

Continued on Next Page...

Table A.1 – Continued

Year	Data	Source	Other details
1926	**Glacier map and area study**	**Ahlmann and Tryselius, 1929**	**German**
1928	Terminus position	Ahlmann and Tryselius, 1929	German
1927-32	Terminus measurements	Ahlmann and Lindbald, 1940	German
1936	Terminus photograph	Ahlmann and Lindbald, 1940	German
1939	Terminus position	Ahlmann and Lindbald, 1940	German
1943	**Glacier Map**	**Wallen, 1948**	**-**
1942-47	**MB study**	**Wallen, 1948**	**-**
1950	Terminus photograph	Holdar, 1957	-
1959	**Glacier map/Aerial photograph**	**University of Stockholm, 1984**	**August photograph**
1961	Glacier Map	Schytt, 1963	-
1973	**Glacier map/Aerial photograph**	**University of Stockholm, 1984**	**July photograph**
1981-82	MB data	Erikkson	Unpublished
1984-85	MB data	Erikkson	Unpublished
1989-91	**MB data**	**Bodin, 1993**	**-**
1991-92	**GPR survey of the glacier**	**Bodin, 1993**	**-**
1991	**Glacier map**	**Bodin, 1993**	**-**
2008	**Satellite Imagery**	**Lantmäteriet**	**July image**
2008-2011	**Winter dGPS and snowpack surveys**	**University of Leeds**	**Unpublished**
2009	**GPR survey of the glacier**	**Rippin et al., 2011**	**-**
2010	**Glacier map**	**This study**	**-**

Appendix B

Select long term geodetic glacier studies

The following table presents a sample of geodetic glacier monitoring/reconstruction studies as discussed in section 2.4.1 of chapter 2.

Table B.1: A selection of geodetic glacier assessments and reconstructions, highlighting data acquisition methods and associated issues

Study period	Country	Glacier	$\bar{x}$ glacier size (km^2)	Climate	Data acquisition	Issues and other details	Author
1969 - 1998	Austria	96% of Austrian glaciers	-	Alpine	Aerial photogrammetry	Advance during the 1970s due to assumption of stationarity regarding glacier area. Linear interpolation will have resulted in similar issues from 1985 - 1998. Volume assessment must account for errors introduced by scaling methods used to derive bed elevations.	Abermann, Kuhn and Fischer (2011)
1880 - 2006	Spitsbergen	Scott glacier	4.75	Polar	Aerial photography, GPS (1987 onwards - direct measurements of extent 2000 onwards)	Difficulty discerning between the glacier and moraine. Area of visible ice assumed as being glacier surface.	Zagrski and Bartoszewski, 2004; Zagrski et al. 2008

Continued on Next Page...

Table B.1 – Continued

Study period	Country	Glacier	$\bar{x}$ glacier size (km^2)	Climate	Data acquisition	Issues and other details	Author
1919 - 2006	Canada	Glaciers in the Canadian Rocky Mountains	1.60	Alpine	Topographic maps (1: 62500 - methods including aerial photography 1903-1924); Landsat (TM and ETM+) imagery	Older maps georeferenced using GCPs identified from Landsat imagery with respective errors in northing and easting of 12.2 m and 11.5 m. Vertical errors associated with the maps used ranges from ±10 m - ±40 m. Errors in area assessments ranged from 9.8 - 12.6%.	Tennant et al., 2012
1919 - 2009	Canada	Columbia icefield	8.22	Sub-Polar	Topographic survey maps (1919), aerial photography (1948-1993), satellite imagery (1999-2009)	Errors present from different data available and accounted for within analysis.	Tennant and Menounos, 2013

Continued on Next Page...

Table B.1 – Continued

Study period	Country	Glacier	$\bar{x}$ glacier size (km^2)	Climate	Data acquisition	Issues and other details	Author
1710 - 2009	Norway	Outlet glaciers of Josteldals-breen and Folgefonna	13.05	Sub-Polar	Pictoral evidence (pictures, engravings, planar photographs), topographic maps, written accounts, satellite imagery	Spatial errors pertaining to disagreements between historical and contemporary locations resulting in georeferencing issues.	Nussbaumer et al. 2011
1962 - 1995	India	Dokriani glacier	7.00		Topographic maps (aerial photography 1962 and 1995), field observations of terminus (1991-1995), GPR measurements for thickness	-	Dobhal et al., 2004

Continued on Next Page...

Table B.1 – Continued

Study period	Country	Glacier	$\bar{x}$ glacier size (km^2)	Climate	Data acquisition	Issues and other details	Author
1944 - 1986	Patagonia	Outlet glaciers of the Southern Patagonia Icefield	234.56		Oblique photographs, aerial photographs, Landsat TM, SPOT and Landsat MSS imagery	Remotely-sensed data limited due to cloud cover. Landsat TM images corrected geometrically and combined to which all other data was located due to the poor topographic map coverage of the area.	Aniya et al. 1996, Aniya et al. 1997
1926 - 1991	Sweden	Kårsa		Sub-Polar	Topographic maps, field measurements and aerial photography.	-	Bodin, 1993

Continued on Next Page...

Table B.1 – Continued

Study period	Country	Glacier	$\bar{x}$ glacier size (km^2)	Climate	Data acquisition	Issues and other details	Author
1961 - 2005	Svalbard	Austre Brøggerbreen, Grønfjordbreen, Midtre Lovénbreen, Albrecht-breen, Gullfak-sebreen and Slakbreen	27.33	Arctic	Stereo-aerial photographs and LiDAR imagery	Oblique photographs (1930s) were available but not used due to poor quality. Errors constrained for aerial photographs as information from the calibrated metric cameras used available. GCPs identified and enhanced from contemp. LiDAR imagery were used to locate aerial photographs. Historic DEM quality assessed by comparing off-ice positions expected to have undergone little physical change.	Murray et al., 2012
1968 - 2006	Garhwal Hi-malaya	Glaciers in the Bhagi-rathi and Saraswati/ Alaknanda basins	3.70 (Saraswati/ Alak-nanda) 13.7 (Bha-girathi)		CORONA, Landsat MSS & TM , Cartosat-1 and ASTER imagery	Mean accuracy of data sets used ˜19.2 m. Best resolution was 2.5 m compared to the pororest at 90 m (ASTER).	Bhambri et al., 2006

Continued on Next Page...

Table B.1 – Continued

Study period	Country	Glacier	$\bar{x}$ glacier size (km^2)	Climate	Data acquisition	Issues and other details	Author
1981 - 2006	Italian Alps	112 glaciers within the Ortles-Cevedale group	˜0.68	Alpine	Landsat imagery, aerial photogrammetry, LiDAR	2-4% discrepancies found with Landsat data relating to debris covered glacier margins. Uncertainties relating to the vompared DEMs a consequence of the different procedures used by the different data acquisition methods.	Carturan et al., 2013
1912 - 2011	Tanzania	Kilimanjaro glacier	1.76	Tropical	Terrestrial photogrammetry, aerial photography, Landsat (MSS and TM) , QuickBird and Kompsat imagery	To extend study fully, old and new mapping methods had to be integrated. Maps available in 1912 and 1962 at 1:50 000. Errors quantified for satellite imagery based on GCP agreement. Errors of topographic maps not quantified. Glacier boundaries were reassessed for some past mapping efforts based on photographic and geomorphological evidence.	Cullen et al., 2013

Continued on Next Page...

Table B.1 – Continued

Study period	Country	Glacier	$\bar{x}$ glacier size (km^2)	Climate	Data acquisition	Issues and other details	Author
1958 - 1998	Washington, USA	All glaciers in the North Cascades	0.34		Oblique and vertical aerial photography	Topographic maps available from 1958 updated for the region but only in terms of man-made structures. Glacial and topographic features not updated. ASTER imagery experimented with but resolution too coarse (15 m^2) for small cirque glaciers (>0.5 km^2) being studied. SRTM data not used due to cloud cover and radar shadowing. C-band synthetic apeture radar (SAR) not used due to presence of large amounts of wet snow which SAR cannot penetrate.	Granshaw et al., 2006
1975 - 2012	Northern central Andes, Peru	Glaciers in the Cordillera Vilcanota	-	Tropical	Landsat MSS, TM, ETM+; ASTER and Corona KH-9 imagery and SRTM data	Study not restricted just to glaciers, also including lake area change. Images frequently obstructed by cloud cover.	Hanshaw and Bookhagen, 2013

Continued on Next Page...

Table B.1 – Continued

Study period	Country	Glacier	$\bar{x}$ glacier size (km^2)	Climate	Data acquisition	Issues and other details	Author
1992 - 2010	Alaska, USA	Bering glacier system			TOPEX/ Poseidon Geophysical Data Record(GDR) and Sensor Data Record from a 10-day repeat cycle 9364 (1992-2002) and Envisat RA-2 GDR	Study assessed elevation changes. Methods used previously only for ice sheets as mountain glaciers proved issuous due to steep and rough terrain clashing with the large footprint of radar altimetry tracks. Method specific to glaciers that are >7 km wide.	Lee et al., 2013
1973 - 1999	Switzerland	930 glaciers in Switzerland	1.05 (SGI)	Alpine	Topographic maps (1973); Landsat TM imagery	Results extrapolated to other regions in the Alps. Data taken from the Swiss Glacier Inventroy (SGI) not as well represented due to snow cover inhibiting glacier quantification campaigns.	Paul et al., 2004

Continued on Next Page...

Table B.1 – Continued

Study period	Country	Glacier	$\bar{x}$ glacier size (km^2)	Climate	Data acquisition	Issues and other details	Author
1969 - 1992	Austria	235 glaciers in the Tyrol	0.80	Alpine	Topographic maps and aerial photography (used for the Austrian Glacier Index (AGI)), Landsat TM images	Errors in area associated with debris cover and misinterpretation of debris/ glacier extent, resulting in a 3% area error. Issues related to shadowing, resulting in removal of certain glaciers from the study. Difficulties in area change introduced by varying temporary snow conditions, present on available imagery. Topographic maps had a much better spatial respolution than the TM imagery, the latter causing apparent area increases (approx. 5% for a 0.1 km^2 glacier).	Paul, 2002

Continued on Next Page...

Table B.1 – Continued

Study period	Country	Glacier	$\bar{x}$ glacier size (km^2)	Climate	Data acquisition	Issues and other details	Author
1990 - 2003	Svalbard	Finster -walderbreen	29.60	Polar	Photogrammetry, GPS profiling	GPS methods provide high resolution (*pm* 0.10-0.15 m) vert. accuracy and prove a useful tool for mass change, providing a larger spatial coverage than would be associated with traditional stake methods. Problems associating changes identified by GPS profile changes with MB change and change at a point incurred by glacier flow.	Hodgkins et al., 2007
1990 - 2007	New Zealand	Tasman Glacier	-		Aerial photography (1986 - from which DEM is derived); Landsat ETM+, TM; ASTER.	Study more focused on change in flow velocity. Elevations acquired using DEM derived from aerial photgrammetry and another developed using ASTER imagery. respective vertical errors were *pm*10 m (absolute) and *pm*20 m (estimate) which gave a 1.4 m yr^{-1} error on elevation changes.	Quincey and Glasser, 2007

Continued on Next Page...

Table B.1 – Continued

Study period	Country	Glacier	$\bar{x}$ glacier size (km^2)	Climate	Data acquisition	Issues and other details	Author
1950 - 2008	Russia	Glaciers in the Polar Urals	<1.0	Polar	Aerial photography, theodolite survey, ASTER, Landsat ETM+, GPS, DGPS.	Errors from a number of sources due to variety of data integrated. Aerial photographs of high resolution (1-3 m). Older maps (devloped using a theodolite) had a vertical error of $pm2.5$ m. Orthorectification accuracy tested via GCP collection and resultant position comparison. Further error introduced by interpolation, especially in areas of greater slope angles.	Shahgedanova et al., 2012

Continued on Next Page...

Table B.1 – Continued

Study period	Country	Glacier	$\bar{x}$ glacier size (km^2)	Climate	Data acquisition	Issues and other details	Author
1861-2004				Alpine	Aerial photography and topographic maps (Siegfried maps 1860-1890)	Non-glacierized areas accounted for in map compilation, providing numerous control points, increasing ability to fit maps as accurately as possible. All data interpolated on regular grids enabling DEM comparison. Long time scale of the DEMs available allowed for observations of multiple advance and recession periods.	Bauder et al., 2002

Appendix C

Select glacier surface energy balance modelling studies

The following table presents a sample of grid-based mass balance model approaches as discussed in section 2.5.3 of chapter 2.

Table C.1: Selected distributed MB models - key objectives, findings and results. The *Geom.* column refers to whether the model calculates geometry dynamically as a function of surface lowering.

Approach	Location	Glacier	Climate	Objectives and methods	Key findings and issues	Geom.	Author
Grid SEB	Swiss Alps	Haut Glacier d'Arolla	Alpine	Spatial approach at calculating SEB whilst considering both the glacier geometry and surrounding topography/ Surface aspect and slope values derived from a DEM were integrated into calculations of shortwave radiation on a cell by cell basis/ Hillshade calculated as a function of surrounding topography	Modelled values compared to observations made along the centre line in 1990, against which there was good agreement (correlation coefficients of 0.99, 0.85 and 0.81 for elevation, albedo and ablation change)/ Error and uncertainty related to paramterisation of albedo within the model (see model entry for Brock *et al.* (2000a))	No	Arnold et al. 1996
Grid SEB	Sweden	Storglaciären	Sub-polar	Developed for assessment of spatial melt and discharge patterns/ MB model coupled with a three tier linear reservoir model/ Hillshade and atmospheric transmissivity, cell slope and aspect accounted for/ Spatial distribution of model allowed for effective accountance of varying hillshade patterns.	Hourly assessment of discharge for the melt seasons of 1993 and 1994 achieve/ Two bulk approaches were used to calculated turbulent fluxes, both taking account of surface geometry, resulting in very different melt water estimates - links to uncertainty of bulk aerodynamic approaches	No	Hock and Noetzli, 1997

Continued on Next Page...

Table C.1 – Continued

Approach	Location	Glacier	Climate	Objectives and methods	Key findings and issues	Geom.	Author
Grid SEB	Swiss Alps	Haut Glacier d'Arolla	Alpine	Use the model of Arnold *et al.* (1996) to assess spatial variations in the effect of albedo and aerodynamic roughness lengths for a full ablation season using new paramterisation schemes/ Aspect and slope values were integrated into calculations of shortwave radiation on a cell by cell basis.	Glacier sensitive to variations in albedo and roughness values, particularly with break down of the winter snowpack and the transient snow line/ Spatially, albedo found to vary with elevation whilst summer snow at higher elevations resulted in large changes in roughness compared to at lower, rougher elevations/ Effects of both were most pronounced under high-energy conditions.	No	Brock et al., 2000a
Grid SEB	Swiss Alps	Morteratsch -gletscher	Alpine	Corrects components to surface geometry (slope, aspect and hillshade)/ Geometry fixed to that of the original input DEM	Sw rad. provided most of the energy to the SEB/ Topographic and geometric effects important, especially for shortwave radiation. Ignoring such factors resulted in 37% more Sw radiation and increased melt / Model limited by snow accumulation distribution, fractional cloud cover estimation and albedo paramterisation	No	Klok and Oerlemans, 2002

Continued on Next Page...

Table C.1 – Continued

Approach	Location	Glacier	Climate	Objectives and methods	Key findings and issues	Geom.	Author
Deg-day	Iceland	Vatnajökull (ice cap)	Maritime	Assessment ice cap hydrological and dynamics response to climatic warming/ Degree-day approach combined with a thermo-mechanical ice sheet and a distributed hydrological model/ Geometry is a requirement for the hydrological model and acquired from the dynamics model	A number of parameters were calculated including changing ice cap geometry, mass balance and runoff relative to climatic variability as assessed from a 1961-1990 reference climatology/ Considering a 2°C increase per century, there would be a 13-36 km retreat over 200 years, along with increase surface runoff/ Changing geometry particularly important when considering areas susceptible to increased discharge rates/ Uncertainty in temperature variation across the icecap	Yes	Flowers et al., 2005

Continued on Next Page...

Table C.1 – Continued

Approach	Location	Glacier	Climate	Objectives and methods	Key findings and issues	Geom.	Author
Grid SEB	French Alps	Glacier de Saint-Sorlin and Glacier d'Argentière	Alpine	Developed to reconstruct mass balance for 1981-2004 with model results validated using satellite imagery and geodetic methods/ Based on the Crocus snow model with meteorological reconstruction devised using the SAFRAN meteorological model/ SAFRAN model acquires elevation, slope and aspect values from the input DEM	Effectively considers complex meteorological effects on MB considering surface geometry (fixed)/ The SAFRAN and Crocus models allow for all components contributing to SEB and MB change to be considered/ Use of a constant DEM is acknowledged as a source of error, as it ignores real surface changes (amounting to 20 m in some areas over the 1981-2004 period). Stated that further work would require assessment of the evolution of the various meteorological components considered	No	Gerbaux et al., 2005

Continued on Next Page...

Table C.1 – Continued

Approach	Location	Glacier	Climate	Objectives and methods	Key findings and issues	Geom.	Author
Deg-day	Iceland	Hosjökull and S. Vatnajökull	Maritime	Monthly temperatures driven Degree-day model is coupled with an finite, vertically integrated ice flow model/ Considers precipitation-elevation feedback excluded in other studies such as Flowers *et al.* (2005)/ Model reference period is 1981-2000 and projected climate change variables are then used to force the model	Glaciers projected to melt slowly initially, speeding up as climate warms further, resulting in annual average runoff increasing and volume modelled to halve within 100-150 years/ MB sensitivity is calculated as part of the study, assessing sensitivity to future changes, although calculation does not account for time dependent changes in geometry	Yes	Adalgeirsdóttir et al, 2006

Continued on Next Page...

Table C.1 – Continued

Approach	Location	Glacier	Climate	Objectives and methods	Key findings and issues	Geom.	Author
Grid SEB	Spitsbergen	Midre Lovénbreen	Polar	Application of SEB over a high resolution LiDAR derived DEM for the ablation season of 2000/ Used to consider the effect of topography as well as glacier slope and aspect on solar radiation receipt ergo surface melting/ The use of LiDAR is key as many DEMs in other studies are derived from contour maps, the method by which many small scale features are smoothed out	Model preforms well compared to in-situ stake derived mass balance measurements for the same period/ Topography found to play a key role in spatial patterns of energy flux distribution/ Slope and aspect barely had an effect on total calculated energy but were extremely important in terms of cross-glacier variation and spatial patterns of melt/ These observed radiation effects were further affected by other feedbacks relating to temperature and snow thickness	No	Arnold et al., 2006

Continued on Next Page...

Table C.1 – Continued

Approach	Location	Glacier	Climate	Objectives and methods	Key findings and issues	Geom.	Author
Grid SEB	French Alps	Saint Sorlin Glacier	Alpine	Developed to reconstruct mass balance for 1981-2004 coupled together with an ice flow model, with model results validated using satellite imagery and geodetic methods/ Uses Crocus and SAFRAN models as in Gerbaux *et al.* (2005)/ Unlike Gerbaux *et al.* (2005), geometry change is considered time	Modelled values found to largely match observed values/ Results show that the glacier will undergo rapid decay under IPCC projections, being non-existant by 2070	Yes	Le Meur et al., 2007
Temp-index	Swiss Alps	Glacier de Zinal, Glacier de Moming and Glacier de Weisshorn	Alpine	MB calc. using a coupled accumulation/ temperature-index model/ DDF factors vary according to direct solar radiation, thus accounting for cell specific slope, aspect and topog. shading, taken from Hock (1999)/ MB model is one of a number of components of the GERM glacio-hydrological model, applied here to assess future runoff for the period 2007-2100	Retreat expected to be considerable, with hydrological regimes altering from being ice melt to snow melt dominated/ Runoff peaks expected in autumn and spring, being at their lowest in summer/ Experiments with keeping the glacier geometry fixed (a reference balance type approach), as opposed to letting it be dynamic, result in runoff values at the end of the 21st century being twice as large	Yes	Huss et al., 2008

Continued on Next Page...

Table C.1 – Continued

Approach	Location	Glacier	Climate	Objectives and methods	Key findings and issues	Geom.	Author
Grid SEB	Austrian Alps	Goldberg -kees	Alpine	Uses the module based Alpine 3D model of Lehning *et al.* (2006) to model hourly discharge and glacier mass balance/ Wind, temperature, humidity and precipitation are interpolated across the surface/ Radiative fluxes and interaction with atmospheric and terrain effects are calculated on a cell by cell basis using the "Complex terrain radiation module" of Alpine3D	Main observed MB patterns reproduced by the model, although in total, loss was overestimated/ Overestimates explained by a lack of mass redistribution within the model (including wind drifting and avalanches)/ Topography recognised as an important factor considering spatial MB change patterns	No	Michlmayr et al, 2008

Continued on Next Page...

Table C.1 – Continued

Approach	Location	Glacier	Climate	Objectives and methods	Key findings and issues	Geom.	Author
Grid SEB	Norway	Hardanger -jøkulen	Maritime/ Continental transition	Developed to assess glacier response through the 20th century and to projected climate changes/ Mass balance model coupled with an ice dynamics model with SEB functionality taken from (Klok & Oerlemans, 2002)/ Glacier geometry is continuously updated in accordance with MB change	Coupling of the mass balance and ice dynamics model allowed for feedback processes between the glacier and climate to be modelled, allowing for realistic assessment of glacial change/ Assuming a projected 3°increase over the next century, the glacier would be expected to disappear/ Large errors were associated with ice thickness values (up to 50 m) which resulted in issues with volume calcs. But model result variability was not of a large enough value to be affected	Yes	Giesen and Oerlemans, 2010

Continued on Next Page...

Table C.1 – Continued

Approach	Location	Glacier	Climate	Objectives and methods	Key findings and issues	Geom.	Author
Grid SEB	NWT, Canada	North Glacier and South Glacier	Alpine	Study to assess model transferability between glaciers/ Slope and aspect derived from DEM to modify individual cell shortwave radiation calculations	Model parameters found to be transferable to within a ¡10% uncertainty/ Model parameter and meteorological function transfer in space found to create large errors in ablation/ Errors can be minimised where local variables (such as albedo) can be retained, resulting in improvements of leq15%	No	MacDoughall and Flowers, 2010
Grid SEB (RB)	Swiss Alps		Alpine	Assesses importance of geometric change on a large selection of glaciers using reference DEMs for the years 1850 and 1973/ Uses a reference balance approach	50-70% of MB response to climate change hidden within geometric adjustment of glaciers, with it being possible to only model/reconstruct 30-50% / Area reduction reduces negativity of balance (0.45 m w.e. less negative) whereas elevation lowering increases negativity (average 0.05 m w.e. more negative)/ Shading also found to be important, increasing over the terminus and resulting in less negative balance values	Yes	Paul et al., 2010

Continued on Next Page...

Table C.1 – Continued

Approach	Location	Glacier	Climate	Objectives and methods	Key findings and issues	Geom.	Author
Temp-index (RB)	Swiss Alps	36 glaciers	Alpine	Uses both a conventional and reference balance approach to assess MB change over time/ MB change driven by a coupled accumulation/temperature-index model taken from Hock (1999)	First study to account for reference MB on a large scale/ Geometry effects found to be very important/ Differences in MB found to increase over time when considering both fixed and adapting geometry, indicating the geometry effect is time dependent/ Geometry not the only thing that controls MB change, with other factors including the correlation between the glacier tongue area with long term MB	Yes	Huss et al., 2012

Appendix D

Model parameter values

The tables below provide the values for all model parameters as detailed in chapter 5. Where values are stated to be a user input, this is implicit of data input from field studies (i.e. these are not constants). Grid inputs imply data is in the form of a matrix - in this study, grid inputs are in the format of ESRI GRID/ASCII files.

Table D.1: Fixed model parameter values

Parameter	Symbol	Value	Unit
Snowfall threshold	T_{Thresh}	1.5	°C
Latent heat of fusion	L_f	3.34 x 10^5	J kg^{-1}
Solar constant	I_0	1368	Wm^{-2}
Ice density	ρ_{ice}	900	kg m^{-3}
Winter snow density	ρ_{snow}	407.13	kg m^{-3}
Summer snow density	ρ_{snow}	200	kg m^{-3}
Water density	ρ_{water}	1000	kg m^{-3}
Temperature lapse rate	Γ	0.0065	Km^{-1}
Mean sun earth distance	Rm	149, 597, 870, 700	m
Instantaneous sun earth distance	R	149, 597, 870, 700	m
Albedo (snow)	α_{snow}	0.70	
Albedo (ice)	α_{ice}	0.39	%
Wind factor	$wind$	0.5	

Table D.2: Dynamic model parameter values. These values will be continuously updated from different sources. The snow thickness (end of season) value is used to initialise daily snow thickness values.

Parameter	Symbol	Value source	Unit
Air temperature	T_a	User input	°C
Solar declination	δ	User input	°
Latitude	η	User input	°
Solar hour angle	ω	User input	°
Solar zenith	θ	User input	°
Solar azimuth	ϕ	User input	°
Surface aspect	A	Internally calculated	°
Surface slope	β	Internally calculated	°
Melt energy	Q	Internally calculated	Wm^{-2}
Rain precipitation	-	User input	m
Snow precipitation	-	User input	m
Ice surface Elevation	$z_{icesurface}$	Grid input	m a.s.l.
Glacier thickness	$z_{glacierthickness}$	Grid input	m a.s.l.
Bed elevation	z_{bed}	Grid input	m a.s.l.
Snow thickness (end of season)	-	Grid input	m
Snow thickness (daily)	-	Internally calculated	m
Hillshade value	i	Grid input	%
Cell volume	V	Internally calculated	m^3

Table D.3: Model run specific parameter values for τ, c ($Wm^{-2}K^{-1}$), ψ_{min} (Wm^{-2}) and T_{Tip} (°C). Runs 1-3 equate to parameters used for Midtdalsbreen (Norway), Storbreen (Norway) and Kongsvegen (Svalbard) respectively, as used in Giesen & Oerlemans (2012).

Model run	τ	c	ψ_{min}	T_{Tip}
1	0.54	8.7	-25	-1.5
2	0.48	8.4	-19	+0.2
3	0.55	10.8	-33	-0.8

Appendix E

Model GUI images

Here are displayed a number of screen shots of the SEB model GUI as described in chapter 5. Screen shots are used to: illustrate the option menus for opening surfaces and input data (which would be in the form of ASCII and CSV files for surfaces and meteorological data respectively (figure E.1); surface visualisation of uploaded surfaces within the main viewing pane (figure E.2); the model type option pane whereby each model available allows a full run depending on the data upload method (also possible through the use of pre-developed configuration files) and varies the level of surface geometric update (figure E.3); the tools available within the programme to investigate changes in the surface (such as regarding elevation change, thickness change and volume updates) which are printed out for the user to see both on screen and in TXT files (figure E.4).

Figure E.1: Data upload options

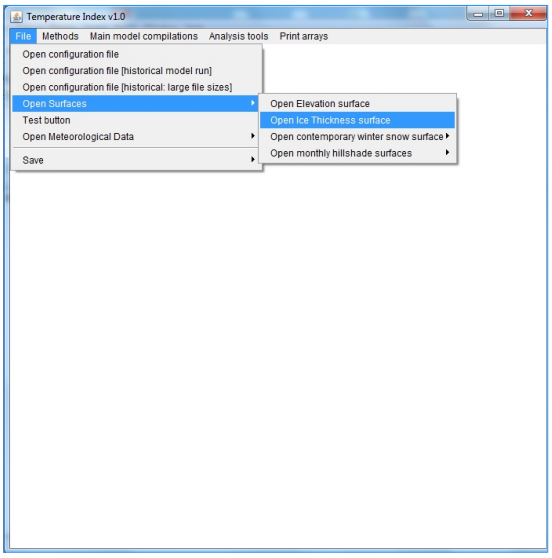

Figure E.2: Surface upload visualisation

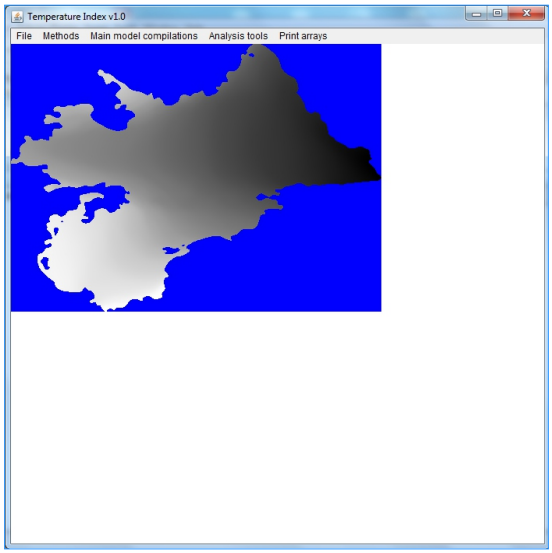

Figure E.3: Model run options

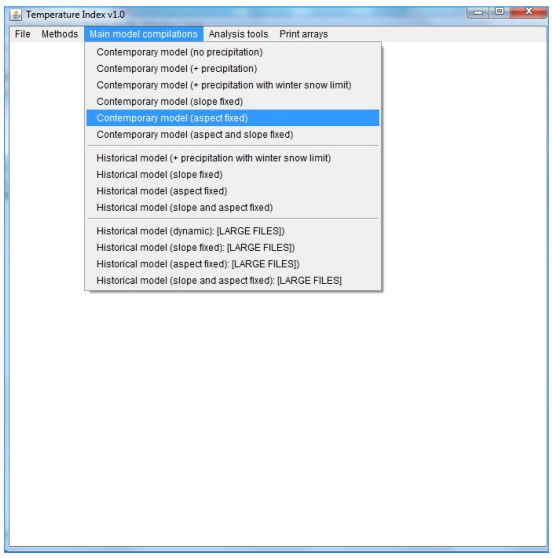

Figure E.4: Inbuilt tool options

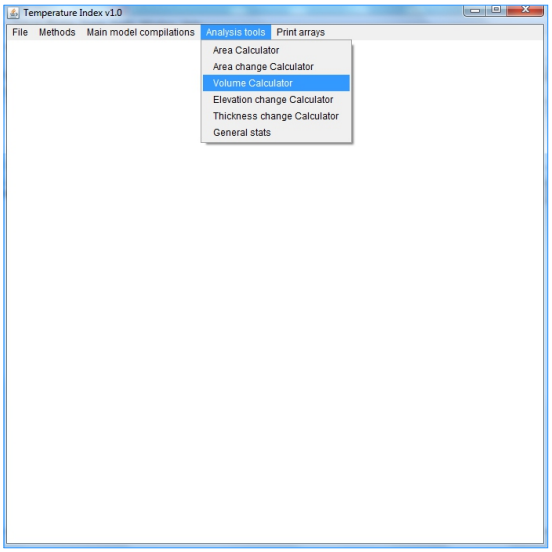

Appendix F

GNU license details

The details below regard the GNU General Public License (Version 2) under which the SEB model developed for this study, available at (`https://github.com/Chris35Wills/SEB_model_java_files`) is registered.

```
                    GNU GENERAL PUBLIC LICENSE
                       Version 2, June 1991

 Copyright (C) 1989, 1991 Free Software Foundation, Inc., [http://fsf.org/]
 51 Franklin Street, Fifth Floor, Boston, MA 02110-1301 USA
 Everyone is permitted to copy and distribute verbatim copies
 of this license document, but changing it is not allowed.

                            Preamble

  The licenses for most software are designed to take away your
freedom to share and change it.  By contrast, the GNU General Public
License is intended to guarantee your freedom to share and change free
software--to make sure the software is free for all its users.  This
General Public License applies to most of the Free Software
Foundation's software and to any other program whose authors commit to
using it.  (Some other Free Software Foundation software is covered by
the GNU Lesser General Public License instead.)  You can apply it to
your programs, too.

  When we speak of free software, we are referring to freedom, not
price.  Our General Public Licenses are designed to make sure that you
have the freedom to distribute copies of free software (and charge for
this service if you wish), that you receive source code or can get it
```

if you want it, that you can change the software or use pieces of it in new free programs; and that you know you can do these things.

To protect your rights, we need to make restrictions that forbid anyone to deny you these rights or to ask you to surrender the rights. These restrictions translate to certain responsibilities for you if you distribute copies of the software, or if you modify it.

For example, if you distribute copies of such a program, whether gratis or for a fee, you must give the recipients all the rights that you have. You must make sure that they, too, receive or can get the source code. And you must show them these terms so they know their rights.

We protect your rights with two steps: (1) copyright the software, and (2) offer you this license which gives you legal permission to copy, distribute and/or modify the software.

Also, for each author's protection and ours, we want to make certain that everyone understands that there is no warranty for this free software. If the software is modified by someone else and passed on, we want its recipients to know that what they have is not the original, so that any problems introduced by others will not reflect on the original authors' reputations.

Finally, any free program is threatened constantly by software patents. We wish to avoid the danger that redistributors of a free program will individually obtain patent licenses, in effect making the program proprietary. To prevent this, we have made it clear that any patent must be licensed for everyone's free use or not licensed at all.

The precise terms and conditions for copying, distribution and modification follow.

GNU GENERAL PUBLIC LICENSE
TERMS AND CONDITIONS FOR COPYING, DISTRIBUTION AND MODIFICATION

0. This License applies to any program or other work which contains a notice placed by the copyright holder saying it may be distributed under the terms of this General Public License. The "Program", below, refers to any such program or work, and a "work based on the Program"

means either the Program or any derivative work under copyright law:
that is to say, a work containing the Program or a portion of it,
either verbatim or with modifications and/or translated into another
language. (Hereinafter, translation is included without limitation in
the term "modification".) Each licensee is addressed as "you".

Activities other than copying, distribution and modification are not
covered by this License; they are outside its scope. The act of
running the Program is not restricted, and the output from the Program
is covered only if its contents constitute a work based on the
Program (independent of having been made by running the Program).
Whether that is true depends on what the Program does.

  1. You may copy and distribute verbatim copies of the Program's
source code as you receive it, in any medium, provided that you
conspicuously and appropriately publish on each copy an appropriate
copyright notice and disclaimer of warranty; keep intact all the
notices that refer to this License and to the absence of any warranty;
and give any other recipients of the Program a copy of this License
along with the Program.

You may charge a fee for the physical act of transferring a copy, and
you may at your option offer warranty protection in exchange for a fee.

  2. You may modify your copy or copies of the Program or any portion
of it, thus forming a work based on the Program, and copy and
distribute such modifications or work under the terms of Section 1
above, provided that you also meet all of these conditions:

    a) You must cause the modified files to carry prominent notices
    stating that you changed the files and the date of any change.

    b) You must cause any work that you distribute or publish, that in
    whole or in part contains or is derived from the Program or any
    part thereof, to be licensed as a whole at no charge to all third
    parties under the terms of this License.

    c) If the modified program normally reads commands interactively
    when run, you must cause it, when started running for such
    interactive use in the most ordinary way, to print or display an
    announcement including an appropriate copyright notice and a

notice that there is no warranty (or else, saying that you provide
a warranty) and that users may redistribute the program under
these conditions, and telling the user how to view a copy of this
License. (Exception: if the Program itself is interactive but
does not normally print such an announcement, your work based on
the Program is not required to print an announcement.)

These requirements apply to the modified work as a whole. If
identifiable sections of that work are not derived from the Program,
and can be reasonably considered independent and separate works in
themselves, then this License, and its terms, do not apply to those
sections when you distribute them as separate works. But when you
distribute the same sections as part of a whole which is a work based
on the Program, the distribution of the whole must be on the terms of
this License, whose permissions for other licensees extend to the
entire whole, and thus to each and every part regardless of who wrote it.

Thus, it is not the intent of this section to claim rights or contest
your rights to work written entirely by you; rather, the intent is to
exercise the right to control the distribution of derivative or
collective works based on the Program.

In addition, mere aggregation of another work not based on the Program
with the Program (or with a work based on the Program) on a volume of
a storage or distribution medium does not bring the other work under
the scope of this License.

3. You may copy and distribute the Program (or a work based on it,
under Section 2) in object code or executable form under the terms of
Sections 1 and 2 above provided that you also do one of the following:

a) Accompany it with the complete corresponding machine-readable
source code, which must be distributed under the terms of Sections
1 and 2 above on a medium customarily used for software interchange; or,

b) Accompany it with a written offer, valid for at least three
years, to give any third party, for a charge no more than your
cost of physically performing source distribution, a complete
machine-readable copy of the corresponding source code, to be
distributed under the terms of Sections 1 and 2 above on a medium
customarily used for software interchange; or,

c) Accompany it with the information you received as to the offer to distribute corresponding source code. (This alternative is allowed only for noncommercial distribution and only if you received the program in object code or executable form with such an offer, in accord with Subsection b above.)

The source code for a work means the preferred form of the work for making modifications to it. For an executable work, complete source code means all the source code for all modules it contains, plus any associated interface definition files, plus the scripts used to control compilation and installation of the executable. However, as a special exception, the source code distributed need not include anything that is normally distributed (in either source or binary form) with the major components (compiler, kernel, and so on) of the operating system on which the executable runs, unless that component itself accompanies the executable.

If distribution of executable or object code is made by offering access to copy from a designated place, then offering equivalent access to copy the source code from the same place counts as distribution of the source code, even though third parties are not compelled to copy the source along with the object code.

4. You may not copy, modify, sublicense, or distribute the Program except as expressly provided under this License. Any attempt otherwise to copy, modify, sublicense or distribute the Program is void, and will automatically terminate your rights under this License. However, parties who have received copies, or rights, from you under this License will not have their licenses terminated so long as such parties remain in full compliance.

5. You are not required to accept this License, since you have not signed it. However, nothing else grants you permission to modify or distribute the Program or its derivative works. These actions are prohibited by law if you do not accept this License. Therefore, by modifying or distributing the Program (or any work based on the Program), you indicate your acceptance of this License to do so, and all its terms and conditions for copying, distributing or modifying the Program or works based on it.

6. Each time you redistribute the Program (or any work based on the Program), the recipient automatically receives a license from the original licensor to copy, distribute or modify the Program subject to these terms and conditions. You may not impose any further restrictions on the recipients' exercise of the rights granted herein. You are not responsible for enforcing compliance by third parties to this License.

7. If, as a consequence of a court judgment or allegation of patent infringement or for any other reason (not limited to patent issues), conditions are imposed on you (whether by court order, agreement or otherwise) that contradict the conditions of this License, they do not excuse you from the conditions of this License. If you cannot distribute so as to satisfy simultaneously your obligations under this License and any other pertinent obligations, then as a consequence you may not distribute the Program at all. For example, if a patent license would not permit royalty-free redistribution of the Program by all those who receive copies directly or indirectly through you, then the only way you could satisfy both it and this License would be to refrain entirely from distribution of the Program.

If any portion of this section is held invalid or unenforceable under any particular circumstance, the balance of the section is intended to apply and the section as a whole is intended to apply in other circumstances.

It is not the purpose of this section to induce you to infringe any patents or other property right claims or to contest validity of any such claims; this section has the sole purpose of protecting the integrity of the free software distribution system, which is implemented by public license practices. Many people have made generous contributions to the wide range of software distributed through that system in reliance on consistent application of that system; it is up to the author/donor to decide if he or she is willing to distribute software through any other system and a licensee cannot impose that choice.

This section is intended to make thoroughly clear what is believed to be a consequence of the rest of this License.

8. If the distribution and/or use of the Program is restricted in

certain countries either by patents or by copyrighted interfaces, the original copyright holder who places the Program under this License may add an explicit geographical distribution limitation excluding those countries, so that distribution is permitted only in or among countries not thus excluded. In such case, this License incorporates the limitation as if written in the body of this License.

9. The Free Software Foundation may publish revised and/or new versions of the General Public License from time to time. Such new versions will be similar in spirit to the present version, but may differ in detail to address new problems or concerns.

Each version is given a distinguishing version number. If the Program specifies a version number of this License which applies to it and "any later version", you have the option of following the terms and conditions either of that version or of any later version published by the Free Software Foundation. If the Program does not specify a version number of this License, you may choose any version ever published by the Free Software Foundation.

10. If you wish to incorporate parts of the Program into other free programs whose distribution conditions are different, write to the author to ask for permission. For software which is copyrighted by the Free Software Foundation, write to the Free Software Foundation; we sometimes make exceptions for this. Our decision will be guided by the two goals of preserving the free status of all derivatives of our free software and of promoting the sharing and reuse of software generally.

NO WARRANTY

11. BECAUSE THE PROGRAM IS LICENSED FREE OF CHARGE, THERE IS NO WARRANTY FOR THE PROGRAM, TO THE EXTENT PERMITTED BY APPLICABLE LAW. EXCEPT WHEN OTHERWISE STATED IN WRITING THE COPYRIGHT HOLDERS AND/OR OTHER PARTIES PROVIDE THE PROGRAM "AS IS" WITHOUT WARRANTY OF ANY KIND, EITHER EXPRESSED OR IMPLIED, INCLUDING, BUT NOT LIMITED TO, THE IMPLIED WARRANTIES OF MERCHANTABILITY AND FITNESS FOR A PARTICULAR PURPOSE. THE ENTIRE RISK AS TO THE QUALITY AND PERFORMANCE OF THE PROGRAM IS WITH YOU. SHOULD THE PROGRAM PROVE DEFECTIVE, YOU ASSUME THE COST OF ALL NECESSARY SERVICING, REPAIR OR CORRECTION.

12. IN NO EVENT UNLESS REQUIRED BY APPLICABLE LAW OR AGREED TO IN WRITING

WILL ANY COPYRIGHT HOLDER, OR ANY OTHER PARTY WHO MAY MODIFY AND/OR REDISTRIBUTE THE PROGRAM AS PERMITTED ABOVE, BE LIABLE TO YOU FOR DAMAGES, INCLUDING ANY GENERAL, SPECIAL, INCIDENTAL OR CONSEQUENTIAL DAMAGES ARISING OUT OF THE USE OR INABILITY TO USE THE PROGRAM (INCLUDING BUT NOT LIMITED TO LOSS OF DATA OR DATA BEING RENDERED INACCURATE OR LOSSES SUSTAINED BY YOU OR THIRD PARTIES OR A FAILURE OF THE PROGRAM TO OPERATE WITH ANY OTHER PROGRAMS), EVEN IF SUCH HOLDER OR OTHER PARTY HAS BEEN ADVISED OF THE POSSIBILITY OF SUCH DAMAGES.

END OF TERMS AND CONDITIONS

Appendix G

Other project outputs

In addition to this thesis, there have been a number of other outputs which are listed here.

Published articles

- Rippin, D.M., Carrivick, J.L., Williams, C., (2011). Evidence towards a thermal lag in the response of small Arctic glaciers to climate change. Journal of Glaciology 57(205), pp895-903.

Proposed articles

- Williams, C., Carrivick, J.L., (in prep). Evaluating mountain glacier change and mass balance sensitivity in Northern Sweden 1926-2010 (target journal: Journal of Glaciology).
- Williams, C., Carrivick, J.L., Carver, S., (in prep). Retreating glaciers and ice sheets: user specific assessments (target journal: Journal of Glaciology).
- Williams, C., Carrivick, J.L., Evans, A., (in prep). A user friendly glacier melt model: its wider application in research and teaching.
- Holmlund, P., Jonasson, C., Williams, C., (in prep). The interaction between perennial snow fields and small glaciers in a sub-Arctic environment in a global change context.

Conference abstracts

- Williams, C., Carrivick, J., Evans, A., Numerical modelling of the effect of changing surface geometry on mountain glacier mass balance (Accepted abstract at AGU 2012, San Francisco, USA).
- Williams, C., Carrivick, J., Evans, A., Carver, S., Changing glacier morphology and glacier mass balance (Leeds University School of Earth and Environment postgraduate Conference, March 2012).

- Williams, C., Carrivick, J., Evans, A., Carver, S., Evaluating mountain glacier change over the 20th and early 21st century utilising a multi-scale approach (International Glaciological Society British Branch meeting, Cambridge, September 2011).
- Williams, C., Carrivick, J., Evans, A., Carver, S., Evaluating mountain glacier change over the 20th and early 21st century utilising a multi-scale approach (UK Arctic Science Conference, University of Leeds, September 2011).
- Williams, C., Carrivick, J., Evans, A., Carver, S., Effects of changing glacier morphology on glacier mass balance (Leeds University School of Geography postgraduate Conference, March 2011).
- Williams, C., Arrell, K., Carrivick, J., Feedbacks between glacier morphology and mass balance (RGS-IBG Annual Conference, September 2010).

Associated grants

- School of Geography (University of Leeds) Research Development Fund (£1400) (January 2012)
- INTERACT (EU-FP7) funding with Dr David Rippin and Dr Jonathan Carrivick (£8000) (May 2011)
- RGS Peter Fleming Award, with Dr David Rippin and Dr Jonathan Carrivick (£9000) (June 2010)
- Royal Society research grant with Dr David Rippin and Dr Jonathan Carrivick (£10,350) (February 2010)
- School of Geography (University of Leeds) Research Development Fund (£1400) (January 2010)
- School of Geography (University of Leeds) Research Development Fund (£800) (January 2009)